ISBN: 978-623-7525-15-8

2019

ICOIRS

THE FIFTH INTERNATIONAL CONFERENCE OF INDONESIAN SOCIETY FOR REMOTE SENSING (ICOIRS) AND MAPIN CONGRESS

17-20 September 2019, ITENAS-Bandung, West Java Indonesia

"The Revolution of Earth Observation for a Better Human Life"

PROCEEDINGS

penerbit itenas

Proceeding *The Fifth International Conferences of Indonesian Society for Remote Sensing (ICOIRS)* 2019

Themes:
The Revolution of Earth Observation for a Better Human Life

Reviewer Team:
1. Prof. Dr. Ir. Dewayany Sutrisno, M.App.Sc. (Indonesia)
2. Dr. Ir. Bambang Edhi Leksono (Indonesia)
3. Dr. Dewi Kania Sari, M.T. (Indonesia)
4. Prof. Dr. Ketut Wikantika, M.Sc (Indonesia)
5. Dr. Agustan (Indonesia)
6. Prof. Wataru Takeuchi (Japan)
7. Prof. Chao-Hung Lin (Taiwan)
8. Prof. Dr. Mazlan Hashim (Malaysia)
9. Tanakorn Sritarapipat, Ph.D., ME., BE (Thailand)

Editor Team:
1. Dr. Henri Kuncoro, M.T.
2. Dr. Eng. Anjar Dimara Sakti, M.Sc.
3. Dr. Lili Somantri, S.Pd., M.Si.
4. Dr. Lissa Fajri Yayusman
5. Rika Hernawati, S.T., M.T.
6. Gusti Ayu Jessy Kartini, S.T., M.T.
7. Nurul Yuhanafia, S.T., M.T.
8. Thonas Indra Maryanto, S.Kel., M.T.
9. Monica Maharani, S.T., M.Eng.
10. Anggun Tridawati, S.T.

Committee:
General Chair : Dr. Soni Darmawan, M.T.
Secretary : Rika Hernawati, S.T., M.T.
Technical Program : Dr. Henri Kuncoro, M.T.
Web Master : Abhi Adhiguna, S.T.

ISBN : 978-623-7525-15-8
First Print : September 2019
Publisher : Penerbit Itenas

Address:
Jl. P.K.H. Mustapha No. 23, Bandung 40124
Telp: +62 22 7272215,
Fax: +62 22 7202892
Email: penerbit@itenas.ac.id

2019

ICOIRS

THE FIFTH INTERNATIONAL CONFERENCE OF INDONESIAN SOCIETY FOR REMOTE SENSING (ICOIRS) AND MAPIN CONGRESS

"The Revolution of Earth Observation
for a Better Human Life"

17-20 SEPTEMBER 2019
BALE DAYANG SUMBI
INSTITUT TEKNOLOGI NASIONAL BANDUNG
WEST JAVA - INDONESIA

FOREWORD

Assalamualaikum Warahmatullahi Wabarakatuh.

First, I would like to say thanks to all committee, sponsor, our students, and our colleague for supporting The Fifth International Conferences of Indonesian Society for Remote Sensing (ICOIRS) and Indonesian Society for Remote Sensing Congress.

The 5th ICOIRS and MAPIN Congress was organized by collaboration of Indonesian Society for Remote Sensing (ISRS/MAPIN), Institut Teknologi Nasional (ITENAS), Center for Remote Sensing Institut Teknologi Bandung, Universitas Pendidikan Indonesia, Universitas Winaya Mukti and Universitas Pajajaran and supported by Ministry of Researh, Technology and Higher Education (RISTEKDIKTI), Geospatial Information Agency (BIG), Indonesian National Institute of Aeronautics and Space (LAPAN), Agency for the Assessment and Application of Technology (BPPT), The Ministry of Agrarian Affairs and Spatial Planning/National Land Agency (ATR/BPN) and Meteorological, Climatological, and Geophysical Agency (BMKG). This event bring together researchers, policy makers, and practitioners from developed and developing countries to share insights into the challenges and opportunities of remote sensing technology and its application in solving the problems of Indonesia especially and South East Asia countries. It showcase cutting-edge research from around South East Asia, cutting-edge research from around South East Asia, focusing on themes of equity and risk, learning, capacity building, methodology, and possibly investment approaches in remote sensing. It explore practical adaptation policies and approaches, and share strategies for decision making to support global cooperation for conserving the earth and for a better human life.

The four-day conference among others consist of plenary, technical and poster sessions, panel discussions, congress of ISRS/MAPIN, exhibition, talk show, workshop, hands on training and city tour. We invite you to join us full time on The 5th ICOIRS and MAPIN Congress and make a successful conference on the application of Remote Sensing, Photogrammetry, GIS, GPS/GNSS, and other related digital mapping technologies in Indonesia and South East Asia.

Hopefully this technical programme can help and guide all of you to absorb all new things on this conference.

Please enjoy it. Thanks…

Wassalamualaikum warahmatullahi wabarakatuh.

Sincerely
Dr. Soni Darmawan
(General Chair of ICOIRS2019 Organizing Committee)

KEYNOTE SPEAKERS

H. M. Ridwan Kamil, S.T., M.U.D.
Governor of West Java

Prof. Hasanuddin Z. Abidin
Head of Indonesian Geospatial Agency (BIG)

Dr. Orbita Roswintiarti, M.Sc
Deputy of Remote Sensing (LAPAN)

Prof.Dr.Ir. Dewayany Sutrisno, M.AppSc
President of Indonesian Society for
Remote Sensing (ISRS/MAPIN)

Prof. Chao-Hung Lin
National Cheng-Kung University, Taiwan

Prof. Wataru Takeuchi
Institute of Industrial Science, The University of Tokyo, Japan

Prof. Tian-Yuan Shih
National Chiao Tung University, Taiwan

Prof. Josaphat Tetuko Sri Sumantyo, Ph.D.
Chiba University, Japan

Prof. Sr. Dr. Mazlan Hashim FASc
Universiti Teknologi Malaysia (UTM), Malaysia

Dr. Gay Jane Perez
University of The Philippines, Philippines

Li Zhang, Ph.D
Co-chair of the Coastal Zone Working Group of the Digital Silk Road
International Scientific Program (DBAR)
Chinese Academy of Sciences, China

Tanakorn Sritarapipat, Ph.D., ME., BE
Suranaree University of Technology, Thailand

Dr. Firman Hadi
Geoinformatics Centre – AIT, Thailand

INVITED SPEAKERS

Prof. Dr. Ir. Bangun Muljo DEA.DESS
Institut Teknologi Sepuluh Nopember

Prof. Projo Danoedoro
Universitas Gajah Mada

Prof. Dr. Ketut Wikantika
Institut Teknologi Bandung

Prof. Dr.-Ing Fahmi Amhar
Badan Informasi Geospasial (BIG)

Prof. Lilik Prasetyo
Institut Pertanian Bogor

Dr. Agustan
Pusat Teknologi Inventarisasi Sumber Daya Alam (PTISDA), BPPT

Dr. Soni Darmawan
Institut Teknologi Nasional Bandung

MAIN PROGRAMME

	07.30 - 08.30	08.30 - 09.45	09.45 -10.00	10.00 - 12.00	12.00-13.00	13.00-15.00	15.00-16.00	17.00-20.00
Day 1 - Tuesday (17th Sep 2019)	Registration	Opening Ceremony			Lunch	Commercial Session / Poster session	Technical Session	Gala Dinner for Invitation
						Technical Session I	Technical Session I	
						Technical Session II	Technical Session II	
						Technical Session III	Technical Session III	
						Workshop GEE	MAPIN Training	
						Commercial Session	Commercial Session	
Day 2 - Wednesday (18th Sep 2019)		Keynote Speaker	Coffee Break	Keynote speaker	Lunch	Commercial Session / Poster session	Technical Session	
				Technical Session I		Technical Session I	Technical Session I	
				Technical Session II		Technical Session II	Technical Session II	
				Technical Session III		Technical Session III	Technical Session III	
				Geomatics Scientific Meeting		Geomatics Scientific Meeting	Geomatics Scientific Meeting	
				Commercial Session		Commercial Session	Commercial Session	

	07.30 - 08.30	08.30 - 09.45	09.45 -10.00	10.00 - 12.00	12.00-13.00	13.00-15.00	15.00-16.00	17.00-20.00
Day 3 - Thursday (19th Sep 2019)		Keynote Speaker	Coffee Break	Talkshow Technical Session I Technical Session II Technical Session III Technical Session Commercial Session	Lunch	Talkshow Technical Session I Technical Session II Technical Session III MAPIN Congress Commercial Session	Closing Ceremony	Gala Dinner for MAPIN Committee and invitation
Day 4 - Friday (20th Sep 2019)	Preparation	**CITY TOUR**						

Information:

- Main Hall at Bale Dayang Sumbi
- At second floor of Bale Dayang Sumbi
- At second floor of Bale Dayang Sumbi
- At second floor of Bale Dayang Sumbi
- At Audio Visual, Building No. 12
- Demonstration stage at Bale Dayang Sumbi
- At Cafe Cinde

TABLE OF CONTENTS

Conference Organization ..... **ii**

Foreword ..... **iv**

Keynote Speakers ..... **v**

Main Programme ..... **viii**

Table of Contents ..... **x**

Effect of Object Homogeneity on Agisoft Processing Success 1
Anna Charieninna, Hary Nugroho and Monica Maharani

Relative Bathymetry Extraction Using SPOT 7 Satellite Imagery 10
Kuncoro Teguh Setiawan, Devica Natalia BR. Ginting, Masita D. M. Manessa, Surahman, Gathot Winarso, Nanin Anggraini, Abdul Basith, Wikanti Asriningrum, Syamsu Rosi and A. Harsono Supardjo

Utilization of Remote Sensing Satellite Data to Predict Future Cloud Cover in Indonesia: A Preliminary Study 17
Ahmad Luthfi Hadiyanto, Ketut Wikantika, Ary Setijadi Prihatmanto and Nurjanna Joko Trilaksono

Mangrove Biomass Estimation Based on Vegetation Height Through Lidar and Terrasar-X Data Approaches 23
Nanin Anggraini, Atriyon Julzarika, Dian Rachmawati and Iwan Erik Setyawan

Asset Identification of Belitung Timur District Government using Geospatial Information Approach 29
Fahrudin and Nurul Mustofa

Urban Building Land Mapping and Monitoring Using Approach Normalized Difference Built-up Index (NDBI) (Case Study: Bandung City, West Java) 36
Felita Larissa Nathania and Rika Hernawati

Correlation Analysis of PM2.5 Air Pollution with NDVI (Normalized Difference Vegetation Index) Based on Landsat-8 (Case Study: Bandung City, West Java) 49
Anis Septi Pratiwi, Rika Hernawati and Soni Darmawan

The Analysis of Correlation Between Pm10 Air Pollution Parameter with The Number of Motored Vehicles Using Landsat Satellite Imagery in Bandung City 56
Anisa Maulidina, Rika Hernawati and Soni Darmawan

Detection of Vegetation Changes Using Landsat Satellite Images in Bandung, Indonesia..... 63
Ichwan Altarans and Rika Hernawati

The Effect of Building Density on Surface Temperature Based Landsat-8 in Bandung City, West Java..... 70
Dery Chahyanto and Rika Hernawati

Strain Analysis Lombok Island Based on GNSS Observation Data 1996 – 2018..... 81
Ardita H Pancanugroho, Henri Kuncoro and Hary Nugroho

Remote Sensing Data for Atlas of Volcanic Landscape Resources..... 93
Fakhruddin Mustofa, Mulyanto Darmawan, Amanah Anggun Prabandari and Zidni Farhati Silmi

Updating Homecoming Route Map (Case Study: Java and Bali Islands)..... 105
Arief Rahman Hakim and Soni Darmawan

The Importance Of Geospatial Information: As a Content in Information Technology Era 120
Asep Karsidi, Samsul Hadi and Totok Sediyantoro

The Comparison of Point Cloud Registration Quality on Maptek I-Site Studio and Cloud Compare..... 129
Fathur Rahman, G A Jessy Kartini and Hary Nugroho

Scanning of Isola UPI Building using Terrestrial Laser Scanner with Cloud to Cloud and Traverse Registration Methods..... 139
Kurniawan Djamal, G A Jessy Kartini and Hary Nugroho

Comparative Study of 3D Geographic Information System and Building Information Modeling for Facility Management..... 146
K N Fadhila, D Suwardhi and S W Trisyanti

Prototype of Remote Sensing Data and Information System Based on Open Source Technology to Support Disaster Management..... 156
Muhammad Priyatna, Ahmad Sutanto, Taufik Hidayat, Aby Al Khudri, Iskandar Effendy, Rokhis Khomarudin and Sastra Kusuma Wijaya

Land Cover Changes Research Level Subpixel A Case Study of Tasikmalaya City on Multitemporal Landsat Image..... 164
Ridwana R, P Danoedoro, S Herumurti, S Himayah and L Somantri

The Effect of Landuse Changes on Peak Discharge Using Cook Method in Sari Watershed West Nusa Tenggara..... 169
R R Suryandari and Sudaryatno

Utilization of Himawari-8 Satellite Data for Estimated Rainfall with Various Methods (Case Study of Heavy Rain Jayapura 16-18 March 2019)..... 182
A R Sagala, H Salawane and A K Silitonga

Field Spectral Reflectance Measurement Distance Effect to the Mangrove Species (Avicennia sp.) Mapping..... 191
T Kanekaputra and M Kamal

Calculation of Total Economic Value of Peatland Burnt Area in Pangkalan Lanpam Sub-district, Ogan Komering Ilir (OKI)..... 200
Tiara Grace F, Riissiyani, Anisah and Dionysius Bryan S

Rapid Mapping for Disaster Recovery (Case Study: Petobo, Palu)..... 207
Z Afif, W Gomarga and B E Leksono

Change Detection of Mangrove Forest using Soil Adjusted Vegetation Indices Based on multitemporal Images Case Study: East Coast of Lampung Province..... 215
N Simarmata, T A Tarigan and T K Ermanto

The Application of a Method Normalized Difference Vegetation Index (NDVI), Normalized Difference Moisture Index (NDMI) and Parameter Physical to Zoning Prone Landslide in Bandar Lampung City..... 222
Tamara, Bambang Edhi Leksono and Nirmawana Simarmata

Application of Lyzenga Algorithm on Sentinel-2B and SPOT-7 Imagery for Estimation of Coral Reef Condition, Capacity and Presence (Case Study: Kapo-Kapo Island and Soetan Island, Pesisir Selatan Regency, West Sumatera Province)..... 236
Tessa Khairani Ermanto, Bambang Edhi Leksono and Nirmawana Simarmata

Vertical Accuracy Evaluation of National DEM Data at Buru Island..... 248
Maundri Prihanggo, Rofiatul Ainiyah and Rofiqoh

Multi Data Digital Terrain Model for Waterlogging Analysis in Institut Teknologi Bandung Ganesha Campus..... 253
K N Fauzan, D Suwardhi and I Gumilar

Determining the Zone of Potassium in Muria Mountain Using Landsat-8 Oli By Spectral Angle Mapper..... 266
A Zakiya, M Rindianingrum and N A H Harahap

Geodatabase Masterplan of Mangrove Forests in Indonesia Based on the Indonesian Geographical Element Catalog..... 271
Yusuf Hary Saputro and Soni Darmawan

Land Suitability Analysis Using Analytical Hierarchy Process and Geographic Information System for Coffea arabica Linn. In Benguet Province, Philippines..... 285
Richard Dein Diaz Altarez, Elvert Bugnosen Lucas, John Christian Recana Pabustan, Cyrx Delos Reyes Ermel Concepcion, Maricor Coquilla Pabillaran, Jerome Gardiola Maglinao and Alexandrio Aloguin Ramirez

Total Suspended Solid Mapping Using Remote Sensing: Accuracy Comparison of Absolute and Relative Atmospheric Correction..... 297
Maria Roswita Kartika Sari Bawono and Pramaditya Wicaksono

A New Chapter in Participatory Mapping in Indonesia..... 305
Franko Jhoner, Rahmat Kurniadi Dewantara and Fajar Harnowo

Effect of Object Homogeneity on Agisoft Processing Success

Anna Charieninna[1]*, Hary Nugroho[1], Monica Maharani[1]

[1]Geodesy Engineering, Institut Teknologi Nasional, 23 PH.H. Mustofa Street, 40124, Bandung, Indonesia

*Corresponding author's e-mail: annacharieninna@ymail.com

Abstract. Bosscha Observatory is one of the cultural preservations that needs to be preserved by making a three-dimensional (3D) model. The method that can be used to create 3D models is Close Range Photogrammetry. This method can produce 3D models of objects with shapes and colors that match the real conditions of the object. The vehicle used for photographing the building is an Unmanned Aerial Vehicle (UAV) that has been equipped with a camera. Shooting is done tilting with converging and vertical camera configuration. Photographs of shooting are processed to produce a 3D model using Agisoft software that applies the Structure from Motion technique. This technique reconstructs the photos together with similar features to produce a 3D model. The homogeneity of objects in photos can affect the results of 3D models. On the wall of the Bosscha Observatory which has a color and texture that tends to be homogeneous, causing a lot of noise caused by failed matching when matching photos with each other. Meanwhile, the roof of the Bosscha Observatory is modeled perfectly, because the roof has heterogeneous colors and textures.

Keywords: Bosscha 3D Observatory Model, Close Photogrammetry, Structure from Motion, Failed Matching, 3D Model Accuracy.

1. Introduction

Observatorium Bosscha is the largest observatory in Indonesia that functions as an Indonesian Astronomy research and education institution which currently belongs to the Bandung Institute of Technology (ITB) [1]. Bosscha Observatory is a cultural heritage needs to be protected as a dynamic effort to maintain and to fulfill and need to be respected by protecting, developing and utilizing it. This building has a homogeneous wall with pure white color and fine-teztured that supports poles with the same distance from each other. Otherwise, Bosscha Observatory has a half-ball roof and a cylindrical wall. One of efforts to preserve cultural heritage is to do digital construction on the interior and exterior parts of the building. One of the ways to make digital is to create a three-dimensional (3D) model of a cultural heritage building. 3D models present sizes of length, width, and height according to the original requirements in the field [2]. The same thing was also stated by [3] that the making of 3D model documents is carried out for planning, management.

One method that can be used to document 3D models is Close Range Photogrammetry [4, 5]. Close Range Photogrammetry represents photogrammetry that uses photos as a measurement of instrument with a distance of fewer than 300 meters [6, 7]. Regarding to the Bosscha Observatory, this building will be modeled using the Close Range Photogrammetry method. The chosen method, is designed to be able to present all parts of the Bosscha building effectively and remained by field conditions. This paper will discuss how to use object homogeneity against 3D models produced using Agisoft Metashape Professional software that uses Structure from Motion techniques.

Structure from Motion is a method of forming a three-dimensional (3D) model which is determined by the feature equation of several photographic images taken from different points and angles. SfM has the principle of stereoscopic photogrammetry where 3D models are formed from a series of overlapping images. According to [8] SfM photogrammetry is different from traditional photogrammetric approaches, because the determination of geometry is based on camera position and orientation

automatically without the need of predetermined set of "ground controls". SfM has several advantages, namely relatively low costs and high levels of accuracy. This method is a passive 3D reconstruction method, where images or photos that are representations of objects on the surface are recorded from various angles (line of sight) using a digital camera, processed using the Scale Invariant Feature Transform (SIFT) algorithm which later projects objects into three-dimensional shapes. Illustration of the SfM method can be seen in Figure 1.

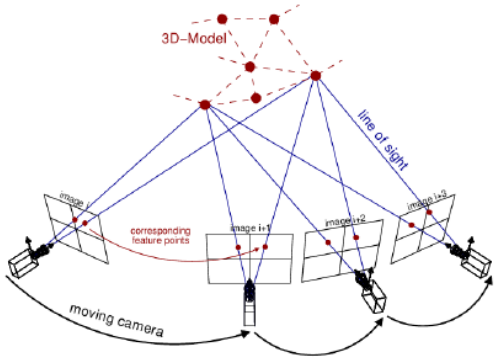

Figure 1. Illustration of Structure from Motion Works.

2. Methods

Cultural heritage building, Bosscha Observatory located in Lembang, Bandung Barat Districts, Jawa Barat Province, Indonesia with geographic coordinates 107º 37'BT and 6º 49 'LS. Bosscha Observatory can be seen in Figure 2.

Figure 2. Bosscha Observatory.

2.1. Data Collection

The data acquisition is the only phase of the process taking place in the field. It comprises 2 steps, (i) the recording of ground control points coordinates and (ii) imaging of the building using close-range photogrammetry.

2.2. Data processing

Using Agisoft, a 3D model can be generated in a fully auto-mated three-step process [9, 10], comprising (i) the alignment of the photographs, (ii) the calculation of a dense 3D surface and finally (iii) the texture mapping of the model. The processing of the 3D model starts by aligning the photographs. During this step (i) a 3D sparse point cloud is generated representing the geometry of the scene (Figure 3 and Figure 4), For the processing of the alignment, Agisoft uses a structure from motion approach [11], see also [12].

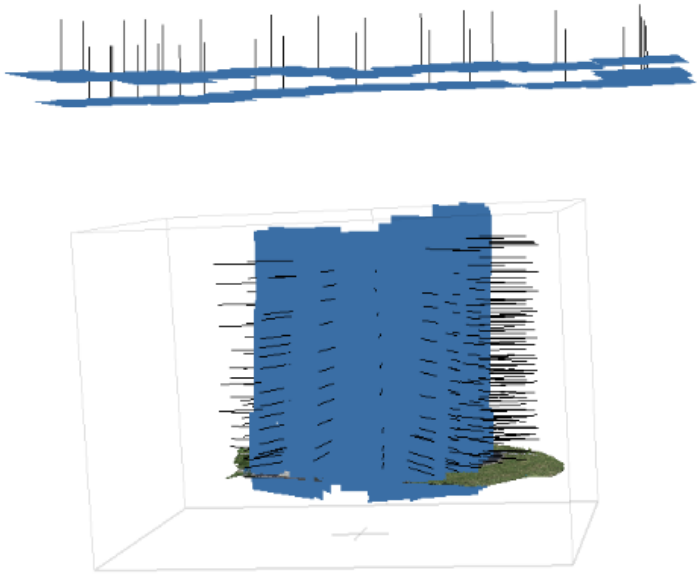

Figure 3. Camera Positions.

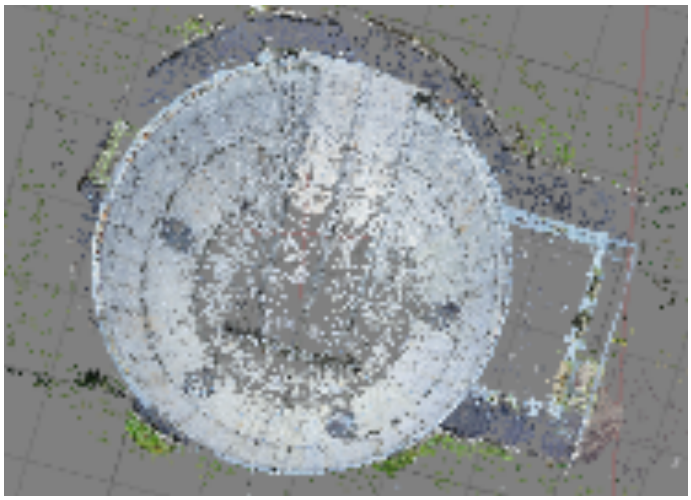

Figure 4. Sparse Point Cloud.

Figure 5. Dense Point Cloud.

(ii) The next step is absolute orientation or georeferencing by input the ground control poins coordinate. And then doing for (iii) the relative orientation of camera position at the moment of image acquisition is determined and (iv) the internal camera parameters (focal length, principal point location, skew, radial and tangential distortion coefficients) are computed. (v) Generating dense point cloud, to produce a very tight point (Figure 5). After a dense point cloud is generated, the next step is (vi) making mesh, which is to collect 3D from point cloud resulting from the process of building dense point clouds. The concept of mesh formation is the result of the capture of a triangular net from dots formed from dense cloud. This net creates interrelated polygons creating a surface from a 3D model. This stage is done to bind a collection of cloud that has not been arranged, so that they close each other (Figure 6). (vii) The last step is making 3D models in this research is texture making. This stage aims to give texture and color to the 3D model so that it can approach the actual state of the object. Parameters chosen based on recommended settings by software developers and test-and-trial (Table 1).

Figure 6. Meshing.

Table 1. Parameters Used in Agisoft Software.

Photo Alignment Parameters	
Accuracy	High
Reference preselection	Enabled
Point Limit	274.728
Camera Accuracy	
Marker Accuracy	
Scale Bar Accuracy	
Projection Accuracy	
Tie Point Accuracy	
Fit f	Enabled
Fit cx, cy	Enabled
Fit k1	Enabled
Fit k2	Enabled
Fit k3	Enabled
Fit k4	Enabled
Fit b1	Enabled
Fit b2	Enabled
Fit p1	Enabled
Fit p3	Enabled
Fit p4	Enabled
Building dense point cloud	
Quality	High
Depth Filtering	Mild
Calculate point colors	Enabled
Building mesh	
Source data	Dense Cloud
Surface type	Arbitrary (3D)
Face count	High
Calculate vertex colors	Enabled
Building Texture	
Mapping Mode	Generic
Blending Mode	Mosaic
Texture size/ count	8192 x 1
Enable hole filling	Enabled
Enable ghosting filter	Enabled

3. Results

A total of 362 overlapping photos were used to reconstruct the 3D model (Figure 7). Overall, approximately 28 hours of processing were required, including computational processing time and interactive adjustments. The root mean quare error for the 3D model, as calculated from the subset of 38 ground control points, was 0.009 m (x), 0.007 m (y) and 0.006 m (z). Ground Sample Distance (GSD) obtained from the results of the formation of this 3D model is very thorough with a value of 1.67 mm/pix. This 3D model is compared to the actual conditions in the field. This comparison can be seen in the Figure 8 which are seen in terms of shape, detail, texture and color.

Figure 7. Bosscha Observatory 3D Models using Close Range Photogrammetry Method.

4. Discussions

From the 3D model formed, it can be seen that the model almost represents the actual structure in the field. Figure 8 images prove that the details on the building were successfully represented on the 3D model. In the first photo in Figure 8 that can be seen in the details in the front of the building has doors, windows, roofs, and stairs modeled on a 3D model but is not perfect due to the noise. In terms of form, these objects have presented the real situation. However, on the part of the ladder on the right side, the shape is not modeled quite well due to plants blocking. In Figure 8 you can see the appearance of pipes, windows and some rust that have been successfully modeled on the 3D model. In terms of color and texture, the two images are presented almost exactly like the real conditions. However, the cylindrical parts of the building produced from 3D models are not perfectly modeled especially in the shape of the wall poles.

This matching failure is caused by the Structure from Motion (SfM) technique applied to Agisoft Metashape software processes all photos simultaneously so that it produces a lot of noise. The cause of this noise comes from photographs of the photoshoot on the cylindrical part of the Bosscha Observatory building which has a homogeneous and smooth color so that the software is difficult to match photos (Figure 9). Unlike the roof that is modeled very well in terms of shape, texture and color that resembles the actual shape. This is because the roof of the Bosscha Observatory has a fairly rough texture and there are distinguishing objects such as curved iron and windows. The 3D model roof is compared to the roof according to the conditions in the field is shown in Figure 8.

Figure 8. Visual Comparison of Bosscha Observatory 3D Models(left) with the real condition (right).

Figure 9. Bosscha Building Walls.

5. Conclusions

In the making of 3D model Bosscha Observatory using close-range photogrammetric methods almost presents the actual shape. However, in the cylindrical part of the building there are many wall poles which are not modeled due to a lot of noise. Noise due to failed matching during data processing. Bosscha has a homogeneous shape, color, texture so Agisoft software that applies structure from motion techniques where photos are processed together with similar features difficult to match photos with each other.

6. References

[1] Observatory, B. *Sejarah Observatorium Bosscha*. 2016 [cited 2019 23 February]; Available from: https://bosscha.itb.ac.id/id/index.php/tentang-bosscha/sejarah-Observatorium-bosscha/

[2] Mulyadi, Y., *Mengoptimalkan Zonasi Sebagai Upaya Pelestarian Cagar Budaya.* Balai Pelestarian Purbakala Makassar, Makasar, 2012.

[3] Barsanti, S.G., et al., *Critical factors and guidelines for 3D surveying and modelling in Cultural Heritage.* International Journal of Heritage in the Digital Era, 2014. **3**(1): p. 141-158.

[4] Park, H.S., et al., *A new approach for health monitoring of structures: terrestrial laser scanning.* Computer-Aided Civil and Infrastructure Engineering, 2007. **22**(1): p. 19-30.

[5] Yilmaz, H.M., et al., *Importance of digital close-range photogrammetry in documentation of cultural heritage.* Journal of Cultural Heritage, 2007. **8**(4): p. 428-433.

[6] GJ, I.N.H., *PEMBUATAN MODEL TIGA DIMENSI CANDI GEBANG MENGGUNAKAN METODE FOTOGRAMETRI JARAK DEKAT*. 2014, Universitas Gadjah Mada.

[7] Luhmann, T., Robson, S., Keyle, S., Harley, Ian, *Close Range Photogrammetry Principles, Techniques dan Applications*. 2006, Scotland, UK: Whittles Publishing.

[8] Mozas-Calvache, A., et al., *Method for photogrammetric surveying of archaeological sites with light aerial platforms.* Journal of Archaeological Science, 2012. **39**(2): p. 521-530.

[9] AgiSoft, L., *AgiSoft PhotoScan User Manual: Standard Edition, Version 0.8. 4.* AgiSoft LLC, 2011.
[10] Verhoeven, G., *Taking computer vision aloft–archaeological three-dimensional reconstructions from aerial photographs with photoscan.* Archaeological prospection, 2011. **18**(1): p. 67-73.
[11] Ullman, S., *The interpretation of structure from motion. Proceedings of the Royal Society of London.* Series B. Biological Sciences 203 (1153), 1979. **405e426**.
[12] Szeliski, R., *Computer Vision: Algorithms and Applications*. 2011, Springer, London: Texts in ComputerScience.

7. Acknowledgments

The authors are grateful for funding from PT. Zenit Era Utama Servizio (ZEUS). We would like to big thanks Geodesy Engineering National Institute of Technology Big Family.

Relative Bathymetry Extraction Using SPOT 7 Satellite Imagery

Kuncoro Teguh Setiawan [1]*, Devica Natalia BR. Ginting[1], Masita D. M. Manessa[2], Surahman[3], Gathot Winarso[1], Nanin Anggraini[1], Abdul Basith[4], Wikanti Asriningrum[1], Syamsu Rosid[5], A. Harsono Supardjo[5]

[1]Remote Sensing and Applications Center, LAPAN
[2]Department of Geography, Indonesia University
[3]Hidrography and Oceanography Center, Indonesia NAVI
[4]Department of Geodetic Engineering, Universitas Gadjah Mada
[5]Department of Physics, Indonesia University

*Corresponding author's e-mail: kunteguhs@gmail.com

Abstract. Bathymetry is information on the depth of the sea that can describe the hydrographic conditions of the seabed. Satellite derived bathymetry has several methods that can be applied to the batimetric extraction process using optical satellite images. One of the satellite images that can be used is SPOT 7. The image is the latest generation of SPOT which has 4 multispectral channels with a spatial resolution of 6 meters so that it can be extracted to obtain information on shallow water bathymetry. The bathymetry extraction method uses the Van Hengel and Spitzer methods, 1991. The VS method is the principal component analysis method of three bands with respect to the rotation transformation factor. The purpose of this study is to extract SPOT 7 satellite image data to produce relative bathymetry information in shallow seas using the VS algorithm. The location of the study was carried out on Karimunjawa Island, Jepara Regency, Central Java. The data used is SPOT 7 imagery that was acquired May 18, 2017. The extraction algorithm is used the VS 1991 method. The results show that from SPOT 7 images produce depth index values ranging from 0.0985 to 0.6378.

Keywords: Bathymetry, SPOT 7, Karimunjawa Island.

1. Introduction

The bathymetry extraction method using satellite image data is the development of satellite remote sensing technology. The method takes into account the principle of the propagation of light waves in water and the intensity of incident light that decreases in accordance with the increase in depth traversed. Since 1970, satellite remote sensing technology has been adopted as an alternative to minimize the mapping bathymetry [1]. Depth measurement with remote sensing technology can be performed by analyzing spectral values of each channel from satellite imagery. Shorter wavelength light penetrates water deeper than those with longer wavelength [2, 3]. Lambert's law explains that the absorbance of light is expotentially increased to the thickness of media through which the light is transmitted [4, 5] mentions that blue band has the ability to penetrate 25 meters deep, green band to penetrate 15 meters, red band to penetrate 5 metres. The sunlight that enters the body of water in intensity continuously decreases exponentially with increasing depth [6]. Multispectral sensor, especially green and blue bands, can penetrate up to 20 meters below the sea surface in a clear water condition [7-9].

Bathymetry was generally obtained by measuring the distance between the average of sea surface to the sea floor. Preliminary technique of bathymetry measured using heavy ropes or cables lowered from the ship side. The main limitation of this technique is only able to perform one measurement in one position and is strongly influenced by the movement of the vessel and flow that is considered inefficient. In addition, the use of ecosunder that utilizes sound waves is also used to measure the depth of waters. Echosounders work by sending sound waves that will propagate through the medium of water and reflect waves after touching the water base. The main parameter in the bathymetry measurement process using

the acoustic method is the time difference between when sound waves are emitted and received again. Each block will get depth information of one point so that when each point is connected it will produce depth profile and when the ship moves it will produce images that illustrate the surface of the sea floor. This technique is also less efficient for obtaining bathymetry information for a very wide area and has a weakness for very shallow waters due to the limitations of ships to reach the area. Alternatively, remote sensing images can be used in coastal and shallow water bathymetric mapping is considerably cost effective [10, 11].

The challenge of utilizing remote sensing technology to obtain depth information is the accuracy of the information. Various data extraction and resolution methods are used. The previous research that used remote sensing data to derive depth information such as [12-14] using Landsat 8 OLI data. [15-20] using better spatial resolution, Worldview.

Futhermore, the methods used to extract water depths such as [12] using the stump method, [18, 19] using a method developed on worldview data. Otherwise, there are still many other methods used to extract water depths using remote sensing data. However, in this study the Van Hengel and Spitzer (VS) Algorithm method, 1991 will be used. This method has been applied by [21] using LANDSAT 7 ETM + imagery data in Pari Island, DKI Jakarta Province by comparing the combination of red, green and blue bands. V-S (1991) introduced an algorithm to generate bathymetry information by using the rotational transformation matrix. Based on research conducted by [21], the tree band combination showed the best results for estimating the depth of shallow waters on Pari Island by the Van Hengel and Spitzer Algorithm method.

The purpose of this study is to extract SPOT 7 satellite image data to produce relative bathymetry information in shallow seas using the V-S algorithm. SPOT -7 had four channels such as spectral blue, l green, red, and near infra red. Blue spectral channels are channels that are more sensitive to the identification in the territorial waters when compared with other spectral channels. The choice of location in the Karimunjawa Island in Jepara Province of Central Java because the island had a clearwaters which is also is one of the National park areas so that it becomes one of the tourist destinations so the results of this study can be used to support marine tourism especially for bathymetric mapping information.

2. Methodology

This research was conducted in the Karimunjawa Island, Jepara, Province of Central Java who are geographically located at coordinates 5º44'18.16"- 5º55'22.76" LS and 110º24'37.85"- 110º31'03.06" BT (Figure 1). The data used in this study is the SPOT-7 imagery acquisition date of May 18, 2017 which channels in the visible wavelengths. The relative bathymetry extraction method in this study uses the Van Hengel and Spitzer algorithm. Stages of the research conducted is summarized in the flow diagram in Figure 2.

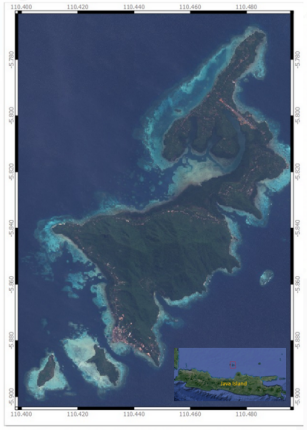

Figure 1. Area of Study.

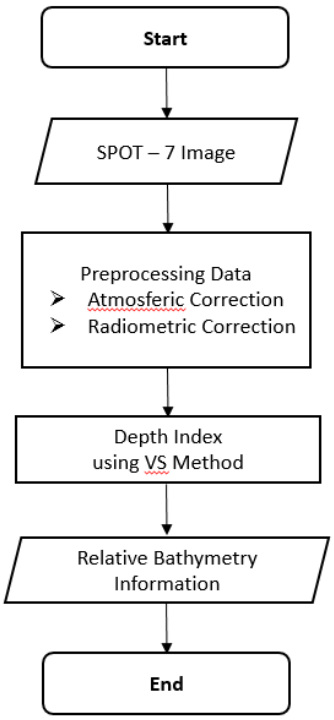

Figure 2. Flowchart of Research.

Algorithm V-S (1991) is the development of previous algorithm popularized by Lyzenga (1981). This algorithm produces relative depth index value as it is defined in equation (1).

$$Y1 = (\text{Cos}\,(r) \times \text{Sin}(s) \times X1) + (\text{Sin}(r) \times \text{Cos}(s) \times X2) + (\text{Sin}(s) \times X3) \quad (1)$$

$$r = arctan\,(Ur + \sqrt{Ur^2 + 1}\,) \quad (2)$$

$$s = arctan\,(Us + \sqrt{Us^2 + 1}\,) \quad (3)$$

$$Ur = \frac{Var\ x2 + Var\ x1}{2\ Cov\ x1x2} \quad (4)$$

$$Us = \frac{Var\ x3 + Var\ x1}{2\ Cov\ x1x3} \quad (5)$$

Where :

Y1	:	Depth Index
X1	:	Reflectance value of band 1
X2	:	Reflectance value of band 2
X3	:	Reflectance value of band 3
Var X1	:	Variance of 30 data of band 1
Var X2	:	Variance of 30 data of band 2
Var X3	:	Variance of 30 data of band 3
Cov X1X2	:	Covariance of 30 data of band 1 and band 2
Cov X1X3	:	Covariance of 30 data of band 1 and band 3

3. Results

Processing begins with collecting SPOT 7 image data and proceed with the data correction process. Data correction process carried out includes atmospheric and radiometric corrections. Atmospheric correction is useful for eliminating or reducing the effects of the atmosphere. Therefore, after the correction process the digital value received by the sensor is the result of reflection from the surface bottom. Radiometric correction is done to provide stability of the digital reflection value of each object that is based on water. The radiometric process is carried out by changing the digital value of each pixel into a reflectance value. Reflectance values of blue, green, and red channels of bathymetry from SPOT-7 imagery in the waters of Karimunjawa Island, shown in Figure 3.

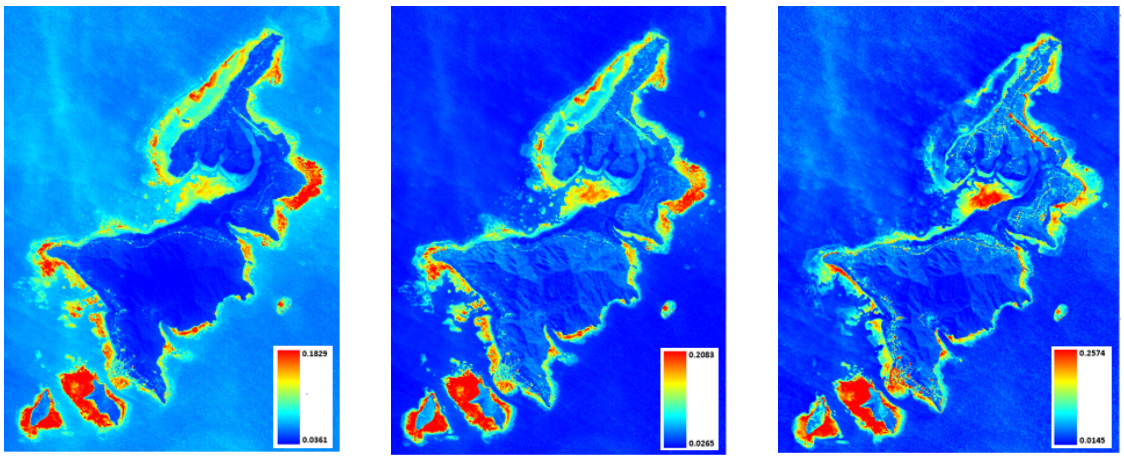

Blue Band Green Band Red Band

Figure 3. Reflectance SPOT 7 imagery.

Bathymetry extraction is a process to produce depth information values from a water location. The data used in the extraction process is the reflectance value of the wavelengths owned by the SPOT 7 image. The wavelengths of the SPOT 7 Image used are the blue band, green band and red band. From the three bands the depth index is generated using the VS algorithm. The algorithm is a model developed using rotational transformation. In bathymetry extraction using the VS algorithm is the determination of the two transformation angles r and s used. Determination of the two transformation angles through a pair of wavelength values. The angle r is obtained from the pair between the band's value and the green band. The angle s is obtained from the pair between the blue band and the red band. The two pairs of bands are then calculated the value of each variant and the covariance of each pair. The formula for calculating the angle r and s values follows the equations found in no (2) and (3). Determination of the transformation Ur and Us according to equation no (4) and (5). Furthermore, the determination of the depth index using the VS algorithm in accordance with equation (1).

The first pair consisting of the blue band and the green band produced a variant value of 0.000572 and 0.001011 respectively and covariance of 0.000729. The second pair consisting of the blue band and the red band produced a variant value of 0.000572 and 0.000155 respectively and a covariance of 0.000218. The two pairs the band produces a rotation transformation angle of 68.667° and 74.512°. The equation used to produce the depth index value is according to the following equation:

$$\text{Depth Indeks} = (0.36379 * 0.96369 * X1) + (0.93148 * 0.26704 * X2) + (0.96369 * X3) \quad (6)$$

The results of the depth index values using the VS algorithm using SPOT 7 image data are shown in Figure 4.

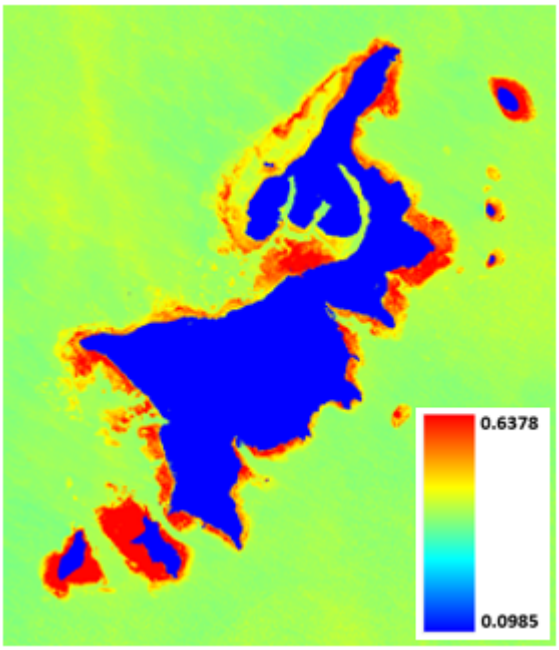

Figure 4. Depth Index.

The next processing is modeling making depth class. The depth class is created based on the resulting depth index value. From this index five classes of depth were produced. Determination of the class is made based on the division of depth index range. The process is extraction of SPOT 7 satellite imagery to produce bathymetric information in relative terms.
The depth index value generated from the VS algorithm is 0.0985 to 0.06378 as shown in Figure 4. From the depth index value is made into five depth classes. The five classes are very shallow, quite shallow, shallow, quite deep and deep (Figure 5). The depth welding is done by grouping the depth index values generated by the VS algorithm. Very shallow class has a depth index value of 0.5786 - 0.6378, quite shallow class has a depth index value of 0.4586 - 0.5785, shallow class has a depth index value of 0.3386 - 0.4585, quite deep class has a depth index value of 0.2186 - 0.3385, deep class has an index value depth of 0.0985 - 0.2185. A very high depth index value results in a very shallow depth class, whereas a very low depth index value results in the deepest depth class.

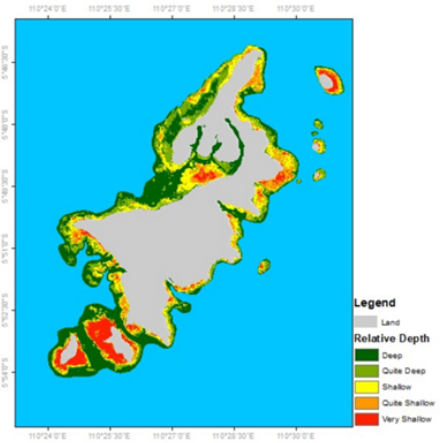

Figure 5. Bathymetry information.

The use of the VS algorithm has been done using LANDSAT TM imagery data. By using of LANDSAT ETM+ image with VS algorithm transformation may generate depth information up to -22.5 m with R^2 value of 0.62 on Menjangan Island, Bali Province. [21] used LANDSAT ETM+ imagery with the same algorithms was able to extract depth information up to -15 m with value R^2 value of 0.67 on Pari Archipelago, Kepulauan Seribu, DKI Jakarta Province. Another research had been performed by [1] by using spectral bands correlation of SPOT-4 satellite imagery data to predict bathymetry of shallow waters in Ratai Bay, Pesawaran Regency, Lampung Province. The data can only estimate to approximate depth of 18 meters. Meanwhile, according to results of [5] LANDSAT TM on clear waters is able to extract depth value up to -25 m.

The results of this study aim to provide depth information that is still realistic in qualitative classes. Quality depth classification is done to get preliminary information on shallow sea depth conditions in coastal areas. With the information on bathymetry, it is hoped that it will be useful for the regional or central government to manage the inventory planning of natural resources. The results of this study need to be continued with quantitative depth determination and accuracy calculation. To produce this information, data on depth of field around shallow sea waters is certainly needed. Field depth data is used to build empirical models to produce quantitative depth and accuracy calculations.

4. Conclusions

The SPOT-7 image acquired on 18 May 2017 can be used to extract relative bathymetry information on Karimunjawa Island in Jepara, Central Java Province. Batimetri information relatively produces 5 depth classes consisting of very shallow, quite shallow, shallow, quite deep and deep. The bathymetry information is expected to be useful as preliminary information to support the management of coastal resource management.

5. References

[1] Arief, M., *Pendekatan Baru Pemetaan Bathimetric Menggunakan Data Penginderaan Jauh Spot Studi Kasus: Teluk Perigi Dan Teluk Popoh (The New Approach To Mapping Bathimetric Using Spot Remote Sensing Data Case Study: The Bay And Popoh Gulf).* Jurnal Teknologi Dirgantara, 2012. **10**(1).

[2] Lyzenga, D.R., N.P. Malinas, and F.J. Tanis, *Multispectral bathymetry using a simple physically based algorithm.* IEEE Transactions on Geoscience and Remote Sensing, 2006. **44**(8): p. 2251-2259.

[3] Hutomo, A., *Aplikasi Citra Quickbird Untuk Pemetaan Batimetri Dan Pemetaan Objek Dasar Perairan Dangkal (Studi Kasus : Gobah Panggang, Kepulauan Seribu).* 2010.

[4] Bukata, R.P., et al., *Optical properties and remote sensing of inland and coastal waters*. 2018: CRC press.

[5] JUPP, D.L. *Background and extensions to depth of penetration (DOP) mapping in shallow coastal waters*. in *Proceeding of The Symposium on Remote Sensing of the Coastal Zone Queensland*. 1988.

[6] Jerlov, N.G., *Marine optics*. Vol. 14. 1976: Elsevier.

[7] Poerbandono, N.D.E., *Djunarsjah, 2005.* Survei Hidrografi. Refika Aditama Bandung. **162**.

[8] Sutanto, *Penginderaan Jauh Jilid I*. 1986, Yogyakarta: Fakultas geografi Universitas Gadjah Mada.

[9] Sutanto, *Penginderaan Jauh Jilid 2*. 1992, Yogyakarta: Gadjah Mada Press.

[10] Lillesand, T., R.W. Kiefer, and J. Chipman, *Remote sensing and image interpretation*. 2015: John Wiley & Sons.

[11] Mumby, P.J. and A.R. Harborne, *Development of a systematic classification scheme of marine habitats to facilitate regional management and mapping of Caribbean coral reefs.* Biological conservation, 1999. **88**(2): p. 155-163.

[12] Jagalingam, P., B. Akshaya, and A.V. Hegde, *Bathymetry mapping using Landsat 8 satellite imagery.* Procedia Engineering, 2015. **116**: p. 560-566.

[13] Vinayaraj, P., V. Raghavan, and S. Masumoto, *Satellite-derived bathymetry using adaptive geographically weighted regression model.* Marine Geodesy, 2016. **39**(6): p. 458-478.
[14] Pushparaj, J. and A.V. Hegde, *Estimation of bathymetry along the coast of Mangaluru using Landsat-8 imagery.* The International Journal of Ocean and Climate Systems, 2017. **8**(2): p. 71-83.
[15] Arya, A., G. Winarso, and A.I. Santoso, *EKSTRAKSI KEDALAMAN LAUT MENGGUNAKAN DATA SPOT-7 DI TELUK BELANGBELANG MAMUJU (THE BATHYMETRY EXTRACTION USING SPOT-7 DATA AT THE BELANGBELANG BAY WATERS MAMUJU).* GEOMATIKA, 2017. **22**(1): p. 09-20.
[16] Kanno, A. and Y. Tanaka, *Modified Lyzenga's method for estimating generalized coefficients of satellite-based predictor of shallow water depth.* IEEE Geoscience and Remote Sensing Letters, 2012. **9**(4): p. 715-719.
[17] Kanno, A., Y. Koibuchi, and M. Isobe, *Shallow water bathymetry from multispectral satellite images: Extensions of Lyzenga's method for improving accuracy.* Coastal Engineering Journal, 2011. **53**(04): p. 431-450.
[18] Manessa, M.D.M., et al. *Lyzenga multispectral bathymetry formula for Indonesian shallow coral reef: evaluation and proposed generalized coefficient*. in *Remote Sensing of the Ocean, Sea Ice, Coastal Waters, and Large Water Regions 2016*. 2016. International Society for Optics and Photonics.
[19] Kanno, A., et al., *Generalized Lyzenga's predictor of shallow water depth for multispectral satellite imagery.* Marine Geodesy, 2013. **36**(4): p. 365-376.
[20] Guzinski, R., et al., *Exploring the utility of bathymetry maps derived with multispectral satellite observations in the field of underwater archaeology.* Open Archaeology, 2016. **2**(1).
[21] Wahyuningrum, P.I., I. Jaya, and D. Simbolon, *Algoritma untuk Estimasi Kedalaman Perairan Dangkal Menggunakan Data Landsat-7 ETM+.* Buletin PSP, 2008. **17**(3).

Acknowledgments
This research was supported by The National Innovation System Research Incentive Program (Insinas) 2019, collaborate between The Ministry of Research, Technology and Higher Education and Remote Sensing Application Center (PUSFATJA) LAPAN.

Utilization of Remote Sensing Satellite Data to Predict Future Cloud Cover in Indonesia: A Preliminary Study

Ahmad Luthfi Hadiyanto[1,2,6]*, Ketut Wikantika[1,2,7], Ary Setijadi Prihatmanto[3,4], Nurjanna Joko Trilaksono[5]

[1]Center for Remote Sensing, Faculty of Earth Sciences and Technology, Bandung Institute of Technology
[2]Remote Sensing and GIS Research Group, Faculty of Earth Sciences and Technology, Bandung Institute of Technology
[3]School of Electrical Engineering and Informatics, Bandung Institute of Technology
[4]Research Center on Information and Communication Technology, Bandung Institute of Technology
[5]Atmospheric Science Research Group, Faculty of Earth Sciences and Technology, Bandung Institute of Technology
[6]Parepare Remote Sensing Ground Station, National Institute of Aeronautics and Space
[7]Indonesian Young Researcher Forum (ForMIND), 10 Ganeca Street, Bandung, Indonesia

*Corresponding author's e-mail: a_luthfi@lapan.go.id

Abstract. Information of cloud cover, especially rain cloud, affect human activity. People take decision in agriculture and outdoor activity frequently based on rain information. In decision making, predictive information is usually more valuable. Therefore, future prediction of rain cloud cover become important. The common technology in cloud prediction use Numerical Weather Prediction method. The method needs high performance computation system because of complexity of the model. It depends on the knowledge of dynamical process in atmosphere, while the process is very complicated in tropical region. Then many other methods still have potential to be explored. Some of the methods are statistical, i.e. analog prediction and time series prediction. The other method implements artificial intelligence using machine learning. All those methods use historical data and has their own characteristic in handling the data. It is shown that machine learning has more flexibility to handle non-linear data. Therefore, machine learning is proposed to utilize historical satellite images to predict future cloud cover. Moreover, to estimate rain information, rain cloud can be differed from detected cloud in satellite images.

Keywords: prediction, machine learning, satellite images.

1. Introduction

People is getting aware to weather forecast especially for severe weather. This kind of weather cause destruction. People try to avoid and anticipate its occurrence. The information of severe weather is very important, but information of normal weather is also important. People often make decision based on weather information. The information is needed for the success in many aspects of life, i.e. agriculture, construction work, socioeconomic activity etc. Weather forecasting provide prediction of many parameters in atmospheric dynamics. Some of the parameters are used to generate information of rainfall, cloud fraction etc. Rainfall and cloud fraction, both are very related. Detection of cloud fraction or cloud cover, with ability to differentiate cloud convection, can be an option to provide information related with rain. Technology in remote sensing satellite has shown that spectral characteristic of cloud retrieved from satellite can be used to estimate the existence of significant rainfall [1]. Since rainfall information is important in calculating planting time, pattern, variety, crop growth and irrigation [2, 3], then cloud cover can provide similar idea.

Weather forecasting techniques have gone through a lot of improvement using Numerical Weather Prediction (NWP). The state of the art of this technique uses ensemble forecasting, result in probability

density function of occurrence. However, this technique implements the knowledge of physical processes in atmosphere dynamics to build the numerical model. Thus, the model become very complex. In tropics, formulation of the model is more difficult because the air circulation in tropics is more complex. It had been shown, in short term scale, that weather forecasting in tropics have poor skill. In contrary, seasonal forecasting is skillful in tropics. Although it is skillful, the weather around Indian ocean has the lowest predictability [4]. Indonesia is a maritime continent which lies between Indian and Pacific-ocean, thus some parts of Indonesia have lower predictability than others. Moreover, the topography in Indonesia affect the complexity of atmosphere dynamics [5]. As an alternative to avoid difficulty in modelling atmosphere dynamics in tropics, empirical data driven model is an option. The use of this model is potential to reduce processing time needed in numerical model[6].
In this paper, we explore methods and data to create data driven model. Satellite remote sensing images is selected due to its wide coverage.

2. Proposed Data Driven Model

Analysis in empirical data driven model can be performed by statistical algorithm or machine learning. Statistic use mathematics to find relationship between variables or examine the pattern of the data. Based on the knowledge of the data, machine learning is used to build the model instead of statistical model. Machine learning based model is better to handle multivariate nonlinear non-parametric data set [7]. Multivariate means the data set contain more than one variable. Non-parametric means the data are not assumed to fit a normal distribution. The issue in all kind of models are dimension, but a technique to reduce dimension can be applied by selection of significant data [8].
In many practical weather forecasting, machine learning is often used to improve the result of NWP in post processing [9, 10], but it is also used in forecasting algorithm itself. Many methods in machine learning have proven to predict future condition. Some examples of the methods are neural network which was used to predict monthly temperature [11], Support Vector Machine which was used to predict rainfall [12] and Random Forest algorithm which was used to predict precipitation [13]. In cloud forecasting, neural network had been used for very short-term scale of forecasting [14]. The implementation of machine learning in operational forecasting algorithm is still less popular than analog forecasting. Analog forecasting statistically search for similarity of current condition in historical data [15]. Machine learning work in similar way, but the historical data is used to train the model. In machine learning we can build the model as a black box without knowing exactly the physical process. Therefore, the use of machine learning is very potential.
In this paper we propose to use remote sensing satellite images as the data, because the coverage of satellite images can reach remote area. Remote area can be difficult to observe with ground instrument [5]. The basic requirement of the data to be used in predicting future cloud cover is the sensitivity of the observation tool to clouds. Some remote sensing optical imagery have spectral channels with ability to detect clouds [16, 17]. Cloud generally can be characterized with higher reflectance and lower temperature than other object on the earth's surface [17]. Therefore, simple algorithm can be implemented using visible and infrared channel to detect clouds. Visible and infrared channel are available from many operational satellites like Terra, Aqua, NPP Suomi, MTSAT, Himawari-8/9 and NOAA-18/19/20. Satellite images had been used in data assimilation for numerical model [10, 18], but some research also use satellite images as main data in forecasting algorithm [14, 15]. Figure 1 shows the forecasting system utilizing remote sensing satellite data in the proposed model.
This paper emphasizes to have a look on characteristic of several satellite images, including availability of historical data, spectral resolution, spatial and temporal resolution and availability of cloud detection algorithm.

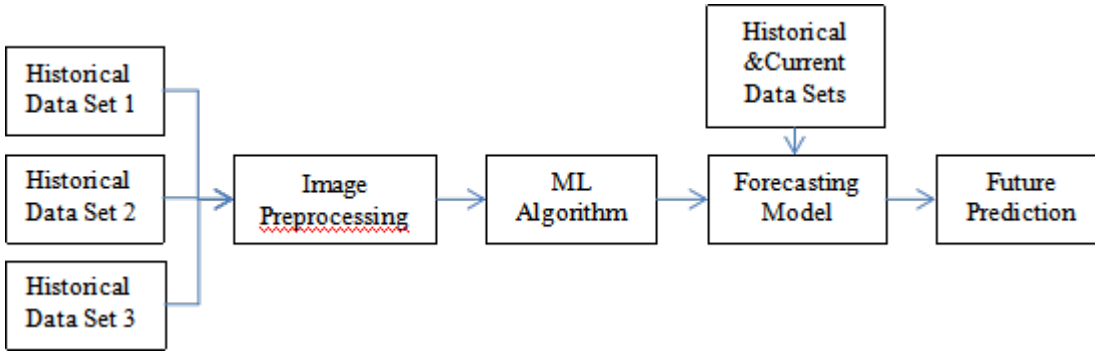

Figure 1. Machine Learning (ML) based forecasting system model.

2.1. Terra and Aqua

Both satellites were launched to provide data for environmental monitoring over land, ocean and low atmosphere. Terra was launched in December 18, 1999 with descending orbit. Aqua was launched in May 4, 2002 with ascending orbit. Both are still operational but was designed with 6 years of design life. They have Moderate-Resolution Imaging Spectroradiometer (MODIS) sensor on board.

2.1.1. Spectral, Spatial and Temporal Characteristic

MODIS acquire image with 36 spectral bands. Bands 20-25 and 27-36 are thermal emissive bands which have spectrum in mid-wavelength infrared (MWIR) and long-wavelength infrared (LWIR) band. Bands 1-19 and 26 are reflective solar bands which have spectrum in visible, near-infrared (NIR) and short-wave infrared (SWIR) band. The spatial resolution varies from 250 m, 500 m and 1000 m. Bands 1-2 have 250 m spatial resolution. Bands 3-7 have 500 m spatial resolution. Band 8-36 have 1000 m spatial resolution. With repeat cycle in 16 days and swath width of 2330 km, both satellites can cover entire earth's surface every 1 to 2 days.

2.1.2. Cloud Detection

MODIS processing software produce level-2 cloud products: MOD06/MYD06 and MOD35/MYD35. MOD06/MYD06 is cloud product which contain information of cloud optical and physical parameters. Cloud top temperature, cloud top height, effective emissivity, cloud phase and cloud fraction are derived from infrared channel (MWIR and LWIR). Cloud optical thickness, effective particle radius and cloud shadow effect are derived from visible radiance. NIR reflected radiance is used to derive cloud particle phase. MOD35/MYD35 is cloud mask product generated at 1 km spatial resolution and 250 m spatial resolution at nadir. The 1 km resolution product utilize visible and infrared thresholding in the algorithm. The 250 m cloud mask is derived based on 250 m visible data only.

2.2. MTSAT 1R/2, Himawari 8/9

MTSAT geostationary satellite series were launched for weather services. MTSAT-1R was launched in February 26, 2005 and operational until December 2015. MTSAT-2 was launched in February 18, 2006 and operational until March 2017. Himawari satellites replace the mission of MTSAT. Himawari-8 was launched in October 7, 2014 and Himawari-9 was launched in November 2, 2016. Both satellites are operational and provide images for disaster risk reduction.

2.2.1. Spectral, Spatial and Temporal Characteristic

MTSAT data has 5 spectral bands, consist of 1 visible band and 4 infrared bands (MWIR and LWIR). Himawari data has 16 spectral bands, consist of 3 visual bands, 3 NIR/SWIR bands and 10 infrared bands (MWIR/LWIR). Spatial resolution of MTSAT data is lower than data acquired from Himawari. MTSAT data has 1 km spatial resolution for visible band and 4 km spatial resolution for infrared bands. Himawari data 1 km and 0.5 km spatial resolution for visible bands, 1 km spatial resolution for NIR

band and 2 km spatial resolution for SWIR, MWIR and LWIR bands. MTSAT data are acquired every 30 minutes, while Himawari data can be acquired every 10 minutes.

2.2.2. Cloud Detection
Algorithm for cloud detection was built for MTSAT-1R data by Japan National Meteorological Satellite Center. The algorithm utilizes the concept that cloud have high reflectance and low brightness temperature value[19]. MTSAT-2 has different imagery but there is no difference in spectral characteristic. The Meteorological Satellite Center also built algorithm to produce cloud mask from Himawari-8 data. The algorithm detects clouds based on comparison of satellite observation and clear sky data calculated from Numerical Weather Prediction [20]. The algorithm can be implemented in Himawari-9 which has the same imagery.

2.3. NOAA-18/19
NOAA-18 was launched in May 20, 2005 and NOAA-19 was launched in February 6, 2009. Both satellites are still operational with their mission to provide meteorological data. They have Advanced Very-High Resolution Radiometer (AVHRR) sensor on board.

2.3.1. Spectral, Spatial and Temporal Characteristic
NOAA's AVHRR has 5 spectral bands, consist of visible red band, NIR, SWIR and 3 thermal bands (MWIR and LWIR). Spatial resolution for AVHRR data is 1.1 km at nadir with swath width of 2400 km. Both NOAA 18 and NOAA 19 can have full global coverage twice daily.

2.3.2. Cloud Detection
Cloud mask algorithm named Enterprise Cloud Mask was built to run on varied satellite data, including on AVHRR data [21]. The algorithm utilizes Naïve Bayesian idea of clear/cloudy pixel detection.

2.4. Suomi NPP and NOAA-20
Suomi NPP and NOAA-20 are currently operational for environmental monitoring purpose. Suomi NPP was launched in October 28, 2011 and NOAA-20 was launched in November 18, 2017. NOAA-20 (originally named as JPSS-1) and with Suomi NPP are part of Joint Polar Satellite System (JPSS) constellation. Both satellites have Visible Infrared Imaging Radiometer Suite (VIIRS) sensor on board.

2.4.1. Spectral, Spatial and Temporal Characteristic
VIIRS data consist of 21 visible/infrared bands, and 1 panchromatic band (visible). There are 16 bands in visible/infrared spectrum which have 750 m spatial resolution. Panchromatic and 5 bands in visible/infrared spectrum have 375 m spatial resolution. Both Suomi NPP and NOAA-20 cover full global coverage twice daily with swath width of 3060 km.

2.4.2. Cloud Detection
VIIRS Cloud Mask (VCM) algorithm was built for Suomi NPP data [22]. The algorithm can be implemented in NOAA-20 VIIRS data. Another algorithm namely Enterprise Cloud Mask which run on AVHRR is also adopted to run on NOAA-20 data.

3. Discussion
Algorithm to detect clouds is available for all the satellite data, and the data had been used in any research or operational of cloud forecasting. Evaluation to select the most suitable satellite data is based on several criteria:

- Availability of historical data
- Spectral, spatial and temporal resolution
- Acquisition time

MODIS historical data from Terra and Aqua is available for a long period of time. Data from the series of MTSAT and Himawari is either. So does the data from NOAA-18/19 satellites. Due to the old age of Terra and Aqua, Suomi NPP and NOAA-20 can be an option to replace them as the source of historical data when both Aqua and Terra are inactive.
Concerning spectral resolution, MODIS and VIIRS are the best option. Although Himawari 8/9 have good spectral information, their predecessor MTSAT doesn't have the same sensor. Suomi NPP and NOAA-20 have the best spatial resolution, but their period of historical data is less than the others. The best option for temporal resolution is the series of MTSAT and Himawari.
Concerning acquisition time, only NOAA-18/19 which do not pass Indonesian region at noon. They usually pass earlier in the morning and pass later in the afternoon than other satellites.
Combination of satellite data can be a good practice to explore forecasting performance. MODIS and MTSAT/Himawari are good choice since each of them has their own superiority. Due to the size and variety of the data, the issue of big data become another challenge. It covers the challenge in data warehousing, processing and visualization.
In data processing, apart from the selection of prediction method, there are still many issues which need further research:

- Specify the period of historical data
- Select type of operation, pixel-based or region-based
- Specify the period of prediction (short term, medium term and long term) depend on the purpose
- Consider the use of additional parameters which influence the formation of clouds, like topography, surface temperature, land cover, wind, distance from ocean and sun intensity represented by latitude.
- Consider the use of data from active sensor (radar)

As final discussion, although cloud is related with rainfall and we can retrieve rainfall data easily from satellite, information of cloud prediction has many benefits not only for agriculture. Information of cloud prediction is also needed by aviation, ground station and planning of solar power system development. To relate cloud from satellite data with rainfall, rain cloud or convective cloud can be differentiated by their optical thickness and cloud top pressure information [23].

4. Conclusions

Satellite data are potential for cloud forecasting using machine learning because of its wide coverage and availability of historical data. MODIS data, MTSAT and Himawari data are selected in this study. MODIS data has superiority in its spectral resolution. MTSAT and Himawari data has their superiority in temporal resolution. Many issues still need further research. When shorter period of historical data is suitable for forecasting algorithm, the use of Suomi NPP and NOAA-20 data is a better option to replace MODIS data.

5. References

[1] Meyer, H., et al., *Comparison of four machine learning algorithms for their applicability in satellite-based optical rainfall retrievals*. Atmospheric research, 2016. **169**: p. 424-433.
[2] Badan Penelitian Pengembangan Pertanian Kementerian Pertanian. *Kalender Tanam Terpadu, Penelitian, Pengkajian, Pengembangan, dan Penerapan* 2013.
[3] Han, E., A.V. Ines, and W.E. Baethgen, *Climate-Agriculture-Modeling and Decision Tool (CAMDT): A software framework for climate risk management in agriculture*. Environmental modelling & software, 2017. **95**: p. 102-114.
[4] Scaife, A.A., et al., *Tropical rainfall predictions from multiple seasonal forecast systems*. International Journal of Climatology, 2019. **39**(2): p. 974-988.
[5] Islam, M., et al., *Effects of El-Niño, Indian Ocean Dipole, and Madden-Julian Oscillation on Surface Air Temperature and Rainfall Anomalies over Southeast Asia in 2015*. Atmosphere, 2018. **9**(9): p. 352.

[6] Berkhahn, S., L. Fuchs, and I. Neuweiler, *An ensemble neural network model for real-time prediction of urban floods*. Journal of Hydrology, 2019. **575**: p. 743-754.
[7] Pillai D K., *Big Data Analytics for Satellite Image Processing and Remote Sensing*, P. Swarnalatha. and P. Sevugan., Editors. 2018, IGI Global. p. 133-150.
[8] Fu, T.-c., et al. *An innovative use of historical data for neural network based stock prediction*. in *9th Joint International Conference on Information Sciences (JCIS-06)*. 2006. Atlantis Press.
[9] Tuba, Z. and Z. Bottyán, *Fuzzy logic-based analogue forecasting and hybrid modelling of horizontal visibility*. Meteorology and Atmospheric Physics, 2018. **130**(2): p. 265-277.
[10] Gultepe, I., et al., *A review of high impact weather for aviation meteorology*. Pure and Applied Geophysics, 2019. **176**(5): p. 1869-1921.
[11] Ise, T. and Y. Oba, *Forecasting climatic trends using neural networks: An experimental study using global historical data*. Frontiers in Robotics and AI, 2019. **6**: p. 32.
[12] Du, J., et al., *A prediction of precipitation data based on support vector machine and particle swarm optimization (PSO-SVM) algorithms*. Algorithms, 2017. **10**(2): p. 57.
[13] Min, M., et al., *Estimating summertime precipitation from Himawari-8 and global forecast system based on machine learning*. IEEE Transactions on Geoscience and Remote Sensing, 2018. **57**(5): p. 2557-2570.
[14] Lee, S., et al., *Detection of deterministic and probabilistic convection initiation using Himawari-8 Advanced Himawari Imager data*. Atmospheric Measurement Techniques, 2017. **10**(5): p. 1859-1874.
[15] McDermott, P.L. and C.K. Wikle, *A model-based approach for analog spatio-temporal dynamic forecasting*. Environmetrics, 2016. **27**(2): p. 70-82.
[16] Rillo, V., et al. *Detection and forecast of convective clouds using MSG data for aviation support*. in *2015 IEEE Metrology for Aerospace (MetroAeroSpace)*. 2015. IEEE.
[17] Ackermann S A., e., al, , *Handbook of Weather, Climate, And Water ed Potter T D andColman B R*, ed. I. (New Jersey: John Wiley and Sons. 2003: Wiley Online Library.
[18] Sawada, Y., et al., *Assimilating Every-10-minute Himawari-8 Infrared Radiances to Improve Convective Predictability*. Journal of Geophysical Research: Atmospheres, 2019. **124**(5): p. 2546-2561.
[19] Japan National Meteorological Satellite Center., *Algorithm Theoretical Basis Document For Cloud Detection*. 2012, National Meteorological Satellite Center: Japan.
[20] Imai, T. and R. Yoshida, *Algorithm theoretical basis for Himawari-8 cloud mask product*. Meteorol. Satell. Center Tech. Note, 2016. **61**: p. 1-17.
[21] Heidinger A., Botambekov D., and Walther A., *Algorithm Theoretical Basis Document: A Naïve Bayesian Cloud Mask Delivered to NOAA Enterprise*. NOAA Nesdiscenter For Satellite Applications And Research, 2016
[22] Godin, R., *Joint Polar Satellite System (JPSS) VIIRS cloud mask (VCM) algorithm theoretical basis document (ATBD)*. Joint Polar Satellite System (JPSS) Ground Project Code, 2014. **474**: p. 474-00033.
[23] Punay J P. and Perez G J P., *valuation of MODIS Cloud Products-Derived Rainfall Estimates 35th* Asian Conference on Remote Sensing, 2014 E.

Acknowledgments
The author would like to thank Kemenristekdikti who provide Saintek 2018 Scholarship as financial support. The authors would like also to thank Bandung Institute of Technology for the facility provided in this research.

Mangrove Biomass Estimation Based on Vegetation Height Through Lidar and Terrasar-X Data Approaches

Nanin Anggraini[1]*, Atriyon Julzarika[1,2], Dian Rachmawati[3], Iwan Erik Setyawan[4]

[1]Remote Sensing Applications Center, LAPAN, Indonesia
[2]Geodesy Geomatics Enginering, UGM, Indonesia
[3]Directorate of Soil and Water Conservation, Ministry of Environment and Forestry, Indonesia
[4]Geospatial Information Agency, Indonesia

*Corresponding author's e-mail: nanin_rain@yahoo.com

Abstract. One of the mangroves roles is as carbon reserves. Calculation of carbon stocks can be done based on mangrove biomass. Biomass estimation can be estimated by the vegetation height approach derived from LIDAR and TerraSAR-X data. The study purpose was to estimate mangrove biomass based on LIDAR and TerraSAR-X data in Kubu Raya West Kalimantan. The data used are LiDAR (ICEsat / GLAS) and TerraSAR-X data. The method of estimating biomass used is Above Ground Biomass and Below Ground Biomass with a vegetation height approach. Vegetation height was obtained from the difference between TerraSAR-X Digital Surface Model (DSM) and Digital Terrain Model (LiDAR). The location and extent of mangroves was obtained from the National One Map Mangrove data. Based on the temporary processing results, the area of mangrove in Kubu Raya is 129,308 ha, with biomass (AGB and BGB) ranges from 51.5 - 203 Mg and 13.2 - 81.2 Mg. At least 9 mangroves species were found in Kubu Raya which is dominated by *Rhizopora sp* and *Nypa fruticans* species.

Keywords: mangrove biomass, vegetation height, LiDAR, TerraSAR-X, One Map Mangrove.

1. Introduction

Carbon stocks can be defined as the amount of organic carbon stored in an ecosystem of known size and consists of one or more carbon sources [1]. One source of carbon stocks is coastal area and it is known as the blue carbon. Blue carbon is the carbon stored in mangroves, salt tidal marshes, and seagrass meadows within the soil, the living biomass aboveground (leaves, branches, stems), the living biomass belowground (roots), and the non-living biomass (eg, litter and dead wood) [2]. Mangroves are very high provider of blue carbon compared to tidal salt marsh and seagrass. According to [3], mangroves have average carbon stock of 386 Mg/ha.

Carbon stocks of mangrove estimation can be done with biomass derived approach from vegetation height. The vegetation height of mangrove can be estimated using remote sensing data, including Light Detection and Ranging (LiDAR) from ICEsat/GLAS) and TerraSAR-X. Digital Terrain Model (DTM) can be extracted LiDAR and Digital Surface Model (DSM) is extracted from TerraSAR-X. The difference between DTM and DSM is vegetation height. This vegetation height information can be used to estimate biomass either on the surface or belowground biomass.Biomass estimation using LiDar data has also been carried out by [4] with research area in Africa.

This research aim is to estimate mangrove biomass based on LiDAR (ICEsat/GLAS) and TerraSAR-X data in Kubu Raya, West Kalimantan.

2. Methods

2.1. Data and location

The data used are LiDAR (ICEsat / GLAS), TerraSAR-X, Landsat 8, mangrove data from the National One Mangrove Map, and field data. Field data were obtained from the results of a field survey conducted on 7-13 August 2018. The location of the study was in the District of Kubu Raya, West Kalimantan (Figure 1).

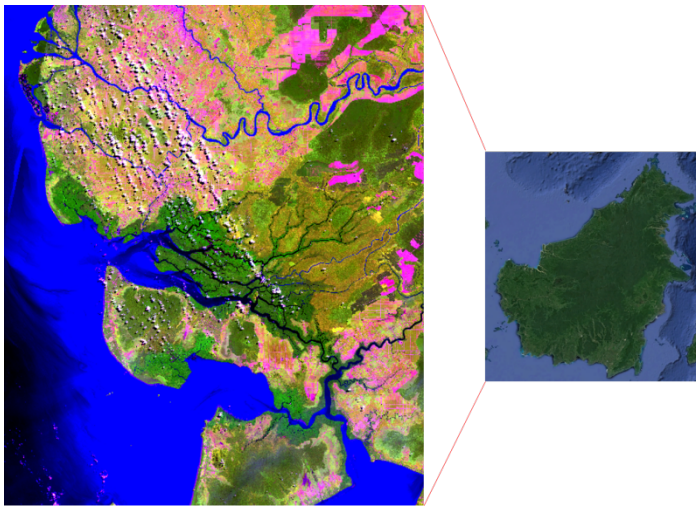

Figure 1. Kubu Raya, West Kalimantan.

Estimation of mangrove locations in Kubu Raya is based on visual interpretation of the Landsat 8 data mosaic with path rows 121 060, 121 061, and 122 060 on the acquisition date on February 12th, 2018 and on July 15th, 2018. Composite of Red Green Blue (RGB) SWIR-1 NIR Red shows the location mangrove. A side from being visual, the estimation of the location and extent of mangroves in Kubu Raya is based on data from the One Mangrove National Map. One Map Mangrove information is created using data from SPOT, SPOT 6/7 and some information from ground survei data.

2.2. Biomass

Biomass estimation (Above Ground Biomass and Below Ground Biomass) uses vegetation height approach that derived from LiDAR and TerraSAR-X data. LiDAR actively provides information related to the parameters of the earth's surface in the form of height and canopy from the earth's surface [5, 6] TerraSAR-X is high-resolution radar that has an accuracy of up to 1 m. TerraSAR-X has Spotlight, StripMap, and ScanSAR imaging modes [7]. Information obtained from LiDAR is DTM and from TerraSAR-X is DSM. DTM and DSM are derived by the DSM2DTM method [8]. Difference from DTM and DSM produces vegetation height information.

AGB Estimation uses allometric equation with mangrove height approach [9]. This allometric equation was built using 43 field data that were distributed globally with $R^2 = 0.77$ and RMSE = 43.8.

$$AGB = 10.8 \text{ x } H + 34.9 \quad (1)$$

where:

AGB : Above Ground Biomassa (Mg)
H : Mangrove Height (m)

BGB estimation uses an equation developed by [10]. BGB is obtained from the conversion of AGB values:

$$BGB = 0.073 \text{ x } AGB^{1.32} \quad (2)$$

where:
BGB : Below Ground Biomassa (Mg)
AGB : Above Ground Biomassa (Mg)

3. Results and Discussion

Identification of the location of mangroves in the Kubu Raya area is done visually using RGB SWIR-1 NIR Red data from Landsat 8 data. The RGB composite results show the location of mangroves in Kubu Raya. Mangroves look greener compared to other vegetation (Figure 2). This is due to the influence of the SWIR-1 band which is sensitive to moist soil [11]. Based on data from the Kalimantan One Map Mangrove, the area of mangroves in Kubu Raya reaches 129,308 ha. A field survey conducted on 7-13 August 2018 showed the condition of mangroves in Kubu Raya. The results of the field survey showed that there were around 9 mangrove species and were dominated by *Rhizophora sp* and *Nypa fruticans* (Figure 3).

Figure 2. Mangrove research area.

Based on the processing results of LiDAR and TerraSAR-X data, DTM and DSM information is extraction. DTM provides the spatial information related to terrain height or ground level while DSM describes the surface height of objects. The difference in value between DTM and DSM is the object height (mangrove tree height). The mangroves height in Kubu Raya varies between 1.54 - 15.6 m. Mangroves with a height of 4 - 10 m dominate in Kubu Raya with frequencies reaching 250. Mangrove height with a range of 1.54 - 10.7 m dominates in the Teluk Pakedai Subdistrict, height with a range of 8.85 - 15.6 m dominates in the Batuampar and Kubu Districts (Figure 4).

AGB with the approach of mangrove height has values ranging from 51.5 - 203 Mg and BGB ranges from values 13.2 - 81.2 Mg. AGB with a value of 7-10 Mg dominates with frequencies reaching 250 and BGB is dominated at values 30-40 Mg with frequencies up to 350 (Figures 5 and 6). High values on AGB and BGB illustrate the potential for carbon stocks from mangroves in Kubu Raya. Therefore, the existence of mangroves in Kubu Raya needs to be maintained.

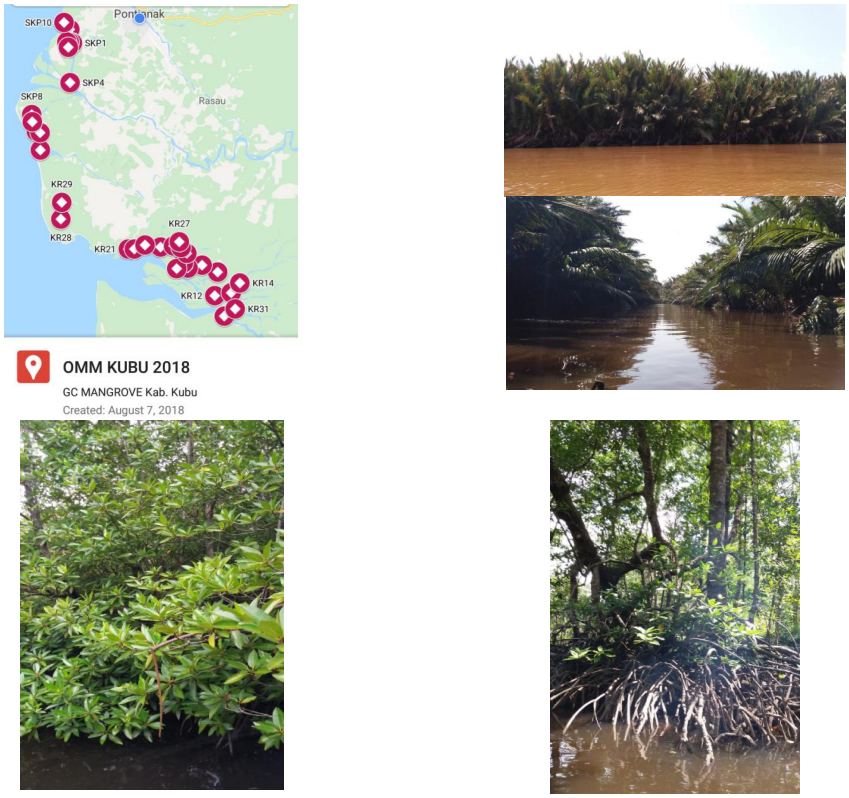

Figure 3. Ground survey of *Nypa fruticans* and *Rhizophora sp.*

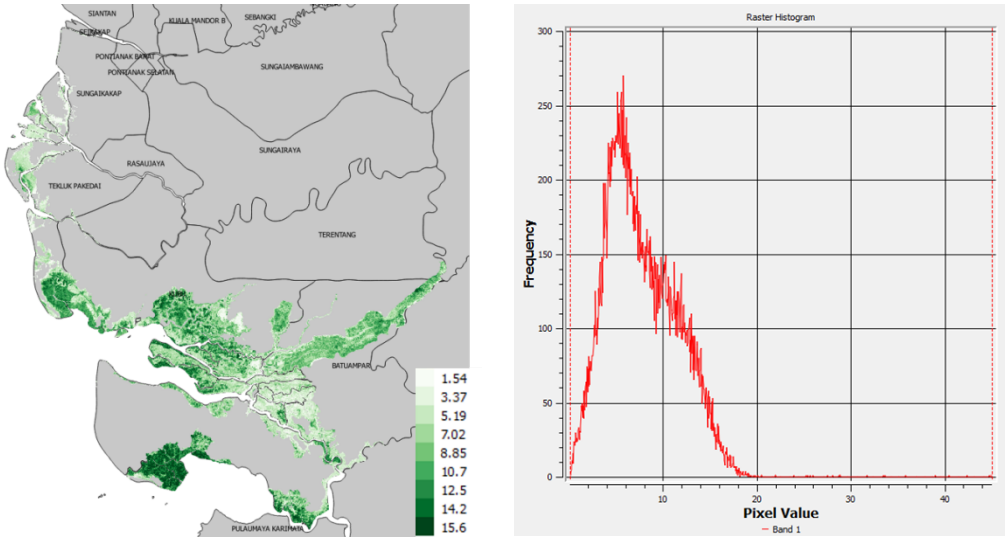

Figure 4. Mangrove height distribution.

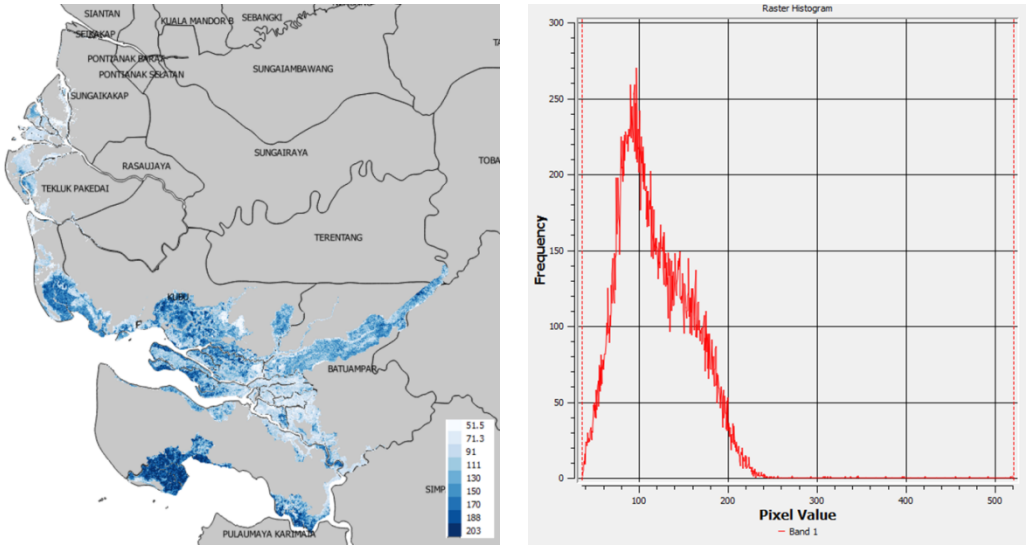

Figure 5. AGB distribution.

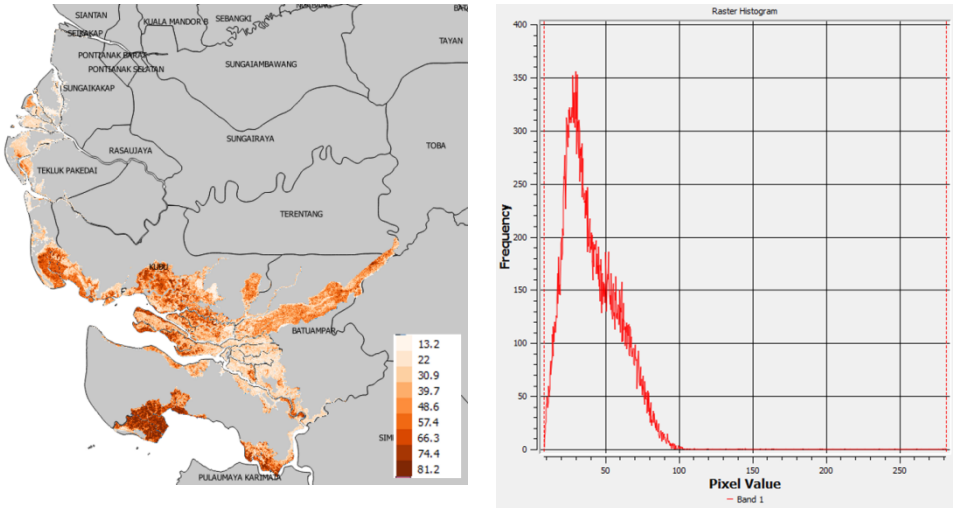

Figure 6. AGB distribution.

4. Conclusions

Vegetation biomass (AGB and BGB) can be estimated using an approach of vegetation height. Vegetation height can be obtained from the difference between DTM and DSM. DTM was extracted from LiDAR data while DSM was extracted from TerraSAR-X. AGB and BGB in Kubu Raya range between 51.5 - 203 Mg and 13.2 - 81.2 Mg.

5. References

[1] Howard, J., et al., *Coastal blue carbon: methods for assessing carbon stocks and emissions factors in mangroves, tidal salt marshes, and seagrasses.* 2014.

[2] Mcleod, E., et al., *A blueprint for blue carbon: toward an improved understanding of the role of vegetated coastal habitats in sequestering CO2.* Frontiers in Ecology and the Environment, 2011. **9**(10): p. 552-560.

[3] Kennedy, H.H., et al., *Coastal wetlands*, in *2013 Supplement to the 2006 IPCC Guidelines for National Greenhouse Gas Inventories: Wetlands. IPCC, Switzerland*. 2014, IPCC.

[4] Fatoyinbo, T.E. and M. Simard, *Height and biomass of mangroves in Africa from ICESat/GLAS and SRTM.* International Journal of Remote Sensing, 2013. **34**(2): p. 668-681.
[5] Los, S., et al., *Vegetation height and cover fraction between 60◦ S and 60◦ N from ICESat GLAS data, Geosci. Model Dev., 5, 413–432, doi: 10.5194*. 2012, gmd-5-413-2012.
[6] Rosette, J., P. North, and J. Suarez, *Vegetation height estimates for a mixed temperate forest using satellite laser altimetry.* International Journal of Remote Sensing, 2008. **29**(5): p. 1475-1493.
[7] Defence, A., *Space (2014) TerraSAR-X image product guide.* Airbus Defence and Space, Geo-Intelligence, Friedrichshafen.
[8] Julzarika, A. and Rukhmana. *GLOBAL DEM – GDEM++*. 2019; Available from: http://www.potretudara.com/global-dem-gdem/.
[9] Saenger, P. and S.C. Snedaker, *Pantropical trends in mangrove above-ground biomass and annual litterfall.* Oecologia, 1993. **96**(3): p. 293-299.
[10] Hutchison, J., et al., *Predicting global patterns in mangrove forest biomass.* Conservation Letters, 2014. **7**(3): p. 233-240.
[11] Landsat, U., *8 (L8) operational land imager (OLI) and thermal infrared sensor (TIRS)*. 2013.

Acknowledgement
Thanks to DLR and NASSA for the LiDar and TerraSAR-X data. The main contributor in this paper are Nanin Anggraini and Atriyon Julzarika.

Asset Identification of Belitung Timur District Government using Geospatial Information Approach

Fahrudin[1]*, Nurul Mustofa[1]

[1]Public Works and Spatial Planning Services of Belitung Timur District, Indonesia

*Corresponding author's e-mail: fahrudinmanggar@gmail.com

Abstract. This study aims to identify the asset of Belitung Timur District government based on geospasial information approach. Identification the real asset area includes analysis of the coordinate points because both area and the coordinate points data are very necessary to be used as input data in Regional Management Information System (SIMDA). Because previous surveying and mapping seem inaccurate with the Indonesian Geospatial Reference System (SRGI), newer surveying and mapping is needed for reconstructing the mark boundary in order to make it compatible with SRGI i.e., switching UTM Zone from 48S to 49S reference system. In the reconstruction of this asset boundary, the linier interpolation method is used and then combined with Digital Theodolite and GPS receiver. Overlay analysis is also used to measure the real assets of Belitung Timur. After being analyzed using geospatial information approach, the total assets were not exactly 431.71 Ha as recorded by Audit Board of the Republic of Indonesia (BPK-RI), but the total area is below 431.71 Ha, and also the coordinates are updated.

Keywords: Asset, SRGI, Geospatial Information.

1. Introduction

Based on the decree of the regent of Belitung Timur number 991/24/KEP/I/2003, Belitung Regency Government office area is ± 500 Hectare (Ha) located in the Padang village of Manggar sub-district. The location is only a designation so the map is only an indicative map yet the map has been georeferenced in accordance with the provisions one because the purpose of the decree is for establishment of a new district as prerequisite by the Ministry of Home Affairs (MENDAGRI), which is at least ± 500 Ha (Figure 1). The map did not have right referencing system because of the lack of mapping database and absence of laws and regulations that regulate mapping issues such as Geospatial Information Law number 4 of 2011 and Indonesian Geospatial Reference System (SRGI) 2013.

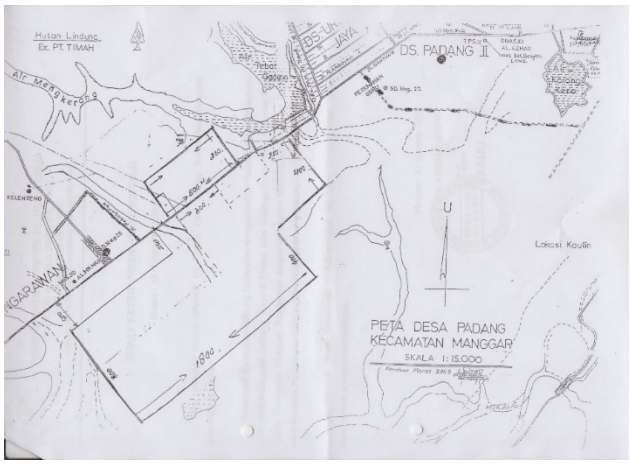

Figure 1. Early map of the Belitung Timur District Government.

In 2008, Planning and development agency [1] of Belitung Timur had surveyed and mapped Belitung Timur District government area. The purpose of the activity was to obtain coordinate data and an integrated office area of East Belitung Regency Government in all. Furthermore, boundary structuring of office areas is carried out in the form of installing boundary stakes in the field. This activity has succeeded in making the coordinates of the boundary markers and installing them in the area of 449.21 Ha. However, there are some differences in these activities such as the suitability between the stake in the field with the reported coordinates. This may be due to a lack of data bases and related regulations to geospatial information. So that there are many inconsistence coordinate points obtained by field boundary stakes based on the results of ground truth conducted by Boundary Team of Belitung Timur Regency in 2019. So, it is necessary to update the coordinate data in previous document with real boundary markers in the field by referring to the coordinates of points obtained from geospatial analysis in this study. The checks are carried out by comparing coordinate data with orthorectified high-resolution satellite imagery (CSRT) from BIG and enhanced by the latest CSRT of LAPAN. Both BIGS's Geodetic Control Network [2] and CORS area also used in this research.

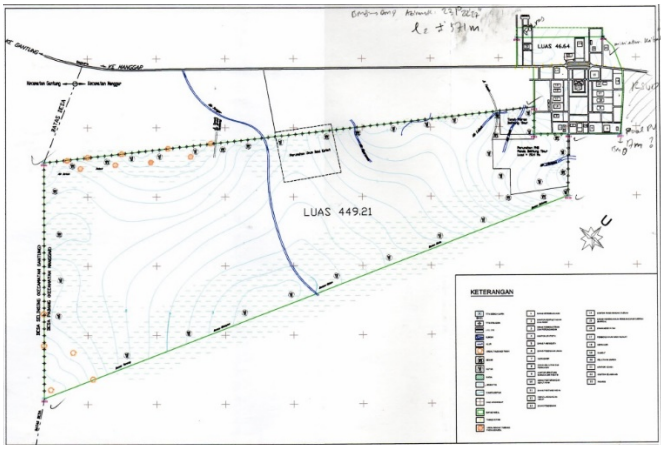

Figure 2. Map of Belitung Timur District Government after re-survey by BAPPEDA in 2008.

In addition, [3] had provided a study of the extent of the existing ± 500 Ha with details. The calculation is based on a calculator count of the total land area of the ± 500 Ha minus the parcels that have been granted to third parties. The information is not based on the true geographic space where the land is located. The current development turns out that the regency's land based on geospatial is not as large as 431.71 Ha because the data used is not based on proper geospatial information. Therefore, it is necessary to do a research based on geospatial information approach to the one of Belitung Timur government assets to identify the actual size of that parcel.

Besides that, the correct measurement is important because the true area will be included in regional management information system (SIMDA). Before input in SIMDA the data must meet minimum requirements i.e., right area and coordinate points of the area of interest (AOI). The study area, shadowed one, is shown as figure follow (Figure 3).

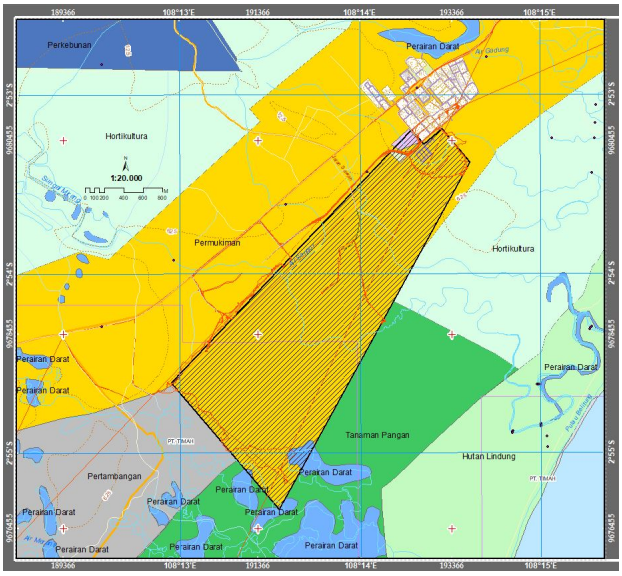

Figure 3. Area of Interest (AOI).

2. Research Methodology

The first step in this study is data collecting both spatial and attribute data such as regent's decree of Belitung Timur and also collecting raster and vector data used as input data. Data from the previous survey conducted by BAPPEDA was also used as input data to model boundary stakes in the field and analyzed using computer as on desktop study step. On desktop study was conducted to compile a survey design for data acquisition in the field based on data obtained from BAPPEDA's surveying report so that it can be seen whether the boundary stakes in the field is still relevant or not. Orthorectified satellite imagery of Belitung Timur District issued by BIG in 2019 are used to model the direction of the stake in the field and then look for the azimuth and also true coordinate points. Previous coordinates point is not match with Indonesian Geospatial Reference Systems (SRGI) because the coordinate system is UTM Zone 48S in which it must be transformed to UTM Zone 49S. One reason is SRGI was issued in 2013 by BIG so before 2008 it was not yet issued. A geographic coordinate system defines a framework for identifying locations and also has a spheroid which sets size and shape. Each geographic coordinate system is also tied to the earth in a particular way. Because of this, the same location on the ground will have different coordinate values in different geographic coordinate systems. Displaying data in a projected coordinate system can exaggerate the differences which can be from a few centimeters to hundreds of meters. So, it will need to set a geographic, or datum, transformation.

Many damaged and even missing boundary marks have been reconstructed using theodolite after being analyzed by adjusting computation with simple interpolation, namely linear interpolation because the study area is relatively straight and not bent. A linear interpolation approach is used to reconstruct the boundary mark in the area of interest. So, the azimuth and the distance of the lost stakes can be recovered using this recipe as formulae below.

$$x_{n-1} = x_n + d_{n,n+1} \sin \theta_{n,n-1} \quad (1)$$

$$Y_{n-1} = Y_n + d_{n,n+1} \cos \theta_{n,n-1} \quad (2)$$

Where

x_{n-1} = Sougth abscissa
Y_{n-1} = Sougth ordinate
x_n = Known abscissa
Y_n = Known ordinate
$d_{n,n+1}$ = distance between the known point and the sougrt point
$\theta_{n,n-1}$ = azimuth between the known point and the sougrt point

The stakes were successfully reconstructed according to the model obtained from a combination of analytical data with digital theodolite that was used where navigation was also carried out with the help of a GPS navigation receiver to make it easier to route the stake points surveyed. Surveying data are processed by geospatial analysis, one of which is overlay analysis. Overlay analysis can find out which identities are contained in the assets of the Belitung Timur regency government totaling 431.71 Ha from the (BPK RI) report. As a geoprocessing result, the measurement results were obtained with different areas compared to the results of the BPK-RI calculation. In addition to the availability of the area, the coordinates of the results of this research update were also obtained. Area calculation is based on formulae in equation 3.

$$L = \frac{1}{2} \sum_{n=1,2,}^{n+1} (X_n Y_{n+1} - X_{n+1} Y_n) \quad (3)$$

Where:
L = Area calculated
n = vertex number
n + 1 = the next point, the last point must meet the first one
Note: The area obtained from the coordinates of the calculated results will be more precise than the measurement results from the map

Finally, the output of this research is the true assets of Belitung Timur District Government based on geospatial information. In the fact, there is an overlap with other parties based on overlay analysis. This output includes adjusted area and coordinates which is ready to input to SIMDA. The following is research methodology flow chart of the identification assets of Belitung Timur District Government.

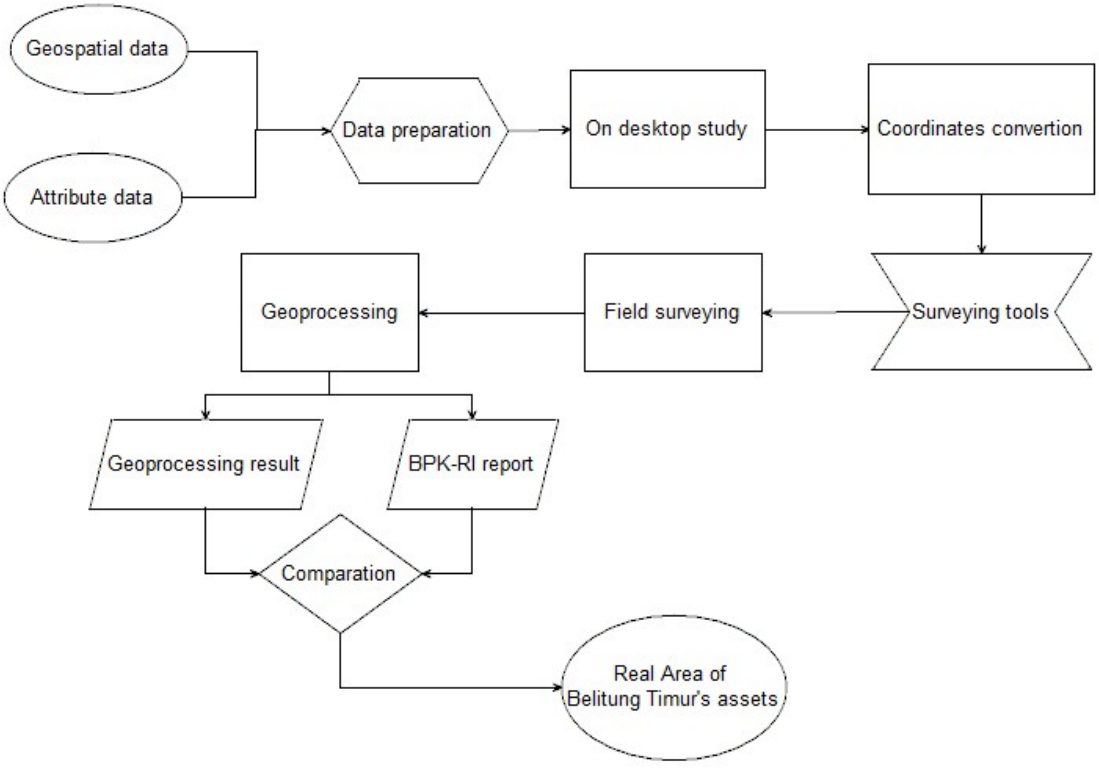

Figure 4. Research Methodology.

3. Results and Discussion

3.1. Updating Boundary Markers of Coordinate Points

There is a significant difference between the survey results and in the field boundary markers. Benchmark Point 1 (BM1) survey results experience a very far translation compared to the real boundary markers. The translation is ± 32.59 meters with azimuth $308^0 28'23''$ measured from BM1 report (model) to BM1 boundary marker (realworld). BM1 report position in the corner near to Belitung Timur District Government's pool office and this is one-way validation that the coordinates from the report is not right because the existing one is on the corner of food stalls (Figure 5).

Figure 5. Benchmark of previous surveying.

Other Validation is done by matching the GCP-M03 tie point which is a survey point with the Geodetic GPS receiver gained from measurement report of BAPPEDA in 2016 with the coordinates 192980,806 Easting and 9680522,238 Northing UTM Zone 49S with an elevation of 30,831 m. Based on desktop study, azimuth and distance measured from GCP-M03 to BM3 exiting are respectively $316^0 54'38''$ and 89,259 m and this information is accurate with in the field surveying using digital theodolite DT200. Precise coordinate points of BM3 is also gained by theodolite measurement (Figure 6).

Other coordinate points can be created from coordinate point of BM3 as reference by using geoprocessing method. Output coordinate points of geoprocessing are the right ones because they match with satellite imagery of BIG & LAPAN, and Geodetic GPS receiver data. Resulted coordinate points are different from previous coordinate points gained from previous surveying and mapping report. The bias between the data contained in the 2008 survey documents and in the field boundary markers is also found at points adjacent to BM1 and other boundary points.

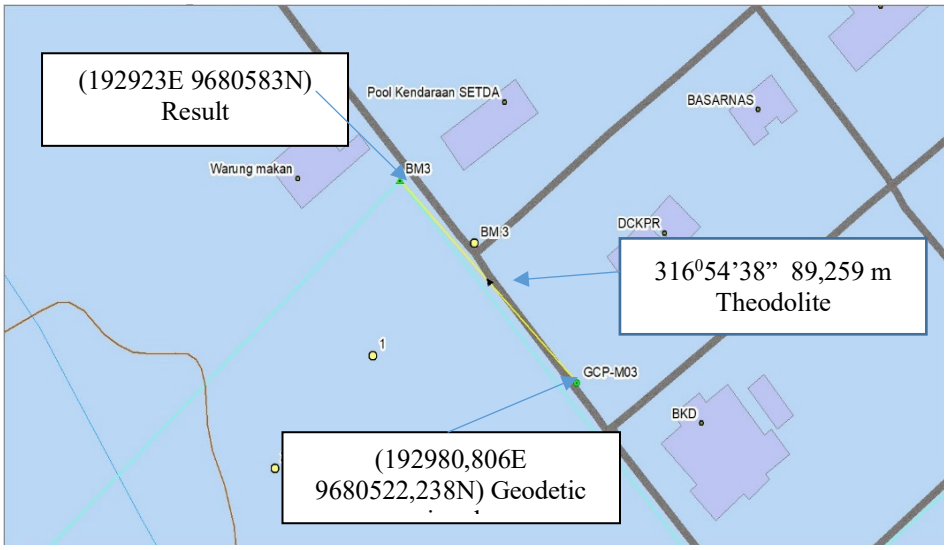

Figure 6. Coordinate Acquisition of BM3.

Table 1. Comparison between the study and the 2008 surveying report coordinates.

Points	Easting	Northing	Points	Easting	Northing	Points	Easting	Northing	Points	Easting	Northing
BM1	193237	9680596	PB43	191438	9679025	BM 1	193264	9680575	43	191470	9679004
BM2	193046	9680435	PB44	191405	9678990	BM 2	193077	9680417	44	191436	9678968
BM3	192920	9680587	PB45	191369	9678952	BM 3	192946	9680567	45	191402	9678931
BM4	190463	9677971	PB46	191337	9678917	BM 4	190480	9677955	46	191367	9678895
BM5	191541	9676708	PB48	191269	9678844	BM 5	191587	9676654	48	191298	9678822
BM6	193545	9680227	PB49	191235	9678807	BM 6	193549	9680234	49	191265	9678786
PB4	192775	9680445	PB50	191200	9678768	4	192808	9680421	50	191230	9678750
PB8	192632	9680302	PB52	191133	9678696	8	192671	9680276	52	191161	9678677
PB9	192598	9680266	PB53	191100	9678660	9	192636	9680239	53	191127	9678640
PB10	192564	9680229	PB57	190950	9678499	10	192603	9680203	57	190990	9678495
PB11	192529	9680192	PB58	190917	9678463	11	192568	9680167	58	190956	9678458
PB21	192188	9679829	PB61	190814	9678350	21	192225	9679803	61	190853	9678350
PB23	192120	9679756	PB68	190578	9678096	23	192156	9679731	68	190613	9678096
PB24	191981	9679609	PB105	193493	9680289	24	192121	9679695	105	193517	9680273
PB25	191947	9679573	PB106	193460	9680329	25	192088	9679658	106	193485	9680311
PB26	191880	9679501	PB107	193429	9680367	26	192053	9679622	107	193453	9680350
PB40	191545	9679142	PB108	193399	9680402	40	191573	9679113	108	193421	9680388
PB42	191469	9679059	PB110	193332	9680483	42	191504	9679040	110	193357	9680464
Study						2008 Surveying Report					

The comparison of the coordinates of the study results with the coordinates of the 2008 survey report is shown in Table 1. The study coordinate points are the pegs that still exist in the field taken by using appropriate measuring instrument while the coordinates of the surveying results are BAPPEDA's survey reports in 2008. The study coordinate points are the truth ones because they had been validated with satellite imagery orthorectified by BIG, CSRT LAPAN, and also BIG's JKG.

3.2. Updating Area Calculation of Assets

The regency's asset area is 449.21 Ha from the Bappeda survey while the area of research results is 449.51 Ha, which corresponds to the actual size of the regency's assets. The wide difference in the results of the 2008 Bappeda measurement with the research results is not too significant, only different in the decimal. However, as explained in the sub-section updating the coordinates of the delineation area of the 2008 Bappeda measurement results is too biased. This bias occurs because the point of the results of the report contained in the document does not match the point in the field. Therefore, in this research

the area of the area was adapted to follow the area of the boundary markers found in the field. Not all boundary markers in the field were found only between BM3 and BM 4, BM 1 and BM6 while BM4 and BM5 and BM5 and BM6 were not found so that these stakes were made with markan point.

Table 2. 500 Ha Area of Belitung Timur District based on SK No. 991/24/KEP/I/2003.

No	Entity	Decree area (Ha)	Measured area (Ha)	Area (Ha)	Note
1	Bappeda	± 499,21			Surveying report in 2008
2	Awakened area		± 29,68		Kompleks Pemkab Beltim Existing
3	Vertical Instance		± 7,42		
4	PT. Jaya Harapan Aristama		± 0,72		Manggar Trade Center (MTC); SK No. 590/210/KEP/I/2009
5	PT. Jaya Harapan Aristama		± 15		
6	PT. Truetech Cipta Sarana		± 14,96		Rumah PNS; SK No. 590/479/KEP/I/2008
	Remain area			± 431,71	No. 700/23/LHP/ BPK-RI/INPT-I/2018
Inspection report of BPK - RI					

No	Entity	Decree area (Ha)	Measured area (Ha)	Area (Ha)	Note
1	Boundary Team	±449,51			Surveying report in 2019
2	PT. Jaya Harapan Aristama		± 15		Manggar Trade Center (MTC); SK No. 590/210/KEP/I/2009
3	PT. Truetech Cipta Sarana		± 14,96		Rumah PNS; SK No. 590/479/KEP/I/2008
4	Polres of Belitung Timur		± 3.075		
	Remaining area			± 416.475	
5	IUP PT. Timah		± 183,18		
	Remain area			± 233.295	Lahan Pemkab Beltim
Study result					

BPK-RI counts that total asset is ± 431.71 Ha where it includes area for PT. Jaya Harapan Aristama 0.72 Ha so if 431.71 Ha which is minus this area the total area is 430.99 Ha (Table 2). It is because area 0.72 Ha is outside the asset 449.51 Ha and this study only review the area inside 449.51 Ha. The study proves that area of Belitung Timur District Government assets is not ± 431.71 Ha but ± 449.51 Ha which overlaps with other parties, namely PT. Truetech Cipta Sarana (Manggar Residence) = ± 14.96 Ha, PT. Jaya Harapan Aristama (Telaga Bulan Residence) = ± 15 Ha, and Polres of Belitung Timur = ± 3.075 Ha. So, the total area based on the study is 416.475 Ha. If Mining license (IUP) PT. Timah tbk = ± 183.18 Ha is inputed in overlay study, the total net area is ± 233.295 Ha. PT. Timah tbk maybe will give the IUP to the District but not all area potential to take over because there are many mining activities in there.

4. Conclusions and Recommendations

Asset identification with a geospatial information approach using the right input data such as geospatial information from an orthorectified imagery and using meticulous measuring instrument and also geoprocessing method can produce precise and accurate measurement results.

It is likely if Belitung Timur District Government wants to calculate the area of any asset using geospatial information identification approach for obtaining the appropriate area value combined with precise measuring instrument and geoprocessing. After obtaining the area of assets with that method than value of assets including the coordinates are ready to submit into the Regional Management Information System (SIMDA).

5. References

[1] Timur, B.B., *Survei dan Pemetaan Kawasan Perkantoran Terpadu dan Perdagangan* 2008, PT. Putri Siantan Belitung Timur.

[2] BIG. *Informasi JKG*. 2019 [cited 2019 August 1]; Available from: http://srgi.big.go.id/srgi2/jkg.

[3] Belitung, B.-R.P.B., *Laporan Hasil Pemeriksaan (LHP) Tahun Anggaran 2018 Belitung Timur*. 2018, BPK-RI.

Urban Building Land Mapping and Monitoring Using Approach *Normalized Difference Built-up Index* (NDBI) (Case Study: Bandung City, West Java)

Felita Larissa Nathania[1]*, Rika Hernawati[1]

[1]Geodesy Engineering, Institut Teknologi Nasional, 23 PH.H. Mustofa Street, 40124 Bandung, Indonesia

*Corresponding author's e-mail: felitanathania1@gmail.com

Abstract. Bandung is the capital of West Java Province which is one of the largest metropolitan cities with a very dense population due to urbanization. Population density causes the importance of the need for a decent place to live, resulting in the use of urban built land. The significant change in urban built land can be felt long ago until now, in 1990, 2000 and 2018 where changes were felt like the replacement of plantation land into housing, high-rise buildings, and industrial area. Monitoring changes in urban built land can be important information about spatial planning in the city of Bandung. Remote sensing applications from Landsat 5 and 7 Imagery products use the Normalized Difference Built-up Index (NDBI) approach method to determine changes and the extent of urban built areas in the city of Bandung. The results of this study indicate that the city of Bandung experienced a significant change in built-up land at 1990, 2000 and 2018 with accuracy test using confussion matrix table an overall accuracy 90% and kappa accuracy 86.67%.

Keywords: Landsat 5, Landsat 7, Remote Sensing, NDBI.

1. Introduction

Bandung City is the largest metropolitan city in West Java Province, as well as being the capital of the province. The city is located 140 km southeast of Jakarta, and is the largest city in the southern part of Java Island. The total area of Bandung City is 16,729.65 Ha, where at the end of 2007 it had a population of 2,329,928 people. Urban population growth which exponentially increases both naturally and due to urbanization causes problems in natural characteristics, namely Land Use or Land Cover [1]. Land use in the city of Bandung based on data in 2007 was dominated by land use types in the form of settlements with an area of 9,290.28 hectares or around 55.5% of total land use. The development of the built area in the city of Bandung is still in the old city center area in the city square of Bandung [2].

Based on the Regional Regulation of Bandung City Number 18 of 2011 concerning the spatial plan of the City of Bandung that the importance of spatial planning sees the city of Bandung as a stand-alone metropolitan area and functional interrelationships associated with regional infrastructure network systems which are integrated with population and development [3].

Satellite imagery with remote sensing methods can be used to monitor and detect changes in built-up areas that often occur in urban areas and suburbs as a consequence of incessant urbanization. Built areas can be mapped through the Normalized Difference Built-up Index (NDBI) algorithm by using Landsat image data [4].

This research refers to several previous studies conducted by [5] using Landsat 8 imagery to determine settlement density using two parameters, namely, Object Base Image Analysis (OBIA) and Normalized Difference Built-up Index (NDBI), research by [6] using Landsat 8 OLI imagery for mapping urban built land with the Normalized Difference Built-up Index (NDBI) and Semi-Authatic approaches, [7] use five parameters, namely, Normalized Difference Built-up Index (NDBI) , Normalized Difference Vegetation Index (NDVI), Modified Normalized Difference Water Index (MNDWI), Normalized Difference Water Index (NDWI), Soil Adjusted Vegetation Index (SAVI), and [8] use MODIS imagery

to monitor urbanization in combination. three parameters, namely, Visible-Infrared Imager-Radiometer Suite Day / Night band (VIIRS DNB), Normalized Difference Vegetation Index (NDVI), Normal ized Difference Built-up Index (NDBI), where the final results of the four studies are how much the land changes are built in terms of the parameters used.
Based on the research conducted by [5-8]
this study will apply the Normalized Difference Built-up Index (NDBI) approach to see how much urban land development changes multitemporal. This study will produce a map of the growth of built-up land in the city of Bandung in 1990, 2000 and 2018. This activity plays an important role in monitoring the increase in urban built land, in order to reduce spatial planning for land to be built in the future.

2. Methodology

2.1. Method

Research methodology is the flow of research implementation starting from determining the location of Bandung City, West Java Province, collecting Landsat Satellite image data downloaded through the USGS website, preprocessing Landsat Image data which includes geometric correction, radometric correction. Furthermore, Landsat Image data is ready to be used to identify built-up land in the city of Bandung. This study uses the *Normalized Difference Built-up Index* (NDBI) algorithm.

2.2. Research Data and Location

The data used in this study are Landsat 5 Image data in 1990 and Landsat 7 Image data in 2000 and 2018, Bandung City administrative boundary map, and Bandung City land cover map. Landsat 5 and 7 imagery are the main data that will be used to determine density built, Bandung Citr administrative boundary map that will be used to crop area of interest, and Bandung City land cover map that will be used to build total data. Description of research data can be seen in Table 1**.**

Table 1. Data.

Data	Information	Source
Landsat 5 Imagery Data	9 July 1990	www.earthexplorer.usgs.gov
Landsat 7 Imagert Data	28 July 2000	www.earthexplorer.usgs.gov
	6 July 2018	www.earthexplorer.usgs.gov
Map of Bandung City Administrative Limits	Scale 1: 50000	www.tanahair.indonesia.go.id
Map of Bandung City Land Cover	Scale 1: 25000	www.tanahair.indonesia.go.id

In this study using Landsat 5 and 7 imagery data where each satellite image has different spectral spesification, to produce NDBI calculations, it is necessary to calculate Band contained in these satelllite images. As in the picture below, the sepecifications of satellite imagery will be used in this study can be seen in Table 2**.**

Table 2. Specifications of Landsat 5 and Landsat 7.

Details of Landsat 5-TM Satellite Images

Band Number	Spectral Range (μm)	Spatial Resolution (m)	Band Name
1	0.450-0.515	30	Blue
2	0.525-0.605	30	Green
3	0.630-0.690	30	Red
4	0.760-0.900	30	Near IR
5	1.550-1.750	30	Mid IR
6	10.400-12.500	120	Thermal
7	2.080-2.350	30	Mid IR

Details of Landsat 7-ETM Satellite Images

Band Number	Spectral Range (μm)	Spatial Resolution (m)	Band Name
1	0.45-0.51	30	Blue
2	0.52-0.60	30	Green
3	0.63-0.69	30	Red
4	0.76-0.90	30	Near IR
5	1.55-1.75	30	Mid IR I
6	10.40-12.50	30	Thermal
7	2.09-2.35	30	Mid IR II
8	0.52-0.90	15	Pancromatic

To clarify the stages of this research, flowchart methodology is shown in Figure 1. Data on Landsat 5 and Landsat 7 Bandung City can be downloaded on NASA's USGS official website page www.earthexplorer.usgs.gov. The results of downloading Landsat 5 and Landsat 7 Bandung City data, which can be seen in Figure 2, Figure 3, and Figure 4, while Bandung City Administrative can be seen in Figure 5.

From the results of the Landsat Image 5 in 1990 there were few clouds in the South and West areas of Bandung City, Landsat 7 in 2000 there were clouds in almost regions of Bandung City, while Landsat 7 in 2018 were different appearance where there is stripping in all areas of Bandung City which is a mistake in tools when recording data or scan line corrector (SLC) off. Especially in Indonesia, where most of the territory is tropical and is the location of clouds. The reason for choosing Landsat Image 5 and 7 is because researchers want to know the phenomenon of changes density-built Bandung City in 1990-2018 and caused climate change since time series years in the city of Bandung.

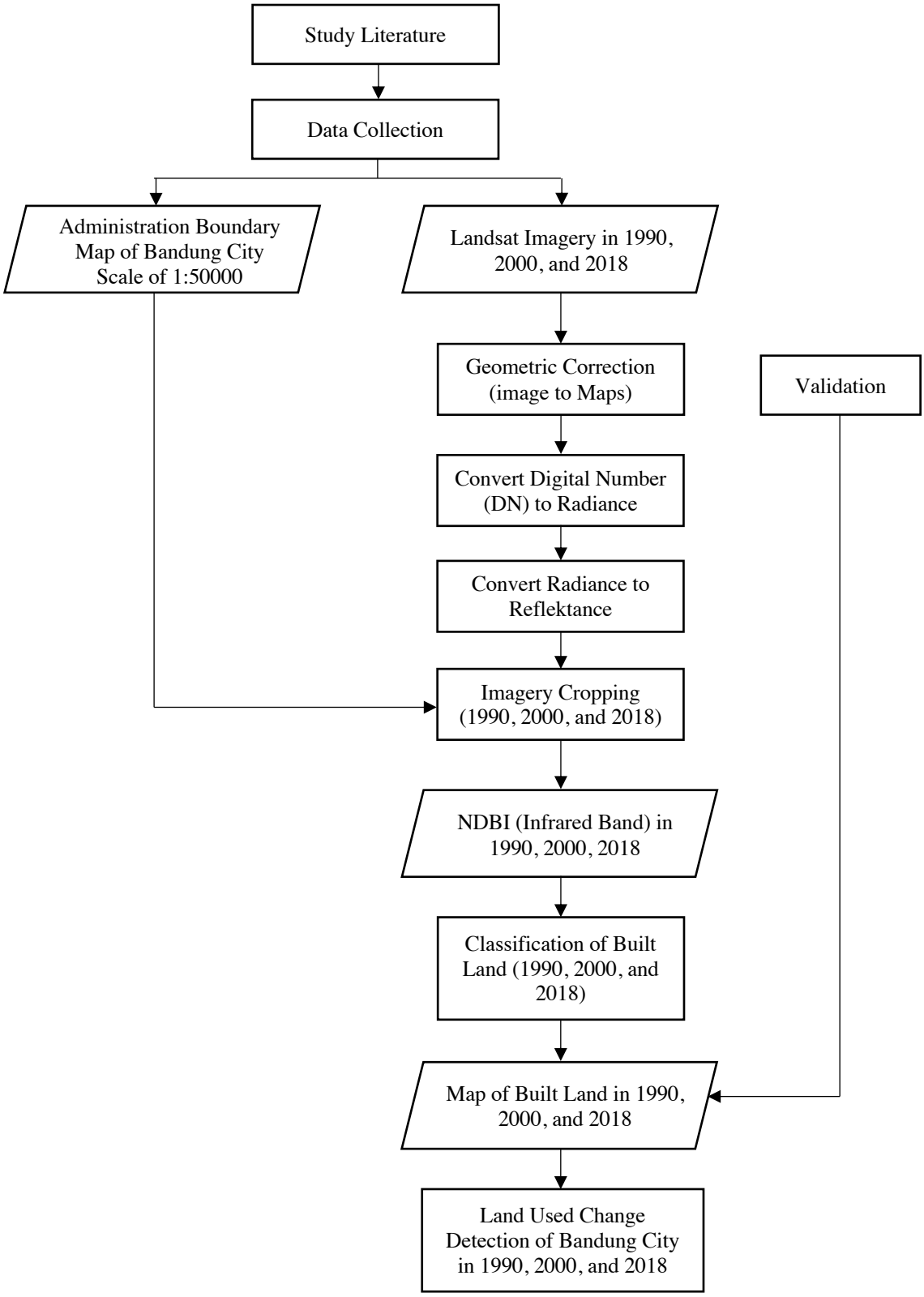

Figure 1. Flowchart Methodology.

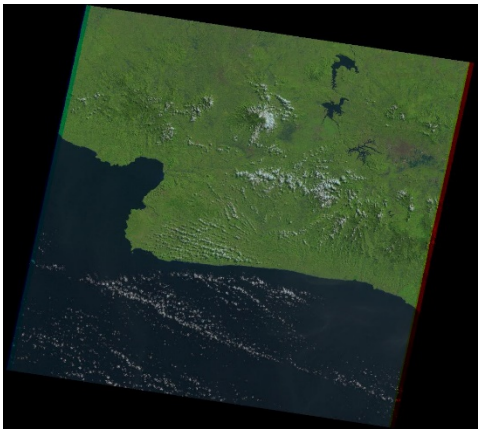

Figure 2. Citra Satellite Landsat 5 in 1990 area of Bandung.

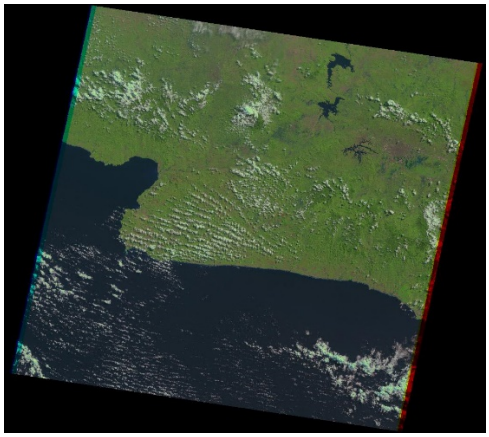

Figure 3. Citra Satellite Landsat 7 in 2000 area of Bandung.

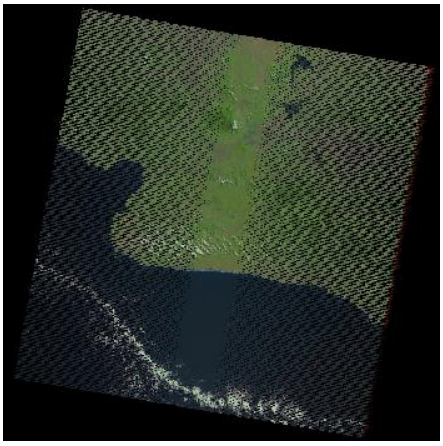

Figure 4. Citra Satellite Landsat 7 in 2018 area of Bandung.

Figure 5. Bandung City Administrative Limits.

2.3. Data Processing

Before the data is used to identify land built-up, preprocessing steps are carried out first which includes geometric correction and radiometric correction which consists of converting the digital number value to radians and then conversion of radians to reflectance values. Next step is cutting the image based on AOI (Area of Interest), then enter the NDBI algorithm, classification NDBI.

2.3.1. Geometric Correction

To eliminate image geometry errors that cause the position of the object in the image does not match the actual position in the field, it is necessary to have geometric correction. Geometric correction will re-place pixel positions in the image according to the actual position. In this study geometric correction was carried out by the image to map method where land cover map became the base / reference for determining GCP points would be corrected geometrically.

2.3.2. Radiometric Correction

Radiometric correction is intended to increase correction values. Correction is needed on the basis of two reasons, namely to improve image quality and at the same time improve pixel values that do not match the reflectance values or actual spectral rays of the object [9]. The radiometric correction process

is first converted from Digital Number to Radical Value, then conversion from radians to reflectance values. This study uses the FLAASH method in the radiometric correction process.

2.3.3. Cropping
Image cutting use administrative boundary of Bandung City is done so that the data processing process is more focused on the observed area so that it can facilitate image analysis.

2.3.4. Normalized Difference Built-up Index (NDBI)
To calculate the concentration of land built-up with satellite images NDBI algorithm is used as in the following formula (1);

$$\text{NDBI} = \frac{b_{mi} - b_{ni}}{b_{mi} + b_{ni}} \quad (1)$$

The parameters used in the algorithm are:
NDBI = *Normalized Difference Built-up Index*
B_{mi} = *Mid-Infrared* for Landsat 5 & 7 (1,550-1,750) µm
B_{ni} = *Near-Infrared* for Landsat 5 & 7 (0,760-0,900) µm

The value of Aerosol thickness was obtained through NASA's official website called AERONET. NDBI spectral range values from -1 to 1 [10], but NDBI range values obtained range from -1 to 0,3 [11] can be seen in Table 3.

Table 3. NDBI Spectral Range Values.

No	Range NDBI	Classification Range NDBI Index
1	-1 – 0	Non-Building
2	0 – 0.1	Low Building Density
3	0.1 – 0.2	Mid Building Density
4	0.2 – 0.3	High Building Density

2.3.5. Building Density
Building density data is categorized into three classes, namely low, medium and high. The building density category is obtained by calculating the building density using the equation Formula (2) [12]:

$$Building\ Density = \frac{Total\ Building}{Area\ (Ha)} \quad (2)$$

Categories of building density data obtained using the Equation formula (2) are classified based on three classes with conditions according [13] can be seen in Table 4.

Table 4. Category Building Density.

No	**Category**	**information**
1	Low Building Density	<32 Unit/Ha
2	Mid Building Density	32-57 Unit/Ha
3	High Building Density	>57 Unit/Ha

2.3.6. Accuracy Test
Confussion matrix table that connects the classification pixels and data whose information can be taken from field data or maps that have been verified or commonly referred to as ground truth. There is some information that can be taken from the confusion matrix including overall accuracy, user accuracy, producer accuracy, tau coefficient, and kappa coefficient. Error matrix [14] can be seen in Table 5.

Table 5. Error Matrix.

Reference Class	Sample Date			Total Pixel	Produsen Accuracy
	A	B	C		
A	X_{11}	X_{12}	X_{13}	X_{1+}	X_{11}/X_{1+}
B	X_{21}	X_{22}	X_{23}	X_{2+}	X_{22}/X_{2+}
C	X_{31}	X_{32}	X_{33}	X_{3+}	X_{33}/X_{3+}
Total Pixel	X_{1+}	X_{2+}	X_{3+}	N	
User Accuracy	X_{11}/X_{1+}	X_{22}/X_{2+}	X_{33}/X_{3+}	X_{ii}	

$$User\ Accuracy = \frac{X11}{X+1}\ x\ 100\% \quad (3)$$

$$Produsen\ Accuracy = \frac{X11}{X1+}\ x\ 100\% \quad (4)$$

$$Overall\ Accuracy = \frac{\sum_{i=1}^{r} Xii}{N}\ x\ 100\% \quad (5)$$

$$Kappa\ Accuracy = [(N \sum_{i=1}^{r} Xii - \sum_{i=1}^{r} X1+X+1) / (N^2 - \sum_{i=1}^{r} X1 + X + 1)]\ x\ 100\% \quad (6)$$

The parameters used in the algorithm are:
N = Total pixel
X_{1+} = Total pixel in line-i
X_{+1} = Total pixel in column-i
Xii = Diagonal value from kontigensi matrix line-i and column-i

3. Results and Discussion

3.1. Normalized Difference Built-up Index (NDBI) in Bandung City

The results obtained from this study were in the form of the change of land built-up use NDBI algoritm in Bandung City in 1990, 2000, 2009, and 2018, respectively shown in Figure 6.
The land built in the city of Bandung in July 1990 was still dominated by purple, namely the non-residential class because in that year there was still little land built but more vegetation, whereas for 2000 the dominating colors were red settlement class very tight because in 2000 the land waking up has increased so that vegetation is reduced, and in 2018 the dominant color is green which is a medium building density class and red is a high building density class while purple is a non-building class experiencing a significant reduction because in 2018 the built land already dominates compared to non-building.

3.2. Built Area NDBI Result

NDBI Classification produces an area for each range that is visualized in various colors. The extent of each range is generated from the data processing in ENVI 5.1 software, the results of the area shows the division of the area in accordance with the provisions of the range sourced from Adeanti, et al. (2018) where each color has a different class according to its category. The calculation of the area of the NDBI classification results is done to see the area in each range according to its category, where information will be obtained about changes in the area in each range. The area for each range in July 1990, 2000 and 2018 can be seen in Table 6.

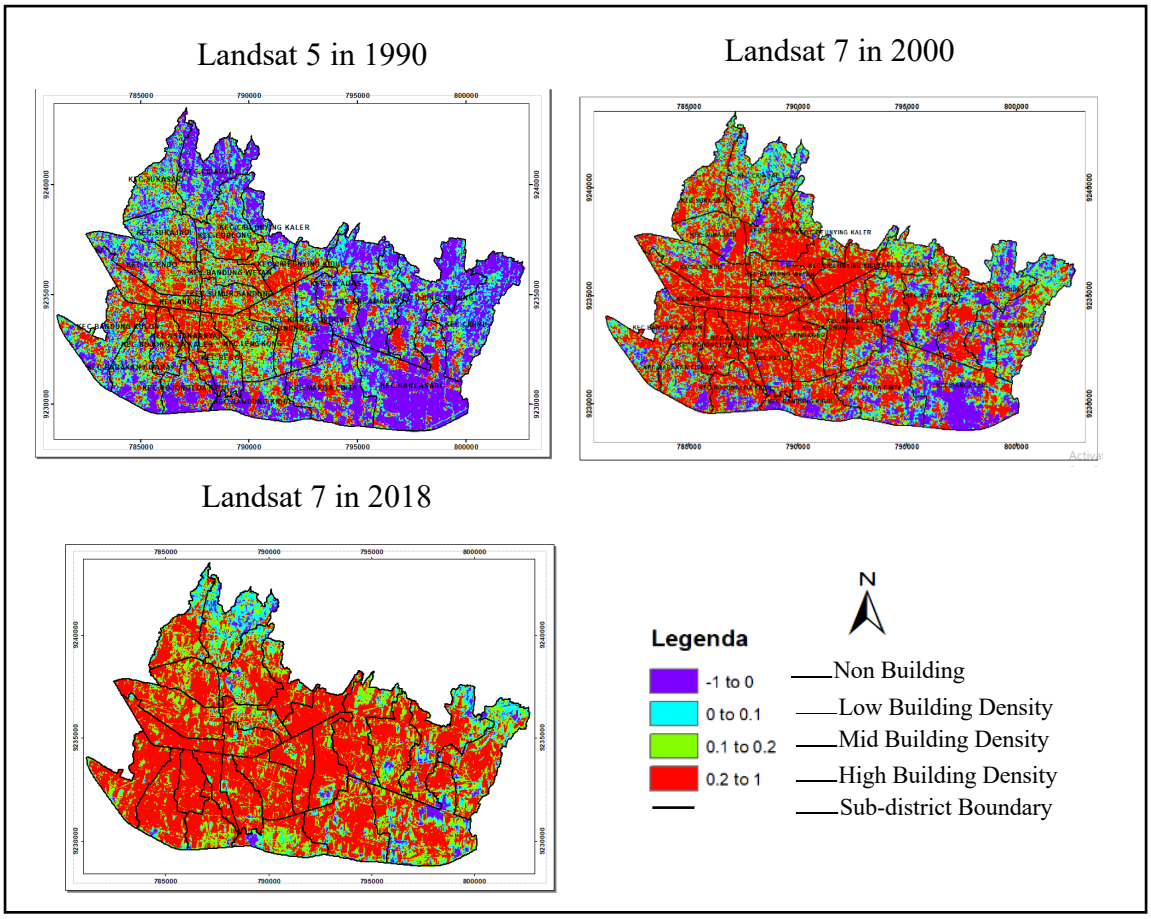

Figure 6. Visualization of NDBI.

Table 6. Area of NDBI in Each Range.

Years	Classification Indeks Value Range	Area (Ha)
1990	-1 - 0	4964.9
	0 – 0.1	5548.1
	0,1 – 0.2	3206.9
	0.2 - 1	3136.1
2000	-1 - 0	2425.4
	0 – 0.1	2361.6
	0.1 – 0.2	3682.4
	0.2 - 1	8385.7
2018	-1 - 0	554.9
	0 – 0.1	1558.8
	0.1 – 0.2	4079.2
	0.2 - 1	10663.2

Based on the calculation of built-up land area using NDBI in Table 6 above, it can be concluded that in 1990, it can be concluded that in 1990 it began to be dominated by the category of low building density with a value of 5548.1 Ha but still has a large non-building class with a value of 4964.9 Ha, medium building density with a value of 3206.9 Ha and high building density with a value of 3136.1 Ha. So that for the year 1990 has started to be dominated by the built land but there are still many non-buildings. For 2000, it was dominated by the category of high building density with a value of 8385.7 Ha, while non-buildings had been greatly reduced from 1990, namely with a value of 2425.4 Ha, low building density with a value of 2361.6 Ha, and medium building density with a value of 3682.4 Ha. So, it can be concluded in 2000 that the category of non-building and low building density decreased significantly, while the density of medium buildings and high-density buildings experienced a significant increase seen from the results of the area which was dominated by the category of high building density and reduced vegetation or non-building.
The year 2018 was dominated by the category of high building density with a value of 10663.2 Ha and the category of medium building density with a value of 4079.2 Ha, while for the low building density with a value of 1558.8 Ha and non-building with a value of 554.9 Ha experienced a reduction. So it can be concluded that the increasing number of years seen from 1990, 2000, until 2018 the category of non-building and low building density has decreased significantly, while the category of medium building density and high building density has increased very rapidly.
This can be seen from the actual conditions on the ground that more land is being built with a large number of industrial estates, shopping centres and other high-rise buildings causing non-building or vegetation to decrease. In addition to seeing changes using the table, a histogram is also made according to the area in each range. The results of changes in the area built by histogram making can be seen in Figure 7.

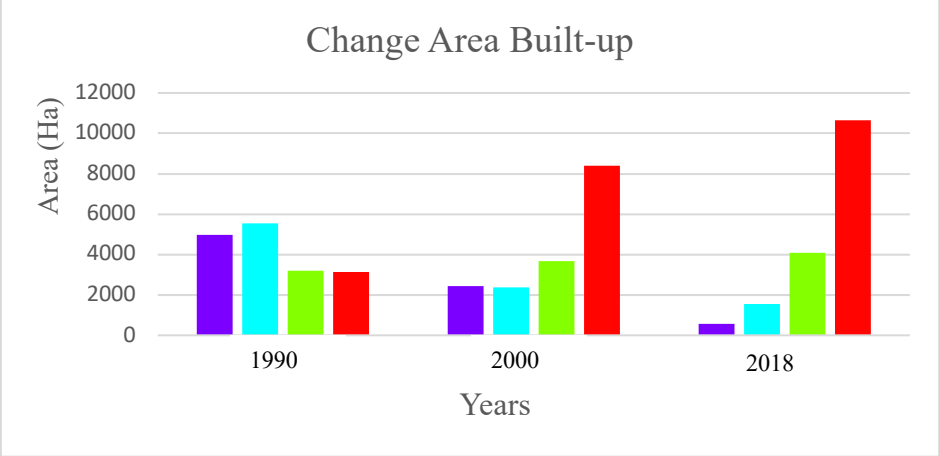

Figure 7. The results of changes in the area built.

In addition to seeing changes in each range, a histogram was nade thae focused only on changes in non-built and built-up land un 1990, 2000, and 2018 can be seen in Figure 8.

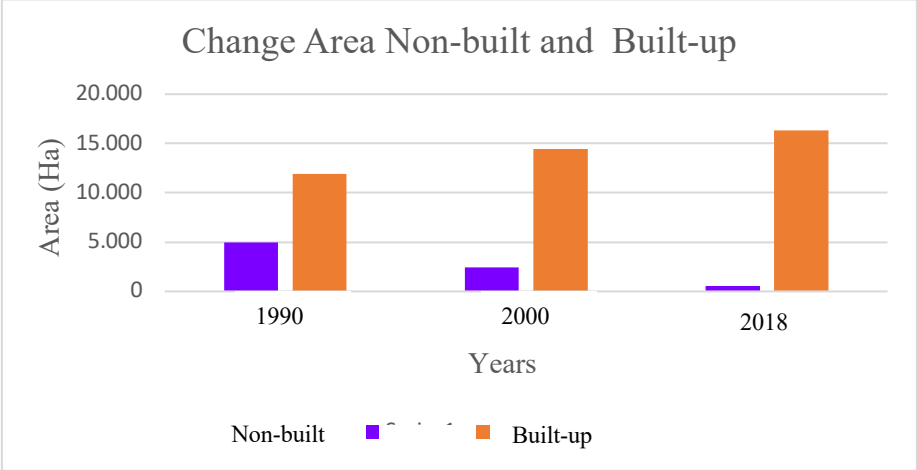

Figure 8. The results of changes in the non-built and built-up

Based on Figure 8, a percentage calculation was made for non-built and built-up land in 1990, 2000, and 2018 can be seen in Table 7.

Table 7. Percentage non-built and built-up.

No	Years	Non-built	Percentage Non-built (%)	Built-up	Percentage Built-up (%)
1	1990	4.965	0.003	11.891	0.007
2	2000	2.425	0.001	14.430	0.009
3	2018	555	0.000	16.301	0.010
Percentage Change (%)			0.157		0.843

3.3. Building Density

Building density is divided into three categories, namely low building density, medium building density, and high building density. Calculation of building density is done using the equation (2), where the data on the number of buildings in each category is obtained from the metadata map of Bandung City land cover while the area value is obtained from the areas of category NDBI in Ha units, data on the number of buildings in each category can be seen in Table 8.

Table 8. Total Building.

No	Category	Building Total (Unit)
1.	Low Building Density	18520
2.	Mid Building Density	176890
3.	High Building Density	659962

- Low building density$=\frac{18520\ (\text{Unit})}{1558.8\ (\text{Ha})}=12$ Unit/Ha
- Mid building density$=\frac{176890\ (\text{Unit})}{4079.2\ (\text{Ha})}=43$ Unit/Ha
- High bulding density$=\frac{659962\ (\text{Unit})}{10663.2\ (\text{Ha})}=62$ Unit/Ha

3.4. Change Detection NDBI

From the results of processing NDBI from Landsat Satellite Images and NDBI from Google Earth, make a table change detection using software ENVI in 1900 and 2018. Change detection result can be seen in the following Table 9.

Table 9. Change Detection NDBI in Pixel During 1990 and 2018.

NDBI 2018 / NDBI 1990	Non-Building	Low Building Density	Mid Building Density	High Building Density
Non-Building	21	234	1302	4609
Low Building Density	254	1224	4707	11135
Mid Building Density	1949	13711	17207	12457
High Building Density	52942	46477	12416	6645
Class Changes	55145	60422	18425	28201
Image Difference	-49000	-44326	9692	83864

Based on Tabel 9, high building density has a dominating value of 83634 pixel, while medium building density has a value of 9692 pixels, low building density has decreased by 44326 pixel, and non-building has decreased significantly which is equal to 49000 pixels. This change shows that the change in land developed in 1990 to 2018 experienced a very rapid increase resulting in a very significant decrease in non-buildings.

3.5. Accuracy Test

Accuracy test is carried out only on Landsat Image 7 in 2018 because 2018 is the latest image data used in processing the NDBI classification, so it can be seen the actual conditions in the field to facilitate the analysis of classification results. Accuracy make shapefile is determined in the form of sample points.

Table 10. Confussion Matrix.

		Data (Google Earth)					
	Reference Class	Non-Building	Low Building Density	Mid Building Density	High Building Density	Total Pixels	Producer Accuracy
Data (Image)	Non-Building	14	0	0	0	14	93.33
	Low Building Density	1	14	0	0	15	93.33
	Mid Building Density	0	1	13	2	16	86.67
	High Building Density	0	0	2	13	15	86.67
	Total Pixels	15	15	15	15	60	
	User Accuracy	100	87.50	81.25	86.67	54	

Overall akurasi = $\frac{54}{60}$ x 100% = 90 %

Kappa Accuracy = $\frac{(60x54)-(900)}{60^2-(900)}$ = 0.8667 x 100% = 86.67% (fulfill tolerance)

4. Conclusions

Based on the results of the research that has been done, it can be concluded that the analysis of change detection using Normalized Difference Built-up Index (NDBI) algoritm based on Bandung City Landsat Satellite Imagery in 1990, 2000, and 2018 is as follows:

- Built land with remote sensing applications is determined using the normalized difference built-up index (NDBI) approach method in 1990, 2000, and 2018, where the use of the method produces four classifications according to the NDBI range of -1 to 0 is non-building, 0 to 0.1 are low building density, 0.1 to 0.2 are mid building density, and 0.2 to 0.3 or 1 are high building density. The results of identification of the built up land were tested for accuracy by using a matrix confusion table to see the categories of objects included in the NDBI classification, where the overall accuracy of 90% and kappa of 86,67%, looking at these results it can be concluded that the identification data has met the tolerance.
- Based on the results of processing using the normalized difference built-up index (NDBI) approach, the developed land in 1900, 2000, and 2018 experienced a significant increase in built-up land, causing non-built to decrease. The constructed land can be seen based on the category of building density, where the building density is divided into three namely low building density, medium building density, and high building density. Significant changes to built up land can be seen in the actual conditions on the ground in 2018, many shopping centers, industrial estates and other high-rise buildings have been built, causing non-buildings or vegetation to experience rapid decline.

5. References

[1] A, P. *Kondisi Gegorafi Kota Bandung*. 2017 [cited 2019 March 12]; Available from: https://www.geografi.org/2017/12/kondisi-geografi-kota-bandung.html.

[2] Umum, G., *Gambaran Umum Kota Bandung*. 2013.

[3] Sasky, P., S. Sobirin, and A. Wibowo. *Pengaruh Perubahan Penggunaan Tanah Terhadap Suhu Permukaan Daratan Metropolitan Bandung Raya Tahun 2000–2016*. in *Prosiding Industrial Research Workshop and National Seminar*. 2017.

[4] Handayani, M.N., B. Sasmito, and A.P. Wijaya, *Analisis Hubungan antara Perubahan Suhu dengan Indeks Kawasan Terbangun Menggunakan Citra Landsat (Studi Kasus: Kota Surakarta)*. Jurnal Geodesi Undip, 2017. **6**(4): p. 208-2018.

[5] Fariz, T.R., *OBIA CLASSIFICATION AND BUILT-UP LAND INDICES NDBI FOR ESTIMASTION OF SETTLEMENT DENSITY IN PONTIANAK CITY.* Jurnal Geografi: Media Informasi Pengembangan dan Profesi Kegeografian, 2018. **14**(2): p. 36-44.

[6] Hidayati, I.N., S. Suharyadi, and P. Danoedoro, *Pemetaan Lahan Terbangun Perkotaan Menggunakan Pendekatan NDBI dan Segmentasi Semi-Automatik.* 2017.

[7] Hidayati, I.N., R. Suharyadi, and P. Danoedoro, *Kombinasi Indeks Citra untuk Analisis Lahan Terbangun dan Vegetasi Perkotaan.* Majalah Geografi Indonesia, 2018. **32**(1): p. 24-32.

[8] Li, H., et al., *Interaction between urban heat island and urban pollution island during summer in Berlin.* Science of The Total Environment, 2018. **636**: p. 818-828.

[9] Danoedoro, P., *Pengantar penginderaan jauh digital.* Yogyakarta: Andi, 2012.

[10] Zhang, Y., I.O. Odeh, and C. Han, *Bi-temporal characterization of land surface temperature in relation to impervious surface area, NDVI and NDBI, using a sub-pixel image analysis.* International Journal of Applied Earth Observation and Geoinformation, 2009. **11**(4): p. 256-264.

[11] Adeanti, M. and M.C. Harist. *ANALISIS SPASIAL KERAPATAN BANGUNAN DAN PENGARUHNYA TERHADAP SUHU Studi Kasus di Kabupaten Bogor*. in *Seminar Nasional Geomatika*. 2019.
[12] Poli, T.P.A., P.P. Egam, and S. Tilaar, *SEBARAN LOKASI PERMUKIMAN KUMUH DI KOTA MANADO.* SPASIAL, 2015. **2**(3): p. 102-111.
[13] Sujatmiko, R., *Kejadian Kebakaran Permukiman Kota Bekasi Tahun 2010.* Universitas Indonesia. , (2012).
[14] Jaya, I., *Analisis Citra Digital: Perspektif Penginderaan Jauh untuk Pengelolaan Sumber Daya Alam. Teori dan Praktek Menggunakan Erdas Imagine*. 2007, Bogor: Fakultas Kehutanan IPB.

Correlation Analysis of PM2.5 Air Pollution with NDVI (Normalized Difference Vegetation Index) Based on Landsat-8 (Case Study: Bandung City, West Java)

Anis Septi Pratiwi[1]*, Rika Hernawati[1], Soni Darmawan[1]

[1]Geodesy Engineering, Institut Teknologi Nasional, 23 PH.H. Mustofa Street, 40124 Bandung, Indonesia

*Corresponding author's e-mail: anisseptipratiwi@gmail.com

Abstract. Air pollution in the city of Bandung is a major problem that causes a decrease in air quality and can endanger health and the environment. Air quality has been declining continuously over the past few years, as a result of a surge in the number of motorized vehicles and human activities (BPLHD, 2015). The main source in reducing air pollution is PM2.5. PM2.5 (Particulate Matter 2.5) is a particle that is less than 2.5 μm in size and particles that are very dangerous in air quality. This study aims to determine the distribution of PM2.5 with NDVI correlation. PM2.5 monitoring can be done using Landsat Satellite Imagery with several parameters namely AOT, NDVI, LST, and TVDI. The results of this study indicate that the city of Bandung has not exceeded the threshold value issued by PP No. 41/1999 which is 65 μgram / m^3, the results of processing obtained a maximum value of 24.6 μgram / m^3. These results are regressed resulting in, the higher the pollution the lower the vegetation density index. The result showed that the vegetation index has been improved to a medium quality of pollutant.

Keywords: Landsat, NDVI, LST, TVDI dan PM2.5.

1. Introduction

Air pollution in the city of Bandung is a major problem that causes a decline in air quality and can harm health and the environment. Air quality has experienced a continuous decline over the last few years, in 2013 Bandung City ranked one as the city with the lowest pollutants and in 2014 there was a decline to be ranked sixth, it resulted from the surge in the number of motor vehicles and human activity [1]. The main sources in the decline in air pollution are (CO_2, NO_2, and PM 2.5).

Pollutants can be measured and monitored using satellite technology and remote sensing is a new way of monitoring air quality with wide coverage. Compared to land-based measurements, remote sensing has large spatial coverage and can provide an effective way to monitor air quality at large and periodic scale. One of the remote sensing products that support this research is imagery of Landsat satellite.

PM 2.5 (Particulate Matter 2.5) is a particle measuring less than 2.5 μm and a very dangerous particle in air quality PM2.5 also known as fine particles. PM 2.5 derived from soil abrasion, street dust (dust from tires or brake shoes). PM 2.5 is very influential in human health such as asthma, bronchitis outside respiratory diseases, such as diseases: alzaheimer, cardiac, diabetes and cancer. The impact of PM2.5 goes beyond human health. A recent study found evidence that high levels of PM2.5 in the atmosphere can block out sunlight, reducing the rate of photosynthesis, and therefore growth, in crops [2].

Based on the research conducted by [3], the study used image Landsat 8 to estimate the concentration of PM2.5 on the ground surface using 3 parameters (Aerosol Optical Thickness (AOT), Land Surface Temperature (LST), Temperature Vegetation Dryness Index (TVDI)). In this research will be different from the research of Chen dkk where this study of AOT used is obtained from NASA site namely AERONET and this research will be correlated with vegetation density index, so the result of this research is the concentration of PM 2.5 was correlated with the vegetation density index in the city of Bandung in 2019.

2. Methodology

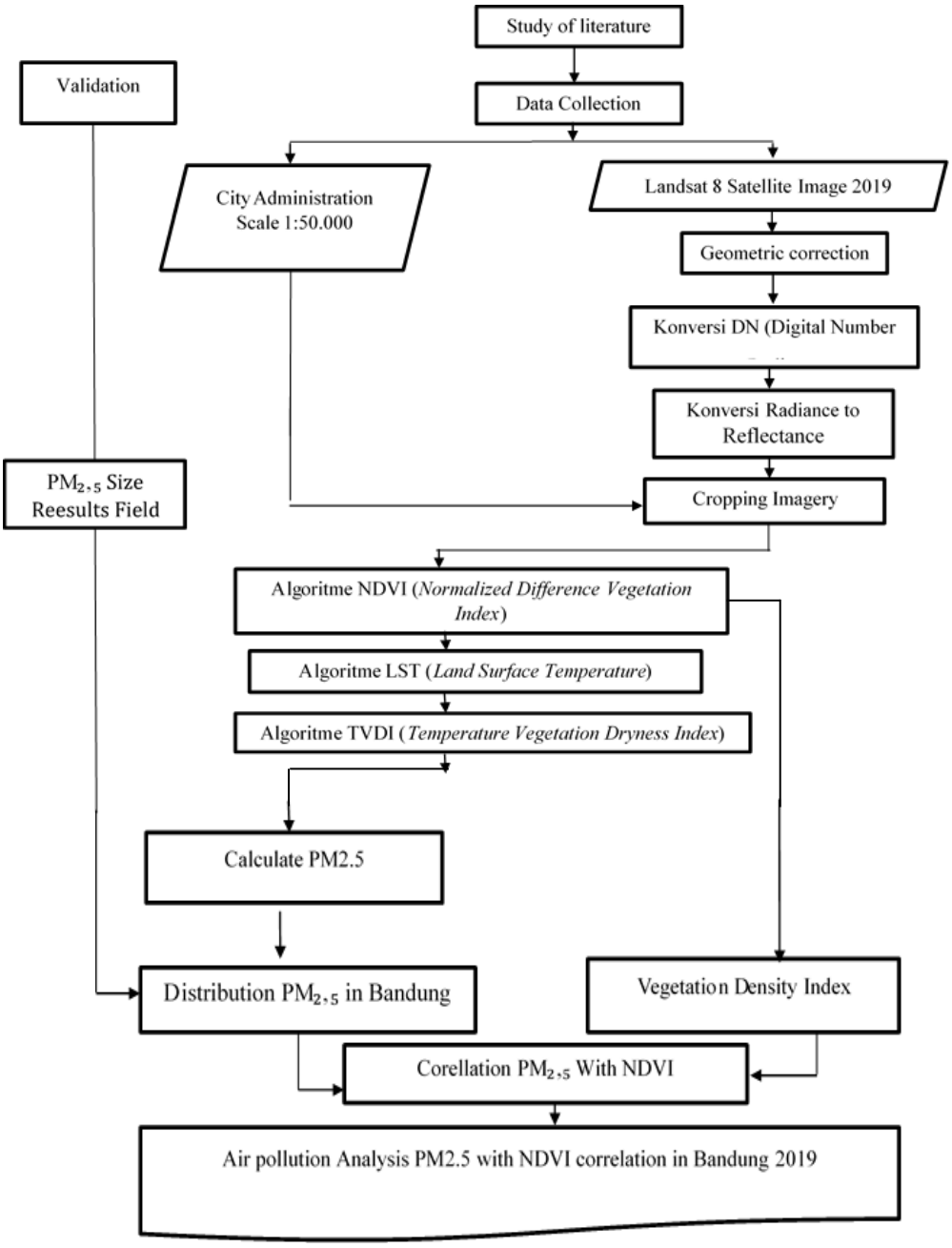

Figure 1. Methodology.

2.1. Method

Data processing of PM 2.5 air pollution and vegatation density index, performs geometric correction, conversion of digital number to radiance, from Radiance to Reflectance, then performs the processing of PM 2.5 and the vegetation density index.

2.2. Research Data and Location

Table 1. Data used.

Data	Information	Source
Landsat Satellite 8 Image	22 Mei 2019	www.earthexplorer.usgs.gov
City Administration in Bandung	Scale 1: 50000	www.tanahair.indonesia.go.d
AERONET	CSV format	www.aeronet.gsfc.nasa.gov

The location of this research took on the area of Bandung, West Java province with an area of 16,729.65 Ha. The research site is an area that belongs to one city with a crowded population and activities.

Figure 2. Location.

2.3. Geometric Corretction

This geometric correction is done for the overall image used in the study. Geometric correction is done using 14 GCP with image to image method, Citra Landsat 8 used as base and image to be corrected as GCP point warp should be spread evenly throughout the image that is placed at the edges of imagery, beach side and large rivers. The overall RMSE value of GCP for each image used, must follow the true rule of less than 0.5 pixels.

2.4. Radiometric Correction

The radiometric correction of an image is performed so that the spectral radiating values of the represented objects have a value that corresponds to that object's spectral character. The initial stage before making corrections to these atmospheric effects is to first convert the digital number into spectral radiancy and reflectance to obtain physical parameters that form the magnitude of solar energy reflected by Objects on the Earth's surface. Radiometric correction using the FLAASH method.

2.5. Data Processing

To get the estimation of PM2.5 this research refers to [3] which is the algorithm using NDVI, LST and TVDI parameter, formula PM2.5:

$$PM2.5 = e^{box} (\boldsymbol{AOT})^{bAOT} \times \boldsymbol{TVDI}^{bTVDI} \times (\boldsymbol{LST})^{bLST} \quad (1)$$

AOT Data are retrieved from situs NASA AERONET, LST is land surface temperature (LST) retrieved from the thermal infrared band data (band10) of the Landsat 8 data using Image-based Method. β0,

βAOT, βTVDI and βLST are regression coefficients for AOT, LST, TVDI and other factors, respectively. Before calculating PM2,5, first compute NVDI, LST and TVDI.

2.6. Calculation of Normalized Difference Vegetation Index

Normalized Difference Vegetation Index (NDVI) Algorithm At this stage data processing is carried out using the Normalized Difference Vegetation Index (NDVI) method to produce a vegetation index. (Carlson Td., 1997).

$$NDVI = \frac{(NIR-Red)}{(NIR+Red)} \quad (2)$$

Where, NIR and Red are the DN value of band NIR and band Red, respectively. To NDVI, the larger the value, the higher the vegetation coverage is, while the smaller the value, the closer the bare soil. In order to improve the accuracy of NDVI.

Table 2. NDVI Classifications.

NDVI	Classification Class
-1.0 - 0.11	No Vegetation
0.11 - 0.25	Very Low Vegetation
0.25 - 0.33	Low Vegetation
0.33 - 0.45	Medium Vegetation
0.45 - 1	High Vegetation

The NDVI value between vegetation and bare soil indicates that the pixel consists of a certain percentage of vegetation and a certain percentage of bare soil. So, we determined the vegetation coverage of every pixel in the image with the following formula [3]:

$$Pv = [(\text{NDVI-NDVIs})/(\text{NDVIv-NDVIs})]^2 \quad (3)$$

Where:
Pv = Proportion of Vegetation
NDVI = DN values from NDVI Image
NDVI min = Minimum DN values from NDVI Image
NDVI max = Maximum DN values from NDVI Image

In this study, ε of water surface pixels is 0.995, ε of town and natural surface can be calculated with the following formula:

$$\varepsilon = 0.985Pv + 0.960\,(1-Pv) + 0.06Pv\,(1-Pv) \quad (4)$$

Where:
ε = Land Surface Emissivity
P_V = Proportion of Vegetation

2.7. Land Surface Temperature

Where, ε surface is the land surface emissivity of natural surface, and ε town is the land surface emissivity of town surface. In this study, band10 on Landsat 8 to retrieve the brightness temperature of the land surface, and then calculated the land surface temperature using ε. The land surface brightness temperature can be calculated with the following formula:

$$Tb = \frac{K_2}{In(+\frac{K_1}{L\lambda}+1)} \quad (5)$$

Tb = Brigthness Temperatur satelit (ºC)
K_1 = Band calibration constant 10 (Landsat 8)
K_2 = Band calibration constant 10 (Landsat 8)
Lλ = Radiance spectral TOA (watts/m^2 Srad μm)
Finally, land surface temperature (Ts) was calculated as:

$$Ts = \frac{Tb}{1+(\frac{\lambda Tb}{\delta})ln\varepsilon} \quad (6)$$

Ts = Land Surface Temperature (ºC)
Tb = Temperatur Brightness (ºC)
λ = Mid-wavelength value band 10
δ = hc/σ= 1.438 x 10^{-2} mK
h = Konstanta Planck (6.26 x 10^{-34} Jsec)
c = Speed of light (2.998 x 108 m s-1)
σ = Konstanta Stefan-Boltzman (1.38 x 10^{-23} J K-1)
ε = Emisivitas objek

2.8. TVDI (Temperature/Vegetation Condition Index)
A simplified water stress index called the TVDI, based on an empirical interpretation of the NDVI–Ts space, was suggested by [4]. The TVDI is related to the soil moisture status so that high values indicate dry conditions and low values indicate moist conditions. The TVDI is a no-moisture index, reaching values of 1 at the dry edge (water limited condition) and 0 at the wet edge (adequate water availability). Based on remotely sensed observations, the TVDI can be formulated as:

$$TVDI = \frac{Ts-Tsmin}{(a+b \times NDVI-Tsmin)} \quad (7)$$

Ts = Land Surface Temperature
Tsmin = Land Surface Temperature minimum
Tsmax = Land Surface Temperature maximum (a + b × NDVI)

3. Results and Discussion

3.1. PM2.5 (Particulate Matter) in Bandung City basic on Landsat 8
The result of this study is the distribution of PM 2.5 in the city of Bandung in the year 2019, respectively, shown in Figure 3.

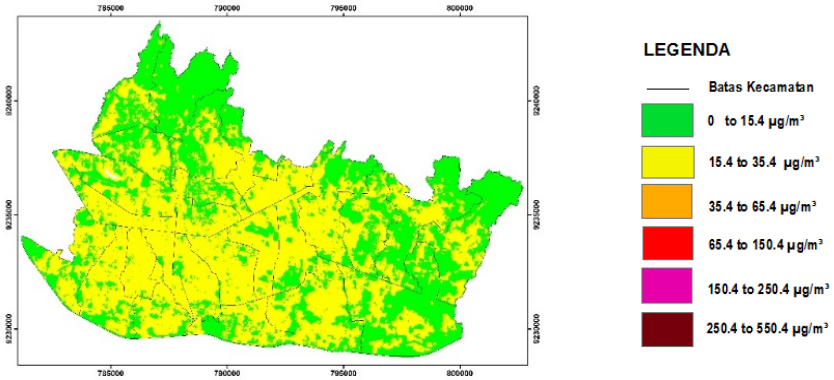

Figure 3. PM2.5 in 2019.

Based on Figure 3 it can be seen that the concentration of PM 2.5 in the year 2019 there is a difference annually. PM 2.5 in Bandung city is still in good quality with the concentration obtained by 24.6 µg/m^3 which means the value is still under the threshold of government regulation of the Republic of Indonesia No 41 year 1999 IE 65 µg/m^3. In the year 2019 medium air quality is on the area of 9902.07 Ha and good air quality is the area 6925.41 Ha. Medium air quality, more than good air quality.

3.2. *Vegetation Density Index Bandung 2019*

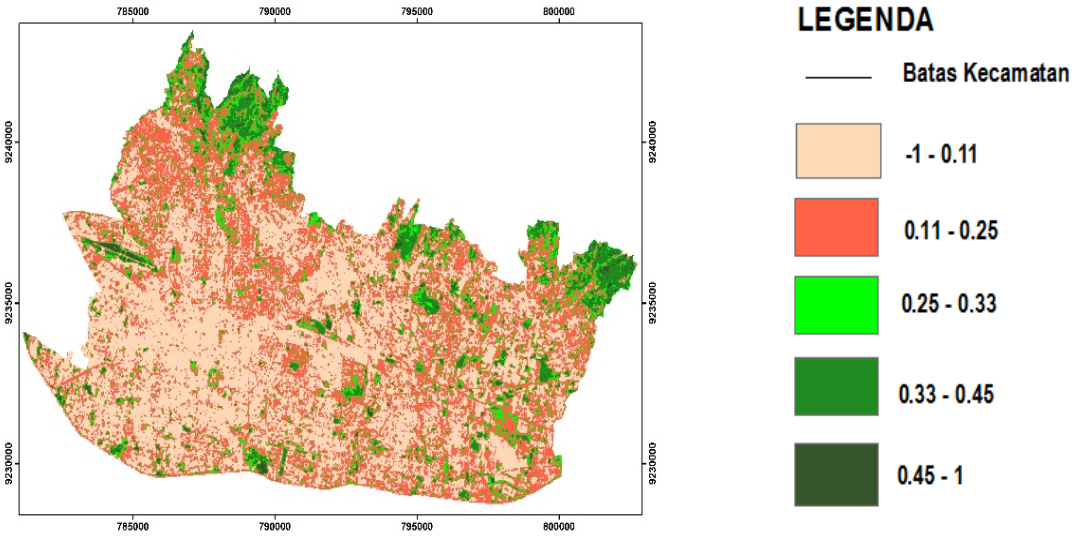

Figure 4. Index Vegetation 2019.

Based on the results of NDVI processing in year 2019 can be seen tendency to decline vegetation annually. In Figure 3 can be seen that the class spread of non-vegetation year 2019 more annually and high vegetation class has been very little, this is due to change of land function that occurred in the year 2008 where most of city land Bandung (55.5%) Used as residential land.

3.3. Correlation of PM2.5 NDVI from Landsat Satellite Image Processing

From the results of the processing of NDVI and PM 2.5 with LANDSAT satellite imagery carried out linear regression to see the relationship between the two variables using multiple samples. The following results in a linear regression of PM 2.5 with NDVI can be seen in Figure 5.

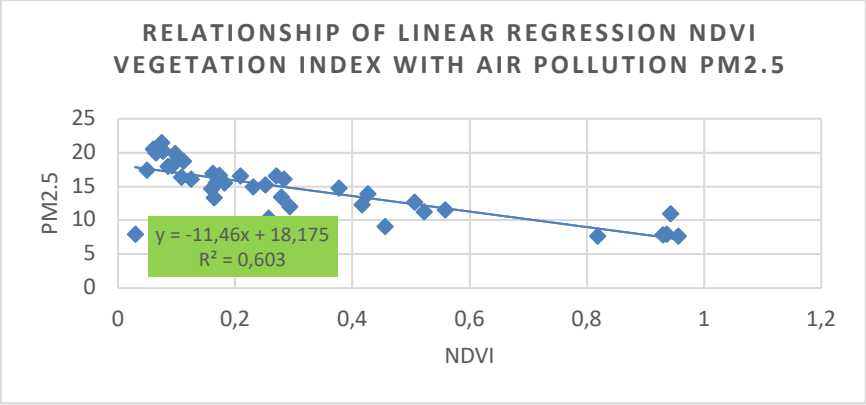

Figure 5. Relationship of Linear Regression NDVI Vegetation Index with Air Pollution PM2.5.

Table 3. Correlation Coefficient Value.

Number	Nilai Koefisien Korelasi	Information
1	0.90 < R < 1.00 atau -1.00 < R< -0.90	Verry Strong
2	0.70 < R < 0.90 atau -0.90 < R < -0.70	Strong
3	0.50 < R < 0.70 atau -0.50 < R < -0.70	Moderate
4	0.30 < R < 0.50 atau -0.30 < R < -0.50	Weak
5	0.0 < R < 0.30 atau -0.30 < R < 0.0	Very weak

The relationship between vegetation density index and PM 2.5 s strong with a value of R: 0.7765. The value of the koefesien regression of the five imagery is negative or inversely proportional which means that the higher density of vegetation then PM 2.5 will be lower.

4. Conclusions

Air pollution PM 2.5 in Bandung City in the year 2019 is still in good condition and temperate. Air pollution of PM 2.5 is still below the threshold determined by NAB which is 65 μg/m^3. In 24.63 μg/m^3 with an average value of 15,708 μg/m^3. Vegetation density index results from NDVI there are 5 classes among others i.e. non vegetation, very low vegetation, low vegetation, temperate vegetation and high vegetation. Judging by the spread of Bandung city that underwent the change of vegetation 2019, almost all of Bandung has undergone a change in the green level. Year 2019 high vegetation area of 124.56, the area that is still temperate and high vegetation is in the district Cidadap and Cibiru Sub-district of Bandung and the non-vegetation region is the center of Bandung and Based on a linear regression coefficient between NDVI and PM 2.5 in 2019 using a LANDSAT image coefficient that produces negative value means the higher the vegetation density index then the air pollution of PM 2.5 is getting smaller. Conversely if the vegetation density index is low then PM 2.5 is getting higher.

5. References

[1] Badan Pengelolaan Lingkungan Hidup Daerah., B.P.L.H.D. *Kondisi Udara di Kota Bandung* 2015; Available from: https://jabarprov.go.id/index.php/pages/id/1321

[2] Helthcare, G. *The impact of PM2.5 beyond respiratory health* 2019; Available from: https://www.gelifesciences.com/en/us/solutions/lab-filtration/knowledge-center/pm2-5-beyond-respiratory-health.

[3] Chen, Y., et al. *Estimating ground-level PM2. 5 concentration using Landsat 8 in Chengdu, China*. in *Remote Sensing of the Atmosphere, Clouds, and Precipitation V*. 2014. International Society for Optics and Photonics.

[4] Carlson, T.N. and D.A. Ripley, *On the relation between NDVI, fractional vegetation cover, and leaf area index*. Remote sensing of Environment, 1997. **62**(3): p. 241-252.

The Analysis of Correlation Between Pm10 Air Pollution Parameter with The Number of Motored Vehicles Using Landsat Satellite Imagery in Bandung City

Anisa Maulidina[1]*, Rika Hernawati[1], Soni Darmawan[1]

[1]Geodesy Engineering, Institut Teknologi Nasional, 23 PH.H. Mustofa Street, 40124 Bandung, Indonesia

*Corresponding author's e-mail: anisamaulidina07@gmail.com

Abstract. Bandung is the capital of West Java Province with high population density and rapid development progress that cause the rise of motorized vehicles related to the number of emissions as the cause of air pollution. One of the parameters that cause air pollution is Particulate Matter (PM10). This study aims to determine the distribution of PM10 in Bandung and the correlation between the number of motorized vehicles. The monitoring of PM10 can be carried out by remote sensing technology using Landsat Imagery and the coeficient of Aerosol Optical Thickness (AOT) parameters using AERONET and bands reflectance. The Result showed that PM10 concentration in Bandung is categorized healthy with PM10 rage of 0-50 micrograms. Based on the correlation between PM10 level and the number of motored vehicles in Bandung was indicates a strong correlation. It means that if the value of motorized vehicles is increase than the PM10 concentration is going to increase.

Keywords: Landsat, AERONET, Particulate Matter 10, Motorized Vehicles.

1. Introduction

Bandung is the capital of West Java Province with the dense population. The population density is also followed by very rapid development progress which encourages the increase in industrial development, economy, and the number of vehicles related to the number of emissions as the cause of air pollution.

Air quality is monitored based on 5 parameter indicators, one of which is *Particulate Matter* (PM10). *Particulate Matter* (PM10) is a parameter to state the amount of dust in the air [1]. Particulate Matter (PM10) is an airborne particle with its size less than 10 microns (micrometers). The Threshold Limit Value (TLV) is the limit value of air pollution allowed in ambient air. NAB PM10 = 150 µgram / m^3 [2].

According to the Regional Environmental Management Agency, one of the PM10 sources that are scattered in the atmosphere comes from fumes of incomplete combustion processes of motorized vehicles. Motorized vehicles add to the level of PM10 by exhaust emissions, brake and tire abrasion, road wear and resuspension of road dust and soil [3]. High PM10 levels are particularly found in urban areas with heavy traffic and dense population. It causes the number of exposed people is high, which worsens the health impact of PM10 emissions. The Monitoring of air pollution to determine PM10 value is conducted by observation stations which are only available in certain locations. The observation station in Bandung is only found in Dago. To be able to monitor almost the entire area of Bandung, the monitoring is carried out using remote sensing technology.

This study refers to the numerous researches on the identification of PM10 air pollution using Landsat-8 Imagery which was previously examined by [4] with the title *Estimation of PM10 From AOT of Satellite Landsat-8 Image Over Hanoi City*. The study used the AOT (Aerosol Optical Thickness) parameter which then obtained the result of PM10 air pollution estimation from Landsat-8 Imagery.

Referring to the research conducted by [4], this study identifies PM10 air pollutant using Landsat-8 Imagery with AOT (Aerosol of Thickness) parameter from AERONET and correlated to the number of

vehicles in Bandung. The AERONET (Aerosol Robotic Network) project is a federation of ground-based remote sensing aerosol networks established by NASA (https://aeronet.gsfc.nasa.gov/). This research showed the PM10 distribution in Bandung in 2000, 2004, 2009, 2014 and 2019 and analyzes the correlation between PM10 and the number of vehicles in Bandung in 1999, 2004, 2009, 2014 and 2019. This study plays an important role in monitoring the condition of air pollution, especially the PM10 parameter in Bandung to anticipate the impact of air pollution in the form of Acute Respiratory Infections.

2. Methodology

2.1. Method

The methodology is the research flow started from determining Bandung, West Java, as the location, collecting the data of vehicles from Bandung Samsat government agencies, collecting Landsat imagery data downloaded through the USGS website, preprocessing Landsat Imagery data which includes the geometric and radiometric correction. Then, Landsat Imagery data are ready to identify the Particulate Matter 10 (PM10) concentrations in Bandung. This study uses a PM10 algorithm with AOT parameter and reflectance values for a blue band, red band, and green band in Landsat imagery. To clarify the stages of this study, a flow chart of the study process is shown in Figure 1.

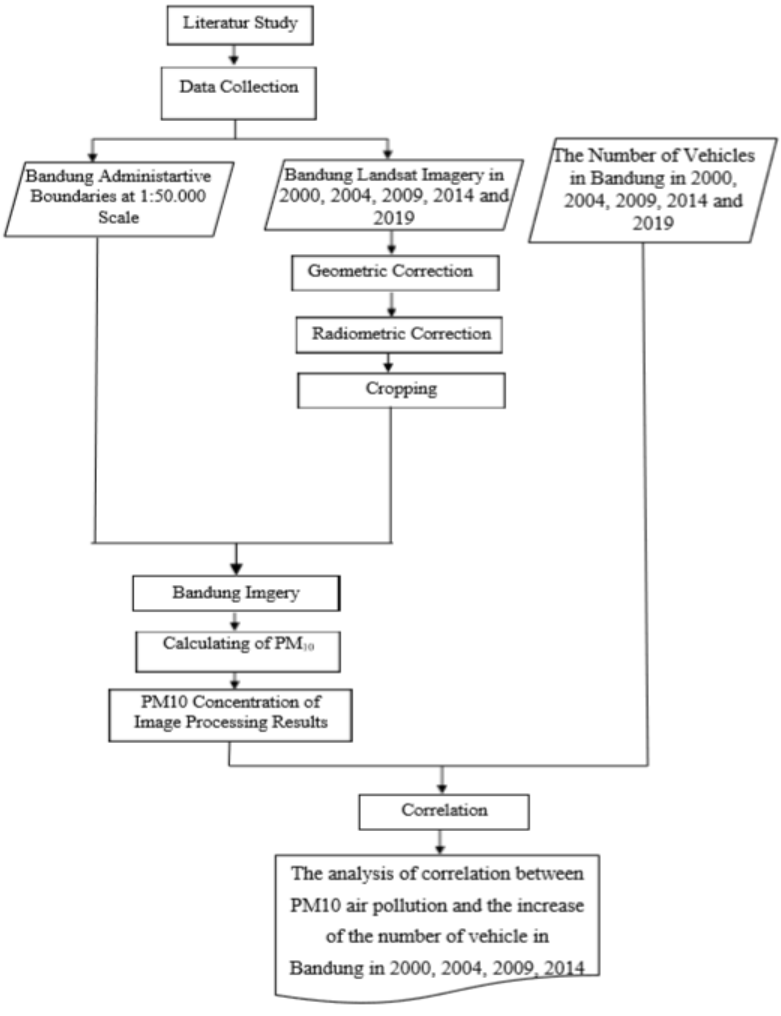

Figure 1. Research Flow Chart.

2.2. Data and Location of Research
The data used in this study are:

Table 1. Data

Data
Satellite Imagery Landsat-5 in 2000
Satellite Imagery Landsat-7 in 2004 and 2009
Satellite ImageryLandsat-8 in 2014 and 2019
Bandung Administrative Boundaries at 1:50000 scale
District administrative boundaries at 1:50000 scale
Number of Motorized Vehicles in 2000, 2004, 2009, 2014 and 2019

The study is conducted in Bandung, geographic coordinates: 107° 36' E and 6° 55' S with an area of 167.7 km^2. Administratively, Bandung is bordered by several regencies/cities, the north is bordered by Bandung Regency and West Bandung Regency, the west is bordered by West Bandung Regency and Cimahi, the east is bordered by Bandung regency and the south is bordered by Bandung Regency.

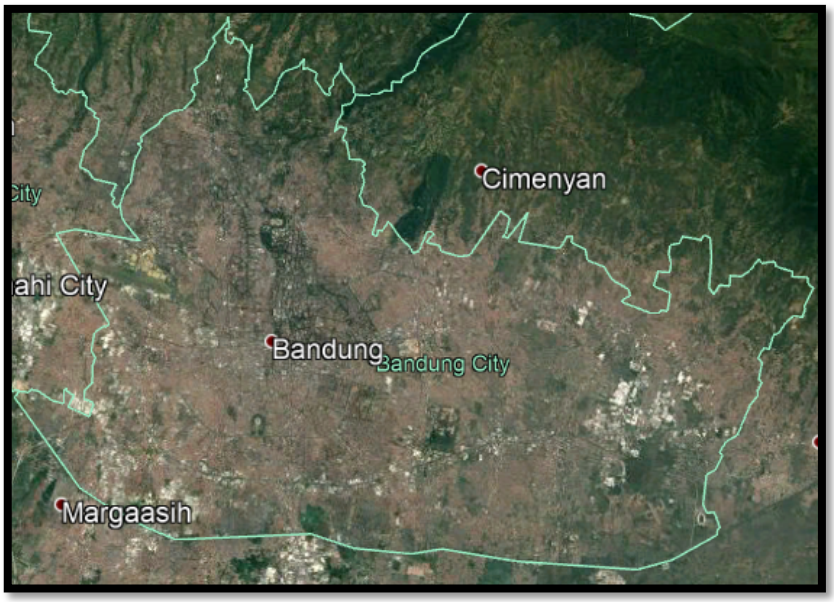

Figure 2. Study Location.

2.3. Data Processing
Before the data are used to calculate PM_{10} concentrations, the preprocessing steps are carried out. It includes geometric and radiometric correction consisting of converting the digital number value to radians and then converting the radians to reflectance values. The next steps are cropping the image based on AOI (Area of Interest), then entering the PM_{10} algorithm with AOT (Aerosol Optical Thickness) parameter which then shows the distribution value of one of the air pollution parameters, Particulate Matter (PM_{10}).

2.3.1. Geometric Correction. To remove geometric distortion that causes a mismatch between object imagery position and object actual position, it is necessary to have a geometric correction. It establishes the pixel position of imagery to the actual position. In this study, geometric correction is carried out by

the image to image method where Landsat-8 become the base/reference to determine GCP on Landsat which will be corrected geometrically.

2.3.2. Radiometric Correction. Radiometric correction was undertaken to correct the pixel values so those can match the actual values, considering atmospheric disturbance factor as the primary source of error. The Atmospheric effect causes the value of object reflection on the surface of the earth recorded by the sensor is not the original value, but it becomes larger due to the scattering or smaller due to absorption process [5]. The radiometric correction process is first converting Digital Number to Radians, then converting radians to reflectance values. This study using FLAASH method in the radiometric correction process.

2.3.3. PM_{10} algorithm. To calculate PM10 concentration with satellite imagery, PM10 algorithm is used as in the following formula [6].

$$PM10 = ax\, R\lambda 1 + ajR\, \lambda 2 + a2R\, \lambda 3 \quad (1)$$

The parameters used in the algorithm are:
ax = Aerosol Optical Thickness value (AOT)
Rλ1 = Band reflectance value used
The value of Aerosol thickness was obtained from NASA's official website, AERONET. The reflectance values used are the reflectance values of the red, green, and blue (RGB) bands.

3. Results and Discussion

3.1. PM10 (Particulate Matter) in Bandung City
The result of this study shows the distribution of PM_{10} in Bandung in 2000, 2004, 2009, 2014, and 2019, respectively, shown in Figure 2.
The Classes of air quality level based on the range of values referring to the Pollutant Standard Index are classified to different colours. The health Class is visualized in green colour, the moderate class is visualized in blue, the unhealthy class is visualized in yellow, very healthy class is visualized in red, and hazardous class is visualized in black. Based on the result of PM10 management, there is a difference in PM10 distribution. As shown in Figure 3, the dominant PM10 distribution is classified as a healthy class with PM10 range of 0-50 µg/m³ visualized in green. However, it also shows that the distribution of moderate class in blue with PM10 range of 51-100 µg/m³ significantly increases from 2000 to 2019.

3.2. *Linear Regression Analysis between PM10 and The Number of Motored Vehicles*
One of the biggest sources of PM10 comes from the exhaust gas produced by motorized vehicles. Based on motor vehicle data obtained from various agencies, the number of vehicles in the city of Bandung has increased every year. The number of motorized vehicles in the city of Bandung can be seen in Table 2.

Table 2. Number of motorized vehicles.

Time	Number of motorized vehicles
2000	463627
2004	654979
2009	1452504
2014	2857215
2019	3033511

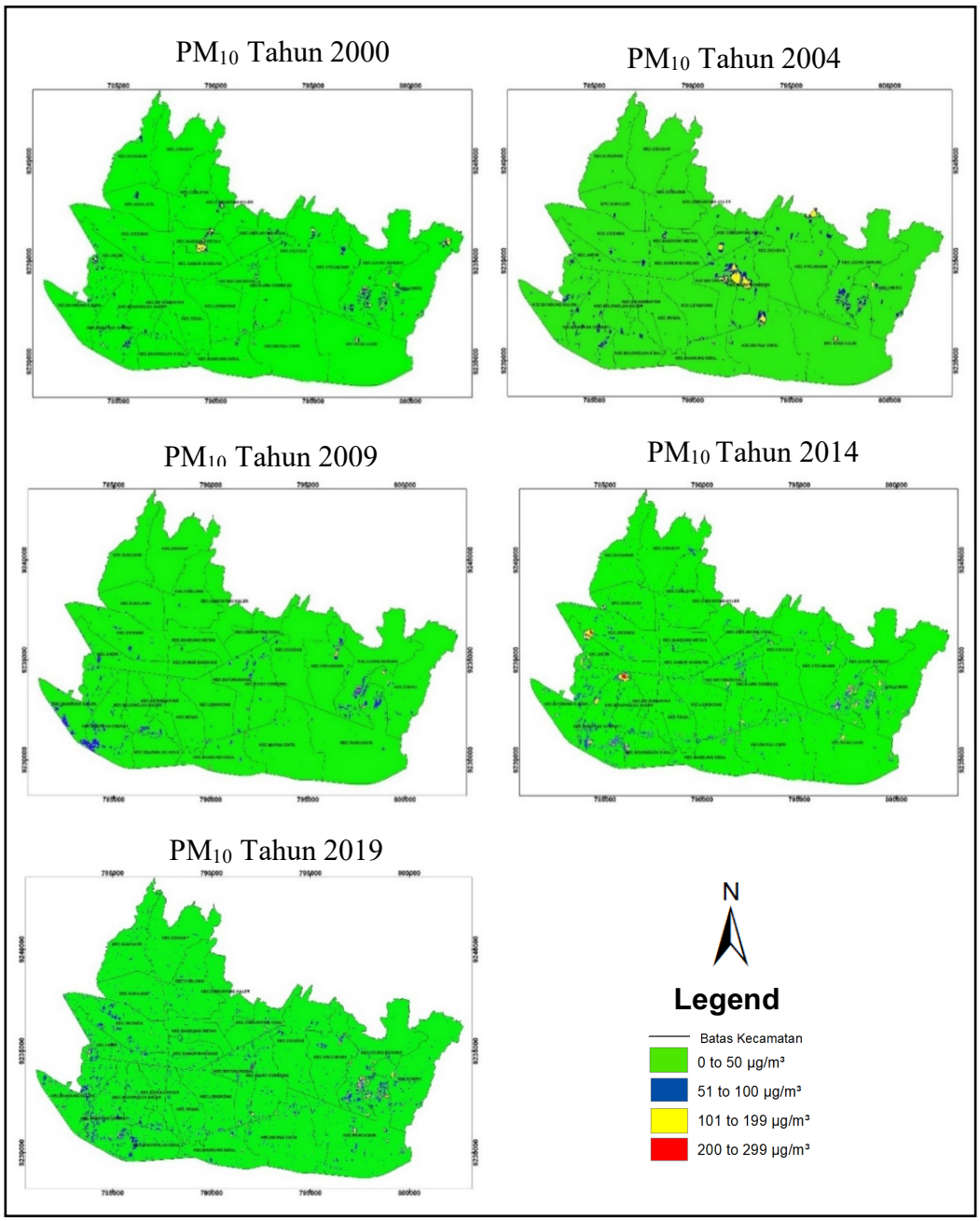

Figure 3. Visualization of PM10.

PM10 averages of Landsat imagery is analyzed using linear regression with the number of vehicles to find out the correlation between those variables by taking the average of PM10 concentrations. The following is the result of linear regression analysis between PM10 of Landsat imagery and the number of vehicles in 2000, 2004, 2009, 2014, and 2019.

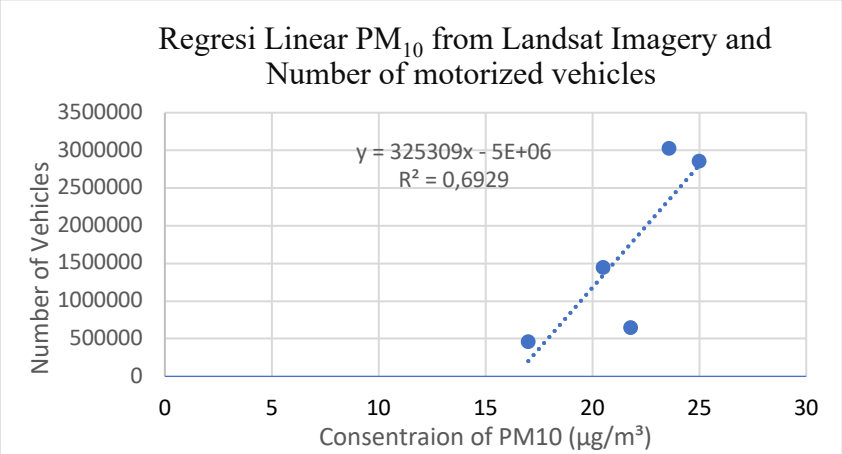

Figure 4. Correlation ff PM_{10} Image Processing and Number of Motorized Vehicles.

The scatter plot shows that the regression coefficient value is positive, the increase in the number of vehicles leads to an increase in PM10 concentration. The coefficient of determination value in the regression analysis above is 0.68464. To find out the value of the correlation coefficient the determination coefficient is rooted so that it gets a value of 0.82742. This means that the number of vehicles and PM10 concentrations has a strong relationship.

4. Conclusions

Based on the results, it can be concluded that the analysis results of PM10 air pollution with the number of motorized vehicles in Bandung based on Landsat Satellite Imagery in 2000, 2004, 2009, 2014 and 2019 are as follows:

- The levels of PM10 air quality based on PSI are divided into 5 classes, healthy, moderate, unhealthy, very unhealthy, and hazardous. The distribution of PM10 in 2000, 2004, 2009, 2014, and 2019 shows that the air quality in Bandung is still considered healthy with PM10 concentration average of 0-50 µg/m³. Even though there are several spatial distribution patterns in moderate air quality level with PM10 concentration range about 51-100 µg/m³, it is not dominant like healthy class, but the distribution of moderate class had increased in the period 2000 to 2019.
- Based on the linear regression coefficient PM10 equation with the number of positive motorized vehicles, it means that the higher the number of motorized vehicles, the PM10 concentration will increase. The maximum value of PM10 concentrations from 2000 to 2019 has also increased. From the linear regression relationship, it can be concluded that PM10 and motorized vehicles have strong relationships.

5. References

[1] Chrisdayanti, B., dan Suharso, *Forecasting the Content of Particulate Matter (PM10) in the Ambient Air of Surabaya Using Double Seasonal ARIMA (DSARIMA).* Faculty of Math and Science. Journal of Science and Art, Sepuluh Nopember Institute of Technology (ITS), 2015. **Vol. 4**(No.2): p. 2337-3520

[2] Badan Metereologi, K., dan Geofisika (BMKG) [cited 2019 March 3]; Available from: https://www.bmkg.go.id/kualitas-udara/informasi-partikulat-pm10.bmkg.

[3] Malina, C. and F. Fischer, *The impact of low emission zones on PM10 levels in urban areas in Germany*. 2012, CAWM Discussion Paper, Centrum für Angewandte Wirtschaftsforschung Münster.

[4] Nguyen, N.H. and V.A. Tran, *Estimation of PM10 from AOT of satellite Landsat image over Hanoi city.* 2014.
[5] Danoedoro, P., *Introduction to remote sensing*. 2012, Publisher of Andi: Yogyakarta.
[6] Othman, N., M.Z.M. Jafri, and L.H. San, *Estimating particulate matter concentration over arid region using satellite remote sensing: A case study in Makkah, Saudi Arabia.* Modern Applied Science, 2010. **4**(11): p. 131.

Detection of Vegetation Changes Using Landsat Satellite Images in Bandung, Indonesia

Ichwan Altarans[1], Rika Hernawati[1]*

[1]Geodesy Engineering, Institut Teknologi Nasional, Bandung

*Corresponding author's e-mail: rikah@itenas.ac.id

Abstract. In this era land use and development rates are getting faster in the city of Bandung, this cause to reduced vegetation land. Vegetation is a part of life that is composed of plants that occupy an ecosystem. One component of vegetation monitoring can be with remote sensing technology, using the NDVI (Normalized Difference Vegetation Index) method. The data was using are Landsat satellite images in the year of 2000, 2005, 2010, 2015, 2018, and 2019. The purpose of this study was to detect differences in the density of vegetation and provide information about the level of greenery in the city of Bandung. Vegetation density classified into five classes, therewere: non-vegetation class, very low greenish class, low greenness, medium greenish, and high greenness. The density of vegetation in the city of Bandung was decreased significantly in the last 19 years are 94.02 km^2.

Keywords: Vegetation Change, NDVI Image, Landsat.

1. Introduction

The level of land use and the rapid development that occurs in the city of Bandung can result in reduced green open land area. The land use includes the construction of highways, residential development, land clearing for living rooms including apartments, hotels and others. This can reduce the level of environmental ecosystems and drastic changes in land use change.

The principle of green open space has the benefit of improving the quality of the urban environment and as a means of protecting the urban environment. The increase in population from year to year by the distribution is one of the causes of the lack of green open land. According to [1] changes especially in urban vegetation areas will cause increasingly complex environmental problems. In general, land cover change studies, one of which is to monitor and detect vegetation density, can be done quickly, accurately, and efficiently and covers a large enough area to utilize remote sensing technology [1].

Vegetation index is an algorithm applied to satellite imagery, to highlight aspects of vegetation density or other aspects related to density [2]. One of the vegetation densities can be determined using the NDVI (Normalized Difference Vegetation Index) technique. One of them uses Landsat satellite imagery by decreasing the value of vegetation density index using NDVI (Normalized Difference Vegetation Index) technique to detect the level of vegetation density in an area. NDVI reduction is obtained from the calculation of Near Infrared (NIR) channels with red channels reflected by plants [3]. Detection of changes in vegetation density using vegetation index parameters, can provide information about the percentage of vegetation cover, plant index (Leaf Area Index), plant biomass, fAPAR (Photosynthetic Active Radiation fraction), photosynthetic capacity, and estimation of carbon dioxide absorption [4].

In this study, by detecting changes in vegetation in the city of Bandung by determining the value of NDVI 2000 and 2019 using DNDVI (Differencing NDVI). DNDVI is a technique for comparing and calculating NDVI values between two images with different recording times [5]. DNDVI is a technique of image difference based on cell reduction between different images in a time series. This technique applies the difference between the image and the characteristics of the vegetation from a distance, and the difference in the index originating from the difference in the light of the image, which is the result of NDVI (Normalized Difference Vegetation Index) or change vectors [6].

2. Study Area and Data Description

2.1. Study Area

Bandung City is the capital of West Java Province, with an area of 167.7 km^2. The city of Bandung is located at the confluence of the road axis, from west to east which facilitates relations with the national capital, while from north to south which facilitates traffic to the plantation area (Subang-Pangalengan).

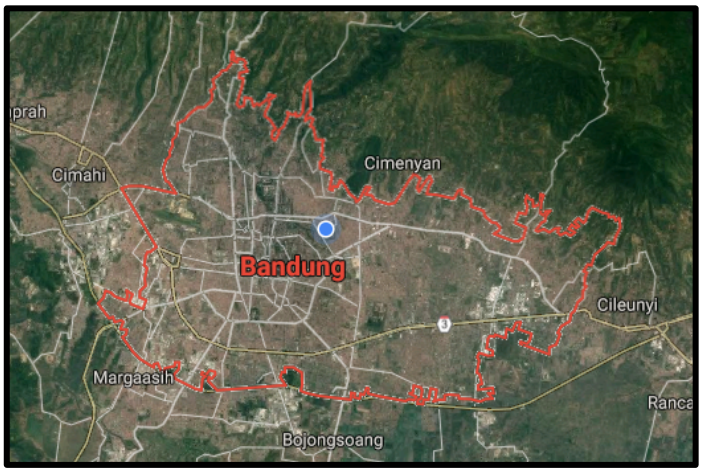

Figure 1. Research Location.

2.2. Data

In this study using Landsat imagery the year of 2000, 2005, 2010, 2015, 2018, and 2019. The Bandung administrative boundary data, and rainfall data in the city of Bandung.

Table 1. Types of Data.

Number	Data Type	Format	Source
1	6 Landsat Satellite Image data for 2000, 2005, 2010, 2015, 2018 and 2019	TIFF	Earthexplorer.usgs.gov
2	Bandung administrative boundary the scale of 1: 50,000	.shp (Shapefile)	tanahair.indonesia.go.id
3	Daily rainfall data for 2000 to 2019	Ms. Excel	Data.onlinebmkg.go.id

3. Methodology and Processing Data

3.1. Methodology

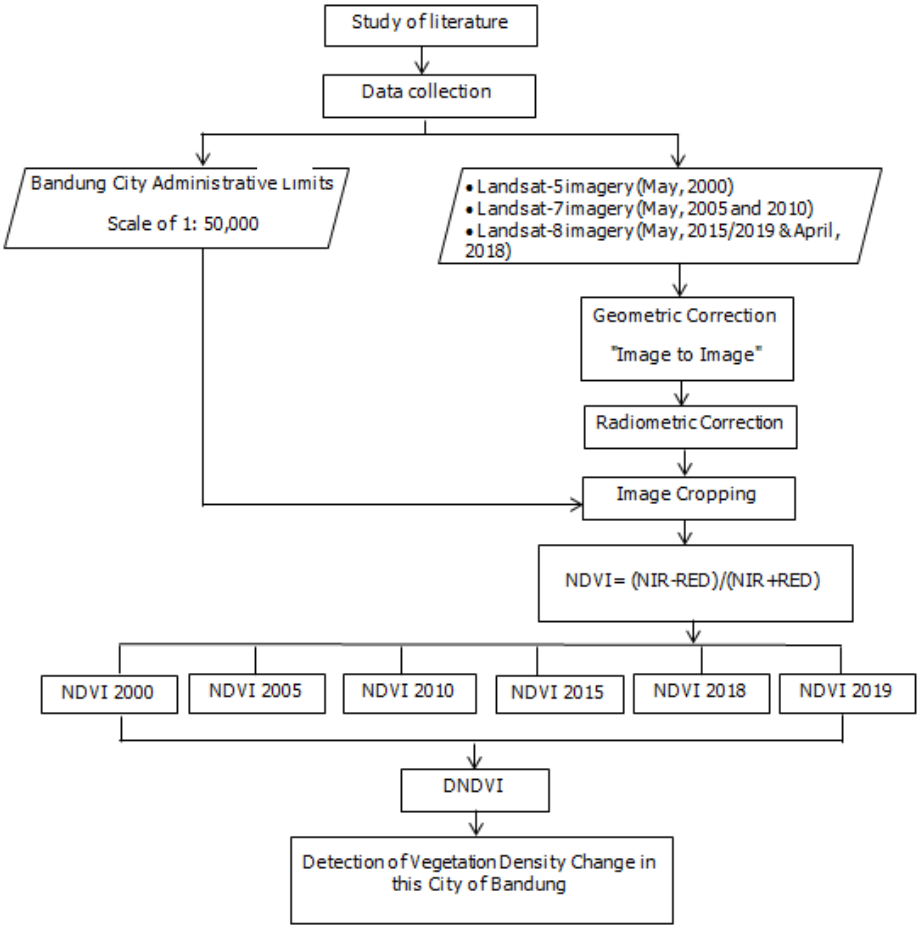

Figure 2. Diagram of Methodology.

3.2. Processing Data

3.2.1. Geometric Correction. Geometric correction is generally carried out for rectification of geometric images. Errors from the geometry of this image cause the pixel position of the satellite data does not match the actual situation. The image-to-image correction process starts by selecting the coordinate pair point on each image (row-column). This process is by comparing pairs of points that can be easily identified in the two images. Image to image geometric correction also requires the position of the points in each image to be spread evenly on the sides, this also affects the shape of the image after correction.

3.2.2. Radiometric Correction. Radiometric correction used in Landsat-5, Landsat-7, and Landsat-8 images is using the flaash technique. Flaash method used to perform Atmospheric Corrections that would correct wave displays from Visible to Near Infrared and SWIR channels. These atmospheric corrections include correcting images by suppressing or eliminating the effects of water vapor, oxygen, carbon dioxide, methane, ozone and molecular and aerosol scattering.

3.2.3. NDVI (Normalized Difference Vegetation Index). The result of cutting the image that has been corrected geometrically and radiometrically, then the vegetation index calculation can be done in this case is the Normalized Difference Vegetation Index (NDVI). According to [7] NDVI is a combination of penis technique with image reduction techniques. Which is where the calculations produced from the infrared channel are close to the red channel on the Landsat satellite as shown in Figure 3.

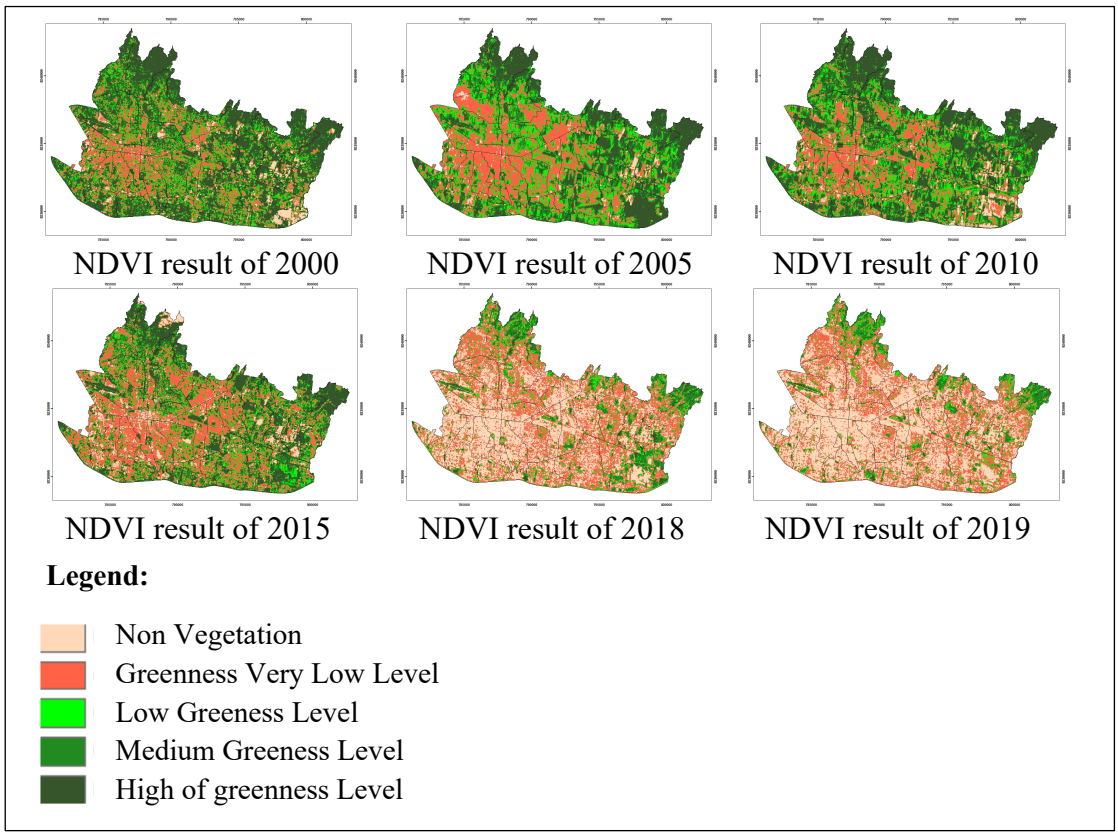

Figure 3. The Result of NDVI.

$$\text{NDVI} = \frac{\text{Near infrared} - \text{red}}{\text{Near infrared} + \text{red}} \quad (1)$$

As for the NDVI results obtained, according to [8], the distribution of NDVI values is made in 5 classes of Vegetation Greeness Index (VGI) in Table 2.

Table 2. Vegetation Greenness Index (VGI) Classification.

NDVI	Classification
NDVI ≤ 0.11	Non Vegetations
0.11 ≤ NDVI ≤ 0.25	Greenness Level Very Low
0.25 ≤ NDVI ≤ 0.33	Low Greeness Level
0.33 ≤ NDVI ≤ 0.45	Medium Greeness Level
NDVI ≥ 0.45	High level of greenness

Source: Sari et al., 2005

3.2.4. NDVI Differences (DNDVI). According to [5] NDVI differencing (DNDVI) is carried out to measure changes in biomass. This technique compares and calculates NDVI values between images

obtained on two different dates. To apply NDVI distribution differences, NDVI distributions from each date are generated with a range of values from -1 to +1. The results of the comparison of the two NDVI issued values range from 0-255 (Al-doski et al, 2013). Step difference NDVI (DNDVI) through reducing NDVI images one date from that on another date. In this study, the distribution of NDVI 2019 is reduced from the distribution of NDVI 2000 as shown in the equation as follows:

$$DNDVI = NDVI\ 2019 - NDVI\ 2000 \quad (2)$$

4. Results and Discussion

Changes vegetation density from the year of 2000, 2005, 2010, 2015, 2018 and 2019 is one of the impacts of land use both for development and land use functions. Apart from the influence of land use factors, natural factors also affect changes in vegetation density, namely the level of rainfall activity. The low rainfall rate affects the decrease in the level of vegetation density, this can be seen in the rainfall data in table 4. The highest rainfall on May 7, 2005 and May 21, 2010 is consistent with the results of NDVI in 2005 and 2010 with high high vegetation. While the vegetation density in 2018 and 2019 that predominates is non-vegetation class, this can be seen from the absence of rainfall activities in 2018 and 2019.

Table 3. Results of NDVI Distribution Areas in 2000, 2005, 2010, 2015, 2018 and 2019 (km^2).

Tahun	NDVI Value Range (km^2)				
	-1 – 0.11	**0.11 – 0.25**	**0.25 – 0.33**	**0.33 – 0.45**	**0.45 – 1.0**
2000	6.93	41.02	26.34	29.54	64.71
2005	3.72	54.83	33.97	33.20	42.85
2010	6.56	45.05	30.61	33.17	53.14
2015	12.65	63.94	25.93	25.25	40.80
2018	63.17	69.20	15.34	17.13	3.73
2019	77.65	64.34	12.90	12.44	1.25

Then the next process is to calculate NDVI Differencing was to determine the rate of change in vegetation density from 2000 to 2019 for 19 years.

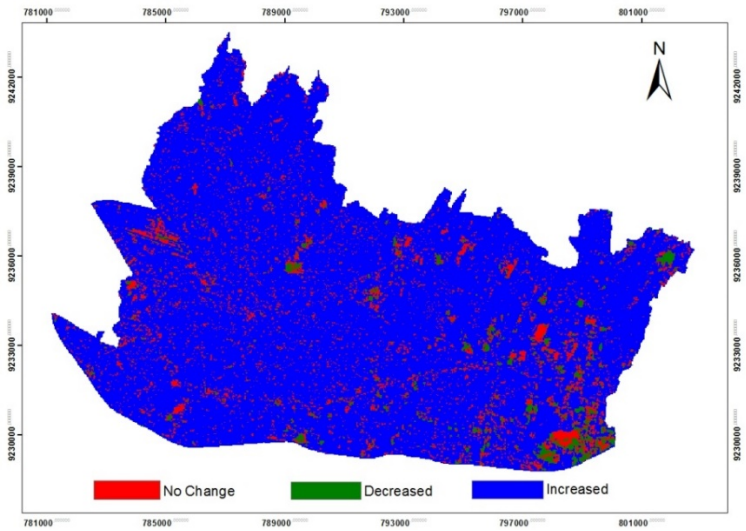

Figure 4. Result of DNDVI.

Figure 4 shows the results of the NDVI difference (DNDVI) with a reduction in the distribution of NDVI in 2019 with the distribution of NDVI in 2000. The DNDVI results resulted in three (3) classification classes, namely the class did not change in the range (0-1) with an area of 15.26 km², the class decreased with a range (1-251) with an area of 4.2 km² and class increasing with a range of grades (251-255) with an area of 149.11 km².

Table 4. Detection of NDVI Changes in 2000 and 2019 (km^2).

2000 **2019**	**-1 to 0.11**	**0.11 to 0.25**	**0.25 to 0.33**	**0.33 to 0.45**	**0.45 to 1**	**Row Total**
-1 to 0.11	4.39	31.6	15.7	12.16	13.73	77.58
0.11 to 0.25	1.84	8.26	9.46	14.89	29.72	64.17
0.25 to 0.33	0.34	0.65	0.73	1.49	9.59	12.81
0.33 to 0.45	0.32	0.44	0.39	0.84	10.34	12.33
0.45 to 1	0.04	0.04	0.04	0.08	1.03	1.23
Class Total	6.93	41.02	26.34	29.54	64.71	0
Class Changes	2.54	32.76	25.61	28.7	63.68	0
Image Difference	70.71	23.32	-13.45	-17.11	-63.46	0

5. Conclusions

In the NDVI process it uses the near infrared channel and the red channel on the Landsat image. The range of NDVI values from -1 to 1, are classified in five classification classes, namely non vegetation (-1.0 - 0.11), very low vegetation (0.11 - 0.25), low vegetation (0.25 - 0.33), moderate vegetation (0.33 - 0.45), and high vegetation (0.45 - 1.0). The results obtained in 2000 vegetation index (low, medium and high greenness) of 120,591 km^2. In 2019 the level of vegetation (green, low, medium and high) has decreased very significantly, this can be seen from the vegetation area of only 26,577 km^2.

Then the NDVI data for 2000 and 2019 can be seen the change using NDVI Differencing (DNDVI), by calculating NDVI after (2019) and NDVI before (2000). DNDVI calculations produce three class categories namely unchanging, decreasing, and increasing. Where the increasing category has an index value in the range (0-1), decreases (1-251) and increases (251-255). The results of calculations using the DNDVI (NDVI Differencing) method show the extent of increased vegetation index in this case which is most clearly seen in the non-vegetation index and very low vegetation. The total area of vegetation index increases 149 149 km^2. This can be proven by increasing the vegetation index in classes -1 - 0.11 (non-vegetation) in 2019 due to land use and sustainable infrastructure development. After calculating NDVI on Landsat satellite imagery data in the Bandung City area, Landsat imagery data can meet the criteria and be valid in meeting the results of this study. And it can be identified that the calculation of NDVI can be derived from Landsat imagery in 2000 and 2019. The results of the NDVI show significant changes in vegetation density from 2000 to 2019 in a period of 19 years of 94.02 km^2.

6. References

[1] Wahyuni, N.I., D.I.D. Arini, and A. Ahmad, *Identifikasi Perubahan Kerapatan Vegetasi Kota Manado Tahun 2001 Sampai 2015.* Majalah Ilmiah Globe, 2017. **19**(1): p. 65-74.

[2] Nugroho, A., *Analisis Kerapatan Vegetasi di Kecamatan Ngaglik tahun 2006 dan 2016 Menggunakan Teknik Penginderaan Jauh.* Geo Educasia-S1, 2017. **2**(3): p. 306-320.

[3] Hernawati, R. and S. Darmawan, *Analisis Kerapatan Vegetasi Berbasiskan Data Citra Satelit Landsat Menggunakan Teknik NDVI di Kota Bandung Tahun 1990 dan 2017.* 2018.
[4] Horning, N., *Global Land Vegetation; An Electronic Textbook.* NASA Goddard Space Flight Center Earth Sciences DirectorateScientific and Educational Endeavors (SEE). Maryland-USA, 2004.
[5] Al-Doski, J., S.B. Mansor, and H.Z.M. Shafri, *NDVI differencing and post-classification to detect vegetation changes in Halabja City, Iraq.* IOSR Journal of Applied Geology and Geophysics (IOSR-JAGG), 2013. **1**(2): p. 01-10.
[6] Oppenheimer, C., *S CHOWENGERDT, RA 1998. Remote Sensing. Models and Methods for Image Processing, xiv+ 522 pp. San Diego, London: Academic Press. Price US $75.00 (hard covers). ISBN 0 12 628981 6.* Geological Magazine, 1999. **136**(6): p. 697-711.
[7] Danoedoro, P., *Introduction to digital remote sensing.* Indonesia), Yogyakarta: Andi, 2012.
[8] Sari, D.K., E.T. Hermawan, and G. Hudman. *Study on vegetation cover changes in the province of south Kalimantan using RGB-NDVI unsupervised classi fi cation method*. in *Map Asia Conference. Jakarta*. 2005.

The Effect of Building Density on Surface Temperature Based Landsat-8 in Bandung City, West Java

Dery Chahyanto[1]*, Rika Hernawati[1]

[1]Geodesy Engineering, Institut Teknologi Nasional, 23 PH.H. Mustofa Street, 40124 Bandung, Indonesia

*Corresponding author's e-mail: Chahyantoodery@gmail.com

Abstract. Developments of urban area is a process of land use changed to meet the needs of urban communities for infrastructure and facilities. Continuously development without regard to the percentage between the built up space and green open space will result building density and temperature changes in Bandung city. The main objective of this research was using remote sensing methods to identified building density quickly and accurately was using the Normal Difference Built-Up Index (NDBI) algorithm. NDBI is an effective transformation to mapping area of land with built in urban areas properly using Landsat 8. The results of this research showed the value of building density in Bandung city in the year of 2014, 2016, and 2019. The value of building density generated through the NDBI algorithm and then correlated with the surface temperature obtained through the Land Surface Temperature method. NDBI values showed a decrease in the high density class in 2014 to 2016 by 0.5% and show an increase of 6% in 2019. The value of relationship coefficient shows R = 0.91 in 2014, R = 0.95 in 2016, and R = 0.91 in 2019, It can be concluded that the NDBI building density value and the LST soil surface temperature value have a very strong relationship.

Keywords: Development, Built Up, Temperature, Landsat 8, NDBI, Brightness, Temperature.

1. Introduction

Bandung city is one of the biggest cities in Indonesia that has a density population cause have strategic location and the economic center of West Java. A region always grow and develop with social and economic life in that region. In the process, urban development often eliminated the ecological value of land to be exchanged with more economical functions. Increasing population results in a high area of built-up space and reduced green open space. This causes changes temperature in Bandung city cause unbalanced land use changes between built up space and green open space.

The parameters can be used to knows the temperature changes is land surface temperature (LST). LST is an important parameter in studying behavior thermal and urban areas. The rise and fall of LST in temperatures under the atmosphere layer are important factor to know surface radiation [1]. To identify the density of built up land using can be use remote sensing technology. That method is NDBI (Normal Difference Built-Up Index). NDBI is a spectral reflection involving SWIR and NIR channels, NDBI is also an effective transformation to mapping areas of urban built land well using Landsat 8 OLI images. Referring to the study conducted by [2] where the study showed changes in land surface temperature in Shuzou City and the factors that influenced it. To identify these factors a calculation algorithm is needed to knows the values of each index which is used as a parameter to create analysis. The index value needed to determine these factors is the value of the vegetation index by Normal Difference Vegetation Index (NDVI), the value of building density represents the population density intended by Normal Difference Built-Up Index (NDBI), and value of Normal Difference Water Index (NDWI). The three data are correlated with Land Surface Temperature data to find out how the relationship between the index value of the land surface temperature. But In this research was using 2 perameters to identified land surface temperature changes. The parameters used in this research were NDBI and LST with Mono Windows Brightness Temperature algorithm.

2. Methodology

2.1. Method

The methodology used in this study starts with data collection, including Landsat 8 imagery obtained from the USGS and administrative boundary of Bandung city. Pre-processed images are carried out that include geometric correction, radiometric correction, and image cropping, and then the processing including the NDBI algorithm to determine the value of the building density index and to identified values of LST using Mono Windows Brightness Temperature algorithm, and then the value of building density generated through the NDBI algorithm and then correlated with the surface temperature obtained through the Land Surface Temperature method. To clarify the stages of this study, a flow chart of the study process is shown in Figure 1.

2.2. Data and Location of Research

The data used in this study are:

Table 1. Data.

Data
Satellite Imagery Landsat 8 in 2014, 2016 and 2019
Bandung Administrative Boundaries at 1:50000 scale
District administrative boundaries at 1:50000 scale
Bandung City Temperature from Dapartment of Meteorology, Climatology, and Geophysics

The study was based in Bandung with an area of 167.7 $km^{2.}$ Bandung is bordered by several regencies/cities, the north is bordered by Bandung Regency and West Bandung Regency, the west is bordered by West Bandung Regency and Cimahi, the east is bordered by bandung regency and the south is bordered by Bandung Regency.

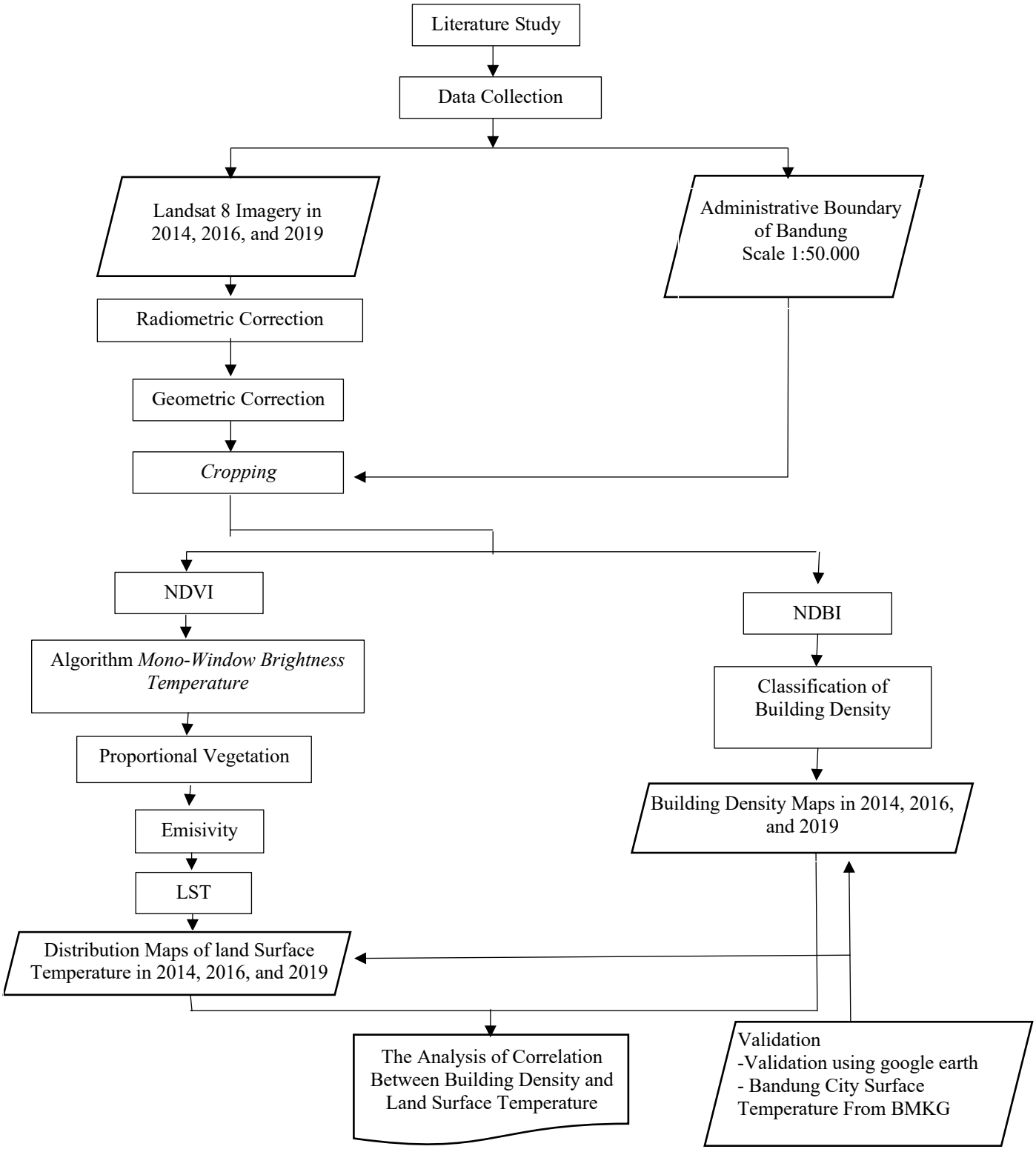

Figure 1. Research Flow Chart.

Figure 2. Study Location.

2.3. Data Processing

Before the data are used to calculate value of building density and land surface temperature, the preprocessing steps are carried out. It includes geometric correction and radiometric correction consisting of converting the digital number value to radians and then converting the radians to reflectance values. The next steps are cropping the image based on AOI (Area of Interest), then calculate LST used mono windows brightness temperature algorithm and calculate value of building density used NDBI algorithm.

2.3.1. Geometric Correction. To remove geometric distortion that causes a mismatch between object imagery position and object actual position, it is necessary to have a geometric correction. It establishes the pixel position of imagery to the actual position. In this study, geometric correction is carried out by the image to image method where Landsat-8 become the base/reference to determine GCP on Landsat which will be corrected geometrically.

2.3.2. Radiometric Correction. Radiometric correction was undertaken to correct the pixel values so those can match the actual values, considering atmospheric disturbance factor as the primary source of error. The Atmospheric effect causes the value of object reflection on the surface of the earth recorded by the sensor is not the original value, but it becomes larger due to the scattering or smaller due to absorption process [3] The radiometric correction process was converting Digital Number to Radians, then converting from radians to reflectance values. This study was using the FLAASH method in the radiometric correction process.

2.3.3. Normal Difference Vegetation Index (NDVI). To calculate NDVI on Landsat 8 Imagery used band NIR and band RED. NDVI algorithm was used as in the following formula.

$$NDVI = \frac{(NIR-RED)}{(NIR+RED)} \quad (1)$$

The parameters used in the algorithm are;
NIR = Near Infrared
RED = Red

2.3.4. Mono Windows Brightness Temperature. This method used to analyze temperature by converting digital numbers into spectral radiance, Mono Windows Brightness Temperature is used as in the following formula:

$$Tb = \frac{K2}{ln\frac{K1}{L\_\lambda+1}} \quad (2)$$

The parameters used in the algorithm are;
Tb = Brightness Temperature Satelite
K1 = Constanta Calibration in Spectral Radiance
K2 = Constanta Calibration in Spectral Radiance
L_λ = Spectral Radiance in Wm−2sr−1mm−1.

2.3.5. Proportional Vegetation. To knows the value of vegetation cover fraction needs the minimum NDVI and maximum NDVI values, therefore the NDVI value must first be known.

$$Pv = (\frac{NDVI-NDVImin}{NDVImax-NDVImin})\text{^}2 \quad (3)$$

The parameters used in the algorithm are;
Pv : Proportional Vegetation
NDVI : Normalized Difference Vegetation Index
NDVImax : Normalized Difference Vegetation Index maximum
NDVImin : Normalized Difference Vegetation Index minimum

2.3.6. Normal Difference Built-Up Index (NDBI). Value of building density index using band NIR and band SWIR on Landsat 8. The NDBI value in this study was obtained by adopting a calculation method from [4]

$$NDBI = \frac{(SWIR-NIR)}{(SWIR+NIR)} \quad (4)$$

The parameters used in the algorithm are;
NIR = Near Infrared
SWIR= Short Wave Infrared

3. Results and Discussion

3.1. Normal Difference Built-Up Index
The result of this study showing the distribution of Building Density Maps in 2014, 2016, 2019 as shown as Figure 3.

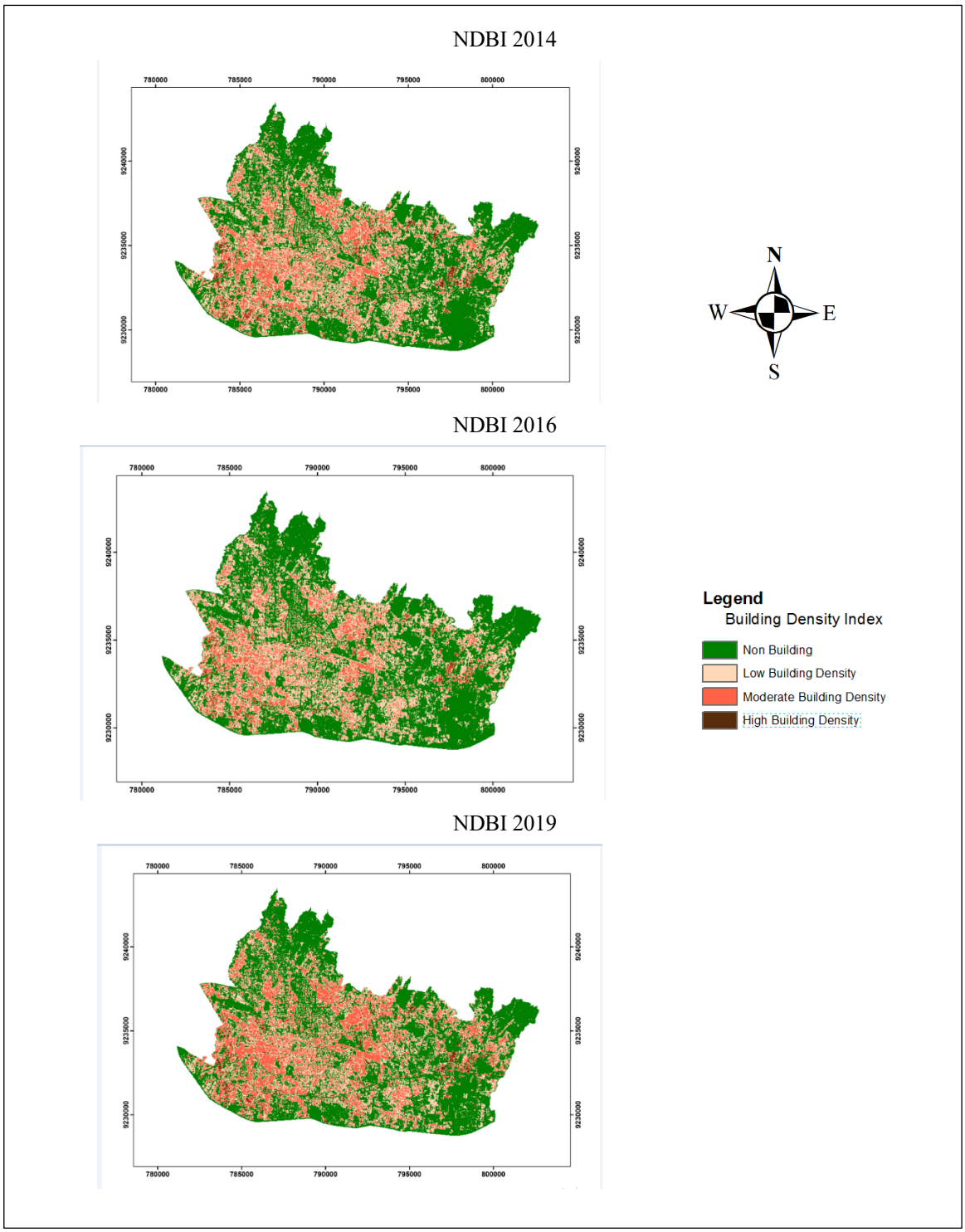

Figure 3. Visualization of NDBI.

3.2. Land Surface Temperature

The result of this study showing the distribution of Land Surface Temperature in 2014, 2016, 2019 as shown as Figure 4.

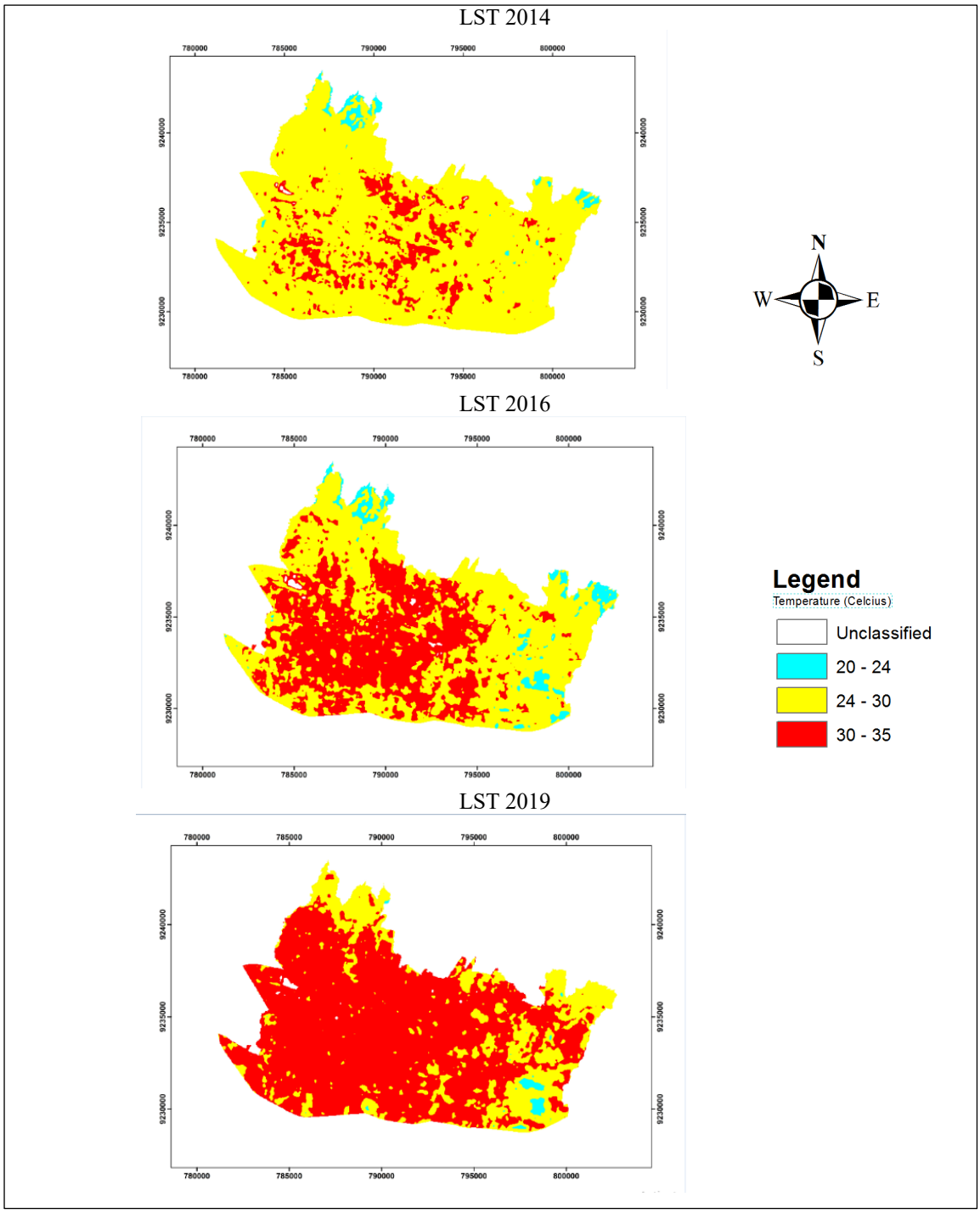

Figure 4. Visualization of LST.

3.3. Visualization of NDBI and LST

Figures 5, 6, and 7 show the visualization of NDBI and LST processing. Sampling was choosen in Rancasari Regency because that region illustrates the density of built area weren't so tight and their located in the suburbs of Bandung.

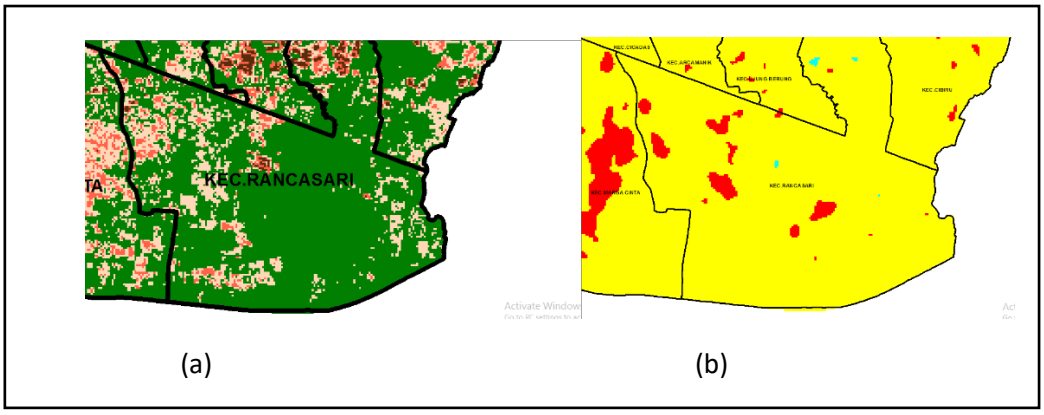

Figure 5. (a) NDBI building density index and (b) LST estimated results in 2014.

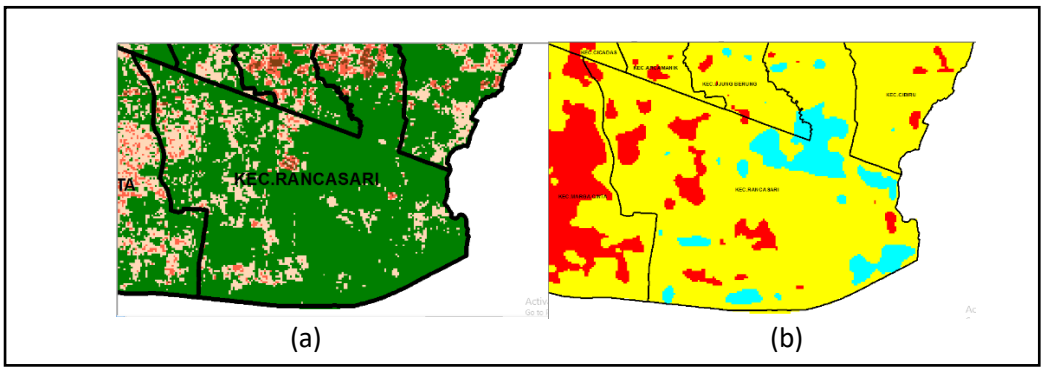

Figure 6. (a) NDBI building density index and (b) LST estimated results in 2016.

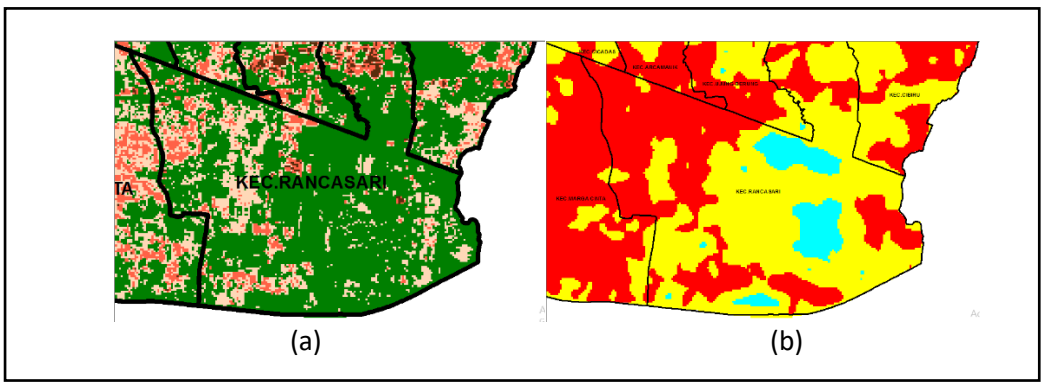

Figure 7. (a) NDBI building density index and (b) LST estimated results in 2019.

3.4. Validation of Builtding Density

Validation is needed to determine whether the results of processing same with the actual conditions. Validation was using google earth, The validation process only in 2019 as a sample to identified the accuracy of the processing results. The results of image processing in 2019 showed Bandung that has an area 16865.1 Ha. The results of extensive built-up land area from processing is 8521.74 Ha or 50.56% of the total area.

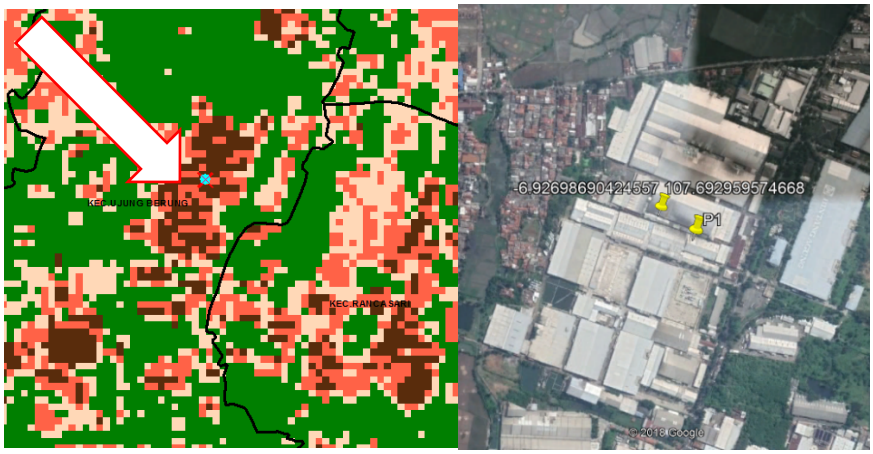

Figure 8. Validation of High Building density.

Figure 9. Validation of Moderate Building density.

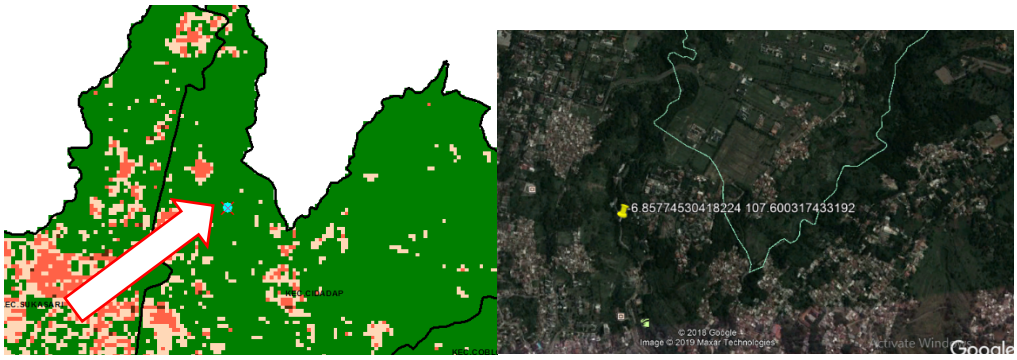

Figure 10. Validation of Low Building density.

3.5. Correlation Analysis between NDBI and LST

Correlation is an analysis used to find out how much the strength of the relationship between two or more variables. Correlation analysis is done by taking a random sample with stratified method where this method was to select stratified samples to represent each surface temperature value.

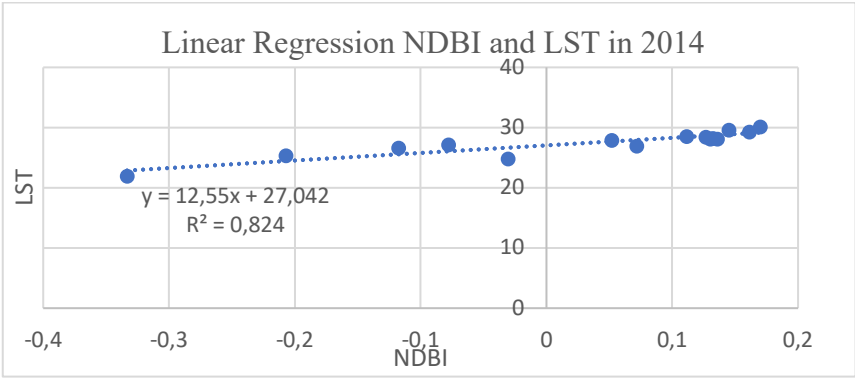

Figure 11. Linear Regression NDBI and LST in 2014.

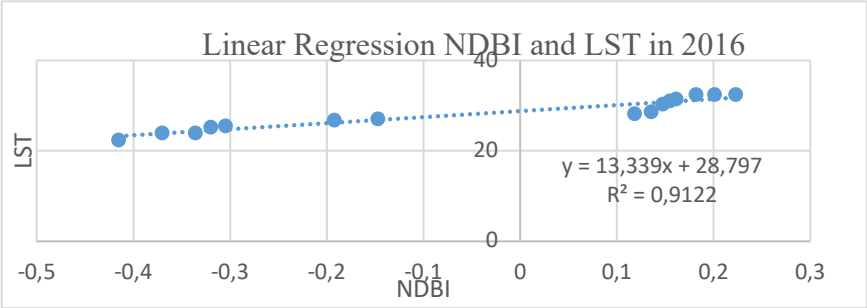

Figure 12. Linear Regression NDBI and LST in 2016.

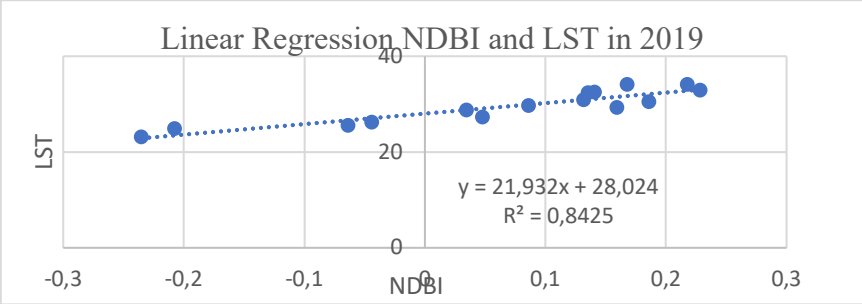

Figure 13. Linear Regression NDBI and LST in 2019.

Results of the scatterplot show the regression coefficient value is positive, where the higher the level of the building density index, the surface temperature value of the ground will be higher too, and conversely if the level of the building density index in an area is low, its value from the surface temperature of the land in this area is low. The equation of the coefficient of determination in 2014 was 0.824 and 2016 was 0.9122, while in 2019 had a value 0.8425 thats means the effect of building density on surface temperature was 82.4% for 2014, 91.22% in 2016, and 84, 25% for 2019. According to [5], the meaning of the correlation value if it shows the value of r = 0.90 <r <1.00 or -1.00 <r <-0.90, that's means has a very strong relationship. It can be concluded that the NDBI building density value and the LST soil surface temperature value have a very strong relationship.

4. Conclusions

Based on the results, it can be concluded that the analysis results of built-up density with land surface temperature in Bandung based on Landsat Satellite Imagery has a very strong influence on the surface temperature of land in Bandung. This is proven by random sampling using the strata method. To find out how to influence building density at land surface temperature, the linear regression method is used.

The results of linear regression showed the value of $R^2 > 0.80$ occurred in each regression table, this explains the ability of the independent variable to explain the variance of the dependent variable is 80% and the remaining 20% is explained by other factors outside the variables in the regression equation.

5. References

[1] Voogt, J.A., *Urban Heat Island*. Journal of Geographic Information System, 2002. **3**: p. 06 – 666.
[2] Feng, Y., et al., *Spatial patterns of land surface temperature and their influencing factors: a case study in Suzhou, China*. Remote Sensing, 2019. **11**(2): p. 182.
[3] Danoedoro, P., *Introduction to remote sensing*. 2012, Yogyakarta: Andi.
[4] Zha, Y., J. Gao, and S. Ni, *Use of normalized difference built-up index in automatically mapping urban areas from TM imagery*. International journal of remote sensing, 2003. **24**(3): p. 583-594.
[5] Kusumawati, W.I., *Simulasi Produksi dan Distribusi Pelayanan Permintaan Sarung Tenun Dengan Metode Monte Carlo*. 2011.

Strain Analysis Lombok Island Based on GNSS Observation Data 1996 - 2018

Ardita H Pancanugroho[1]*, Henri Kuncoro[1], Hary Nugroho[1]

[1]Geodesy Engineering, Institut Teknologi Nasional, 23 PH.H. Mustofa Street, 40124 Bandung, Indonesia

*Corresponding author's e-mail: arditahadi@gmail.com

Abstract. Based on gravity and bathymetry data analysis, [1] stated that the area of Bali - Lombok and Sumbawa Island is in the subduction of the Indo - Australian Plate in the South and the Fault Zone Rising Flores in the North. This area is an active geological structure with relative Western-Eastern direction of movement. In addition to the fault zone, the straits between the islands are also separated by the presence of horizontal faults (oblique) which cause fracture segments in the area. The purpose of this study is to determine the magnitude of the Lombok Island plate strain prior to the earthquake by utilizing GNSS data in 1996 - 2018. The deformation velocity of Lombok Island in the period 1996 - 2018 has an average speed for E component 31.2mm/year, N component 3,869 mm/year. From the results of the deformation velocity it can be seen that the direction of shift for E component goes east and N component to the south. So, it can be concluded that the direction of the shift towards the Southeast, this indicates that the southern subduction movement is relative to the movement of the Eurasian plate. The strain pattern produced in the 8 strainrate models shows that the dominant strain is the compression strain, where this strain is affected by the activity of the Flores Rear Arc Up and Indo-Australian Subduction. The value of the resulting model has a value of 10^{-6}, in this study it is assumed that it cannot be used because it produces a significant strain model.

Keywords: Lombok Island, Strain Rate, Velocity, GNSS.

1. Introduction

The territory of Indonesia is not a stand-alone geological unit from geotechnical point of view, but rather a geological center that stretched between Southeast Asia and Australia and between the Pacific Ocean and the Indian Ocean. Indonesia itself is located between the four main plates of the world, namely: 1) Pacific plate which moves to the Southwest, 2) The Indo-Australian Plate which moves to the East and North, 3) The Philippine Plate which moves to the West, and 4) Plate Eurasia which moves to the Southeast. The movement of the plates form into some pattern, namely: the movement of subducted plates, the movement of plates away from each other and the movement of plates sliding each other [2]. The one effect of plate movements is the occurrence of earthquakes. An earthquake caused by plate movement is called a tectonic earthquake caused by strains accumulation of the earth's tectonic plates. In range July 29 - September 2, 2018 the Meteorology and Geophysics Agency (2018) has recorded 46 tectonic earthquakes occurred on Lombok Island and its surroundings with a strength above 5.0 SR (Richter Scale). The biggest tectonic earthquake occurred on August 5, 2018 in Loloan with a strength of 7.0 SR which resulted in 401 people dead (National Disaster Management Agency, 2018).

Tectonic earthquakes cause changes in natural and man-made objects. This event is often known as the deformation of an object. Deformation is an activity to change the shape and location or position of objects that are influenced by nature and humans on a time and space scale. Earth Plate movement is one example of absolute and relative change activity which is moved by nature which has an impact on natural objects changing position, man-made or the earth's plate itself.

[3] monitors the tectonic deformation of Lombok Island based on GNSS observation data from 2013-2016. This study explains that deformation has occurred with the plate shifting speed of 5.57 mm/th to 21.86 mm/y with the direction of moving towards the Northeast. This research was conducted by analyzing data from recording at 12 stations spread on Lombok Island. [4] a deformation analysis of the geometric aspects of the Mentawai segment was carried out due to the tectonic earthquake of July 10, 2013 in the intersismic, coseismic, and post-seismic phases. This research explains that the SuGar (Sumatran GPS Data Array) station deformed horizontally and vertically in the 3D cartesian coordinate system. The horizontal shift speed direction of the SuGar station in the interseismic phase tends to move towards North - Northeast indicating energy accumulation. The horizontal shift speed direction of the SMGY and TRTK stations in coseismic phase has shift in the opposite direction of the interseismic phase.

This research analyzed the deformation or strain rate of tectonic plates before the Loloan earthquake in 2018 (M 6.9). The data used are the results of GNSS observations from 1996 to 2018 in 16 points scattered at Lombok Island region, 16 points are divided into 2 parts, 12 points are the campaign data by [5] in observation year 2013 - 2016 and 3 data campaign points are the Geodetic Control Network data in observations from 1996 - 2015, 1 continuous data point which is recording with the CORS system by BIG (Badan Informasi Geospasial) at the end of 2013 and mid-2018. The results expected from this research are to determine the strain rate Lombok Island horizontally so the surface deformation pattern is known that caused by elastic deformation from the subduction boundary.

2. Research Implementation

2.1. Research Data

The data used are the results of GNSS observations from 1996 to 2018 in 16 points scattered at Lombok Island region, 16 points are divided into 2 parts, 12 points are the campaign data by [5] in observation year 2013 - 2016 and 3 data campaign points are the Geodetic Control Network data in observations from 1996 - 2015, 1 continuous data point which is recording with the CORS system by BIG (Badan Informasi Geospasial) at the end of 2013 and mid-2018 described in Tables 1 and 2.

Table 1. Observation Data Information of BIG GPS Campaign at Lombok Island.

Station	2013		1994	1996	2002	2003		2004		2013		2015	
	September	October	January	November	April	May	October	January	March	March	April	May	June
	DOY												
N1.3071	268 269 271												
N1.3072	268 269	 274											
N1.3073	269 271												
N1.3074	266 268 269		27							295			175 176
N1.3075	264 266 268			315 316 317							296 297		
N1.3076	266 268 269												
BLMB					100 101 102 103	133 134	282 283 284 285	4 5	66			141 142	

Table 2. Information of GPS Campaign Data PVMBG at Lombok Island.

Station	2013	2014		2015		2016
	September	March-April	October	April	October	April
			DOY			
KDOO	270	88	298	99	282	96
	271	89	299	100	283	97
MDRI	268	90	298	100	281	98
	269		299	101	282	99
				102		100
MJRW	268	88	296	97	279	94
	269	89	297	98	280	95
					281	
MKYG		89	300	100	283	98
		90	301	101	284	99
				102		
				103		
MMTR	268	90	298		279	98
	269	91	299		280	99
						100
MPCR		88	296	97	279	95
			297		280	94
					281	
MPGB	268	88	298		280	94
	269		299		281	95
MPKT	267	86	296	97	279	92
	268	87	297		280	93
MPNJ		86	295	97	279	92
			296	98	280	93

Table 3. List of IGS Stations Used.

Station	City	Country	Manager	Longitude	Latitude
BAKO	Cibinong	Indonesia	BIG	106.8500	-6.4900
XMIS	Christmas Island	Australia	GA	105.6885	-10.4500
COCO	Cocos (kelling) Island	Australia	GA	96.8339	-12.1883
KARR	Karattha	Australia	GA	117.0972	-20.9814
DARW	Darwin	Australia	GA	131.1327	-12.8437
TOW2	Cape Ferguson	Australia	GA	147.0557	-19.2693
ALIC	Alice Springs	Australia	GA	133.8855	-23.6701
CEDU	Ceduna	Australia	GA	133.8098	-31.8667
DGAR	Diego Garcia Island	Australia	GA	72.3702	-7.2697
SEY1/2	La Misere	Seychelles	JPL	55.4795	-4.6737
IISC	Bangalore	India	JPL	77.5704	13.0212
HYDE	Hyderabad	India	NGRI	78.5509	17.4173
KMNM	Kinmen	Taiwan	NLSC	118.3886	24.4638
SHAO	Sheshan	Cina	JPL	121.2004	31.0996
CUSV	Patumwan	Thailand	JPL	100.5339	13.7359

2.2. Method

The research was carried out through several stages described in Figure 1. that GNSS data processing is processed using GAMIT software to obtain daily solutions, then proceed to processing GLOBK to get the coordinates and accuracy of each observation year by transforming from the WGS84 datum framework to ITRF14. For calculation of strain rate using the triangle strain algorithm method in MatLab software and plotting to analyze strain results using GMT.

3. Results and Discussion

3.1. GPS Time Series

Obtaining a deformation velocity value plotting time series steps is needed. This is done to get a linear equation between the observation time (x axis) of the shift or movement of the point (y axis) in units of mm / year, this equation value which will be the velocity deformation value of each observation point. In its application, linear plotting time series is carried out using MatLab software. This software is needed a plugin called tssum, which is a plugin to process the plotting time series until it gets velocity values. The change in this value represents the movement of the plate under the observation point. The plotting time series is plotting dN (difference North) coordinates, dE (difference East) and dU (difference Vertical). This coordinate point is the relative movement point coordinate to the epoch reference point that has been transformed from a geocentric coordinate system to a topocentric system. The epoch reference point is the middle coordinate value of the observation range.

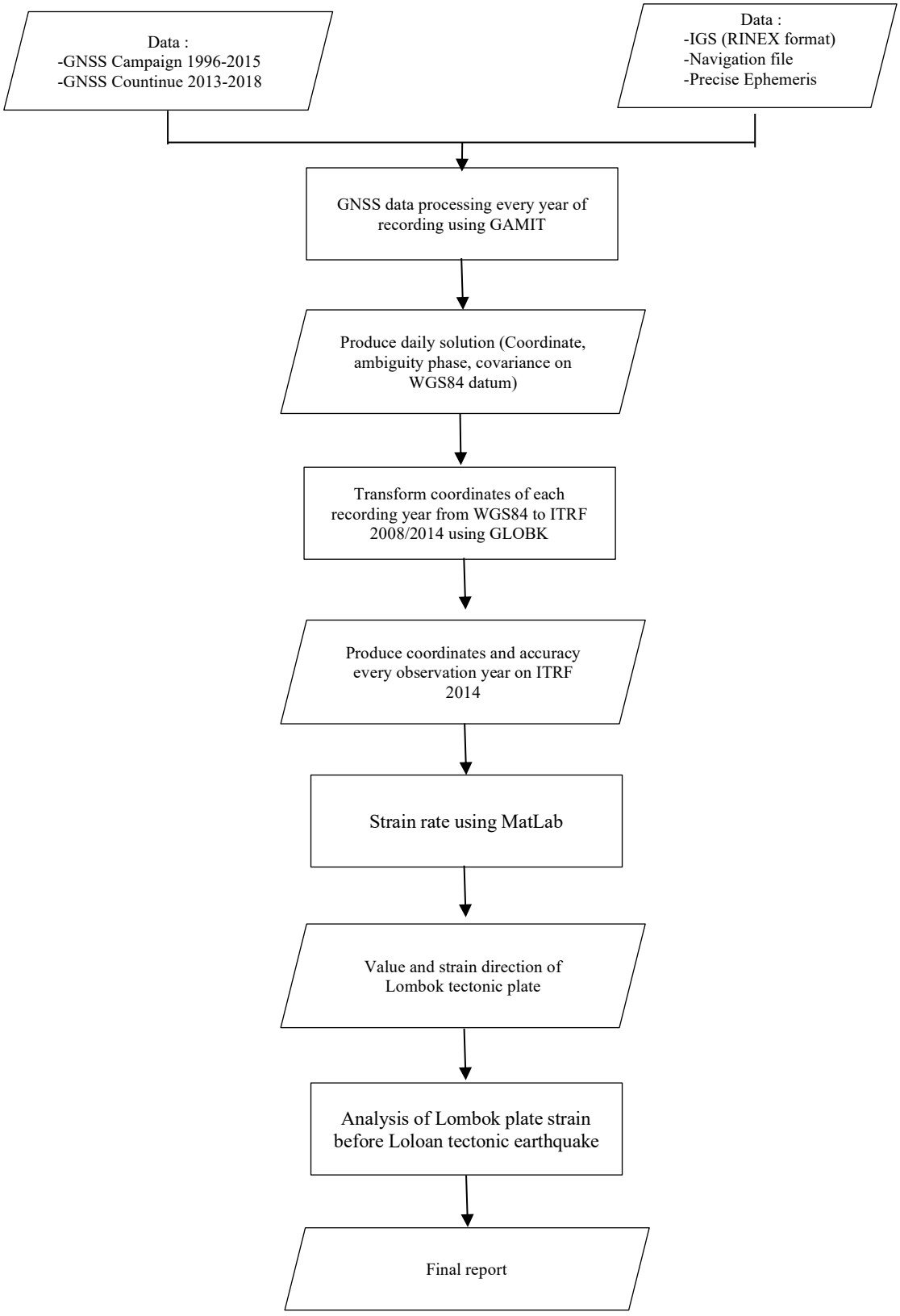

Figure 1. Research Methodology.

The removal or deletion of data outliers is an initial step before conducting a time series analysis. Outliers data itself is a data whose value is outside the value of the linear line that should be. Outliers appear among other things, there is a smaller amount of data compared to other data or the time span of the first observation with the last one is very far away. This is explained in Figure 2, where the range of observations is very far, starting from the beginning of observations in 1996 doy 315 and subsequent observations in 2013 doy 297. However, this can be tolerated because the data that is the result of episodic observations have a time span a long time from one observation to the next and has a small amount of data, but can be used as a deformation analysis data with several conditions, including the number of observations of more than three observational data in one observation station point.

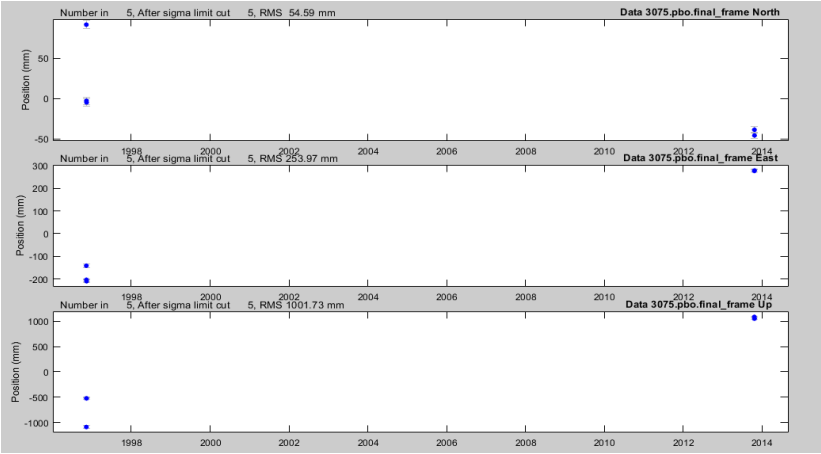

Figure 2. Display Plotting Time Series N1.3075 station.

Table 4. Time Series Coordinate Points N1.3075 station.

N1.3075						
dN (milimeter)	**dE (milimeter)**	**dU (milimeter)**	**Se (milimeter)**	**Sn (milimeter)**	**doy**	**Tahun**
91.33	-14.18	-1.09	5.14	7.45	315	1996
-2.71	-203.06	-0.52	4.71	5.12	316	1996
-4.69	-209.10	-0.52	4.67	5.56	317	1996
-38.46	275.48	1.08	4.37	5.53	296	2013
-45.48	277.88	1.05	3.76	5.80	297	2013

Based on the discussion above, the observation data for the removal of outliers was not carried out. Table 4 explains that the results from the plotting time series for the campaign data are quite good. One of them is at station N1.3075 which has the farthest observation time range producing a standard deviation value for the N component (north) of 7.45 mm and the E component (east) of 5.14 mm for doy 315 observations in 1996 and for 297 years doy 2013 showed the value of component E was 3.76 mm and component N was 5.8 mm. This value is very good considering that each result is required to have a value of accuracy to the millimeter fraction.

In contrast to the CMAT point which has continuous observational data starting at the end of 2013 until July 2018. In this data there are almost no data outliers. The large number of observational data is one of the reasons this data does not have data outliers, this proves that the quality of the data from observations is quite good and also explains that the more data and meeting points on the trend line will be better. Figure 3 explains that at this station it is necessary to erase the value of outliers in the 2018 observation year which coincides with the occurrence of tectonic earthquakes. This was done because in this study only analyzed strain values before the occurrence of tectonic earthquakes in July 2018.

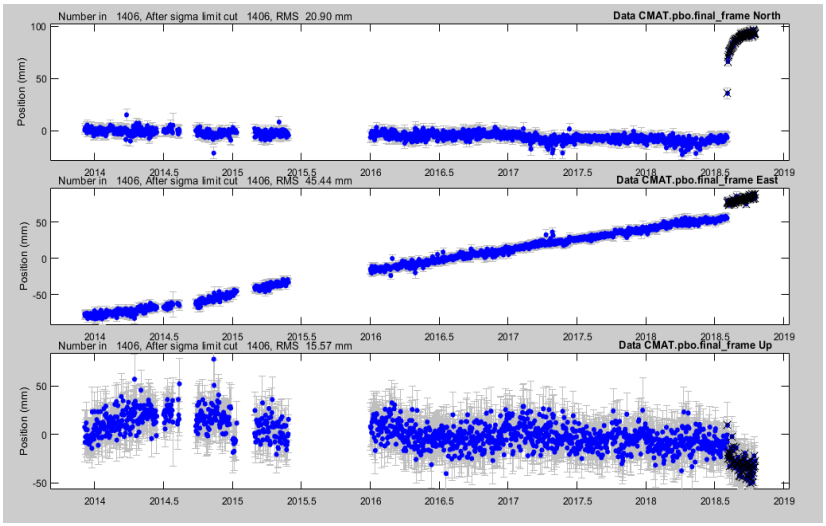

Figure 3. Display Plotting Time Series CMAT station.

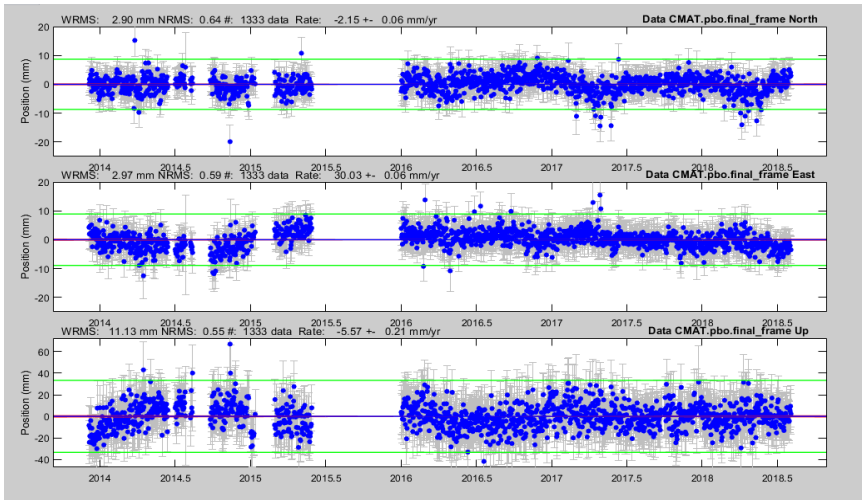

Figure 4. Display Plotting Time Series CMAT station after Outliers removal.

3.2. Velocity Vector Shift Every Observation Point

According to [6] shifting speed is the amount that states the change in a monitoring point in a certain time interval so that it can be an indicator of deformation in the area of observation. To get the velocity value one way is by using the Tsview plugin in the MatLab software. The velocity for each observation point comes from daily coordinates that are free from the value of outliers, where the velocity is calculated in the North and East components. Table 5 explains the velocity value of each observation point with respect to the time of observation of the value of the horizontal component and the magnitude of the error ellipse or standard deviation obtained from the daily coordinates of each observation point that is free from the outlier value. The value of the vertical component is not estimated because it has a very large error ellipse value. All information about deformation on Lombok Island depends on several factors that affect the quality of the results, such as data accuracy, observation geometry, observation strategies, and data processing [8].

Table 5. Velocity and Standard Deviation Every GNSS Observation.

Station	E (meters)	N (meters)	Z (meters)	E velocity (mm/yr)	Uncertainty (mm/yr)	N velocity (mm/yr)	Uncertainty (mm/yr)
KDOO	450298.24	9086319.19	47.69	25.70	0.37	-6.92	0.50
MKYG	418700.56	9087533.35	55.53	27.64	1.63	-3.02	1.65
PGRJ	447465.55	9076145.67	1181.69	25.47	0.88	-5.66	1.56
MPGB	458798.07	9053268.01	73.59	28.74	1.63	-2.70	1.10
MPCR	447530.60	9044217.02	212.68	28.66	0.93	2.04	2.58
N1.3074	429635.90	9045435.03	370.18	26.51	0.17	-5.51	1.93
MTTL	426176.98	9046749.46	44.58	41.22	3.32	2.38	2.37
MTJG	402504.14	9073384.78	52.08	34.50	2.77	5.56	2.65
N1.3075	401080.68	9053511.73	4.04	27.69	1.39	-3.94	2.12
CMAT	400701.85	9051127.16	51.46	30.30	0.06	-2.15	0.06
MMTR	399510.24	9051476.03	12.51	35.27	1.97	-3.17	1.21
MPNJ	416476.93	9033018.94	26.33	42.39	4.57	3.66	5.68
BLMB	398375.04	9035116.38	34.08	29.93	0.31	-2.86	1.27
MDRI	396707.77	9021583.95	38.41	31.76	1.52	-4.89	1.98
MPKT	420385.86	9017491.65	33.27	34.44	3.83	-3.07	4.10
MJRW	442996.13	9022325.64	53.77	29.04	0.95	-4.38	1.83
Average (mm/yr)				31.20	1.64	3.87	2.04

Figure 5 shows that all point vectors are fairly uniform in the southeast direction, this is supported by the recognition of [8] in which part of the Sunda block area is relative to the movement of Eurasia to the southeast. There are two points of view that indicate different directions and large error large ellipses at the MPNJ and MTJG observation points. This is very related to the quality of data carried out systematically on the value of the results of processing. An explanation of the quality of data at the station is discussed in Table 6 and Table 7. The error values explained in columns Se (easting standard deviation) and Sn (northing standard deviation) and time series coordinates are determined in the dN, dE, and dU columns. Table 6 explains the error value at the MPNJ station evaluating the 2014 Doy 29 assessment with a value of Se 6.02 millimeters and Sn 7.99 mm. The MTJG station error value is recommended at the assessment of 100 in 2016 with Se values of 5.82 and Sn 7.14. Table 6 also shows that 100 observations in 2015 are better than 2016 observations, which are shown with a default deviation of less than 5 millimeters in 2015.

3.3. Strain Analysis (strainrate)

The results of this strain analysis use the calculation of the Triangle Strain Algorithm in which this theory uses triangles whose sides are the length of the baseline between one station point and the other. In this study produced 20 models and only 12 models that can be analyzed. The strain values in these 12 models are shown in Table 8. Strain values for compression movements are shown in columns Eigen1 and Eigen2 show the value of extension movements with microstrain units / year (μεx10-6 / year). The smallest value is shown in strain1 model generated from the calculation of observation stations KDOO, PGRJ, and MKYG with Eigen1 value = -0.12 μstrain / year and Eigen2 value = -0.03 μstrain / year. Explanation of the value of this model shows an incorrect value, this is indicated by the Eigen1 value

for the compression motion that should be positive. Thus, producing a very small strain model and resulting strain analysis on this model cannot be done.

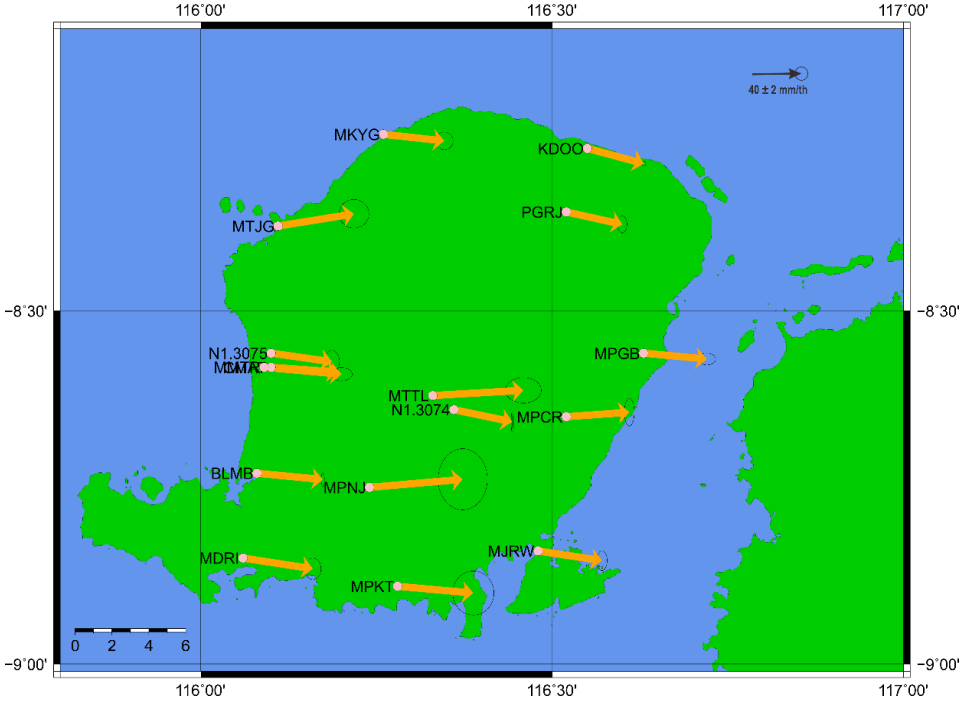

Figure 5. Vector Speed for Each GPS Station. Orange Arrow Shows Direction and Circle Shows Standard Deviation or Elliptical Error.

Table 6. Time Series Coordinates and standard intersections of MPNJ Station.

MPNJ						
dN (milimeter)	**dE (milimeter)**	**dU (milimeter)**	**Se (milimeter)**	**Sn (milimeter)**	**doy**	**year**
3.41	-31.99	-9.09	6.02	7.99	296	2014
-6.85	-4.7	5.92	2.98	3.62	280	2015
1.2	0.75	0.68	4.57	5.96	281	2015
2.23	35.94	2.49	3.46	4.2	93	2016

Table 7. Time Series Coordinates and standard intersections of MTJG Station.

MTJG						
dN (milimeter)	**dE (milimeter)**	**dU (milimeter)**	**Se (milimeter)**	**Sn (milimeter)**	**doy**	**year**
-1.29	-17.37	13.78	4	4.73	100	2015
-3.92	-8.82	-7.4	3.43	4.64	101	2015
-0.3	-16.41	8.06	2.95	3.67	102	2015
-0.63	-18.17	1.56	3.62	4.59	103	2015
2.74	18.64	14.02	3.34	3.93	98	2016
8	17.68	-2.97	3.25	3.82	99	2016
-4.59	24.46	-27.04	5.82	7.14	100	2016

This modeling is also influenced by systematic errors from data quality to produce velocity values, elliptical errors or standard deviations to the value of the strain itself. There are several stations that cannot be used including MTJG, MTTR, MTTL, N1.3075, and MPNJ. The greatest value is shown in the stran12 model resulting from the calculation of observations of MPGB, MPCR, and MJRW stations with an Eigen1 value of 0.7 µstrain / year and an Eigen2 value of -0.22 µstrain / year. This value indicates that there is a large compression due to interactions in the Flores Rear Arc Rise fault which are mutually pressing with the Indo-Australian fault. The existence of the extension value cannot be analyzed with certainty, given the need to know the analysis of the occurrence of movement that shows the existence of extension movements on the base fault that is in the strait base.

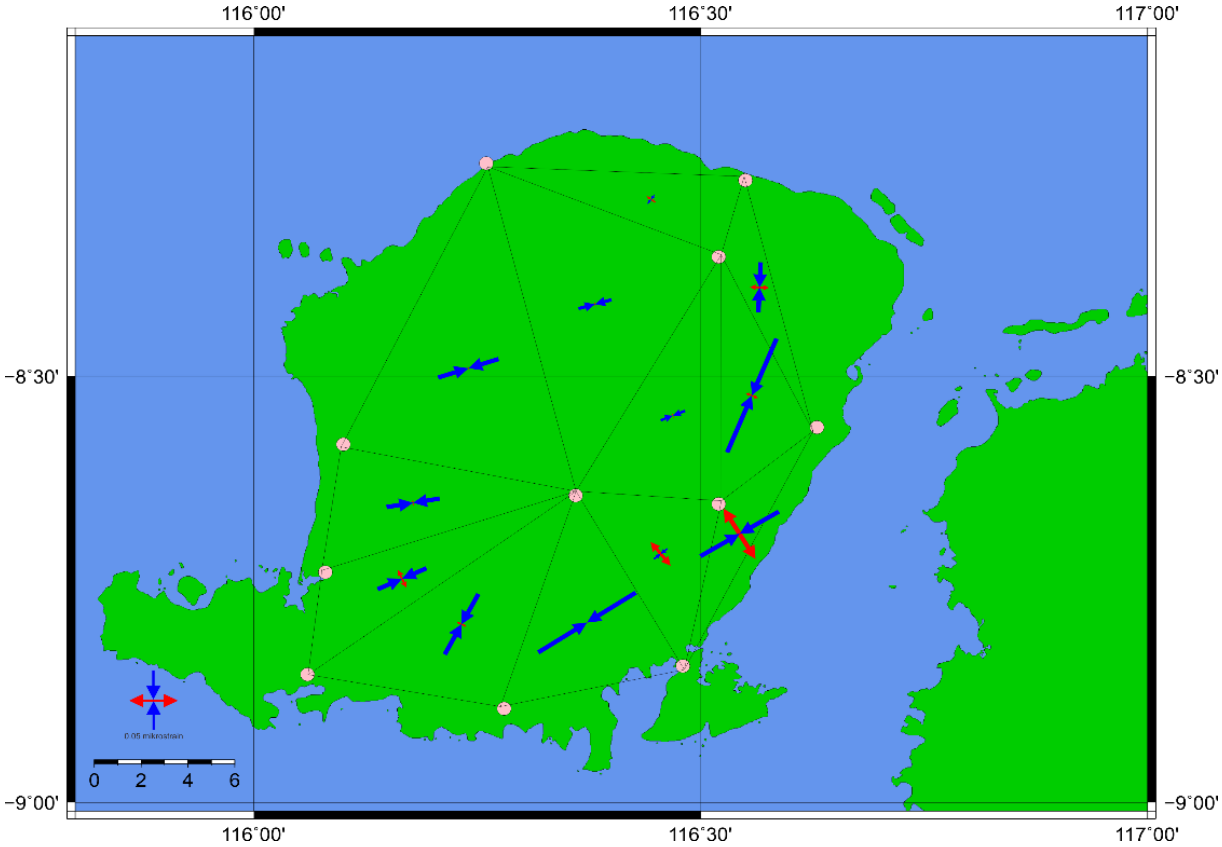

Figure 6. The Main Level of Strain for Each Centroid in A Triangle.

Figure 6 shows the results of strains or strains on Lombok Island. The direction of the red arrow indicates a compression motion and the blue color indicates the extension. Strain analysis shows the extension more indicated by the results of the calculation of 12 strain models. The strain analysis shown in Figure 6 explains that the movement occurring on Lombok Island is largely influenced by the activity of the northern Flores Flores Back Arc Fault and the southern Indo-Australian Subduction. This model also shows the direction of compression strain that leads to the west which explains the influence of the Lombok Strait fault. However, this analysis cannot be ascertained correctly considering the need for data analysis that shows the movement of the Lombok Strait fault itself. The size of the model image is an explanation of the strain calculation results shown in Table 8.

Table 8. Strain Rate.

Triangle Strain	Longitude (◦)	Latitude (◦)	Eigen 1 (mikrostrain/tahun)	Eigen 2 (mikrostrain/tahun)	Azimuth (◦)
Strain 1	116.44	-8.29	-0.12	-0.03	215.94
Strain 2	116.57	-8.40	0.21	-0.13	182.51
Strain 3	116.56	-8.52	0.15	- 0.31	202.39
Strain 4	116.47	-8.55	0.06	-0.06	67.78
Strain 5	116.38	-8.42	0.05	-0.08	74.30
Strain 6	116.24	-8.49	0.05	-0.15	72.09
Strain 7	116.18	-8.65	0.06	-0.13	80.41
Strain 8	116.17	-8.74	0.23	-0.13	245.67
Strain 9	116.23	-8.79	0.12	-0.17	207.86
Strain 10	116.37	-8.79	0.01	-0.28	57.14
Strain 11	116.46	-8.71	0.36	-0.04	51.14
Strain 12	116.54	-8.69	0.70	-0.22	239.01

4. Conclusions

The research result on strain analysis of Lombok Island based on observation data of GNSS in 1996 - 2018 it can be concluded that:

- Velocity of deformation Lombok Island in the period of 1996 - 2018 has an average velocity for E component 31.2 mm / year, N component 3,869 mm / year.
- From the results of the deformation speed it can be seen that the direction of shift for E component goes east and N component to the south. So that it can be concluded that the direction of the shift towards the Southeast, this indicates that the southern subduction movement is relative to the movement of the Eurasian Plate.
- The strain pattern produced in 12 strainrate model shows that compression strain is more dominant, where this strain is affected by the activity of the Flores back arc thrust and Indo-Australian Subduction. The value of the resulting model has a value of 10^{-6}, in this study it is assumed that it cannot be used because it produces a significant strain model.
- Model values were considered in the calculation results of the three observation stations MKYG, KDOO and PGRJ with Eigen1 -1.20x10-7 microstrain / year and Eigen2 -2.82x10-8 microstructure / year. Explanation of the value of this model shows an incorrect value, this is revised to the value of Eigen1 for displacement that gets a positive value. While the value of the model is significant in the calculation results of MTTL, N1.3074, and MJRW observation stations with Eigen1 values 1.14x10-8 microstrain / year and Eigen2 -7.27x10-6 microstructure / year. The result of the variation in the value of the strain model is also by the systematic error of the quality of the data to produce a velocity value, the error ellipse or the standard deviation to the strain value itself.

5. References

[1] Widiyantoro., Zubaidah., and Suhaimi., *Kajian Geodinamika Lombok dan Mekanisme Gempa Yang Terjadi*. *Seminar*, P.S.G.B.G. KESDM., Editor. 2014: Bandung.

[2] Pratama. A., *Monitoring Deformasi Tektonik Pulau Lombok Berdasarkan Data Pengamatan GNSS Tahun 2013 – 2016*, in *Fakultas Teknik Sipil dan Perencanaan, Teknik Geodesi*. 2018 Itenas: Bandung.

[3] Sriyono., *Geologi dan Geomorfologi Indonesia*. 2014, Yogyakarta: Ombak.

[4] Ulinnuha, H., A. Sunantyo, and N. Widjajanti, *Analysis of the July 10th 2013 Tectonic Earthquake effect on the Coordinates Changes of Mentawai Segment Monitoring Station*. JGISE: Journal of Geospatial Information Science and Engineering, 2018. **1**(2).
[5] Geologi, P.V.d.M.B., *Penelitian Pendefinisan Sumber Gempa Bumi di Pulau Lombok, Provinsi NTB*, B. Geologi, Editor. 2016: Bandung.
[6] Andriyani, G., et al., *Kajian Regangan Selat Bali Berdasarkan Data GNSS Kontinu Tahun 2009-2011*. Jurnal Geodesi Undip, 2012. **1**(1).
[7] Abidin, H.Z., *Penentuan Posisi dengan GPS dan Aplikasinya*. 2007, Jakarta: PT Pradnya Paramita.
[8] Bock, Y., et al., *Crustal motion in Indonesia from global positioning system measurements*. Journal of Geophysical Research: Solid Earth, 2003. **108**(B8).

Acknowledgement
We would also like to show our gratitude to the Volcanology and Geological Disaster Mitigation Center and Geospatial Information Agency for providing this research data, and we thank the two reviewers (Sumarno, Ir., M.T. and Rinaldy, S.T, M.T.) for what which is called their insight. We are also very grateful to the academic staff and Geodesy Engineering staff of the Institut Teknologi Nasional Bandung, for their support.

Remote Sensing Data for Atlas of Volcanic Landscape Resources

Fakhruddin Mustofa[1]*, Mulyanto Darmawan[1], Amanah Anggun Prabandari[1], Zidni Farhati Silmi[1]

[1]Center for Spatial Planning Mapping and Atlas, Geospatial Information Agency, Jakarta-Bogor Street Km.46, Bogor, Indonesia

*Corresponding author's e-mail: mustofa@yahoo.com

Abstract. The existence of volcanoes is often associated with disasters. It cannot be avoided because volcanoes will always carry out eruption activities. The bigger the eruption means more victims, loss of property, and infrastructure damage. In the other side, there are many positive impact of the existence of active volcanoes in Indonesia. One of them is the wealth of land resources that scattered in the volcanic landscape. These resources are forest resources, springs, plantations and fertile agriculture also cultural wealth around volcanoes. In the context of the Sustainable Development Goals, the existence of the mountain become the highlight of the Goal 15 : "Life on Land". Goal 15 target 15.4 is "By 2030, ensure the conservation of mountain ecosystems, including their biodiversity, in order to enhance their capacity to provide benefits that are essential for sustainable development". Based on these targets, ecosystems and land resources are important parts that need to be maintained. In the other side, land degradation is still occured, such as a deforestation rate. This is a contradiction with the target of SDGs. As part of an effort to support this target, geospatial information is needed to provide an overview of volcanic land resources, one of them is atlas. Compilation of this Atlas use integration method between remote sensing data, spatial data, and survey. The result is "Atlas of Eastern Java Volcanic Landscape Resources", which can be guidance about land resources condition of 3 (three) volcanic area : Mount Kelud Area, Mount Bromo-Semeru Area, and Mount Ijen Raung Area.

Keywords: Remote Sensing, Spatial, Atlas, Volcanoes, Landscape.

1. Introduction

Indonesia has 129 active volcanoes that stretching from the tip of Sumatra, Java, Bali, Nusa Tenggara, Banda Islands and Maluku, to northern Sulawesi. This amount is almost occupying 30 percent of the world's alignment of volcanoes known as "ring of fire". Its existence cannot be separated from the impact of three tectonic plates in Indonesia. No wonder, the incident after the disaster of volcanic eruptions often occurs in the archipelago. The impact of the eruption often caused losses in the form of casualties, property losses, and infrastructure damage. But the existence of volcanoes in Indonesia is not only seen as one of the sources of disaster, but is a blessing of nature for the lives of living creatures around it [1]. Furthermore, after the danger period has passed, volcanoes provide benefits or luck to the surrounding community [2].

A source of blessing for life is abundant natural resources around the landscape of volcanoes, both from the peak landform (crater / caldera) to the slopes of its feet. These resources include forest resources, springs, plantations and fertile agriculture, as well as thousands of cultural wealth around volcanoes that have remained sustainable today. In each form of volcanic land, natural resources are stored that need to be known by the public in order to have a good understanding of the importance of their existence. The importance of volcanoes is highlighted in the Sustainable Development Goals. Based on Goal 15 "Life on Land", especially Target 15.4 "By 2030, ensure the conservation of mountain ecosystems, including their biodiversity, in order to enhance their capacity to provide benefits that are essential for sustainable development". Based on these targets, ecosystems and land resources are an important part that all parties need to preserve. Identifying spatial information on each

ecosystem is important so that the resource is sustainable according to the mandate of the SDGs until 2030.

The use of remote sensing data to identify landscape information is an important part of supporting the goals of the SDGs. Components of landscape content consist of landscapes and cultural landscapes [3]. Remote sensing datas are ranging from medium to high resolution which are very supportive for identifying both components. The form of presentation of this information can be tangible of spatial data, image maps, thematic maps of natural resources as a result of image interpretation, DEM (Digital Elevation Model) volcanoes, and intensive analysis of narrative information packaged in the form of atlas. Atlas is a collection of geographic and coherent data and information. Through the atlas media, it is expected that most information about the landscape of land resources is conveyed to the public systematically and chronologically between the contents of the atlas.

An important part of the landscape of volcanic land in Indonesia is located in eastern Java, starting from the Mount Kelud Area, Mount Bromo-Tengger-Semeru Area, to the Mount Ijen Area and its surroundings. The volcanic activity of the three mountains is still intensive. In the other side, natural resources are very abundant for the lives of the surrounding community, in the form of forests, plantations and agriculture, abundant water. The tourism sector is growing rapidly in all three volcanic area. Mulyaningsih, 2015 [4] emphasizes that there are at least two main resources from volcano, namely resources for the development of science and technology or scientific benefits, as well as resources to increase income. From the ecological aspect, volcanoes are useful as soil fertilizers, hot springs, rain-forming factors, and water stores [5].

Based on the background above, a study and efforts to identify the landscape of volcanic land resources are needed. This study aims to identify the landscape of the third area of the volcano, the form of land and general resources in it, starting from the crater to the slopes of the volcanic foot. The use of multiresolution remote sensing data is very necessary to obtain information on the extent of land resources in the three areas. The results of the identification are manifested in an Atlas of Eastern Java Volcanic Landscape Resources, in the form of prints and e-books. In the end, literacy about the span of volcanic land resources became one of the important outcomes of the results of this study.

2. Data and Method

2.1. Data

Atlas contains maps, images, pictures, and narratives which are arranged systematically. The data used in the preparation of the atlas includes Geomorphology Map on scale 1: 1,000,000, Indonesian Topographic Map of Eastern Java Region on scale 1:50.000, SRTM Imagery, Landsat 8 OLI Image path / row 117/65, 117/66, 118/65, 118 / 66, 119/65, 119/66 composite 567 to highlight the topographic aspect, SPOT 6 imagery, secondary data related to resources, and data from field survey results: observations & results of drone shots in the sample area.

2.2. Method

This atlas illustrates various potential land resources in the volcanic area. The research location focuses on the type A volcano area in Eastern Java. Type A volcano is a volcano which has been recorded as having erupted or having magmatic eruptions at least once after 1600. Type A volcanoes in Eastern Java include Kelud volcanoes, Arjuno-Welirang, Bromo, Semeru, Lamongan, Raung, and Ijen. Furthermore, the grouping of volcanic areas was carried out based on the proximity of the location, into the volcanic area Kelud-Arjuno-Welirang, Bromo-Tengger-Semeru-Lamongan, and the Ijen-Raung area.

Geomorphological maps and remote sensing data are used to identify landscape conditions in general and the interpretation of semi-detailed landscape units. This landscape unit is used as a basis for analyzing land resource potential and determining the location of sample points. In addition to using spatial data, identification and analysis of land resources also utilizes non-spatial secondary data, such as articles and books. The survey was conducted to observe the potential of volcanic land resources in

the field. The sample points are based on the landscape units that have been identified, starting from the cone, upper slope, middle slope, lower slope, foot plains, and alluvial volcanic plains.

2.3. General Flowchart

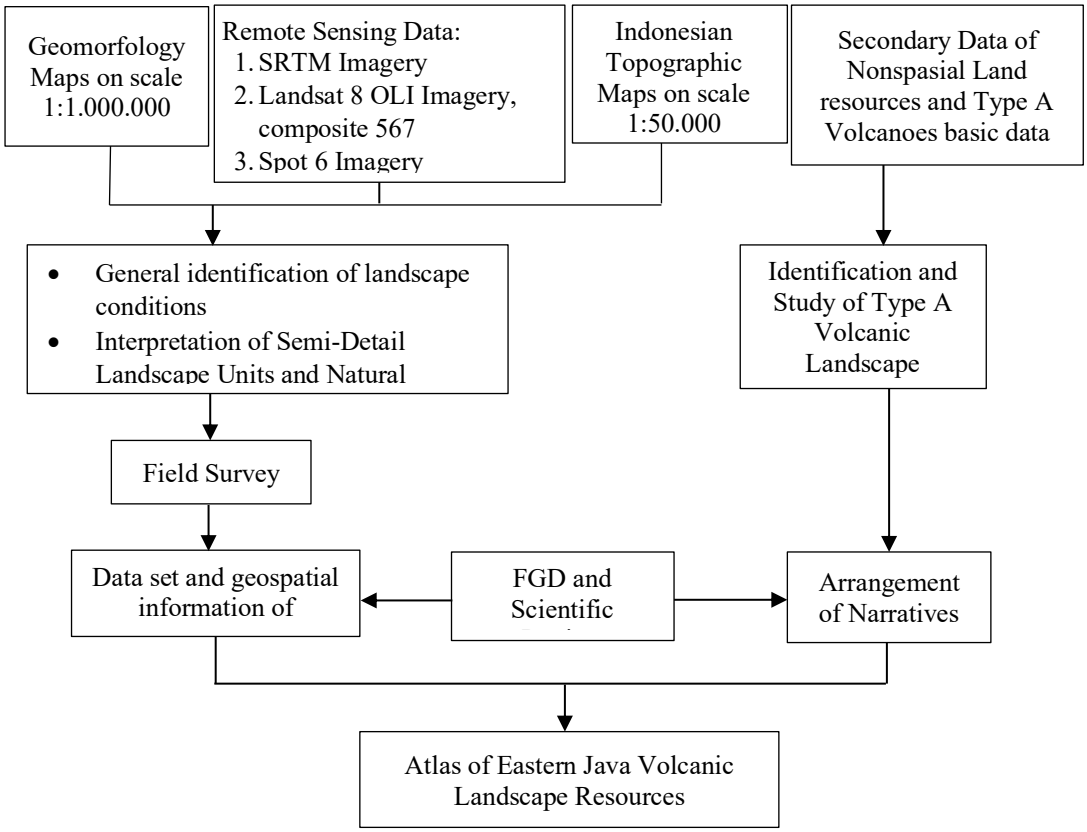

Figure 1. General Flowchart of the Atlas Production Method.

2.4. Study Area

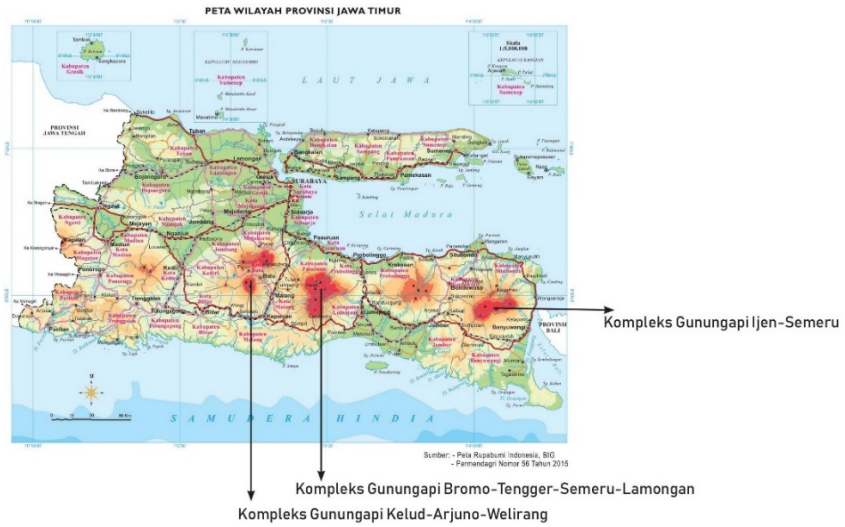

Figure 2. Study area.

2.5. Atlas Presentation Structure

One of the advantages of atlas is its structured presentation, interrelated between each part. This is because the basic consept of an atlas is not a single map, but rather the integration of various maps forming certain thematic geospatial information. The Atlas Range of Volcanic Land Structure structure is presented in Table 1 below.

Tabel 1. General Atlas Presentation Structure.

Part	Contents Information
The beginning	Book Start Page
	Foreword
	Welcome Speech
	Table of Contents
	Geospatial Information Landscape of Java Island
	Landscape Resources of Eastern Java Volcano
Fill in	Landscape Resources of Kelud and Arjuno Welirang Volcano
	Landscape Resources of Bromo-Tengger-Semeru and Lamongan Volcano
	Landscape Resources of Ijen-Raung Volcano
Closing	Invitation for Conservation ofcVolcanic Land Resources
	Data Sources and Glossaries
	Index
	References

3. Results and Discussion

3.1. General Condition of Landscape

In a regional context, in general the central zone of Java is a volcanic landform, both classified as type A or type B. These landscapes are consist of some volcanoes start from Lawu to Ijen-Raung area is in the central zone of the Eastern Java Geomorphology. Most of volcanoes in Eastern Java are located in East Java Province. The three study areas in Eastern Java are type A volcanic area or volcanoes which have been recorded having magmatic eruptions at least once since AD 1600. For example, Mt. Kelud erupted on February 14, 2014. The impact of that eruption even reached Yogyakarta and several airports were closed due to the effects of volcanic ash. From the map information in Figure 3 below, is clearly described the central zone of Java in general is a volcanic landscape.

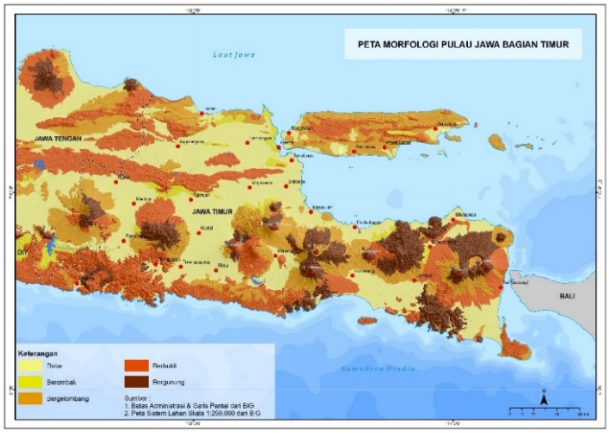

Figure 3. Middle Zone of Eastern Java is Volcanic Landscape.

There are two aspects of volcanic landform in Eastern Java which are physical landscape and cultural landscape that need to be described. The discussion about volcano isn't limited to the physical aspect, but a volcano has become an inseparable part and become a social-economic and a cultural life for Eastern Java society. Many social, economic, and cultural activities are closely related to the existence of volcano. For the example some temple relics around Mt. Kelud and their religious ceremony. Another example is a mountain tourism that become an economic generator for the local people.
Physical and cultural landscapes of three volcanic area are resource assets that have a positive impact on environmental sustainability. The discussion isn't clearly separated, but integrated with each other. Resources assets (both physical and cultural), starting from the crater / caldera to the foot slope are abundance of fores resources, plantations and agriculture, water resources, mineral resources, and cultural resources that invaluable. In this context, the integration between landscape and its resources use the term: landscape resources.

3.2. Landscape Resources of Kelud - Arjuno – Welirang Volcanic Area

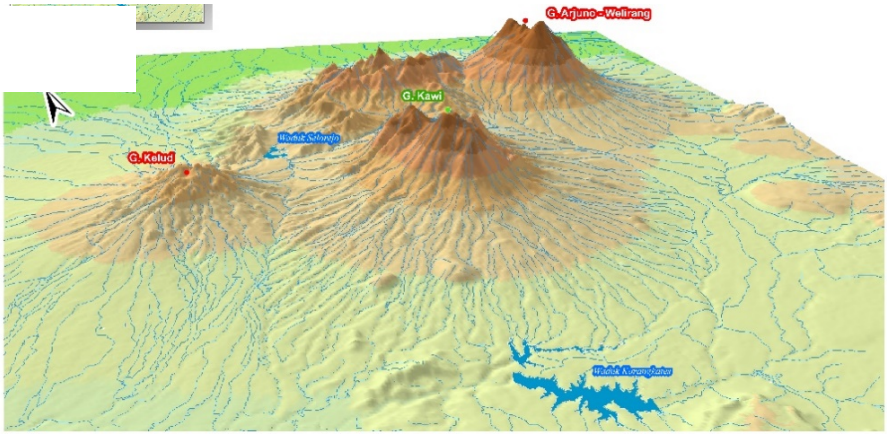

Figure 4. 3D Imagery of Kelud and Arjuno – Welirang Volcanic Area.

Volcanic landscape of Mt. Kelud and Arjuno-Welirang (include Mt. Kawi and Butak) are in Kediri, Blitar, Malang, Batu, Jombang, Mojokerto, and Pasuruan Region. Volcanic activities in Mt. Kelud - Arjuno-Welirang are still intensive (type A), while Mt. Kawi and Butak are relatively inactive (type B). Those volcanoes are nearby, separated by inter-mountain valleys around Batu City, Pujon, and Ngantang.
The impact of the existence of these volcanoes make these areas very fertile and rich of natural resources. One of the important natural resources for life are ground water, springs, and surface water. Spesifically the surface water as seen from the data in Figure.4 is three dimensionals data which show surface flow pattern sourced from those volcanoes to the Brantas River. It means those volcanoes are upstream and water source for life. Flow pattern of Brantas river is quite unique because it surrounds those volcanoes before finally ending in Sidoarjo region. A sufficient water supply from the upstream area makes the Brantas river become an epicodic stream flowing throughout the year. Water from Brantas river is mainly used to irrigate rice fields that flowed from some dams, especially in the middle and downstream. For example is Ir. Sutami or Karangkates dam that can irrigate thousands hectares of rice fields.
At certain points, the part of the flow pattern is a waterfall because of the extreme difference between grooves. Waterfalls are mainly located in the middle slope and foot slope of volcano. In the local term, waterfall is called "Coban". Some examples of waterfalls that easily accessible and become tourism place are Coban Rondo, Coban Talun, Coban Putri, Coban Sewu, Coban Manten, and Coban Kethak. The existence of waterfalls is not only seen from the physical aspect but has aroused local tourism. For

example, Batu City which are very crowded because of mountain tourism. The local government relies on tourism as a source of regional revenues.
Other abundant natural resources are forest, agriculture, and plantation. The forest usually is located around the crater and upper-middle slope of the volcano. The existence of a forest is important in maintaining mountain ecosystem. Agricultural land and plantation are located in foot slope to aluvial plain. Volcanic ash from Kelud eruption fertilized those land. Landuse digitazion from SPOT imagery and field survey shows that in the foot slopes of those volcanoes are mainly plantation and agriculture area. Plantation areas can be seen in Figure 5. Some plantation products in these regions are coffe, cloves, rubber, chocolate, and sugar cane which have been cultivated since Dutch colonial period. One of those plantations is coffe plantation in Karanganyar, Blitar Region (southern Kelud), shown in Figure 6.

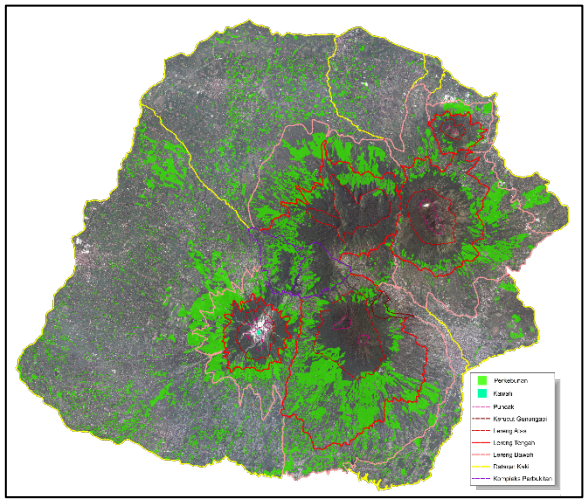

Figure 5. Green is a Plantation Areas.

Figure 6. Coffee Factory Since the Dutch Period.

Mineral resources that are found around Mt. Kelud are sand mining. Sand comes from the volcanic mudflow of Kelud, flowing to the west on Bladak river. Thousand tons of sand are mined in this river is mainly for building materials supply in Kediri, Tulungagung, and surrounding regions. The result of field survey using drone (Figure 7) around the Bladak river showed that residents were mining sand and several trucks were carrying sand. These natural resources have positive impact on local people as a source of income. But mining activities should consider the environtmental aspects and minimize the landslide.

Figure 7. Drone Imagery of Sand Mining in Bladak River, Western Kelud.

In cultural context, foot slope landscape of Kelud was the central area of Hindu – Buddhist kingdom. It is used to be the core center of Javanese civilization around 929-1486 [6]. Most of the royal relics are temples and waters / ponds that are well maintaned. The existence of temples around volcano isn't separated from Hindu-Buddhist belief that place with high topography is a holy place. Some temples were even founded below the surface due to sedimentation from volcanic activity and alluvial processes. Examples of the temple are Penataran Temple, Dorok Temple, Gambarwetan Temple, Sawentar Temple, Sumberagung Temple, Wringinbranjang Temple, Sirahkencong Temple, Tepas Temple, Songgoriti Temple, and Plumbangan Temple.

3.3. Landscape Resources of Bromo – Tengger - Semeru Volcanic Area

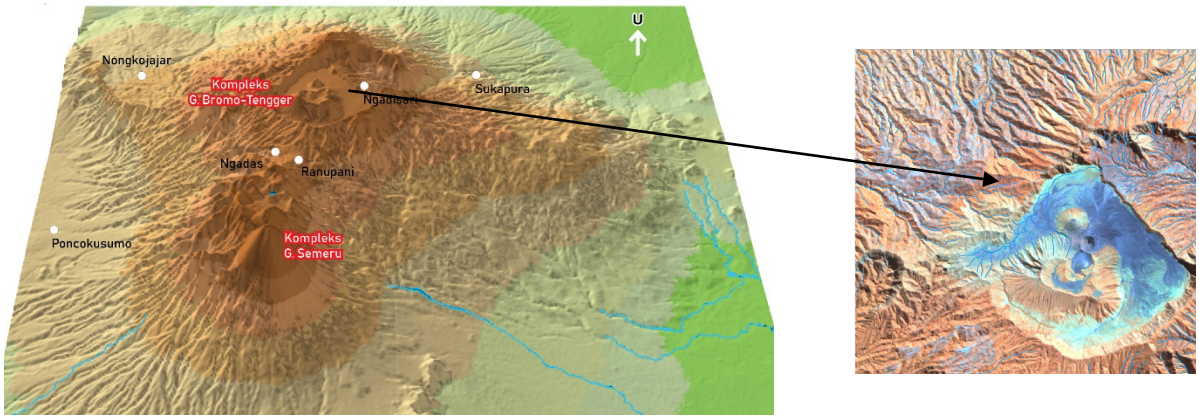

Figure 8. 3D imagery and Landsat 8 in Bromo – Tengger caldera.

Bromo – Tengger - Semeru landscape is very stunning from every sides. One interesting side is Penanjakan (2.100 m asl) among Cemorolawang, Ngadisari, Probolinggo Region. Everydays at dawn, many tourists enjoy the sunrise, due to the landscape factor in this active volcano area. From Penanjakan's observation point, there is a large caldera (8 x 9 km) with active volcanoes in the middle, one of them is Bromo volcano. Volcanic activity which is still occurred is a forming of several Bromo volcano cone and its surrounding. The large caldera is formed by several periods of the great eruption of Old Tengger Volcano thousand years ago. The Bromo caldera is younger than the previous caldera formation around Ngadisari [7]. On the southern part outside the caldera, there is Semeru Volcano which is the highest mountain in Java.

Figure 9. 3D imagery of waterfalls around Bromo, Tengger, and Semeru Volcanoes.

The land resources wealth outside of Mt. Bromo-Tengger caldera and around Mt. Semeru is a gift for the local people, such as forest resources, water, mineral, plantations, and agriculture. Forest resources

are controlled of Bromo-Tengger-Semeru National Park Office. From Landsat imagery, the dense forest area is on the upper and middle slopes of Semeru and the southern Bromo caldera. Forests on those volcanoes become a water resource for their lower areas. Several waterfalls (Coban) which are having quite heavy can be found on the middle and lower slopes of Bomo, Tengger, Semeru Area (Figure 9). These Cobans become tourism magnet and improve local economy.
Some intensive agriculture lands and plantations are generally located in northern, western, and eastern Bromo caldera. Some agricultural products are onion, potato, carrot, cabbage, mustard green, and chili. From the field observation, agricultural activities are usually carried out on quite steep or steep (45-80%). For example in Ngadas Village, Argosari Village, Tosari Village, and Ngadisari Village. Agricultural products an income for local people, but landslides also threat for them. Some landslides often occur on these agricultural areas.

Figure 10. Drone imagery of steep slope agriculture in Ngadas, Malang.

Cultural landscape of Bromo can't be separated from the existence of Tengger Tribe who lives around Bromo caldera. Bromo Volcano is integrated with Tengger's life. Tengger Tribe lives in Malang, Pasuruan, Probolinggo, and Lumajang Region. During a certain period, they held a sacred ceremony in Bromo crater and become an attractive and a popular tourism. Some of Tengger Tribe communities live in "enclave" Bromo-Tengger-Semeru National Park, like in Ngadas Village, Malang Region and Ranupane Village, Lumajang Region (Figure 11).

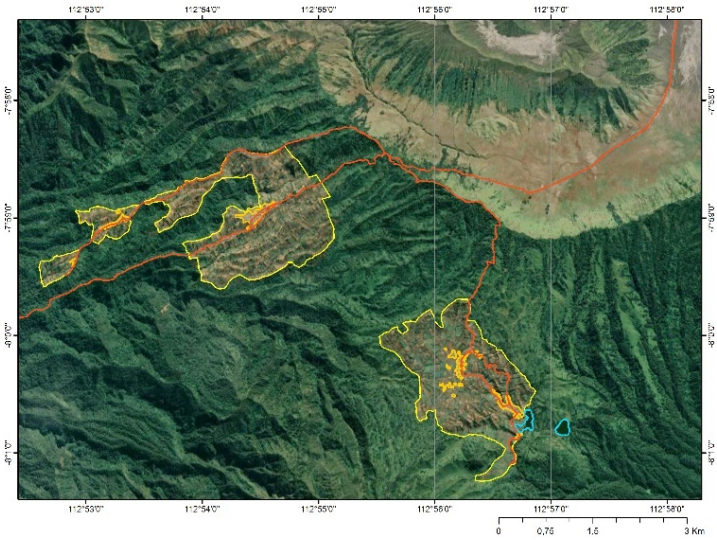

Figure 11. Tengger's settlement and agricultural land in Ngadas and Ranupani (yellow polygons).

Lamongan Volcano (1671 m asl) is located in Eastern Bromo-Tengger-Semeru Area. The description about Lamongan volcano landscape resources can't be separated from the existence of volcanic lake. Many holes aprroximately 100 – 800 meters in diameter forming some small lakes around Lamongan Volcano. Those holes are formed by volcanic process that occured for thousand years. In earth science, known as 'maar'. Many holes filled with water become natural lakes that contain fish and source of irrigation. Maar or Ranu give economic impacts for local people. Many important benefits from these holes affect local people especially in Klakah, Ranuyoso, Ranuagung (Lumajang Regency) and Tritis (Probolinggo Regency). Agriculture, fishery, and tourism are three main sectors in Ranu utilization. They give positive impact especially increasing the community prosperity and economy.

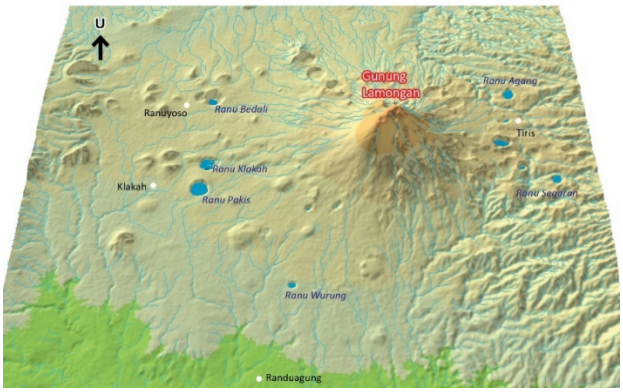

Figure 12. Lamongan Volcano and Maar.

Table 2. Distribution of Type 'Maar' Lakes Around Lamongan Volcano.

No	Name	Coordinat		Location	Landcover
		S	W		
1	Ranu Pakis	7^0 59' 54"	113^0 16' 22"	Klakah, Lumajang	Watery
2	Ranu Klakah	7^0 59' 08"	113^0 16' 17"	Klakah, Lumajang	Watery
3	Ranu Lading	8^0 00' 31"	113^0 18' 45"	Klakah, Lumajang	Watery
4	Ranu Yoso	7^0 56' 59"	113^0 15' 55"	Ranuyoso, Lumajang	Farm
5	Ranu Air	7^0 56' 42"	113^0 19' 21"	Ranuyoso, Lumajang	Shrub
6	Ranu Bedali	7^0 57' 03"	113^0 16' 16"	Ranuyoso, Lumajang	Berair
7	Ranu Gunungparang	7^0 55' 39"	113^0 18' 39"	Ranuyoso, Lumajang	Moor
8	Ranu Wurung	7^0 56' 08"	113^0 18' 50"	Ranuyoso, Lumajang	Moor
9	Ranu Kembarsalak	8^0 00' 29"	113^0 19' 25"	Ranuagung, Lumajang	Watery
10	Ranu Wurung/Legung	8^0 02' 31"	113^0 18' 25"	Ranuagung, Lumajang	Watery
11	Ranu Semokah	7^0 56' 39"	113^0 20' 42"	Tiris, Probolinggo	Shrub
12	Ranu Kembar (1)	7^0 57' 02"	113^0 21' 50"	Tiris, Probolinggo	Shrub
13	Ranu Kembar (2)	7^0 57' 06"	113^0 22' 09"	Tiris, Probolinggo	Shrub
14	Ranu Katak	7^0 55' 58"	113^0 21' 79"	Tiris, Probolinggo	Moor
15	Ranu Gedang	7^0 56' 30"	113^0 22' 49"	Tiris, Probolinggo	Watery
16	Ranu Segaran	7^0 57' 03"	113^0 23' 43"	Tiris, Probolinggo	Watery
17	Ranu Betok	7^0 57' 54"	113^0 23' 35"	Tiris, Probolinggo	Watery
18	Ranu Agung	7^0 58' 36"	113^0 23' 26"	Tiris, Probolinggo	Watery
19	Ranu Segaranmerah	7^0 59' 23"	113^0 23' 48"	Tiris, Probolinggo	Watery
20	Ranu Segaranduwes	7^0 59' 45"	113^0 24' 36"	Tiris, Probolinggo	Watery

In agriculture sector, some Ranus are the irrigation source for fieldrice, such as technical irrigation from Ranu Klakah and Ranu Pakis managed by Public Works and Water Resources Office, East Java Province. Those Ranus supply water for rice fields around Kalakah Subdistrict. Water flowing heavily through outlet toward irrigation which are located in southern Ranu Pakis and western Ranu Pakis. Second sector is fishery: fishpond and fishing pond. Fisheries business raises the local economy. One of the indicators is the fish supply in markets around Klakah is from fishpond in Ranu.

3.4. Landscape Resources of Ijen-Raung Volcanic Area

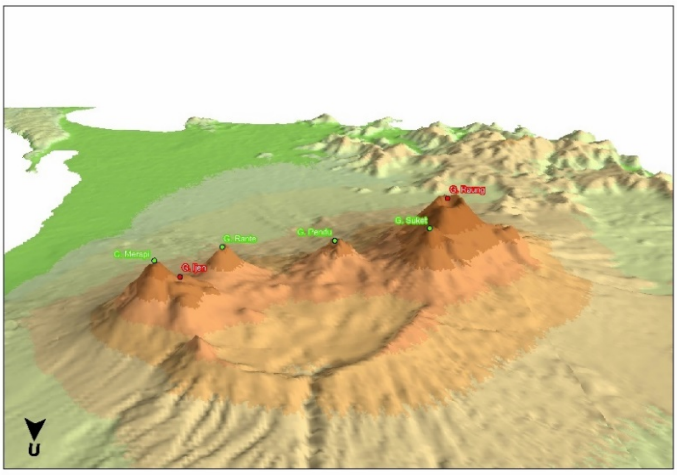

Figure 13. Ijen-Raung Volcano Area.

Administratively, the Ijen-Raung Volcano area is located in four districts in East Java, which are Banyuwangi, Bondowoso, Situbondo, and Jember. There are at least 2 large regional areas, called the Ijen and the surrounding volcanic cones and the Raung Volcano area. The first area is classified as ancient volcanoes which have erupted violently leaving traces of eruptions in the form of oval-shaped Ijen caldera measuring approximately 14x16 Km. The traces of ancient volcanic cones can also be seen from intermediate resolution of remote sensing images, in the northern part of the caldera there is still a relatively perfect cone shape.

Volcanic activity still occurs around the caldera, at least can be observed Ijen crater (Figure 14). From the bottom of the crater is still continuously producing solfatar smoke in high intensity and is quite dangerous for human breathing. Sulfur chunks are produced from the crater. These sulfur mineral resources are a source of livelihood for traditional miners. Sulfur is brought down from the top of Ijen downward by foot for approximately 2.5 Km. This activity back and forth becomes a part of interesting attractions, in addition to the bluefire phenomenon around the crater.

The extensive stretch of the Ijen caldera (approximately 1/3 of the total area of DKI Jakarta Province) is a dry zone. But on the north side in the central area of Sempol, there are resources in it, including coffee plantations, dry land agriculture, and hot springs. The Arabica type of coffee is in a high quality and is one of the culinary attractions in Ijen. Dryland farming is often found in Asembagus, part of ancient volcanic cones on the northern side of the Ijen caldera. This area has a small rainfall intensity, making it famous as the driest area on Java. While many plantation resources are located on the south and east side of the Ijen-Raung Volcano Area in the Banyuwangi Regency area (Figure 15).

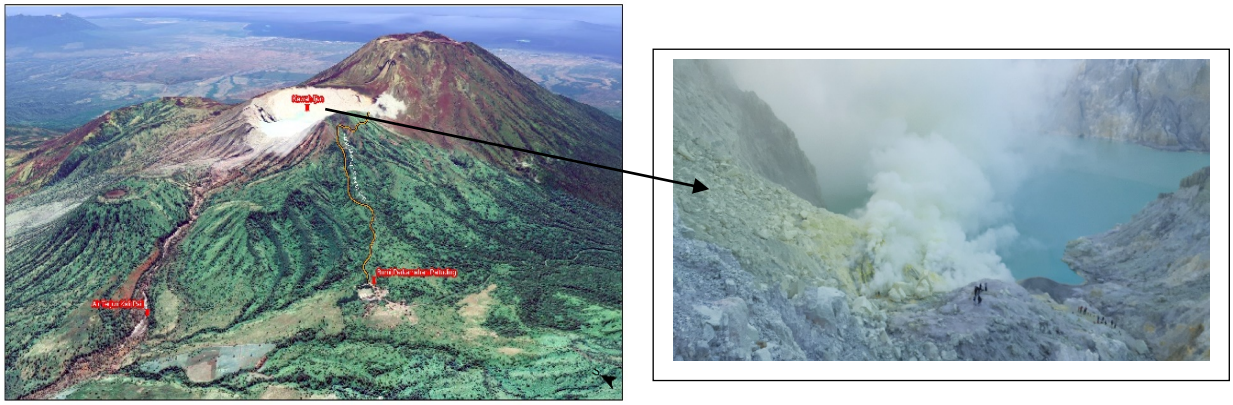

Figure 14. 3D satellite imagery of Mount Ijen and sulfur resources in the Ijen crater.

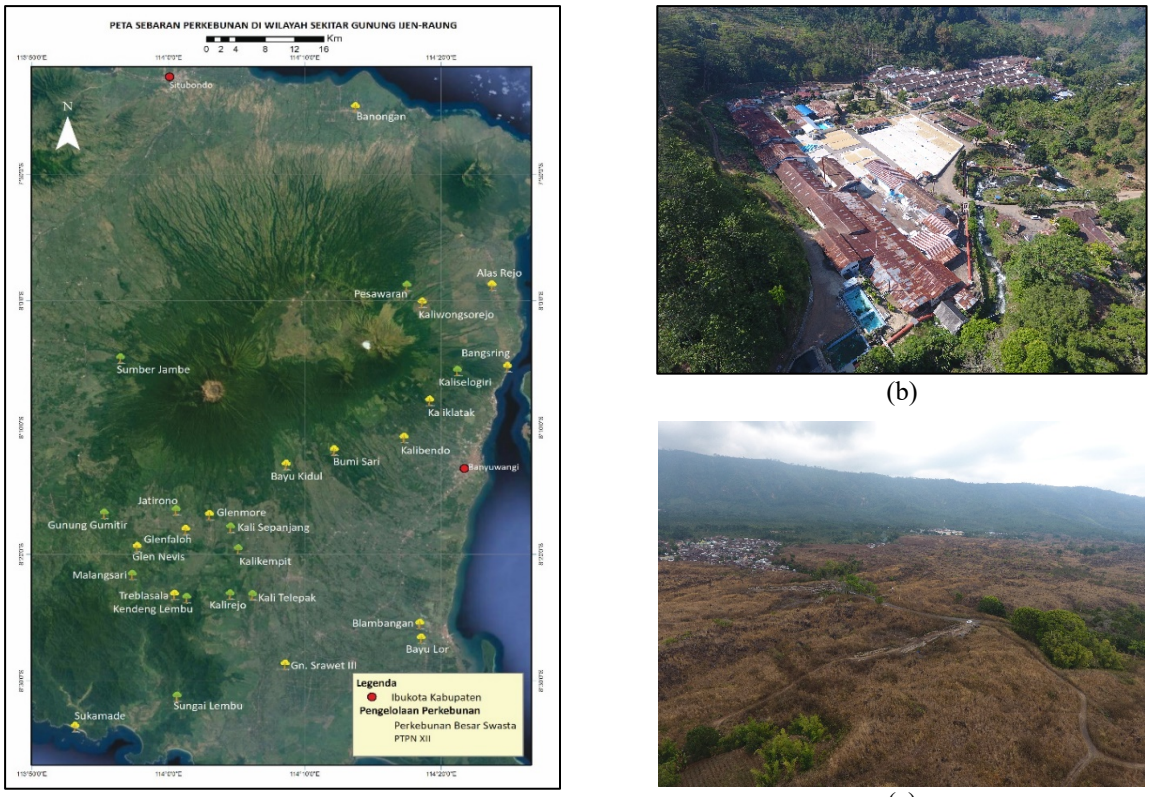

(a)

(b)

(c)

Figure 15. (a) Distribution of plantation resources on the south and east side of Ijen-Raung; (b) Drone Imagery of Coffee Factory of PTPN XII Belawan; (c) Drone Imagery of Ijen Dry Zone.

4. Conclusions

- Atlas of Volcanic Landscape Resources as an important part of delivering geospatial information related to land resources volcanoes as well as a platform for geoliteration for the public, especially for education, tourists and prospective tourists who will visit the volcanic region.
- Extraction of information on land resources from multiresolution remote sensing images is more maximal. Medium resolution satellite imagery can recognize volcanic areas on a

regional basis, while high resolution satellite imagery can recognize phenomena in more detail.

- The landscape of the volcanic area in Eastern Java can be considered not limited to the landscape, but it is integrated with its cultural landscape due to many people live around the volcano.

5. References

[1] Naryanto, S.P.N., Lilik K and Ikawati *Indonesia diantara Berkah dan Musibah*, M.o.R.a.T.o.t.R.o. Indonesia., Editor. 2009.
[2] O, A. and Priatna, *Lempeng Tektonik, Ancaman Bencana, dan Kreativitas Budaya. Hidup di Atas Tiga Lempeng Gunung Api dan Bencana Geologi.* 2014: Bandung.
[3] Santoso, L.W. and L. Muta'ali, *Bentang Alam dan Bentang Budaya*, ed. P.K.K.L.P. Bentanglahan. 2014, Gadjah Mada University Press.
[4] Mulyaningsih, S., *Vulkanologi.* Yogyakarta: Ombak Publisher, 2015.
[5] S., S.O., *Ekologi, Lingkungan Hidup dan Pembangunan.* Jakarta: Djambatan Publisher., 2004.
[6] Rahardjo, S., *Peradaban Jawa dari Mataram Kuno sampai Majapahit Akhir.* Jakarta: Komunitas Bambu Publisher., 2011.
[7] Verstappen, H., *Garis Besar Geomorfologi Indonesia.* Gadjah Mada University Press, Yogyakarta., 2014.

Acknowledgments

The author's team would like to thank to Prof. Dr. Junun Sartohadi and the UGM Team, Dra. Niendyawati, M.Sc., and the Technical Team of the Field of Atlas and Social Mapping of the Geospatial Information Agency, who have worked together to complete the Atlas of Eastern Java Volcanic Landscape Resources book.

Updating Homecoming Route Map (Case Study: Java and Bali Islands)

Arief Rahman Hakim[1]*, Soni Darmawan[1]

[1]Department of Geodesy Engineering, National Institute of Technology, 23 PH.H. Mustofa Street, 40124 Bandung, Indonesia

*Corresponding author's e-mail: ariefrahmanhakim06@gmail.com

Abstract. Homecoming is a necessity, and as if an obligation if left there will be something missing when the Eid Mubarak arrived. Though homecoming was not identified in religious teachings, in other words, it was an indigenous tradition and culture that developed in Indonesia Generally homecoming was carried out by all Muslims who were overseas or live far from their hometowns. In carrying out homecoming, a homecoming map was needed as a consideration in determining the homecoming route to be taken as well as supporting information in helping homecoming. Currently, there were two versions of the map made by Itenas Bandung, but it must be updated to be used by users. The purpose of this research was to analyze the elements must be changed, identify aspects that need to be considered so that visualization of the cartographic map design of the homecoming was obtained by the cartographic rules and made evaluations of the results from updating homecoming route maps through the making of questionnaires. The method used was the identification of elements needed in updating, by processing data in stages starting from classification, editing, and generalization, adding supplementary information, to collecting questionnaires as an evaluation material for homecoming map 2019. The results of this research were in the form of visualization of cartographic designs of the homecoming maps of Java and Bali in 2019 which have been added by considering the cartographic aspects and evaluating them by digitally collecting questionnaires.

Keywords: Homecoming, Homecoming Map, Updating, Visualization of cartographic design, Evaluation.

1. Introduction

Homecoming is a necessity, and as if an obligation if left there will be something missing when the Eid Mubarak comes. Though homecoming was not identified in religious teachings, in other words, it was an indigenous tradition and culture that developed in Indonesia [1]. Generally, homecoming was carried out by Moslems who were overseas or live far from their hometowns. This habit was carried out at 7 days before Eid to 7 days after it. The duration of people's homecoming and returning process is different each other. It was depended on the vacation period given by their work place in the city. The period of the week before Eid to a week after was the longest time used by homecomers [2].

According to the Ministry of Transport, the number of homecomers in 2018 was estimated at 19.5 million people [3]. According to the prediction, the possibility of homecomers in 2019 will be around 19.5 million. With a large number of Indonesian homecomers, it would be better if this moment was prepared earlier in order to minimize the accident and traffic jam increasing. The accident occurred during Eid holiday in 2018. For instance, until four days after Eid (Tuesday, June 19, 2018), there were 1559 accidents dominated by land route cases. Besides, the accident occurred during Eid holiday has killed 346 people. But, the number has decreased since last year. It was stated by the Public Relation Divison of National Police Headquarters quoted by [4].

Based on the available data, there were 10 congestion-prone points in Java Island during homecoming flow in 2018. The first congestion point was along Cikampek toll road. The second one was in the path after Nagreg, precisely in Malangbong Garut route, Limbangan Kendal route, and Linkar Gentong Tasikmalaya. The fifth was Gandulan or Kertasari. Furtermore, the congestion point was in Kalikuto

and Krapyak Semarang. After that, there was also in South Brebes to Purwokerto, in Tonjong Market precisely. Then, the last two ones were at Merak-Bakauheni and Gilimanuk-Ketapang crossings. Those crossings areas were prone for congestion because there was a long line leading to crossing location. It was stated by the Head of the Traffic Corps of National Police, Irjen.Pol. Royke Lumowa and quoted by [5].

There are various steps taken to minimize traffic accidents and reduce traffic jams. One of them is making and updating homecoming atlas map in some regions in Indonesia, including Java and Bali Island. Homecoming atlas map updating is a process to update the map in 2019. In this case, it updates various informations about Java and Bali Region such as the information related to spatial and other supporting information.

The previous study was conducted by [6] in 2018 about "Kajian Aspek Kartografis Peta Mudik 2018". The data used in the study were spatial and attribute. In the research, the data were processed trhough some steps. It was started from collecting data, selecting and data generalization in order to present suited map with the users' necessity. Editing data used ArcGIS software, and classifying the homecoming route in accordance with Law Number 38 of 2014 concerning Roads. Thus, this research produced "Homecoming Map 2018" as the second version of same map issued by GeoSpatial Information Agency and made jointly by Intenas Bandung with relevant agencies. In this research, the researchers can see an example of homecoming atlas map visualization; including simbolization and every data displayed on the homecoming map.

The purpose of this research was to analyze the elements must be changed, identify aspects that need to be considered so that visualization of the cartographic map design of the homecoming was obtained by the cartographic rules and made evaluations of the results from updating homecoming route maps through the making of questionnaires.

2. Methodology

The method of this research was carried out by some steps. They include tool and material preparation, and literature studies collecting process. The identification step on substance and aspect of homecoming map cartography includes searching, finding, and analyzing everything that must be updated in Homecoming Atlas map 2019 making process. The data collecting was carried out by Spatial and attribute data, data classification, editing and data generalization, adding supplementary information, to homecoming map cartography design. The result is homecoming map and homecoming map evaluation in questionnaire form. The research methodology can be viewed in Figure 1.

2.1. Identification of Element Should be updated

This identification makes Java-Bali homecoming map 2018 as reference for adding elements and adjusting carthograpy aspcets that will be used in homecoming atlas map 2019 cartographic design for Java and Bali regions. The elements should be updated in this map were road network, POI (Point of Interest), coast and sea boundaries administration, and supplementary information supporting the map. Besides, the cartographic aspects that will be updated including Generalization, symbol and colour selection, map and writing layout determining.

2.2. Data Collecting

The data used in this research includes spatial and attribute. The spatial was road network data obtained from the Ministry of of Public of Works and Housing (PUPR). POI data was obtained from GeoSpatial Information Agency (BIG). The Attribute was supplementary information obtained from the Ministry of of Public of Works and Housing. The source of those data was obtained from stakeholders in accordance with the capacity and authority in providing data related to making homecoming map as presented in Table 1.

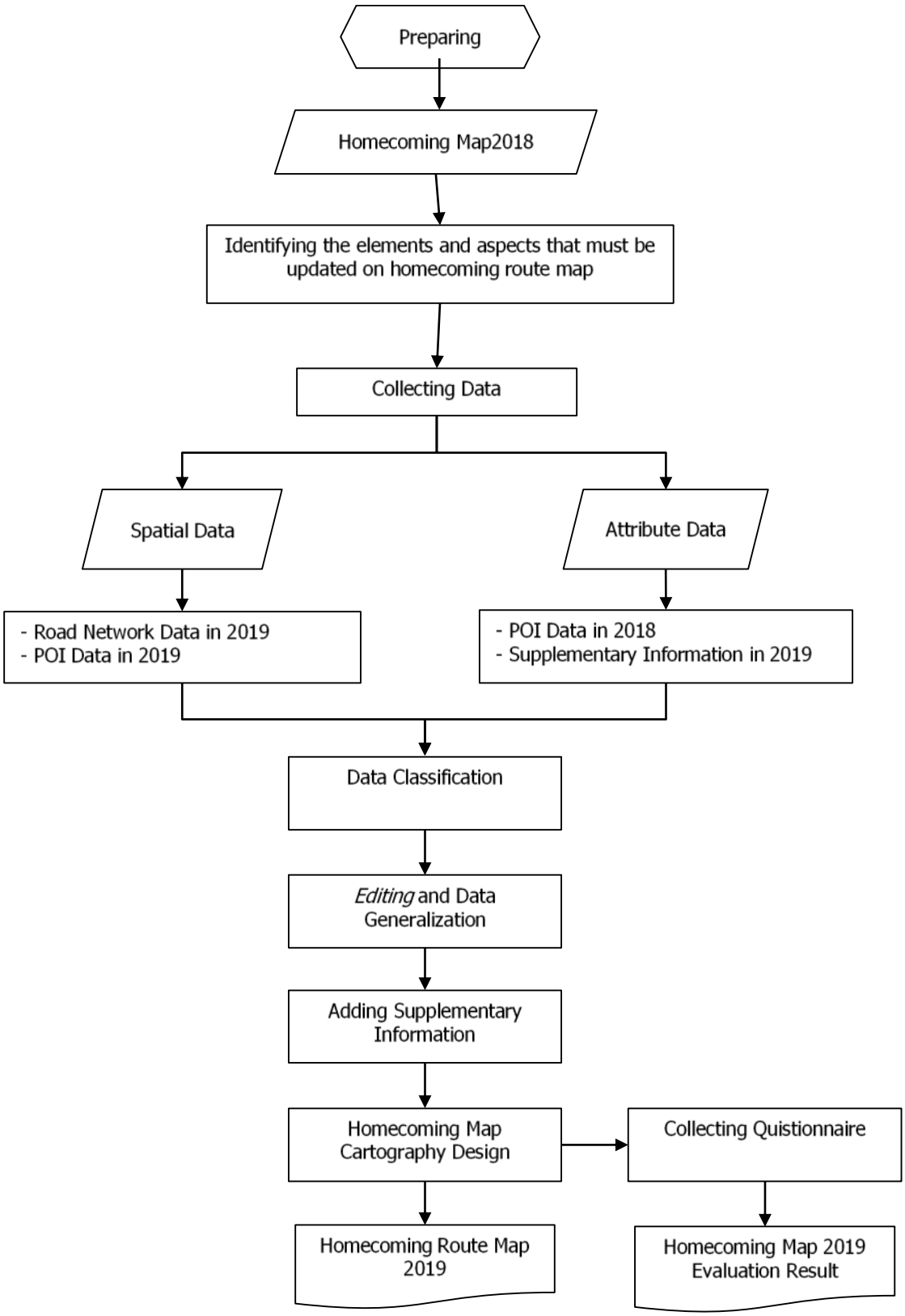

Figure 1. Flowchart Methodology.

Table 1. Research Data.

No.	Data	Data Form	Data Source
1.	Road Network Data in 2019: • Toll road • Artery Road • Collector Road • Local Road • Railway	Spatial Data	Ministry of Public of Works and Housing
2.	Point of Interest Data in 2018: • Airport • Port • Police Office • Toll Road Gateway • Gas Station • *Rest Area* • Tour Object • Hospital/Clinic	Spatial Data and Attribute	Compiler Team
3.	Topography Data	SRTM Res 90 m	http://srtm.csi.cgiar.org/
4.	Prone Data in 2018: • Accident Prone • Disaster Prone (flood and slide)	Spatial Data	BNPB Compiler Team
5.	District Administration Data in 2018: • Province Capital • City/Regency Capital • Sub-District Capital • Mountains • Province Boundaries • Lake, Coast, and Sea Boundaries	Spatial and Attribute Data	GeoSpatial Information Agency (BIG) Earth Scale Map at 1:25000
6.	The distance scheme between homecoming lane segments in 2017	Spatial Data	The Ministry of Public of Works and Housing
7.	Supplementary Information in 2019 • Toll Road Information • Toll Road Fare Discount • Functional Toll Road Information • Toll Road Exit Gate Information	Attribute Data	Ministry of Public of Works and Housing Waskita Toll Road

2.3. Data Classification

Data classification aimed to display data in certain class forms according to its type. This classification activitiy is needed to display data in accordance with certain categories or classes. Therefore, the collected data is arranged in table form according to its statistic rules, so that the mapping process is easier, faster to be used, and minimize the error possibility caused by irregular data. Data classification was carried out on road network, topography, and sea.

Classification is done on ArcGIS 10.5 software using Symbology based on Categories of the type of road shown in Figure 2.

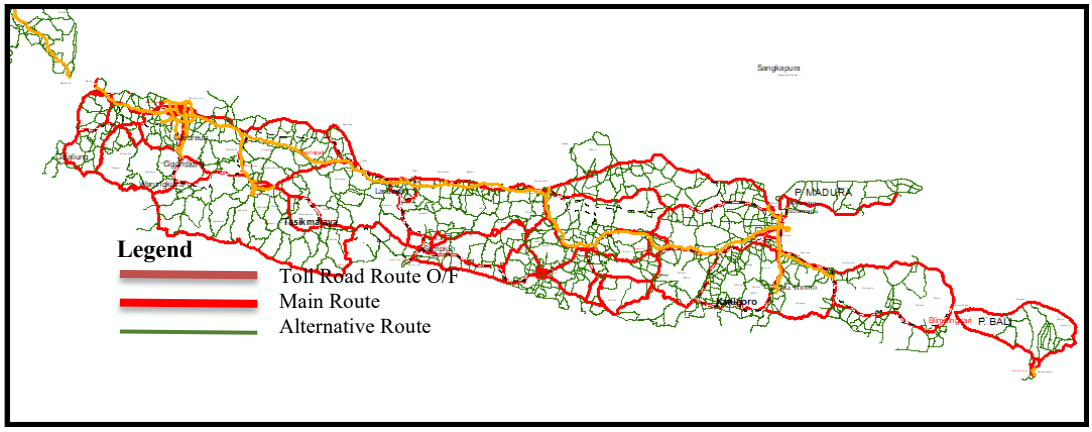

Figure 2. Road Network Classification.

The data used in the background of Java and Bali are topographic data from the SRTM (Shuttle Radar Topography Mission). Symbology uses classified types with the number of classes of 5 shown in Figure 3.

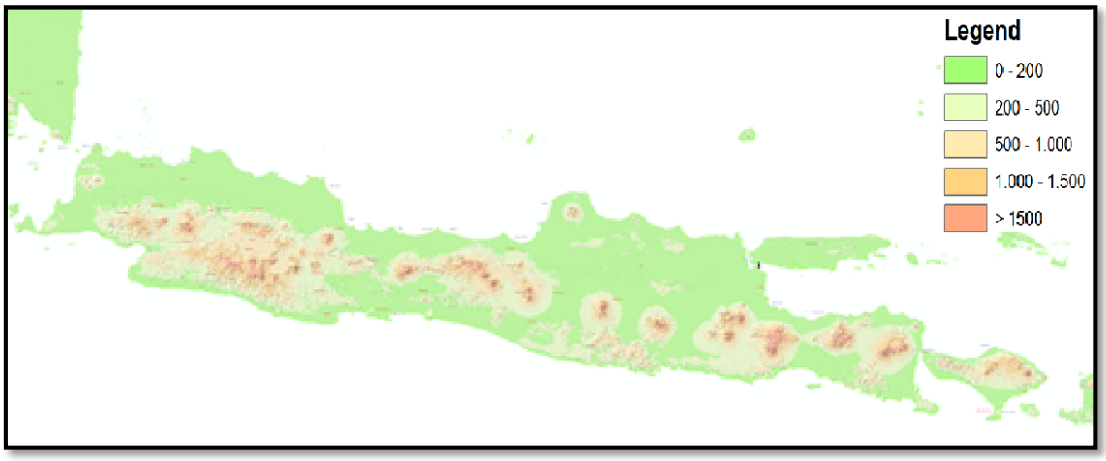

Figure 3. Topography Data Classification.

Marine data were classified into depth values using Symbology types categories with 7 depth values shown in Figure 4.

Figure 4. Sea Depth Data Classification.

2.4. Editing and Generalization

Editing data includes checking and repairing. They were done by shifting or moving points that are deemed necessary by considering the density data on map face. Data Generalization includes selection, simplification, combination, and enlargement. Those data were very needed to obtain simple data so that it can be displayed well. It is according to the face map size which depending on limited paper media. Data Generalization is carried out on road network data, POI (Point of Interest), and other supplementary informations. The selection of the road is done by selecting the road to be used as an alternative way back and forth and delete unnecessary shown as shown in Figure 5. before generalization and Figure 6. after generalization.

Figure 5. Roda Network Data before Generalization.

Figure 6. Road Network Data after Generalization.

The selection and editing stages of POI data are shown in Figure 7 (before generalization) and Figure 8 (after generalization).

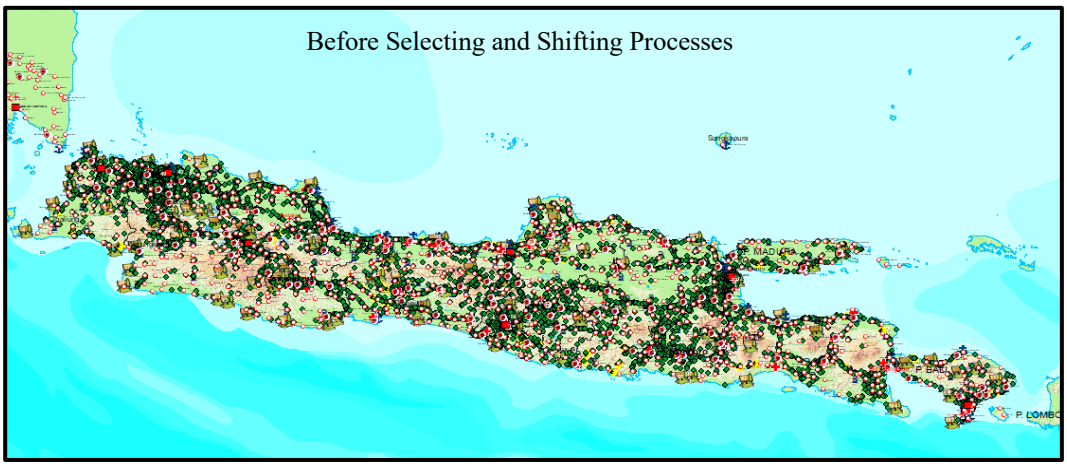

Figure 7. POI Data before Generalization.

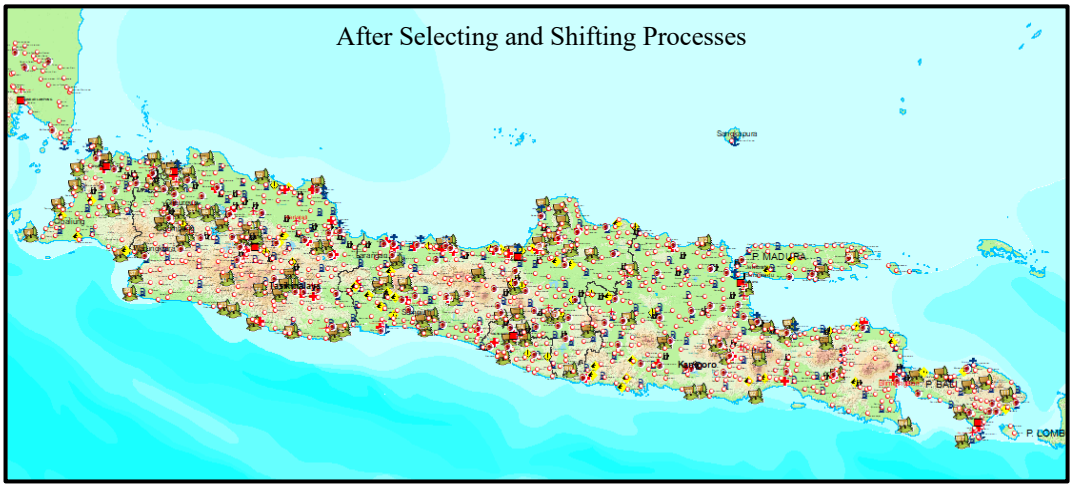

Figure 8. POI Data after Generalization.

Data selection is carried out in the sub-district capital that is not traversed by the homecoming route by taking into account the density of existing data as shown in Figure 9.

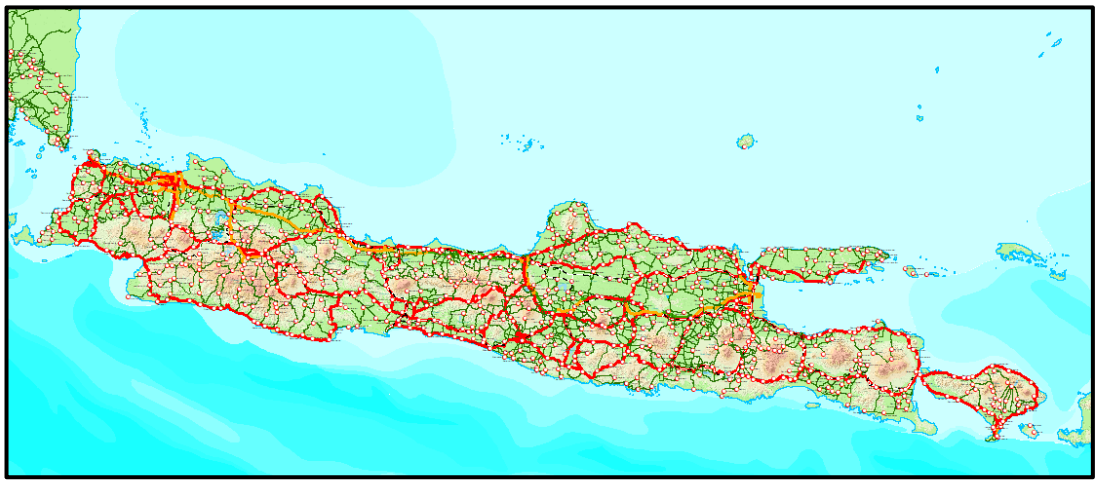

Figure 9. The Selecting and Shifting Processes of Sub-District Capital.

The processing phase of vulnerability data is by selecting and shifting the points of vulnerability to be displayed. The vulnerability data are shown in Figures 10., Figure 11. and.Figure 12.

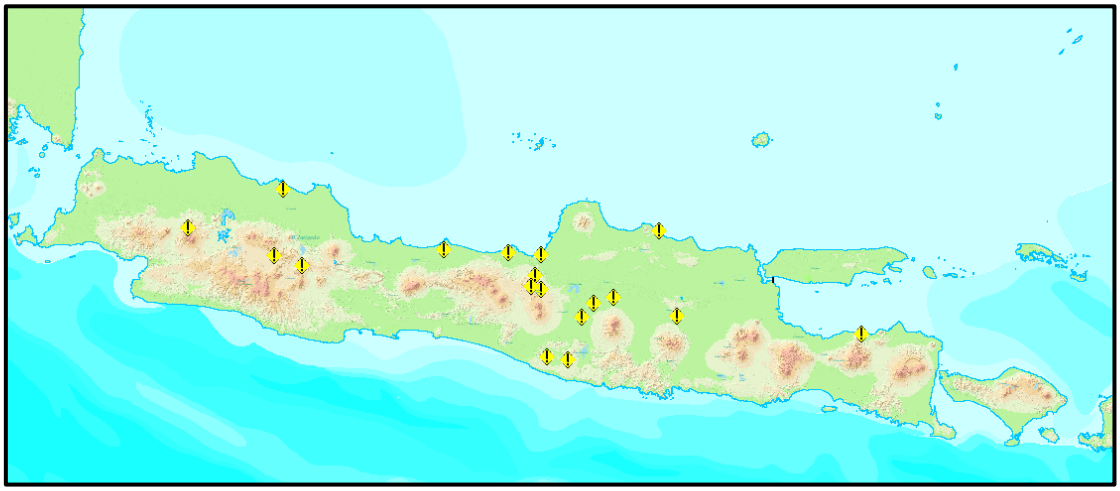

Figure 10. The Vurnerabilty Data (Accidential Prone).

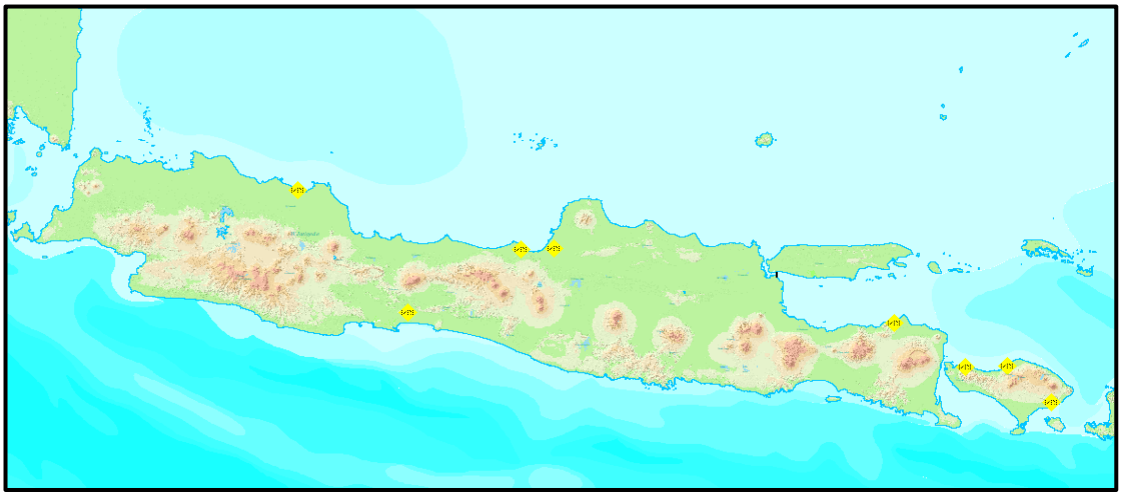

Figure 11. The Vulnerability Data (Flood Prone).

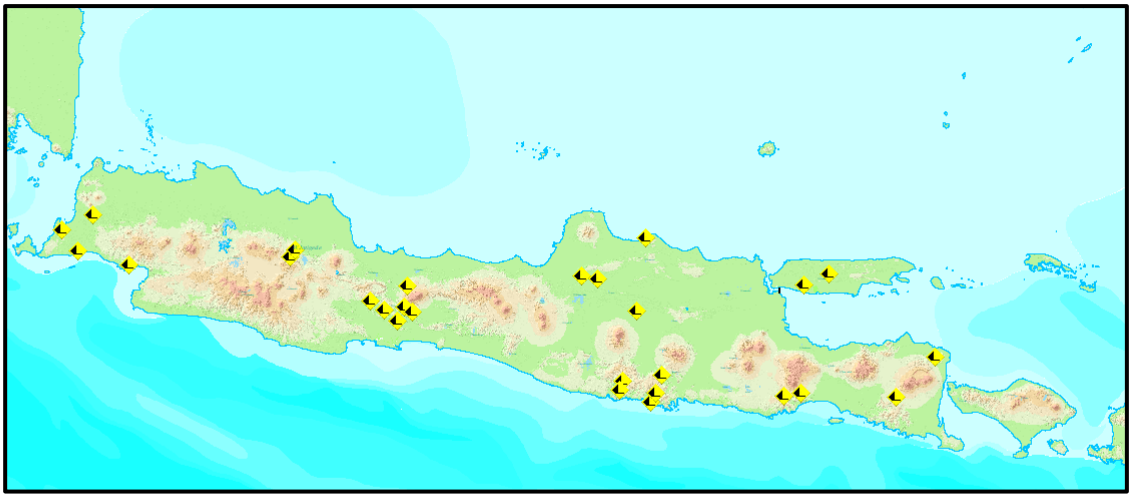

Figure 12. The Vulnerability Data (Slide Prone).

2.5. The Addition of Supplementary Information

The supplementary Information includes toll road and alternative road details, and descriptive information related to homecoming activity. Those details were used to clarify to the users about the information of toll and alternative roads. These informations need special space so that it can be presented completely. Descriptive information was created to display supplementary information about homecoming, to clarify and add available information on map face. The descriptive informations consist toll road fare from The Ministry of Public of Works and Housing, Call Center from BPJT, and tour object shown in Figure 13.

Figure 13. Supplementary Information.

2.6. Homecoming Route Map

The homecoming map cartography design in this research was map layout determining on presented map to be. [7] in their book entitled "Kartografi", said that there was one part of map sheet can be distinguished on map face, map boundary information, and map edge information.

The face of the map is part of the map that presents the mapped area, bounded by the edge of the map which can be in the form of grid lines or free lines.

Map boundary information provides data relating to the face of the map, generally the data presented on the map boundary information are numbers from the coordinate data whose area is on the face of the map.

Map edge information is part of a map sheet that provides information about matters relating to the contents of the map, so that map users can evaluate and interpret the map concerned. Map edge information on the homecoming atlas consists of supplementary information placed at the front and at the back of the map.

3. Results and Discussion

The result of Homecoming Atlas Map 2019 updating for Java and Bali Regions consist of updated elements. The cartography aspect was updated on the map in order to suit users' necessary. Besides, this

research evaluates on map usefulness and suitability for users in order to know their response on the made map. The next homecoming map can be adjusted with users' necessity.

3.1. The Result of Elements Updating on Homecoming Route Map 2019

The result of elements updating, through processing step, on Homecoming Atlas Map 2019 occurs on POI element. They are tour object and sea administration boundary elements. POI element such as tour object was added by attribute and tour object information that placed on homecoming map. For updated toll road network data can be seen in Figure 14.

3.2. The Result of Updated Carthograpy Aspect Analysis

The The updating cartography aspect, which carried out on Homecoming Atlas Map 2019, was on map layout part such as in legend and other supplementary informations. The aspect that need to be considered in map's making in to order to suit cartography rule include Generalization, symbol and color selecting, and map layout.

The Generalization process includes selection and smoothing on road network element. According to the data from The Ministry of Public of Works and Housing, the displayed road network was less informative to be used in the map. Therefore, there were selections to determine the alternative and main routes for homecoming. Then, the unselected network would be eliminated. The symbol used in this map was as similar as the Java-Bali map issued by BIG and Itenas previously. The color selection was used in data classification process so that the differences are seen in its each class. This selection was carried out on Sea classification and Topography using subtractive color. These colors were obtained from the color combination based on ink media on paper. This model was also referred as CMYK (Cyan, Magenta, Yellow, and Black) Color System. The layout does not have rule for thematic map, but it should be made with interesting and informative for suiting the users. Thus, it can be used as a media to determine the best route for homecoming trip.

3.3. The Result of Homecoming Route Map Analysis

The result of "The Updating of Homecoming Atlas Map for Java and Bali Islands" was available in softcopy form. It was a digital map. The map softcopy was available in pdf format and it was a digital map that can be accessed in official website of Itenas Homecoming Atlas Route (https://www.itenas.ac.id/atlas-jalur-mudik-2019/). This Atas Map was divided into 3 parts. They are map face, map boundary information, and map edge information. The information of map edge was available on the front and back pages. The obtained map face scale was 1:1.230.000. The homecoming map design mostly follows SNI on its Earth Map displaying. It also has been validated by BIG team, Itenas, and The Ministry of Public of Works and Housing. The Atlas Map face presents Java and Bali Islands incluing the information about homecoming activity as below, the result shown in Table 2.

Brebes-Semarang Toll Road before *updating* process

Brebes-Semarang Toll Road after *updating* process

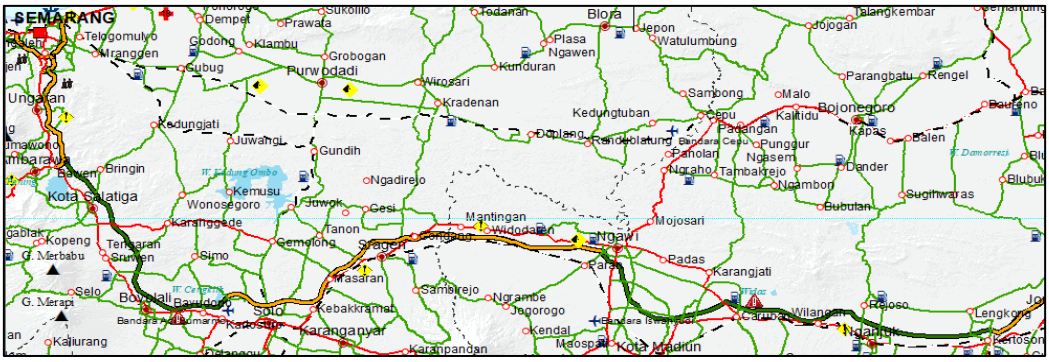

Salatiga and Ngawi-Kertosono Toll Roads before *updating* process

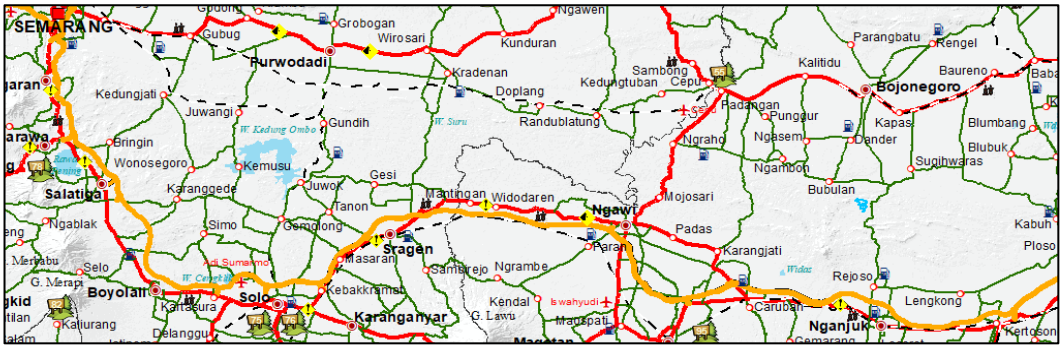

Salatiga and Ngawi-Kertosono Toll Roads after *updating* process

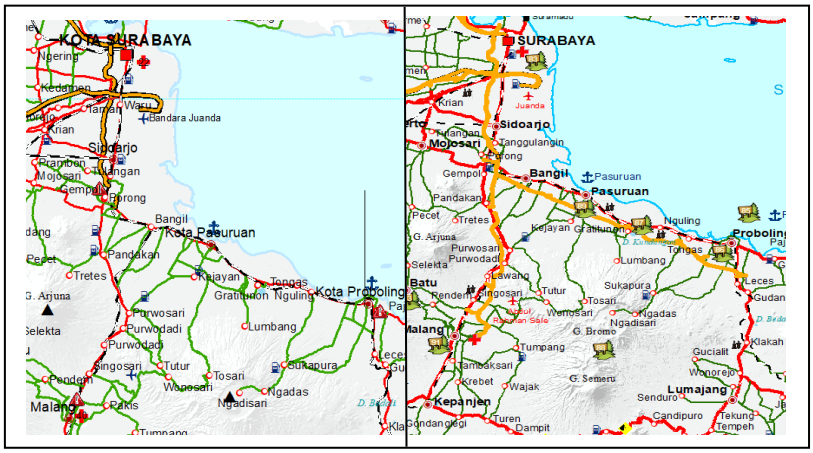

Pandaan-Malang and Gempol-Pasuruan Toll Roads, before and after *updating*

Figure 14. The Result of Element Updating.

Table 2. The Result of Homecoming Route Map.

No.	Element	Information
1.	The Road Networks of Java and Bali Islands	- Alternative Road - Toll Road - Homecoming Main Road - Railway
2.	POI (Point of Interest)	- Tour Object with its name - Port with its name - Airport with its name - Rest Area - Gas Station - Hospital/Clinic - Mountain with its name
3.	The Administration Boudary of Java and Bali Islands	- Province Capital with its name - City/Regency Capital with its name - Sub-District with its name - Province Boundary - Sea with its name - Lake with its name - Coast Boundary

The map boundary information presents coordinate data in degree, minute, and second forms with interval on 2 degrees. The front part of suppelementary information contains:

- Province Tour Object Information
- Itenas' Adress information
- Website and Itenas Social Media's Contact List Information

The back part of suppelementary information contains:

- Toll Road Exit Gate Information
- Emergency Call Information
- Map History Information
- Toll Fare Information
- Non-Fare Toll Information
- The Toll Route Map of Jakarta-Bandung-Tegal
- The Toll Route Map of Merak-Jakarta
- The Toll Map Route of Brebes-Semarang
- The Toll Map Route of Batang-Jombang
- The Toll Map Route of Ngawi-Probolinggo
- The Toll Map of Semarang City
- The Toll Map of Surabaya City
- The distance scheme between homecoming lane segments (North and South)

The result of "The Updating of Homecoming Atlas Map for Java and Bali Islands", which is designed as similar as cartography rules, was presented in Figure 15.

3.4. The Result of Quistionnaire Analysis

The evaluation result of "The Updating of Homecoming Atlas Map for Java and Bali Islands" was done trhough questionnaire, namely "Survey of Homecoming Map Usage" in digital form. It was shared online among some Itenas students with 38 questions and 59 respondents. This evaluation result was categorized into 4 question categories. They include elements on Homecoming Atlas Map 2019, cartography aspect and visualisation design displayed in the map, the required cartography elements on the map, and some questions about the map's usage and suitability with users' necessity.

1. The data result was the question about the map's suitability with users' necessity. There were still many respondents who need the directional help application on their mobile devices to determine the homecoming route. More than half of respondents have ever used homecoming map and most of them used Java and Bali ones. Many of them felt helped by the map. Besides, many of them considered that digital homecoming map version was more effective to be used. Thus, most of them also considered that the map made by Itenas Bandung team was interesting and its information was more useful during homecoming activity. Therefore, they considered that Itenas's map should be updated for next year.
2. The respondent's data result was the question about homecoming atlas map elements. The main route and prone points were the best helper elements for respondents in homecoming trip. As for alternative routes, prone points, and toll fare information were three main elements that are judged to be incompatible with the actual condition. In this case, most of respondents argued that it was a necessary to add or improve on the homecoming map's elements.
3. The respondent's data result was the question about the map's cartographic aspect. The respondents considered that symbolization was a less informative cartographic aspect in map presentation. Most of them argued that the visualisation display of Java and Bali homecoming atlas map was interesting. Thus, they also stated that cartographic aspects presentation (in this case were legend, symbol, color, text, map scale, and layout) was interesting and it was necessary to add or improve on the cartographic aspect or map design.
4. The respondent's data result was the question about the homecoming atlas map element. All respondent argued that those map elements should be included. Thus, they also argued that the other map elements (in this case were title, sub-title, legend, compass' point direction, the date of map making, the maker, the bar scale, and line edge) also should be included in homecoming atlas map.

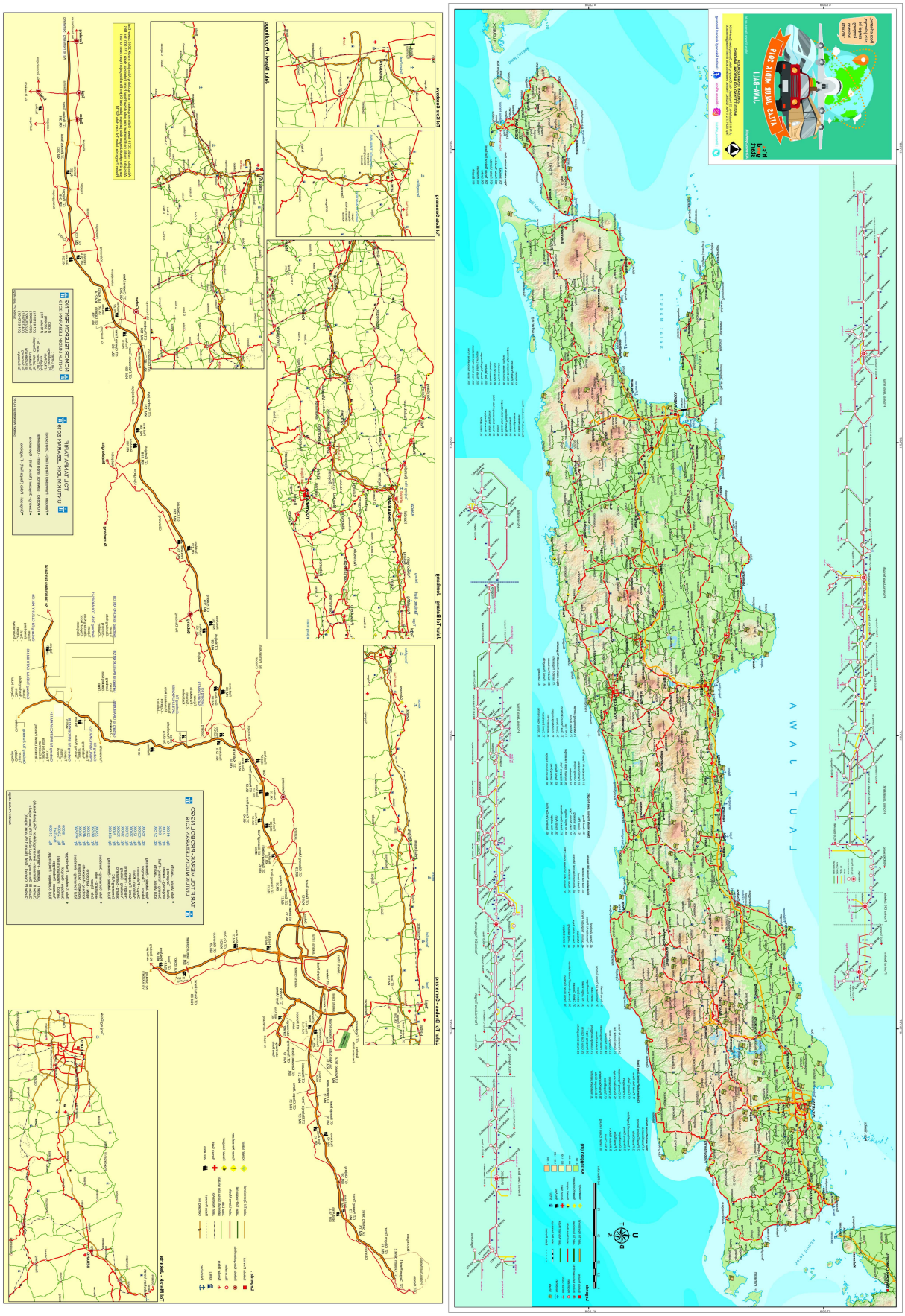

Figure15. The Result of The Homecoming Route Map 2019.

4. Conclusions

Based This research produced Homecoming Atlas Map 2019 for Java and Bali Island which has been updated by considering the cartographic aspects and presented in digital map with pdf form. The conclusions of this research were as follows:

1. The updated elements on the map were the newest road network in 2019. It was the toll roads. The toll road network data were obtained from The Minstry of Public of Works and Housing. The data form was shp which contained operational and fungtional toll roads throughout Indonesia. The supplementary information included toll road 2019 detail information, toll fare 2019 information, and descriptive information. The supplementary data were obtained from PT Jasa Marga. It was attribute contained detail information about Trans Java 2019 toll road, Trans Java toll road fare information, and toll roads' status (including operational and fungtional).
2. The cartographic aspects that need to be considered in the map updating processes were Generalization, symbol and color, map layout, text or writing arrangement. The updated cartographic aspect in this updating map was the the map's back face part and its inset size for back part.
3. The result evaluation of Homecoming Atlas Map 2019 for Java and Bali Islands was obtained through collecting quistionnaires that produced an assessment on the elements, aspects, display, and suitability of the homecoming atlas map 2019. It has been made through 5 assessment levels. The evaluation also produced critic and suggestion for the information's unsuitability between the homecoming maps with the actual situation. The respondent also argued that it is necessary to update the map for the next years.

5. References

[1] Arribathi, A. H., Kajian Aspek Kartografis Peta Mudik 2018. Jurnal CICES. STMIK Raharja. Tangerang. 2018.

[2] Soebyakto, B. S., *Mudik Lebaran (Studi Kualitatif)*, Jurnal Ekonomi Pembangunan. 9,2:61-67. 2011.

[3] Apfia, T. B., *Tahun Ini, Pemudik Diprediksi Mencapai 19,5 Juta Orang*, Diakses dari http://www.tribunnews.com/bisnis/2018/06/07/tahun-ini-pemudik-diprediksi-mencapai-195-juta-orang, pada tanggal 11 Maret 2019.

[4] Satrio, D. A., *Mudik Lebaran 2018, 346 Orang Meninggal Dunia Dalam 1.559 Kecelakaan*, Diakses dari https://news.okezone.com/read/2018/06 /20/337/1911863/mudik-lebaran-2018-346-orang-meninggal-dunia-dalam-1-559-kecelakaan, pada tanggal 11 Maret 2019.

[5] Habibie, N., *Kakorlantas sebut ada 10 titik rawan kemacetan aru mudik 2018 di Pulau Jawa*, Diakses dari https://www.merdeka.com/peristiwa/ kakorlantas-sebut-ada-10-titik-rawan-kemacetan-arus-mudik-2018-di-pulau-jawa.html, pada tanggal 11 Maret 2019.

[6] Anesya, K., *Kajian Aspek Kartografis Peta Mudik 2018*, Penelitian Geodesi Itenas, Bandung. 2018.

[7] Soendjojo, H. and Riqqi, A., *Kartografi*. Penerbit ITB. Bandung. 2012.

The Importance Of Geospatial Information: As a Content in Information Technology Era

Asep Karsidi[1]*, Samsul Hadi[1], Totok Sediyantoro[1]

[1]Dewan Geospasial Indonesia

*Corresponding author's e-mail: askarsidi@gmail.com

Abstract. The era of Industry 4.0 is characterized by the development of digital-based Information technology and its utilization in various fields of activity. Entering the era of digital-based information technology and supported by high-speed communication infrastructure, easily accessible, larger in volume, several types and more detailed. The content of Information is challenging to be managed properly and correctly including information that relates to aspects of the earth space (Geospatial data). The Geospatial Data is the data that is very much needed as long as we carry out activities on the Earth. In the current information age, the high demand for detailed and accountable Geospatial data is very much needed in term of "The Science of Where". Questions about Where? bring implications that "Content" of information concerning aspects of the location of an object (Geospatial Information) is important. Supported by the development of remote sensing technology, the acquisition of the contents of the earth's objects can now be done easily and quickly. Indonesia has a One Map Policy, Geospatial Information Development and Implementation of a one map policy on a large scale are expected to guarantee the availability of quality and reliable Geospatial Information for the development process in this era of digital technology.

Keywords: Geospatial Information, GIS, Remote Sensing, Satellite, One Map Policy, Geo-portal, Indonesia.

1. Introduction

The Industrial 4.0 is characterized by the development of digital-based Information technology and its utilization in various fields of business activities. With the availability of digital-based information technology and supported by high-speed communication infrastructure, the flow of information will faster, large in volumes, many types and more detailed in content. The content of information that is challenging to be managed properly and correctly includes content that relates to aspects of the earth space (Geospatial Data / Information).

Geospatial is a spatial aspect that shows the location and position of an object or phenomenon that is below, on or above the earth's surface expressed in certain coordinate [1]. Furthermore, it is also stated that geospatial is more concerned with location precision in many context of geospatial information, because it is used in terms of not only graphical representation or maps as information, but also equipped with attributes that are bound to the coordinates of the object [2].

Geospatial data and information in the form of maps or corrected images, presents the fact of an object or phenomenon based on spatial, so that the guarantee of the validity of the content is very necessary. In the era of digital, the process of constructing content of geospatial information must involve a competent science in the field of Geosciences. Geospatial Information Development is not just the use of computer sophistication and information technology, but to develop the content of geospatial information must be supported by the earth science knowledge.

The Geospatial terminology as a combination of Geomatic and Geographic Information System (GIS), is an application of earth science in the era of computer-based digital. As an example of the use of geospatial information in development, such as for early warning systems of natural disasters, predictions or projections on climate change, land use and land cover change, spatial planning, natural resource management are all integrated in GIS [3-5]. GIS is a system that consisting of hardware,

software, geographic data and human resources that work together effectively to enter, store, improve, update, manage, manipulate, integrate, analyze and display data in a geographic-based information [6, 7].

The Geospatial data is very much needed as long as we carry out activities on the Earth. In the current information age, the high demand for detailed and accountable Geospatial data / information is related with recently terminology of the "Science of Where". Questions about "Where"? bring implications for the need of the "Content" of information concerning aspects of the location of an object, that is the information containing in Geospatial Information. Valid and accountable Geospatial Data or Information, good structured in digital format is very effective in supporting the implementation of economic development including industrial processes in the industrial era 4.0. The government of Indonesia committed with sustainable development base and to meet the targets of SDGs (Sustainable Development Goals), is need of structured, valid and accountable Geospatial Data or Information. The Indonesia Government already has Ministries and Institutions which are among the main tasks and functions of providing Geospatial Data or Information such as: Geospatial Information Agency has duties and functions as the organizer of the development of Basic Geospatial Information (Basic IG) including the integration of Thematic Geospatial Information (IG Thematic) created by the Ministry and other institutions or individuals. The implementation of the development of Geospatial Information, both Basic IG conducted by BIG, and Thematic IG created by the Ministries and other institutions including individuals in practice still faces many obstacles. The lounching of the "One Map Policy" and "One Data" is the Government's efforts to maximize the utilization of Geospatial Data or Information that is equipped with statistical data as its attributes, in the implementation of National development including supporting of Industry 4.0 which will involve Big Data which is content in volume and diversity is very large and varied.

The following article reviews the importance of Geospatial Information for development and supports the development of industry in the digital era. Starting with a description of the development of geospatial information technology to the importance of geospatial information in the implementation of national development, including supporting the era of Industry 4.0.

2. Geospatial Information Technology

Nowday not only an agency is utilizing geospatial information, but almost all people have understood and need information concerning aspects of the earth's space in the form of maps. These are range from everyday needs, for example for traveling, to find out area of interest, and to more complex purposes such as for regional or physical planning. With the support of digital-based information technology, the required geospatial information content is necessary and increasing, including information of the traffic to facilitate finding alternative roads, information about interesting locations to visit such as the resort, restaurant, accommodation and others.

There are at least three satellite technologies that support the development and utilization of geospatial information (Figure 1):

- Observation and Altimetry Satellite
- Satellite Positioning
- Satellite communication

The first, “observation satellites”, these satellites orbit the earth to record the condition of the earth's surface, ranging from Geostationary Weather satellites with a resolution of 1000 m to satellites with high resolution of 50 cm and even 30 cm like WorldView-3 Digital Globe satellites (spatial resolution 30-50 cm) and GEOFEN11 Satelite with 10c spatial resolution. Through this observation satellite allows us to obtain data and information the earth's surface condition. This observation satellite has been orbiting in space and continues to be developed more high spatial resolution and real time. The second is satellite positioning, the satellite “Global Positioning System (GPS)”, via GPS satellites the position of objects on the earth is recorded in coordinate making it easier to monitor and locate the object. GPS satellite expected to have better accuracy. Coupled with the availability of satellite altimetry, the

condition of the high and low of the earth surface can be identified through the record of the height of the object from the mean sea level.
The third is the presence of communication satellites, it makes us able to communicate even in the remote areas. All data or information, whether in the form of text or images and videos, can be disseminating and sharing. Through this communication stellite we can easily and quickly to share information (including data and information related to Geospatial), between individuals and communities where ever they located. Therefore communication satellites are expected to have a wide range of communication.

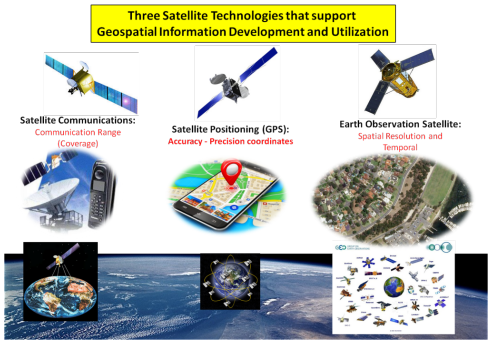

Figure 1. Three types of Satellites.

3. New Paradigm of Geospatial Data

There has been shifting paradigm of maps as a source of geospatial data, from 2 dimensions to 4 dimensions. Today, geospatial information is not only presented in a 2D map but in 3D digital format and even in 4D as a time dimension (Figure 2), make it enriching understanding of the earth characteristics (physical, social, cultural and even political and economic) [8-10].

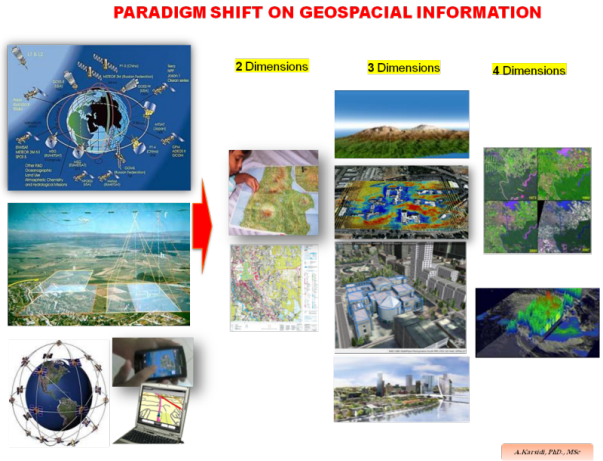

Figure 2. Shifting Paradigm of Geospatial Information.

In the era of globalization and 4.0 industry era, geospatial data has been widely used by various sectors (social, economic, cultural) and at various levels of interest (government and private) [11-13]. Utilization of digital geospatial data must be done correctly, if the method of use, processing and analysis is done in an inappropriate way, it will become a problem.
The spatial element of geospatial data also functions as a common identifier to integrate various types of data and information in an area such as population, economy, natural resources, agriculture, education, history of disaster events and so on. This means that a variety of data and information in the same area can be spatial base analyzed.

Geospatial data through GIS devices have been used in various applications such as managing buildings and facilities, managing transportation systems, mapping disasters, managing natural resources and prediction[5, 14, 15]. The use of geospatial data includes planning the future of a city or region have to be more careful in understanding the physical condition of the environment, because city or regional planning must be based on facts in the field (geospatial data) and supported by Geographical Knowledge. The deeper the understanding of the geographical conditions of a region and the more detailed the descriptions outlined in various geospatial themes, the more complete and dynamic the design and planning process [5, 8, 16].

Today the demand for geospatial data is not only the availability, accuracy and high resolution, but also the ease of access including the up-to-date data. The demand is at a real time level. With supporting by various application devices, the availability of geospatial data must be able to compensate for the fulfillment of real time data or near real time. For example, in monitoring the movement of an object, real time data is needed. Another example such as precise agricultural activities, by integrating GPS satellites and communication satellites including sensors, such as planting processes, maintenance until harvesting can be carried out accurately automatically.

4. Importance of Geospatial Information in 4.0 Industry Era

The notion of industry 4.0 is a trend in the industrial world that combines automation technology with cyber technology [17]. The era of Industry 4.0 is characterized by the development of digital-based Information technology and its utilization in various fields of activity. In industry 4.0, manufacturing technology has entered the trend of data automation and exchange. These include cyber-physical systems, internet of things (IoT), cloud computing, and cognitive computing.

Considering that all the activities takes place on the earth, the geospatial data and information are needed. Data and information of Geospatial are presented the spatial elements with information about the location, will provide a better understanding than data that is only presented in the form of text, tables and graphs. This is because the spatial element presents the distribution of data and information based on its coordinate. Therefore the content of geospatial data is important.

The trend of automation and data exchange with supported by cyber systems need to be supported with the availability of the good quality and structured content of geospatial data. The content is challenging to be managed properly and correctly includes content of Geospatial Data.

This Geospatial data is unique because it involves location aspects that are bound to a particular coordinate system. Geospatial data are divided into three categories where each category represents objects according to the scale of the map. The three categories are [18]:

- The Fisrt is *Point,* point which is representing an object that has uniqe and singgle coordinat. With an object that has coordinat make it easy to be monitor their movment by supporting GPS satellite.
- The scond is *Line,* line is consist of many points represent elongated object such as roads, rivers, telephone lines, electricity lines etc.
- The third is *Polygon*, polygon is an object in the form of a collection of coordinates on a close line. This object can be a sport field, a large building, a plantation area.

Geospatial data that has high precision / accuracy is the main and important key in developing industries related to location, both service industries such as transportation services without drivers and freight forwarding services and other industries. *This activity requires geospatial data with high up to the centimeter or milimiter level of spatial resolution and high accuracy on Positioning.*

Supported by devices such as smart watches or other gadgets, the availability of digital geospatial data that is accurate to the centimeter level *or millimeter* allows to track the movement of that object. Conversely, analog-based geospatial data is not possible to be utilized directly in today's digital era.

On the other hand combine with sensor technology, the position and movement of objects can be monitored in real time or near real time. Digital geospatial data will be easily integrated and utilized in various business pillars born in this era of industrial revolution 4.0. The utilization of future geospatial data will include several activities including [19]:

- Biosecurity and health informatics.
- Biostatistics and health risk appraisals.
- Geospatial patterns of health behaviors and outcomes.
- Geospatial patterns of disease treatment and outcomes.
- Urban health, education, crime, and economic development.
- Computation spatial statistics and social-environmental synthesis.
- Geospatial urban planning and development.
- Geospatial civil engineering.
- GIS for traffic analysis and engineering applications.
- Environmental and food security on both a regional and global scale.
- Transport of contaminants in soil and water.
- Geospatial trends in air pollution.
- Food and water security.
- Regional climate response and agricultural forecasting.

All of this is a trend of activities in the industrial 4.0 era that requires the support of geospatial data that anticipates the diversification of businesses or activities.
To fulfill the above, the geospatial data must be seriously built, detailed, systematic, accurate and in a database system that is easy to manage and integrate.

5. Geospatial Information Development Process in Indonesia

The development of geospatial information in Indonesia has been intensively carried out since the Law No. 4 of 2011 about Geospatial Information law in Indonesia issued on April 2011. In this case BAKOSURTANAL transforms into Badan Informasi Geospatial (BIG) [1].
This law mandates to ensure the availability of accountable geospatial data and geospatial information. It means Geospatial must be built systematically and sustainably. Also mandated that Basic Geospatial Information is the main thing as a reference for develeopment of Thematic Geospatial Information, therefore the development of Basic Geospatial Information is the top priority that must be implemented. The Basic Geospatial Information consists of: Geodetic Control (Vertical, Horizontal and Gravity) and Base Maps from 1: 1,000,000 scale maps up to 1: 1,000 scale consisting of Indonesian Earth Map (Topography map), Indonesian Coastal line Map and National Marine Environment Map. Basic Geospatial Information development is BIG's main task, in addition to conducting guidance in the development of IGT by the relevant agencies [20].

The Indonesian government is currently prioritizing the development of Medium and Large scale maps to support the operational activities of sector development and development in the region. The prioritized medium 1: 50,000 scale map is needed as a basic map for the development of thematic maps that will be built by the sector, including the preparation of spatial plans and the operationalization of forest and environmental management.
The Development program for larger scale map, such as a map of 1: 5,000 to 1: 1,000 scale is also being accelerated. This map is needed for the process of preparing detail spatial planning, but it takes a long time considering the Indonesia territory is too large. Utilization of the latest technology that is able to acquire including high-resolution DEM is needed to accelerate the making large scale base maps complete with high resolution of contours line.
Another important step and needs attention is in the development of geospatial information such as the integration of thematic geospatial information that is built by various agencies or even by individuals. This integration begins with designing a standard geospatial database structure that is sourced from one reference, namely one basic geospatial information. The development process must follow the principles of building a geospatial database that are standardized and understood together.
Steps have been taken in the framework of developing thematic Geospatial information development are include [20]: Preparation of Thematic Geospatial Information Norms, Standards, Guidelines and

Criteria; Thematic Geospatial Information Development Guidance at the National level; Development of Thematic Geospatial Information Development in Regions in the frame of one map policy.

6. One Map Policy or "Kebijakan Satu Peta" and "One Data" in Indonesia

One map policy was born from the many discrepancies in geospatial data and information generated from various agencies in national and in regions level. For example, data on protected forest area issued by the Ministry of Forestry is different from the protected forest area issued by the Ministry of Environment (when this ministry has not been merged). This difference occurs because the two agencies calculate the forest area from their thematic maps which are sourced from different base maps.

The importance of developing thematic maps must come from the same basic map. Bakosurtanal, who is now transforming into a Geospatial Information Agency (BIG) is a government institution in Indonesia that has been mandated by the Geospatial Information (GI) Law to build basic geospatial information as a reference for every person or institution (both central, regional and private government institutions) in arranging thematic maps [9, 21].

This One Map Policy is a policy that directs the development of Geospatial Information and its utilization must fulfill four things, namely: ***one reference, one standard, one geodatabase, and one geoportal*** [21] (Figure 3).

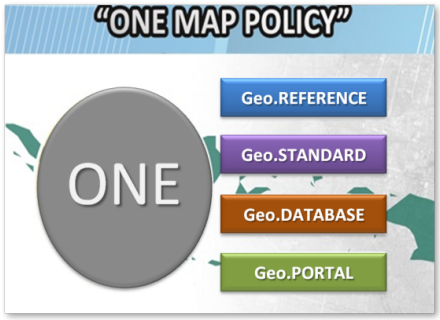

Figure 3. The Principle of One Map Policy.

6.1. One Reference

In the process of building geospatial information will not be separated from the survey and mapping activities to produce a map. The implementation must refer to one standard reference. This reference was built by BIG as the only institution that built Basic Geospatial Information. The Basic Geospatial Information consists of vertical and horizontal Geodetic Control and Base Maps.

6.2. One Standard

In order for thematic maps have uniform formats, both content, form and type of presentation, the development process must meet the standard rules such as the Indonesian National Standard consist of the Norms and Criteria. For example in the preparation of thematic maps containing elements of object classification, the aggregate classification must refer to the standard class of objects that have been set in accordance with the map scale that is compiled. As a guideline at this time various references have been issued in the form of Indonesian National Standard classification of land cover types according to map scale.

6.3. One Geo data base

Geospatial information is an integration between spatial data and statistical data or other data as information or attributes. Therefore, the builder must also go through the same database system, known as the standard geospatial database system (Standard Geodatbase), to make easily to integrate among any types of data.

6.4. One Geoportal

Geospatial information must be easily accessed and shared so there needs an infrastructure. In accordance with the mandate of the GI Law and Presidential Regulation No.27 of 2014, it is necessary to establish a National Geospatial Information Net (NGINet). Through this NGINet, a National Geospatial Portal, known as Ina Geoportal (Indonesia Geospatial Portal) was built as a geospatial data and information sharing platform. Through this portal easily to do searches, integrate, analyze, create and publish of geospatial information.

7. National Geospatial Data Infrastructure for Geospatial data sharing in Indonesia

In the GI law, in addition to ensuring the availability of GI, it is also mandated that GI must be easily accessed. In an effort to fulfill the mandate, Presidential Regulation No. 27/2014 was issued concerning the National Geospatial Information Network (NGIN) as an improvement to Presidential Regulation No.85 of 2007 concerning the National Spatial Data Network in Indonesia (NSDI) [21].

The national geospatial information network is built as an infrastructure to access and share usage about geospatial data nationally [20, 21]. These infrastructures include a National Geospatial portal known as Ina Geoportal (http://tanahair.indonesia.g.id), which is a portal, website and repository for GIS content [3]. Users can use this portal for GIS applications and share maps among user.

At the national level, the National Geospatial Data Center was built and supported by the construction of network nodes in local institutions and governments in the form of institutional strengthening that handles the construction of geospatial data. Each node has responsibility for the development of thematic geospatial data content in accordance with its competence [21] For example, the geospatial data network node in the Ministry of LHK, the network node here is a thematic geospatial data processing center that concerns the forestry and environmental sectors.

The node in the LHK Ministry is responsible for updating geospatial content with the theme in accordance with the Ministry of LHK's competence. Whereas the national geospatial data center is located at the BIG office in Cibinong as a connecting node (Hub) for national network nodes scattered in the agencies and local governments (Figure 4).

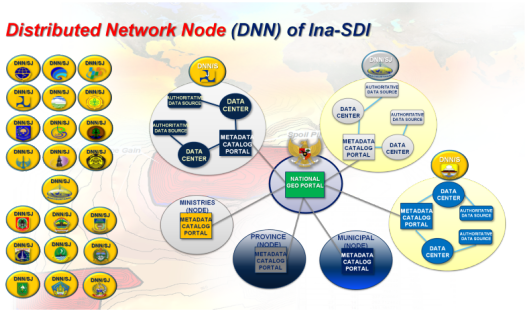

Figure 4. Distribution of Network Nodes.

8. Conclusions

The era of Industry 4.0 is characterized by the development of digital-based Information technology and its utilization in various fields of activity. As far as activities and implementation of development take place on the earth, geospatial information is necessary because it contains information relating to spatial elements that presents the distribution of data based on locations recorded in coordinate sytem. Geeospatial data providing better understanding than data which is only presented in the form of text, tables and graphs.

Geospatial information is useful in supporting the development process which consists of natural resource management, handling natural disasters (emergency response and management), asset management, tax management and various business sectorsto support 4.0 Industry era .

Supported by devices such as smart watches or other gadgets, the availability of digital geospatial data *including positioning that* is accurate to the centimeter-milimeter level allows to track the movement,

and combine with sensor technology, the position and movement of objects can be monitored in real time. Digital geospatial data will be easily integrated and utilized in various business pillars born in this era of industrial revolution 4.0.

The development of geospatial information in Indonesia intensively carried out since the Law No. 4 of 2011 about Geospatial Information, issued on April 2011, which mandates that it must ensure the availability of reliable geospatial data.

In development of geospatial information in Indonesia, the Basic Geospatial Information was develop intensively and systematically as well as integrating Thematic Geospatial Information through one map policy and Ina Geoportal as platform for sharing Geospatial data and information among stake holder or users.

Many difficulties regarding with the ability in accelerating to provide large scale base map due to limitation of technology that can produce contours line on high resolution. In addition, the integration of thematic geospatial information that develops by different agency is very difficult considering that each agency has an own policy in sharing data.

9. References

[1] Indonesia, R., *Undang-Undang Nomor 4 Tahun 2011 tentang Informasi Geospasial.* Sekertaris Negara: Jakarta, 2011.

[2] De Smith, M.J., M.F. Goodchild, and P. Longley, *Geospatial analysis: a comprehensive guide to principles, techniques and software tools*. 2007: Troubador publishing ltd.

[3] Dave., P. *Building a GIS*. 2014.

[4] Nyerges, T.L., et al., *Understanding the scope of GIS: Its relationship to environmental modeling*. 1993: Oxford University Press.

[5] Karsidi, A. and A.B. Wijanarto, *URBAN GROWTH PREDICTION USING LOGISTIC REGRESSION MODEL.* MAJALAH ILMIAH GLOBE, 2011. **13**(2).

[6] Aceh-Nias, G.K., *Modul Panduan ArcGIS*. 2007, Pemda Aceh.

[7] Karsidi, A. and S. Rahardjo. *Sistem informasi geografis: makalah pelatihan*. 1996. Universitas Indonesia, Fakultas Matematika dan Ilmu Pengetahuan Alam ….

[8] Karsidi, A. *Membumikan Informasi Geospasial; Kumpulan Pemikiran Dr. Asep Karsidi*. 2012. 134.

[9] Karsidi, A., *Paradigma Baru tentang Peta - Semua Orang Bisa Buat Peta Secara Interaktif*. 2012, Majalah Sains Indonesia.

[10] Karsidi, A., *The role of the Ina-SDI in supporting the development of the geospatial industry in Indonesia.* Geografia-Malaysian Journal of Society and Space, 2017. **8**(1).

[11] Karsidi, A., *BIG Bantu Atasi Berbagai Persoalan DKI Jakarta*. 2013 Majalah Sains Indonesia. p. 90–93.

[12] Karsidi, A. *Kebijakan dan Strategi Penyediaan Informasi Geospasial Dalam Perspektif Membangun Kecerdasan Spasial Nasional*. 2013. Banjarmasin: Prosiding PIT XVI IGI

[13] Woldai, T. *Geospatial data infrastructure: the problem of developing metadata for geoinformation in Africa*. in *Proceedings in 4th AARSE Conference on geoinformation for sustainable development in Africa*. 2002.

[14] Guzmán, J.M., *The use of population census data for environmental and climate change analysis.* Population dynamics and climate change, 2009: p. 192.

[15] Karsidi, A., *Now or Never ; Informasi Geospasial untuk SDG'S* Post 2015, Majalah Sains Indonesia. p. 90-93.

[16] A., K. *Kumpulan Paparan Kepala Badan Informasi Geospasial Infrastuktur Data Geospasial dan One Map Policy BIG*. 2013.

[17] A., K., *One Map Policy; Dapat Cegah Konflik Lahan* in *Majalah Sains Indonesia*. 2013. p. 26–28.

[18] Clare, V.Z. *Impliction of Industry 4.0 for geospatial professionals, EE Publiser, June 2017[20]*

[19] Longley, P.A., et al., *Geographic information systems and science*. 2005: John Wiley & Sons.
[20] Karsidi, A., *Kebijakan Satu Peta (One Map Policy) Roh Pembangunan dan Pemanfaatan Informasi Geospasial di Indonesia.* Bogor: SAINS PRESS Sarana Komunikasi Utama, 2014.
[21] Behm, D., et al., *The Past, Present and Future of Geospatial Data Use.* Trajectory, February, 2018. **1**: p. 2018.

The Comparison of Point Cloud Registration Quality on Maptek I-Site Studio and Cloud Compare

Fathur Rahman[1], G A Jessy Kartini[1]*, Hary Nugroho[1]

[1]Geodesy Engineering, Institut Teknologi Nasional, 23 PH.H. Mustofa Street, 40124 Bandung, Indonesia

*Corresponding author's e-mail: ayujessy@itenas.ac.id

Abstract. Data registration is one of the critical methods of point cloud processing. Point cloud processing software would have different results, both from quality registration and meshing results. The objective of this research is to find how much different the quality of registration and meshing shape between Maptek I-Site Studio and Cloud Compare. In this study, the registration method used is cloud to cloud. The experimental object is the KOPEL building in the Bosscha Observatory area, Lembang which has a cylindrical shape. The quality of registration of Maptek I-Site Studio software is 0.002 m on all scan worlds. However, the registration quality of cloud Compare in the range of 0.004 m-0.011 m. Based on the single point accuracy is 0.069, the RMSE of Maptek I-Site Studio is better than Cloud Compare. In the meshing process, Could Compare displays better results compared to Maptek I-Site Studio.

Keywords: Point Cloud, Registration, Cloud to Cloud, Meshing, Maptek I-Site Studio, Cloud Compare.

1. Introduction

The development of a complete survey and mapping world makes it a variety of mapping techniques at a particular location or objects. One of them is the Terrestrial Laser Scanner (TLS), which is used to map objects and produce 3-dimensional (3D) shapes. Terrestrial Laser Scanner (TLS) is a mapping technology that utilizes laser beams to provide 3D coordinates for objects appearing automatically and in real-time by using active sensors [1].

The TLS process consists of several steps, including data acquisition, data processing, and 3D model presentation. Before we start data acquisition, we need to make a plan to put the TLS. The results of data acquisition are point cloud and can form a 3D surface modeling [2]. Each point has a 3D coordinate value (x, y, z) and an intensity value (i). Intensity value (i) is a value that represents the reflection of the object that is treated by the laser but does not represent the original color of the object being scanned, due to the inability of TLS to acquire colors that match the original color [3]. After data acquisition in the field, the data processing is carried out in this process which involves data registration, data filtering, meshing, and 3D modeling where the results of 3D object modeling become the final result in mapping 3D objects with TLS.

Data registration is a process of combining TLS recording data from various standing positions (scan world) into one or the same coordinate system [4]. According to Reddington (2005), there are four methods, namely 1) cloud to cloud, 2) target to target, 3) combination and 4) traverse method. This study uses a cloud to cloud registration method. Basically, the cloud to cloud method combines some of the world scan data (SW) by determining the same cloud point and recorded on the SW data to be combined. This method can produce proper registration if when weeding between the two SWs to be registered, the overlap area is generally 30% -40% [2].

This research will use Maptek I-Site Studio software and Could Compare software. The choice of the software is because both are often used and become quite a favorite choice in processing point cloud data. Both software has different categories for Maptek I-Site Studio is software that has a license, while for Could Compare is open-source software.

This research was conducted at the KOPEL building in the Bosscha Observatory area. This building is a cultural heritage in Indonesia. In addition, KOPEL buildings are cylindrical and have a high level of detail so that they can show significant differences when the results of the meshing process are generated in each software.
From the explanation above, what we want to know in this research is the accuracy of the value of Root Mean Square Error (RMSE) on each registration result of software used for the same type of tool in the process of data acquisition. The similarity in shape and degree of completeness produced by the meshing process in each software compared to the original form of the KOPEL and can provide information about the registration and meshing process in the software used.

2. Methodology
Cloud to Cloud Registration is a registration method using the Iterative Closed Point (ICP) technique to synchronize data from two contiguous SW [5]. This technique requires the operator to select at least 3 points corresponding to the data point cloud. By selecting 3 points that are approximately corresponding, the ICP algorithm system will iteratively check the distance from all point clouds and estimate the transformation to align the two SWs to produce the minimum possible correction [2] as shown in Figure 1.
In making measurements using this method, there is one condition that must be met to get a good registration result, SW from each position has a 30-40% overlap [2].

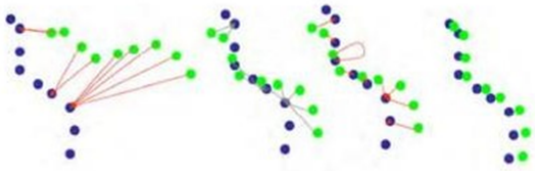

Figure 1. Illustration of cloud to cloud registration [6].

The parameter used for comparison on the results of registration between software is the RMSE value generated. In this study the tolerance of the RMSE value used is the tolerance obtained from the TOPCON GLS-2000 tool specifications. According to [7], to find out whether the registration RMS value meets tolerance or not, it can be done by calculating single point accuracy. Based on the specifications of the TLS tool used, the magnitude of the error value on the Y axis is identical to the distance measurement error which is 3.5 mm, while the error value on the X axis and Z axis is identical to the angle measurement error of 6 arcsecond. The value of dx and dz at a distance of 10 m can be determined as follows [7].

It is assumed that:
dx = dz = sin (6 arcsecond) 10 m = 0,29 mm.

The value of single point accuracy can be determined as follows:

$$SPA = \sqrt{dx^2+dy^2+dz^2}$$
$$= \sqrt{0.29^2+3.5^2+0.29^2}$$
$$= 3.52 \text{ mm}$$

Information:
SPA = *Single Point Accuracy*
dx = Error measuring distance on axis x
dy = Error measuring distance on axis y
dz = Error measuring distance on axis z
The amount of fault tolerance is determined based on a 95% confidence level, as follows [7]:

Error tolerance value = 1.960 SPA
= 1.960 (3.52 mm)
= 6.90 mm ≈ 6.9 mm

From the above calculation it can be concluded that the data resulting from the registration process can be declared to meet error tolerance if the registration RMSE value obtained is "≤" 6.9 mm.
Meshing is the process of aiming to form a solid, closed surface on an object. According to [8] meshing consists of a collection of vertices, edges, and polygonal that approach the surface of the object, can be seen in Figure 2. The type of meshing that is often used is the shape of a triangular polygon.

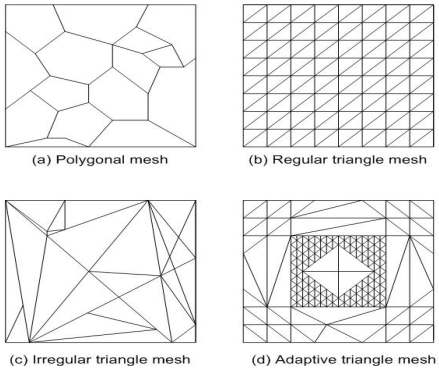

Figure 2. Polygonal Mesh Representation [8].

The methodology to be carried out in this research can be seen in Figure 3.

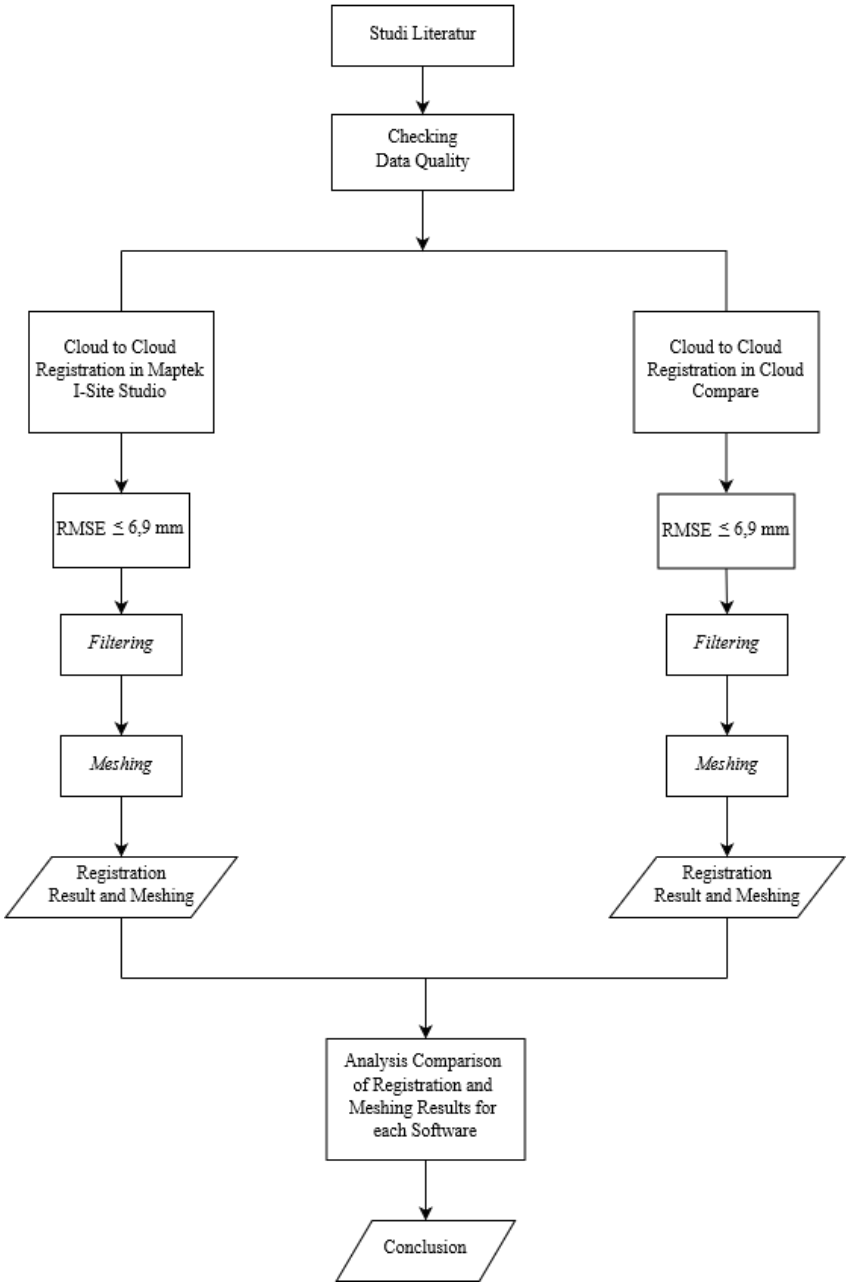

Figure 3. Research Methodology.

3. Maptek I-Site Studio Registration and Data Filtering Results

The results of data registration and filtering can be seen in Figure 4, which shows the results of the four sides of the KOPEL building.

(a) (b) (c) (d)

Figure 4. (a) Front View, (b) Back View, (c) Right View, and (d) Left View.

Maptek I-Site Studio software produces good registration when viewed visually. In addition to showing the visual form of the object in the registration process, it will also display the RMSE accuracy value for each SW, which can be seen in Figure 5 below.

	Data	Warning	Error	Matched point pair count	Sampled point count	Proportion of matched sampled points	Warning	Error	Registered RMS separation	Overall summary
1	ATP9_SCN0001	10.000000%	5.000000%	195	100	195.000000%	0.010m	0.020m	0.002m	✓
2	ATP7_SCN0001	10.000000%	5.000000%	144	100	144.000000%	0.010m	0.020m	0.002m	✓
3	ATP6_SCN0001	10.000000%	5.000000%	100	100	100.000000%	0.010m	0.020m	0.002m	✓
4	ATP5_SCN0001	10.000000%	5.000000%	101	100	101.000000%	0.010m	0.020m	0.002m	✓
5	ATP4_SCN0001	10.000000%	5.000000%	87	100	87.000000%	0.010m	0.020m	0.002m	✓
6	ATP3_SCN0001	10.000000%	5.000000%	150	100	150.000000%	0.010m	0.020m	0.002m	✓
7	ATP2_SCN0001	10.000000%	5.000000%	106	100	106.000000%	0.010m	0.020m	0.002m	✓
8	ATP1_SCN0001	10.000000%	5.000000%	183	100	183.000000%	0.010m	0.020m	0.002m	✓
9	ATP8_SCN0001	10.000000%	5.000000%	197	100	197.000000%	0.010m	0.020m	0.002m	✓

Figure 5. Report on Maptek I-Site Studio Registration Results.

In the report on the above registration results can be seen that all SWs get the same accuracy value that is equal to 0.002 m, which results show that Maptek I-Site Studio software entered into a predetermined tolerance that is 0.069 m based on the single point accuracy of the tool used.
The factor that makes the value of each SW in this software small and within tolerance is the ICP process that runs well at each stage, so there are no deficiencies in the ICP process. The ICP process went well as evidenced by the number of point clouds when data acquisition in the field amounted to 5,103,104 points, after the ICP process the number of point clouds became 5,100,509 points. This shows that the ICP process in Maptek I-Site Studio software runs according to all stages by removing several point clouds that do not have a partner. Maptek I-Site Studio software has the advantage of being able to do repetition in the cloud to cloud registration process, so repetition of the registration process is very helpful in getting the final result RMSE accuracy value is very minimal.
After registering cloud to cloud data to prove that the data generated by TLS is included in the tolerance or not used statistical calculation of distribution T. In this study using a confidence interval of 95%. The results of the calculation of the T distribution can be seen in Table 1.

Table 1. T-Student Test for Maptek I-Site Studio.

ID	Distance between objects		X (m)	σ (m)	95% Confidence Level		Information
	Measuring Tape (m)	TLS *(m)*			*Lower*(m)	*Upper*(m)	Accepted/Not
D1	1.280	1.2775	1.27875	0.003606	1.272	1.283	Accepted
D2	1.000	1.0020	1.00100	0.003162	0.997	1.007	Accepted
D3	1.550	1.5510	1.55050	0.002000	1.548	1.554	Accepted
PB1	0.450	0.4490	0.44950	0.001414	0.447	0.451	Accepted
PB2	0.543	0.5435	0.54325	0.002236	0.540	0.547	Accepted
PB3	1.680	1.6810	1.68050	0.002000	1.678	1.684	Accepted
TB1	2.121	2.1210	2.12100	0.004243	2.114	2.128	Accepted
TB2	0.199	0.1970	0.19800	0.002828	0.193	0.201	Accepted
TB3	0.249	0.2460	0.24750	0.004472	0.239	0.253	Accepted
TB4	2.720	2.7215	2.72075	0.003536	2.717	2.726	Accepted
PD1	1.850	1.8495	1.84975	0.001000	1.848	1.851	Accepted
B1	1.000	1.0015	1.00075	0.003000	0.997	1.006	Accepted

Based on table 1 it can be seen that all distance data generated by Maptek I-Site Studio software can be received statistically. Therefore, the distance data in Maptek I-Site Studio software does not have a significant difference with the distance measured by measuring tape in the field. Based on the results of the RMSE and T distribution statistical tests it can be stated that the results of data processing carried out at Maptek I-Site Studio have good and appropriate accuracy and precision, where the level of accuracy is seen based on the RMSE results while the level of precision is seen based on the results of the T distribution statistics test.

4. Cloud Compare Registration and Data Filtering Results

The results of registering and filtering data using Could Compare software can be seen in Figure 10 to Figure 6 below.

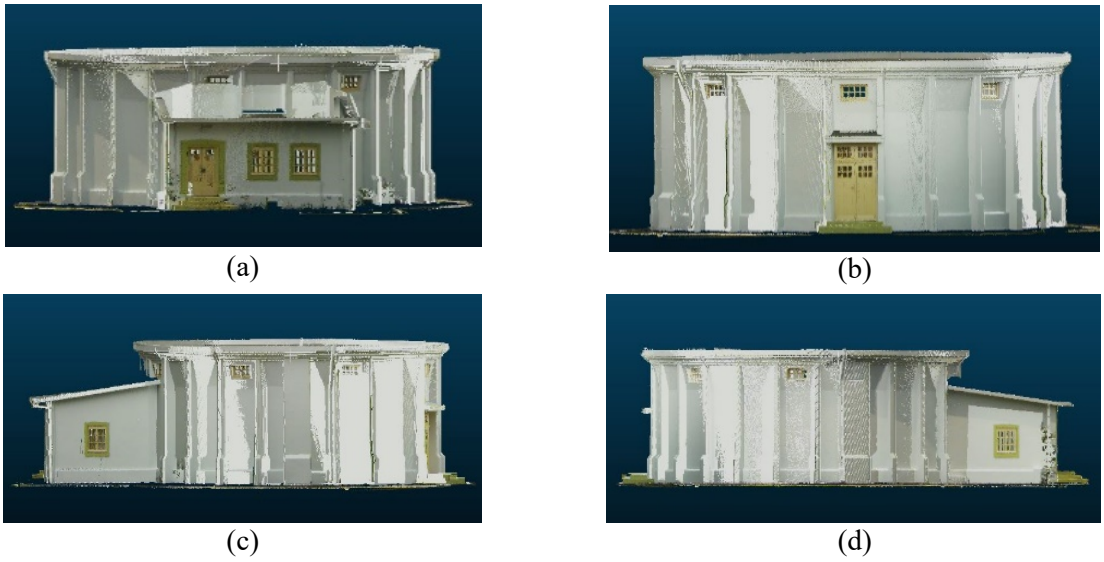

(a) (b) (c) (d)

Figure 6. (a) Front View, (b) Back View, (c) Right View, and (d) Left View.

The Cloud Compare software displays visual results as well as the Maptek I-Site Studio software, it can be seen that the Cloud Compare registration results provide the same visuals as in the field. When viewed from the report the results of the Cloud Compare registration still have a SW that does not fall within the tolerance that can be seen in the following Table 2.

Table 2. Report the Registration Results Could Compare.

Data Scan World	Final RMSE
ATP1_SCN0001-ATP8_SCN0001	0.004 m
ATP1_SCN0001-ATP8_SCN0001-ATP9_SCN0001	0.004 m
ATP1_SCN0001-ATP8_SCN0001-ATP9_SCN0001-ATP7_SCN0001	0.004 m
ATP1_SCN0001-ATP8_SCN0001-ATP9_SCN0001-ATP7_SCN0001-ATP6_SCN0001	0.008 m
ATP1_SCN0001-ATP8_SCN0001-ATP9_SCN0001-ATP7_SCN0001-ATP6_SCN0001-ATP5_SCN0001	0.010 m
ATP1_SCN0001-ATP8_SCN0001-ATP9_SCN0001-ATP7_SCN0001-ATP6_SCN0001-ATP5_SCN0001-ATP4_SCN0001	0.011 m
ATP1_SCN0001-ATP8_SCN0001-ATP9_SCN0001-ATP7_SCN0001-ATP6_SCN0001-ATP5_SCN0001-ATP4_SCN0001-ATP2_SCN0001	0.010 m
ATP1_SCN0001-ATP8_SCN0001-ATP9_SCN0001-ATP7_SCN0001-ATP6_SCN0001-ATP5_SCN0001-ATP4_SCN0001-ATP2_SCN0001-ATP3_SCN0001	0.010 m

In the table above the RMSE value generated in the last 5 stages cannot meet the established tolerance that is equal to 0.069 m, the first cause that makes the RMSE value not meet tolerance is when determining the point cloud pair is not so accurate because the overlapping area is part of the wall from the building so it is difficult to identify each point cloud pair that is used as a reference. Another thing that makes the RMSE value not included in tolerance is because the ICP process that occurs in Cloud Compare is not going well, because there are stages that are not implemented, namely the weighting and rejecting stages. The cause of these stages is not going well because the Cloud Compare software cannot accommodate large data at the time of processing so that the number of point cloud data acquisition results in the field is equal to the number of cloud points after the cloud to cloud registration process, the number of point cloud is 5.103.104 point.

The weakness of this software is that it can only register once and cannot be repeated so as to make point cloud matching less than optimal, and the weakness of this software is that the registration process is done in an aligned manner (manually) so that the user must determine point pairs will be used as a reference manually, because inaccuracies in the selection of point pairs cause the results of the RMSE value will be greater.

On the results of registration of the Cloud Compare software distance comparison is also done using T distribution statistical tests such as Maptek I-Site Studio software. The results of the calculation of the T distribution statistics can be seen in the following Table 3.

Table 3. T-Student Test for Cloud Compare.

ID	Distance between objects		X (m)	σ (m)	95% Confidence Level		Information
	Measuring Tape (m)	*TLS* (m)			Lower (m)	Upper (m)	Accepted/Not
D1	1.280	1.2775	1.27875	0.005000	1.270	1.285	Accepted
D2	1.000	1.0070	1.00350	0.010296	0.991	1.023	Accepted
D3	1.550	1.5575	1.55375	0.011180	1.540	1.575	Accepted
PB1	0.450	0.4490	0.44950	0.003162	0.444	0.454	Accepted
PB2	0.543	0.5365	0.53975	0.009849	0.521	0.552	Accepted
PB3	1.680	1.6800	1.68000	0.007071	1.669	1.691	Accepted
TB1	2.121	2.1205	212075	0.005000	2.113	2.128	Accepted
TB2	0.199	0.2080	0.20350	0.012728	0.188	0.228	Accepted
TB3	0.249	0.2520	0.25050	0.005099	0..244	0.260	Accepted
TB4	2.720	2.7210	2.72025	0.007382	2.710	2.732	Accepted
PD1	1.850	1.8500	1.85000	0.004243	1.843	1.857	Accepted
B1	1.000	1.0070	1.00350	0.010296	0.991	1.023	Accepted

Based on Table 3 it can be seen that all distance data generated in the Cloud Compare software can be received statistically where the distance value used is at the minimum and maximum values determined based on a 95% confidence interval. Therefore, the distance data in the Cloud Compare software does not have a significant difference with the distance measured with a measuring tape in the field.

Based on the results of the RMSE and T distribution statistical tests, it can be stated that the processing data carried out on Cloud Compare has an inaccurate accuracy because the RMSE values generated in cloud to cloud registration in the last 5 stages cannot be included in the specified tolerance so they still have a value poor accuracy, while for the level of precision of data seen based on the results of the T distribution statistics indicate a good level of data precision because all distance data used can be accepted all. It can be stated that the Cloud Compare software has good precision but does not have a good level of accuracy.

5. Meshing Results

In Maptek I-Site Studio software, the results of meshing Triangulation on Original Point are better and provide more interpretation in accordance with the actual form compared to the results of meshing Triangulation on Projected Point. In the results of the Triangulation on Original Point meshing, all detail forms in the building can be produced expressly where the most visible on the wall really matches the original shape, there are no bends or bends.

The process of meshing with a surface with a complex topology performed on Maptek I-Site Studio software is represented based on irrengular triangle mesh, where the reference of the representation is viewed based on [8], irrengular triangle mesh produced by Maptek I-Site Studio can be seen in figure 7(a). Meshing results obtained in this software still have shortcomings because it can be seen at the front of the building that has not been formed solidly. This is due to the use of feature size that is still not appropriate so that the formation of irrengular triangle mesh to the data point cloud is still not bound or formed.

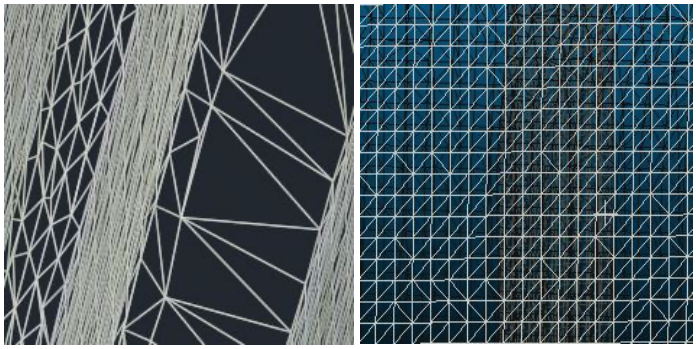

Figure 7. (a) Representation of Maptek I-Site Studio Meshing (b) Representation of Cloud Compare Meshing.

Meshing processing in the Could Compare software results in better meshing compared to Maptek I-Site Studio. Using the Poison Surface Reconstruction process to display complex results yields good results.
In the software Compare Compare the shape representation of the polygon used is Regular Triangle Mesh, where the representation structure displays a neat and orderly surface, and the value given to the octree depth used is very precise so that it can produce a meshing shape that matches the actual shape of the building and have a good level of detail too. The shape of the Regular Triangle Mesh representation can be seen in Figure 7(b).
A comparison of the two software with the actual form of the KOPEL building can be seen in Table 4. In the table it can be seen that the two software have similarities with the actual shape of the KOPEL building but both software still has shortcomings, such as the Could Compare software that produces a form that very solid compared to Maptek I-Site Studio still has shortcomings, especially that seen in the front window of the building there is still such a triangle mesh stacking which is due to the large amount of point cloud data that is not erased. While in Maptek software it is clearly seen that the front is not yet solid so that this software cannot represent the building optimally.

6. Conclusions

Based on the results of research and discussion described in the previous chapter, the following conclusions can be drawn that Maptek I-Site Studio software has better RMSE accuracy than Cloud Compare software. All RMSE values in each SW in Maptek I-Site Studio meet tolerance with an RMSE value of 0.002 m and a tolerance of 0.069 m. On the results of the comparison between the distance between Cloud Compare and Maptek I-Site Studio with the results of validation stipulates that the distance generated by the two software can be accepted and is within the range that has been determined statistically. Meshing results that are very good and in accordance with the original are the results of meshing from Cloud Compare, because all parts of the building are solid, and the details displayed are very in accordance with the actual shape of the building.

7. References

[1] Mills, J dkk. 2003. An Addendum to the Metric Survei Specifications for English Heritage– the collection and archiving of point clouds data obtained by terrestrial laser scanning or other methods. Version 11/12/2003.
[2] Quintero, M. S., Genechten, B. V., Bruyne, M. D.,Ronald, P., Hankar, M., dan Barnes, S. 2008. Theory and practice on Terrestrial Laser Scanning. Project (3D Risk Mapping). University of Applied Sciences St. Lieven, Belgium.
[3] Vidyan, Y., et al., *Pemanfaatan metode TLS (Terrestrial Laser Scanning) untuk pemantauan deformasi gunung api. Studi kasus: kerucut sinder Gunung Galunggung, Jawa Barat*. Jurnal Lingkungan dan Bencana Geologi, 2013. **4**(1): p. 49-69.

[4] Wibowo, H.W., *Pengukuran Plant Satellite Nilam 2 Pt. Vico Indonesia Menggunakan Laser Scanner Scanstation 2 Dengan Registrasi Metode Target To Target*. 2013, Universitas Gadjah Mada.
[5] Simbolon, A.B.S., B.D. Yuwono, and F.J. Amarrohman, *Analisis Perbandingan Ketelitian Metode Registrasi antara Metode Kombinasi dan Metode Traverse dengan Menggunakan Terrestrial Laser Scanner dalam Pemodelan Objek 3 Dimensi*. Jurnal Geodesi Undip, 2017. **6**(4): p. 285-294.
[6] Pfeifer, N. 2007. Overview of TLS System, Overall Processing and Applications. ISPRS Summer School. Ljubljana, Slovenia.
[7] Nandaru, A., B. Sudarsono, and B.D. Yuwono, *Studi Registrasi Point Cloud Pada Pemrosesan Data Terrestrial Laser Scanner (Tls)(Studi Kasus: Jembatan Gading Batavia, Kelapa Gading, Jakarta Utara)*. Jurnal Geodesi Undip, 2014. **3**(4): p. 201-2011.
[8] Abdelmajid, Y., *Investigation and comparison of 3D laser scanning software packages*. 2012.

Acknowledgments
We thank to Geodesy Research Group, Institut Teknologi Bandung for helping us provide a place for processing laser scanner data.

Scanning of Isola UPI Building using Terrestrial Laser Scanner with Cloud to Cloud and Traverse Registration Methods

Kurniawan Djamal[1], G A Jessy Kartini[1]*, Hary Nugroho[1]

[1]Geodesy Engineering, Institut Teknologi Nasional, 23 PH.H. Mustofa Street, 40124 Bandung, Indonesia

*Corresponding author's e-mail: ayujessy@itenas.ac.id

Abstract. The ongoing maintenance of old buildings (heritage) needs to be considered, for this reason it is necessary to consider documentation to ask for the authenticity of old buildings that are included in the building of cultural heritage. To support this in terms of documentation, it is necessary to do 3D modeling to support the structural planning process by the three-dimensional building model. Technological developments in the field of surveying and mapping are now very well developed, both in 2D and 3D modeling. One of them is Terrestrial Laser Scanner (TLS), which can conduct data acquisition quickly and efficiently. TLS tool is able to provide 3D form visualization with a high point density on each object to be taken. There are 4 TLS Measurement methods: Cloud to Cloud method, Target to Target method, Traverse method, and Combination method. In research conducted at the Isola Building UPI uses a combination of traverse and cloud to cloud methods. The final result of this research is a 3-dimensional model of the Isola UPI Building in the form of a point cloud. The amount of RMS registration from the combination of two traverse methods and cloud to cloud is 0.010 m. Total error from a combination of two registration methods (RMSE) of 0.013 meters.

Keywords: Heritage Building, Terrestrial Laser Scanner, Traverse Method, Cloud to Cloud Method, 3D Model.

1. Introduction

The Rectorate Building of the Indonesian Education University (UPI) or commonly known as the Isola Building, is a Dutch heritage building designed by CP Wolf Schoemaker in 1933 which is included in the Cultural Heritage building. The government regulates cultural heritage buildings in Law No. 11 of 2010 Article 1 and Bandung City Regulation Number 21 of 2009 concerning maintaining and protecting the existence of cultural heritage in an effort to maintain it. Old buildings that are still suitable to be occupied have been transferred to various functions such as government offices, museum government, research objects and research laboratories. The ongoing maintenance of historic buildings needs to be considered, for this reason there is a need to document 3D Building Isola UPI. To support this in terms of documentation, it is necessary to hold 3D modeling to support the structural engineering planning process by architects on the three-dimensional model of the Isola UPI Building.

Technological developments in the field of surveying and mapping are now very well developed, both in 2D and 3D modeling. One of them is Terrestrial Laser Scanner (TLS), which can conduct data acquisition quickly and produces high accuracy. The TLS tool is able to provide 3D form visualization with high point densities on each object to be measured. The working principle of TLS itself uses electromagnetic waves that are emitted to objects then reflected back and received by the tool. The results of the recording using a laser scanner in the form of millions of accurate X Y Z coordinate points, with a very high point density in a short time which makes it a potential for large-scale applications in 3D mapping such as tunnels, bridges, and historic heritage buildings.

In making 3D models of an object using Terrestrial Laser Scanner, it cannot only be done with a single tool standing, it must be several times a device. The results of weeding each tool stand (scan world) are combined or registered. The registration process is a stage that combines several different world

scans of the data acquisition process which then becomes a unified point cloud [1]. Basically, the level of accuracy of the TLS tool cannot be separated from the registration process in use. According to [2], registration can be divided into 3 methods, namely cloud to cloud method, target to target, combination, and traverse. In research conducted at the Isola Building UPI uses two methods, the traverse method and cloud to cloud. The results obtained are 3D visualization of the Isola UPI Building in the form of a point cloud which can later be useful as preliminary data in architectural planning on the formation of the 3D model of the Isola UPI Building and for the purposes of conserving old buildings (heritage) and documenting historic buildings that are already included in the cultural preservation.

2. Research Methodology

The research was carried out in one of the buildings that have been included in the list of Cultural Heritage, namely the ISOLA Building, Universitas Pendidikan Indonesia (UPI). The Isola UPI building is located on Jl. Dr. Setiabudi No. 229, Sukasari, Bandung West Java 6° 51' 40.11" S - 107° 35' 39.00" E. The research method used in this study can be seen in Figure 1.

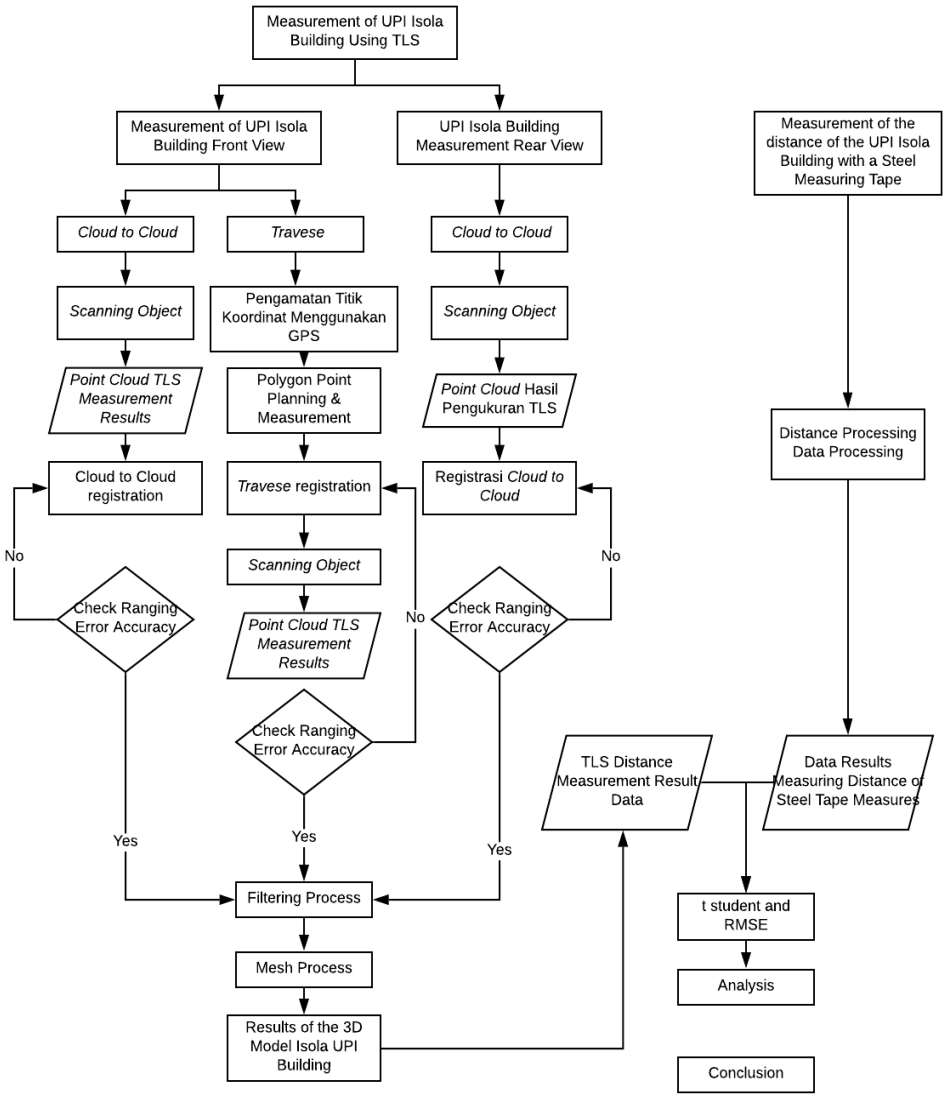

Figure 1. Implementation Flow Chart.

The stages of the research methodology carried out are as follows:

- Data Retrieval.
- Pre-Processing.
- Registration data, at this stage of registration is the stage where the process of combining the same point-clouds from different positions (stand points), or at this registration process is changing the coordinates of common point-clouds from different positions into the same coordinate system. Traverse method registration is done at the time of measurement in the field, because the measurement principle of this method uses global coordinates or the coordinates of the original field data filtering, at this stage of filtering is done to eliminate objects that are not needed such as trees, humans and so forth. This filtering process uses software that is available as a package for the processing of point-cloud data. The final results of this study are in the form of 3D point cloud Gedung Isola UPI.
- Data Analysis, comparing distances from 3D results of Isola UPI Building with field size results.

3. Results and Discussion

3.1. Front and Rear View of Isola UPI Building Results

In the research conducted in the making of the 3D model of the Isola UPI Building using Terrestrial Laser Scanner, it was carried out with a combination of two methods at the time of measurement and registration. In the process of registering the traverse method when processing data requires a known point coordinates, so that when merging the world scan is done automatically. The results of the front view of the Isola Building 3D point cloud model can be seen in Figure 2.

Figure 2. 3D Front View of the Isola UPI Building.

The process of weeding using the cloud to cloud method is relatively easy because the position of the TLS tool is free to be placed anywhere as needed. Unlike the traverse method that requires coordinate points before weeding. Scann world registration process using the cloud to cloud method is done manually, which is to equate the form of the object world scan results with one another. For example, the object chosen at the time of registration is usually the corner of a building, window or door. The results of the 3D point cloud model appear behind the Isola UPI Building can be seen in Figure 3.

3.2. Analysis of Registration of the Combined Traverse and Cloud to Cloud Method

The advantage of using the traverse method is that measurements for complex surface shapes and measurements of distances between scan worlds are quite long, because this method makes it easy to register. This method is possible if the coordinates of each TLS stand location are known, either through measurements with the Total Station or with previous GPS [3].

.

Figure 3. 3D Rear View of the Isola UPI Building.

From the scan to scan registration process the size of the Root Means Square (RMS) generated using the traverse method with four times weeding using a laser scanner of 0.011 meters. For the traverse method, errors are usually caused by several factors when measuring in the field, such as incorrect during the centring tool stage, errors when measuring prism height and errors when making backsight measurements.

Cloud to cloud method data registration process in this study, carried out with 6 different weeding points including FC6, FC7, FC8 FC0, FC11 and FC12. The amount of RMS generated using this method is affected by the distance of each world scan or overlap resulting from two world scans, quoting from [3] this method can produce good registration if when weeding between two world scans to be registered must have overlap the area is generally 30% -40%. In the registration process this method can be done repeatedly to produce the desired RMS, because this method uses local coordinates that are different from the traverse method that uses a binding point. The RMS value from the cloud to cloud method is 0.055 m. The cloud to cloud yield is smaller than the traverse method because registration with the cloud to cloud method can be done repeatedly while traversing cannot. The results of the combined registration RMS report of the traverse and cloud to cloud methods can be seen in Figure 4.

Overview

	Data	Proportion of matched sampled points	Registered RMS separation	Overall summary
1	F11ISOLA_SCN0001	53.000000%	0.006m	✓
2	F12ISOLA_SCN0001	73.000000%	0.007m	✓
3	FC0ISOLA_SCN0001	72.000000%	0.011m	✓
4	FC6ISOLA_SCN0001	80.000000%	0.010m	✓
5	FC7ISOLA_SCN0001	106.000000%	0.010m	✓
6	FC8ISOLA_SCN0001	31.000000%	0.011m	✓
7	P1ISOLA_SCN0001	153.000000%	0.009m	✓
8	P3ISOLA_SCN0001	167.000000%	0.009m	✓
9	P4ISOLA_SCN0001	65.000000%	0.012m	✓
10	P5ISOLA_SCN0001	127.000000%	0.012m	✓

Figure 4. Traverse & Cloud to Cloud Report Results.

In the registration of measurement results in the field, the amount of the RMS value will be seen after registration is complete. In Maptek RMS software results are shown with green, yellow and red indicators. The green color indicates that the registration result is within tolerance, the value limit for this green indicator is ≤0,100 m. The yellow color which means warning indicates that the registration result is not perfect, the range limit for this yellow indicator is ≥0,100 m and ≤0,200 m. The red color

means the error indicates that the registration result is bad, the tolerance value is ≥0,200 m. From figure 4, the two methods of traversing and cloud to cloud combined the value of RMS has entered tolerance with a value of ≤0,100 m, the average total size of RMS from the combined method of traverse and cloud to cloud in this study is 0.009 m.

3.3. Distance Comparison Analysis Using the T-Test

Statistical testing in this study aims to determine whether the measurement results using TLS and steel measuring tape have a significant difference and data results from TLS can be accepted or not statistically. With the difference in distance data, statistical tests are needed so that the quality of the data can be accepted or rejected. Accuracy test in this study was conducted by the t-distribution method. In statistical testing in this study, the sample data used were 14 samples, because the data samples used were small so the statistical test used was the t-distribution test method. Statistical test results can be seen in Table 1.

Table 1. Statistical Data Test Results by the T-Distribution Method.

No.	Point	Distance		X (m)	σ (m)	Confidence Level (95%)		Status
		Measuring Tape (m)	TLS (m)			Lower (m)	Upper (m)	
1	T1	2.992	2.9938	2.9929	0.00219	2.9911	2.9965	Accepted
2	T2	3.005	3.0014	3.0041	0.00417	2.9980	3.0084	Accepted
3	T3	2.983	2.9887	2.9844	0.00649	2.9778	2.9939	Accepted
4	T4	2.971	2.9616	2.9683	0.00867	2.9553	2.9769	Accepted
5	T5	3.019	3.0171	3.0181	0.00199	3.0153	3.0203	Accepted
6	D1	1.056	1.0543	1.0552	0.00241	1.0519	1.0579	Accepted
7	D2	1.056	1.0541	1.0551	0.00331	1.0507	1.0589	Accepted
8	D3	1.033	1.0398	1.0343	0.00802	1.0261	1.0462	Accepted
9	D4	1.050	1.0416	1.0475	0.00869	1.0347	1.0564	Accepted
10	L1	0.220	0.2284	0.2221	0.00912	0.2128	0.2356	Accepted
11	L2	0.220	0.2208	0.2202	0.00464	0.2146	0.2262	Accepted
12	L3	0.250	0.2546	0.2512	0.00759	0.2428	0.2618	Accepted
13	L4	0.250	0.2500	0.2503	0.00256	0.2474	0.2538	Accepted
14	L5	0.240	0.2401	0.2400	0.00538	0.2334	0.2468	Accepted

From the t-distribution result table using 95% confidence interval above shows that all values of the TLS measurement result and steel measuring tape can be accepted, therefore both data collection methods can be received statistically and there is no significant difference.

3.4. Data Accuracy Test

Each measurement must not be free from errors, as well as in the processing of size data, namely the registration process which is also not free from errors. To find out the total error resulting from TLS in making the 3D model of Isola UPI Building with a combination of traverse and cloud to cloud methods in this study can be calculated using the RMSE formula. The mathematical definition of RMSE is similar to the standard deviation, which is the square root of the average number of residual squares [4]. RMSE is the difference between the actual value and the measured value. After obtaining a distance from the size of the 3D point cloud model of the Isola Building UPI and the measurement of the distance of the steel measuring tape in the field, an RMSE accuracy test is then performed. The

amount of RMSE generated from measurements using TLS with a combination of traverse and cloud to cloud methods of 0.003 m is validated with a steel measuring tape.

3.5. Analysis of 3D Models

After obtaining the results of the 3D Isola UPI Building model using TLS tools with a combination of traverse and cloud to cloud methods, it can be seen that the shape of the 3D Building Isola UPI measured using TLS is approaching the original form in the field, and there are some parts of the UPI Isola Building look that are not scanned such as the roof, the canopy and the window affected by obstruction. Obstruction is noise from the measurement using TLS which is caused by several factors, including flowers or trees covering the object, humans standing near the object. On the roof itself many are blocked by plants located on building windows and the ability of TLS tools that do not cover the roof. However, on the façade of Gedung Isola UPI on the first floor it has been acquired well with TLS so it can be maintained its authenticity for the maintenance of old buildings (heritage). As in Figure 5 the results of the 3D point cloud façade of Isola UPI Building and photos of the Isola UPI Building.

(a) (b)

Figure 5. (a) Point Cloud 3D Façade Results of Isola UPI Building (b) Results of the Photo Gallery of the Isola UPI Building.

In Figure 5, the roof of the building was not acquired because the range of the TLS tool's camera for vertical viewing only covers 270 ° and field conditions are blocked by trees so it is not possible in the weeding process. Due to the fact that the roof did not acquire well so that it was problematic during the meshing process, the meshing process itself was carried out using cloud compare software that interpolates adjacent cloud points. On the roof when interpolated, it becomes bubbly due to inaccurate point cloud data filtering. Placement of the tool's standing position is also very influential in the formation of 3D models using TLS, the process of weeding using TLS is best done in the morning to evening because it affects the lighting on objects. The results of the UPI Isola Building meshing can be seen in Figure 6.

Figure 6. 3D Point Cloud Mesh Results of the Isola UPI Gedung Building.

4. Conclusions

Based on the results of research that has been done, the following conclusions can be drawn:

- From the results of the comparison of the accuracy of the distance between the TLS and the measuring tape produces an RMSE of 0.013 meters so that the accuracy obtained is still suitable for use in the conservation of the UPI Isola Building facade as a type of small structure.
- Based on the form of the UPI Isola Building facade produced by TLS close to the original form, but the roof and canopy of the upper window has not been well described.
- Based on the shape of the rear view of the Isola Building, UPI produced by TLS is close to the original form, but the roof is not well described.
- In 3D modeling with a combination of traverse and cloud-to-cloud methods, the average total RMS of the two methods is 0.009 m and the registration tolerance is less than 0.100 m.

5. References

[1] Vosselman, G. and H.-G. Maas, *Airborne and terrestrial laser scanning*. 2010: CRC press.
[2] Reddington, J., *HDS traing manual*. Leica Geosystem, 2005.
[3] Van Genechten, B., *Theory and practice on Terrestrial Laser Scanning: Training material based on practical applications*. 2008.
[4] Soeta'at, *Fotogrametri Analitik*, in *Jurusan Teknik Geodesi*. 1994: Fakultas Teknik Universitas Gadjah Mada.Yogyakarta.

Comparative Study of 3D Geographic Information System and Building Information Modeling for Facility Management

K N Fadhila[1]*, D Suwardhi[1]*, S W Trisyanti[1]*

[1]3D Modeling and Information System Division, Remote Sensing and GIS Research Group, Faculty of Earth Sciences and Technology, Institut Teknologi Bandung, 10 Ganesha Street, 40135, Bandung, Indonesia

*Corresponding author's e-mail: kavitanurfadhila@gmail.com, deni@gd.itb.ac.id, shafarina.wahyu@gmail.com

Abstract. Geospatial information is not only essential for the commercial sector and our daily lives, but also the foundation for many e-government applications, such as utility management and building smart cities. Currently, geospatial information is available in the form of 2-dimensional maps and 3-dimensional maps. Two 3-dimensional geospatial information technologies have started to be developed in various applications, namely Building Information Modeling (BIM) and 3D Geographic Information System (3D-GIS). 3D-GIS represents a 3-dimensional model of a large area such as a landscape, while BIM is intended for management planning, construction to maintenance of a building. The open standard data model and data exchange format for storing 3D-GIS models are called CityGML, while IFC is a popular data format for BIM. Both of these models can be used for a variety of requirements, for example, facility management. Currently, ITB Campus is developing an Information System for asset and facility management. Furthermore, problems arise in the 3D model that will be stored, whether using the CityGML or IFC models. In this study, a 3-dimensional model of simple house building using BIM and 3D-GIS will be conducted. The software used in this study is CMDBuild which uses BIMServer and PostgreSQL. The 3DCityDB is implemented as the new schemas in CMDBuild database. The two models will then be compared in terms of data structure and database so that the most appropriate 3D model can be determined for facility management. The result of this research shows that BIM is more effective than 3D-GIS for facility management.

Keywords: CityGML, IFC, 3DCityDB, BIMServer, 3D-GIS, BIM.

1. Introduction

The need for geospatial information is increasing along with the development of technology. It is because technological development also accompanied by geospatial information needs in every aspect. Moreover with the development of the Smart City concept, making geospatial information as a mandatory component in fulfilling various kinds of human needs. One example of these requirements is the need to manage facilities in the surrounding environment. In the previous era, facility management had been well unmeasured and was unconcerned with the spatial aspects of it. As a result, management of facilities carried out is less effective because it does not contain geographic information.

At present, there are two 3-dimensional spatial information technologies that are being researched and used in various applications, namely Building Information Modeling (BIM) technology and 3D Geographic Information System (GIS) technology. 3D-GIS represents a 3-dimensional model of a large area such as a landscape and is commonly used to map pre-existing objects, while BIM is intended for management planning, construction, and maintenance of a building from an architectural and construction point of view [1]. Both of these models can be used for a variety of needs, one of which is for facility management.

This study aims to compare 3D-GIS and BIM in terms of data structure and database. In terms of data structure, these two models will be compared in semantic, geometry, topology, and visual aspects. After

that, CityGML and IFC as open data models and 3D-GIS and BIM data exchange formats will be imported into the database for spatial query. The database used for importing CityGML is the 3D City Database, while the database used for importing IFC files is BIMServer. The result obtained from this study represents the most appropriate 3D model for facility management needs. The first section of this paper discusses CityGML and IFC in general and the provisions that apply in it. The second section explains the materials and methods used in this paper. The third part of this paper explains data structure of CityGML and IFC. The last section of this paper explains the characteristics of the two data models after being imported into the database and spatial query carried out for facility management.

2. CityGML and IFC

2.1. City Geographic Markup Language (CityGML)

One method that commonly used in 3-dimensional modeling is 3D-GIS. 3D-GIS (Geographic Information System) is used to model and analyze spatial data of urban environments from a geographical perspective [2]. To build the 3-dimensional model, a data format that is suitable for 3D-GIS is used. CityGML is an open standard data model and exchange format that can store 3D models of cities and landscapes based on Geography Markup Language (GML), as identified by the Open Geospatial Consortium (OGC) in the Extensible Markup Language (XML) format [3]. CityGML has several uses, including urban planning, management of utilities and facilities in a building, disaster risk analysis and determination of disaster evacuation, navigation, and so forth.

Modeling in CityGML is divided into 5 different levels of detail (LOD). This study only focuses on CityGML in building modeling. The lowest level of CityGML modeling is represented in LOD0. LOD0 illustrates the footprint of each building and usually covers regional and landscape areas. LOD1 is a form of primitive building that has not been described in detail, usually only in the form of blocks or cubes and covers the city or region. The buildings in LOD2 have already seen the details and have begun to differentiate between roofs, buildings, and land. The LOD2 area covers a city district project. LOD3 is the development of LOD2 which already has an opening in the form of doors and windows. The area covers architectural models (outside) and landmarks. As for the highest level of detail, LOD4 is the development of LOD3 which is equipped with a building interior. LOD4's area covers architectural models (interior).

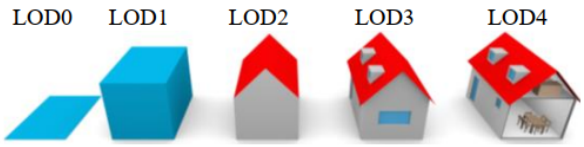

Figure 1. The Five Level of Details Defined by CityGML [4].

2.2. Foundation Classes (IFC)

Besides 3D GIS, one of the other 3-dimensional models that are often used to model a building is Building Information Modeling (BIM). BIM is a building model that is often used in architecture and construction to exchange information about project activities, both in terms of the 3d model in detail and terms of project implementation management. One data format that is often used in BIM is Industry Foundation Classes (IFC). IFC describes the BIM model information scheme into very detailed objects. IFC can model a building up to 700 objects. Modeling in IFC is represented in the Level of Development (LOD). This level of development describes the IFC model at each level of project development. So that this Level of Development does not clearly explain the scope of the object modeled by IFC.

2.3. 3D City Database (3D CityDB)

As more cities and countries use CityGML to model their territories, the need for databases used to store these data models is increasing. One database that can be used to store CityGML data is the 3D City Database (3DCityDB). 3DCityDB is an Open Source software that allows users to import, manage, analyze, visualize, and export virtual 3D city models according to CityGML standards (Yao, et al., 2018). Database schema results from mapping the object-oriented CityGML data model to a spatially improved relational database management system (RDBMS) that is usually connected with PostgreSQL and PostGIS. The 3DCityDB can be accessed by using CityGML Importer / Exporter or directly accessing database tables whose relational structure is known.

2.4. BIMServer

BIMServer is made by Graphisoft which is intended for architects, interior designers, and planners. Graphisoft BIM Server acts as central file storage, document management, and framework to facilitate interaction and collaboration between users via the Internet. BIMServer is based on IFC open standards. BIMServer is open source which can also be used by commercial software. Therefore, BIMServer is ideal for supporting the development of architectural, engineering, and construction projects.

3. Data and Methods

The data used in this study is a 3D model of a simple house building. This simple house consists of 2 floors with 7 rooms. The 3D GIS data used in this study is CityGML LOD4 regardless of its appearance. CityGML LOD4 is a 3D model with the highest level of detail. The selection of LOD4 is because in the management of facilities the object being modeled must be detailed so that management of each object in the house can be carried out. While the BIM model used is in the IFC format. The detailed information of the IFC model is following the detailed information in 3DCityDB so that the objects analyzed from these two models are the same. The following is a complete explanation of the data used which is presented in tabular form.

Table 1. Data Source.

	Source	**Website**
CityGML LOD4 FZK-Haus	Karlsruhe Institute of Technology (KIT), Applied Computer Science Institute.	www.citygmlwiki.org
IFC (2x3) FZK-Haus	Karlsruhe Institute of Technology (KIT), Applied Computer Science Institute.	www.ifcwiki.org

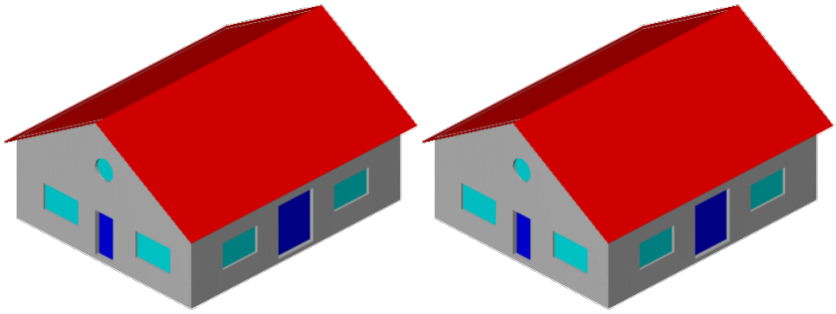

Figure 2. CityGML LOD4 FZK-Haus (left) and IFC (2x3) FZK-Haus (right)**.**

The two models are then processed by understanding the data structure. Understanding data structures can be done by understanding existing programs in CityGML and IFC. This model is displayed in Notepad ++. After understanding the data structure, the next step is to import the two models in the

database. The process of importing CityGML into a database can be done using 3D City DB Importer / Exporter. While the process of uploading IFC to BIMServer can be done through mapping IFC to BIMServer via a database scheme in PostgreSQL. Uploading CityGML to 3DCityDB is done automatically by 3D CityDB Importer / Exporter while uploading IFC to BIMServer is done manually by selecting what objects we want to upload to the database.
After uploading to the database, the next step is to compare the data structure and database of the two models. In terms of data structure, CityGML and IFC will be compared in terms of semantics, geometry, and topology and visualization. While in terms of databases, the two models will be compared in terms of relations, attributes, and spatial analysis. Spatial analysis is carried out in the form of spatial queries relating to facility management.

4. The difference between CityGML and IFC Data Structure

4.1. Semantic aspects

The semantic aspects of CityGML are realized as classes in CityGML that are used to model buildings. The CityGML data structure in terms of semantics is shown in the following figure. The semantic aspects mentioned in the diagram below are semantic aspects of CityGML modeled in LOD4.

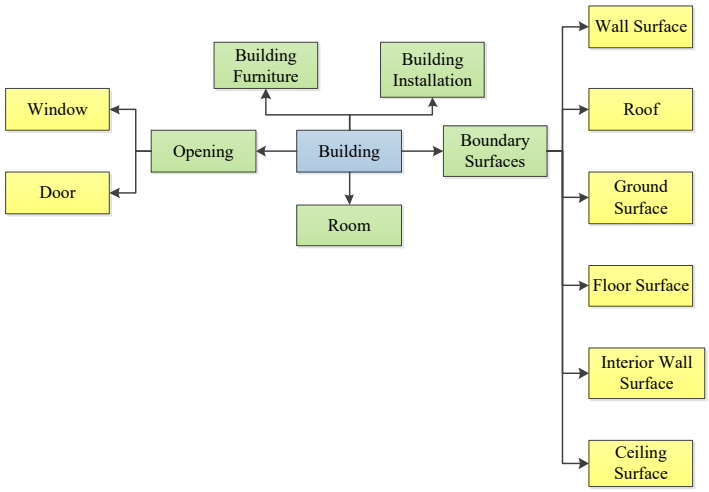

Figure 3. Semantic Aspects of CityGML LOD4**.**

Room in CityGML is an abstract form of a room. A room can be used to perform spatial queries such as the number of openings in a room, calculation of the volume of a room, calculation of wall area, and so forth. A room in CityGML is limited by BoundarySurface in the form of *InteriorWallSurface, Ceiling,* and *Floor*. *BoundarySurface* in a room is associated with a special function called *Solid*. Whereas *WallSurface, RoofSurface,* and *GroundSurface* are the boundaries for building entities. So, this entity acts as a barrier in a building.
Opening in CityGML can refer to Outer Boundary and Inner Boundary. In the CityGML data structure, defining opening is only done once either in the Outer Boundary or the Inner Boundary. If a previous definition has been made, both in terms of coordinates and relationships to other entities, then in another Boundary it is sufficient to be connected or called using the Xlink function.

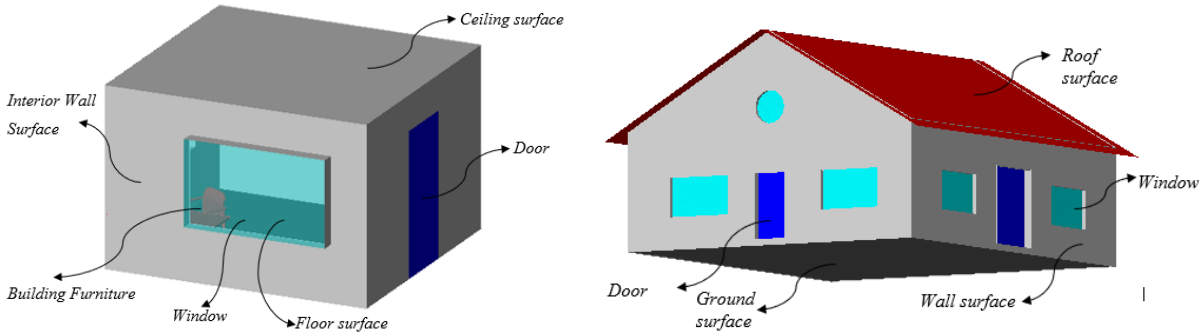

Figure 4. Visualization of *Room 2* FZK-Haus (left) and Visualization of *Outer Boundary* FZK-Haus (right)**.**

The semantic aspects of the IFC data structure are as follows:

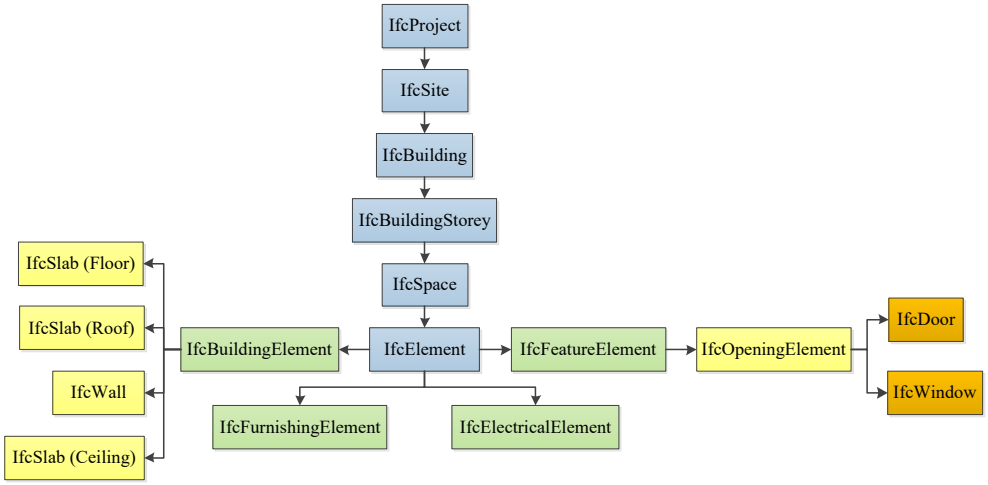

Figure 5. IFC Data Structure**.**

Just like CityGML, the data structure in IFC is also hierarchical. The entity with the highest level in IFC is IfcProject. IfcProject defines all matters relating to the project being worked on, whether related to geometry or other attributes in IFC such as building history information. IfcProject is then explained further by IfcSite about its geometrical aspects. Then IfcBuilding defines the geometrical aspects of a building in the project. IfcBuildingStorey defines the geometry of the floor in a building. From IfcBuildingStorey then proceed with IfcSpace to define every space in the building. In IfcSpace several entities are in that room. These entities are incorporated in IfcElement. Then the indoor entities in IfcElement are divided into other IFC elements such as *IfcWall, IfcDoor, IfcWindow, IfcSlab (Roof), IfcSlab (Ceiling),* and *IfcSlab (Floor). IfcWall, IfcSlab (Roof), IfcSlab (Ceiling),* and *IfcSlab (Floor)* function as boundaries between spaces in IfcSpace. Whereas IfcDoor and IfcWindow function as opening or opening in buildings.

Although the hierarchy is the same, in CityGML the modeling is divided into detailed levels in each LOD (Level of Detail) which is clear. However, at IFC, building modeling is not divided into a clear level of detail. Whereas in IFC, LOD is the Level of Development which shows the level of ongoing project development. This is because IFC as a standard data model for BIM was initially used for construction and architecture purposes.

The IFC model used in this study is a simplified model. So that the semantic aspects modeled in this study are only the basic semantic aspects. However, the IFC model, in general, can model semantic

aspects to very detailed levels. A very detailed IFC model can model up to the opening parts such as door handles, door frames, and so on. As a result, the IFC model is a more appropriate model to be used as facility management from semantic aspects.

4.2. Geometric Aspects

Apart from the semantic aspect, the difference in data structure between CityGML and IFC can also be seen from the geometric aspect. Broadly speaking, the geometry comparison of each object in CityGML and IFC is explained in the following table:

Table 2. Geometric Aspects of CityGML and IFC.

	CityGML	**IFC**
Building	Solid	GeometricCurveSet, Brep
Building Storey	-	GeometricCurveSet, Brep
Room/Space	Solid	Curve2D, GeometricCurveSet, SweptSolid, Clipping, Brep
Wall	MultiSurface	SweptSolid, SurfaceModel, Brep, Clipping, BoundingBox
Window	MultiSurface	Curve3D, GeometricCurveSet, Annotation2D, SweptSolid, SurfaceModel, Brep
Door	MultiSurface	Curve3D, GeometricCurveSet, Annotation2D, SweptSolid, SurfaceModel, Brep
Floor	MultiSurface	SweptSolid, Brep, Clipping, MappedRepresentation, BoundingBox
Ceiling	MultiSurface	SweptSolid, Brep, Clipping, MappedRepresentation, BoundingBox
Roof	MultiSurface	SweptSolid, Brep, Clipping, MappedRepresentation, BoundingBox
Ground	MultiSurface	SweptSolid, Brep, Clipping, MappedRepresentation, BoundingBox

In LOD4 CityGML Building is modeled in Solid geometry which is connected by external references (Xlink) with the geometry of building boundaries, such as *Wall Surface, Roof Surface, Ground Surface, Outer Ceiling Surface, Floor Surface, Door,* and *Window*. The second semantic aspect, *Ground Surface,* is modeled in *MultiSurface* geometry. *Ground Surface* consists of several surfaces that are visible from outside the building as a boundary of a building. Just like *Ground Surface*, other semantic aspects such as *Wall Surface, Roof Surface, Outer Ceiling Surface,* and *Outer Bottom Surface* are also modeled in *MultiSurface* geometry which is seen from outside the building as a barrier of a building. This *MultiSurface* geometry has also been mentioned explicitly in the CityGML data structure. As for the last semantic aspect, the room is represented by *Solid* geometry because it is limited by the other entities that surround it.

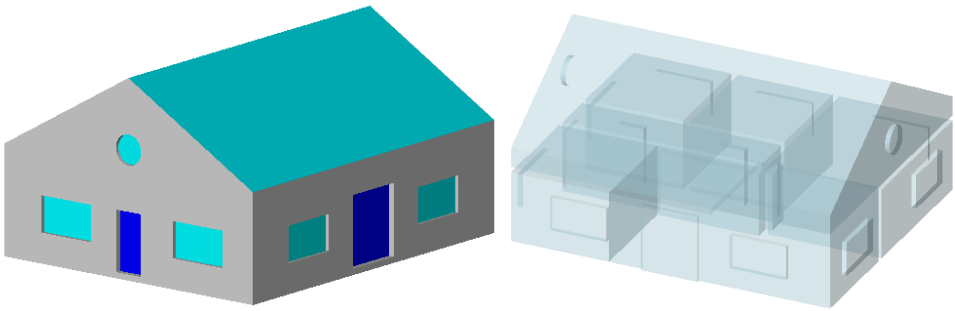

Figure 6. Solid in a building and a room**.**

One of the differences in the structure of CityGML and IFC lies in the wall. In CityGML there are 2 types of walls namely *WallSurface* and *InteriorWallSurface*. Whereas in IFC there is only *IfcWall*. *WallSurface* defines the outer walls of buildings, while *InteriorWallSurface* defines walls in parts of a building. Meanwhile, at IFC both the inner and outer walls are only defined by *IfcWall*. However, for facility management, this is not very influential considering that facility management carried out for a wall does not cover the total number of walls.

4.3. Topology Aspects

The topology aspect of CityGML is influenced by the geometry of each object being modeled. *Wall, Window, Door, Ceiling, Floor, Roof,* and *Ground* are represented by *MultiSurface* topology. This is because each object is composed of several surfaces that are not connected. Each of these geometries can be connected to any spatial relationships such as disjoint, overlap, touching, or disconnected. However, multisurface does not have clear rules regarding spatial relations between objects.

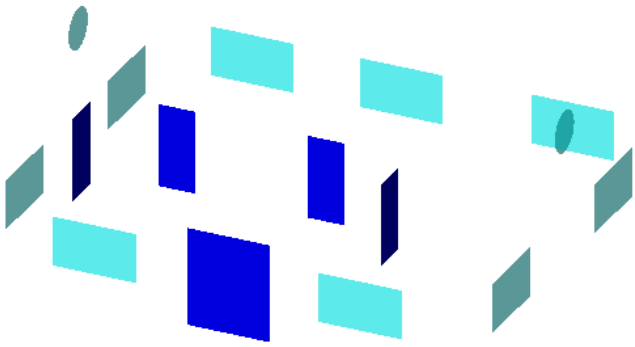

Figure 7. Multisurface of Door and Window in CityGML LOD4 FZK-Haus**.**

Besides *Multisurface*, CityGML is also equipped with Xlink topology. This Xlink mechanism functions to call the geometry of an object that has been defined elsewhere. Example 1 door can be used in 2 different rooms. As a result, to avoid redundantly, the mention of a door in another room only needs to be done by calling the same door object in the previous room using XLink. In IFC, there is also a topological relationship between entities. The topology in CityGML and IFC can also be explained in Figure 3 and Figure 5. The two figures show the sequence scheme of each semantic aspect that is modeled in both models. From the two images, it can be seen that the data structure of CityGML and IFC is in the form of a hierarchy. However, even though both forms are hierarchical, the topology of IFC is more difficult to understand and requires in-depth knowledge to be able to understand it. As a result in terms of topology, IFC is more difficult to use compared to CityGML.

5. The Difference Between 3D City Database and BIMServer

5.1. Relational Database Schema Aspects

The process of uploading CityGML to 3DCityDB is relatively easier because there is no need to use a special program. Also, when uploading CityGML to 3DCityDB there were some simplifications which caused several classes in CityGML to be merged into a new class in 3DCityDB. Classes in CityGML are mapped to 3DCityDB by inserting these classes into tables that are already available. These tables are then linked together to form a relation table. Tables that function as a link to all the tables in 3DCityDB are called objectclass tables. In this table, all classes in 3DCityDB are defined. Then to complete the attribute table object class cityobject table is used to store the attributes that exist in each class. The complete 3DCityDB database scheme is shown in the following figure:

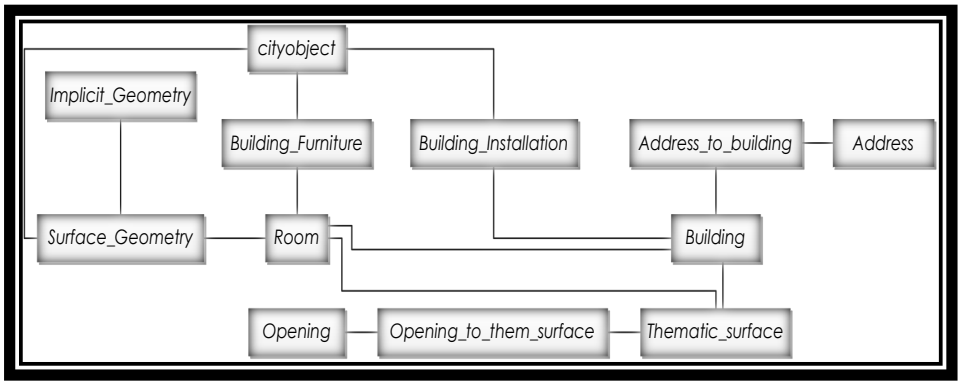

Figure 8. 3D City Database Schema**.**

BIMServer provides *Domains* to create relationships between classes in BIMServer. Because the classes in BIMServer are determined by themselves through the import mapping mechanism, making relations is done by themselves through *Domains*. In brief, the relational database schema in BIMServer is described as follows:

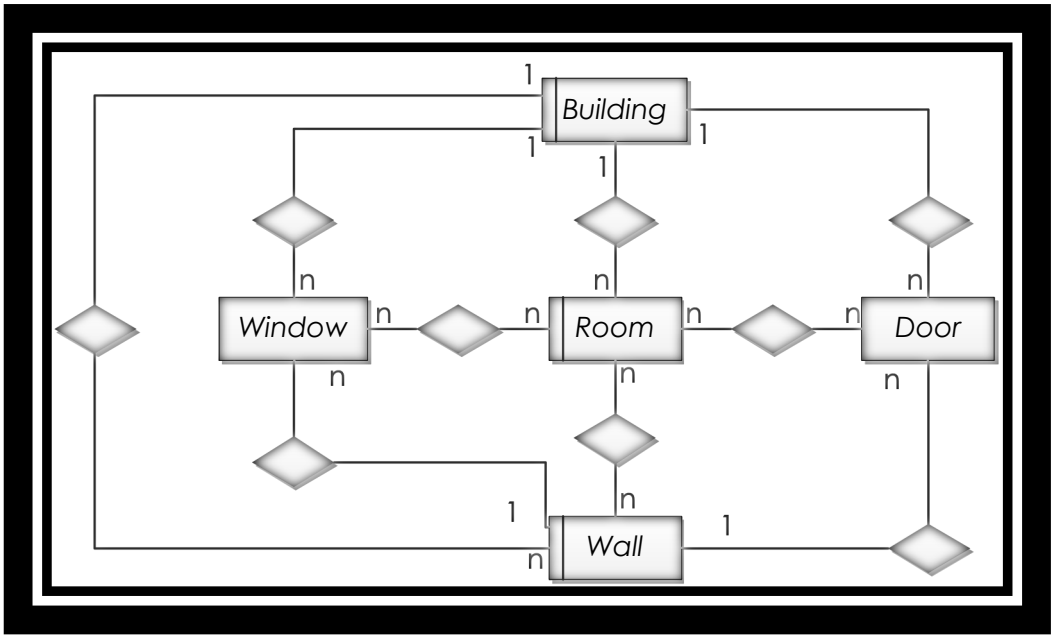

Figure 9. Relational Database Schema in BIMServer.

The difference of attribut in 3DCityDB and BIMServer are: 3DCityDB has been available in accordance with the provisions in 3DCityDB. It has a primary key and foreign key. While the BIMServer is customized by the user according to their individual needs.
From the explanation above, it can be concluded that the database schema contained in the 3D City Database follows the existing rules, whereas in BIMServer the database schema used can be made by the user. As a result, the data stored in BIMServer is more flexible and can be made according to needs. This advantage can be used to save storage space because data that is not used will not be stored in a database.

5.2. Attribute Aspects
The attributes in 3DCityDB are adjusted to the tables that are formed after uploading CityGML to the database. The attributes in this table can be the primary key that acts as the id of each table. Besides, there is a foreign key that functions to connect tables arranged in a relation table. Then, other attributes that do not function as primary keys and foreign keys are also available to store other information that can be used for spatial queries. Existing attributes in BIMServer are adjusted by the user. This is because the tables in BIMServer are made by themselves so that the attributes that are made are adjusted to the needs.

5.3. Spatial Query Aspects
The spatial query is intended to determine the quality of the model in carrying out facility management, the spatial query in question, among others: the total number of windows in a building, the number of doors in one room, wall area, and floor area. When calculating the number of windows in a building in 3DCityDB, the total number of windows generated is 32. Even though if counted manually there are only 16 windows. This is because the opening is called twice in defining the data structure. Defining 2 this time includes defining the window in each room. However, the calculation of the number of windows and doors at BIMServer is following the original conditions. While the calculation of the number of doors in each room is following actual conditions. Comparison of wall and floor area calculations is shown in the following table:

Table 3. Wall Area Calculation.

No.	CityGML (m^2)	IFC (m^2)
1	24.3	24.2
2	31.8	29.5
3	32.4	31.2
4	43.2	40.92
5	37.2	27.9
6	33.5	27.8
7	53.0	51.9

Table 4. Floor Area Calculation.

No.	CityGML (m^2)	IFC (m^2)
1	13.0	17.4
2	13.0	13.0
3	12.5	12.5
4	22.0	22.0
5	29.5	24.9
6	12.3	11.5
7	91.4	91.0

In general, the difference in the area of the wall between each room is not so big. But for rooms 1 and 5, this wide difference is quite large. This is because between room 1 and room 5 there is no dividing wall. Also, the CityGML and IFC models have differences in defining boundaries between the two rooms. As a result, the results of spatial queries in these two rooms for the CityGML model and the IFC model have significant differences. However, if we combine rooms 1 and 5 by adding up the results of the spatial query in the two spaces, the difference in the results of the spatial query in CityGML and IFC is not much different. This also applies to the calculation of floor area.
There is a slight difference in the calculation of the wall area in each room using IFC and CityGML. This is because there are slightly different geometric shapes in the two wall models. The difference in geometry can be seen in the following image.

6. Conclusions

From the comparison of data structures and databases that have been done, it can be concluded that BIM is better for facility management use compared to 3D GIS. However, the data structure in BIM is more difficult to understand so that a sufficiently in-depth understanding of the BIM model is used.

7. References

[1] Liu, X., et al., *A state-of-the-art review on the integration of Building Information Modeling (BIM) and Geographic Information System (GIS)*. ISPRS International Journal of Geo-Information, 2017. **6**(2): p. 53.
[2] Sani, M.J. and A.A. Rahman, *GIS and BIM integration at data level: A review*. International Archives of the Photogrammetry, Remote Sensing and Spatial Information Sciences, 2018. **42**(4/W9).
[3] Deng, Y., J.C. Cheng, and C. Anumba, *Mapping between BIM and 3D GIS in different levels of detail using schema mediation and instance comparison*. Automation in Construction, 2016. **67**: p. 1-21.
[4] Gröger, G., et al., *OGC city geography markup language (CityGML) encoding standard*. 2012.

Acknowledgments

The authors would like to thank the 3D Modeling and Information System Group for helping data processing.

Prototype of Remote Sensing Data and Information System Based on Open Source Technology to Support Disaster Management

Muhammad Priyatna[1]*, Ahmad Sutanto[1], Taufik Hidayat[1], Aby Al Khudri[1], Iskandar Effendy[1], Rokhis Khomarudin[1], Sastra Kusuma Wijaya[2]

[1]Remote Sensing Applications Center – National Aeronautics and Space Agency (LAPAN), Indonesia
[2]Indonesia University, Depok, Indonesia

*Corresponding author's e-mail: mpriyatna@lapan.go.id

Abstract. Fast, precise and accurate remote sensing information is expected to increase support for disaster management in building an accountable disaster management system, as well as being a reference in disaster emergency response activities, according with Law No.24/ 2007 about disaster management. One of the functions of the Remote Sensing Utilization Center (Pusfatja) is to disseminate remote sensing information to users according to the Law Number 21 of 2013 Article 22 paragraph 1. The purpose of this project is to analyze the web-based information and disaster data systems. The method is used in this project is to make this system using open technology. The steps are taken in this project are identification of technological components and general architecture evaluations to facilitate the development, design and implementation of the system by updating, repeating testing and integrating open source software. The results showed that the system using prototype could implement and teste successfully. The prototype fully operate can be developed so that it can use for decision makers as a response to disaster activities in Indonesia and also as a reference in innovating technology and Geospatial information.

Keywords: Disasters, Emergency Response, Dissemination, Web Mapping, Opensource, Geospatial.

1. Introduction

The State of Indonesia has geographical, geological, hydrological and demographic conditions that enable disasters, whether caused by natural factors, non-natural factors or human factors resulting in human casualties, environmental damage, property loss and psychological impact. In accordance with the mandate of Law No.24 of 2007 on disaster management, the government and regional governments are responsible for the implementation of disaster management, from the pre-disaster stage, during the disaster to after the disaster [1]. The use of geospatial data and information in Indonesia is currently still experiencing various obstacles, one of which is the aspect of geospatial data and information. Many mapping activities that have produced geospatial data and information have been carried out, but the management system has not been given enough attention so that for the development and construction of a disaster management system there are many obstacles and there is still a lack of information and difficulties in accessing. The National Aeronautics and Space Agency in this case the Remote Sensing Application Center (Pusfatja) is ready to carry out the dissemination function of remote sensing information for the users according to the Law of Space Number 21 of 2013 Article 22 paragraph 1.

To overcome the problems mentioned above and support the development of data and information based on remote sensing data to the user in Indonesia. It is therefore necessary to develop the Disaster Management of the National Earth Monitoring System. This system is one of the main supporting facilities for the development and development of disaster mitigation in Indonesia as well as the service process of exchange and dissemination of geospatial data and information on natural disasters between institutions and the wider community both central and local government. One of the technologies that can be used to support it is Remote Sensing Technology and Spatial Information and

Communication Technology. The advantage of such technology is to have a wide, actual, and fast coverage and have excellent historical data. Spatial Information Technology and Communications allow users to obtain remote sensing information easily, quickly and accurately. It is a challenge for Pusfatja to continue to develop methods on the system of data presentation and spatial information remote sensing, especially better disaster information that can be trusted. This study aims to analyze the availability of data management and spatial information in disaster emergency response in Indonesia. So that will know the process of management of data availability and spatial information disaster good and efficient for disaster emergency response information user.

2. Research Methods

This Application Development is carried out with *Prototyping Development Methodology With Open Source Software* [2]. The implementation emphasized on the integration and practicality for the needs of users in the form of multi-application GeoFOSS (*Geospatial Free and Open Source Software*) through a process of revamping various building components to obtain a simple system with the term reengineering, namely the process of technology analysis to identify component components and their relationships and develop systems in a new form.

The stage of gathering requirements or initial requirements in the prototype with Open Source Based Software is carried out by searching for components that can be integrated.

In this study the steps taken are:

- Identify technological components and evaluation of the general architecture to facilitate the development.
- Rapid design and system implementation with repeated test updates and Open Source Software Integration.
- Implementation of prototypes into complete systems that operate in full.

2.1. General Architecture

This system adopts the general architecture of Spatial Information Infrastructure by following the conceptual Software Three-Tiers Archiatecture, compatible with proposal of Geospatial Free and Open Source Software (GeoFOSS) for Spatial Data Infrastructure (SDI) as shown in Figure 1 [3].

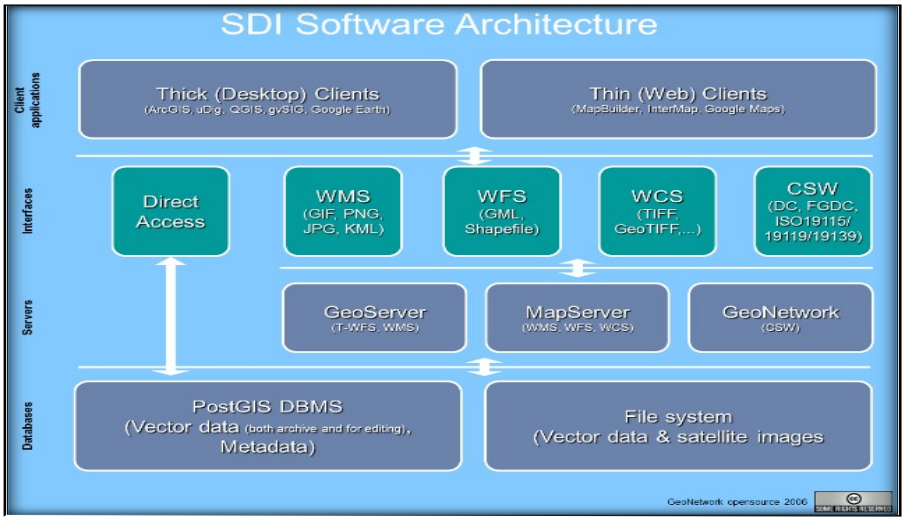

Figure 1. SDI Software Architecture [3].

The architecture is an established design pattern and software architecture, where the functional logical storage process, data access and user interface are developed and maintained as free modules

on separate platforms. *Tier* or *layer* on the architecture allows to be upgraded or replaced independently.
The read operation describes the access flow of information in an architecture, starting from the database layer through the server layer and interfacing to the Desktop GIS application layer or Web Browser. The Write operation describes the reverse information access flow from read operations.
The following sub-section discusses the components and functions of each tier or layer and logical structure of the read and write operations process information.

2.1.1. Data Base Layer. At the bottom tier or layer, integrated, compiled and customized storage in the form of database server and remote sensing information file system in order to achieve more efficient data management.
PostgreSql/PostGIS software [4, 5] is used as a Spatial Database Management System (DBMS) The server is compiled and customized for remote database management of remote sensing information and File governance systems or satellite image raster files in GeoTiff format.

2.1.2. Interface and Server Layer. In the middle layer is compiled, customized and integrated all services that help accessibility to the spatial information repository utilization Remote sensing. The middle layer also provides direct access services to remote sensing information databases with advanced queries and information load analysis. Spatial Information Infrastructure has 3 (Three) main server, namely: Map Server; Web Service Server; and Catalog Server.
Servers distribute and serve the contents of remote sensing information to the web, based on standard interfaces (eg Web Map Service (WMS), Web Feature Service (WFS), Web Coverage Service (WCS), ISO (19115/139) to facilitate access and use of information remote sensing online.

2.1.3. Application Layer. At the top layer are users and applications. Access to the information content of remote sensing utilization is possible either through the Desktop as well as the Web client. Desktop clients can be software packages with Geovisualization capabilities and GIS Desktop functions, such as GIS software packages (ArcGIS and Quantum GIS) or Map Viewer (Google Earth).
Suatu aplikasi Web GIS terdiri dari tumpukan perangakt lunak (stack of software) yang mampu melayani informasi penginderaan jauh melalui web. Struktur arsitektur akan mempertimbangkan dan mengacu pada komponen-komponen perangkat lunak lengkap untuk memenuhi kebutuhan atau persyaratan yang ditentukan oleh Model Pelaksanaa FreeGis [6].

2.2. Open Technology Survey
The open source technology survey focused on Open Source Software packages released under the General Public License (GPL) -like license, adopted by an active community, supports standard, stable and reliable formats [7].
The main technology and the Implementation Model are chosen in order to manage, discover, analyze and disseminate information, so that the System can be built and operated easily. The following software is considered and involved in the design of the prototype of the above-mentioned system. [6]**:**

- PostgreSQL Software (http://www.postgresql.org/). PostgreSQL is a very sophisticated open source DBMS,
- PostGis Software (http://Postgis.refractions.net/). PostGis adds support for geographic objects to the PostgreSQL DBMS, following OpenGIS Simple Features Specification for SQL,
- Geoserver Software (http://geoserver.org) is the most widely used WebGIS software.
- PyWPS Software (http: //pywps.wald.org intevation.org). PyWPS implements Web Processing Service (WPS) standards, provides geoprocessing functions,
- GeoNetwork Software (http://geonetwork-open source.org/), GeoNetwork is a catalog application for managing spatially referenced resources,
- OpenLayers Software (http://openlayers.org/). OpenLayers provides the Javascrtipt Application Program Interface (API) to integrate dynamic maps into web pages with ease.

- GeoNode software. GeoNode is a Geospatial Content Management System. GeoNode is built from open source project components: PostGis, GeoServer, Pycsw - CSW Metadata Catalog, Geospatial Pyton Libraries and OpenLayers-GeoEx

2.3. Web GIS Application Method

There are several stages done in the development of geographic information system application of this geography, namely: 1) Define the system - Development of GIS Web applications and the arrangement of integration and presentation of dynamic spatial visualization of geospatial information; 2) Determine the software component - This activity only takes into account GeoFOSS; 3) Building a prototype - This activity is intended to develop prototypes that have been defined by Installed, configured and Customize; 4) Determining and populating information - sets of information used in the form of geospatial information as well as integrating into GIS Web applications; 5) Test and evaluation - this activity is carried out to ensure all functions of the system are available and running as expected; 6) Operation and system support - GIS Web Application enters the operational and support stage. During the operation of the GIS Web application needs support in the form of maintenance.

Soft-line technology used in data presentation systems and remote sensing information is OGC-rated software, namely: GeoNode application. GeoNode is a geospatial content management system, a platform for the management and publication of geospatial data. It is a more mature and stable open source software project under a consistent and easy-to-use interface that allows users to share data and create interactive maps.

GeoNode is an open source project developed to support the development of web-based geographic information platform information and spatial data infrastructure [8]. GeoNode [9] is designed to be further developed and can be integrated on existing platforms and can be one of the nodes application of spatial data infrastructure (IDS).

GeoNode is built from the open source project component, the GeoNode component is: 1) PostGis - Spatial Databases [4, 5]; 2) GeoSever - OGC services [10]; 3) Pycsw - CSW Catalog metadata [11]; 4) GeodDjango [12]; 5) OpenLayers and GeoExt [13].

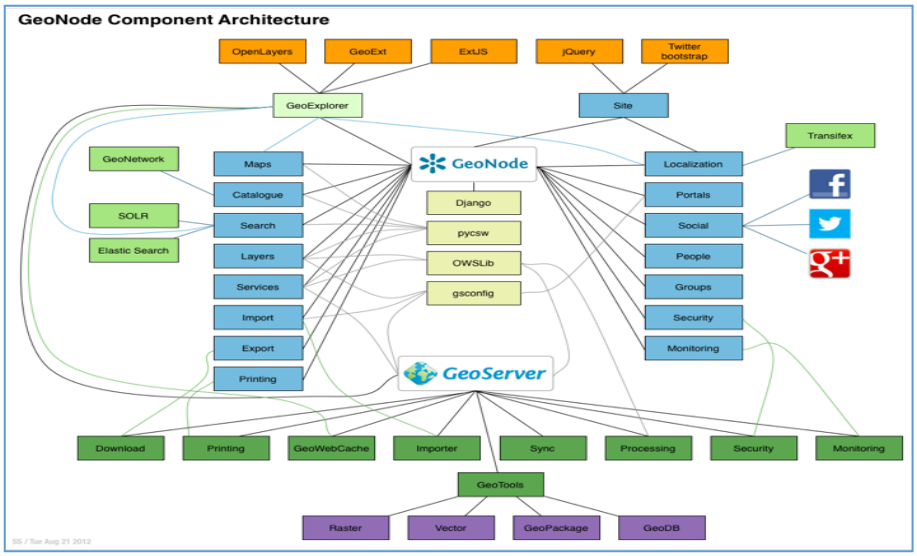

Figure 2. Geonode Architecture.

GeoNode applies GeoServer as an application that functions as a webGIS service. GeoServer allows us to publish data from various sources using protocols and standards from OGC.

The Catalog and metadata system is also supported by GeoNode by applying pycsw as a catalog and metadata service provider. GeoNode supports OGC standard services: 1) Web Map Service (WMS) for map drawing; 2) Web Feature Service (WFS) for vector information; 3) Web Coverage Service (WCS) for raster information; 4) Catalog Service for Web (CSW) for catalog information.
GeoNode is built using authentication framework and integrated with GeoServer. Layer and map ownership and permissions can be used to share data. These rights include, read, write, and make changes to the permissions. Data can be presented publicly or specifically to other users or user groups. GeoNode allows users to upload and manage spatial data over the web.
The uploaded spatial data can be used as web service according to OGC standard ie WMS and WFS [14]. Such spatial data may be available and may be processed by other users in creating maps and cartography. Supported features include: GeoExtpoler client, cartographic editor, interactive multi layer map, and can share and include maps in other web.
GeoNode can serve as a geospatial portal that provides spatial data exploration and search. GeoNode makes it easy to do visualization and use of the spatial data and allows users to upload and manage spatial data over the web.

3. Results and Discussion

Prototype system for presenting data and remote sensing information to support disaster management. This system is built on the web by using GeoNode application.
With this system is expected the user can access the spatial information disaster quickly and accurately online through the web browser. Spatial information is stored in a DBMS spatial database that uses PostGis software. Spatial information is in the form of layers, thematic maps, and some documents.

3.1. Layer

Layer is the main component of GeoNode. Layers are publication resources that represent spatial data sources in the form of raster data or vector data. Layers can be associated with metadata, ratings, and comments.
These layers are grouped by specific categories that include: Climatology Meteorology Atmosphere, Elevation, Environment, Farming, Location, Oceans. These layers contain the results of information extraction from remote sensing satellite imagery that has been widely used by the community. The following is an example of a layer view.

3.2. Map

The Map is one of the main components of GeoNode. Map consists of various Layer and style/Legend of the layer. Layers can be spatial data contained in local servers in GeoNode as well as spatial data coming from servers outside of GeoNode served from other WMS (Web Map Services) servers or by web service layers like Google or MapQuest. WMS is part of the Open Geospatial Consortium standard that manages the delivery of processed data to users via tools. By clicking on the map link, we will get a list of all published maps.
Maps can be created based on uploaded layers, combine them with existing layers and layers coming from web services, then share the resulting map for public view. Figure 3 sample map view (map) designed on the system. The Map (Map) in Figure 3 is constructed from the tsunami and earthquake disaster response layers in Palu (Central Sulawesi). Another example picture of 4 maps made tsunami disastern response layers in the Sunda Strait. Figure 5 flood disaster response map in Cilacap.

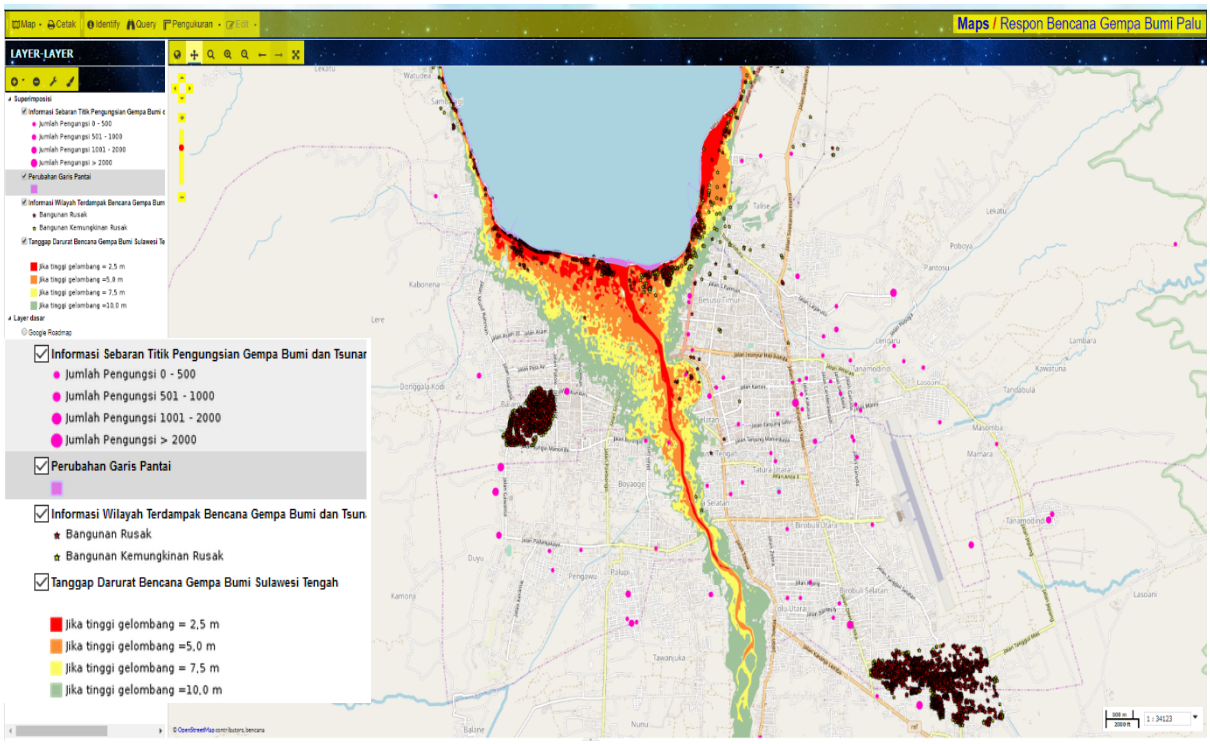

Figure 3. Map of earthquake disaster response in Palu (Central Sulawesi).

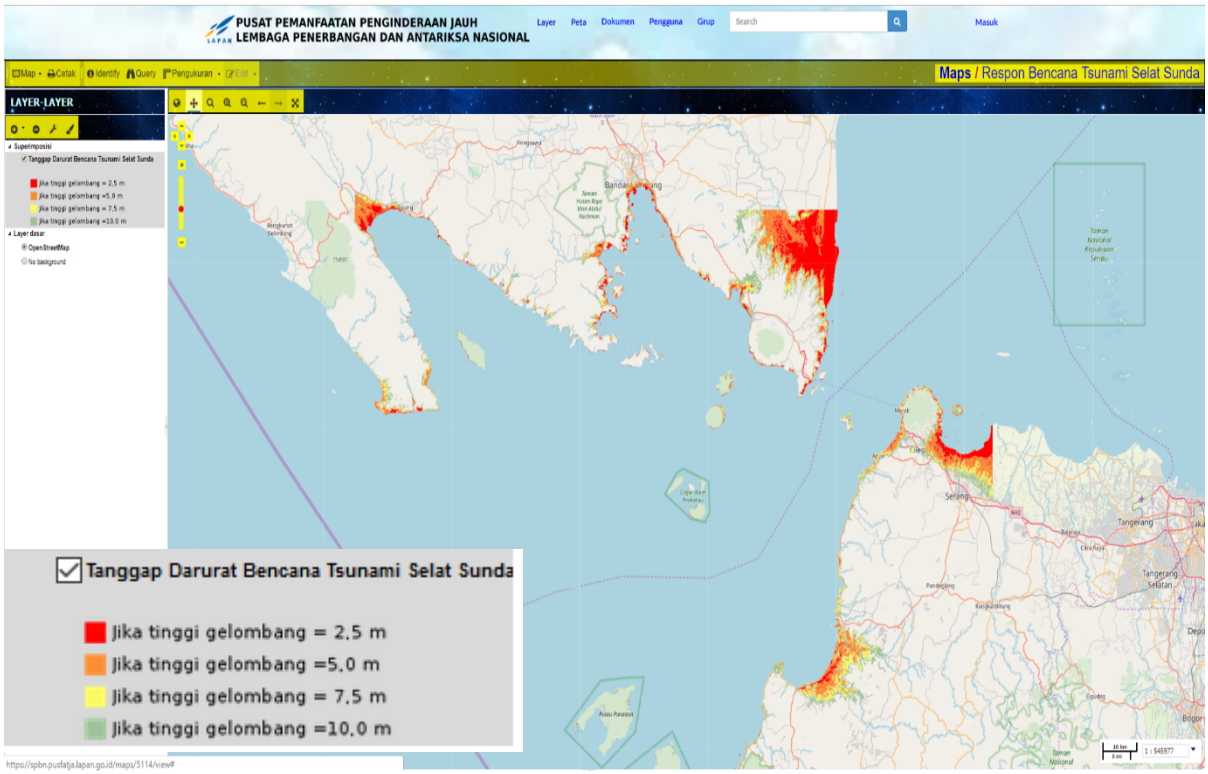

Figure 4. Map of Tsunami Disaster respones on sunda strait.

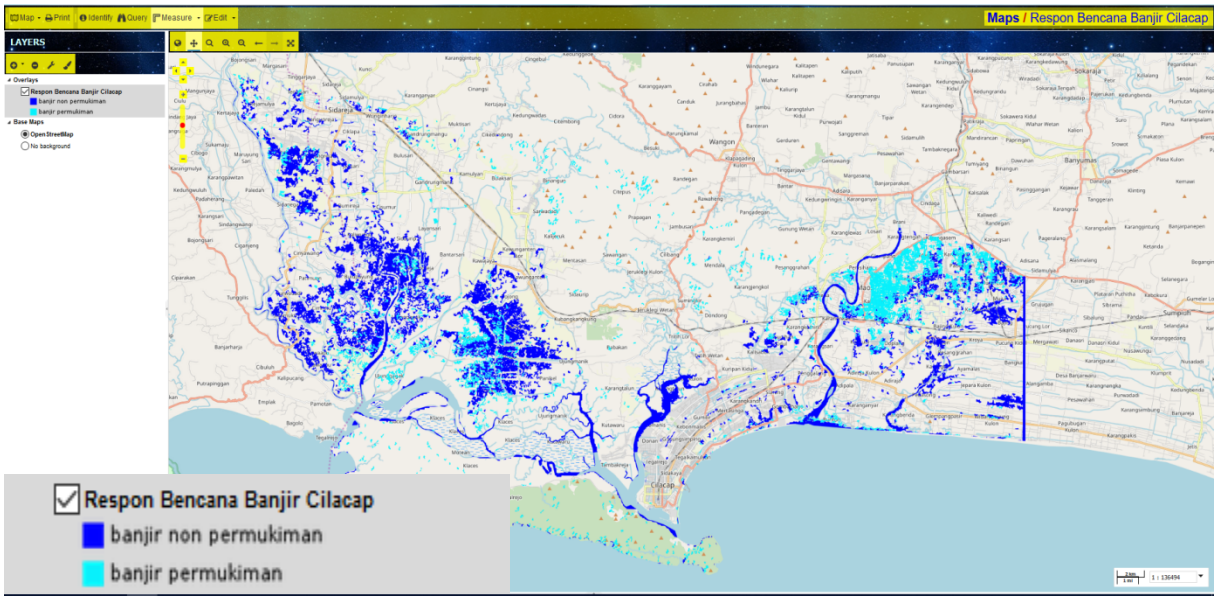

Figure 5. Flood disaster response map in Cilacap (Central Java).

In Map view there are a number of facilities / tools such as facilities based on export map into image file or html; facilities for printing maps; facility for object layer identification based on attribute table; facility to perform Query based on attribute table; facilities to measure distance and extent;

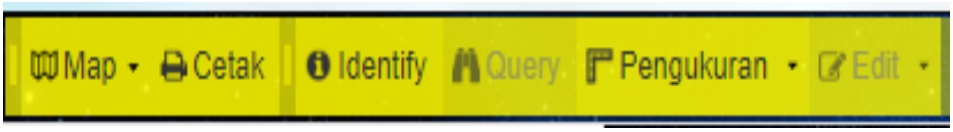

Figure 6. Facilities / Tools in Map.

4. Conclusions

Application of data presentation system and remote sensing information based on open source is expected to disseminate spatial and textual information of remote sensing utilization result implemented by Pusfatja LAPAN. This system integrates all the information results of remote sensing utilization and provides ease of access that is widely reachable by the user community.

Users can easily apply dynamic spatial visualization presentations, perform web mapping operations functions and spatial analysis of remote sensing-related information utilization to support and realize disaster preparedness and response so that management of Indonesian goes well.

Presentation system application of data and information based on Open Source allows its users to create and innovate in modifying the system according to the needs and characteristics of each. It is expected that this system can bridge between the users concerned especially in the scope of the utilization of national remote sensing.

5. References

[1] Bencana, B.N.P., *Peraturan Kepala Badan Nasional Penanggulangan Bencana Nomor 07 Tahun 2012 tentang Pedoman Pengelolaan Data dan Informasi Bencana Indonesia*. 2012, Jakarta.

[2] Hilton, B.N., *Open source software, web services, and internet-based geographic information system development*. 2014, Claremont Information and Technology Institute School of Information Science. 2014.

[3] J, T. *SDI Software Architecture*. 2007.
[4] Obe, R.O. and L.S. Hsu, *PostGIS in action*. Vol. 2. 2011: Manning Greenwich.
[5] Postgis, T., *Postgis 1.5. 1 Manual*. 2017.
[6] Francesco, D., et. al., *Analysis of the Free GIS Software Applications in respect to INSPIRE services and OGC standards.* 2011.
[7] McArdle, G., et al., *An open-source web architecture for adaptive location based services.* The International Archives of the Photogrammetry, Remote Sensing and Spatial Information Sciences, 2010. **38**(2): p. 296-301.
[8] Pickle, E., *GeoNode–A New Approach to Developing SDI*. 2010: na.
[9] Contributors, G., *Geonode–open source geospatial content management system*. 2015.
[10] Contributors, G., *Geoserver–open source server for sharing geospatial data*. 2015.
[11] Kralidis, T. and A. Tzotsos, *pyCSW–Metadata Publishing Just Got Easier*. 2014.
[12] Contributors, G. *A worldclass geographic web framework. Django Software Foundation*. 2014.
[13] Contributors, G. *JavaScript Toolkit for Rich Web Mapping Applications. GeoExt Community*. 2014.
[14] Mehdi, S.A., et al., *How to implement a governmental open source geoportal.* Journal of Geographic Information System, 2014. **6**(04): p. 275.

Land Cover Changes Research Level Subpixel A Case Study of Tasikmalaya City on Multitemporal Landsat Image

Ridwana R[1*], P Danoedoro[2], S Herumurti[2], S Himayah[1], L Somantri[1]

[1]Departemen Pendidikan Geografi, Universitas Pendidikan Indonesia, Jl. Dr. Setiabudi 229, Bandung 40154, Indonesia
[2]Penginderaan Jauh dan Kartografi, Fakultas Geografi, Universitas Gadjah Mada, Yogyakarta 55281, Indonesia

*Corresponding author's e-mail: rikiridwana@upi.edu

Abstract. The complexity of land cover region that could be mapped using terrestrial survey and high resolution satellite image. Although precision better but limited to the broad scope and scale produced. More than the need related to information on land cover changes in 1990 which required data based on two different times and the unavailability of high-resolution imagery. Therefore, the image of a relatively lower spatial resolution is still needed. Compilation problems that arise using intermediate resolution imagery such as Landsat with the presence of mixed pixels as a variety of differences in land cover in urban region. Mixed pixels will reduce the level of accuracy in multispectral classification, so analysis of the level sub-pixels is needed. Information on changes in land cover in sub-pixels, can be resulted through Linear Spectral Mixture Analysis, a pixel in Landsat imagery will be collected into four parts, namely impervious surface, vegetation, water, and bare soil. The results obtained showed endmember it was well received, in 1994 the accuracy rate was 94.44% and in 2003 the accuracy was 97.81%. Land cover impervious surface increased by 0.63% from the whole area, landcover of vegetation decreased by 0.81%, water land cover decreased by 18.25% and bare soil increased by 33.23%.

Keywords: Multitemporal Landsat Imagery, Linear Spectral Mixture Analysis, Change Detection.

1. Introduction

Land cover and the dynamics of displacement in urban areas are complex, because they are closely related to human factors and the physical environment. The expansion of the city also often occurs due to an increase in social and economic activities, for example urbanization has a great importance on the economy of the local community. Changes in land cover are also an important component of changes that are natural in nature so they have a broad impact on world climate change [1].

Land cover in urban areas is more difficult to identify with spectral compared to rural areas, due to heterogeneity in physical appearance in urban areas [2, 3]. The causes of this are related to vegetation cover, number of buildings, as well as the composition and composition of the building [4]. Like challenging spectral reflections from wetlands, rocky soils, and buildings will be very difficult to distinguish from Landsat images.

The remote sensing data contained in it is mixed pixels can only be confirmed into one class using conventional algorithms such as Algorithms, ParallelPiped, Minimum Average Distance Algorithms, and Maximum functioning Algorithms. Therefore, the regular classification used to classify pixels can reduce the quality of modeling, eliminate information, and reduce the accuracy results of classification. [5] To solve the problem of mixed pixels, there are many techniques that can be selected, incorrectly released using Linear Spectral Mixed Analysis. This method can be used for analysis at the subpixel level so that it can extract information in one pixel not just one class. This solution is suitable to be applied to Landsat imagery for urban studies which choose very diverse land cover. The spectral mixture analysis method is already quite widely applied in advanced countries, but in developing country such as Indonesia itself there are not too many. This research is needed to improve the level of understanding

of this method in analyzing changes in land cover in Tasikmalaya city and its surroundings based on Multitemporal Landsat imagery.

2. Methods

The method used in this study is digital analysis of multitemporal landsat images to determine land cover changes in the city of Tasikmalaya surrounding area with Linear Spectral Mixture Analysis. The process of detecting land cover changes is done by utilizing data from similar sensor systems, ranging from geometry, radiometry, spatial resolution, recording time, and number of bands [6, 7]. Land cover changes was obtained through a change detection analysis that produced information on vary in each land cover fraction at the subpixel level consisting of impervious surface, vegetation, water, and bare soil. Research locations in Tasikmalaya city and surrounding area. The study area was taken 700 x 700 pixels in which a pixel represented 30 x 30 m^2, the amount research region was 44,100 ha, Tasikmalaya city and its surroundings which could representative land cover fractions, impervious surface, vegetation, water, and bare soil.

3. Results and Discussion

3.1 Linear Spectral Mixture Analysis

The Linear Spectral Mixture Analysis process is capable of being a solution that is compatible with pixels contained in intermediate resolution images in the urban area. The principle in one pixel can be changed into some information that corresponds to linear reality. The results of this process form the fractions of land cover images according to the root mean square error. The image that discusses each fraction uses percentage pixels with gray levels in the range 0-1. This value means presenting most of the cover choices in pixels, simply the value of 0 means 0% and the value of 1 means 100% land covers a certain area in pixels. More details look at tables 1 and 2.

Table 1. Classification Results Endmember Abundance Value Linear Spectral Mixture Analysis the 1994 Landsat

Endmember	Maximum	Minimum	Average	Standart Deviation
Impervious Surface	9.714310	-0.925292	0.346260	0.487136
Vegetation	1.529173	-5.715897	0.582147	0.438726
Water	2.882548	-1.016518	0.204753	0.276664
Bare Soil	3.394641	-4.965809	-0.174264	0.450384
Root mean Square Error	0.144384	0.000022	0.011910	0.009937

Table 2. Classification Results Endmember Abundance Value Linear Spectral Mixture Analysis the 2003 Landsat

Endmember	Maximum	Minimum	Average	Standart Deviation
Impervious Surface	1.066640	-0.331535	0.313510	0.312493
Vegetation	1.351876	-0.314326	0.687762	0.323244
Water	2.090995	-1.363634	0.279264	0.282010
Bare Soil	1.621522	-0.825249	-0.114500	0.237515
Root mean Square Error	0,397505	0,000000	0,023684	0,017847

Statistics show a good value on the image endmember fractions 1994 (Table 1) and image endmember fraction in 2003 (Table 2) are not in the range of values 0 - 1 This can happen because the study area and surrounding urban form has a diversity of land cover which includes not the input endmember consisting of impervious surface, vegetation, water, and bare soil, but there are another object than classified into endmember input of land cover adjusted.
Having done some times in the selection of iteration input endmember, and then obtained results endmember fraction images (impervious, vegetation, bare soil, and water) with an average value of the lowest RMS error which is worth 0,011 for 1994 and for 2003 is worth 0, 02 (table 1 and table 2). The results of this statistical mean RMS error, this methods able good classify land cover. Fraction values at each endmember in a pixel if added together result a value same to one, that means that meets the limit function of a linear model of spectral separation.
Regardless of the reliability owned, please note that there are also weaknesses in this method. The weakness is that is tied to the amount of the input endmember linear, but in the field where the land cover is not only limited to the vegetation, impervious surface, bare soil, and water. So the pixel mixture where the most diverse land cover such as urban areas, have the highest error value. In addition to processing the Linear Spectral Mixture Analysis has been done, the value of the reflection of the water that has similarities with the bare soil endmember classifiable into bare soil, as well as cloud object, who has similarities with the endmember value impervious surface cover participate classifiable into impervious surface region. another weakness of the Linear Spectral Mixture Analysis which has actually been minimized through accurate determination of endmember.

3.2 Accuracy Test

Test the accuracy of this fact occurs in two stages. The first stages of the vast proportion of each sample measurement in the field and interviewing locals for the results of the Linear Spectral Mixture Analysis 1994 utilizing the second stage of 2002 DigitalGlobe Imagery to the results of the Linear Spectral Mixture Analysis in 2003, and test the accuracy of the RMS Error begins with taking samples were done purposively, with distribution taking evenly on each endmember fraction image results are Linear Spectral mixture Analysis. Total number of samples tested by 30 samples and attempted selected sample has a composition of 100% if all four endmember overlayed. The selection of samples to be tested at least consider objects that are assumed not to change.
Checking the accuracy of the imagery are Linear Spectral Mixture Analysis 1994 against field measurement data sample and interview local people, obtaining an average RMS error for the entire land cover 94.44%. The accuracy test of the imagery are Linear Spectral Mixture Analysis 2003 to DigitalGlobe imagery with a spatial resolution of about 1.1 to obtain average RMS error for the entire land cover is 97.80% with the other methods are Linear Spectral Mixture Analysis has a good accuracy.

3.3 Analysis of Change Detection

The change detection process consists of two inputs, ie, the initial state is the first to be filled with the image of endmember fractions 1994, while for the newer image of the image endmember fractions incorporated into the 2003 state finals. The results of this change detection process in the form of images that have a range of values between (-1) to (+1). This means that the closer the value (-1) and (+1), the greater the change, while the approximate value (0) means almost no change in land cover. Analysis of land cover change detection in the study area produce changes in area land cover that occur in the period of 9 years from 1994 to 2003 Estimates of broad changes can be seen in Table 3 below. In general, broad land cover change detection is done by summing the percentage of each land cover contained in each pixel, in order to obtain the total number of fractions for each land cover in the study area after deducting the cloud and shadow block (area 1198.511 ha).

Table 3. Area of Land Cover Change Every Endmember Results Detection of Changes in Year 1994 - 2003

Endmember Land Cover	1994 (ha)	2003 (ha)	Change (ha)	Change (%)
Vegetation	30.108	29.865	-243	0.81
Impervious Surface	9.256	9.314	58	0.63
Bare Soil	1.612	2.148	535	33.23
Water	1.923	1.572	-351	18.25
Amount	**42.901**	**42.901**		

Results of the land cover change detection analysis showed that the narrowing of vegetation, land cover 0.81% (-243 ha) of the total area, or 0.09% per year, the impervious surface expansion occurs 0.63% (58 ha) or 0.07% per year, on open land cover expansion occurs 33.23% (535 ha), or 3.69% per year, to cover the narrowing land water 18:25% (351 ha), or 2.02% per year. Further result at figure 1.

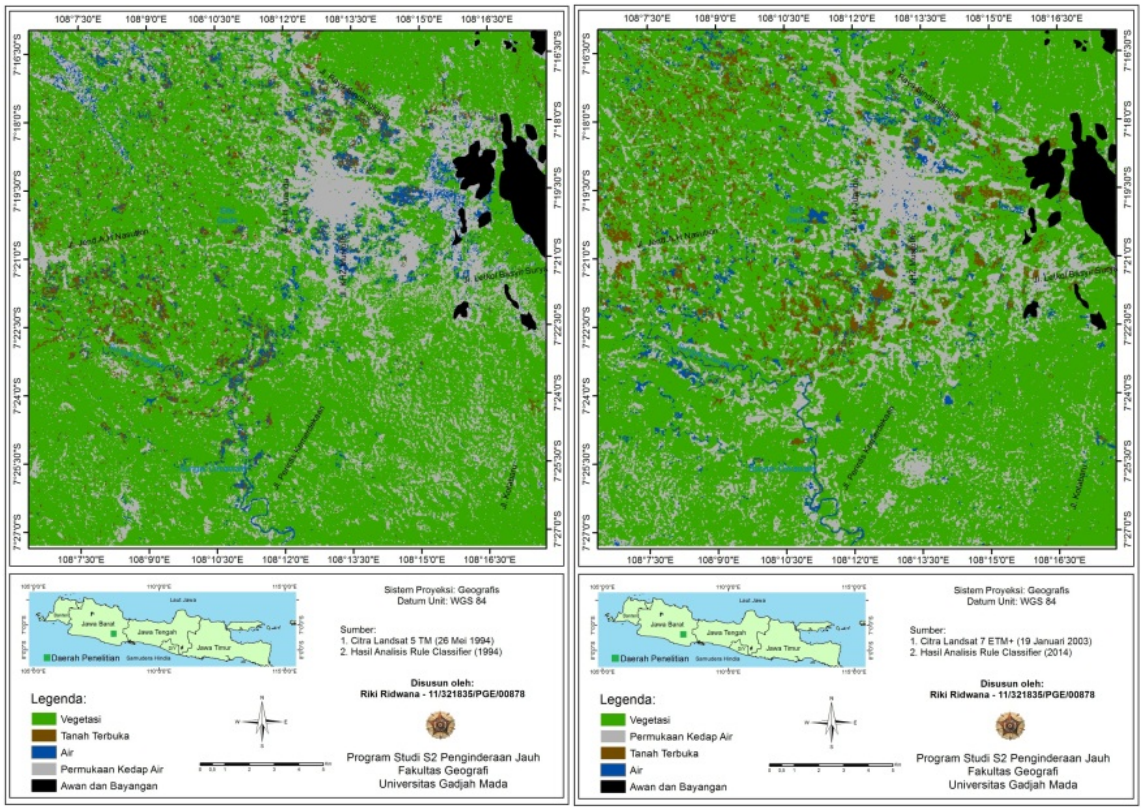

Figure 1. Land Cover Map of Rule Classifier in 1994 and in 2003.

4. Conclusions

The accuracy of the method are Linear Spectral Mixture Analysis in this study were able to achieve a mean accuracy for each pixel, a. 94.44% for the 1994 image (RMSE 0.013) and, b. 97.80% for the 2003 image (RMSE 0.021). The results of the analysis can be seen that in a span of nine years, ie from 1994 to 2003 land cover vegetation narrowing of 0.81% (-243 ha) of the total area, the expansion of impervious surface occurs 0.63% (58 ha), on open land cover expansion occurs 33.23% (535 ha), and the land cover of the narrowing water 18:25% (351 ha).

5. References

[1] Jensen, J.R., *Introductory digital image processing: a remote sensing perspective*. 2015: Prentice Hall Press.

[2] Nurlina, A., *Linear Spectral Mixture Analysis untuk Kajian Perubahan Tutupan Lahan Di Daerah Perkotaan Menggunakan Data Satelit Landsat Multitemporal*, in *Program Pascasarjana Fakultas Geografi*. 2008, Universitas Gajah Mada: Yogyakarta.

[3] Pascari, M.R. and P. Danoedoro, *Linear Spectral Mixture Analysis (Lsma) Untuk Tutupan Lahan Menggunakan Citra Landsat Etm+ Di YOGYAKARTA Dan Sekitarnya.* Jurnal bumi Indonesia, 2013. **2**(2).

[4] B, M. and H. Martin. in *Proceeding of the SPIE 10thInternational Symposium on Remote Sensing*. 8 – 12 September 2003. Barcelona.

[5] W., M.S., *Quantifying Impervious Surface, Vegetation, Soil, and Shade in the Phoenix Metropolitan Area Using Multiple Endmember Spectral Mixture Anlysis.* . 2005.

[6] Jensen, J.R., *Introductory Digital Image Processing: A Remote Sensing Perspectiv,* . 1986: New Jersey: Pearson Prentice Hall. .

[7] Lillesand, T., R.W. Kiefer, and J. Chipman, *Remote sensing and image interpretation*. 2015: John Wiley & Sons.

The Effect of Landuse Changes on Peak Discharge Using Cook Method in Sari Watershed West Nusa Tenggara

R R Suryandari[1]*, Sudaryatno[2]

[1]Department of Geographic Information Science, Universitas Gadjah Mada, Indonesia
[2]Bulaksumur, Sinduadi, Mlati, Sleman Districts, 55281, Special Region of Yogyakarta, Indonesia

*Corresponding author's e-mail: rani.rahim.s@mail.ugm.ac.id

Abstract. The study of land use changes in the Sari watershed was carried out due to the occurrence of flash flood occurring in the Sari watershed in 2016. In addition to rainfall, the flood events could be caused by changes in land use that occurred in the upper Sari watershed. This change in land use directly affects the flow coefficient and flow coefficient is one of the parameters in calculating peak discharge. This study aims to determine the effect of land use changes on peak discharge in the Sari watershed in 2009, 2016 and 2018. Land use was obtained from the maximum likelihood multispectral classification using Landsat 5 and Landsat 8. The peak discharge was calculated using the Rational method where the runoff coefficient calculations using the Cook method. Descriptive analysis was used to determine the effect of changes in land use. The results showed that the largest land use change occurred in the use of forest land into open land from 2009 to 2018. This intensive land change has an effect on the increase in runoff coefficient of 0.037. The increase in runoff coefficient affects the peak discharge, but it is not too significant.

Keywords: runoff, the cook method, flow coefficient.

1. Introduction

Watershed (DAS) is a land area that is topographically limited by backs that collect and store rainwater to then channel it into the sea through the main river [1]. A watershed is a system in the environment in which various activities of living things occur, starting from the hydrological cycle, the growth of plants, animals and humans to socioeconomic activities occurring in a watershed. Decreased land capacity (Land Degradation) in the upstream and middle of the watershed will have an impact on the health of a watershed. Various phenomena that occur in the upstream and middle of the watershed will directly affect the entire watershed. The importance of the study of land use change in the upstream part of the watershed apart from the perspective of the upstream loss, but also affects the middle and downstream areas of the watershed.

Transfer of land functions that occur in the upstream watershed causes the upstream function as a water catchment area will naturally be disrupted. Transfer of land functions can disrupt the hydrological characteristics, especially the infiltration process of the soil. changes in biophysical properties due to land use change can minimize the capacity of water infiltration into the soil. Transfer of land functions that occur in the upstream watershed causes the upstream function as a water catchment area will naturally be disrupted. Transfer of land functions can disrupt the hydrological characteristics, especially the infiltration process of the soil. changes in biophysical properties due to land use change can minimize the capacity of water infiltration into the soil. The high run-off that leads to the main river causes changes in water discharge to be greater than before the change of land use. Flood events can be identified from information on peak flow readings from the water level at a certain time [2]. The peak discharge of a watershed is the result of the accumulation of each sub-watershed in that watershed. This peak discharge analysis can be used to determine the potential of the watershed flood [3]. The flash flood disaster in Bima occurred on 21 December 2016, 23 December 2016, and 2 January 2017.

Remote sensing acts as a source of data in hydrological studies and geographic information systems as a medium used to process an input data into a model or output. Remote sensing data can be extracted to produce data used to identify changes in land use and as a parameter for calculating peak discharge. GIS acts as a media for processing and analyzing the results of image processing so that later it can be used for flood hydrological data modeling. The use of GIS software for analyzing hydrological data with spatial databases can be used to measure and obtain the data needed in the calculation of peak discharge.

1.1. Objective

- Find out the landuse changes in 2009, 2016 and 2018
- Find out the peak debit in 2009, 2016 and 2018
- Find out the effect of changes in land use on peak discharges in 2009, 2016 and 2018

2. Methodology

2.1. Multispectral Classification of the Use of Sari Watersheds in 2009, 2016 and 2018

Land use changes in the Sari watershed in 2009, 2016 and 2018 were identified using Landsat 5 imagery in 2009 and 2017 and Landsat 8 in 2018. Correction of the two images needs to be done to provide geometric and radiometric accurate information from the imagery. Remote sensing image certainly has distortion, so the image pre-processing process needs to be done.

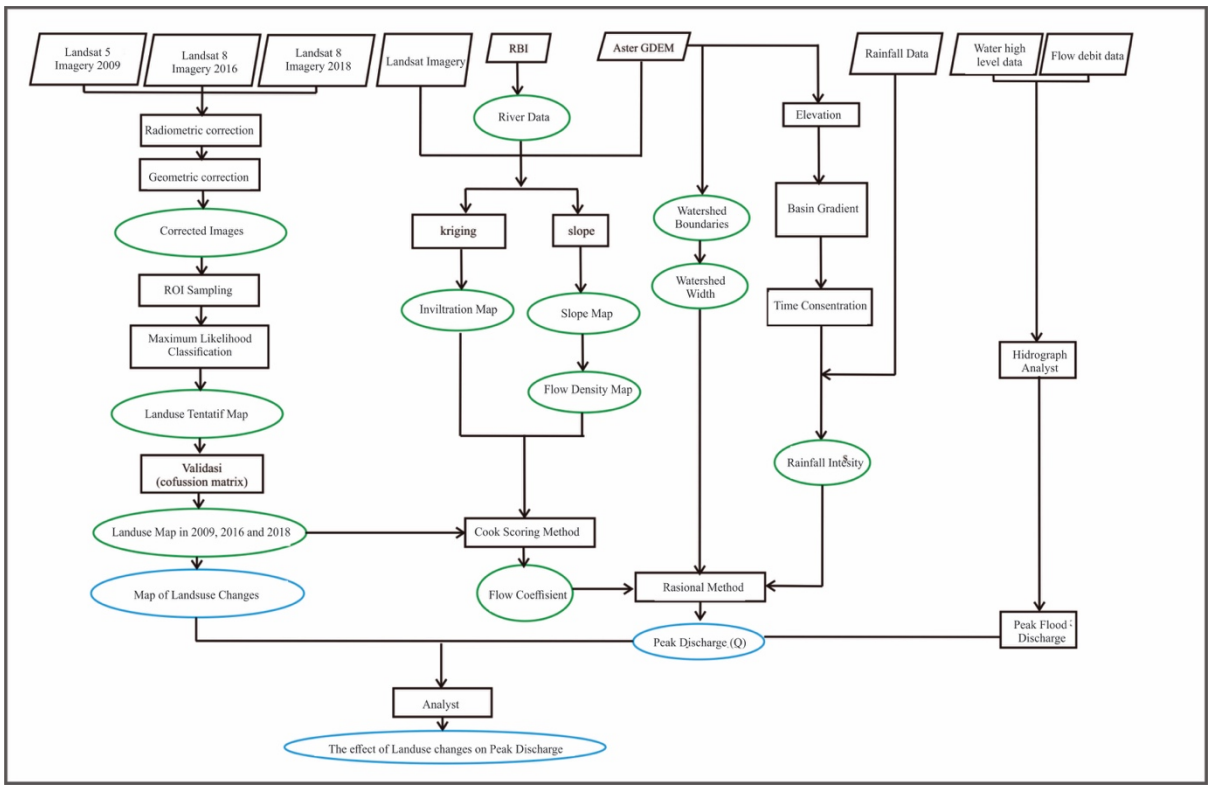

Figure 1. Research Flow Chart.

The corrected Landsat 5 TM and Landsat 8 images were classified as land use. The classification used is the maximum likelihood classification. Classified supervised using object information that is already known, so the classes of objects that appear in the image of the classification results are based on classes that have been determined by the user. The use of land classification based on the above method needs to be tested for accuracy. The accuracy and reality test in the field is carried out using the Confusion Matrix method.

Accuracy test is very important because it strengthens the level of reliability of the classification data. Samples are needed in multispectral classification. The sampling point sampling method will be carried out using the proportional random sampling method. The choice of this method is because the sampling points of the testers are based on new units resulting from overlaying land use maps that produce new units.

2.2. Calculation of Sari Runoff Coefficient in 2009, 2016 and 2018

The runoff coefficient is the sum of all (total scores) of the physical components of the watershed that are considered using the following formula:

$$C = (A1C1 + A2C2 + \cdots + AnCn) / A \quad (1)$$

Where:

C : Watershed runoff coefficient
A1 : The area of the mapping unit 1 (km^2) calculated by the grid system
C1 : Surface runoff coefficient in mapping unit 1
A : Watershed area (km^2)

Table 1. Classification of Land Use for Runoff Coefficient.

Land Cover Characteristics	Criteria	Scores
Land cover that is ineffective, bare, or very rarely Land cover that is ineffective, bare, or very	Open land, built up land	20
Natural land cover that is not so tight Shrubs / shrubs	rarely Open land, built up land	15
Cover close enough to 50% in the form of a mixture of grasses and forest trees Plantation	fields, rice fields	10
The vegetation cover is very good, 90% of the area is covered by tree vegetation or equivalent Hutun meeting	forest dense	5

The slope of Sari watershed is obtained from contour DEM data. The DEM is reduced to slope as a parameter for the runoff coefficient Cook method.

Table 2. Slope Classification for Runoff Coefficients.

Grade slope	Scores
Relatively flat with a slope of <5%	10
Corrugated with an average slope of 5-10%	20
Hilly, with an average slope of 10-30%	30
Steep hilly, heavy terrain, with an average slope of> 30%	40

Classification of soil infiltration for runoff coefficients is presented in Table 3 where infiltration parameters are obtained based on the Sari watershed landform approach which is interpreted from the Landsat imagery.

Table 3. Classification of Soil Infiltration for Runoff Coefficient.

Classification of Soil Infiltration	Infiltration mm / hour	Score
Very low	<2.5	20
Low	2.5 - 15	15
Normal	15-28	10
Height	28 - 53	5

Flow density parameters are obtained through DEM data. DEM data is derived into flow accumution and flow direction so that the flow flow in the Opak Hulu sub-watershed is known. Flow density is measured up to river order 3 which refers to Strahler's ordering. Flow density is the amount of flow length divided by the area of the catchment up to the 3rd order river.

Table 4. Classification of Flow Density for Runoff Coefficient.

Flow Density (km / km²)	Classification according to Linsley	Score
> 5	Extreme sweeping, no inundation, steep slopes	20
2-5	Good flow system and pattern, water flows smoothly	15
1 - 2	Normal, river flow exists, there is inundation but ≤2% of the total area of	10
<1	Poor drainage, always inundated	5

2.3. Rainfall Data Processing

Calculation of peak daily rainfall intensity in this study needs to be done as input to peak discharge. According to the monobone formula [4] the calculation of rain intensity is done by the following formula:

$$I = \frac{P}{24} x \frac{(24)^2}{t} \quad (2)$$

Where:
I : rain intensity (mm / hour)
P : Daily rain (mm)
Q : A large rain period

The duration of rain (t) is considered to be the same as the concentration time (Tc), then Tc is calculated by the Kirpch method as follows:

$$Tc = 0.0078\, L^{0.77}\, S^{-0.385} \quad (3)$$

Where:
T_C : concentration time (hours)
L : travel length / water trajectory (feet)
S : the slope is the same magnitude as H / L, H is the height difference between the farthest point (topmost) of the watershed and the watershed outlets expressed in feet.

2.4. Calculation of Sari Peak Watershed Debit Calculation in 2010, 2016 and 2018

Calculation of flood peak discharge has been done by Ir. A. P. Melchior, Dr. J. Boerema, Ir. F. H. Van Kooten, Ir. J. P. Der Weduwen in the late 19th to early 20th century. The Pascher formula is used as a basis for determining peak discharges which are also based on rational formulas, namely:

$$Qp = 0.278\ C.I.A \quad (4)$$

Where:
Qp : peak flood discharge (m^2 / sec)
A : area of river basin km^2
C : surface runoff coefficient when it rains Iy
0.278 : reduction rate
I : rainfall intensity (mm / hour) whose duration is the same as the time of concentration (Tc)

Runoff coefficient value entered in the Rational formula is the result of calculations with the cook method that has been done before. The results of calculations using the cook method need to be tested for accuracy by comparing the data with the runoff coefficient of the result of flow hydrograph analysis

2.5. Analysis of the Effects of Changes in the Use of Sari Watersheds in 2010, 2016 and 2018
Analysis of the effect of changes in land use of the Sari River Basin in 2010, 2016 and 2018 on peak discharge was carried out by means of descriptive analysis. Land use in 2010 and the peak discharge of the Sari watershed in 2010 compared with 2016 and 2018. Descriptive analysis was carried out by looking at the peak discharge response to changes in land use that occurred. Then from the results of the analysis it can be seen whether the change in land, especially the case study into corn land, has a major role in the change in peak discharge. Table 5 provides a comparison of land use in X, Y and Z which are considered to be changing, while other parameters are considered constant every year.

3. Results
The results of this study were carried out to achieve the main objective of the study, which is to determine the effect of land use changes in the Sari Watershed for 2009, 2016 and 2018 peak discharges. Results schemes are explained coherently according to the results obtained.

3.1. Determination of watershed boundaries
The watershed boundary is determined by drawing a line at the peak of a river in the direction of the flow toward the same valley. The watershed boundary determination is done with the help of digital elevation model (DEM) derivative data, namely TIN (triangulated irregular network). Making TIN basically uses contour lines extracted from DEM data. The appearance of TIN is able to describe the topography of an area more clearly, so that the pulling of watershed boundaries can be done more easily. Withdrawing watershed boundaries is also assisted by river flow to indicate the direction of river flow. Although there are differences in the headwaters of the river, the watershed boundaries provided by BPDAS are still used in the headwaters because the topography tends to be uniform and difficult to draw lines without reference. Differences in drawing watershed boundaries also cause differences in watershed area. The watershed provided by BPDAS has an area of 297.57032 Ha while the delineated watershed has an area of 273,572 Ha where the delineation results tend to be smaller in area.

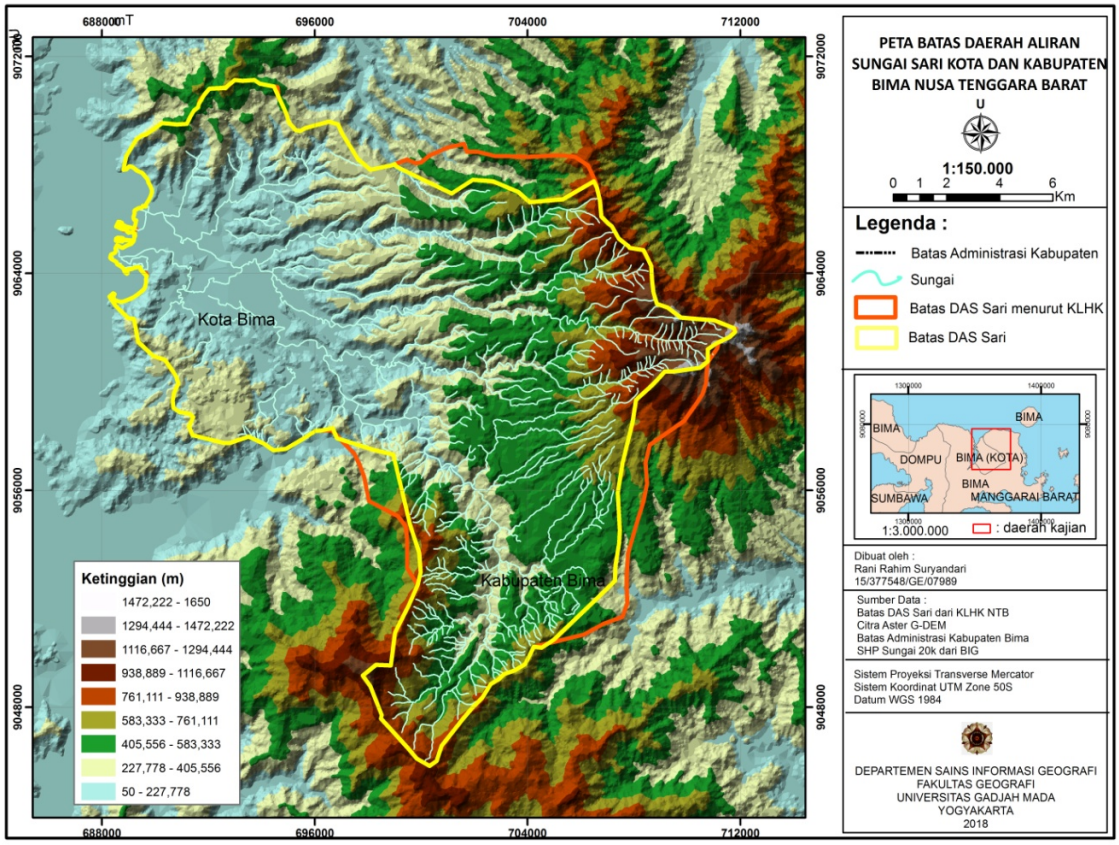

Figure 2. Sari watershed boundaries.

3.2. Multispectral Classification for Land Use and Accuracy Test

Land use classification is carried out using supervised classification methods with maximum likelihood. The results of digital classification will not produce maps with a level of accuracy reaching 100% or exactly the same as reality on the ground. Multispectral classification map results are still in the form of tentative maps where the level of accuracy and accuracy of the map is unknown. To find out the level of accuracy and accuracy, the observations are carried out and check directly in the field. Field observations refer to predetermined sample points, which are 150 points determined by proportional random sampling. Tentative maps of the results of the multispectral classification in 2009, 2016 and 2018 were processed using ArcMap 10.3 to reclassify pixels into pre-determined classes.

Accuracy test using confusion matrix considers accuracy of producer and user. Table 5 shows the value of the overall accuracy (overall accuracy) of the results of the multispectral classification is 83.33%.

Table 5. Accuracy Test with Confussion Matrix.

Kelas		Data Lapangan								
		LTB	LTK	HA	HP	SW	KBC	Jumlah	User Accuracy	Error Com.
Data Klasifikasi Multispektral	LTB	20	0	0	0	0	0	20	100	0
	LTK	0	28	0	1	0	1	30	92	8
	HA	0	2	17	5	1	0	25	68	32
	HP	0	1	0	20	1	3	25	80	20
	SW	0	5	0	1	18	1	25	72	28
	KBC	0	2	0	1	0	22	25	88	12
	Jumlah	20	38	17	28	20	27	Overall accuracy		83,33
	Producer Acc.	100	73,6	100	71,42	90	81,48			
	Error Com.	0	26,4	0	28,58	10	18,52			

3.3. Map of Land Use in Sari Watershed in 2009, 2016 and 2018

The land use classification is divided into 6 main classes, namely natural forests, production forests, mixed gardens, developed land, open land, and rice fields. The digital classification results map results in the Sari, DAS Land Use Map in 2009, 2016 and 2018 which show variations in the extent and distribution of land use types in the Sari DAS.

Table 6. Changes in Land Use.

Tahun/ Jenis PL	LTB (km^2)	LTK (km^2)	HA (km^2)	HP (km^2)	SWH (km^2)	KBC (km^2)
2009	13.0678	25.4534	86.3540	84.1008	10.6254	53.6543
2016	16.1543	50.2941	55.6576	73.6540	7.9210	69.8830
2018	17.2073	73.0772	53.2629	47.6316	7.7310	74.6540

Note: LTB = Land Built; LTK = Open Land; HA = Natural Forest; HP = Production Forest; SWH = Rice field; KBC = Mixed Plantation

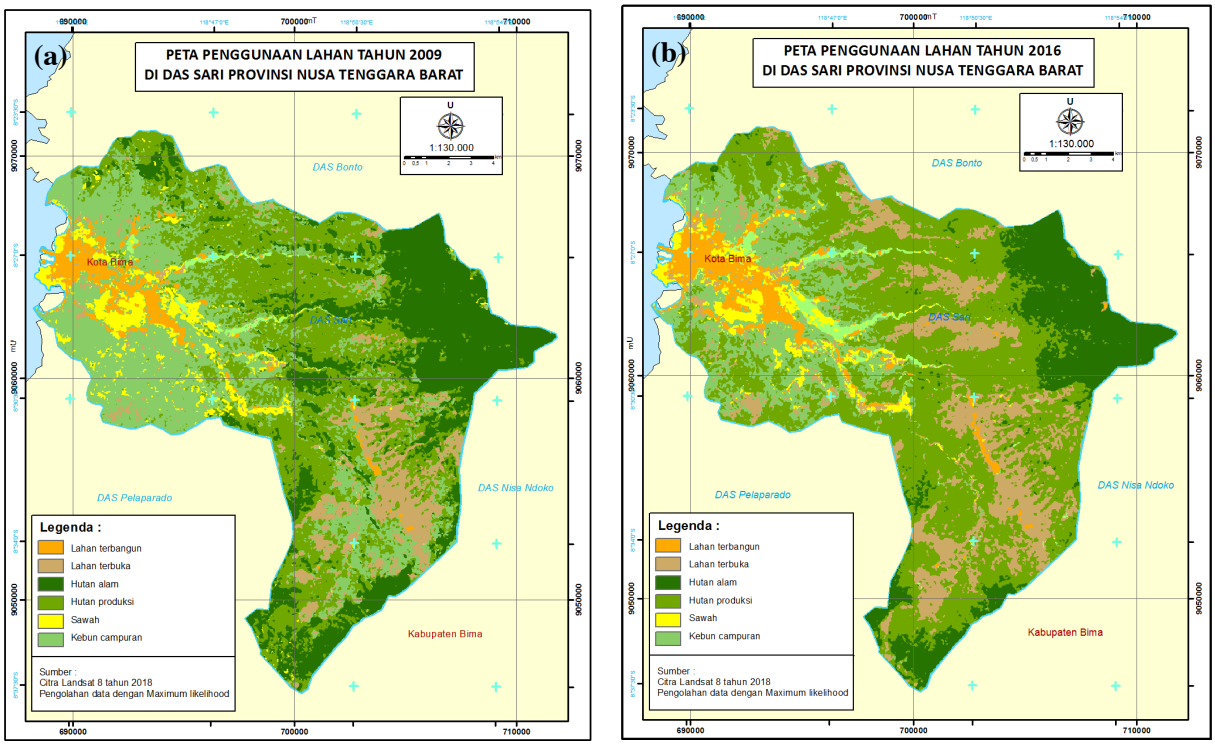

Figure 3. **(a)** Map of Land Use in Sari Watershed in 2009. **(b)** Map of Land Use in Sari Watershed in 2016.

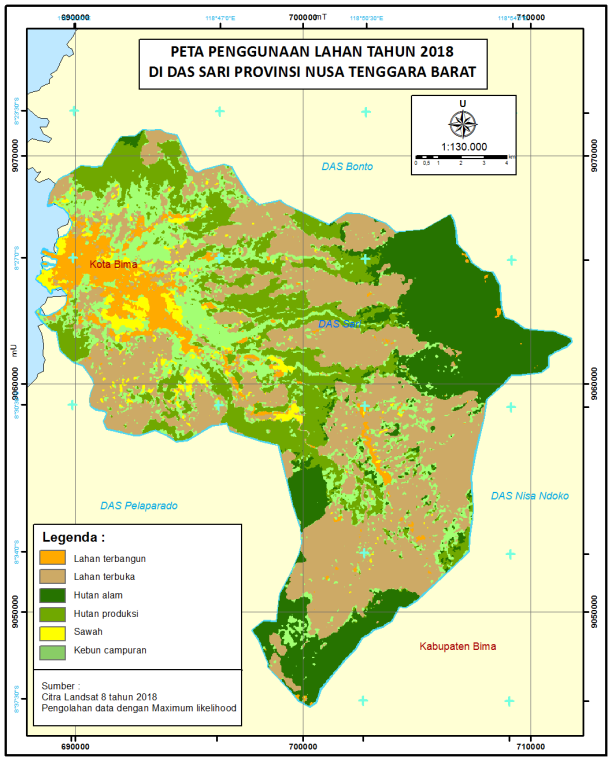

Figure 4. Map of Land Use in Sari Watershed in 2018.

3.4. Map of the slope of the Sari watershed

Slope maps are produced from raster data processing from Aster GDEM images with a resolution of 30 * 30 m. DEM data processing is performed with Arcmap 10.3 software to create image hillshades. The appearance of the previous GDEM Aster image which is only a greyscale (black-and-white hue) with pixel values is then displayed in a hillshade which further highlights the visualization of the slope height difference from the shadows on the igir so that the slope shape of the DEM pixel values appears.

Based on the slope map of the Sari watershed as shown in Figure 4 has quite a lot of slope variations. Slopes with 0 - 5% slope dominate the downstream watershed with relatively flat reliefs with a deep green color on the map. The width of Sari watershed with a slope of 0 - 5% is 208.7307 km^2. The slope that dominates the Sari watershed is 10-30% with an area of 942.9273 km^2. The weighting for this class is also a maximum weight of 40 for its contribution to the runoff coefficient. Upstream characteristics like this need special handling because it can be a threat to the survival of the area underneath.

3.5. Map of Sari Watershed Density Flow

Groove density is one of the parameters in determining the magnitude of the coefficient in a watershed. The channel density needs to be considered because it can show the average river length compared to the extent of a watershed where the higher the density, the more effect on the height of the surface water heights in a particular watershed unit.

The brown sub-watershed has a flow density value of 0.84 miles / mil^2 and is given the smallest score of 5 where this sub-watershed has a poor drainage system and is prone to inundation. For sub-watersheds blue and light blue with a value of 1.64 miles / mil^2 and 1.66 miles / mil^2 given a score of 10 with normal drainage and there are only < 2% of the flooded area. Other sub-watersheds located in the upper reaches of the watershed have a value of flow density > 2 miles / mil^2 so a score of 15 is given where this area has a good system and flow pattern and the water flows smoothly.

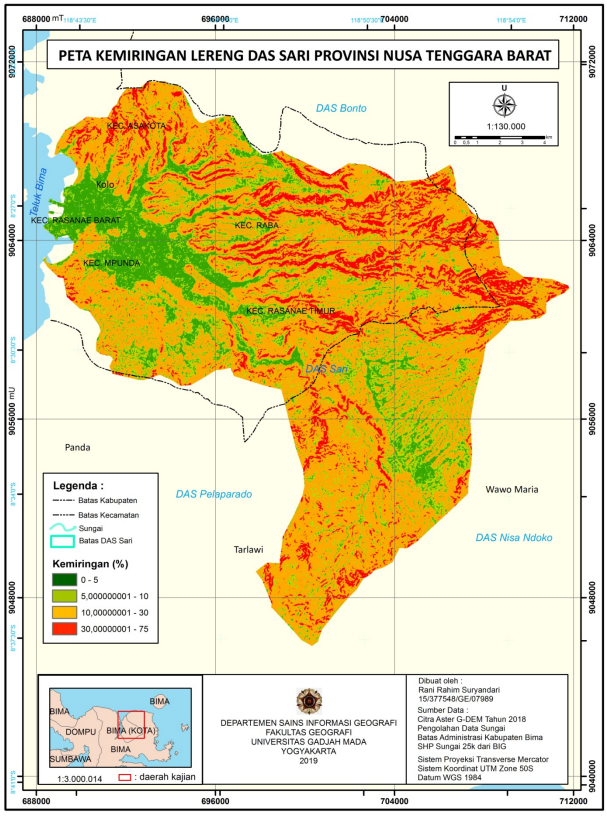

Figure 5. Map of the Slope of the Sari Watershed.

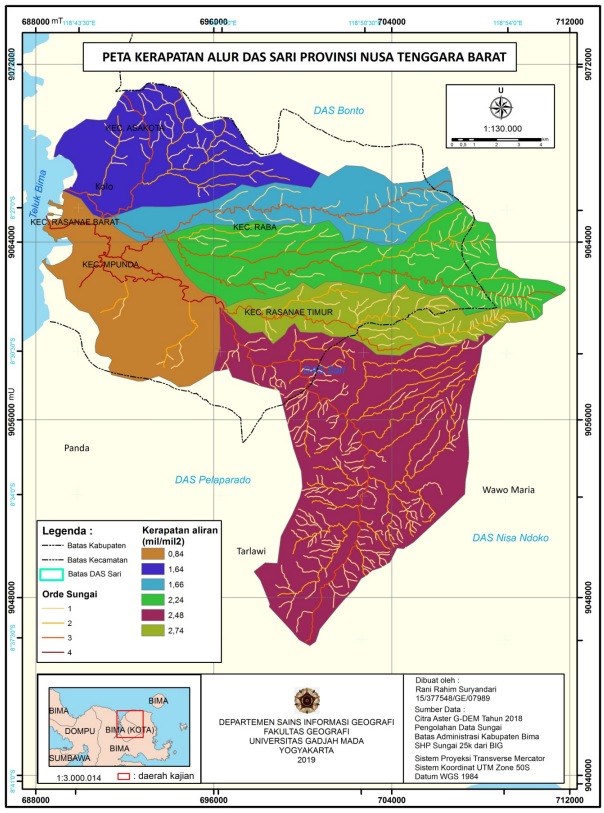

Figure 6. Sari Watershed Density Map.

3.6. Map of Sari River Basin Infiltration Rate

The infiltration rate is obtained from direct measurements in the field by taking several samples to determine the infiltration rate in the Sari watershed. The total points of measurement of the infiltration rate are 21 points spread over almost all watersheds as illustrated in Figure 6. In the pre-field, measurement sample points are planned to be measured in all watersheds but not all measurement points are in accordance with the planned sample measurements, because the terrain is too difficult to reach in the field. But the unreachable sample points are then replaced with other representative sample points. The measurement results are then analyzed by the Horton method. The results of measurement of infiltration rates are presented in Table 6 and Figure 7 shows the variation of infiltration rates that vary in each soil texture class. The highest infiltration rate of 8.27 mm / hour is symbolized in dark green and the highest infiltration rate is 140.522 mm / hour symbolized in red.

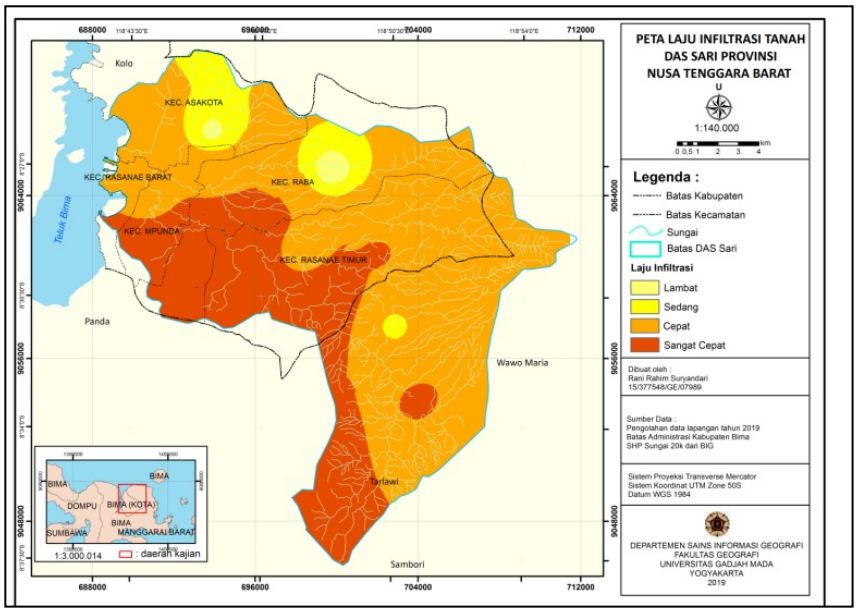

Figure 7. Sari Infiltration Rate Map Sari.

3.7. Map of Sari Basin Watershed Runoff Coefficient

Runoff coefficient is obtained from the overlapping of land use variables, slope slope, channel density, and infiltration rate that have been given a score of each. The results of the overlapping produce land units where each pixel contains information on the results of the addition of the four variables.

The value of the flow coefficient in 2009 was 0.52397. This value indicates that the Sari watershed is in poor condition because 52.4% of rainwater has fallen to surface runoff. The value of the flow coefficient in 2016 is 0.532759 which means there is an increase in the flow coefficient of 0.008789 from 2009. In 2018, the flow coefficient has increased quite significantly to 0.56127 where the difference from 2016 amounted to 0.02851 greater than two folds compared to changes from 2009 to 2016. Good and healthy watershed conditions are characterized by runoff coefficient values close to zero (0) which indicate that most of the rainwater is infiltrated into the ground.

3.8. Rain Data Processing

Rainfall data is one of the data that is very needed in the calculation of peak discharge. The data used are the maximum rainfall data every month in 2009, 2016 and 2018 in several rain posts scattered in the Sari watershed.

Table 7. Rain intensity in the Sari watershed.

No.	Tahun	Stasiun				W_AX	W_BX	W_CX	W_DX	Jumlah
		Wawo (W_A)	Rasa Na'e Timur (W_B)	Raba (W_C)	Teke (W_D)					
1	2016	0,161842276	0,259410503	0,09179	0,007887473	21,44839	35,96461	11,38307	0,807653	69,60373
2	2018					9,823152	10,56284	3,927962	0,552786	24,86674
3	2009		-	-	-	16,30585	16,30585	5,769695	0,495785	38,87717

From table 7 it can be seen that the average maximum rainfall after compared with the area of the polygon produces the highest average maximum rainfall in 2018 that is 69.60373 mm / hour, then in 2009 with a magnitude of 38.87717 mm / hour and 2018 at 24.87717 mm / hour.

3.9. Peak discharge of Sari Watershed

The peak discharge value of the DAS Sari is produced based on a rational method that considers the runoff coefficient, rainfall intensity and watershed area. Peak discharge values in 2009, 2016 and 2018 consider several parameters that continue to change each year, namely rainfall intensity and runoff coefficient.

Table 8 shows the peak discharge values from 2009, 2016 and 2018 with varying values ranges. The 2009 peak discharge value was 154,926 m^3 / second with runoff coefficient of 0.52 and rainfall intensity of 38.87717 mm / hour. The peak discharge value in 2016 was the highest at 282,021 m^3 / second with runoff coefficient of 0.53 and the highest rainfall intensity at 69.60373 mm / hour. The peak discharge value in 2018 is 106.147 m^3 / second with runoff coefficient of 0.56 and rainfall intensity of 24.86674 mm / hour.

Table 8. Peak Debit Value of the Sari Watershed in 2009, 2016 and 2018.

Year	C	I (mm/hour)	A (Km^2)	Q Rasional (m^3/s)	Q Manning (m^3/s)
2009	52.39	38.87717	273.5722	154.926	13.9128
2016	53.27	69.60373	273.5722	282.021	
2018	56.12	24.86674	273.5722	106.147	

Flooding occurs due to surface runoff that flows at the main outlet that cannot be accommodated by the oulter. A river outlet has a maximum capacity to accommodate surface flow where if the flow has a discharge that exceeds the peak flow of the river, the flow will come out of the main outlet and inundate the surrounding area. From the calculation of the manning method, the Padolo river as the main outlet has a capacity of 113.9128 m^3 / sec.

3.10. Effects of Changes in Land Use on Peak Debits

Based on Table 8, it can be seen the magnitude of increased discharge to rainfall with a change in runoff coefficient of 0.1 from 2009 to 2016 and 0.3 from 2016 to 2018. In 2016 a tropical cyclone occurred in the Sari watershed, resulting in unusual rainfall intensities and impacts directly to the increased peak discharge in the Sari watershed. The higher the rainfall, the higher the increase in discharge. In fact, the amount of rainfall that occurs is different and not necessarily the same every time the rainfall occurs so that the change in discharge depends on the size of the rainfall.

Table 9. Extensive Changes in Land Use.

No.	Types of landuse	Area of change (km^2)
1	Open land becomes mix garden	5.0922
2	Open land becomes rice fields	19.9296
3	Forest become mix gerden	5.4036
4	Forest become open land	51.2802
5	Mix garden becomes open land	36.1719

Table 9 presents data on land use changes that indirectly influences changes in peak discharge, but has a direct effect on the runoff coefficient. Surface runoff coefficient in 2009 to 2016 experienced a change of 0.01 but with a large enough rainfall intensity was able to cause flash floods that occurred in Sari watershed on 21-22 December 2016. While in 2018 the changes that occurred from 2016 were quite large namely 0, 03 but the peak discharge tends to be lower due to rainfall that is not so high. However, based on the value of the change in runoff coefficient, the peak discharge of the DAS Sari will experience an increase from 2009, 2016 and 2018 when compared to the same rainfall. Runoff coefficient in 2009, 2016 and 2018 will be 99.1 m^3 / second in 2009, 100.755 m^3 / second in 2016 and 106.14 m^3 / second in 2018 where the rainfall intensity applied will be 24.866 mm / hour. Based on these results, the effect of land use change on peak discharge is significant if the rainfall intensity in a watershed does not change extensively.

4. Conclusions

The conclusions based on the research carried out are as follows:

1. There was a change in land use in the Sari watershed from 2009 to 2018, namely open land into mixed gardens of 5.09 km^2, open land to become rice fields 19.9296 km^2, Forests to Mixed Gardens area of 5.4036 km^2, Forests to Open Land covering an area of 51.2802 km^2, and Mixed Gardens becoming Open Land covering an area of 36.1719 km^2. The change of open land into mixed estate is caused because open land is land that is mostly deliberately opened to be used as production land so that this change is a series of changes from non-developed land to production land so that the change of forest to open land with a large enough area does not rule out the possibility of change back to mixed garden land in the future.
2. Sari's DAS peak discharge respectively from 2009, 2016 and 2018 is 154.926 m^3 / sec, 282.021 m^3 / sec, and 106.147 m^3 / sec whose size is greatly influenced by the intensity of rain in that year.
3. The effect of changes in land use in the Sari watershed in 2009, 2016 and 2018 is not too significant, because the discharge in 2009 is higher than in 2018 which has a greater runoff coefficient. This happened because of the very significant difference in rainfall intensity in the three years. However, if the rainfall intensity value is not extreme, the effect of land use change on peak discharge is quite significant.

5. References

[1] Asdak, C., *Hydrology and Management of Watersheds*. Gadjah Mada University Press.
[2] Sudaryatno, *The Application of Remote Sensing Techniques and Geographic Information Systems for Estimating Peak Discharge in the Garang Watershed (DAS) Semarang*, in *Graduate program*. 2000, Gadjah Mada University: Yogyakarta.

[3] Puspitasari, b., *Utilization of the 2A Sentinal Image and Geographic Information System for Peak Debit Estimation Related to the Evaluation of the Parameters of the Flood Contributors in the Serang Hulu Watershed, Kulonprogo Regency*, in *Faculty of Geography*. 2018, Gadjah Mada University Yogyakarta.
[4] Sosrodarsono, S. and K. Takeda, *Hydrology for Watering*, ed. P. Paramita. 1987, Jakarta.

Utilization of Himawari-8 Satellite Data for Estimated Rainfall with Various Methods (Case Study of Heavy Rain Jayapura 16-18 March 2019)

A R Sagala[1*], H Salawane[1], and A K Silitonga[2]

[1]Meteorological Climatological and Geophysical Agency (BMKG) Angkasa I No.2 Kemayoran Street, 10720 DKI Jakarta, Indonesia
[2]School of Meteorology Climatology Geophysics (STMKG) Perhubungan I No.5 street, 15221 Tangerang Selatan, Banten, Indonesia

*Corresponding author's e-mail: andreassmartest@gmail.com

Abstract. The estimation of rainfall is very important in increasing the accuracy of the weather forecast. An accurate weather forecast will reduce the impact of disaster risks. Jayapura was chosen as the stufy are because in recent times there was heavy rain for three consecutive days which caused various losses. Estimation of rainfall by applying various estimators have been widely carried out but specifically discussing the phenomenon of heavy rainfall is still small. This research was carried out by utilizing the Himawari-8 channel 13 (Infrared1) satellite data as input to estimate rainfall and compared to Authomatic Weather Station Digitation Dok II Jayapura rainfall data. The estimator methods used are Autoestimator, Insat Multispectral Rainfall Algorithm (IMSRA), Non-Linear Relation, Non-Linear Inversion. Cloud top temperature data for three heavy rain events (16-18 March 2019) are converted into rainfall data every hour during the convection process. Phase of cloud development (growing, mature, extinct) based on time series cloud top temperature which indicates a decrease in temperature at growing phase, low maximum in mature phase, and increase in extinct phase. The result of this study shows that the best estimation method for heavy rain in Jayapura base on ranking point (highest correlation and lowest RMSE) is IMSRA.

Keywords: estimation rainfall, Himawari, cloud.

1. Introduction

The auto estimator method is applied to estimate daily rainfall in Jayapura in January-February 2010. The results of the study indicate that in general the auto estimator method is relatively poorly used for estimating rainfall in Jayapura but is good for estimating the number of rainy days. The auto estimator method has been widely used to estimate the amount of rainfall. However, the results of rainfall estimates detected by weather satellites and funds on synoptic observations have a difference or value difference. This is what needs to be assessed for the accuracy of the estimated rainfall using this method. Conventional rain rainfall observation encountered many obstacles, especially when bad weather occurred. This is a problem for the availability of timely, continuous and accurate rainfall data. Therefore, the estimation of rainfall using weather satellite imagery needs to be developed [1].

Rainfall prediction in Indonesia is still very difficult to accurately predict because it has very large spatial and temporal variations with the number of surface observation rainfall observations which is still very limited [2]. The study of heavy rain cases in Jayapura in 2014 showed a significant decrease in the value of cloud top temperatures around -61C and a significant increase in cloud top height. These values and patterns can be used as an indication of the growth of heavy rain-producing clouds in the Jayapura region [3]. Precipitation patterns over sea surface should be more easily estimated than over land since the patterns are probably prompted more by purely atmospheric factors and leey by complex topographic variation, yielding instantaneous distributions of precipitation activeity that are more random than those over land, but average distribution that are less complex [4].

When viewed from the trigger, the shape of the cloud caused by local conditions or the usual shear in the form of one cell cumuliform clouds. Whereas regions, where there are ITCZ or vortex, low, tropical depression, in satellite images, will be seen the formation of cumuliform clouds mixed with stratiform clouds. In this case, the resulting rain will usually have a long and continuous period, which will eventually result in an accumulation of large rainfall. For flood-prone areas, this can be a problem because when the accumulation of rainfall exceeds the extreme weather threshold of the region, flooding will occur [5]. Remote sensing is a science and measurement method to get information on an object or phenomenon using a recording device from a distance without making physical contact with objects or measured/observed phenomena[6]. A wheater satellite, which has wider coverage and faster in generating data than in situ observation, is used to monitor weather in Indonesia to provide atmospheric dynamic information that is related to early warning of extreme weather. It can generate cloud top brightness temperature data to determine the presence and type of clouds, and it also can be used to generate the amount of rainfall [7].

2. Data and Method

The area of study in this study is Jayapura 2 Meteorological Station. The coordinates of this region are 2.53S 140.72E. The characteristic of the Jayapura region is the hills with many green areas. The Dok 2 Jayapura Meteorological Station is right on the coast of Jayapura waters so that the phenomenon of land wind and sea wind can be one of the causes of extreme weather in Jayapura.

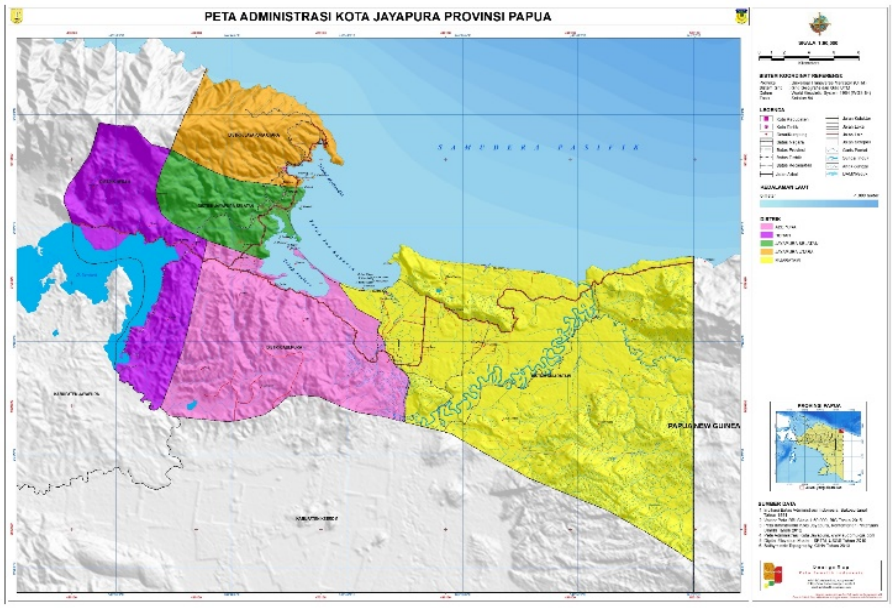

Figure 1. Map of Jayapura source: thematic map of Indonesia.

The data used in this research are Himawari 8 satellite data on 16-18 March 2019 Infrared (IR1) channel with 10 minutes resolution. Data for per 10 minutes for time series cloud top temperatures and per hourly for estimated rainfall. Hourly rainfall data from Authomatic Wheater Station Digitation Dok 2 on 16-18 March 2019.

Cloud top temperature is extracted from the satellite IR channel Himawari-8. The data is then entered into various equations that convert cloud top temperatures into rainfall in this case used 5 equations that have been studied in existing research. Precipitation estimates from various equations are compared to the AWS Digitization Dock 2 rainfall. From these comparisons, the correlation and RMSE values will be obtained. The incidence of heavy rain for three days in a row was compared separately as well as the correlation and RMSE. The ranking table of 3 events will be used to choose the best estimation method with the highest correlation and lowest RMSE.

The frequency of the appearance of CB clouds in Serui, Papua in March 182 events in 2014 and most occurred at 15:00 UTC as many as 26 events. The emergence of CB clouds in Yapen is caused by land wind convergence from the island of Papua and the island of Yapen. This condition lasts from 11:00 UTC to 16:00 UTC. [8] The Himawari 8 and 9 satellites are advanced programs from the MTSAT Satellite, to improve the accuracy of observation and weather prediction developed into 16 bands consisting of 3 visible bands, 3 near-infrared bands (NIR) and 10 thermal bands (IR) with spatial resolution 0 , 5km x 0.5km and 1km x 1km per pixel on visible band data, 2km x 2km per pixel on IR bands and 1km x 1km and 2km x 2km per pixel on the NIR band so the data volume becomes large. Besides, the intensity of observations increases to every 10 minutes, so the data transmission needs to be faster and the volume becomes large. For this reason, JMA will develop a fast data receiver system and for user needs, AHI data will be distributed with a resolution directly via the internet. The increasing number of bands and the increasing temporal and spatial resolution of the Himawari 8 and 9 Satellite data, is very necessary and is expected to provide an opportunity to improve the accuracy of weather prediction in tropical regions such as Indonesia which has rapid weather change dynamics [8] . Himawari 8 and 9 have special meteorological missions, namely: maintaining continuity and increasing weather observations via satellite for disaster prevention and weather forecasting; improve the ability of short-term forecast the next 6 hours or what is known as 'nowcasting', especially for the detection and prediction of bad weather; improve the accuracy of numerical weather predictions; improve climate and environmental monitoring [9].

2.1. Autoestimator

Comparison of GEOS cloud-top temperature in the IR images and visible images against collocated radar images have demonstrated that convective thunderstorms are characterized by very low clud-top temperature (195-210 K) and rapid spatial and temporal changes in the structure of the cloud-top surface. The auto-estimator initially computes rainfall rates based on a nonlinear, power-law regression relationship between cloud-top temperature (10.7 um brightness temperature) and radar-derived rainfall estimates.

$$R = 1{,}1183.10^{11}\exp\left(-3{,}6382.10^{-2}.T^{1.2}\right) \quad (1)$$

Autoestimator uses National Centers for Environmental Prediction (NCEP) Eta Model generated relative humidity (RH) and precipitable water (PW) to analyze the environmental moisture and scale the rainfall amounts accordingly. The auto-estimator has some skill at 1-h time resolution and spatial resolutions of 12 km, and it presents useful results on larger grid sizes (48-km and larger). Cold-top (colder than 280 K) MCSs composed the dataset for this initial validation[10].

Contrast to the reasonale performance of the technique for well-defined and short duration convective systems, poor results are common for stratiform cloud systems. This is especially important during winter season when most of the precipitation comes from cloud tops that are warmer than 230 K. For these cases, danger of flash flooding result from persistent rainfall over long periods of time, not to short-lived intense storms associated with convective systems during the summer. These intense convective systems are the ones for which the auto-estimator was originally developed. We should also be carefull about the use of auto-estimator for 24-h daily rainfall accumulation.

2.2. IMSRA

The IMSRA technique is combination of the IR and MW measurements which benefits from the relative accuracy of the MW-based estimates and the relatively low sampling errors of the TIR-based estimates. This algorithm is developed for the small-scale rainfall estimation over the Indian region.

$$R = 8{,}613098 * exp\left(-\frac{(TB-197{,}97)}{15{,}7061}\right) \quad (2)$$

The development of this algorithm includes two major steps: classification of rain bearing clouds using proper cloud classification scheme utilizing Kalpana-1 TR and WV Tbs; collection of Kalpana-1 IR Tbs

with TRMM-PR suface rainfall rate and establishment of a regression relation between them. Kalpana-1 based rainfall estimate is successfully used for rainfall monitoring during the monsoon and severe weather conditions [11].

2.3. Non-Linear Relation

Information on rainfall is very important because it is needed by various aspects of life, especially in planning agriculture, transportation, plantations to early warnings of old disasters, floods/landslides and droughts. Remote sensing satellites for weather and environmental monitoring can provide weather information every hour in a wide range. The lower the brightness temperature of the cloud, the higher the rainfall, except for cirrus clouds which are not rain-producing but have low temperatures [12].

$$R = 2.10^{25}.x^{10,256} \quad (3)$$

2.4. Non-Linear Inversion

The relationship between the physical properties of the object under study with observational data can be in the form of a mathematical model. This model is used to extract the physical parameters of the object under study from observation data. This process is called inverse modelling [13].

$$R = 1{,}38046.10^{-7}.e^{\frac{3789,518}{x}} \quad (4)$$

The rainfall model obtained using nonlinear inversion based on the cloud top temperature, seen from the comparison graph between the observed rainfall and the estimated rainfall has a relatively similar pattern, but the magnitude of the increase or decrease in rainfall is not the same. This is caused by other factors such as cloud top temperature factors that affect rainfall such as latitude, altitude, a distance of water sources, differences in soil temperature and land area.

3. Results and Discussion

Based on the time series of cloud top temperatures determined the time series of cloud development at the study point, namely at the Jayapura II Meteorological Station. March 16, 2019, the time series which is used as a phase of cloud development is 09.00 UTC-20.00 UTC (12 data). March 17, 2019, the time series as a cloud phase is 12.00 UTC-21.00 UTC (10 data). March 18, the time series used is 12.00 UTC-20.00 UTC (9 data). The choice of time series of this cloud development phase will indirectly filter out other hours where the chance of rain is small because the development of convection clouds is a common cause of rain. Using AWS data can also actually determine the phase of cloud development. High cloud top temperature correlates with high rainfall and generally occurs in the mature phase. Rainfall tops occur at very low cloud top temperatures (mature phase) while in the growing and extinct phases of rainfall are relatively small changed in cloud top temperatures in these two phases are opposite. Based on cloud top temperatures it is determined that the growing phase of clouds on 16, 17, March 18, 2019, is 09.00-09.30 UTC, 12.00-13.30 UTC, 12.00-14.00 UTC. The mature phase of the cloud on 16, 17, 18 March 2019 is 9:30 to 17:00 UTC, 13.30-18.00 UTC, 14.00-19.00 UTC. The extinct phase of the cloud on the 16th, 17th, March 18, 2019, is 17.00-20.00 UTC, 18.00-21.00 UTC, 19.00-21.00 UTC.

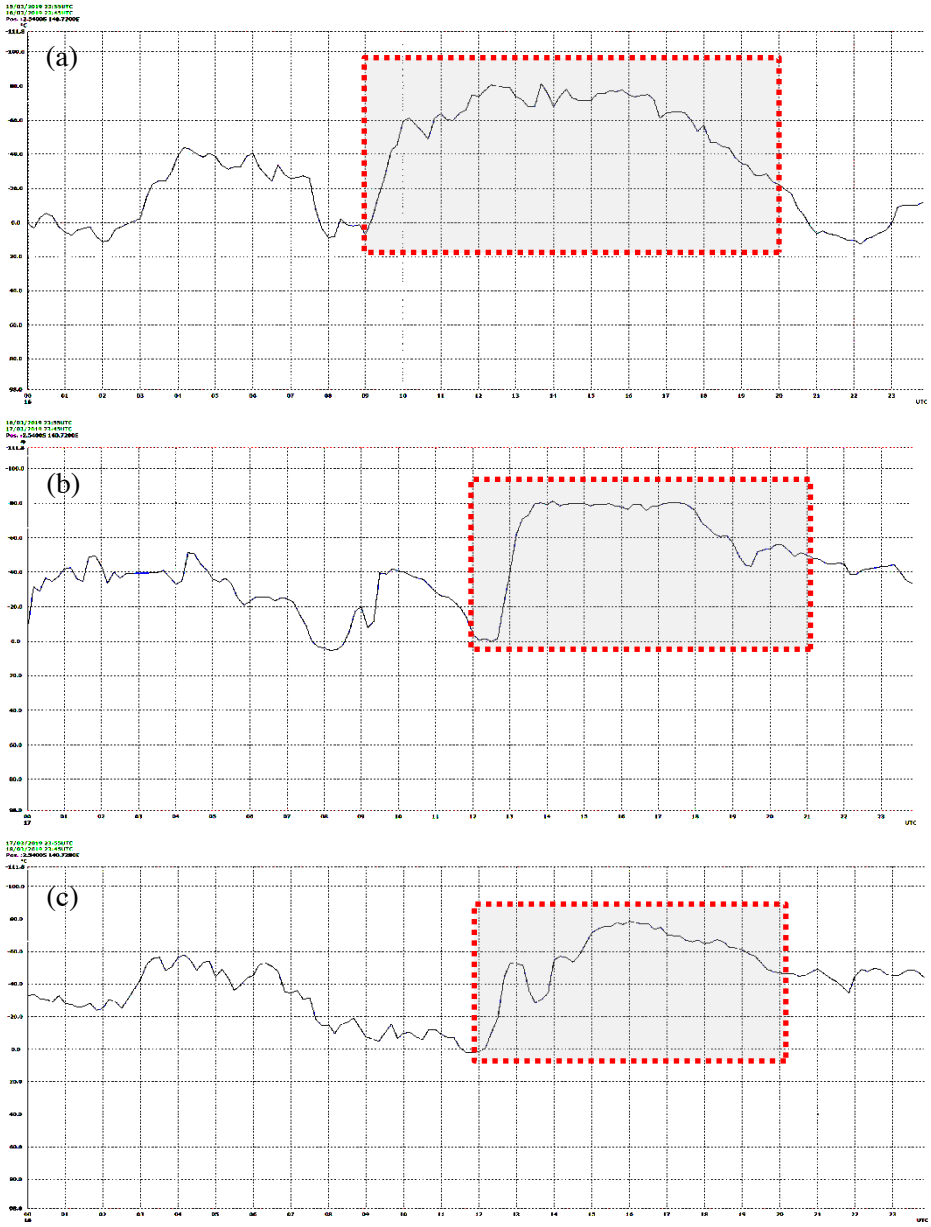

Figure 2. Cloud top temperature (a) March 16, 2019, (b) March 17, 2019, (c) March 18, 2019.

The rainfall at 14:00 UTC is the highest rainfall at 40.8 mm. At this hour, the Autoestimator overestimate method is 43.1 mm against the actual rainfall while the rainfall estimation using the Non-Linear Relation method is closest to the actual rainfall despite underestimation with a rainfall value of 38.3 mm. The Autoestimator method experiences the greatest overestimate at 12, 13, and 16 UTC, which is the phase where the cloud enters the mature phase and goes into extinction. At 18-20 UTC shows the actual rainfall value of 0 mm but the estimated rainfall indicates the precipitation at that hour.

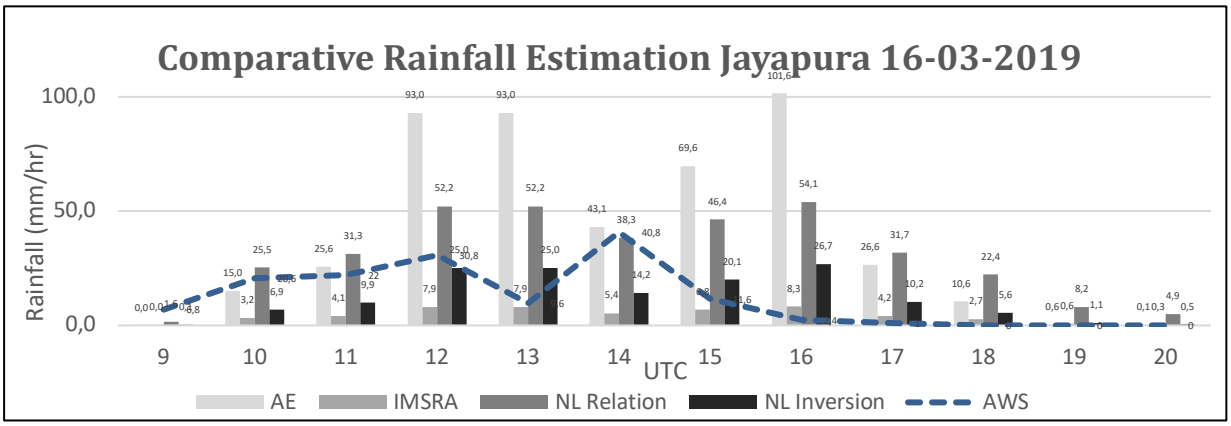

Figure 3. Comparison of rainfall on March 16, 2019.

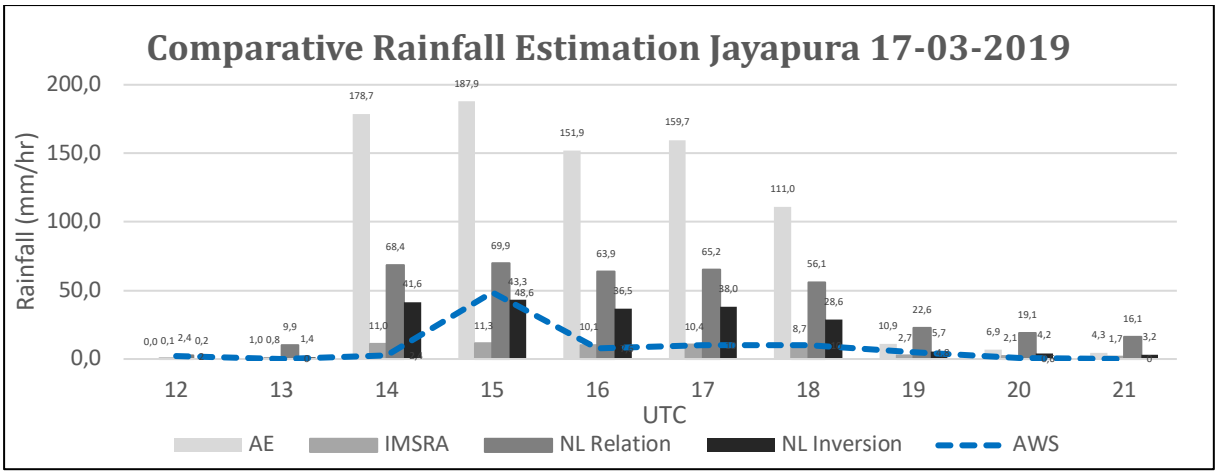

Figure 4. Comparison of rainfall on March 17, 2019.

The rainfall at 14:00 UTC is the highest rainfall at 40.8 mm. At this hour, the Autoestimator overestimate method is 43.1 mm against the actual rainfall while the rainfall estimation using the Non-Linear Relation method is closest to the actual rainfall despite underestimation with a rainfall value of 38.3 mm. The Autoestimator method experiences the greatest overestimate at 12, 13, and 16 UTC, which is the phase where the cloud enters the mature phase and goes into extinction. At 18-20 UTC shows the actual rainfall value of 0 mm but the estimated rainfall indicates the precipitation at that hour.

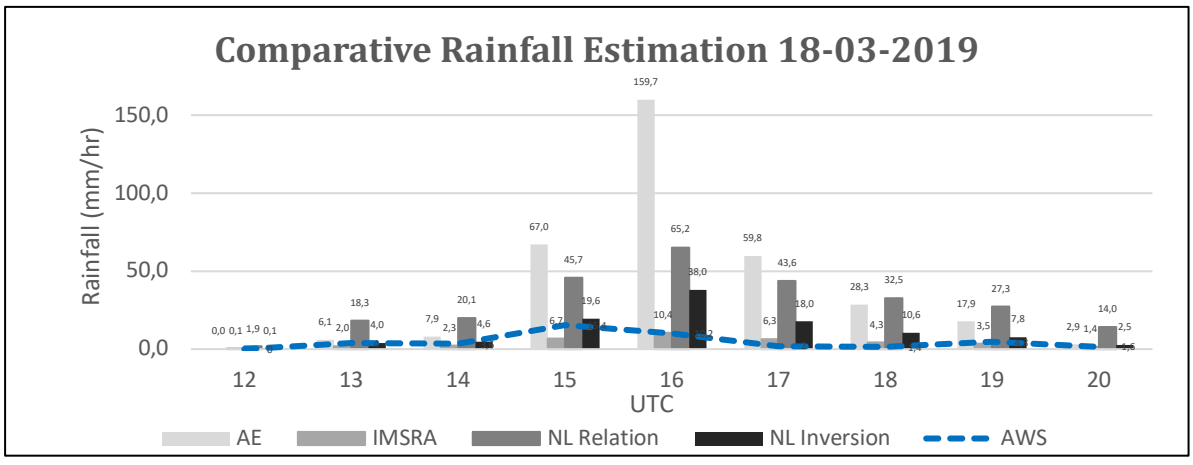

Figure 5. Comparison of rainfall on March 18, 2019.

The rainfall at 15 UTC is the highest actual rainfall which is 15.4 mm. At this hour the Autoestimator overestimate method is 67.0 mm against the actual rainfall while the rainfall estimation using the Non-Linear Inversion method is closest to the actual rainfall even though it is overestimated with a rainfall value of 19.6 mm. In general, the estimated rainfall results overestimate the actual rainfall. The Autoestimator method overestimates with a fairly large value in almost all phases of cloud development, especially at 16.00 UTC which reaches 158.7 mm.

Table 1. Correlation and Rating Estimation Methods.

Methods	Correlation (Scoring)			Average Correlation & Overall Scoring
	16 March 2019	17 March 2019	18 March 2019	
AutoEstimator	0.282 (4)	0.595 (1)	0.634 (4)	0.504 9
IMSRA	0.384 (2)	0.563 (3)	0.676 (2)	0.541 7
NonLinear Realtion	0.398 (1)	0.554 (4)	0.677 (1)	0.543 6 (best correlation)
NonLinear Inversion	0.333 (3)	0.584 (2)	0.658 (3)	0.525 8
Mean	0.349	0.574	0.661	

Precipitation estimates from various methods on 18 March 2019 have the best average correlations compared to 16 and 17 March 2019. Non-Linear Relations Method is the method with the best correlation with the largest average correlation value for 3 occurrences of heavy rain. The estimated rainfall on March 16, 2019, has the lowest average correlation value. Although Autoestimator has the smallest average correlation, this method has the largest correlation on March 17, 2019.

Table 2. RMSE and Assessment of Estimation Methods.

Methods	RMSE (Scoring)			Average Correlation & Overall Scoring
	16 March 2019	17 March 2019	18 March 2019	
AutoEstimator	45.6 (4)	322.5 (4)	57.0 (4)	141.7 12
IMSRA	14.5 (2)	38.6 (1)	3.5 (1)	18.7 4 (Best RMSE)
NonLinear Realtion	25.5 (3)	199.0 (2)	29.4 (3)	84.6 8
NonLinear Inversion	13.3 (1)	59.7 (3)	11.3 (2)	28.1 6
Mean	33.0	206.6	33.7	

Precipitation estimates from various methods on 16 March 2019 have the best average RMSE compared to 17 and 18 March 2019. The IMSRA method is the method with the best RMSE with the lowest average RMSE value for 3 heavy rainfall events. The estimated rainfall on March 16, 2019, has the highest average RMSE value. The largest RMSE value occurred on March 17, 2019, using the Autoestimator method. The lowest RMSE value occurred on March 18, 2019, using the IMSRA method.

Table 3. Total and Rating Estimation Methods.

Methods	Correlation	RMSE	Total	Methods Ranking
AutoEstimator	4	4	8	4
IMSRA	2	1	3	1 (Best Method)
NonLinear Realtion	1	3	4	2
NonLinear Inversion	3	2	5	3

Based on the assessment of the correlation and RMSE in the 4 methods of rainfall estimation, a ranking table is prepared that contains the ranking of each method. The ranking is arranged based on the smallest to largest total value as the best to the worst method. From the table, it can be seen that the rainfall estimation using the IMSRA method was chosen as the best estimation method (highest correlation and smallest RMSE) and Autoestimator as the worst estimation method (smallest correlation and highest RMSE).

4. Conclusions

Various estimator methods have been used to estimate rainfall in the case of heavy rain on 16-18 March 2019 in Jayapura. The results show that the IMSRA method is the best method that can be used to estimate rainfall in Jayapura. This is obtained through an assessment of the correlation rank and RMSE rainfall estimation of the rainfall AWS Digitization Doc 2. It should be noted that when viewed per case occurrence the methods are not consistent in estimating rainfall which means it can show good results in one case but not necessarily the same results are obtained for other cases. By referring to the cloud top temperature which experiences a decrease in temperature in the growing phase, the maximum maximal temperature in the mature phase, and an increase in temperature in the extinct phase indicates that the same temperature in one phase does not produce the same rainfall in the other phases. For this reason, in future studies, estimation of rainfall must involve factors determining the phase of cloud growth to estimate rainfall.

5. References

[1] Swarinoto, Y.S. and H. Husain, *Estimasi Curah Hujan Harian Dengan Metode Auto Estimator (Kasus Jayapura dan sekitarnya).* Jurnal Meteorologi dan Geofisika, 2012. **13**(1).
[2] Hastuti, M.I. and Anniza, *Pemanfaatan Data Satelit Himawari-8 untuk Estimasi Curah Hujan dengan Metode Autoestimator di Kaliangete, Madura* J.S.N.P.J.k.I.p. 447, Editor. 2017.
[3] Kurniawan, P.M.R., *Analisis Cuaca Ekstrem Terkait Bencana Hidrometeorologi di Jayapura (Studi Kasus Hujan Lebat Tanggal 22 Februari 2014).* Jurnal Meteorologi Klimatologi dan Geofisika, 2018. **5**(3): p. 25-36.
[4] Barrett, E.C., *The estimation of monthly rainfall from satellite data.* Monthly weather review, 1970. **98**(4): p. 322-327.
[5] Ginting, N.K., *Estimasi Curah Hujan dari Citra Satelit dengan Menggunakan SATAID dan Autoestiamtor di wilayah Sibolga (Bulan Desember 2012 dan April 2014* 2015, Meteorologi AMG: Tangerang.
[6] Lillesand, T.M. and R.W. Kiefer, *Penginderaan Jauh dan Interpretasi Citra. Terjemahan*. 1990, Gajah Mada University Press. Yogyakarta.
[7] Wandala, A., *Comparative Test of Several Rainfall Estimation Methods Using Himawari-8 Data.* International Journal of Remote Sensing and Earth Sciences (IJReSES), 2017. **13**(2): p. 95-104.
[8] *Pascalis DI Puncak Fase Diurnal Konvektif Awan Cumulonimbus di Stasiun Meteorologi Serui Papua* in *Meteorologi STMKG*. 2015: Tangerang.
[9] Kushardono, D., *Kajian Satelit Penginderaan Jauh Cuaca Generasi Baru Himawari 8 dan 9.* Jurnal Inderaja, 2012. **3**(5).

[10] Vicente, G.A., R.A. Scofield, and W.P. Menzel, *The operational GOES infrared rainfall estimation technique.* Bulletin of the American Meteorological Society, 1998. **79**(9): p. 1883-1898.
[11] Gairola, R., et al., *Rainfall estimation from Kalpana-1 satellite data over Indian land and oceanic regions.* Current Science, 2014: p. 1275-1282.
[12] DS, K.A. and M. Kartasamita, *Penentuan Hubungan Antara Suhu Kecerahan Data Mtsat Dengan Curah Hujan Data Qmorph.* Jurnal Penginderaan Jauh dan Pengolahan Data Citra Digital, 2010. **6**.
[13] Octari, G.R., et al., *Model Estimasi Curah Hujan Berdasarkan Suhu Puncak Awan Menggunakan Inversi Nonlinear.* 2016.

Field Spectral Reflectance Measurement Distance Effect to the Mangrove Species (*Avicennia* sp.) Mapping

T Kanekaputra[1]*, M Kamal[1,2]

[1]Departement of Geographic Information Science, Faculty of Geography, Universitas Gadjah Mada, Yogyakarta, Indonesia
[2]PUSPICS, Faculty of Geography, Universitas Gadjah Mada, Yogyakarta, Indonesia

*Corresponding author's e-mail: tito.kanekaputra@mail.ugm.ac.id

Abstract. *Avicennia* sp. is a major mangrove species which has various benefits for the coastal environment of Karimunjawa National Park, Jepara, Central Java. This species needs to be mapped and monitored to figure out its distribution and abundance in this area, thus support the biodiversity inventory efforts. The spectral reflectance curves from field spectrometer measurements can be used to help distinguishing *Avicennia* sp. from other mangrove species. Spectral reflectance curves could be obtained at different levels (i.e. leaf and canopy level), so that it is possible to produce different spatial distributions of *Avicennia* sp. This research aims to (1) map *Avicennia* sp. using spectral reflectance curves at leaf and canopy level with Spectral Angle Mapper (SAM) and Spectral Information Divergence (SID) classifications, and (2) analyze the effect of using spectral reflectance curves at different levels to *Avicennia* sp spatial distribution in parts of Karimunjawa National Park. Spectral reflectance from field measurements at leaf level were taken from young and old leaves at a measurement distance of 2cm. At the canopy level, spectral reflectance measurements were taken at measurement distance of 10cm, 1m, and 2m. The results of this research are *Avicennia* sp. distribution from SAM and SID classification with spectral reflectance curves at leaf and canopy levels. From these maps, we found that the field measurement distances have greatly affect the result of the distribution map. Closer measurement distance results in a low variability of spectral reflectance curve, and vice versa.

Keywords: *Avicennia* sp, spectrometer measurements, Spectral reflectance.

1. Introduction

Avicennia sp. is a mayor mangrove species which has varios benefits for the coastal environment. This smangrove species has ability to form pure stand and characterize community stricture in domination [1]. *Avicennia* sp. is mangrove species that its existence is less domination at Karimunjawa National Park [2], so this species needs to mapped and monitored to figure out its distribution and abundance in this area, thus support the biodiversity inventory efforts. The using of remote sensing can help to mapping *Avicennia* sp. distribution. Sensor of remote sensing can view a phenomenon with synoptic overview, especially mangrove at species level phenomenon

Remote sensing in this research used very high spatial resolution, that is Worldview-2 imagery. The use of WorldView-2 because mangrove phenomenon at species level has mix distribution, so that is necessary using very high spastial reolution to minimize mixed pixel in this imagery. Worldview-2 imagery also has eight multispectral band that record object in different wavelength [3]. Multispectral band of Worldview-2 imagery can help to mapping the object using its spectral reflectance. Spectral reflectance is ratio of energy that accepted and reflected from an object [4]. Vegetation object with same characteristic also have same spectral reflectance form, especially spectral reflectance of *Avicennia* sp. and other mangrove species. But, between this species to other mangrove species has different of leave structure, both fisiology and morphology [5]. From this different of leave structure it is possible that *Avicennia* sp. to other mangrove species has difereent intensity of spectral reflectance

Spectral reflectance of an object can acquired from field spectral measurement and laboratory spectral measurement [6]. Integration spectral reflectance curves from imagery and field spectrometer measurements can be used to help distinguishing *Avicennia* sp. from other mangrove species. Spectral reflectance curves could be obtained at different levels (i.e. leaf and canopy level), so that it is possible to produce different spatial distributions of *Avicennia* sp. This research aims to (1) map *Avicennia* sp. using spectral reflectance curves at leaf and canopy level with Spectral Angle Mapper (SAM) and Spectral Information Divergence (SID) classifications, and (2) analyze the effect of using spectral reflectance curves at different levels to *Avicennia* sp spatial distribution in parts of Karimunjawa National Park.

2. Method

2.1. Study Site

This study site of this research is located at part of Karimunjawa National Park. This National Park is located at Karimunjawa Sub-District, Jepara District, Central Java Province, Indonesia. Area of mangrove forest in Karimunjawa National Park is 396,4 Ha [2]. This mangrove forest become study site in this research because at this place have 25 mangrove species and this place is one of Indonesian mangrove forest that most varied. *Rhizophora stylosa*, *Ceriops tagal*, and *Lumnitzera racemosa* is mangrove species that dominated in this mangrove forest of Karimunjawa National Park. Map of thisstudy site is showed in **Figure 1**. Mangrove forest of Karimunjawa National Park coordinate is $5^{0}48'0"$ S - $5^{0}50'30"$ S dan $110^{0}26'0"$ E - $110^{0}29'30"$ E.

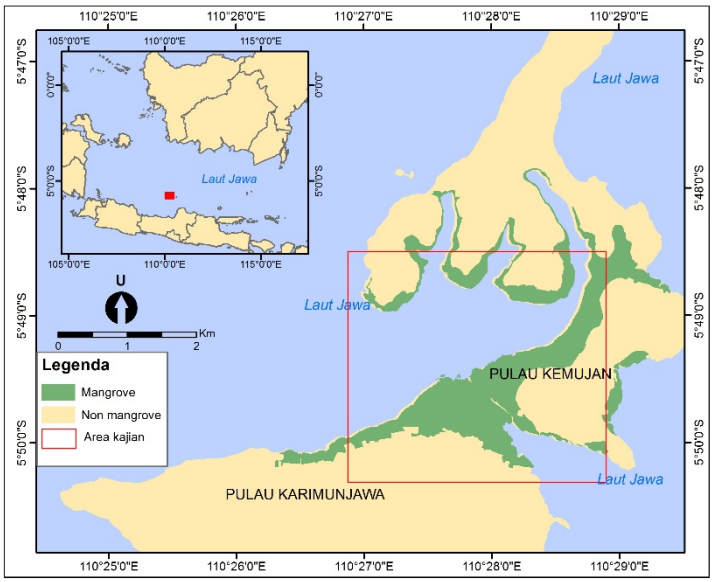

Figure 1. Study Site.

2.2. Field Spectral Reflectance Measurement

Field spectral reflectance measurement starting with spectral reference measurement for equalize field spectral reflectance of *Avicennia* sp. measurement to the actual light condition. Sample of spectral reference is ideal to taking when light condition is change [6]. Spectral reference measurement consist of two steps, taking white reference and dark reference. Taking white reference used to get perfect reflectance from standart lighting, while dark reflection used to get perfect absorpsion from black object. Dark reference measurement is taking with close collimating lens of JAZ-EL350 Spectrometer. White reference measurement using spectralon is showe in **Figure 2**.

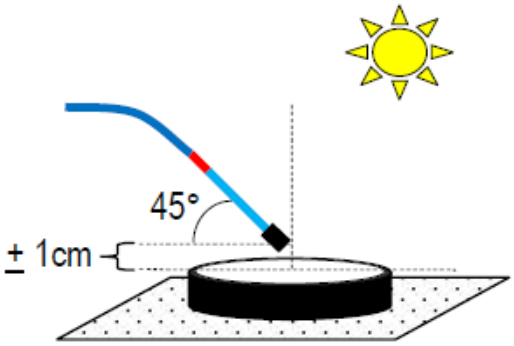

Figure 2. White reference measurement using spectralon.

Field spectral reflectance measurements of Avicennia sp. is measuring at two levels, leaf level and canopy level. First, spectral measurements at the leaf level are measured by choosing two types of leaves, bright young leaves and dark leaves. Measurement at leave level is taking with distnce betweel collimating lens with Avicennia sp. leave is 1-2cm. Meanwhile, because it needs to be measuring at the canopy level, spectral measurement is taking at different spectral measurements between the collimating lens and Avicennia sp. canopy.
Field spectral reflectance measurement is taking three times, measurement with distance of 10cm from the canopy, measurement with distance of 1m from the canopy, and a measurement with distance distance of 2m from the canopy. All measurement of Avicennia sp. spectral reflectance in leave level and canopy level is taking with ten times every item and this result of spectral reflectance is used to built spectral library. Field spectral reflectance measurement at leave level is illustrated in **Figure 3**, that the spectral reflectance taken with distance 1-2cm and Field of View (FOV) 14,250.

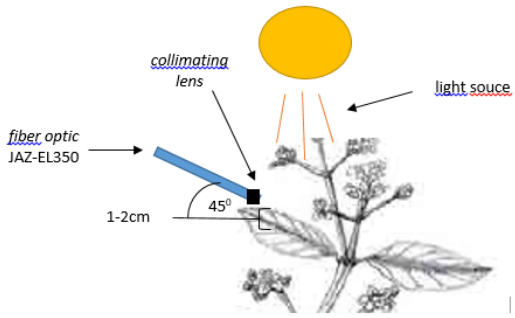

Figure 3. Field spectral reflectance measurement at leave level.

2.3. Spectral Resampling
Spectral reflectance *Avicennia* sp. from filed measurement in the spectral library have different spectral resolutions with WorldView-2 spectral resolution. This requires *Avicennia* sp. spectral reflectance in spectral library conversion to have the same spectral resolution as WorldView-2 imagery by spectral resampling. Spectral resampling for spectral reflectance *Avicennia* sp. measurement field results use two parameters, including center of wavelength and FWHM (Full Width Half Maximum). Information on the center of wavelength and FWHM parameters is in the imagey header. The Worldview-2 image used for resampling spectral library is a corrected image up to at surface reflectance.

2.4. Avicennia sp. Mapping
Avicennia sp. mapping in this research using classifications based on spectral reflectance from Worldview-2 imagery integration with field spectral reflectance measurement. The classifications are Spectral Angle Mapper (SAM) classification and Spectral Information Divergence (SID) classification.

Classification input is performed using spectral reflectance results from resampling spectral processes. Input curve used is Avivcennia sp. spectral reflectance at the leaf level (young leaves and old leaves) and canopy levels (measurements from 10cm, 1m and 2m to the *Avicennia* sp canopy. All spectral reflectance curve inputs for SAM and SID classifications are given a threshold with the same values so that the classification results can be compared.

The use of SAM classification is chosen because it can classify an object not only based on the spectral value of each pixel, but also based on its spectral reflectance curve, while the selection of SID classification because this classification classifies based on differences in spectral reflectance intensity. The results from SID classifications in mapping *Avicennia* sp. distribution can be compared with SAM which only classifies based on its spectral angle between spectral target and spectra reference [7]. SAM classification equation is showed in equation (1) below [8]. SAM classification classifies objects by calculating the spectral angle between the spectral of a pixel to the reference spectral. Smaller the spectral angle between the spectral of a pixel to the reference spectral, the more pixel-like the object being classified. The spectral angle is expressed as α, t_i is spectral in a pixel, r_i is a spectral reference, and n is the number of bands used.

$$\alpha\, cos^{-1} = \left[\frac{\sum_{i=1}^{n} t_i r_i}{(\sum_{i=1}^{n} {t_i}^2)^{\frac{1}{2}} (\sum_{i=1}^{n} {r_i}^2)^{1/2}}\right] \quad (1)$$

SID classification determines the target pixel based on the difference in spectral reflectance information. The smaller of spectral reflectance information difference, the more similar the target pixel to the reference (*Avicennia* sp.). Target pixels that have a value outside the threshold cannot be classified SID classification equation is showed in equation (2) below [9]. The difference in information between the target pixel and the reference is calculated from the number of relative differences in the target pixel to the reference (D (r1 || r2)) and the relative difference in reference to the target pixel (D (r2 || r1)).

$$\mathrm{SID(ri.r2)} = \mathrm{D(r1||r2)} + \mathrm{D(r2||r1)} \quad (2)$$

3. Results and Discussion

3.1. Avicennia sp. Distribution Map from SAM Classification

The results of SAM classification to mapping the distribution of *Avicennia* sp. showed in **Figure 4**. The figure illustrates the distribution of *Avicennia* sp. at the block area of *Avicennia* sp. and *Ceriops tagal* on Karimunjawa Island. The five maps describe the distribution of *Avicennia* sp. resulting from the input of a different spectral reflection curve. All input given same threshold with the value is 0,195. This value is chosen for mapping *Avicennia* sp. distribution using SAM classification because this value resulting the best classification for all spectral reflectance input.

Avicennia sp distribution results. with young leaf input representing the best distribution of *Avicennia* sp. at the block area. The results of the SAM classification with the input curve of the old leaf can represent *Avicennia* sp. distribution but overestimate classification because other vegetation objects are classified all due to high threshold usage. The classification results with input curve at canopy level representative but not optimal because the upper limit of its representation is above the threshold value of 0.195 (for distance canopy of 1m and 2m) and in the canopy with a distance of 10cm the results are underestimate classification.

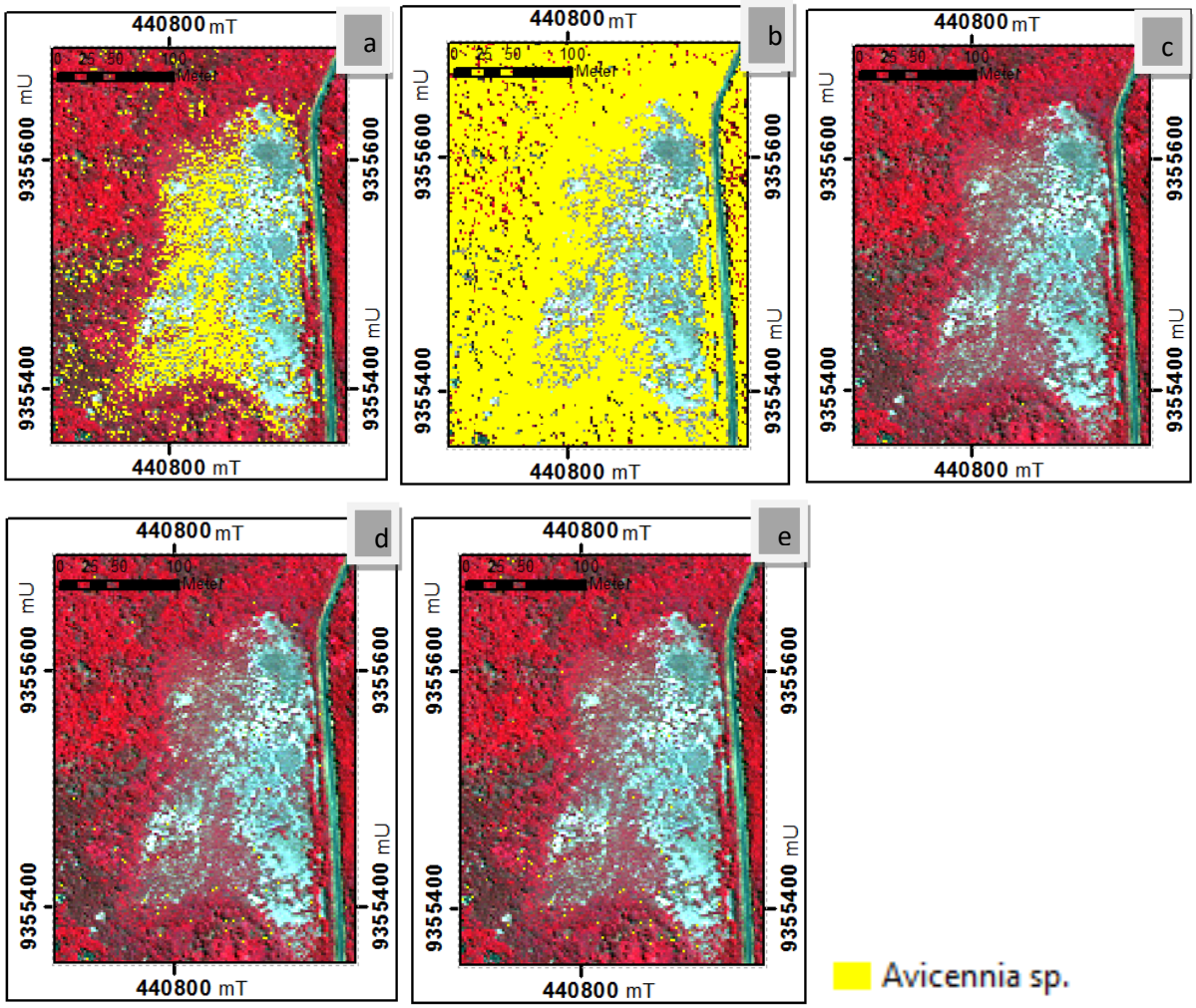

Figure 4. *Avicennia* sp. distribution map result SAM classification using spectral reflectance input from leave level (a) young leave, (b) old leave and canopy level with distance measurement (c) 10cm, (d)1m, (e) 2m.

3.2. Avicennia sp. Dsitribution Map from SID Classification

The results of the SID classification can be seen in **Figure 5**. *Avicennia* sp. from the results SID classification is representative in classifying *Avicennia* sp. at the level of young leaves. This classification results at this level can classify only in the block where the species is located. With the old leaf input the results of SID classification are the same as the results SAM classification, that is overestimate classification. At the canopy level, the results from SID classification overestimate on the canopy input with a distance of 1m because the optimal threshold value is below the value of 0.475. The use of input canopy with a distance of 10cm underestimate because the threshold value is too low to be used. Comparison between SID classification and SAM classification in mapping the distribution of *Avicennia* sp. is the ability to distinguish Avicennia sp. with other species and other objects. It because SAM classification only using spectral angle to distinguish spectral reference (*Avicennia* sp.) with spectral reflectance target (pixel WorldView-2 imagery).

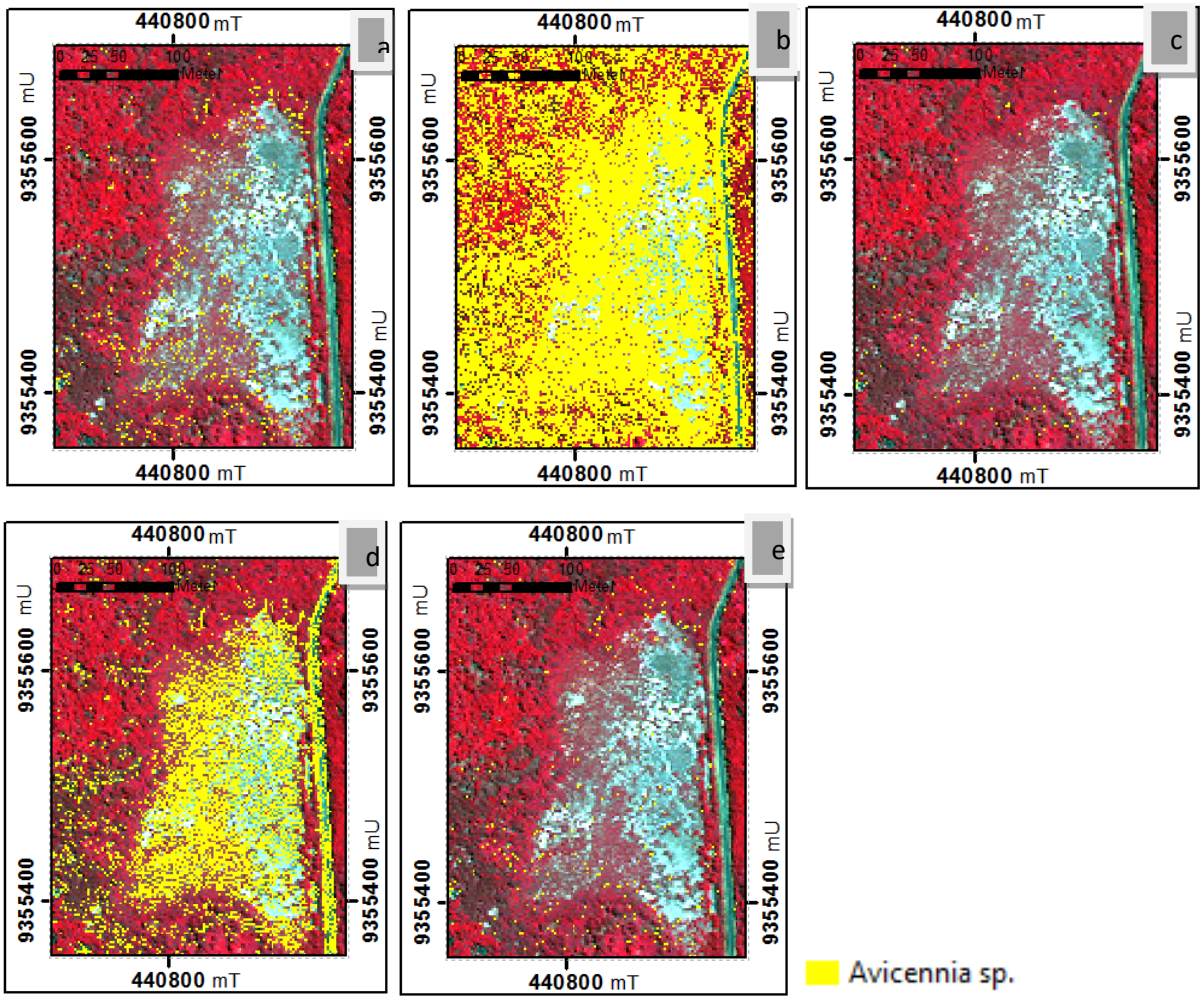

Figure 5. *Avicennia* sp. distribution map result SID classification using spectral reflectance input from leave level (a) young leave, (b) old leave and canopy level with distance measurement (c) 10cm, (d)1m, (e) 2m

3.3. Effect of Field Spectral Reflectance Measurement to Avicennia sp Distribution Map

Input spectral reflectance curves from field measurements withdifferent levels (leaves and canopies) resulting diferrent *Avicennia* sp. distribution map in block area. The difference in field spectral reflectance measurement resulting different spectral reflectance intensities so that both classifications using SAM and SID will also bresulting different *Avicennia* sp distribution. Effect of field spectral reflectance retrieval from leave and canopy level influence in variations of spectral reading curves from ten readings spectral per measuring.

Retrieval from the leaf level effect in a low variation due to the influence of the homogeneity of spectral reflectance measurement close to *Avicennia* sp. leaf. Meanwhile, the effect of spectral retrieval at the canopy level resulted in a high variation of intensity from all spectral readings, where there is a gap in every spectral reading. The gap between all spectral reflectance readings is greater as the distance of measurement increases. This varation of spectral reflectance intensity makes Avicennia sp. distribution with leaf and canopy level input is different. Spectral reflectance curves at leaf and canopy level are shown in **Figure 6.**

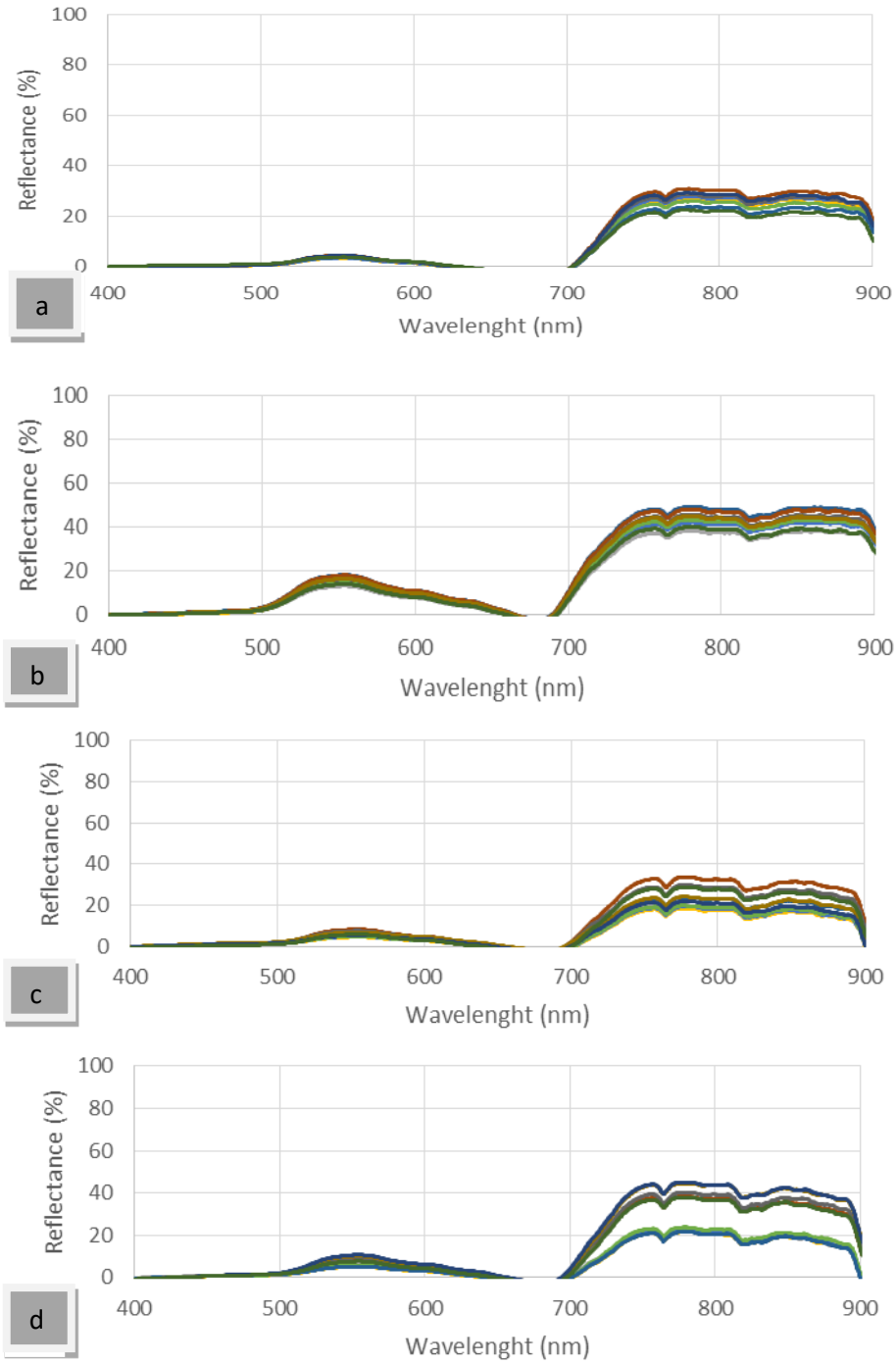

Figure 6. Comparison *Avicennia* sp. field spectral reflectance measurement from leave level (a) young leave, (b) old leave and canopy level with distance measurement (c) 10cm, (d)1m, (e) 2m.

The weakness of using spectral reflectance measurement input at the canopy level is influenced to the reflectance of other objects [10]. Reflectance of other objects such as *Ceriops tagal* spectral reflectance and mangrove background (such as water or soil) will affect the spectral reflectance curve used as an input for mapping *Avicennia* sp. so the distribution results are different. In addition, environmental factors in the measurement will affect the quality of the curve, such as the sun and other factors [11]. Environmental factor and reflectance from other objects make not optimal the use of field spectral

reflectance at the canopy level to mapping distribution of *Avicennia* sp. in mangrove ecosystems that are heterogeneous species [2]. The use of spectral reflectance at the leaf level is more representative because it results spectral reflectance of *Avicennia* sp. without mixture from other objects. However, spectral measurements at the leaf level need to know the dominance of young leaves or old leaves in a canopy. The results of spectral reflectance input with young leaves are more optimal because *Avicenni*a sp. canopy in study site is more dominated by young leaves. *Avicennia* sp. canopy in study site is shown by **Figure 7**.

Figure 7. *Avicennia* sp. canopy ini block area of Karimunjawa Island.

4. Conclusions

The use of fied spectral reflectance with different measurement as input in mapping *Avicennia* sp. results different distributions. Effect of reflectance from other objects and environmental factors on the use of spectral reflectance at the canopy level results in a higher variation of the spectral reading intensity. Meanwhile, at the leaf level it is more optimal to map *Avicennia* sp. which has heterogeneous distribution because the spectral reflectance used has high homogeneity. The dominance of leaf color in a canopy also affected the mapping results of *Avicennia* sp. The use of the spectral reflectance input at the young leaf level is more optimal because of *Avicennia* sp. canopy in the study area dominated by young leaves.

5. References

[1] Tomlinson, P.B., *The Botany of Mangroves*. 1984, Cambride University Press.
[2] Karimunjawa, B.T.N., *Jenis-Jenis Mangrove TN Karimunjawa.* , S.B.T.N. Karimunjawa., Editor. 2012.
[3] DigitalGlobe, *WorldView-2 Spacecraft Information and Specifications*, ed. s.l.D.G. Foundation. 2013.
[4] Danoedoro, P., *Pengantar penginderaan jauh digital.* Yogyakarta: Andi, 2012.
[5] Noor, Y.R., M. Khazali, and S. I NN, *Panduan pengenalan mangrove di Indonesia*. 1999: PKA/WI-IP (Wetlands International-Indonesia Programme).
[6] Kamal, M., N. Adi, and S. Arjasakusuma, *Jaz EL-350 Portable Spectrometer: panduan operasional pengukurandan pengelolaan data pantulan spektral objek.* 2012, Laboratorium Penginderaan Jauh Dasar, Fak. Geografi UGM, Yogyakarta.
[7] Kamal, M. and S. Phinn, *Hyperspectral data for mangrove species mapping: A comparison of pixel-based and object-based approach.* Remote Sensing, 2011. **3**(10): p. 2222-2242.
[8] Jensen, J.R., *Introductory digital image processing: a remote sensing perspective*. 2015: Prentice Hall Press.
[9] Chang, C.-I., *An information-theoretic approach to spectral variability, similarity, and discrimination for hyperspectral image analysis.* IEEE Transactions on information theory, 2000. **46**(5): p. 1927-1932.

[10] Kamal, M., M. Ningam, and F. Alqorina. *The Effect of Field Spectral Reflectance Measurement Distance to the Spectral Reflectance of Rhizophora stylosa*. in *IOP Conference Series: Earth and Environmental Science*. 2017. IOP Publishing.
[11] Blasco, F., et al., *Recent advances in mangrove studies using remote sensing data.* Marine and Freshwater Research, 1998. **49**(4): p. 287-296.

6. Acknowledgement

Authors would like to thank the Karimunjawa National Park Authority for granting permission and providing directions and considerations during the fieldwork for this research. Authors also thanks to DigitalGlobe Foundation for the satellite imagery as a primary data in this research.

Calculation of Total Economic Value of Peatland Burnt Area in Pangkalan Lanpam Sub-district, Ogan Komering Ilir (OKI)

Tiara Grace F[1]*, Riissiyani[1], Anisah[1], Dionysius Bryan S[1]

[1]Center for Regional Resource Development Technology (CRRDT) – Agency for the Assessment and Application of Technology (BPPT), Geostech 820 Building Kawasan Puspiptek, Tangerang Selatan, Indonesia

*Corresponding author's e-mail: tiara.grace@bppt.go.id

Abstract. Peatland fire is mostly triggered by human activities specifically in preparing and managing agriculture, industrial forestry and plantation area. With El Nino event, the fire occurrence in peatland is getting more difficult to handle and cause staggering losses in many aspects like in 2015. Blatant damages were seen in several sectors such as agriculture, forest, health, trade and transportation. Economic valuation is one of methods to assess loss as result of forest or environmental destruction such as peatland fire and it is imperative for gaining knowledge and decision making. According to regulation from Ministry of Environment Republic of Indonesia Number.14 2012 about Guidance for Economic Valuation in Peatland, there are 19 functions and benefits from peatland ecosystem itself namely plantation, agriculture, ecotourism, education, research, water storage, flood/fire prevention, carbon absorbent, carbon storage, oxygen source, fauna breeding, flora/fauna inhabitation, religion activities, transportation services, wildlife conservation and esthetics. One of subdistricts in Ogan Komering Ilir whose burnt area was one of the largest in 2015 was Pangkalan Lanpam subdistrict with total burnt area approximately 7789.84 ha. Specifically, land cover types over peatland which burnt were shrubs with 15.57 hectares, swamp bush with 1211.35 hectares, Industrial Forest with 214.68 hectares, plantations with 238.69, grassland with 1026.73 hectares, barren land with 2483.85 hectares and wildlife conservation area with 2608.97 hectares. Using Economic Valuation method, Total Economic Value (TEV) from burnt area in peatland in Pangkalan Lampang subdisctrict was Rp. 166,580,896,403.77.

Keywords: Economic Valuation, Total Economic Value.

1. Introduction

Fire in peatland has always been initiated by continual anthropogenic factors such as land clearing and draining for agriculture, farmland or industrial forestry, preparing for new settlement development area or even from simple ignorance activity like throwing lit cigarette butts recklessly on dried peat soil. The fire event could be even worse if El Nino Southern Oscillation (ENSO) hit as it would cause prolong fire than ever. Indonesian government itself currently does not really put much concern about law enforcement towards perpetrators of peatland arson even though they cause damages that has effected not only in local region but also regional even in international scope as smoke distribution from this fire is reported to reach other ASEAN countries. Visible damages or impacts caused by severe peatland fires can be seen from the increase of upper respiratory tract infection patients in hospital during fire event, widespread damage of forest and other natural resources, the closing of schools, governmental and administrative activities, transportation system failure even casualties. In larger scope, fire event causes huge losses in economic sector, trade, industry, etc. Considering how massive the damage and the impacts caused by of peatland fire especially in economic view therefore it is important to have a method to accurately measure the economical losses of ecological and ecosystem damages in the aftermath of peatland fires event. Economic valuation is a proper process and method to assess total loss from such event and beneficial as information feed for policy making. In addition, economic valuation can be used as material to file lawsuit against perpetrators. Economic valuation of peatland fire is basically

calculated based on apparent changes or losses in ecosystem or natural resources function. According to Regulation of Ministry of Environment of Republic of Indonesia No.14 2002 [1] concerning Economic Valuation of Peatland Ecosystem, there are 19 functions and roles of Peatland Ecosystem namely energy resources, organic fertilizer medium, industrial forestry, farmland, agriculture, ecotourism, education, research, water retainer, flood or fire prevention, carbon absorption medium, carbon storing medium, oxygen producer, animal breeding ground, fauna and botany, religious activity, transportation services and wildlife conservation. In this research, the focus was in Pangkalan Lanpam subdistrict as this region had one of the largest burnt areas during great peatland fire event in 2015 reaching nearly 7789.84 hectares. Several peatland ecosystem functions that were affected by fire were carbon absorption medium, carbon storing medium, animal breeding ground, fauna, water retainer, fish, flora, timber, water cycle, and hydrology.

2. Methodology

Variables for calculating economic valuation of peatland ecosystem for Pangkalan Lanpam subdistrict as mentioned below.

2.1. Carbon Absorption Medium (11,1)

Formula:

$$Val\,P_{(11,1)} = V_{(11,1,1)} \times V_{(11,1,2)} \times V_{(11,1,3)} \quad (1)$$

Where $V_{(11,1,1)}$ is total amount of carbon absorbed by peatland (ton/m^3 atau ton/ha), $V_{(11,2)}$ is the price of carbon per ton (Rp/ton) and $V_{(11,1,3)}$ is the total burnt peatland volume or area (m^3 atau ha)

2.2. Carbon Storing Medium (12,1)

Formula:

$$Val\,P_{(12,1)} = V_{(12,1,1)} \times V_{(12,1,2)} \times V_{(12,1,3)} \quad (2)$$

Where $V_{(12,1,1)}$ is total amount of carbon released by burnt peatland ((ton/m^3 atau ton/ha), while $V_{(12,1,2)}$ is the price of carbon per ton (Rp/ton) and $V_{(12,1,3)}$ is the total burnt peatland volume or area (m^3 atau ha)

2.3. Animal Breeding Ground (14,1)

Formula:

$$Val\,P_{(14,1)} = \left(\sum_{i=1}^{n}\left(V_{i(14,1,1)} \times V_{i(14,1,2)} \times V_{i(14,1,3)} \times V_{i(14,1,4)}\right)\right) \times V_{(14,1,5)} \times V_{(14,1,6)} \quad (3)$$

Where $V_{i(14,1,1)}$ is total species n per ha (n_species/ha), $V_{i(14,1,3)}$ is the number of frequency each species breed in peatland per year (number of bredd/year), $V_{i(14,1,3)}$ is the number of births for each species in a single breeding period, $V_{i(14,1,4)}$ is the price per individual species (Rp/species) using price market approach or benefit cost transfer approach, $V_{(14,1,5)}$ is the total burnt peatland area (ha) and $V_{(14,1,6)}$ is period it takes to recover for peatland after burnt as animal breeding ground function (year).

2.4. Fauna (15,2)

Formula:

$$Val\,P_{(15,2)} = \left(\sum_{i=1}^{n}\left(V_{i(15,2,1)} \times V_{i(15,2,2)}\right)\right) \times V_{(15,2,3)} \quad (4)$$

Where $V_{i(15,2,1)}$ is total fauna species per hectares (species/ha), $V_{i(15,2,2)}$ is price per individual fauna species (Rp/fauna species) using market price approach or benefit cost transfer approach and $V_{(15,2,3)}$ is total burnt industrial forestry (ha).

2.5. Water Retainer (9,1)
Formula:

$$Val\,P_{(9,1)} = V_{(9,1,1)} \times V_{(9,1,2)} \times V_{(9,1,3)} \times V_{(9,1,4)} \quad (5)$$

Where $V_{(9,1,1)}$ is total precipitation rate in peatland (mm/year), $V_{(9,1,2)}$ is recovery period of peatland (year), $V_{(9,1,3)}$ is the price of waters in peatland and $V_{(9,1,4)}$ is total peatland burnt area (m^2).

2.6. Fish Selling Price in Swamp Peatland (9,2)
Formula:

$$Val\,P_{(9,2)} = \left(\sum_{i=1}^{n}\left(V_{i(9,2,1)} \times V_{i(9,2,2)}\right)\right) \times V_{(9,2,3)} \times V_{(9,2,4)} \quad (6)$$

Where $V_{i(9,2,1)}$ is price for a single individual fish species (*i*) (Rp/kg), $V_{i(9,2,2)}$ is total productivity of single individual fish species (kg/ha/year), $V_{(9,2,3)}$ is years it takes to recover from burnt and $V_{(9,2,3)}$ is total area of inundated peatland or area of swamp in peatland (ha).

2.7. Flora (15,1)
Formula:

$$Val\,P_{(15,1)} = \left(\sum_{i=1}^{n}\left(V_{i(15,1,1)} \times V_{i(15,1,2)}\right)\right) \times V_{(15,1,3)} \quad (7)$$

Where $V_{i(15,1,1)}$ is total flora species per hectare (n_species/ha), $V_{i(15,1,2)}$ is price for single individual flora species (Rp/n_species) and $V_{(15,1,3)}$ is total burnt area of industrial forestry (ha).

2.8. Water Cycle (3,5,1)
Formula:

$$Val\,P_{(3,5,1)} = \left(V_{(3,5,1,1)} - V_{(3,5,1,2)}\right) \times V_{(3,5,1,3)} \times V_{(3,5,1,4)} \times V_{(3,5,1,5)} \quad (8)$$

Where $V_{(3,5,1,1)}$ is mean of precipitation in industrial forestry area before burnt (mm/year), $V_{(3,5,1,2)}$ is mean of precipitation in industrial forestry are after burnt (mm/year), $V_{(3,5,1,3)}$ is years it takes for industrial forestry to recover (years), $V_{(3,5,1,4)}$ is the price of water per m^3 (Rp/m^3) and $V_{(3,5,1,5)}$ is the total area of burnt industrial forestry (m^2).

2.9. Hidrologi (3,5,2)
Formula:

$$Val\,P_{(3,5,2)} = V_{(3,5,2,1)} \times V_{(3,5,2,2)} \times V_{(3,5,2,3)} \quad (9)$$

Where $V_{(3,5,2,1)}$ is total carbon release (ton/m^3), $V_{(3,5,2,2)}$ is carbon price per ton (Rp/ton) and $V_{(3,5,2,3)}$ is the total volume of burnt peatland in industrial forestry (m^3).

2.10. Productive Plantation
Formula:

$$\text{Val } P_{(4,2)} = V_{(4,2,1)}.\left(V_{(4,2,2)} + V_{(4,2,3)} - V_{(4,2,4)}\right) \quad (10)$$

Where $V_{(4,2,1)}$ is total area of burnt plantation (ha). $V_{(4,2,2)}$ is total cost production of plantation (Rp/ha), $V_{(4,2,3)}$ is the total profit of plantatin production (Rp/ha), $V_{(4,2,4)}$ is total profit gained from productive period to burnt event per hectares (Rp/ha).
To get those numerical scores for all variables above and primary data, interviews were conducted to locals in Pangkalan Lanpam sub-district. To complete the data, supplementary data were also gathered from several government institutions such as Local Statistical Agency, Tourism Office, Forestry Office, and etc. The next step was to calculate EV for each variable with following formula below;

$$TEV = EV\,x\,Burn\,Land\,Use \quad (11)$$

Figure 1. Interviewing Locals in Pangkalan Lanpam Sub-district.

Figure 2. Interviewing Local Government Institutions.

3. Results and Discussion

Economic valuation of peatland in Pangkalan Lanpam, OKI Regency was calculated for each burnt land use. There were 7 land use type that were burnt;

3.1. Shrub

Shrubs in Pangkalan Lanpam were burnt up to 15.57 hectares. Shrubs were recognized for its function as carbon absorption medium with economic value Rp. 1,624,000.00 per hectare, carbon storing medium with economic value Rp. 4,408,000.00 per heacter, animal breeding ground with economic value Rp. 193,254.50 per hectare and fauna with economic value Rp. 20,645.16 per hectare.

3.2. Swamp Underbrush

This swamp underbrush had total 1211.35 hectare burnt area and recognized for its function as water retainer with economic value Rp. 10,757,538.17 per hectare, fish selling price with economic value Rp.

1,513,800,.00 per hectars, carbon storing medium with economic value Rp 25,346,000.00 per hectare, animal breeding ground with economic value Rp. 193,254.50 per hectare, flora with economic value Rp. 10,000.00 per hectare and fauna with economic value Rp. 20,645.16 per hectare.

3.3. Industrial Forestry

Industrial Forestry was burnt reaching total 214.68 hectares. This land use type was identified for its functions as timber with economic value Rp. 4,059,549,848.00 carbon absorption medium with economic value Rp. 1,629,800.00 per hectare.

3.4. Plantation

This type had total burnt area 238.69 hectares. Calculation of economic value of this type was delayed because there was no enough data to identify which plantation type that mostly burnt.

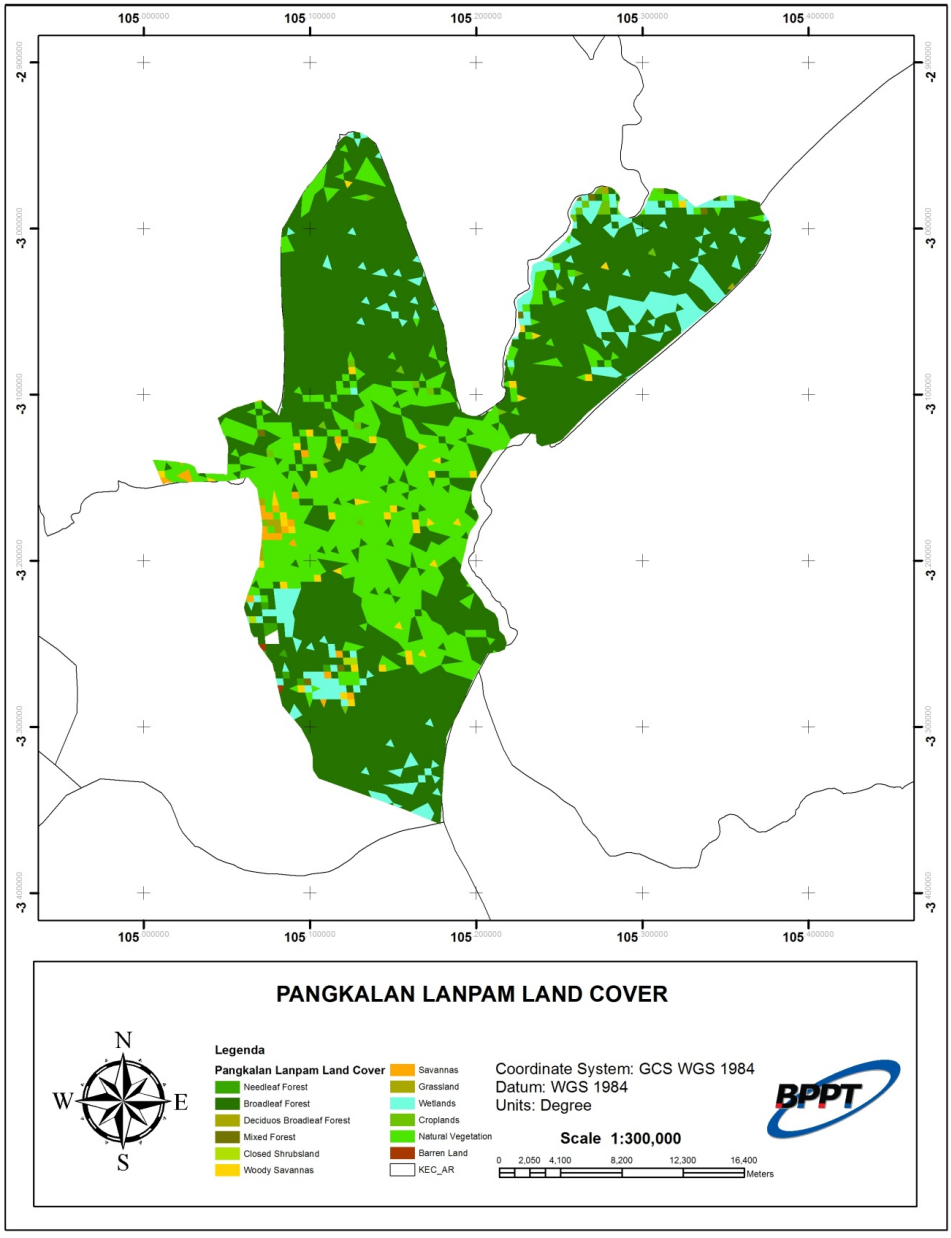

Figure 3. Pangkalan Lanpam Land Cover Map.

3.5. Grassland

Grassland had total burnt area 1026.73 hectares. Similar to plantation, there are no enough data to calculate its economic value.

3.6. Bareland

Bareland had total burnt area 2473.85 hectares. Similar to plantation and grassland, there were no enough data to calculate its economic value.

3.7. Wildlife Conversation

Total burnt area for this type was 2608.97 hectares with functions economic value of timber, Rp. 49,551,059,848.00, carbon absorption medium, Rp. 1,629,800.00 per hectare, fauna, Rp. 20,645.16 per hectare, water cycle, Rp. 2,102,643.86 per hectare and hydrology, Rp. 4,077,400.00 per hectare.

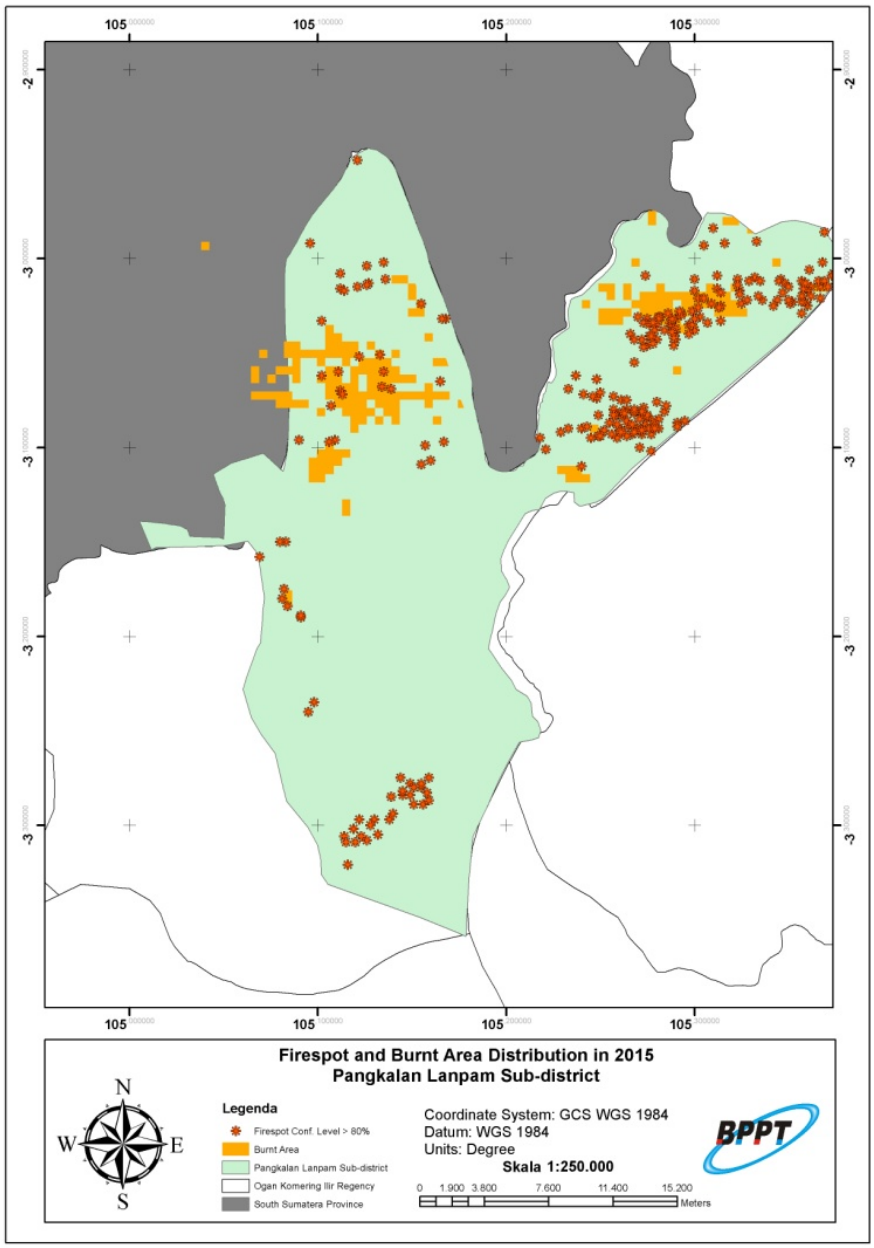

Figure 4. Pangkalan Lanpam Firespot and Burned Area Map in 2015.

Tabel 1. Total Economic Value (TEV) of Pangkalan Lanpam Sub-distict.

No.	Land Use Burned	Area (Ha)	Code	Advantage	EV (Rp/Ha)	TEV (Rp)
1.	Shrub	15.57		Carbon Absorption		
			P(11,1)	Medium	1,624,000.00	25,285,680.00
			P(12,1)	Carbon Storing	4,408,000.00	68,632,560.00
			P(14,1)	Animal Breeding Ground	193,254.50	3,008,972.53
			P(15,2)	Fauna	20,645.16	321,445.16
2.	Swamp Underbrush	1211.35	P(9,1)	Water Retainer	10,757,538.17	13,031,143,856.17
			P(9,2)	Fish	28,419,567.10	34,426,042,609.05
			P(11,1)	Carbon Absorption Medium	1,513,800.00	1,833,741,630.00
			P(12,1)	Carbon Storing	25,346,000.00	30,702,877,100.00
			P(14,1)	Animal Breeding Ground	193,254.50	234,098,835.87
			P(15,1)	Flora	10,000.00	12,113,500.00
			P(15,2)	Fauna	20,645.16	25,008,516.13
3.	Industrial Forestry	214.68	P(3,1)	Timber	-	4,059,549,848.00
			P(3,3,2)	CO2 Absorption	1,629,800.00	349,885,464.00
			P(3,4,2)	Fauna	20,645.16	4,432,103.23
			P(3,5,1)	Water Cycle	2,102,643.86	451,395,582.79
			P(3,5,2)	Hidrology	4,077,400.00	875,336,232.00
4.	Plantation	238.69		Plantation		
5.	Grassland	1026.73				0.00
6.	Bareland	2473.85				0.00
7.	Wildlife Conservation	2608.97	P(18,1)	Timber	-	49,551,059,848.00
			P(18,3,2)	CO2 Absorption	5,643,400.00	14,723,461,298.00
			P(18,4,1)	Flora	10,000.00	26,089,700.00
			P(18,4,2)	Fauna	20,645.16	53,862,606.45
			P(18,5,1)	Water Cycle	2,102,643.86	5,485,734,738.38
			P(18,5,2)	Hidrology	4,077,400.00	10,637,814,278.00
Total Economic Value (TEV) in Pangkalan Lanpam (Rp)						**166,580,896,403.77**

4. Conclusions

Based on analysis above, total TEV was reaching staggering number Rp. 166,580,896,403.77 where the highest TEV value was to be found in Shrub type with Rp. 96,972,212.53 meanwhile the lowest was to be found in Industrial Forestry with Rp. 5,710,599,230.02. TEV above could be interpreted as total economic loss due to severe fire event in Kecamatan Pangkalan Lanpam only. The value of TEV could have been much higher should the data for Grassland and Bareland were completed.

5. References

[1] KLHK, *Peraturan Menteri Negara Lingkungan Hidup Republik Indonesia* in *14.Tahun 2012* P.V.E.E. Gambut., Editor. 2012.

Rapid Mapping for Disaster Recovery (Case Study: Petobo, Palu)

Z Afif[1]*, W Gomarga[1] B E Leksono[2]

[1]Bandung Institute of Technology, Faculty of Earth Science and Technology, Department of Geodesy and Geomatics, Bandung 40116, Indonesia
[2]Survey and Cadastre Reseearch Group Bandung Institute of Technology, Department of Geodesy and Geomatics, Bandung 40116, Indonesia

*Corresponding author's e-mail: zacharyafif@students.itb.ac.id

Abstract. In late 2018, there are spikes of natural disaster occurrence in Indonesia. This occurrence of these natural disasters happened simultaneously in a short period of time. Such events can possess as a threat to civil society. In order to encounter these events, there are needs to produce spatial data about the affected area. This data eventually will be used as primary spatial data for disaster impact analysis in support of the disaster recovery act. The usage of reliable primary spatial data can be obtained by the rapid mapping method. Rapid mapping is a method to produce maps in a short period of time for real-time applications, such as disaster impact analysis. Rapid mapping method emphasizes in generating quick mosaic from the recorded data within minutes right after data acquisition. In order to do such a method, data processing must be done with SFM algorithm on digital photogrammetric software. Results from this method is 1:1000 map (4.12cm/pix). Also, it yields a base product called large scale image product which can be used to generate initial line drawing for further mapping purposes, this method called OBIA (Object-Based Image Analysis) which could be conducted by using feature extraction with result a base map.

Keywords: Rapid Mapping, Disaster Risk Management, UAV.

1. Introduction

As a country highly vulnerable to disasters, Indonesia need any system that manage the reduction and response of every aspect of disasters. Any Implementation on this system has been made to reduce the impact because of the risk of a disaster such as landslide, earthquake and many man-made or natural disaster. Liquefaction and Tsunami strikes Petobo, a district at Palu, Sulawesi in 2019 and made a hugely significant impact on that city and also with their society, a respond plan to the disaster should be made and implemented in order to prevent for further losses caused by the events.

Disaster recovery efforts aim to restore peoples' lives and livelihoods, re-establish institutions, and foster sustainable development [1]. Disaster recovery as part of disaster management become an important issue as a failed disaster recovery process can undermines development of the affected country [1]. Failure of disaster recovery may cause further disaster impact as failed recovery contribute in amplify the disaster effect. Failed recovery resulting the disaster to becoming endemic, cause fuss in the country development, and cause heavy losses. Indonesia now faces a massive scale of disaster particularly in late 2018s that human activities must be adapted not only to reduce the change cause by the disaster itself but also to respond the aftermath.

In order to make the disaster recovery to be effective, disaster recovery need a plan that consider information regarding damages, losses, and existing resources. Such information can be displayed as spatial information and can be acquired with the advance recent development in surveying and GIS (Geographic Information System). As both have been used in response to many disasters that have been occurred.

Rapid Mapping Technology has been developed to help many mitigations and help many developments of the destructed cities as the impact of the disaster and also it helps many disaster relief programs.

Rapid Mapping Technology consists of the usage of a UAV (Unmanned Aerial Vehicle) to create a high-resolution image base map within an hour - day process. The technology behind this technology relies on the integration between the GPS and the acquisition of photographs, each photograph on this system has been processed with the location-based data and it is the most powerful key for a good mechanism to make the orthophotos rapidly. The software that was used to process the image data using the SFM (Structure from Motion) based software.
On rapid mapping process, as the post- processing method, the usage of OBIA (Object-Based Image Analysis) is being used for the object-oriented feature extraction process, this method using artificial intelligence to extract some features on the large-scale image product, the post-processing product that has to be achieved is to make a base map for thematic mapping purpose in order to sustain disaster relief management program.

2. Rapid mapping

Rapid Mapping is a procedure to provide geospatial data by combining immediate data collection and processing with a certain contextual aspect in order to give a quick overview about certain earth phenomena. Rapid mapping method emphasizes in generating quick mosaic from the recorded data within minutes right after data acquisition. Rapid Mapping is a procedure to provide geospatial data by combining immediate data collection and processing with a certain contextual aspect in order to give a quick overview about certain earth phenomena.

3. Data Acquisition

In recent years, Unmanned Aerial Vehicle serve as one of the alternatives for surveying and mapping activity. Particularly in disaster management activity. UAV systems offers many advantages, this system can be used in high risk situations, in accessible areas, and low altitude. Furthermore, UAV system also enabling data acquisition in cloudy weather condition as UAVs can fly below the clouds and has ability for fast data acquisition. The recent development of UAV technology also allows more precise flight from it estimated preflight planning with the usage of GPS system and flight controller. As for the ease of use, certain UAVs, multi rotor type allows vertical takeoff and landing, so it can eliminate the needs of runway. Also, commercial multi-rotor UAV product such as DJI enables the connection from smartphone to the aircraft for mission planning and ground control station.
For this research, DJI phantom 4 Proffesional has been used as it known for it ease of use and mapping capability. DJI Phantom 4 Pro is a multirotor or Vertical Takeoff Landing (VTOL) type UAV. The UAV has a fully complete installed fuselage consist of ESCmotor,propeler,BrushlessTx/Transmitter/ RemotRxReceiver, battery, GPS, IMU, and a camera properly mounted in 3-axis gimbal. The UAV also has main controller (flight controller) so it can enable the ability to autopilot through planned waypoint. The planning of flight waypoint are generated with mission planning software such as dronedeploy.

Figure 1. System Settings and Preliminary Check for DJI Phantom 4.

The UAV system consist of camera with 1" CMOS sensor with 20M effective pixels, camera lens with FOV of 84° and focus at 1 m - ∞, 5472 x 3648 image size, shutter speed in ranging from 8-1/8000 s, 3-axis gimbal system (pitch, roll, yaw), a 5870 mAh Lipo 4S battery with approximately 30 minutes flight time, and GPS/GLONASS positioning system.
The procedure of data acquisition begin with preflight check of UAV system and preflight mission planning. After that, aerial photo data acquisition with UAV is conducted and results 198 photos taken from the total of 71.934 hectares of area covered. Data acquisition with this method did not required a ground control points due to the existence of airborne-GPS that has been installed in the UAV. The airborne GPS yield the position of exposure point and has been geotagged in each photo.

4. Data Processing

The method for generating quick orthomozaic used in this research is structure from motion (SFM). SFM is a recent technological development in the field of photogrammetry that can yield a 3D model data in low cost and user-friendly method. As of conventional photogrammetry, SFM also need overlapping images from different perspective. The main difference in conventional and SFM method is that in SFM method the internal and external orientation is fully calculated simultaneously with bundle adjusment.
The process of SFM begin with identification of image keypoints. Keypoint or point of interest are common feature points identified in each image, then followed by creation of feature descriptor for each point. As this descriptor are unique for it decribe spatial relationship between images location in abitrary 3D coordinate system. The next process is bundle adjustment, the process to transform identified points coordinate into the same local 3D coordinate system, results in sparse point cloud. This point clouds then used for input to generate dense point cloud by implementing Clustering View for Multi- view Stereo (CMVS) and Patch Based Multiview Stereo (PMVS2) algorithm. CMVS used to decomposes large number of images into subsets or cluster of manageable sizes, while PMVS2 used to construct enhanced density point cloud [2]. Next, this density enhanced point cloud processed for 3D surface (mesh) reconstruction or rendering. Then, the mesh transformed from 3D coordinate into 2D coordinate, resulting an orthophoto image. In this research, SFM process conducted in Agisoft Photoscan, a commercial SFM software. In the software, batch process is used to automatically generate orthomozaic images with respect to processing parameters workflow for the batch process are as the following.

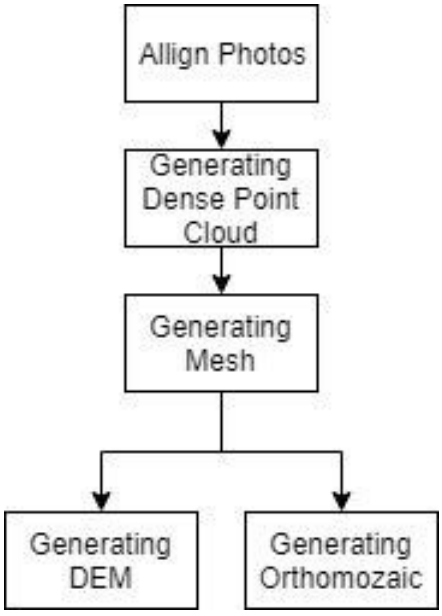

Figure 2. Orthomosaic and DEM Process Workflow.

5. Feature Extraction

A high-quality image product which has been delivered using UAV Photogrammetry acquisition and remote sensing process in order to make a map that has ground accuracy between 4 cm- 5 cm has enabled users to extract more information and more data which have correlation and usage in rapid mapping methods, OBIA which is known as the Object Oriented Image Analysis, according to [3], some features in photogrammetric and remote sensing software using this method to extract building information and analysis form of an object in imagery based on its pixels and clusters of its pixels.

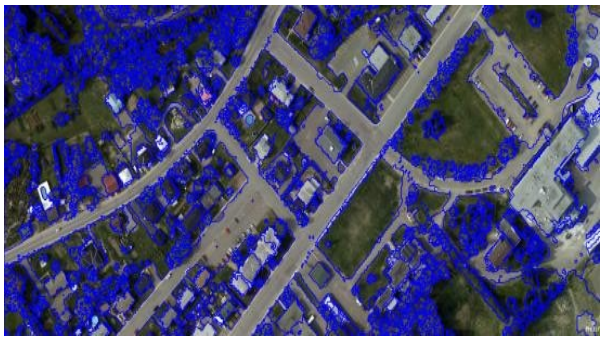

Figure 3. The OBIA Image Segmentation.

In order to make a feature extraction beside using the manual-software digitizing method, with many handicapped conditions, feature extraction has more benefits because it has a less time-consuming strategy which the map results have more accurate segmentation for building or vegetation rather than using a manual-digitizing method. On this figure, the OBIA (Feature Extraction) workflow could be determined.

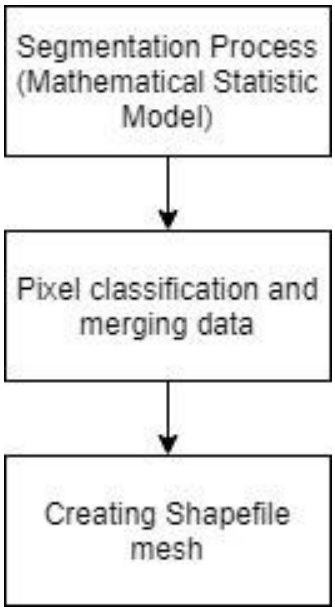

Figure 4. OBIA Image Segmentation Workflow.

The algorithm in OBIA process that been used to determine object features classification is using Edge Algorithm settings and intensity algorithm settings, the use of edge algorithm settings is more preferable because the intensity algorithm settings, classify each object using the edge pixels and the segmentation result in segmenting the edge of the objects. The process on these outputs are vector format or raster format in GIS which are useful to analyze the information about the impact or damage of the disastrous area.

6. Results and Discussion

The process of this research gained from the aerial acquisition using the DJI Phantom 4, results in geotagged images which been used for aligning image process, image matching process, and point cloud or creating mesh process in photogrammetry software such as Agisoft Photoscan. The location data for images geotagging are yields from airborne GPS data that results in errors as the following figure.

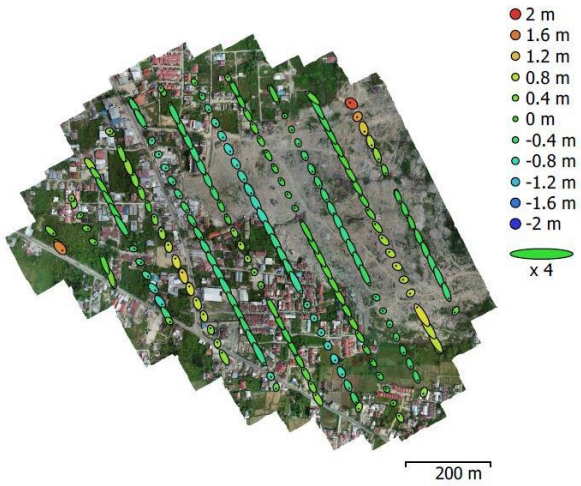

Figure 5. Camera Location Error.

The figure represents location error in error ellipse as vertical (Z) error represented in ellipse color and horizontal (X and Y) error represented in ellipse shape. Estimated camera locations are marked with a black dot. From the error estimation, the average camera location error as follow:

Table 1. Average Camera Location Error.

X (m)	Y (m)	Z/Vertical (m)	XY/Horizontal (m)	Total error (m)
2.777	5.097	0.502	5.805	5.827

The camera location error from the data acquisition are in the total of 5.827 m. This error is likely as the result of GPS-type that has been used. The GPS-type was used an airborne navigation type that only generate single point positioning or absolute positioning. Absolute positioning is expected to be less accurate, as the ionospheric delays which cause position error are not being estimated [4].
The orthomozaic process which was conducted with Agisoft Photoscan according to flow proccess as shown in figure 2 with processing parameters and processing time as follows,

Table 2. Agisoft Image Processing Parameter.

No	Process	Parameter	Elapsed Time
1	Allign Photos	Accuracy: Medium	38 minutes, 38 seconds
2	Build Dense Point Cloud	Quality: Medium	3 hours, 36 minutes, 10 seconds
3	Build Mesh	Surface type: Height Field Face Count: Low	7 Seconds
4	Build DEM	Interpolation: enabled	52 Seconds
5	Build Orthomozaic	Blending mode: Mosaic	Tentative (depends on hard drive)

The results on the process are DEM and Orthophoto in which the DEM shows the actual terrain model. Pair matching was done with medium parameters on matching each digital number between any photos, with result a point matching pair which found between the photos. Point dense cloud was made in order to interpolate the pair point of point cloud to make every detail on the terrain by using spatial interpolation methods.

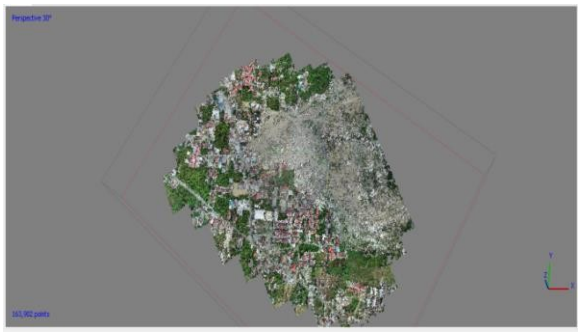

Figure 6. Point Cloud as a result from Image Matching Process.

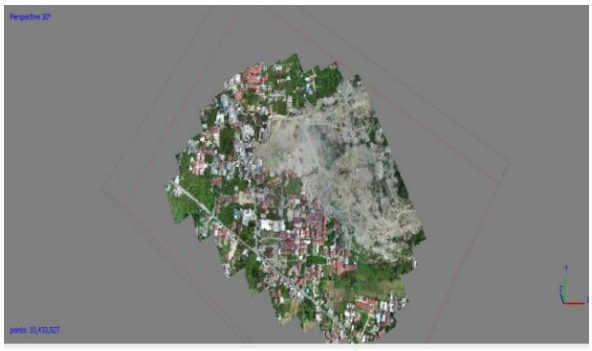

Figure 7. Point dense cloud as a result from Interpolating Process.

By using point cloud, DEM and orthophoto could be erected because on this process each photo which were aligned using the bundle block adjustment with SFM (Structure from Motion) with the results are DEM and Orthophoto, the specification of this orthophoto, it have 4.18 cm/pix GSD (Ground Sampling Distance) and 1:200 scale orthophoto.

Figure 8. Orthophoto which was generated by SFM method.

DEM was made by interpolated point on surface by using point dense cloud interpolation.

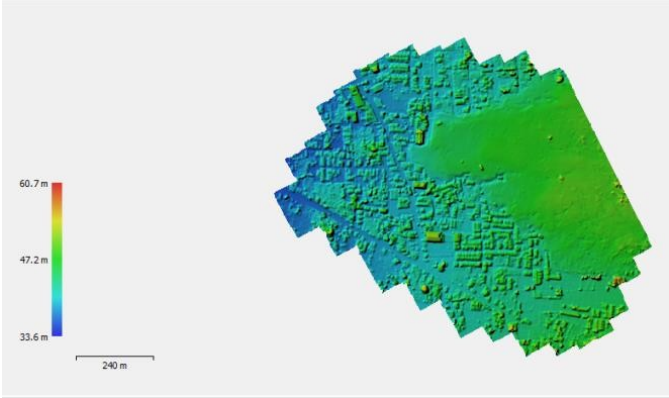

Figure 9. DEM which was generated from dense cloud.

The OBIA (Object-Based Image Analysis) process gave results such as segmented shapefile which gained from edge detection by its algorithm. OBIA (Object-Based Image Analysis) is being used because of its efficiency and fully-automated without any human-based segmentation which is time consuming rather than manual method, by using this method, rapid mapping could be run below one day processing time by using a high specification computer. The input data that were used in this process using the Geo-TIF format which was extracted using The SFM methods, in which the results were orthophoto and DEM (Digital Elevation Model), the feature extraction in OBIA was running in orthophoto processing, meanwhile, the contouring process was running in DEM processing.

Figure 10. Shapefile obtained from OBIA process.

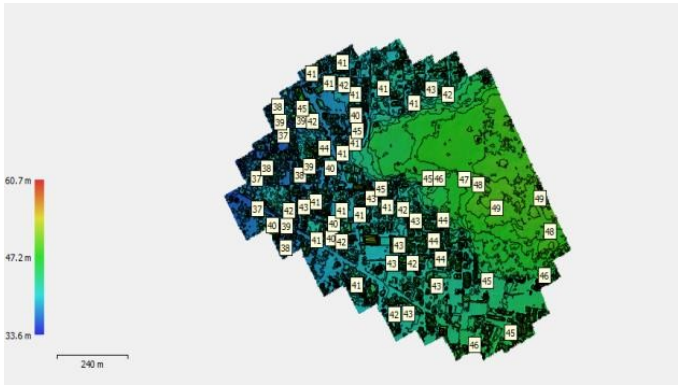

Figure 11. Contour Lines which was generated by using DEM interpolation.

7. Conclusions

The aim of rapid mapping is to produce spatial information data about disastrous or post disaster area within a day or hours. The process of rapid mapping consists of the data acquisition, data processing and data segmentation and analysis which results in base orthophoto and topograhic map for further mapping particularly thematic mapping purposes. The method is useful in disaster and planning management strategy in order to sustain disaster recovery. The parameter that have been used on this research including the medium-photo alignment as shown in table 2, low-photo dense cloud interpolation and low orthophoto process. OBIA was being used in object interpretation process in order to simplify the object identification process to assess the impact of the disaster in Palu, Petobo district.

8. References

[1] UNDP, *Disaster Recovery: Challenges and Lessons.* , in *United Nation Development Programme (UNDP)* N.Y.B.f.P.a.P. Support, Editor. 2016: New York.

[2] Furukawa, Y. and J. Ponce, *Accurate, dense, and robust multiview stereopsis.* IEEE transactions on pattern analysis and machine intelligence, 2009. **32**(8): p. 1362-1376.

[3] Jensen, J.R., *Introductory digital image processing: a remote sensing perspective*. 2015: Prentice Hall Press.

[4] Leick, A., L. Rapoport, and D. Tatarnikov, *GPS satellite surveying*. 2015: John Wiley & Sons.

Change Detection of Mangrove Forest using Soil Adjusted Vegetation Indices Based on multitemporal Images Case Study: East Coast of Lampung Province

N Simarmata[1]*, T A Tarigan[2], T K Ermanto[3]

[1]Geomathic Department of Engineering, Institute of Technology, Sumatra, Indonesia
[2] Department of Ocean Engineering, Institute of Technology, Sumatra, Indonesia
[3]Ryacudu Canal Road, Way yam, Jati Agung, South Lampung, Indonesia

*Corresponding author's e-mail: nirmawana.simarmata@gt.itera.ac.id

Abstract. The characteristic East Coast of Lampung Province is dominated by coastal areas that are muddy and sandy, it is very suitable for mangrove ecosystem. In the fact, mangrove damage in this area is quite severe starting from Bakauheni to Ketapang Lampung. Most of the mangrove damage occurs due to land conversion functions as shrimp farms that are cultivated by the private sector and the community. The impact of damage the mangrove ecosystem is abrasion because there is nothing to hold the waves. The purpose of this study to identify the type and density of mangrove and to detect changes in mangrove cover in a multitemporal manner. Change detection is done by using multitemporal data because it can provide information the land cover that is quite accurate. The data used are SPOT4 and SPOT6/7 recording in 2008 and 2016. The method used to calculate the density of mangroves are the vegetation index MSAVI and SAVI while to detect changes using image classification. This classification uses a maximum likelihood algorithm to distinguish between mangrove and non-mangrove. Based on the results of the analysis using SAVI, the index values were 0.6-0.9 while MSAVI was 0.3-0.6. The results obtained in the mangrove in 2008 it was 272ha, whereas in 2016 it was 586.8ha. Identification of the type of mangrove from the field survey was found by Avicennia Marina. The results of the land cover accuracy test using matrix confusion, land cover classification of 89%. Mangrove areas from 2008 to 2016 increased mangrove forests.

Keywords: Mangrove, SPOT; SAVI; MSAVI; supervised Classification.

1. Introduction

The potential of Indonesian mangrove forest is big enough where Indonesia has extensive mangrove forest in the world. Indonesian mangrove ecosystem be able to absorb carbon in the air as much as 67.7 MtCO2 per year [1]. Per hectare of mangrove forest can store up to four times more carbon than any other tropical forests around the world. One of them in South Lampung regency is an area with a relatively wide cover in Lampung Province. However, the condition of mangrove forests in South Lampung has been a lot of damage. According to WALHI (2010), describes the area has been a decline of mangrove forests. Indonesian mangrove forest area decreased from the initial area of about 4.5 million ha to 1.9 million ha. The decline in mangrove forest area occurs most dominant because of the damage caused by human factors. The utilization of remote sensing data on to provide information on the reduction or the increase of mangrove forest cover. In addition, it can also facilitate building a database in order to manage the mangrove forest as a capital resource and development [2]. Basically, the area calculation to inventory, monitor and manage the mangrove forests can be done with the field measurements using sample plots that tree diameter at breast height (DBH) [3]. The disadvantages of using terrestrial measurements considered less effective because it requires a relatively large time and costs so that the development on the use of remote sensing technology is growing. One of the satellite imagery used to calculate the mangrove forest area that is the image of SPOT-7 with a resolution of 6 meters. The sensor is equipped with red and infrared wavelengths close to that have a high sensitivity

to the object level vegetation. This led to the use of the image of SPOT-7 is good enough to classify mangrove forests in South Lampung Province.

2. Methodology

2.1. Location

The research location is in the mangrove forest area of South Lampung Regency, located in the southern coastal region. Geographically, mangrove forests are in a position between 05°48'48" S until 06°02'20" S and 105°45'06" E until 105°47'0" E. This study uses data Imagery SPOT-7 2016 Lampung Province sourced from National Institute of Aeronautics and Space, Map RBI Indonesia and the survey results.

Figure 1. Location of Research.

2.2. Data

The data used in the analysis of changes in land cover of mangrove forests in the East Coast of South Lampung regency include primary data, secondary and field survey. The research data presented in Table 1.

Table 1. The research data and its uses.

Data Types	Acquisition Date (year)	Data source	Usefulness
SPOT 4 image resolution to 10 meters	2008	LAPAN (National Institute of Aeronautics and Space)	Soil Adjusted Vegetation Indices and Classification of Mangrove Forests
SPOT image 6 6 meters resolution	2016	LAPAN (National Institute of Aeronautics and Space)	Soil Adjusted Vegetation Indices and Classification of Mangrove Forests
Indonesia RBI maps Scale 1: 25,000	2017	BIG (Geospatial Information Agency)	Administrative boundary and Geometric Correction
Sample Data Validation	2018	Field survey	Field verification test

2.3 Methods

Phase of the study was to calculate changes in mangrove forest cover in the East Coast of South Lampung regency. Stages were divided into stages of data collection, pre-processing of data, data processing, test accuracy and analysis of mangrove forest cover change. The data collected are 4 SPOT image recording resolution of 10 meters in 2008, 6 SPOT image recording resolution of 6 meters in 2016 and RBI Indonesia map scale of 1: 25,000. More specifically, the stages of the study are presented in Figure 2.

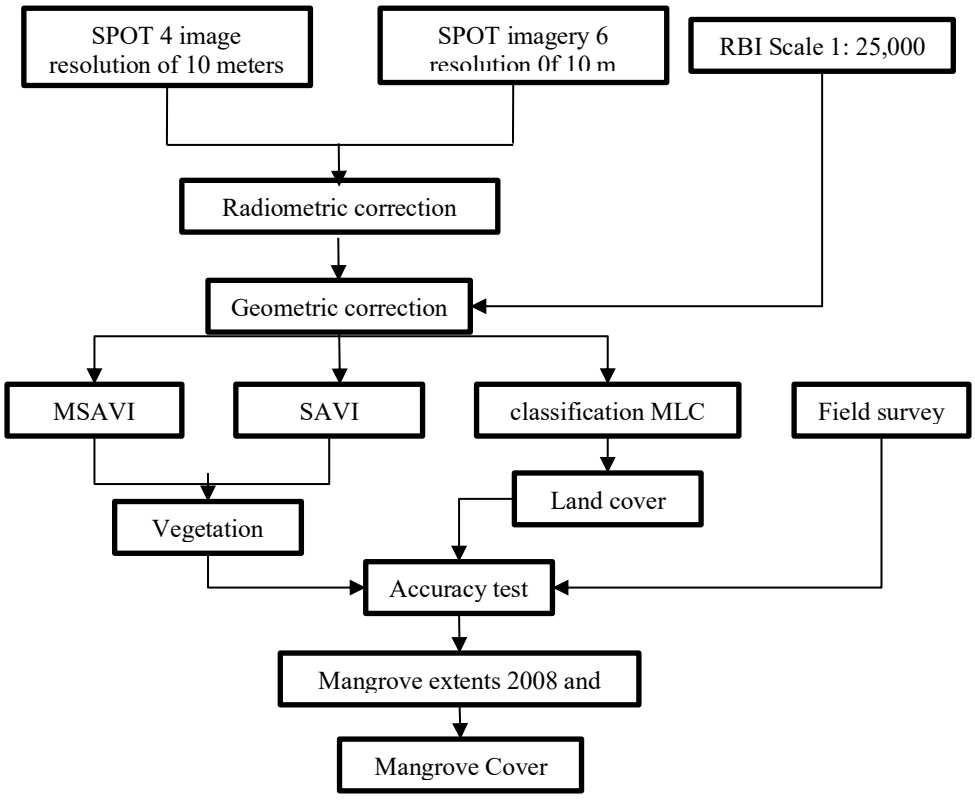

Figure 2. Stages Research.

Pre-processing of data carried out through radiometric and geometric correction for SPOT imagery of 2008 and 2018. The corrected image transformation results using the vegetation index Soil Adjusted Vegetation Indices (SAVI) and Modified Soil Adjusted Vegetation Indices (MSAVI). The formula of transformation SAVI:

$$SAVI: \frac{(IMD-M)}{(IMD+M)} \times (1+0.5) \quad (1)$$

where IMD is the Near Infrared band and M is a red band. As for the transformation MSAVI:

$$MSAVI: \frac{(NIR-RED)}{(NIR+RED+L)*(1+L)} \quad (2)$$

Before you enter the formula, find the value of L first by:

$$L = \frac{2\times S\times(NIR-RED)\times(NIR-S\times RED)}{(NIR+RED)} \ (S = 0.5). \quad (3)$$

On the other hand, to compare the results of the transformation of the forest classification mangrove based on digital classification, this study applied supervised classification with maximum likelihood classification algorithm [4]. Before processing supervised classification done taking the training area with several classes such as: high density vegetation, the vegetation medium density, low density vegetation, ponds, seas, and mangrove. Each training area have 70-100 boundary pixels.
Further to the field survey, the sample points are based on the value of the vegetation index, especially for mangrove forests obtained from the supervised classification method. Then, the result overlaid with closing index value of land in the area of South Lampung Regency East coast.

3. Results and Discussion

Based on the results of geometric correction performed on the SPOT 4 and SPOT imagery 6 obtained respectively RMSE values below 0.5 means that in this case still makes errors in correction fault tolerance. Results corrected image can be used as a basis for further processing that is SAVI and MSAVI and supervised classification.
Results of transformation using the SAVI method and MSAVI performed on both the image of the index values obtained for the image 2008 has a range of values between 0.3 to 0.8. more details MSAVI difference between SAVI and can be seen in Figures 3 and 4. Based on the results of the transformation, there are anomalies on its results because it should lower the value for water with a dark color. But in these results indicate that the body of water has a brighter hue.

Figure 3. SAVI Year 2008 Results.

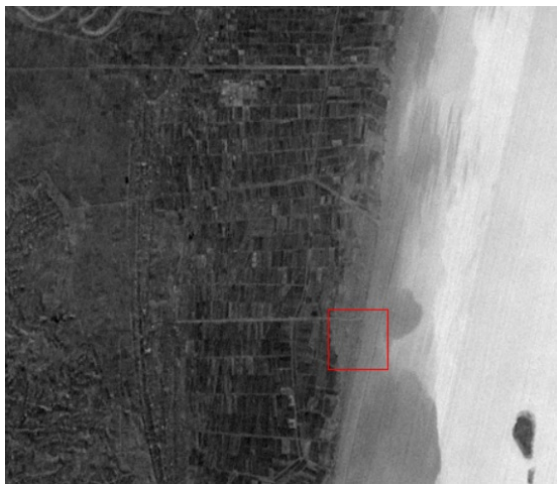

Figure 4. MSAVI Year 2008 Results.

The result SPOT image transformation 6 2016 using SAVI and MSAVI have a fairly significant difference is -1 - 1 while for MSAVI have a value range -0.5 - 0.7. Both these transformation results showed that mangrove forests have bright hue, while the body of water has a very dark hue.

Figure 5. Results SAVI 2016.

Figure 6. Results MSAVI 2016.

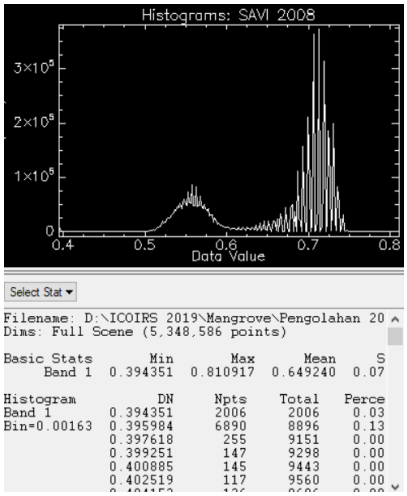

Figure 7. SAVI histogram 2008.

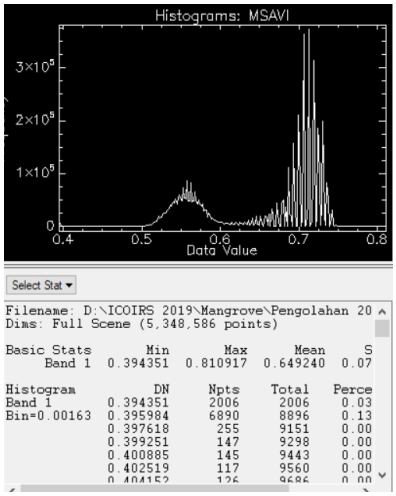

Figure 8. Histogram MSAVI 2008.

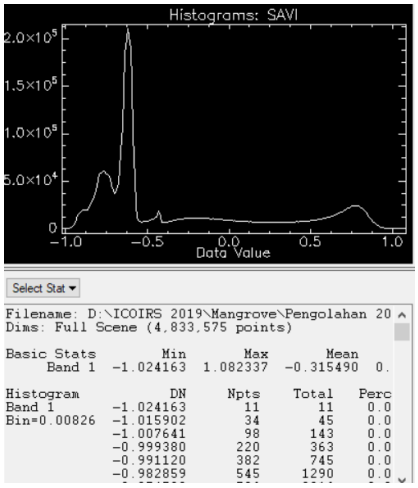

Figure 9. SAVI histogram 2016.

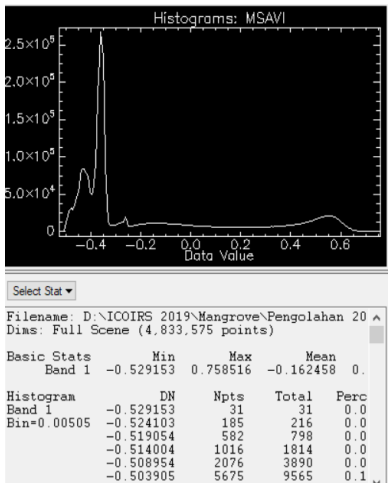

Figure 10. Histogram MSAVI 201.

Land cover classification results show the distribution of mangrove forests in the East Coast Region of South Lampung regency. Based on the results of field surveys showed calcification and mangrove forest area in 2008 covering an area of 272 ha, while in 2016 the range 586.8 ha. More details of mangrove distribution in Region East Coast South Lampung regency served on the image.

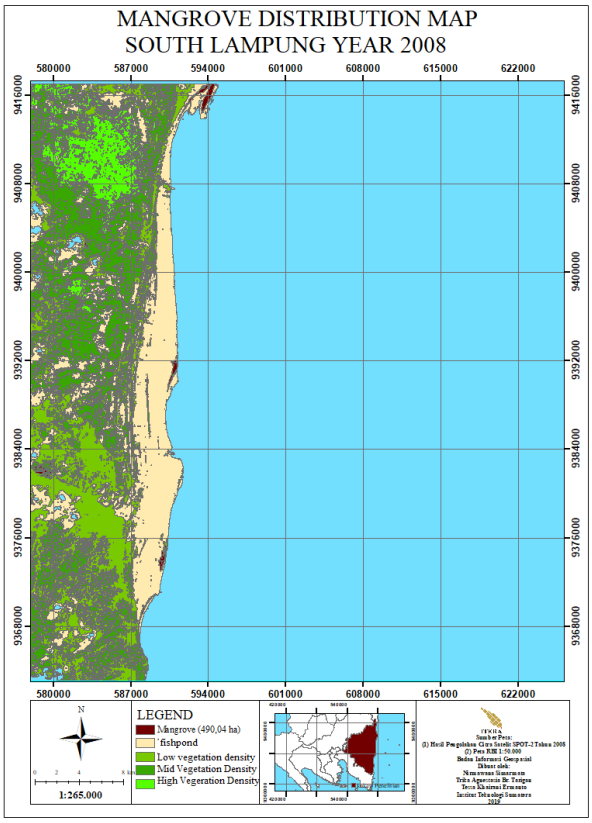

Figure 11. Distribution of Mangrove 2008.

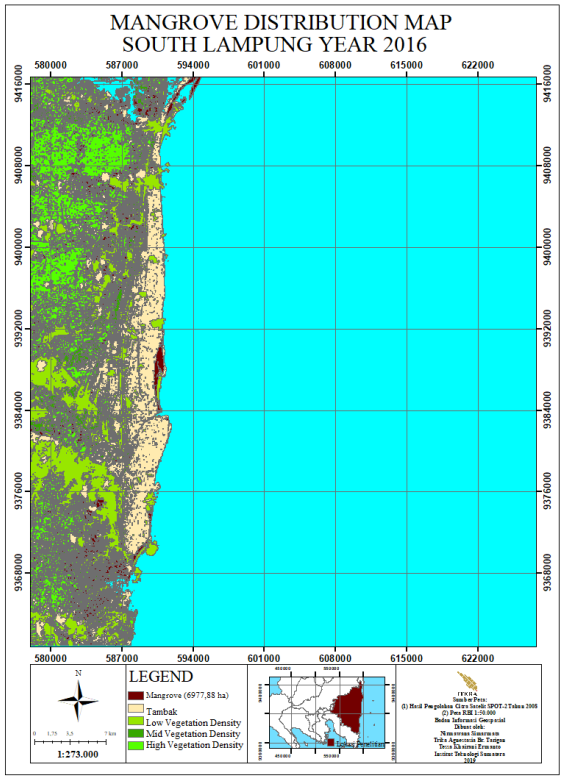

Figure 12. Distribution of Mangrove 2016.

Based on the results, mangrove forest there is an increase in Region East Coast South Lampung regency is 314.8 ha. Based on the results of field surveys and interviews with residents located area of mangrove forests that have been carried out rehabilitation of mangroves. The test results on the accuracy of the map cover / land use using the confusion matrix obtained 89.5% accuracy.

4. Conclusions

Based on the results of image data processing SPOT 4 and SPOT 6 in the East coast of South Lampung regency using SAVI transformation and MSAVI that mangrove forests have an index valueSAVI the value range 0.3-0.6 0.6-0.9 while MSAVI. conservatively measured in2008 measuring 272 Ha, whereas in 2016 about 586.8 ha with an increase in area 314.8 ha. The test results obtained land cover map accuracy 89.5% value.

5. References

[1] Sadelie, A., et al., *Kebijakan pengelolaan sumberdaya pesisir berbasis perdagangan karbon*. Jurnal Hutan dan Masyarakat, 2012. **6**(1): p. 1-11.

[2] Faturrohmah and Marjuki, *Identification of Spatial Dynamics Coastal Mangrove Resources Demak district in Central Java*. Indonesia Geographic magazine, 2017. **31**: p. 36-40.

[3] Kauffman, J.B. and D.C. Donato, *Protocols for the measurement, monitoring and reporting of structure, biomass, and carbon stocks in mangrove forests*. 2012: Citeseer.

[4] Danoedoro, P., *Land-Use Information from the Satellite Imagery: Versatility and Physical Planning* ed. S.L.A. Publishing. 2009.

Acknowledgments
This research was supported by the Directorate General of Higher Education of Indonesia (Higher Education) through the Scheme of the Fund of Beginner Lecturer in 2018.

The Application of a Method Normalized Difference Vegetation Index (NDVI), Normalized Difference Moisture Index (NDMI) and Parameter Physical to Zoning Prone Landslide in Bandar Lampung City

Tamara[1]*, Bambang Edhi Leksono[2], Nirmawana Simarmata[1]

[1]Geomatic Engineering, Sumatera Institute of Technology, Terusan Ryacudu Street, Way Hui, Jati Agung, 35365 South Lampung, Indonesia
[2]Department of Geodesy and Geomatic Engineering, Bandung Institute of Technology, 10 Ganesha Street, 40132 Bandung, Indonesia

*Corresponding author's e-mail: tamaraalwimadina@gmail.com

Abstract. High rainfall intensity caused landslides in several areas of Bandar Lampung City. In general, identification of landslide vulnerability can be known by scoring and weighting methods in spatial analysis using several parameters that cause landslides such as, slope, rainfall, land use, and soil types. The application of the Normalized Difference Vegetation Index (NDVI) and Normalized Difference Moisture Index (NDMI) is used to support the physical parameters of landslide-prone zoning. Based on the classification of NDVI and NDMI values, Bandar Lampung City has a low vegetation density of 37.424% and dry soil conditions of 83.889% of the total area of Bandar Lampung. Land use parameters carried out by the Maximum Likelihood Classification (MLC) method produce an overall accuracy of 91.4%. Landslide Prone Zoning Map consists of three classes, namely low, medium and high. The dominant level of landslide vulnerability is moderate with an area of 11337.2 Ha or 61.880% of the total area of research.The level of landslide vulnerability of low and high class has a percentage of 31.607% and 6.512%, respectively. The results of a spatial analysis on all parameters showed an accuracy of the map 87.5%. High landslide vulnerability is dominated in Sukabumi, Kemiling, and Tanjung Karang Barat Districts. Factors affecting landslides are natural factors such as high rainfall on steep slopes and open land, while human factors indicate the potential for landslides in the rock mining area.

Keywords: Landslides, Sentinel-2, NDVI, NDMI, MLC.

1. Introduction

The landslide occurred on June 26, 2018, in Central Tanjungkarang, Bandar Lampung. The disaster caused six people, five of whom were small children crushed by building rubble. Heavy rains on February 24, 2019, caused landslides at eight points in Kelurahan Pidada, Panjang, Bandar Lampung. The landslide originated from the top of the hill in the settlement. Local people managed to escape, but landslides destroyed two houses. Identification of the existence of landslide-prone areas is needed as a first step to mitigating landslides and is a consideration in the process of spatial planning. In general, landslide-prone areas can be identified by conducting spatial analysis using several parameters that cause landslides such as slope, rainfall, land use, and soil type. In addition to these parameters the presence of vegetation density and humidity affects the stability of the slope, so these parameters are used to support the analysis of landslide-prone areas in Bandar Lampung City.

The use of remote sensing imagery can help identify, interpret, and present the information needed for various phenomena that occur on the surface of the earth without having to make direct contact with terrain or research areas, compared if terrestrial studies have to be done which requires time and cost and energy very big. The application of remote sensing technology can produce parameters of vegetation density, soil moisture, land use, and slope. The identification of vegetation density can be done through the Normalized Difference Vegetation Index (NDVI) method. Absorption of the red band by chlorophyll and the reflection of the near-infrared (NIR) band by the mesophyll tissue on the leaves will make the

brightness values received by the satellite sensor through the band much different. The red band and NIR will produce leaf chlorophyll concentration levels that correlate with the vegetation density based on the spectral value of each pixel. Soil moisture information can be known based on the NIR band and shortwave infrared (SWIR) on the Normalized Difference Moisture Index (NDMI) method. The use of NIR bands can limit the body of water and soil moisture, while the shortwave infrared (SWIR) band can show the composition of plant moisture and soil moisture. The identification parameters of the landslide-prone zoning are integrated with the scoring and weighting method in the spatial analysis of Geographic Information Systems (GIS). GIS as a science and technology can carry out accurate processing in large numbers so that it can obtain new information in identifying areas prone to landslides.

2. Method

2.1. Research Sites

This research was conducted in the city of Bandar Lampung, Lampung. The city of Bandar Lampung is geographically located at 551705 - 568307 M East and 9410469 - 9392030 North M. Bandar Lampung City has an area of 197.22 km2 which is divided into 20 Districts.

2.2. Data

The data used are:

- Sentinel - 2 Resolution 10 m, Date of acquisition 6 August 2018;
- Digital Elevation Model Nasional (DEMNAS) 2018;
- Rainfall data throughout 2018 from BMKG Panjang, BMKG Branti and UPT MKG ITERA;
- Soil Type Map (Scale 1: 25000) from Balai Penelitian Tanah;
- RBI map Bandar Lampung City (Scale 1: 25000) 2018.

2.3. Data processing

This study will use several parameters such as slope, rainfall, land use classification, soil type, vegetation density, and soil moisture. These parameters are generated from several stages of data processing, spatial analysis, field validation tests to achieve the final results in the form of landslide-prone zoning maps. Flowchart of research methodology can be seen in Figure 1.

2.3.1. Digital Image Processing. Sentinel-2 processing begins with pre-processing, namely geometric and radiometric correction. The corrected image was extracted into three parameters, namely land use, vegetation density, and soil moisture. The following stages of digital image processing are carried out in this study:

- Atmospheric Correction
  Atmospheric correction is a process used to eliminate atmospheric influences, namely molecules (rayleigh scattering) and particles (aerosol scattering) recorded by the sensor. Atmospheric correction is done on the SNAP software with Sen2cor tools. This correction is done automatically by inserting Sentinel level 1C images.
- Geometric Correction
  Geometric corrections is a process to correct the position errors of objects recorded on the image caused by geometric distortion. Geometric correction in this study uses the corrected image performed on the ENVI 5.1 software. This process compares pairs of control points that can be easily identified in both images, based on the control points paying attention to the difference along the X-axis and Y-axis. The difference is calculated by the accuracy of the geometry correction results with the formula root mean square error (RMSE).
- Land Use Classification
  The land use classification is produced from corrected Sentinel-2 processing. Classification is done by supervised classification which is guided and controlled mostly or completely by the user in the classification process. The initial stages are carried out with visual interpretation to

determine the training area which is then classified with the maximum likelihood method. The classification technique is carried out using the pixel likelihood method (maximum likelihood), which is the estimation method that maximizes the pixel likelihood function (likelihood). The Bandar Lampung City land use classification that will be used are Forests, Settlements, Industrial Buildings, Estates, Shrubs, Agriculture and Open Land.

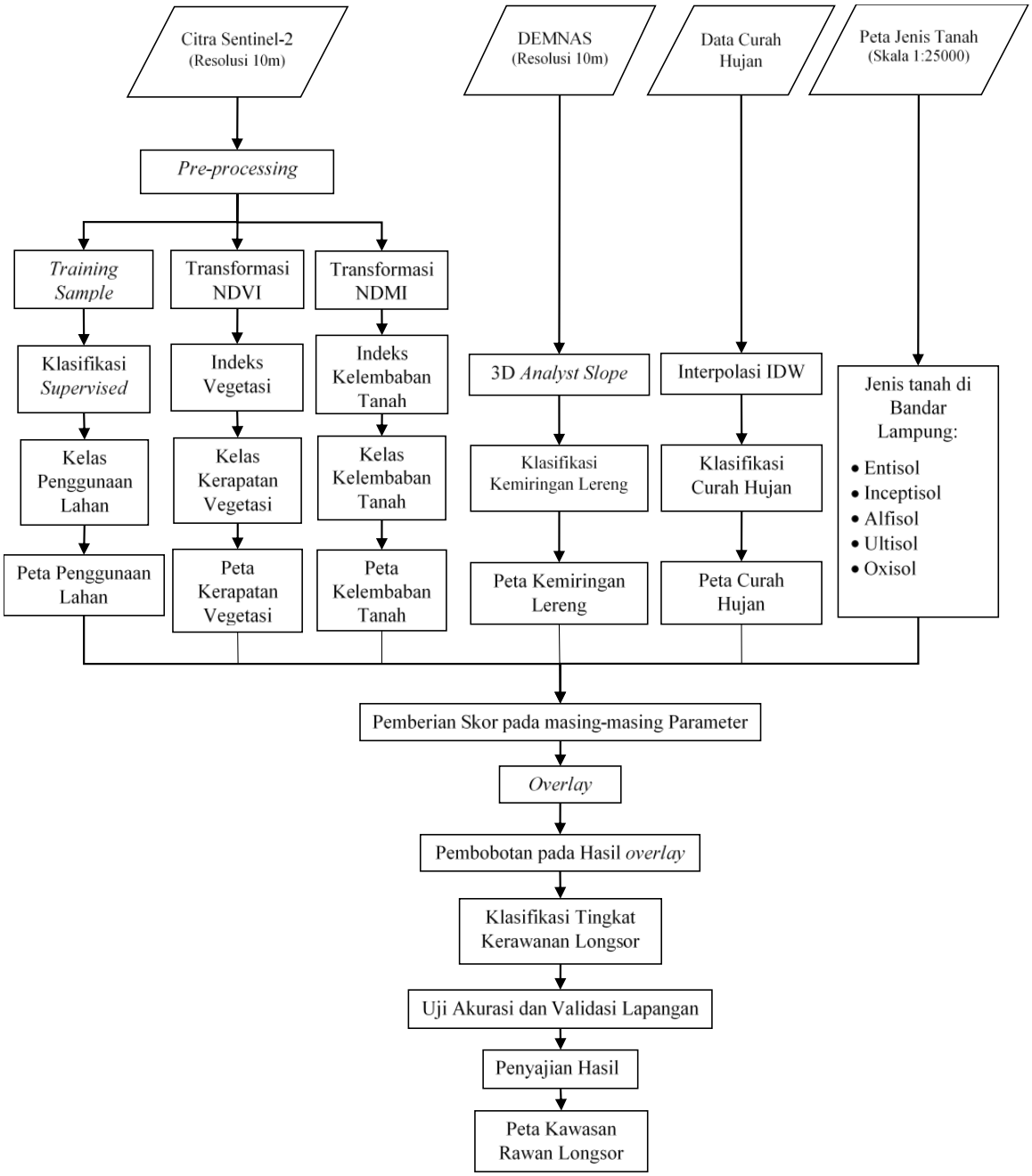

Figure 1. Research Flowchart.

- Normalized Difference Vegetation Index (NDVI)
  NDVI is a value of processing vegetation index from satellite images of the red band and the band near-infrared (NIR). Absorption of the red band by chlorophyll and the reflection of the

near-infrared (λNIR) band by the mesophyll tissue on the leaves will make the brightness values received by the satellite sensor through the band much different. The red band and NIR will produce leaf chlorophyll concentration levels that correlate with the vegetation density based on the spectral value of each pixel. NDVI is formulated in the equation 1:

$$NDVI = \frac{\lambda NIR - \lambda Red}{\lambda NIR + \lambda Red} \quad (1)$$

Vegetation density parameters produced from NDVI transformations on Sentinel-2 images that have been corrected radiometrically or geometrically. Automatically process NDVI on SNAP software. The NDVI transformation pixel values are -1 to 1, where the vegetation class is in the range of 0 to 1 and the non-vegetation class is in the range of -1 to 0.

- Normalized Difference Moisture Index (NDMI)
  NDMI is an index used to detect the humidity of a land surface. NDMI has a median value of spectral obtained from near-infrared (NIR) and shortwave infrared (SWIR) electromagnetic waves. Wavelengths of 0.76-0.90 can distinguish the type of vegetation detected and also the vegetation activity so that it can limit the body of water and soil moisture. Wavelength 1.55-1.75, useful for showing the composition of plant moisture and soil moisture, can also distinguish snow and clouds. NDMI is formulated in the equation 2:

$$NDMI = \frac{\lambda\text{NIR} - \lambda\text{SWIR}}{\lambda\text{NIR} + \lambda\text{SWIR}} \quad (2)$$

  NDMI values range from -1 to +1. A low NDMI value indicates a low humidity level and vice versa a high NDMI value indicates a high humidity level.

2.3.2. Slope. Slope map is generated from DEM data using 3D Analyst tools in ArcGIS software. The DEM is a raster format consisting of pixels so it must take into account the value of surrounding pixels from all directions to determine of the slope.

2.3.3. Rainfall Interpolation. The spatial interpolation method used is IDW (Inverse Distance Weighted). The IDW method is a conventional interpolation method that takes into account distances as weights. The distance in question is the distance (flat) from the data point (sample) to the block to be estimated so that, the closer the distance between the sample point and the block to be estimated the greater the weight, and vice versa .

2.3.4. Spatial Analysis. Spatial analysis in determining landslide-prone zones using the scoring method and weighting on predetermined parameters. Each parameter is divided into several classes that are scored according to the size of the effect on landslides and overlapped with each other to produce new data in the form of the sum of the scores. All parameters that have been overlayed are then categorized by each land unit at the vulnerability level. The level of landslide vulnerability illustrates the tendency of natural slopes for landslides to occur. Mathematical equations by combining scoring and weighting are shown in the equation 3:

$$\text{X} = \sum_{i=1}^{n} (\text{W}_i \text{ x } \text{X}_\text{i}) \quad (3)$$

Explanation:

- X = Vulnerability value
- Wi = Weight for i-th parameter
- Xi = Class score for i-th parameter

Table of values for weighting can be seen in table 1. Based on the Technical Guidelines for the Preparation of Disaster Maps for the District / City Level in 2015, each type of disaster is divided into three classes of potential disasters namely Low, Medium and High. Determination of the interval width of each class is done by dividing as many values obtained by the number of class intervals determined by equation 4:

$$I = \frac{R}{N} \quad (4)$$

Explanation:

- I = class interval
- R = Difference in maximum value and minimum value
- N = Number of classes

Based on equation 4. then the class interval is prone to landslides of 1.3 and is presented in table 2.

Table 1. Scoring and weighting.

Parameter	Class	Score	Weight
Slope	0 – 8	1	30%
	8 – 15	2	
	15 – 25	3	
	25 – 45	4	
	>45	5	
Rainfall	<1500	1	20%
	1500 – 2000	2	
	2000 – 2500	3	
	2500 – 3000	4	
	>3000	5	
Land Use	Forests	1	15%
	Settlements	2	
	Industrial Buildings	2	
	Estates	3	
	Shrubs	3	
	Agriculture	4	
	Open Land	5	
Vegetation Density	*Entisols*	1	15%
	Inceptisols	2	
	Alfisols	3	
	Ultisols	4	
	Oxisols	5	
Kerapatan Vegetasi	0.78 – 1	1	10%
	0.55 – 0.78	2	
	0.25 – 0.55	3	
	0 – 0.25	4	
	-1 – 0	5	
Kelembaban Tanah	-1 – 0	1	10%
	0 – 0.25	2	
	0.25 – 0.50	3	
	0.51 – 0.75	4	
	≥ 0.76	5	

Table 2. The class of landslide.

Class	Interval score	Landslide Vulnerability
I	1.000 – 2.300	Low
II	2.301 – 3.600	Medium
III	3.601 – 5.00	High

3. Results and Discussion

3.1. Land Use Classification

The initial stages are carried out with visual interpretation to determine the training area which is then classified with the maximum likelihood method. Based on the training results in each class area, analysis of separability was carried out. The separability value provides information about the separation of the training area of each class. The lowest separability value is found between agriculture and plantation classes at 1.94386449 with a good level of separability. The accuracy test process aims to obtain information on the accuracy of the results of the land use classification. The calculation of the accuracy test in this study uses an error matrix or confusion matrix. The sample selection method for accuracy testing uses proportional stratified random sampling using 70 samples, confusion matrix tables are presented in Table 3.

Table 3. Confussion Matrix.

Image Classification Data	Reference Data							
	Forests	Estates	Agriculture	Shrubs	Settlements	Industrial Buildings	Open Land	Total
Forests	7	3	0	0	0	0	0	10
Estates	0	10	0	0	0	0	0	10
Agriculture	0	2	7	1	0	0	0	10
Shrubs	0	0	0	10	0	0	0	10
Settlements	0	0	0	0	10	0	0	10
Industrial Buildings	0	0	0	0	0	10	0	10
Open Land	0	0	0	0	0	0	10	10
Total	7	15	7	11	10	10	10	70
Producer Accuracy (%)	100	66.667	100	90.909	100	100	100	
User Accuracy (%)	70	100	70	100	100	100	100	
Overall Accuracy (%)				91.429				

The calculation of confusion matrix in Table 3 shows the overall accuracy result is 91.4% so that the accuracy allowed in the LAPAN land cover classification guidelines is above 75%. The results of land use classification are shown in Figure 2.

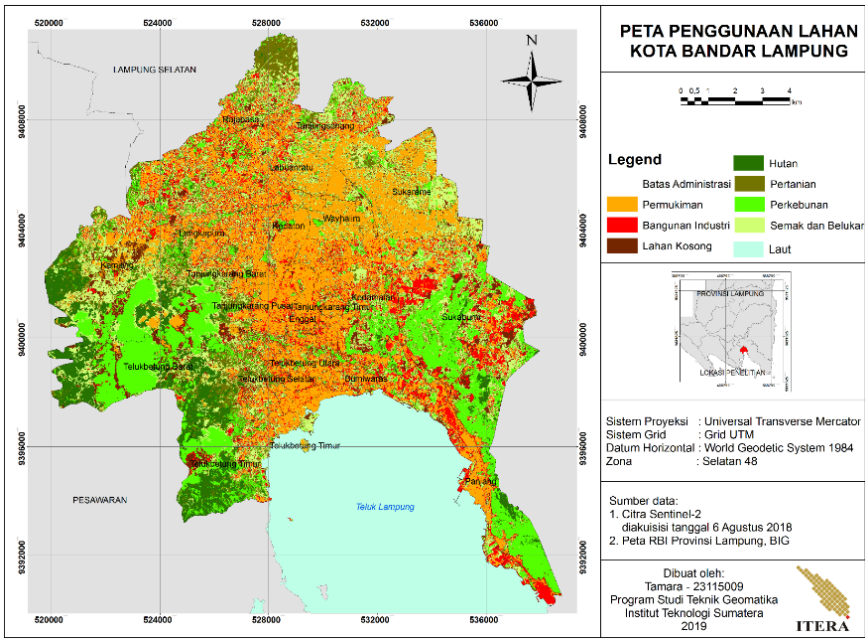

Figure 2. Map of Land Use Classification.

3.2. Normalized Difference Vegetation Index (NDVI)

The transformation of NDVI values is done on Sentinel-2 images that have been radiometrically and geometrically corrected. The results of the NDVI transformation are shown in Figure 3.

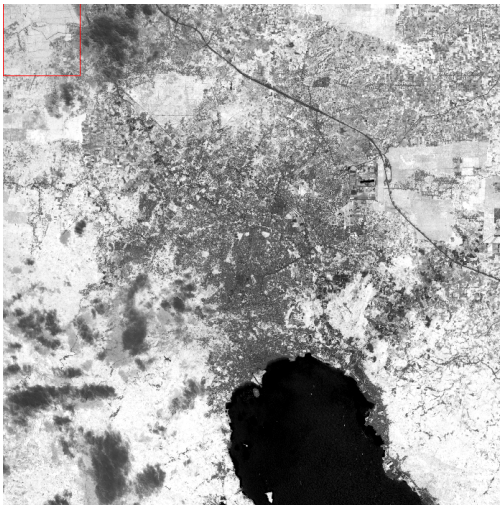

Figure 3. NDVI transformation.

Based on the results of the NDVI transformation, the lowest vegetation index value is -0.550 and the highest is 0.840 as shown in Figure 4.

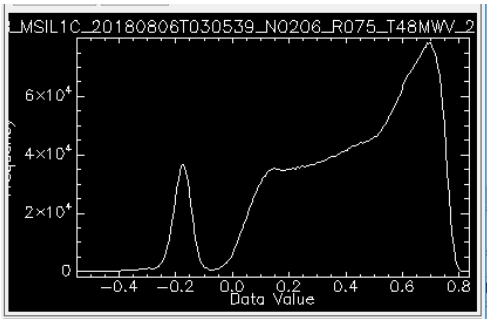

Figure 4. NDVI Histogram.

The results of the NDVI transformation are classified into vegetation index values into five levels: non-vegetation, low, medium, high and very high. The area based on the level is presented in table 4.

Table 4. NDVI.

NDVI	Area (Ha)	Area (%)
Non vegetasi	166.4071	0.907801
Low	6860.251	37.42475
Medium	6719.679	36.65789
High	4559.555	24.87376
Very High	24.8939	0.135804

Bandar Lampung City is dominated by low vegetation density with a percentage of 37.424% of the area of the study site. Low vegetation density is spread throughout the Bandar Lampung City District. As shown in table 4, the most extensive low vegetation density was in Sukabumi District with a percentage of 11.047%. Very high vegetation density occupies the lowest percentage with a value of 0.135% of the area of the study site. The low density of vegetation in an area with a steep slope will affect the stability of the slope because it is not able to withstand the load and soil conditions will be easily saturated if

there is a water flow that has the potential for landslides. Map of Bandar Lampung city vegetation density is presented in Figure 5.

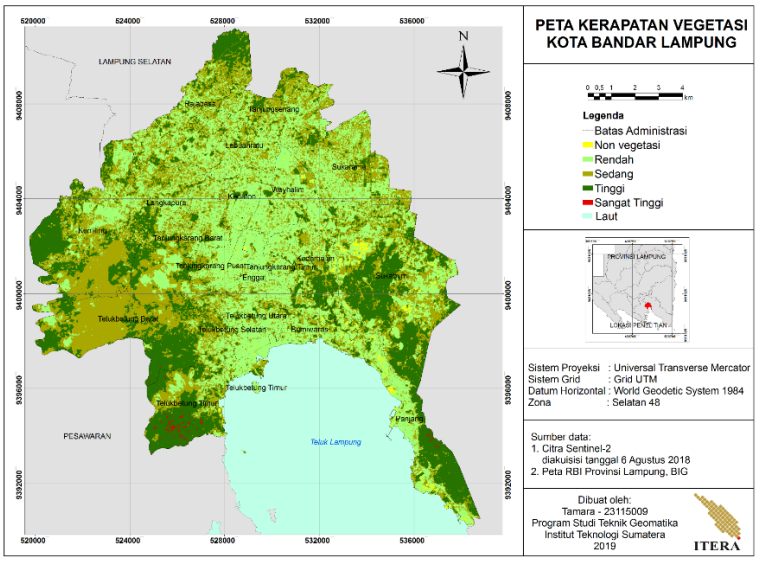

Figure 5. Map of Vegetation Density.

3.3. Normalized Difference Moisture Index (NDMI)

NDMI value extraction was performed on Sentinel-2 images that have been radiometrically and geometrically corrected. The results of the NDMI transformation are shown in Figure 6.

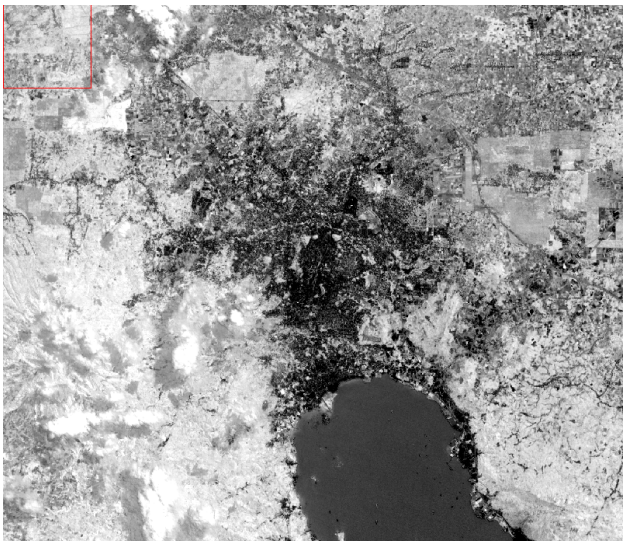

Figure 6. NDMI transformation.

Based on the results of the NDMI transformation, the lowest index value is -3,183 and the highest is 1,323 as shown in Figure 6. Figure 6, shows the NDMI value which is quite high in the range of values -1-0. The area based on soil moisture is shown in table 5. The results of data processing in the city of Bandar Lampung show that the research area is a dry area with a percentage of 83.889% of the area of the study site. A map of soil moisture in Bandar Lampung city is presented in Figure 7.

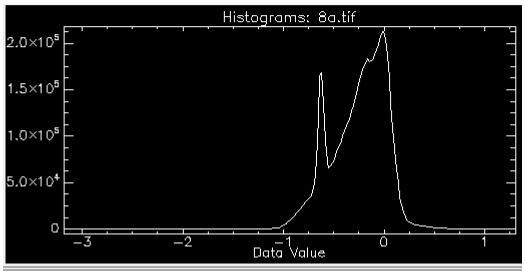

Figure 6. NDMI Histogram.

Table 5. NDMI.

Soil Moisture	Area (Ha)	Area (%)
Dry	15378.51076	83.89461083
Low	2652.918711	14.47250558
Medium	223.871321	1.221288436
High	44.153168	0.240869412
Very High	31.295306	0.170725733

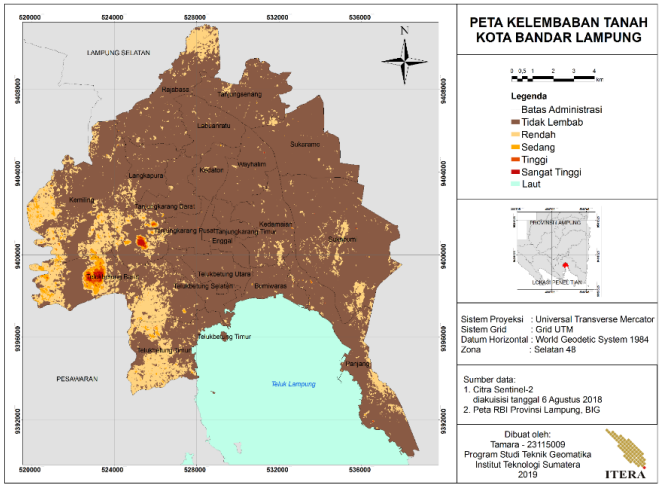

Figure 7. Map of Soil Moisture.

3.4. Slope

Slope is the factor that most influences the occurrence of landslides in an area. The slope parameters are produced from the National Digital Elevation Model (DEM) data processing built from several radar data sources. The area based on the slope is shown in table 6.

Table 6. Slope.

Slope	Area (Ha)	Area (%)
0 - 8%	10634.100	57.996
8 - 15%	2140.280	11.672
15 - 25%	1918.020	10.460
25 - 45%	3127.640	17.057
>45%	515.856	2.813

Based on the results of data processing the city of Bandar Lampung has a varied slope. This is because the topography of Bandar Lampung city covers the lowlands to the hills. The slope with a value of 0 - 8% has the largest area of 10634.100 Ha or 57.996% of the study site. Generally, steep slopes or which have a high percentage of the slope can cause landslides [1]. Based on the results of slope data processing the very steep slope category only has an area of 515.856 Ha or 2.813% of the research location. The

slope of the steep and very steep categories is spread across the districts of Panjang, Sukabumi, Kedamaian, Telukbetung Timur, Telukbetung Barat and Kemiling which are hills. A map of the slopes of Bandar Lampung city is presented in Figure 8.

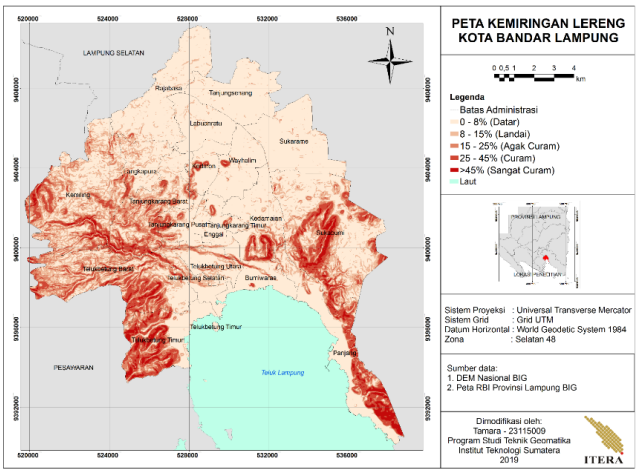

Figure 8. Map of Slope.

3.5. Rainfall Interpolation

Interpolation can be done if it has at least two data, so rainfall interpolation uses data from BMKG Branti, BMKG Panjang, and UPT MKG ITERA. Based on the classification of the Puslittanak rainfall class, the study location has four rainfall classes as shown in table 7.

Table 7. Rainfall.

Rainfall (mm/year)	Area (Ha)	Area (%)
1500 - 2000	2062.309	11.274
2000 - 2500	4075.356	22.279
2500 - 3000	5767.690	31.530
>3000	6387.190	34.917

Rainfall with an intensity of > 3000 mm / year is the rainfall intensity that has the largest area which covers 6387.19 Ha with a percentage of 34.917% of the study site. Extremely high rainfall is found in Sukarame, Tanjungsenang, Wayhalim, Kedaton, Labuanratu and Rajabasa Districts. Rainfall map of Bandar Lampung city is presented in the Figure 9.

3.6. Soil Type

Factor types of soil types have different levels of landslide vulnerability. Landslide sensitivity is the ease or failure of landslides as an interaction of the physical and chemical properties of the soil. As for the properties of the soil that affect landslides are texture, structure, organic matter, depth, soil properties, and fertility levels. Based on the USDA soil type classification, the city of Bandar Lampung has five different types of soil namely Entisols, Inceptisols, Alfisols, Ultisols, and Oxisols. The level of soil development significantly affected the landslide. Developed soils such as Alfisols, Ultisols, and Oxisols give high landslides, while in younger soils there are few landslides . The area and level of landslide vulnerability in each type of soil are presented in table 8.

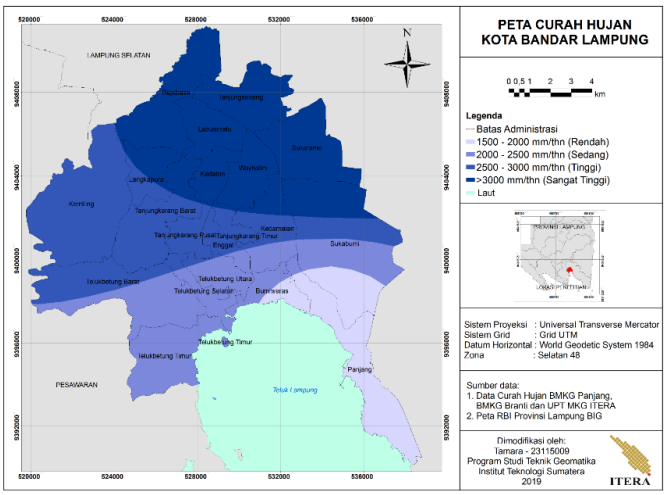

Figure 9. Map of Rainfall Interpolation.

Table 8. Soil Moisture.

Soil Type	Area (Ha)	Area (%)
Entisols	1572.129	8.569
Inceptisols	8117.813	44.245
Alfisols	2453.134	13.371
Ultisols	5154.004	28.091
Oxisols	391.373	2.133
Unclassified	658.773	3.591

Based on table 8, it is known that there are areas that are not classified as soil types, namely in Sukabumi District with an area of 658.773 Ha or 3.591% of the research area. Inceptisols soil type is the type of land with the highest area of 8117.813 Ha or 44.245. Inceptisols soil types have a low level of vulnerability. Based on Figure 10, the types of Inceptisols are found in Sukarame, Wayhalim, Tanjungsenang, Rajabasa, Tanjung Karang Timur and Enggal Districts. Oxisol soil type has a high level of landslide vulnerability, with a total area of 391.373 Ha found in Panjang District. The map of soil types in Bandar Lampung City is presented in Figure 10.

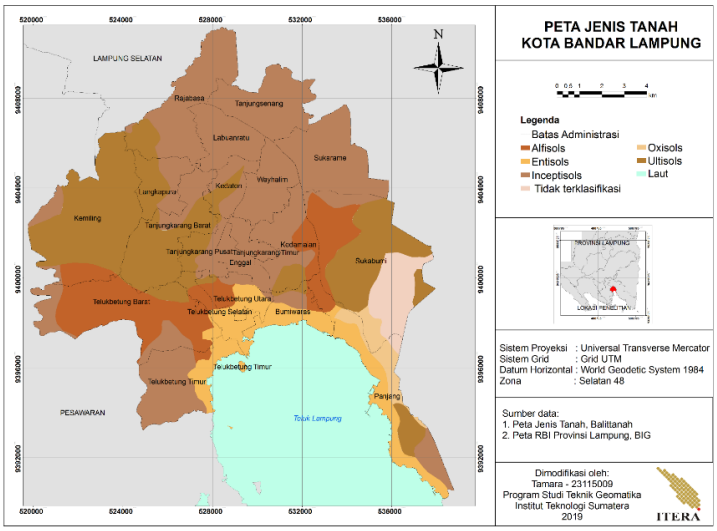

Figure 10. Map of Soil Type.

3.7. Landslide Prone Zoning Map

Zoning of landslide-prone areas is carried out by scoring and weighting methods on parameters which are factors of landslides. All parameters that have been overlayed are then categorized by each land unit at the vulnerability level. Map of Bandalampung City Landslide Zoning Map is presented in Figure 11.

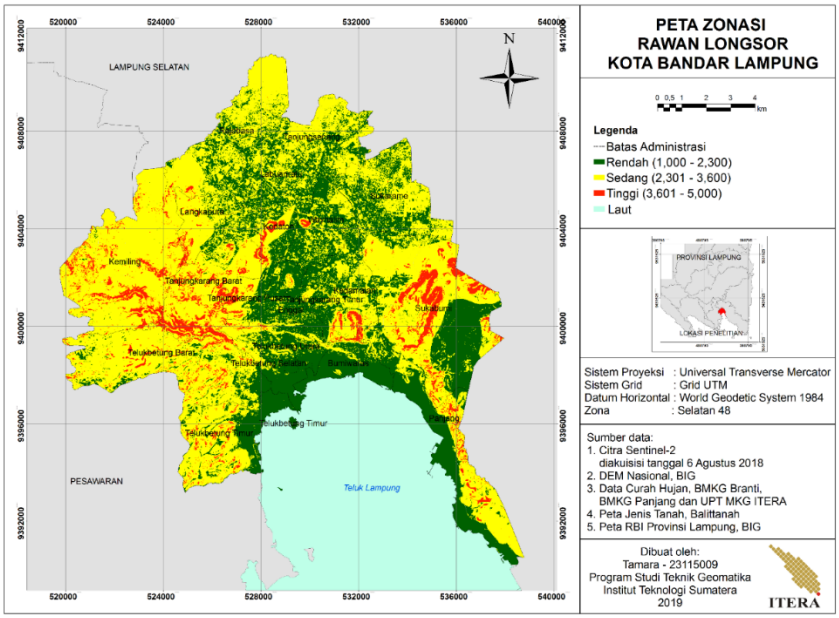

Figure 11. Landslide Prone Zoning Map.

Based on the results of the spatial analysis, the area of landslide vulnerability levels presented in table 9.

Table 9. Landslide Prone Zoning Area.

Prone Level	Area (Ha)	Area (%)
Low	5790.77	31.607
Medium	11337.2	61.880
High	1193.14	6.512

Table 9 shows the area of high landslide hazard level has an area of 1193.14 Ha or 6.512% of the area of the study site. The largest distribution is in the Districts of Sukabumi, Kemiling, and Tanjung Karang Barat. Most of these classes are in areas with steep topography (25 - 45%) with an area of 55343.460 Ha then in very steep topography (> 45%) with an area of 27706.461 Ha. Land cover in the form of open land, plantations, and shrubs dominate in this class with an area of 1039.643 Ha or 79.26% of the total area of high landslide vulnerability. Rainfall that dominates this vulnerability class is rainfall with an intensity of 2500-3000 mm/year with an area of 876.713 Ha. Ultisols soil type is the dominant soil type with an area of 8937.72 Ha. This type of soil is soil that has developed so that it can absorb high water. The absence of vegetation causes water to be absorbed by the soil until the soil becomes saturated and on unstable slopes can cause soil movement.

The application of the Normalized Difference Vegetation Index (NDVI) and Normalized Difference Moisture Index (NDMI) is used to support the physical parameters of landslide-prone zoning based on the presence of vegetation and soil moisture in Bandar Lampung City. The results of the transformation of vegetation index and soil moisture get an index value to be used as a parameter for determining the zoning of landslide-prone areas. The threat of landslides can occur in areas with low vegetation index values and high soil moisture index values. Conditions in these areas cause water to be directly absorbed by the soil to a high level of soil saturation and cause the slopes to become unstable. Based on the results

of the NDVI and NDMI transformation, it can be seen that Bandar Lampung City is dominated by a low vegetation density of 37.424% and has no soil moisture with a percentage of 83.889% of the Bandar Lampung City area.

Accuracy test on the results of landslide-prone zoning mapping in the city of Bandar Lampung was carried out with 24 samples where the determination of samples was carried out by proportional stratified random sampling. The accuracy test calculation is done by calculating the overall accuracy of the confusion matrix. The confusion matrix on the landslide-prone zoning map is presented in table 10.

Table 10. Confusion Matrix.

Classification	Reference Data			Total
	Low	Medium	High	
Low	8	0	0	8
Medium	3	5	0	8
High	0	0	8	8
Total	11	5	8	24
Producer Accuracy (%)	72.73	100	100	
User Accuracy (%)	100	62.50	100	
Overall Accuracy (%)		87.50		

Table 10. shows that the smallest producer accuracy is at the Low vulnerability level of 72.73%, while the lowest user accuracy is at the moderate vulnerability level with a value of 62.5%. The results of the confusion matrix calculation in table 4.14 show that the overall accuracy produced is 87.5%. This value shows that 87.5% of the Landslide Prone Zoning Map is in accordance with the actual conditions. The results of field validation show that landslide events have occurred at some sample points of high hazard level. The event was marked by the fall of trees, material that covered the ground and landslides. Potential landslides in the field validation sample can occur due to natural factors and human factors. Natural factors that are very influential in landslides are high rainfall on steep slopes and open land, while human factors indicate the potential for landslides in rock mining areas. The landslide situation is shown in Figure 12 – 14.

Figure 12. The landslide situation.

Figure 13. The landslide situation.

Figure 14. The landslide situation.

4. Conclusions

Based on the research results that have been described can be concluded that:

- Landslide threats can occur in areas with low vegetation index values and high soil moisture index values. Based on the NDVI transformation, the lowest vegetation index value is -0,550 and the highest is 0.840 while the NDMI transformation is the lowest vegetation index value -3,183 and the highest is 1,323. The classification of NDVI and NDMI values shows that Bandar Lampung City has a low vegetation density of 37.424% and 83.884% is not moist.
- Utilization of remote sensing imagery can obtain several parameters of landslide-prone areas including slope, vegetation density, soil moisture, and land use classification. Land use parameters resulted from the supervised classification with the maximum likelihood method that produces an overall accuracy of 91.4%.
- Spatial analysis results obtained three levels of landslide vulnerability, namely, Low, Medium and High. Spatial analysis results show map accuracy of 87.5%. The dominant level of landslide vulnerability was moderate, 61.880% of the total area of the study. The level of landslide vulnerability of low and high class has a percentage of 31.607% and 6.512%, respectively.

5. References

[1] Arifin, S., I. Carolila, and G. Winarso, *Implementasi Penginderaan Jauh dan SIG untuk Inventarisasi Daerah Rawan Bencana Longsor (Propinsi Lampung).* Jurnal Penginderaan Jauh dan Pengolahan Citra Digital, 2006. **3**(1): p. 77-86.

Application of Lyzenga Algorithm on Sentinel-2B and SPOT-7 Imagery for Estimation of Coral Reef Condition, Capacity and Presence (Case Study: Kapo-Kapo Island and Soetan Island, Pesisir Selatan Regency, West Sumatera Province)

Tessa Khairani Ermanto[1]*, Bambang Edhi Leksono[2], Nirmawana Simarmata[1]

[1]Geomatic Engineering, Sumatera Institute of Technology, Terusan Ryacudu Street, Way Hui, Jati Agung, 35365 South Lampung, Indonesia
[2]Department of Geodesy and Geomatic Engineering, Bandung Institute of Technology, 10 Ganesha Street, 40132 Bandung, Indonesia

*Corresponding author's e-mail: tessakhairani05@gmail.com

Abstract. Coral reefs are some of the most potential ecosystems for the wealth of the oceans and the national development. This potential provides enviromental benefits for biota that lives around coral reefs and also for human life. Kapo-Kapo Island and Soetan Island are one of the islands that has a coral reef habitat, which is used as a tourist destination in Pesisir Selatan Regency. The degradation of the Coral reefs on Kapo-Kapo Island and Soetan Island has been increasing on recent years. It is normally caused by illegal fishing techniques, pollution, careless tourism, other natural phenomena such as coral bleaching, climate change, etc. Using Sentinel-2B and SPOT-7 data of recording year 2018, the coral reefs are classified by means of Lyzenga Algorithm and Mahalanobis Distance method. Based on the results of the image classification, the area of coral reefs obtained from Sentinel-2B imagery is healthy coral reefs was 109.14 ha and unhealthy (dead) coral reefs was 84.08 ha, while healthy coral reefs at SPOT-7 image was 102.96 ha and unhealthy (dead) coral reefs was 71.02 ha. The accuracy test show that the overall accuracy value of Sentinel-2B images was 80% and SPOT-7 image was 87.09%. Between Sentinel-2B imagery and SPOT-7 image, the good accuracy goes to SPOT-7 image, because in addition to the higher overall accuracy value, SPOT-7 imagery has a higher spatial resolution than Sentinel-2B imagery.

Keywords: Coral Reef, Sentinel-2B, SPOT-7, Lyzenga Algorithm, Overall Accuracy.

1. Introduction

Indonesia is the largest archipelagic country in the world with approximately 70% of the sea area and has more than 10,000 islands. Coastal areas and small islands store large potential resources for national development, such as coral reefs. Indonesia has approximately 60,000 km^2 or one-eighth of total area of coral reefs found in all parts of the world. Today, the damage to coral reefs is increasing rapidly, one of which is in Pesisir Selatan Regency.

Pesisir Selatan Regency is one of the districts in West Sumatera Province that has a coral reef ecosystem along its waters. Based on 2011 data, the damage to coral reefs in the South Coastal District has reached 80% of the total area of ~12,721 km^2. The damage was triggered by the rise of fishermen using bombs to catch fish and trawler fishing gear in the waters of the South Coast. Rehabilitation and restoration of coral reefs in the waters of Pesisir Selatan Regency have been carried out by the government and the surrounding communities, especially on Kapo-Kapo Island and Soetan Island.

Kapo-Kapo Island and Soetan Island are one of the small islands which are administratively located in Koto XI Subdistrict, west of Mandeh Village, Pesisir Selatan District, West Sumatra Province. The existence of coral reefs makes Kapo-Kapo Island and Soetan Island as the leading tourist destinations in South Coastal District. This has direct implications for the rapid degradation of coral reefs due to increasing tourism and shipping activities. The process of monitoring coral reefs is an important step in

the conservation of marine resources so that they can know the dynamics of the condition of coral reef ecosystems periodically.
So far, there are still a lot of monitoring of coral reefs in field surveys because they are considered to be the most accurate, but the survey requires considerable time, effort and cost. Along with the development of technology, many methods have been developed to carry out the process of monitoring coral reefs, which is the remote sensing method. Remote sensing methods, especially for the marine sector, are a good alternative for monitoring the condition of coral reefs and other habitats. The ability of this technology to collect data for study areas that are broad and difficult to reach directly in a short time will help in providing information on marine resources.
One of the remote sensing applications is mapping coral reefs using satellite imagery. Satellite image data can sharpen knowledge about threats to coral reefs. Information obtained is in the form of global quality information that is near real-time and provides time-series spatial data that sometimes cannot be obtained based on measurements in the field. Several methods can be used in satellite image processing for coral reef mapping, one of which is the lyzenga algorithm.
The lyzenga algorithm aims to eliminate spectral habitat identification errors due to depth factors. This method produces a basic index that is not influenced by the depth and works well in clear shallow waters such as in the area of coral reef habitat. The problem in identifying coral reefs is the location of coral reefs in the water column, where the water column absorbs most of the electromagnetic wave energy used in remote sensing systems. There are limitations but there are also opportunities because there is a window that allows detecting objects in the water column that is at certain wavelengths that have a low absorption value.

2. Method

2.1. Research Sites

This research was conducted around the waters of Kapo-Kapo Island and Soetan Island, Pesisir Selatan District, West Sumatra Province. Geographically, Kapo-Kapo Island is located at coordinates 653676.95 and 9866741.11 and Soetan Island is located at coordinates 657620.44 and 9865603.04. Administratively it is located in Koto XI Tarusan District, west of Kampung Mandeh, Pesisir Selatan District, Prov. West Sumatra. Kapo-Kapo Island has an area of 316.73 ha and Soetan Island is a small island that has an area of 49.87 ha. The location of this research is right around the waters of Kapo-Kapo Island and Soetan Island.

2.2. Data and Research Tools

The data used in this study area:

- Sentinel-2B satellite image data acquired on June 3, 2018. This data is downloaded from the USGS Earth Explorer website.
- SPOT-7 satellite image data acquired on February 8, 2018.
- Data on the distribution of sample points for the existence of coral reefs around the waters of the acquired Kapo-Kapo Island and Soetan Island using GPS handhelds through field validation tests.

2.3. Data pre-processing

This stage is a process to improve image quality before interpretation. The obtained image has three levels, namely a) the image whose data is still in the form of raw data so that it has not undergone radiometric or geometric correction, b) images that have undergone radiometric correction but have not been geometrically corrected c) images that have undergone radiometric correction and geometric. Sentinel-2B imagery and SPOT-7 imagery are geometrically corrected. Even though the image obtained has gone through a stage of correction, several processes that are commonly performed at this stage are a re-conducting radiometric correction and geometric correction.

2.3.1. Radiometric Correction. Digital Number is a numeric value (1 byte) of pixels. Radiometric correction applied to SPOT-7 satellite images is a correction of the type of conversion of DN values to reflectance values. Electromagnetic waves emanating from satellite sensors interact with the atmosphere, causing a phenomenon such as scattering and absorption of electromagnetic waves. This phenomenon causes information on the spectral value received not to be an actual value and must be corrected. The correction made is to change DN to reflectance value.
Convert DN to radians:

$$L_\lambda = Gain.\ DN + Bias \quad (1)$$

Explanation:

- L_λ = Radian Value
- DN = Digital Number

The gain and bias values can be known through the SPOT-7 image metadata from the recording. The results of calculating radians can be used to calculate the reflectance value as follows:
Radian conversion to reflectance:

$$\rho\lambda = \frac{\pi . L_\lambda . d^2}{E_{sun} . Cos\theta_{sun}} \quad (2)$$

Explanation:

- ρ_λ = Reflectance Value
- L_λ = Radian Value
- d^2 = Earth-Sun Distance
- θ_{sun} = Sun azimuth (°) = 90-$Sun_{elevation}$

2.3.2. Geometric Correction. Geometric correction is done to get the image that matches the map projection by creating GCP points on the image. In this study, geometric correction on Sentinel-2B satellite images is using the image to map the rectification method concerning the SHP of the South Coastal District which already has a coordinate reference system. While the SPOT-7 geometric correction image is done using the image to image method with a reference to the image of the South Coastal District which has been rectified. An image is said to have been geometrically corrected if the RMS-error is not more than 0.5 m.

2.4. Lyzenga Algorithm
Several things are done in the lyzenga algorithm, such as calculating the variance and covariance values of bands 1, 2, and 3. Variance and covariance values are obtained from variant-specific formulas for each band 1, 2, and 3. Variance and covariance values for each band are used to determine attenuation coefficient value (ki / kj). Attenuation occurs because there is a reduction in light intensity due to an increase in water depth.
The magnitude of attenuation differs between wavelengths of light. Attenuation at the red band wavelength (around 700 nm) will be greater than the blue band wavelength (around 400 nm) because absorption at the red band wavelength is greater than the blue band wavelength. The value of the attenuation coefficient (k) will be different at different wavelengths of light. This causes a similar object in the water to have different spectral signature characteristics if it is in a different depth of water.
The attenuation coefficient (ki / kj) is obtained from the calculation of the standard deviation or mean deviation which is the result of the shortest variance of the shortest band with twice the covariance of the band in question.
ki/kj is obtained from the formula:

$$ki/kj = a + \sqrt{a^2 + 1} \quad (3)$$

with a is obtained from:

$$a = \frac{\sigma_{ii} - \sigma_{ij}}{2\sigma_{ij}} \quad (4)$$

Explanation:

- $\sigma_{ii,ij}$ = variant band i or band j
- σ_{ij} = covariant band ij

The DII (Depth Invariant Index) value is calculated after obtaining the ki/kj value for band 1 2, band 1 3, and band 2 3, using the following formula:

$$\text{DII} = ln(Li) - [\left(\frac{ki}{kj}\right).ln(Lj)] \quad (5)$$

Explanation:

- Li = Digital Number from band i
- Lj = Digital Number from band j
- ki/kj = Attenuation coefficient in band i and j

The attenuation coefficient (ki / kj) is used in the real lyzenga algorithm. The bands used are red bands, blue bands, and green bands that will pair up to form pairs of red bands and blue bands, red bands, and green bands, as well as green bands and blue bands. Each pair of bands will produce a new band whose pixel value is not affected by depth and is specific to one type of substrate.

2.5. Classification of Image Results of the Lyzenga Algorithm

Image classification in this study was made based on coral reef habitat cover. Based on SNI: 7645: 2010, the habitat cover is divided into classes such as water, coral reefs, sand, and land. Classification is done by making a training area (ROI) first, according to the appearance. The classification used is supervised classification.

This classification is the process of grouping pixels on images into certain classes based on pixel sample statistics (training) or region of interest. The pixel sample is determined by the user as a reference pixel which is then used by the computer as a basis for classification. A good pixel sample has good average separation between each class as indicated by the separability index value. Separability is a statistical measure between two classes.

The value in the Separability table for all land cover classes is dominated by a value of 2.0 or ranging from 1.9 to 2.0. This shows that the land cover class has the criteria of good and perfect (excellent).

The range of the Separability values can be seen in Table below.

Table 1. Range of Separability Transformation Value.

Separability Transformation Value	Explanation
>2.0	Excellent
1.9 – 2.0	Good
1.8 – 1.9	Fair
1.6 – 1.8	Poor
<1.6	Inseparable

2.6. Field Data Collection

Several stages carried out in carrying out field data collection procedures are 1) Assessment of the condition of coral reefs using the Line Transect Method and 2) Test the accuracy of field samples to see the suitability of the results of the classification of shallow water habitat with actual objects in the field. The Line Transect Method, known as the Line Intercept Transect (LIT) Method, is used to assess

community forms based on the characteristics of lifeforms, especially the morphology of the coral reef community so that the diversity of coral species in the area can be known. This observation is done by scuba diving (swimming using a scuba set) at depths of 3 m and 7 m. This observation is based on a predetermined transect line.
The way LIT works are to spread a 50-meter roll meter perpendicular to the coastline as a transect line, then divide the line into 20 m - 10 m - 20 m. The first 20 m line is photographing coral reefs at depths of 3 and 7 m, then the second 10 m lines is used as a separator between the first and second intervals. Based on the results of field validation, 1 50 m transect has 2 repetitions for each depth.

2.7. Accuracy Test
Accuracy tests were carried out to determine the accuracy of shallow marine habitat cover mapping. Accuracy tests are carried out using a 70% reference in field data. Accuracy testing is done after conducting a survey or fieldwork. The classification results need to be tested to produce acceptable data with a certain level of accuracy.
The accuracy test results are interpreted, all samples from the population are tested for field checking data. The test in question is doing a comparison by compiling a confusion matrix. Tests are carried out on samples representing certain objects in a polygon object with the same location coordinates in the field. Samples that have been taken from the field are compared with the object class results of the classification.

2.8. Reclassify the Cover of Coral Reef Habitat Based on Health
This stage is an image processing activity carried out after image processing (classification) and field surveys. This stage aims to refinement the image classification results. Not all pixel values can be classified or grouped based on their spectral values into habitat classes according to the interpreters' wishes based on their knowledge. This is done to avoid misclassification of objects that experience uncorrected noise/disturbance or different objects but have similar spectral values.
The re-classification of this research is based onthe health of coral reefs. The percentage of live coral cover is calculated from samples obtained in the field. This percentage is calculated by the following formula.

$$L=\frac{Li}{N}\times 100\% \quad (6)$$

Explanation:

- L = Percentage of Coral Cover (%)
- Li = i-i Lifeform Category Length
- N = Transect Length (50 m)

The range for the assessment of coral reef ecosystems according to Keputusan Menteri in 2007 based on the percentage level of live coral is shown in table below.

Table 2. Range of percentage levels of coral cover.

Percentage of Cover	Assessment criteria
0 – 24.9 %	Buruk
25 – 49.9 %	Sedang
50 – 74.9 %	Baik
75 – 100 %	Baik Sekali

3. Results and Discussion

3.1. Lyzenga Algorithm

The lyzenga algorithm is done to eliminate the effect of the water column. The lyzenga algorithm is very important in this study, based on the fact that multispectral classification using original data cannot optimally differentiate the characteristics of benthic objects due to the effect of a water column. The lyzenga algorithm is used to get a better view of the initial image of the basic objects of the waters, especially coral reefs.

The first step is the formation of a training site (region), which is displayed visually in Figure 1. The image used for determining the sample is geometric and radiometric corrected images.

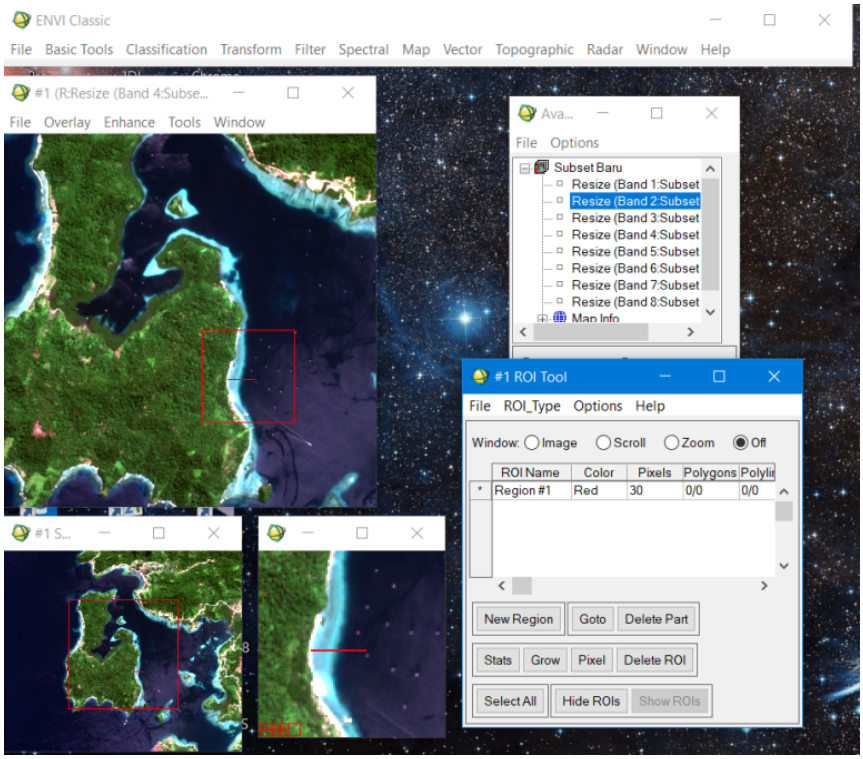

Figure 1. Sampling for Correction of Water Columns in Corrected Images.

The determination of the water column training site starts from shallow water to deep waters as many as 30 points to obtain a variance and covariant values. The image used is a geometric and radiometric corrected image. The next step is to find the per-band variance value of the three bands used, namely the red band (4), green band (3), and blue band (2), by first storing the DN value of each band as a result of the training site. DN data are arranged based on the Npts of each band and are sorted by 30 DN. Before calculating the variance, what is done is correcting the water column in the radiometric and geometric corrected image.

Blue and green bands are commonly used in the correction of water columns. Attenuation in both bands is smaller than the red band because the absorption at the wavelength of the red band is greater. The band used for the correction of the water column in Sentinel-2B Imagery is band 2 (blue) and band 8 (NIR). The combination of the two bands produces a linear regression line graph. The selection of band 2 (blue) and band 8 (NIR) as a regression function in the correction of the water column, because the regression values of these two bands are higher than the green band. This regression graph produces the function x to be input into the math ENVI 5.1 band.

The x function is x = = $\frac{(B1+49.38)}{0.269}$. This value of x has a determinant value (R^2) = 0.603. The regression value explains that 60.3% Y variability can be explained by X variability. The graph is shown in Figure 2 below.

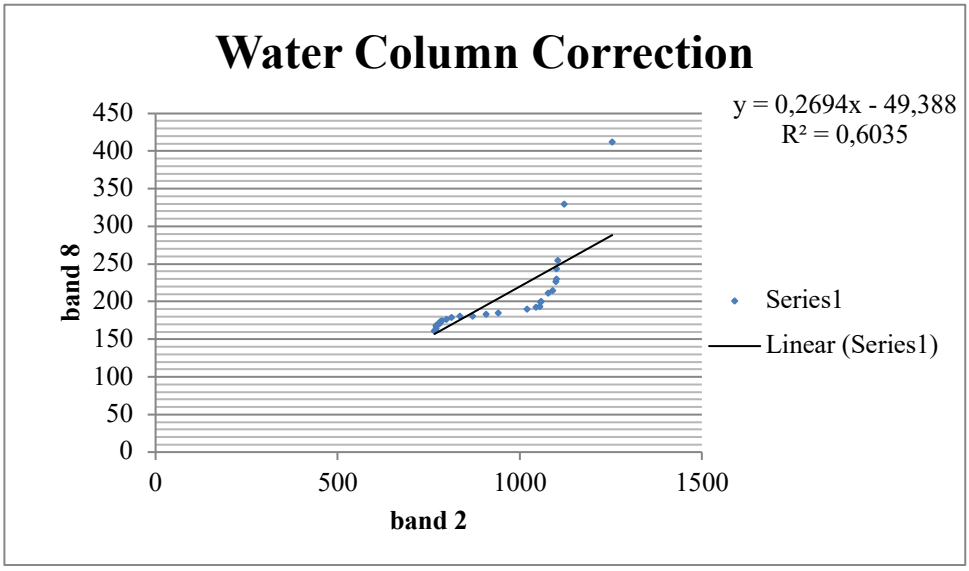

Figure 2. Water Column Correction Linear Line.

Determination of the value of covariance is calculated from the average variance of the band which is a combination of the values of red bands and blue bands, red bands, and green bands, as well as blue bands and green bands. Variant value is a way to measure the spread of image data, while the covariance value is a measure of how strong the relationship between the value of the red band and the blue band, the red band and the green band, and the blue band and the green band.
Image differences before and after applying the lyzenga algorithm lie in visual results. The image from the algorithm raises information found in shallow water. The image results before and after applying the lyzenga algorithm are shown in Figure 3 below.

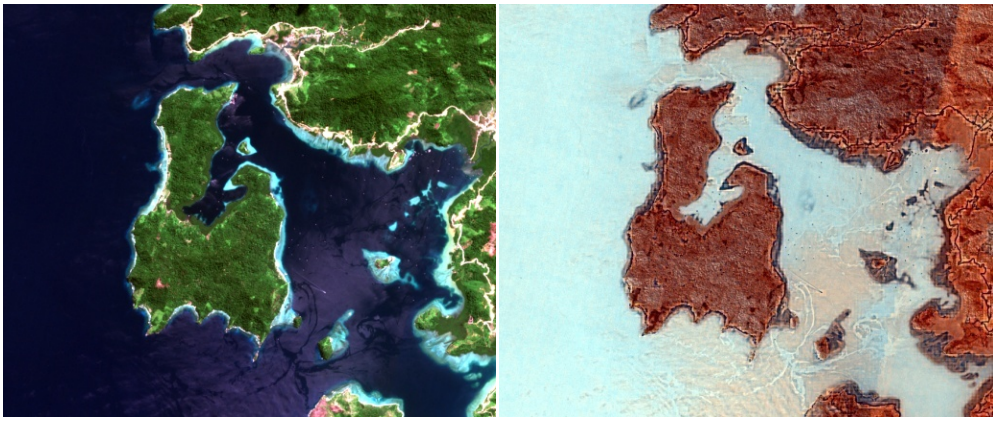

Figure 3. Sentinel-2B Image Before (left) and After (right) Lyzenga Algorithm.

3.2. Land Cover Classification Results
The image from lyzenga transformation is classified into a land cover classification. In this study, the supervised type of Mahalanobis distance, maximum likelihood, and minimum distance were then classified into several classes, such as coral reefs, sand, and land. Classification is done through visual

interpretation. like the example shown in Figure 4¸ the classes are identified from a visual display, namely:

- The stretch of sand is dark blue to black.
- Faded orange coral objects.
- he land is displayed in bright orange and there is an element of sand mixed.

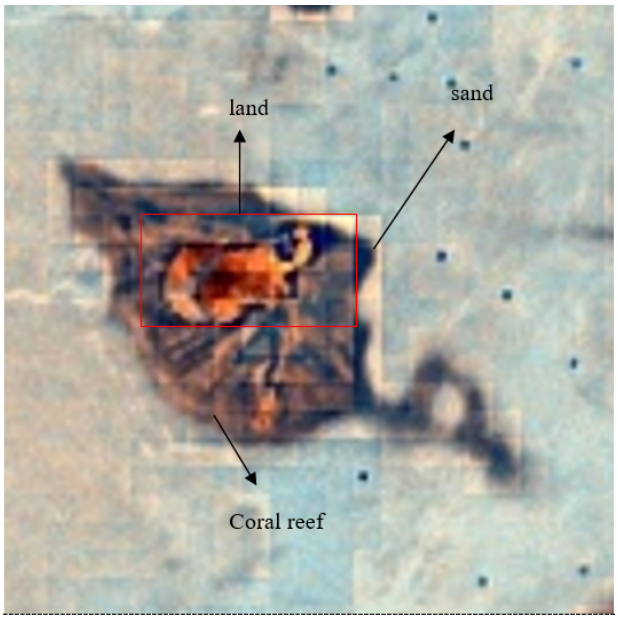

Figure 4. Object Classes in Land Cover Classification.

3.3. Supervised Classification

The results of the guided classification (supervised), Mahalanobis distance are shown visually in Figure 5.

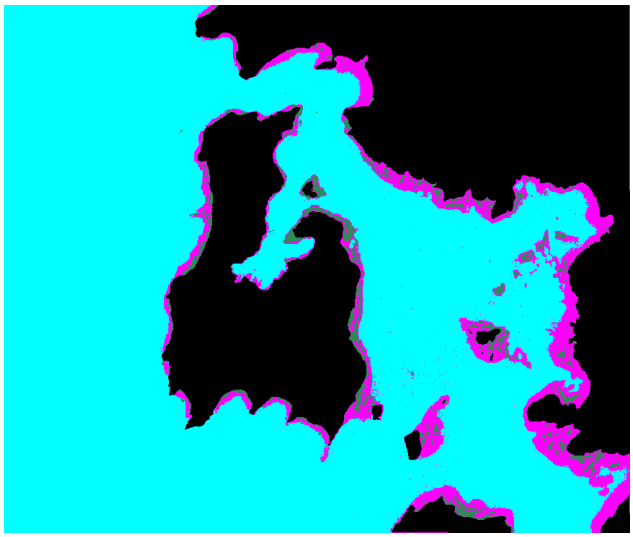

Figure 5. Results of Classification of Mahalanobis Distance.

3.4. Field Analysis Results

The results of this field analysis consisted of results in the form and condition of coral reefs according to the transect method used. The number of transects made in the field is 7 transects with each transect

length of 50 m. Each transect consists of 2 areas divided by 20 m - 10 m 20 m. Illustrations of sampling based on transects, shown visually in Figure 6.

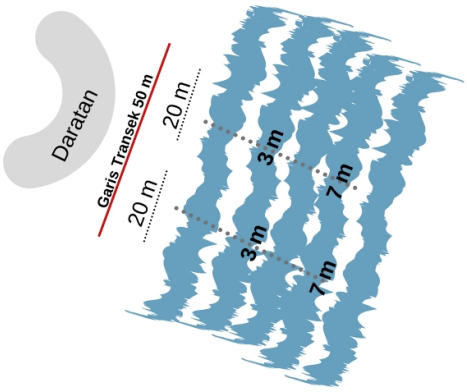

Figure 6. Illustration of Sampling based on Transect Lines.

The determination of the depth depends on the presence of coral at the location at each depth. Generally, it is carried out at three depths namely 3 m, 5 m, and 10 m.

Table 3. Identification of the First and Second Transects of Soetan Island.

Transect	Depth	Repetition	Time (wib)	Date	Temperature (°C)	Brightness (m)	Condition
1	3	1	09.24	14/04/2019	31	3	Damage
		2	09.30	14/04/2019	31	3	Damage
	7	1	09.27	14/04/2019	31	7	Damage
		2	09.33	14/04/2019	31	7	Damage
2	3	1	10.15	14/04/2019	29	3	Healthy
		2	10.35	14/04/2019	29	3	Healthy
	7	1	10.21	14/04/2019	29	7	Healthy
		2	10.38	14/04/2019	29	7	Healthy

3.5. Accuracy Test

Accuracy tests function to measure accuracy in image interpretation. In this accuracy test, the classification results will be compared with the actual conditions in the field concerning points taken in the field, and are considered to represent all categories of percent coral cover.

Table 4. Land Cover Classification Accuracy Table Sentinel-2B Accuracy Test.

Image Classification Data	Reference Data			
	Coral Reef	Sand	Land	Total
Coral Reef	22	0	2	24
Land	2	5	0	7
Sand	3	0	1	4
Total	27	5	3	35
Producer Accuracy (%)	81.48148148	100	33.3333333	
User Accuracy (%)	91.66666667	71.42857	25	
Overall Accuracy (%)		80		
Error (%)		20		
Kappa Coefficient		0.537735849		

Accuracy calculation results using the confusion matrix shown in Table 4, produce an overall accuracy mapping of 80% which indicates that the map has good results. The total sample points in the field were 64 samples, 70% or ± 35 samples were used in the calculation of the accuracy test. A total of 22 points out of a total of 35 samples are coral reefs and 2 points of misinterpretation are land. If seen in the producer accuracy value, the coral reef class has a value of 81.48%. This value indicates that an average of about 81.48% of the survey's reference data on coral reefs will always be confirmed correctly as live corals in the image classification results.
On the user accuracy value of the coral reef class, the resulting value is 91.66%. This value indicates that an average of about 91.66% of the pixel data in the category of coral reefs from image classification will be confirmed precisely on the field as a coral reef. The same statement is also applied to the value of the user accuracy and producer accuracy of the land and sand classes. The value of the overall accuracy and Kappa coefficient represents the image accuracy in general. The Kappa coefficient is more representative for use in comparing accuracy between images.
Table 4 shows that the overall accuracy value and Kappa coefficient on the coral reef class are 80% and 0.53. According to (Altman, 1991) the value of the Kappa coefficient of 0.53 can be interpreted into a fair class. This means that Sentinel-2B only avoids a classification error of 20%.

3.6. Mapping of Land Use
Mapping the use of coral reef habitat is obtained from the results of field validation. A total of 30 samples were distributed in several places on Kapo-Kapo Island and Soetan Island. The results of land use in Sentinel-2B imagery and SPOT-7 imagery are shown visually on figure 7.

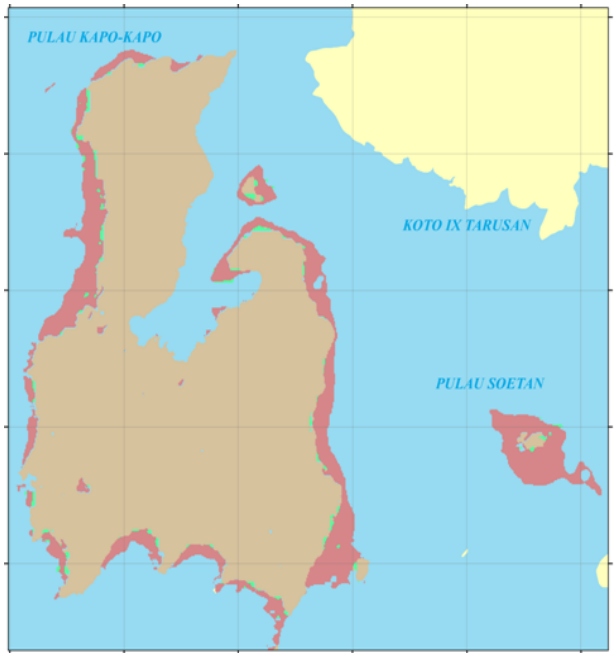

Figure 7. Map of the Sentinel-2B Citra Coral Reef Habitat Use.

The area of coral reefs during the land cover and land use classification gives different results. The area of coral reefs in Sentinel-2B images when the land cover is 105.41 ha and land use results are 161.3 ha, as shown visually on figure 7.

3.7. Mapping of Coral Reefs Based on Health Conditions
Coral reefs scattered around the waters of Kapo-Kapo Island and Soetan Island are in conditions that are mostly healthy and others are damaged. This damage is caused by the following factors.

- The road-widening project in the Mandeh area has a detrimental effect on the life of coral reefs on the islands around the Mandeh area because the remaining material of the project is dumped into the sea.
- High levels of sedimentation in the sea cause sunlight to be closed. Sunlight is needed for photosynthesis by zooxanthellae in coral tissue.
- In 2015, a coral bleaching event occurred as a result of rising sea temperatures. This bleaching process occurs so quickly with a very slow recovery process.
- The effect of temperature increases also affects coral growth. The ideal temperature for coral reefs to live well is around the temperature of 27-29°C.

After validating the field, the condition of the coral reefs in the waters of Kapo-Kapo Island and Soetan Island was categorized into healthy coral reefs and unhealthy coral reefs. Healthy and unhealthy categories of coral reefs are analyzed based on qualitative data, namely the physical conditions of coral reefs and the environmental conditions surrounding coral reefs. Observations on the transect line 1 located on Soetan Island resulted in an analysis that the health of coral reefs in the area was unhealthy. This is seen from the large temperature around the transect 1 area of 31°C and high sedimentation rates.

The coral bleaching event on Soetan Island also caused coral reefs around the transect 1 area to be classified as unhealthy coral reefs. A sign of damage caused by the coral bleaching is the physical condition of the coral reef which is partly white and partly blackened, and the density of coral reefs is relatively low. Besides, the coral bleaching event also caused the least intensity of fish around the waters on transect 1.

The second transect line (2) which is still located on Soetan Island, the condition of the coral reefs around this area, is better than the condition of coral reefs in the transect area one (1). Health analysis on transect 2 is also seen from the amount of temperature, brightness, and sedimentation rate. The temperature of transect 2 is 29°C with good brightness, and low sedimentation rate. The sedimentation rate in this area is different from the transect 1 area because high sedimentation in the transect 1 area is caused by road-widening projects in the area, while transect 2 is far from the road widening project. Besides, coral reefs in area 2 of the transect are still used as a place for snorkeling, so it can be concluded that coral reefs in this area are still considered healthy because of the presence of many fish species.

Accuracy tests using confusion matrix tables are needed in this study to compare the accuracy of Sentinel-2B images and SPOT 7 images using the lyzenga method in identifying coral reef habitats. The distribution of coral reef conditions on Kapo-Kapo Island and Soetan Island using Sentinel and SPOT-7 imagery is shown in Figure below.

The condition of coral reefs on Kapo-Kapo Island and Soetan Island Sentinel-2B imagery is classed into healthy coral reefs and unhealthy coral reefs, as shown visually in Figure 4.39. Unhealthy (dead) coral reefs have an area of 84.08 ha and coral reefs with healthy conditions, the area is 109.14 ha. If added together, the total is 193.22 ha. This amount is compared to the area obtained from the classification of land use of coral reef habitat using the previous Sentinel-2B image, which is 161.3 ha.

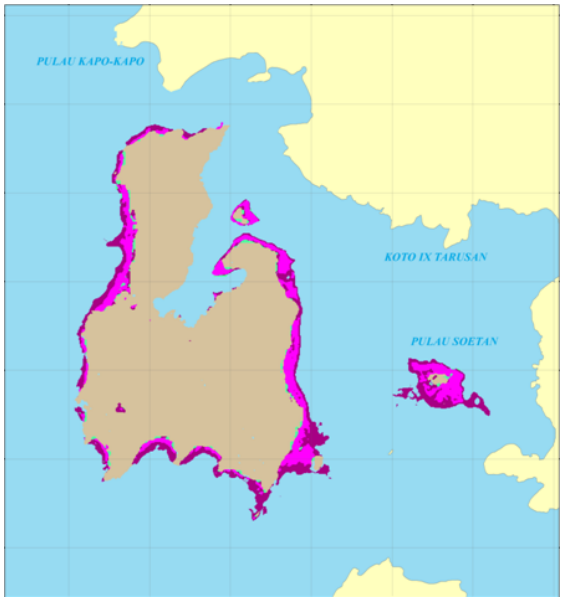

Figure 8. Map of Citra Sentinel-2B Coral Reef Habitat Condition.

4. Conclusions

From the results of the research conducted, it can be concluded:

- The regression value produced by the Sentinel-2B image for the correction of the water column is 0.603. This value is generated from a combination of blue bands (2) and NIR bands (8). In the SPOT-7 image, the resulting regression value is 0.981. This value is generated from a combination of blue bands (3) and NIR bands (4). Linear regression results are said to be good if the determinant results (R2) are almost close to number 1. Correction of the water column is used to correct the depth of the water so that information in shallow water can be detected.
- Effectiveness of Sentinel-2B image and SPOT-7 image in identifying coral reefs, seen from the overall accuracy value and kappa coefficient of each image. The overall accuracy value of the Sentinel-2B image is 80% with its kappa coefficient being 0.53 which is interpreted into a fair class. The overall accuracy value in the SPOT-7 image is 87.09% with a kappa coefficient value of 0.77 which is interpreted into a good class. Technically, SPOT-7 images have a higher Kappa coefficient than Sentinel-2B images given that SPOT-7 has a resolution greater than Sentinel-2B.
- The health of coral reefs is obtained from the results of field validation. The criteria for coral reef conditions in this study are healthy and unhealthy coral reefs. The area of healthy coral reefs in Sentinel-2B imagery is 109.14 ha and unhealthy coral reefs are 84.08 ha. The area of healthy coral reefs in the SPOT-7 image is 102.96 ha and the area of unhealthy coral reefs is 71.02 ha.

Vertical Accuracy Evaluation of National DEM Data at Buru Island

Maundri Prihanggo[1*], Rofiatul Ainiyah[1], Rofiqoh[1]

[1]Geospatial Information Agency of Indonesia, Cibinong, Indonesia

*Corresponding author's e-mail: maundri.prihanggo@big.go.id

Abstract. Indonesia is a very huge country that has a wide vary of topographic landscape therefore Indonesia needs a single elevation data model which is accountable. According to Indonesia Law Number 4 Year 2011, Geospatial Information Agency has the authority to produce geospatial information including national Digital Elevation Model (DEM) that cover all area over Indonesia. The specific purpose of this study is to evaluate the vertical accuracy of Indonesia national DEM at Buru Island. Buru Island is located in Maluku Province and most of its area are covered with forest. The methodology to assess the vertical accuracy of study area is by using independent check point measured by geodetic and terrestrial measurement. There are 30 points measured using geodetic measurement. Geodetic measurement is held along seashore area. The horizontal and vertical accuracy of each point of geodetic measurement is below 10 cm and 15 cm. There are 39 points measured using terrestrial measurement in high and low vegetation. Our main obstacle is points we measured are not well-spread because not every area is accessible. The conclusion of this study is the vertical accuracy of Indonesia National DEM is suitable as the DEM for 1:25,000 scale map or above.

Keywords: National DEM, vertical accuracy.

1. Introduction

Indonesia is an archipelago country which has approximately 1.922.560 km^2 of land area and 3.257.483 km^2 of sea area, having more than 17.504 islands and located on 95° West Longitude to 141°45' East Longitude and from 6° North Latitude to 11°8' South Latitude. In order to support the development in the huge area of Indonesia therefore Indonesian government needs a specific regulation to provide an accessible and responsible of geospatial information. Indonesian Law Number 4 Year 2011 mention that geospatial information consist of base geospatial information and thematic geospatial information. There are two products of base geospatial information, they are base map and geodetic control network. Base map could be present in three dimensional features in the form of Digital Elevation Model (DEM). Geospatial Information Agency is the institution mentioned in President Law Number 94 Year 2011 which has mandate to provide every base geospatial information in Indonesia. By the year of 2018, Geospatial Information Agency already provide an accessible data of Indonesia National DEM, named DEMNAS (DEM *Nasional*), with no charge.

DEMNAS is elevation model that cover all area of Indonesia which built from many types of data sources, such as IFSAR, Terrasar-X and ALOS PALSAR and by adding masspoints from stereocompilation of large-scale map in some location which already has the data. DEMNAS data is present in medium scale sheet-based format, in 1:25,000 scale and 1:50,000 scale, depends on the availability of the data in that location.

The implementation of spatial data is regulated in President Law Number 39 Year 2019 about One Data of Indonesia. It is mentioned in the law that spatial data produced must be accurate, up-to-date, integrated, accesible, responsible and has a good interperobility therefore give benefit to many government agencies by fulfilling data standard, metadata, data interperobility and using reference code. DEMNAS, as one of spatial data products, has to fulfill spesific standard and has to be responsible for the user. The standard used for measuring accuracy of DEMNAS is Geospatial Information Agency Head Law Number 6 Year 2018 about base map accuracy standard. This standard is complied to measure

horizontal and vertical accuracy of the data from small scale map, 1:1,000,000 scale, to large scale map, 1:10,000 scale. Therefore, the purpose of this research is to evaluate the vertical accuracy of DEMNAS data in the study area.

2. Materials and Method

The study area of this research located in Buru Island, Moluccas Province. There are two activities held in this research, they are field survey and data processing. Field survey activity took 7 days. The points of vertical accuracy were spreading most in northern and southern part of the study area, adjusting with the accessibility of transportation available. In the middle part of the study area is a mountainous area that is hard to access the same as in the eastern and western part of the study area that couldn't be accessed by land transportation. Most of the people living there is travelling by boat.

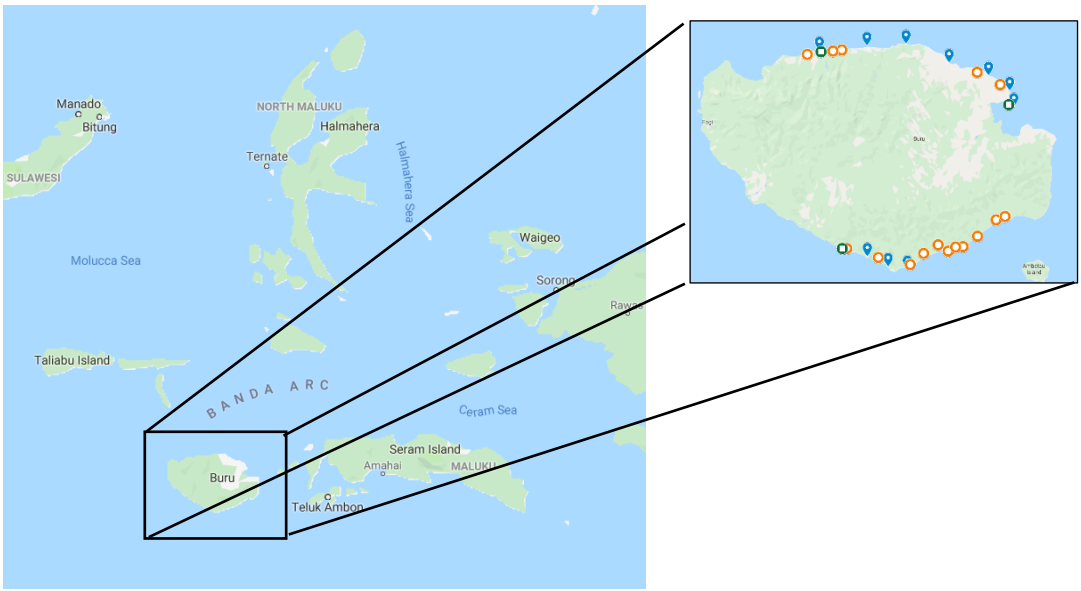

Figure 1. Location of Study Area.

The evaluation of vertical accuracy was using terrestrial and geodetic method. Terrestrial method was held to test di vertical accuracy in the area that covered by vegetation while geodetic method was held on the area that relatively open, such as along sea shore on the estimated lowest tide, highest tide and moment sea tide. Total of points measured by terrestrial method are 39 points while points measured by geodetic method are 30 points, the symbol are shown in figure 1, blue mark is symbol for points measured using geodetic measurement and orange dot is symbol for points measured in terrestrial method. While doing terrestrial method, some extra points need to be measured to tie with the geodetic control network point. As extra tie points, it needs to be measured by geodetic measurement with the duration of measurement adjusting with the distance correspondence the geodetic control points. There are three geodetic control points used and available in the study area, as shown by the green rectangle in the figure 1.

Data processing did to the points measured in geodetic was process in radial method with single baseline to geodetic control points. While points measured in terrestrial method was process by using distance and angle measured on the field. From the processing data we get the orthometric elevation of each check points. Figure 2 shows us the difference between ellipsoid height and orthometric height.

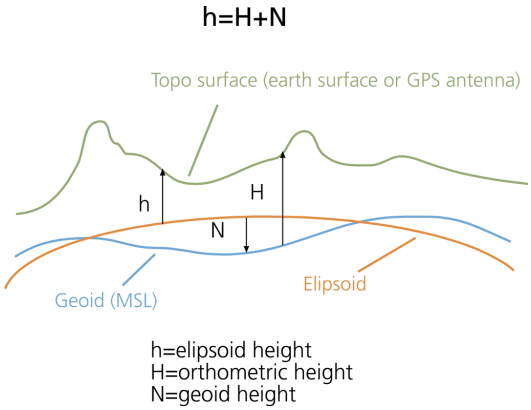

Figure 2. Illustration of Orthometric Height.

3. Results and Discussion

Result from this research could be seen from table 1 and table 2. Table 1 show us the vertical accuracy from points measured by using geodetic method while table 2 show us vertical accuracy from points measured by terrestrial method.

Table 1. Points Measured by Geodetic Measurement.

No.	Site Name	E (m)	N (m)	h_ortho (m)	h_DEMNAS (m)	D(h) (m)	$(Dh)^2$ (m^2)
1	GPS001	265708.109	9654085.730	1.959	N/A	N/A	N/A
2	GPS002	265703.878	9654071.974	3.259	-0.710188	-3.969188	15.75445338
3	GPS003	265699.363	9654027.186	5.224	5.613399	0.389399	0.15163158
4	GPS004	252059.936	9661405.898	1.841	5.199748	3.358748	11.28118813
5	GPS005	252048.839	9661396.536	3.121	6.812749	3.691749	13.62901068
6	GPS006	285387.547	9645963.138	8.925	13.041480	4.116480	16.94540759
7	GPS007	276242.775	9650806.053	4.063	11.755880	7.692880	59.18040269
8	GPS008	285367.338	9645959.784	9.742	14.079570	4.337570	18.81451350
9	GPS009	276253.986	9650819.721	3.989	11.655600	7.666600	58.77675556
10	GPS010	290785.763	9637261.219	2.100	-0.986104	-3.086104	9.52403789
11	GPS011	290731.952	9637323.227	1.888	4.859058	2.971058	8.82718563
12	GPS012	289158.873	9643460.779	1.692	-1.143717	-2.835717	8.04129090
13	GPS013	289123.508	9643401.531	4.137	6.233478	2.096478	4.39522000
14	GPS014	289151.134	9643463.086	2.432	-1.869922	-4.301922	18.50653289
15	GPS015	213908.820	9659063.342	1.507	0.085386	-1.421614	2.02098636
16	GPS016	213884.789	9659049.390	2.392	2.695945	0.303945	0.09238256
17	GPS017	219416.455	9658833.149	4.564	8.877248	4.313248	18.60410831
18	GPS018	219421.991	9658829.878	5.378	9.176649	3.798649	14.42973423
19	GPS019	268064.400	9582624.837	3.378	8.523190	5.145190	26.47298014
20	GPS020	262786.170	9581554.179	3.495	8.690970	5.195970	26.99810424
21	GPS021	265181.391	9580907.870	62.622	60.803000	-1.819000	3.30876100

No.	Site Name	E (m)	N (m)	h_ortho (m)	h_DEMNAS (m)	D(h) (m)	$(Dh)^2$ (m^2)
22	GPS022	268052.314	9582655.355	3.587	9.248400	5.661400	32.05144996
23	GPS023	262791.565	9581570.073	3.328	9.670150	6.342150	40.22286662
24	GPS024	265150.038	9580913.584	62.283	61.571500	-0.711500	0.50623225
25	GPS025	260556.865	9581745.846	7.603	12.851100	5.248100	27.54255361
26	GPS026	256814.275	9580208.885	8.604	14.612600	6.008600	36.10327396
27	GPS027	249894.323	9575794.073	9.010	15.614200	6.604200	43.61545764
28	GPS028	260553.383	9581780.407	7.601	14.539500	6.938500	48.14278225
29	GPS029	256819.583	9580191.085	8.687	15.271600	6.584600	43.35695716
30	GPS030	249876.612	9575811.819	9.489	16.732100	7.243100	52.46249761
RMSe (m)							**4.76972766**
Vertical Accuracy (m)							**7.86957367**

Table 2. Points Measured by Terrestrial Measurement.

No.	Site Name	E (m)	N (m)	h_ortho (m)	h_DEMNAS (m)	D(h) (m)	$(Dh)^2$ (m^2)
1	TS001	219403.674	9658840.870	2.524	9.734784	7.210184	51.98675331
2	TS002	219263.429	9658771.349	0.331	7.146230	6.815230	46.44735995
3	TS003	219469.106	9658729.642	3.589	14.922800	11.333200	128.44142220
4	TS004	219487.985	9658812.046	4.501	12.879300	8.378300	70.19591089
5	TS005	213808.432	9659014.456	3.862	9.760610	5.897810	34.78416280
6	TS006	213929.811	9658944.743	4.921	10.430930	5.509630	30.35602274
7	TS007	213987.914	9658922.664	4.325	10.844140	6.518540	42.49136373
8	TS008	262762.506	9581494.033	3.226	10.210070	6.984070	48.77723376
9	TS009	262809.668	9581531.388	3.473	8.076433	4.603333	21.19067471
10	TS010	262857.154	9581610.049	2.661	8.793503	6.132203	37.60391363
11	TS011	262841.101	9581631.614	3.427	8.354707	4.927007	24.27539798
12	TS012	262733.188	9581503.167	3.900	8.558605	4.658405	21.70073714
13	TS013	265255.679	9580883.906	62.796	47.984520	-14.811780	219.38882680
14	TS014	265252.186	9580920.123	63.047	66.713560	3.665760	13.43779638
15	TS015	265089.217	9580950.174	59.516	67.101230	7.584330	57.52206155
16	TS016	265061.452	9580928.792	59.331	50.726820	-8.605080	74.04740181
17	TS017	268026.782	9582598.680	2.495	11.817690	9.322190	86.90322640
18	TS018	267987.490	9582626.835	3.067	12.386010	9.318110	86.82717397
19	TS019	268002.269	9582696.579	2.776	12.724740	9.948040	98.96349984
20	TS020	268072.099	9582702.825	4.080	10.849100	6.768800	45.81665344
21	TS021	268094.877	9582659.652	2.607	11.229720	8.622020	74.33922888

No.	Site Name	E (m)	N (m)	h_ortho (m)	h_DEMNAS (m)	D(h) (m)	$(Dh)^2$ (m^2)
22	TS022	268096.837	9582619.368	2.474	8.763277	6.289077	39.55248951
23	TS023	260610.606	9581697.795	5.871	13.178700	7.307100	53.39371041
24	TS024	260607.806	9581768.121	6.086	16.690580	10.604080	112.44651260
25	TS025	260602.173	9581828.542	6.324	16.668120	10.344020	106.99874980
26	TS026	260502.262	9581810.436	6.057	13.841450	7.784050	60.59143440
27	TS027	260504.516	9581770.866	6.147	16.228120	10.080620	101.61889960
28	TS028	260509.347	9581711.973	5.649	18.792750	13.143150	172.74239190
29	TS029	256845.598	9580227.382	7.750	14.739590	6.989190	48.84877686
30	TS030	256834.091	9580292.626	9.206	15.676910	6.470910	41.87267623
31	TS031	256776.633	9580212.079	9.363	16.060720	6.697320	44.85409518
32	TS032	256765.895	9580172.856	8.004	16.086860	8.082560	65.32777615
33	TS033	256771.385	9580125.081	8.174	16.216730	8.041830	64.67102975
34	TS034	256868.798	9580146.247	7.587	15.835520	8.248520	68.03808219
35	TS035	249951.285	9575775.581	7.621	13.844090	6.222190	38.71564840
36	TS036	249923.773	9575830.763	8.579	13.801460	5.221860	27.26782186
37	TS037	249846.718	9575876.508	8.087	16.309970	8.222870	67.61559104
38	TS038	249809.061	9575872.534	9.846	16.820960	6.974860	48.64867202
39	TS039	249860.494	9575779.118	7.328	16.789250	9.460650	89.50389842
RMSe (m)							**8.11488830**
Vertical Accuracy (m)							**13.38875420**

On the standard mentioned in Geospatial Information Agency Head Law Number 6 Year 2018, the statistical calculations are based on a 90% linier error (LE90) for the vertical accuracy. It means 90% of the well-defined points that are tested must fall within specified tolerance. LE90 is obtained by multiplying Root Mean Square to factor 1.6449.

$$RMSEz = \sqrt{\frac{\sum(Z_{data}-Z_{check})^2}{n}} \quad (1)$$

$$LE90 = 1.6449xRMSEz \quad (2)$$

From the table 1, we can see that the result of vertical accuracy along sea shore line with 30 points of vertical accuracy tested is 7.869 m and vertical accuracy in vegetated area measured using terrestrial method is 13.388 m. As we see, the result of vertical accuracy is suitable to use in medium scale map, specifically 1:25,000 scale map along sea shore area and 1:50,000 scale map in vegetated area.

Acknowledgement
The authors acknowledge Center for Topographic Mapping and Toponym in Geospatial Information Agency of Indonesia for providing dataset and doing field survey that used in this research.

Multi Data Digital Terrain Model for Waterlogging Analysis in Institut Teknologi Bandung Ganesha Campus

K N Fauzan[1,2]*, D Suwardhi[1,2], I Gumilar[1,3]

[1]Department of Geodesy and Geomatics Engineering, Faculty of Earth Sciences and Technology, Bandung Institute of Technology, 10 Ganesha Street, 40132 Bandung, Indonesia
[2]Remote Sensing and GIS Research Group, Faculty of Earth Sciences and Technology, Bandung Institute of Technology, 10 Ganesha Street, 40132 Bandung, Indonesia
[3]Geodesy Research Group, Faculty of Earth Sciences and Technology, Bandung Institute of Technology, 10 Ganesha Street, 40132 Bandung, Indonesia

*Corresponding author's e-mail: kamal.fauzan55@gmail.com

Abstract. Institut Teknologi Bandung has a vision as a World Class university. One of the strategy to reach the aforementioned vision is the improvement of international standard education and research infrastructure with the sustainable maintenance. Waterlogging is an infrastructure problem that always happens in ITB Ganesha campus. Digital Terrain Model is used to simulate waterlogging in ITB Ganesha campus. Digital Terrain Model can be created using various methods like LIDAR acquisition, photogrammetry acquisition, and terrestrial acquisition. Integration of all data can be used to improve the accuracy of the DTM. The aim of this research is to make accurate DTM from the integration of LIDAR, photogrammetry and terrestrial data with Thin Plate Spline transformation method. This study shows that integrated points cloud can be used to make the accurate Digital Terrain Model with 5 cm vertical accuracy around the control point area and 5-20 cm vertical accuracy outside the control point area. The transformation reliability test shows that Thin Plate Spline method has an accuracy of 20 cm. Multi Data Digital Terrain Model is used to make the simulation of flood and waterlogging in certain regions. The simulation fits to the actual condition when the water channel can be modelled by the Digital Terrain Model.

Keywords: Integration, Point Cloud, Transformation, Thin Plate Spline, DTM, Waterlogging.

1. Introduction

Institut Teknologi Bandung is a University that was founded on the 2nd March 1959. Its main campus is the location of Indonesia's first engineering school. As a university that has been operating for almost a century, ITB has a vision as a World Class University as mentioned in ITB Strategic Plan for 2016-2020 period. One of the strategies used to reach the aforementioned vision is the increase of education infrastructure and international standard research with continuous maintenance. However, the aforementioned strategy has not been implemented to its full extent and still has its weaknesses. A few of these weaknesses are the capacity of education infrastructure and research to optimize academic productivity has not been optimized and the continuous maintenance of education infrastructure has not been carried out.

An infrastructural problem often faced by ITB Ganesha Campus is waterlogging in certain areas after high intensity rain. This phenomenon has a negative impact on the infrastructure of the campus such as damage to the road which may cause the bond between the aggregate and asphalt to weaken [1]. Digital Terrain Model (DTM) data is needed to simulate waterlogging.

At present there are many developing geospatial technologies used to create DTM. Technology LIDAR is a method that is widely used to create the DTM because it has high resolution. But the available LIDAR data has low accuracy of 30-50 cm for horizontal accuracy and 5-15 cm for vertical accuracy. Besides the available LIDAR data from ITB Ganesha Campus is a result of the acquisition in 2013. Other methods that can be used in creating DTM are photogrammetric and terrestrial methods.

Photogrammetric method is widely used because it is easier to use and has a lower cost compared to other methods.
The Digital Terrain Models made from each the method is considered unable to represent the actual situation of the ground, so height data integration is necessary. This is done by integrating the data acquired by LIDAR method with height data acquired by other methods to improve accuracy and suitability of the Digital Terrain Model made. Integration with height data acquired by photogrammetry has the purpose of perfecting regions which changes while integration with height data from the acquisition by terrestrial method has a purpose to improve vertical accuracy of LIDAR data.

2. Data and Method
The primary data used in this study are LIDAR point cloud data, photogrammetric point cloud data, and terrestrial height data. Additional data used are precise undulation data of ITB Ganesha Campus and the Waterlogging that has occurred. The method scheme of this research is as following in figure 1.

2.1. Equalization of Vertical Reference
Ground elevation data from terrestrial acquisition results are in the geoid vertical reference system, while LIDAR point cloud data and photogrammetric point cloud are in the vertical ellipsoid reference system. Therefore, the equalization of vertical reference must be done using the precise undulation data of ITB Ganesha campus. The accurate geoid is obtained by GPS/levelling method.

2.2. Planimetric Validation
Planimetric validation is done to ascertain the values of X and Y coordinates from LIDAR point cloud data, photogrammetric point cloud data, and terrestrial height data are in the same horizontal reference system. The data that was first validated is between cloud photogrammetric point data with terrestrial height data. Validation is done using Agisoft Photoscan software by placing samples of horizontal and vertical control points in ITB Ganesha Campus on Agisoft Photoscan software. Approximate coordinate results obtained from Agisoft Photoscan are compared to the actual coordinates and RMSE values are calculated from the difference in coordinates.
After obtaining an RMSE value that meets tolerance, planimetric validation between photogrammetric data with LIDAR data is done. Planimetric validation is done using Digital Surface Model (DSM) from photogrammetry data with LIDAR data. Validation is done at several roofs of buildings by looking at the cross section formed from both data and compared to the cross-sectional shape formed from both DSMs. From the cross section, the suitability of the planimetric position of the LIDAR point cloud data and photogrammetric point cloud can be seen.

2.3. RMSE of ICP Height Difference Calculation
To test the reliability of the Thin Plate Spline transformation, the transformation process is carried out with different amounts of control points. The first transformation is done using 21 points as GCPs that are spread evenly on all campus areas and other terrestrial points are used as ICPs. The second transformation is done using 54 points as GCPs and other points as ICPs. The third transformation is done by using around 2000 points as GCPs and around 3000 points as ICPs. After transformation with the number of control points as mentioned above, RMSE values are calculated at each ICP point.

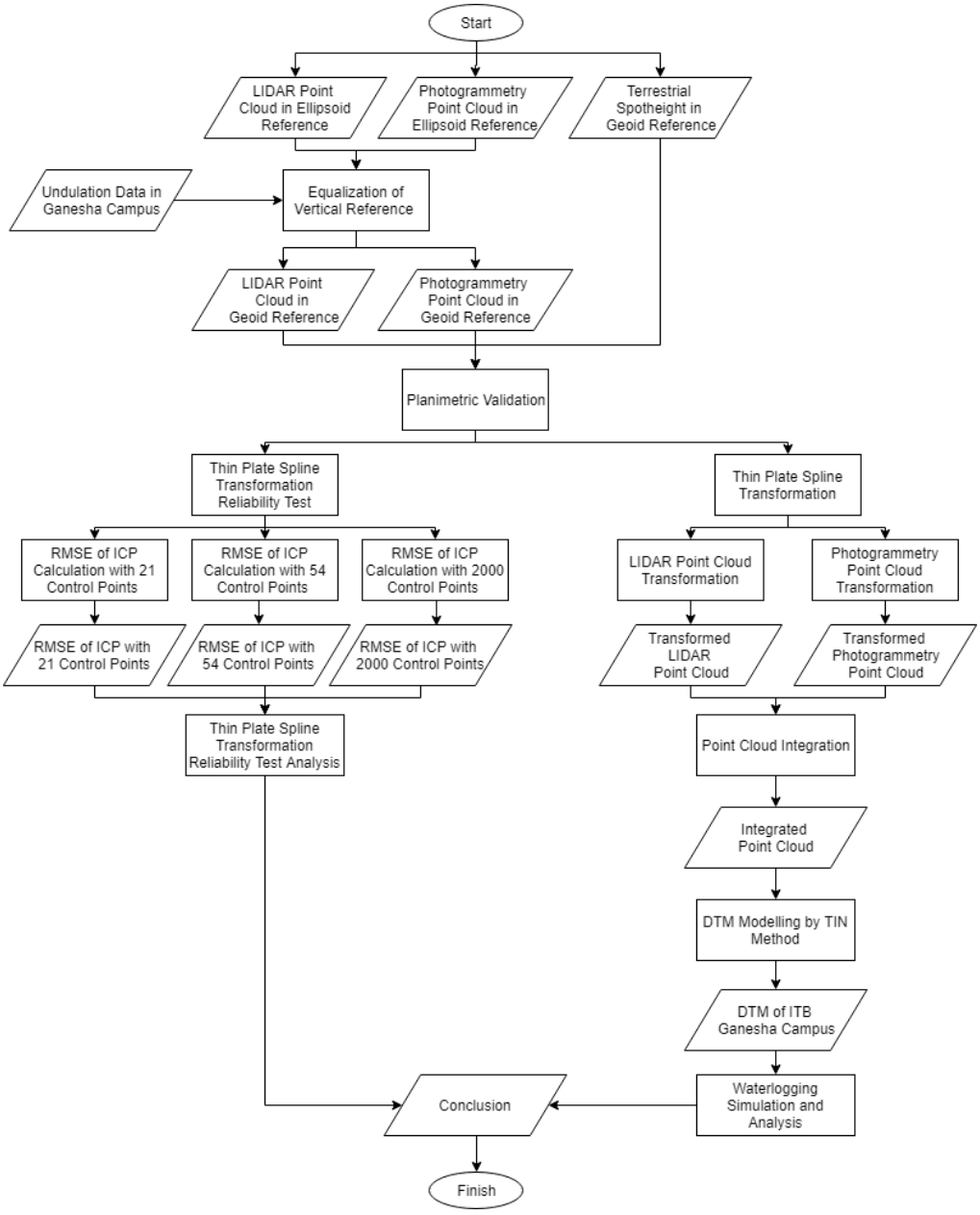

Figure 1. Flowchart of research method**.**

2.4. Thin Plate Spline Transformation Using All Control Points

After testing the reliability of Thin Plate Spline for some control points, then the Thin Plate Spline transformation is carried out using all terrestrial control points available. But in some places there are terrestrial points which have very close distance but have significant difference in height values which affects the transformation process, therefore these points are removed.

After the transformation process is done, the points from LIDAR and photogrammetry have height values equal to terrestrial height values so that it can be assumed that the accuracy of height values from LIDAR and photogrammetry are the same as the vertical accuracy of terrestrial points. LIDAR point cloud data and photogrammetric point cloud data resulting from TPS transformation are compared so that the difference in height is obtained between both data. The height values for both data can be analyzed from the transformation process.

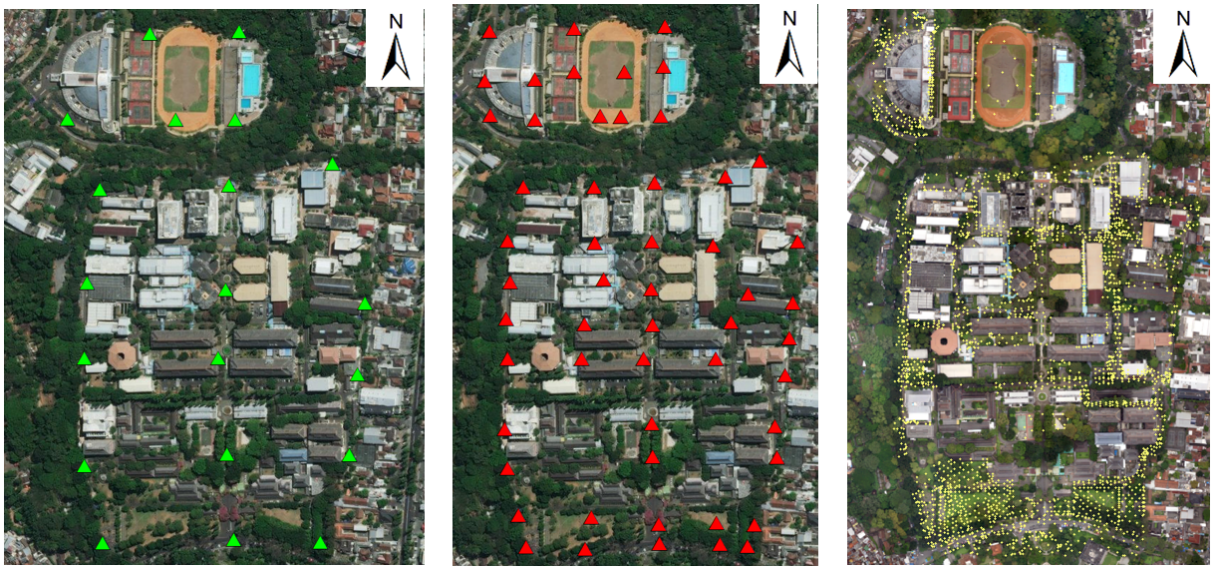

(a) (b) (c)

Figure 2. Distribution of control points for reliability test (a) 21 control points, (b) 54 control points, and (c) 2000 control points**.**

2.5. Integration Process and DTM Modelling by TIN Method

The next process is to integrate the data. Photogrammetric data is used in areas that have complicated details such as tunnels and stairs. In addition, photogrammetric data are used in new buildings because the approved LIDAR data cannot represent the height of these areas due to changes that occur. After getting the data, point clouds that have been integrated, the next step is to do gridding, LIDAR points and photogrammetry that have been transformed using the Global Mapper 17 software.

The gridding process is done using the TIN method. The resulting DTM still has a lot of noise needed to continue the process of smoothing the integrated point cloud data. In addition to the smoothing process, the process undertaken is to approve building breaklines data on the DTM. After the two processes are carried out, the resulting DTM is mostly displayed in the field.

2.6. Waterlogging Simulation

The DTM integration results that have been made are then used to conduct a waterlogging simulation on the ITB Ganesha Campus using the HEC-GeoRAS 10.5 extension on ArcGIS 10.5 software and HEC-RAS software 5.0.7. The area used for flood simulation research is the area of the FITB Building, TL Building, and Boluevard. HECGeoRAS is used to make geometric models of channels or rivers. The geometry illustrated is the channel groove, edge ducts, main grooves and banks, and cross-rivers. The geometry is stored in different layers already available in the HEC-GeoRAS feature. The creation of geometry is done by digitizing the geometries that have been explained earlier. After geometry is formed, all of the geometry is exported in a readable format by HEC-RAS 5.0.7 software.

The geometry that has been made on the HEC-GeoRAS extension is then imported into HEC-RAS 5.0.7 software for flood and Waterlogging simulation. The steps are to make a project from the simulation that has been done, importing channel geometry data, importing river flow data, and finally executing a flow simulation at each channel. The necessary planned simulation parameters are flood discharge, manning coefficient, and current water level during the flood.

After the simulation was carried out on HEC-RAS 5.0.7, the simulation results are displayed on the RAS Mapper menu on the same software. Waterlogging simulation results that are formed can be seen on the RAS Mapper display. Waterlogging simulation results are then compared to the actual situation.

3. Results and Discussion

3.1. Equalization of Vertical Reference System

After the vertical reference equalization process, height difference between data still exists. The statistical difference between LIDAR height with terrestrial height and between photogrammetric and terrestrial heights generated after a vertical reference system equalization can be seen in Table 1.

Table 1. Vertical difference between LIDAR and Photogrammetry Point Cloud to Terrestrial Spotheight.

	LIDAR to Terrestrial	Photogrammetry to Terrestrial
Maximum (m)	3.828	2.044
Minimum (m)	-2.953	-1.885
RMSE (m)	**0.587**	**0.455**

The difference in height can be seen visually from the cross section taken from Global software Mapper 17 in several areas. The blue dashed line shows a cross section of LIDAR data, the dashed red line shows the terrestrial data and the green dotted line shows the photogrammetry data. The cross section can be seen in Figure 3.

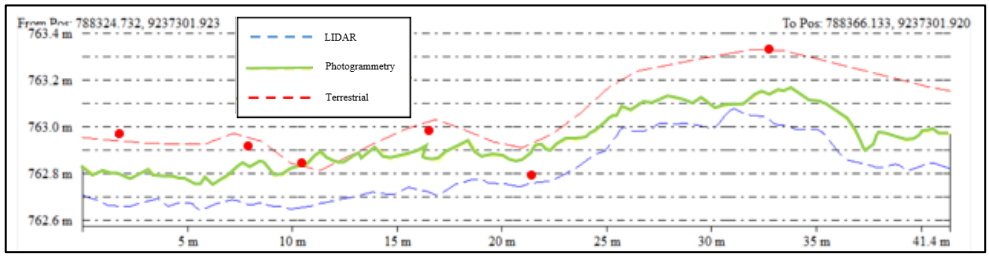

(a)

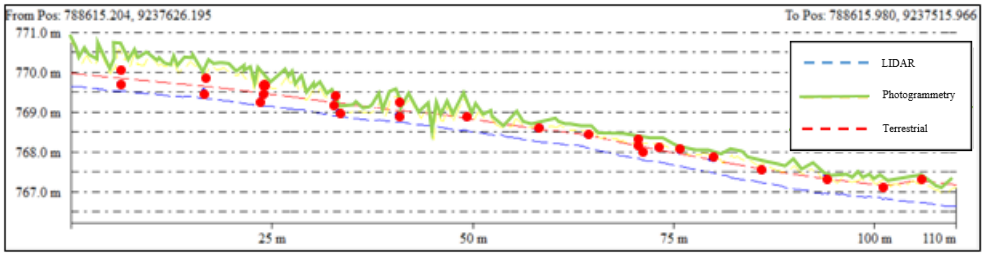

(b)

Figure 3. Cross section from the different place in ITB before transformation (a) Civil Field and (b) J Street.

From the three cross section samples above, it is apparent that there are still significant height differences in data although all three data are already in the same vertical reference system. For this reason, further transformation process is needed so that the height value of the three data the same.

3.2. Planimetric Validation

The planimetric validation process is performed on terrestrial and photogrammetric point cloud height data first. The RMSE value from the difference in horizontal coordinates of terrestrial and photogrammetric data can be seen in Table 2.

Table 2. Horizontal Difference between Terrestrial Spot height and Photogrammetic Point Cloud.

Points Name	Northing Topo	Easting Topo	Northing Photo	Easting Photo	ΔN (m)	ΔE (m)	ΔN²	ΔE²
BM01	9237309.476	788391.911	9237309.401	788391.933	0.074	-0.022	0.0056	0.0004
ITB23	9237334.568	788485.427	9237334.530	788485.456	0.038	-0.029	0.0014	0.0008
ITB28	9237760.415	788495.726	9237760.381	788495.743	0.034	-0.017	0.0011	0.0002
ITB93	9237337.778	788531.147	9237337.753	788531.214	0.025	-0.067	0.0006	0.0040
ITB29	9237777.910	788549.316	9237777.912	788549.360	-0.002	-0.044	0.0000	0.0010
ITB85	9237189.394	788271.539	9237189.220	788271.505	0.173	0.034	0.0300	0.0010
Σ							0.0390	0.0090
∑ / n							0.0060	0.0010
RMSE (m)							0.0800	0.0390
Total RMSE (m)								**0.0634**

Next. planimetric validation process is carried out for LIDAR and photogrammetric point cloud data. The validation process is done using DSMs from both data and seeing the cross section of several roofs of the building at the ITB Ganesha Campus. Roof shape buildings generated by both DSM data can be seen in Figure 4.

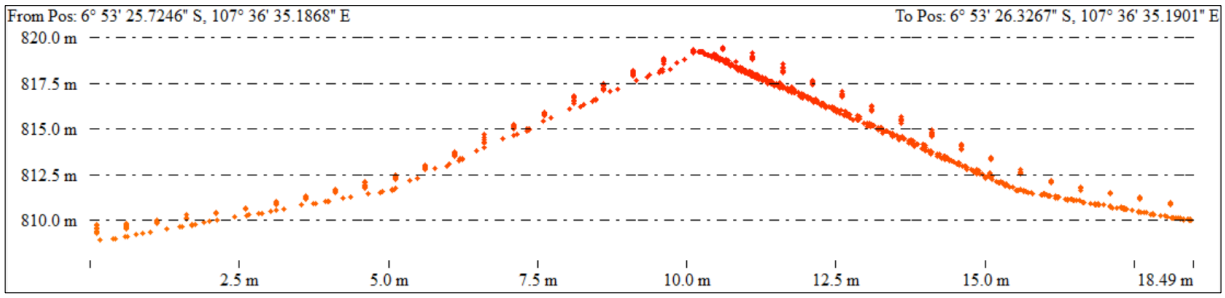

(a)

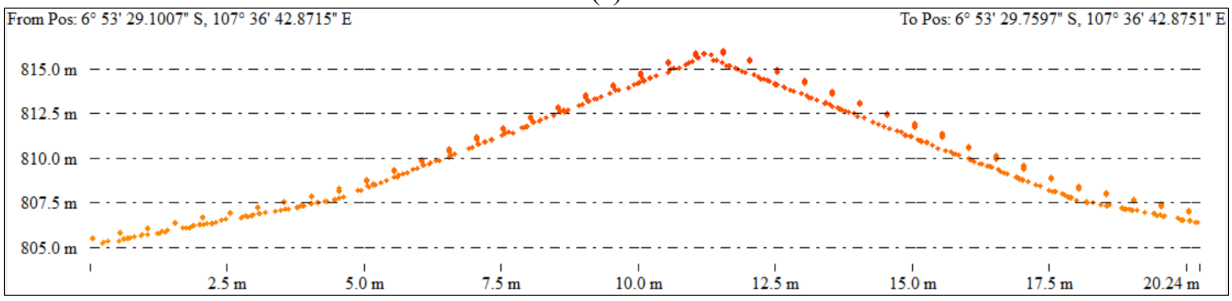

(b)

Figure 4. Cross section of LIDAR and photogrammetric data of building roof (a) Labtek V Building and (b) Labtek IX-C Building.

The horizontal reference system equalization in terrestrial and photogrammetry data is done using Agisoft software. The results of planimetric validation between terrestrial photogrammetry data and terrestrial data can be shown quantitatively so RMSE differences in planimetric coordinates between data can be clearly shown. The RMSE value difference between terrestrial planimetric coordinates and photogrammetry planimetric coordinates is 0.0634 m. This value is considered to already meet the tolerance used which is 2 pixels or equal to 10 cm.

The planimetric validation between LIDAR data and photogrammetric data are shown qualitatively through the roof form of several sample buildings in ITB Ganesha Campus. Validation results cannot be shown quantitatively so the result of validation can not show whether it meets tolerance or not. This is because LIDAR data cannot show clearly the position of the control points from the terrestrial data used.

3.3. Transformation Reliability Test

Transformation method used to transform LIDAR point cloud and photogrammetric point cloud data is the Thin Plate Spline transformation method. To test the reliability of transformation results, the difference in RMSE was calculated between the coordinates of the ICP height as a result of transformation with actual ICP height coordinates. ICP calculations are performed by using different GCP amounts, 21 GCP points, 54 GCP points, and 2000 GCP points. This is done to find out how many GCP points are needed to obtain an ICP RMSE that meets tolerance.

The statistical difference of actual ICP height coordinates with the ICP height coordinates as a result of transformation using 21, 54, and 2000 GCPs can be seen in Table 3.

The first transformation is carried out using 21 points as GCPs and other points as ICPs. The ICP RMSE value obtained is equal to 0.493 m for LIDAR data and 0.596 for photogrammetric data. This value shows that transformation of Thin Plate Spline in an area as large as the ITB Campus Ganesha using only 21 points results in bad transformation. The RMSE value indicates that there is a convex shape on the surface where there are no control points because in principle Thin Plate Spline transformation forces one point on the surface to be the same as the control points in the area causing deformation on the surrounding surface.

Table 3. Vertical RMSE of ICP for (a) 21 control points, (b) 54 control points, and (c) 2000 control points.

(a)

	LIDAR	Photogrammetry
Maximum (m)	1.212	3.660
Minimum (m)	-0.966	-2.780
RMSE (m)	**0.314**	**0.300**

(b)

	LIDAR	Photogrammetry
Maximum (m)	0.874	3.179
Minimum (m)	-0.875	-2.325
RMSE (m)	**0.317**	**0.290**

(c)

	LIDAR	Photogrammetry
Maximum (m)	0.789	2.465
Minimum (m)	-0.974	-2.460
RMSE (m)	**0.218**	**0.112**

Subsequent experiments were carried out using 54 points as GCPs and other points as ICPs. The ICP RMSE value obtained is equal to 0.441 m for LIDAR data and 0.581 m for photogrammetric data. This value is not significantly different with the RMSE ICP value of the transformation process using 21 points. This can be seen from the comparison of the cross section generated by both methods. That surface produced has relatively the same shape and the deformation effect from the surface produced is not significantly different. The cross section can be seen in Figure 4. The cross section is taken from

one control point to another. So, it can be shown that the beginning and the end of the cross section coincide with each other but there are differences in height in the area between the control points.
In the final experiment, the transformation was carried out using 2000 points as GCPs and other points as ICPs. There is a significant decrease in the RMSE value but the RMSE results obtained did not meet tolerance given is 0.273 m for LIDAR data and 0.274 for photogrammetric data. This value is not in accordance with the vertical accuracy of the LIDAR used. Distance between one control point to other control points are in the range of 5-15 m. For obtaining an RMSE value that matches tolerance requires denser control points, around 1-5 m apart from each other. The surface shape as a result of the transformation using 2000 control points is different from the results of the transformation using 21 and 54 control points. This is due to many points on the surface which adjust to the terrestrial control points used.

3.4. All Control Points Transformation

Processing results in the vertical reference equalization step shows there are still significant differences in height coordinates between LIDAR point cloud data with terrestrial data and photogrammetric point cloud data with terrestrial data. So that the transformation process of LIDAR data and photogrammetric data is necessary so that the height values of the two data are equal with terrestrial data. All terrestrial data are used as control points for the Thin Plate Spline transformation.
After the point cloud is transformed, the next step is calculating the residual value of the difference in height of terrestrial control points with the height of LIDAR point clouds and photogrammetric point clouds resulting from transformation. Residual statistics that are generated by the transformation process can be seen in Table 4. The residual value has not met the existing tolerance so that some control points which contain errors are removed.

Table 4. Residual value of GCP in LIDAR and photogrammetry in the first iteration**.**

	LIDAR	Photogrammetry
Maximum (m)	1.125	1.772
Minimum (m)	-1.663	-1.735
Residual (m)	**0.076**	**0.105**

The control points assumed to contain an error are control points that have a short distance but have a very large difference in height so that one data point the control must be removed. In addition to this, dummy control points are added to Sarana Olahraga Ganesha area because there are few control points in the area and affect the results of the transformation.
After the point clouds are transformed, the next step is calculating the residual value of the difference in height of terrestrial control points with the height of LIDAR point clouds and photogrammetric point clouds as a result of transformation.

Table 5. Residual value of GCP in LIDAR and photogrammetry in the second iteration**.**

	LIDAR	Photogrammetry
Maximum (m)	0.194	0.497
Minimum (m)	-0.487	-0.341
Residue (m)	**0.016**	**0.019**

Transformation method used to transform the position of the LIDAR point cloud and the photogrammetric point cloud into terrestrial reference system Thin Plate Spline transformation method. In the first iteration, the transformation process is carried out by using all terrestrial control points overlapping with LIDAR cloud points and photogrammetry cloud points. As explained in the results section that the residual value of the different control points used with the transformation points does not meet the tolerance. The residual tolerance used is 0.020 m. The residue that does not meet the

tolerance is due to points that are close together but have height values that are significantly different which affects the shape of the point cloud produced in the transformation process. Other factors that influence the results of Thin Plate Spline transformation is the density of the control points.

3.5. TIN Method Gridding Result

LIDAR point clouds and photogrammetric point clouds that have undergone the Thin Plate Spline transformation process and already has residual values that meet tolerance are then processed with gridding process on Global Mapper to generate DTM data in TIN format. Gridding of LIDAR data and photogrammetry data can each be seen in Figure and Figure respectively.

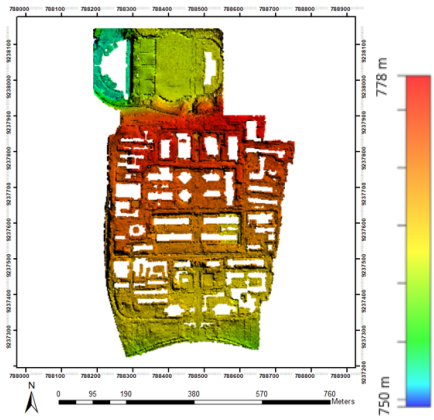

Figure 5. LIDAR Gridding DTM.

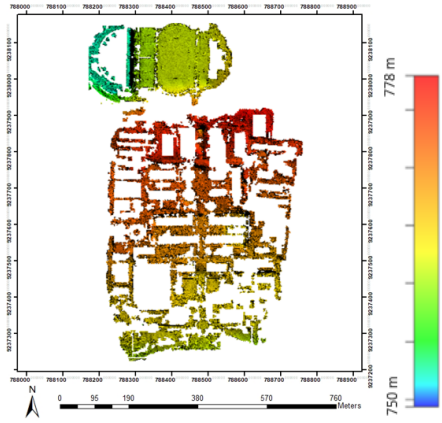

Figure 6. Photogrammetric Gridding DTM.

3.6. Photogrammetry and LIDAR Point Cloud Difference

LIDAR point cloud data and cloud photogrammetric point data have undergone the process of Thin Plate Spline by using all control points are then used to calculate the difference in height between the two data. This difference value is to analyze the Thin Plate Spline transformation that has been done. The RMSE value of the difference in height is 0.402828 m. The results of the transformation can be seen visually from the cross-section transverse taken in Global Mapper 17 software in some regions as samples in Figure 7.

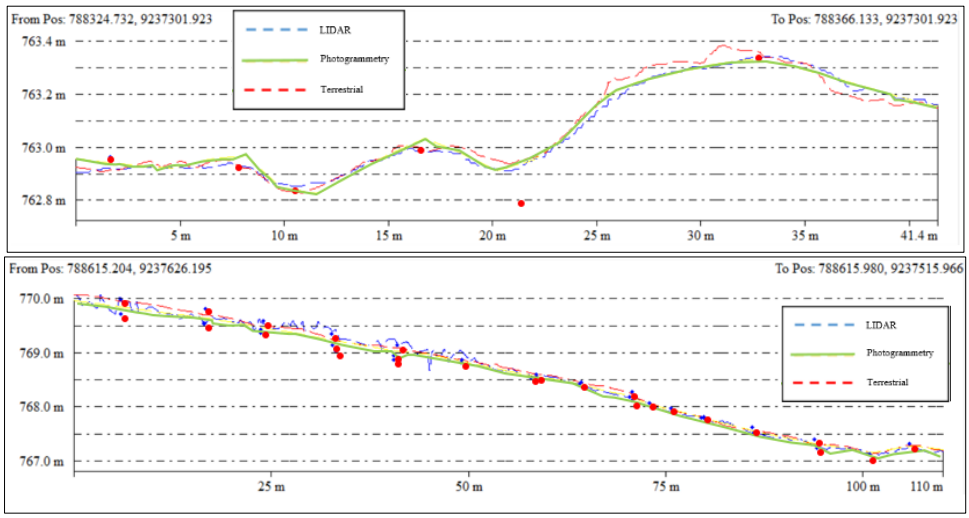

Figure 7. Cross section from the different place in ITB after transformation (a) Civil Field and (b) J Street.

In some places that have a large ICMS RMSE value for example at the boundary between Taman Sari Street and ITB the integration results do not coincide well as shown in Figure 8.

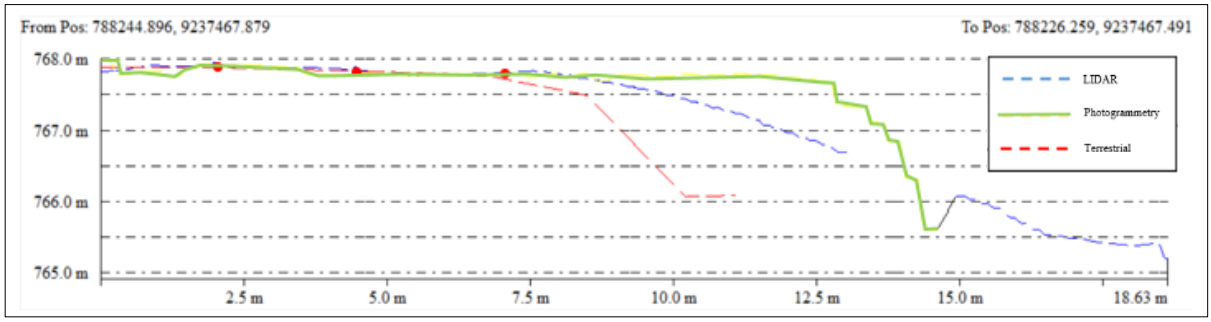

Figure 8. Cross section from the place that has high ICP RMSE.

3.7. Point Cloud Integration

Each data used has its own advantages; hence an integration process is necessary to obtain a representative DTM. Photogrammetric data is used in regions which has complicated details such as tunnels and stairs. In addition, photogrammetric data is used in the building area new because LIDAR data is deemed incapable represents the height of these areas because changes that have occured. Photogrammetric cloud point data which are used in the integration process can be seen in Figure 9.

After the integration process is done, the next process is gridding using the points that have already been integrated. The resulting DTM still has a very rough shape because the number of point clouds used is very large so it must go through a smoothing process. Besides smoothing the DTM also requires building breaklines data which is made continuous. DTM and contour as a result of the addition of breaklines can be seen in Figure 10 and Figure 11.

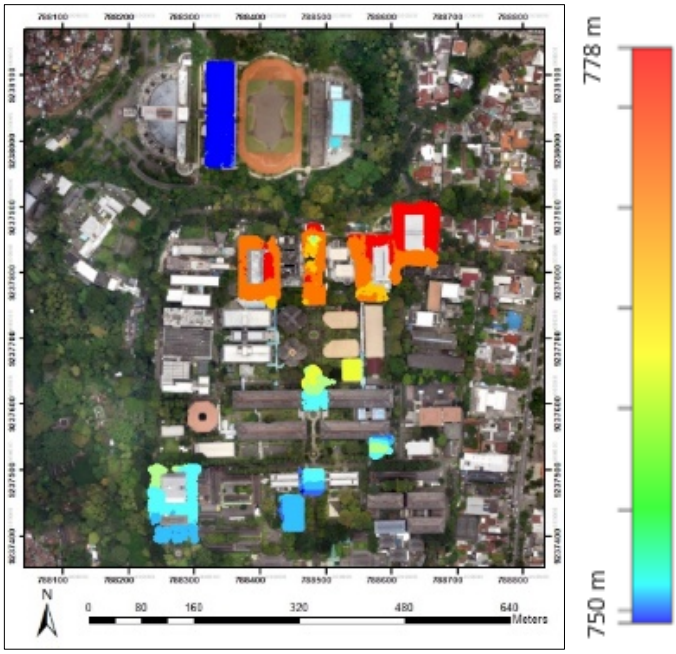

Figure 9. Photogrammetric point cloud that is used in integration process.

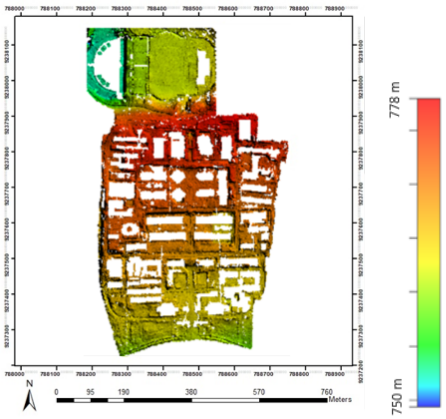

Figure 10. Integrated DTM before smoothing.

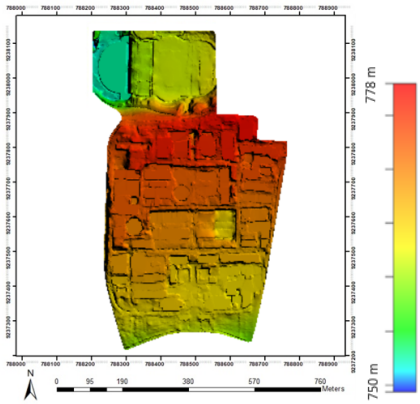

Figure 11. Integrated DTM after smoothing.

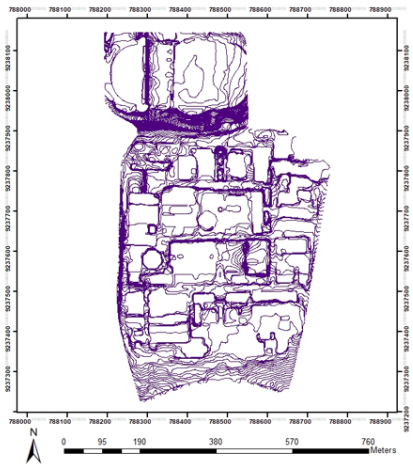

Figure 12. Final contour map.

In this study three different height data were used namely LIDAR point cloud data, photogrammetric point cloud data, and terrestrial height data. Each data has different characteristics. This is due to the acquisition method of each data is different too. In the process of cloud point data integration, selection of cloud point data which represents the actual land surface is done to ensure the resulting DTM has high quality.

Photogrammetry cloud point data has more detailed characteristics compared to LIDAR data. In this case the level of photogrammetry cloud point detail points is better than LIDAR point cloud data which can be seen in certain places such as tunnels, Widya Plaza staircase, boulevard staircase, and Labtek VIII building parking lot. Therefore, in the process of integrating the entire cloud data points on these parts photogrammetric cloud point data is used because it better represents the actual condition of the land.

Photogrammetric cloud point data was acquired in 2016 while the LIDAR point cloud data was acquired in 2013. There is a 3 years times difference from LIDAR cloud point data acquisition to the photogrammetric cloud point data acquisition. In the 3 years difference several building developments occurred. Buildings that were built from 2013 to 2016 are the CADL building, CAS building, CRCS building, and CIBE building. The construction of buildings affects the shape of the ground around it building so that photogrammetric data is more reliable compared to LIDAR data in these areas.

Overall LIDAR point cloud data generates a smoother DTM. Hence, besides the photogrammetric point cloud data, LIDAR point cloud data is used. Besides that, roads are modeled better on the DTM with

LIDAR cloud point data. After the integration process is done, an intact cloud data on the entire ITB Ganesha Campus is formed. But some places which have high canopy cover do not have point cloud data so there is empty data on the area.

3.8. Waterlogging analysis

In the cloud waterlogging process simulation, the geometry is created in the GEC-GeoRAS 10.5 extension installed on ArcMap 10.5 software. The results of channel geometry in several sample regions can be seen in Figure 13. The light blue lines are the geometry of the channel's center line, the red lines are channel edge geometry, the blue lines are river geometry channels, and green lines show the channel's cross sections. The results of the Waterlogging simulation on HEC-RAS software as shown on RAS Mapper is as following.

(a) (b)

Figure 13. Comparison between waterlogging simulation and actual condition (a) FITB Building and (b) Environmental Engineering Building.

Waterlogging simulation in the FITB Building area does not give results that match the actual situation. While simulations carried out in the area TL Building and Boulevard ITB provide appropriate results with the actual situation. Incompatibility of simulation results with the actual conditions in the field are caused by some factors.

The first factor is the shape of the water channel used in when the simulation does not represent the actual state at field. LIDAR cloud point data and photogrammetric cloud point data are unable to model the drains that correspond to original state. This is caused by several causes. The first cause is the horizontal resolution of LIDAR data the result is smaller than the dimensions of water channels on the ITB Campus in Ganesha. According to Alexander (2017) based on existing as built drawing data, the bottom width of the existing channel is 28 cm and the average channel depth is 50.5 cm. LIDAR data which has a horizontal accuracy of 15-30 cm. Photogrammetric cloud point data has a better resolution and can even describe objects that are more detailed still cannot make a good channel model due to many channels on the ITB Campus of Ganesha which are under trees so the channel cloud point cannot be formed.

Other factors beside point cloud data are a few channels on the ITB Campus Ganesha are covered by iron or concrete so that the surface DTM produced does not model the channels properly.

The second factor is the value of flood discharge and manning coefficient used in the simulation on the HEC-RAS software use rough assumptions. The value of water discharge used is 0.0245 m3 / s based on the calculation performed by Alexander (2017) on his Thesis entitled "Study Implementation of Public Policy in Drainage Management in Bandung Ganesha Institute of Technology Campus". The Manning coefficient used is assumed to be the same on all channels. The Manning coefficient value used is 0.018; this value is the manning coefficient of concrete according to Manning (1889).

4. Conclusions

The integration of LIDAR cloud point data, photogrammetric cloud point data, and ITB Ganesha Campus terrestrial height data can produce a Ground Surface Model Digital that can represent the actual

state. To represent the actual situation means that the DTM has the right height value and describe objects correctly. Every data has their respective uses in the integration process. Terrestrial data is used as a reference value height of the LIDAR point cloud and photogrammetric point cloud data. Photogrammetric cloud point data is used in the area of new buildings. Besides this, photogrammetric data is used on complicated objects because photogrammetry has the ability to describe objects in a higher detail. LIDAR data is used in almost all regions because of LIDAR's ability to penetrate trees and form a cloud of ground point beneath it. The method of Thin Plate Spline transformation is not the best method to do point transformations due to producing a large bowl effect. The ICP RMSE using 2000 control points is 0.273 m and that value exceeds vertical accuracy from LIDAR data which is 0.05-0.15 m. The resulting Digital Soil Surface Model can be used for simulations in several places which have fairly large channel shape. While in areas that have dense canopy cover, channel shape cannot form on point clouds produced by photogrammetry as well as on point clouds produced on LIDAR.

5. References

[1] Nurhudayah, *STUDI GENANGAN AIR TERHADAP KERUSAKAN JALAN DI KOTA GORONTALO*. Simposium XII FSTPT, Universitas Kristen Petra Surabaya, 14 November 2009 2009. **XII**: p. 16.

Acknowledgments

The authors would like to thank the 3D MODIS Team, Mr. Irwan Gumilar's squad, and Mapping and Surveying laboratory assistants for helping me in data acquisition.

Determining the Zone of Potassium in Muria Mountain Using Landsat-8 Oli By Spectral Angle Mapper

A Zakiya[1]*, M Rindianingrum[1], N A H Harahap[1]

[1]Department of Geological Engineering, Universitas Diponegoro, Semarang, Indonesia

*Corresponding author's e-mail: askazakiya@gmail.com

Abstract. The abundance of potassium elements contained in feldspatoid minerals is a geological resource that is a prospect for making fertilizers in agriculture. The purpose of writing is to explore and determine the location on Mount Muria with potassium content which have the prospect especially for the people of Pati and around Mount Muria. The method used in this study is the interpretation of DEM and Landsat-8 OLI images using the Spectral Angle Mapper Classification (SAM) method to interpret the presence of mineral potassium from Mount Muria and also mapping around Muria Mountain as primary data. The Geological Agency through the Center for Mineral Resources, Coal and Geothermal Energy (PSDMBP) stated that Pati Regency is estimated have 665.37 million Tons of rock containing Potassium with higher quality than other Districts with K_2O content ranging from 1.92% dd. 8.79% weight. The results of the analysis show the distribution of potassium carrying minerals from rocks with feldspatoid content, namely Adularia, Biotite, Glauconite, Muscovite, Nepheline, and Orthoclase obtained in Landsat Images. It is expected that the potential of potassium carrier rocks in this area can be an alternative substitute for Potassium (NPK) fertilizer which has been imported.

Keywords: Muria, Potassium, SAM.

1. Introduction

Indonesia has considerable potential in terms of the availability of non-metallic minerals which have so many uses, one of which is as a supporter of food security. Non-metal minerals that have the potential to support food security include dolomite, phosphate, potassium-bearing rocks and limestone.

The three most important ingredients in plant growth are Nitrogen, Phosphate and Potassium. Natural fertilizers and factory fertilizers contain these three components. From the market analysis, fertilizer made from potassium is needed. Potassium carrier rocks can be used as raw material for natural potassium fertilizer. Potassium is found in relatively large amounts in most soils. In tropical regions such as Indonesia, potassium is easily lost due to decomposition and washing due to rainfall and high temperatures.

The distribution of potassium in Mount Muria can be known from the Landsat-8 OLI image using the SAM (Spectral Angle Mapper) method in the form of minerals Adularia, Biotite, Glauconite, Muscovite, Nepheline, and Orthoclase. Each of these minerals has a different emission to the image. It is expected that the potential of potassium-bearing rocks in this area can be an alternative to the potassium fertilizer (NPK) which is still imported. Potassium carrier rock is expected to have an impact on increasing agricultural productivity so that it can increase farmers' incomes and reduce government burdens by reducing the country's foreign exchange burden.

2. Experimental Method

The method used in this research is observation using remote sensing imagery as the main research, and taking some rock samples as evidence the presence of these minerals.

2.1. SAM Method (Spectral Angle Mapper)
SAM method carried out on Mount Muria is intended to determine the distribution of potassium minerals that exist in Mount Muria (covering 3 districts). Observation results with remote sensing found 6 types of potassium-carrying minerals, namely the minerals Adularia, Biotite, Glauconite, Muscovite, Nepheline, and Orthoclase.

2.2. Rock Sampling Method
Sampling was carried out at one point on the slopes of Mount Muria, especially in Pati Regency. Samples obtained in the form of lava with porphyry Andesite rock types.

3. Results and Discussion
The results and discussion that will be discussed include the work steps and appearance of each mineral that has been processed from the results of the DEM shapefile (Digital Elevation Model) and a little discussion about the results of primary data collection in the form of porphyry Andesite lava. The SHP / shapefile is entered into the ENVI application together with Landsat-8 OLI by selecting the appearance of images that are clean from clouds and other disturbances. After Landsat is cut with SHP from DEM, then corrections are made using the QUAC (Quick Atmospheric Correction) method for radiometric correction of Landsat images. After radiometric correction, Band Math is performed to enter the formula so that the maximum value on the Compute Statistics curve becomes 1. The Band Math formula is as follows:

$$(b1\ le\ 0)*0+(b1\ ge\ 10000)*1+(b1\ gt\ 0 \text{ and } b1\ lt\ 10000)*\text{float}(b1)/10000 \quad (1)$$

After correction, then do SAM (Spectral Angle Mapper) with the provisions of the spectral library used to import minerals - the minerals come from "usgs_min" on the local disk c. then import all the feldspatoid minerals. The following is the SAM results for each mineral (Figure 1).
After selecting minerals with feldspatoid content, the results obtained as in the picture above. The map consists of three districts, namely Jepara Regency, Kudus Regency, and Pati Regency. In each district has a different abundance. According to data from The Geological Agency through the Centre for Mineral Resources, Coal and Geothermal Energy (PSDMBP) stated that Pati Regency is estimated to have 665.37 million Tons of rock containing Potassium with higher quality than other Districts with K_2O content ranging from 1.92% dd. 8.79% weight. The results of the analysis show the distribution of potassium carrying minerals from rocks with feldspatoid content, namely Adularia, Biotite, Glauconite, Muscovite, Nepheline, and Orthoclase obtained in Landsat Images.
Each mineral shows different SAM intensity, and there is a tendency that in Pati Regency has the spread of the density of feldspatoid minerals which is more abundant compared to the Kudus and Jepara regions. The results obtained from primary data collection as supporting data obtained the presence of porphy Andesite lava (figure 2) consisting of biotite minerals as a support for the presence of feldspatoid. The rock sample was taken in Gembong, Pati Regency.

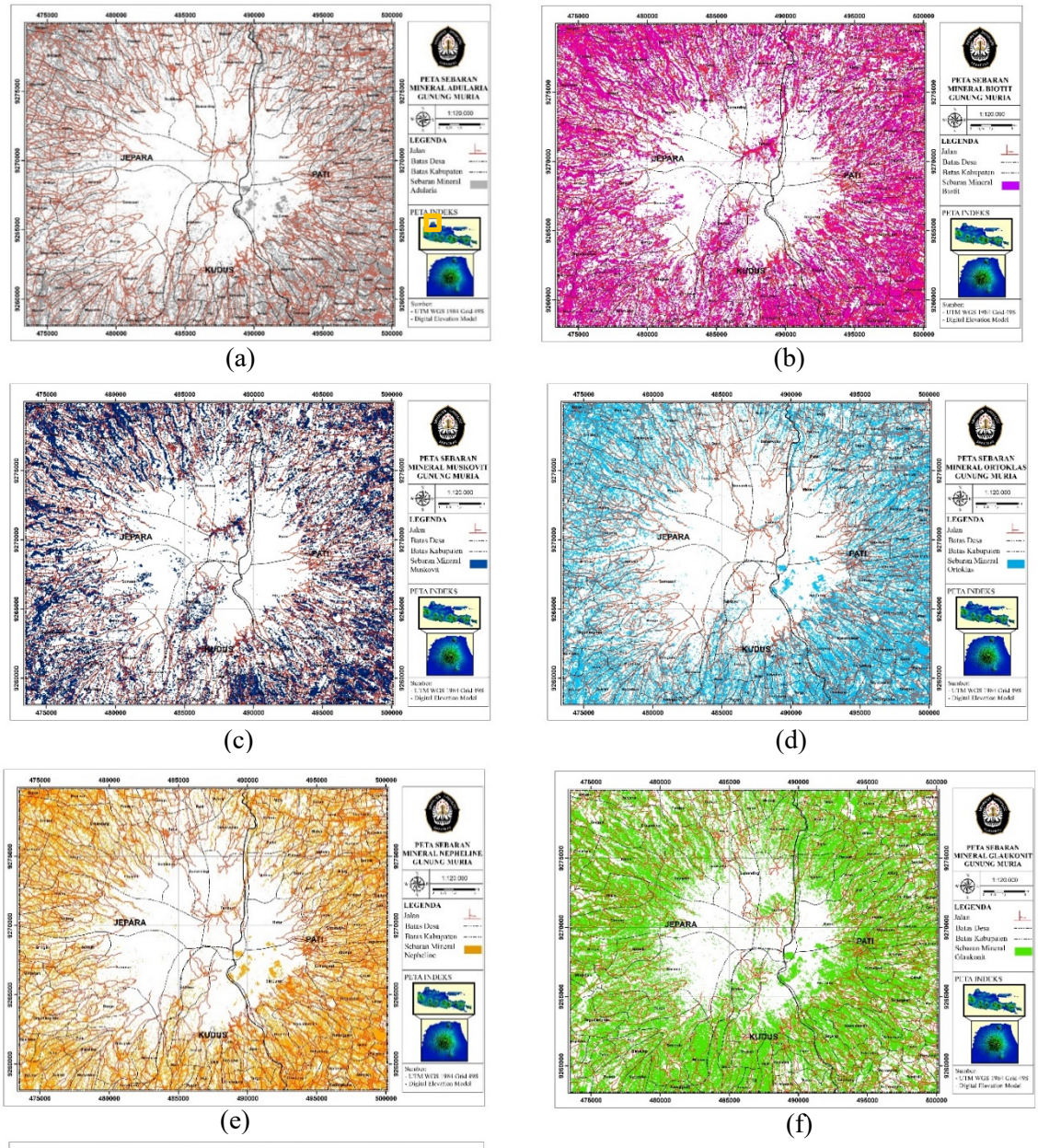

Figure 1. Displays the distribution of potassium-carrying minerals around Mount Muria and its surroundings. Figure (a) distribution of adularia minerals, (b) distribution of biotite minerals, (c) distribution of muscovite minerals, (d) distribution of orthoclase minerals, (e) distribution of nepheline minerals, (f) distribution of glauconite minerals, and (g) distribution of combined mineral potassium carrier minerals.

In the appearance of each mineral, certain locations that have a maximum distribution of feldspatoid minerals are summarized in the following table:

Table 1. Location of Feldspatoid Mineral's Tendency.

Feldspatoid Mineral	Location
Adularia	Jepara: Bangsri, Tengguli, Guyangan, Banjaran, Kepuk, Plajan, Tanjung, Rajekwesi, Datar, Ngroto, Buaran Kudus: Tergo, Cranggang, Menawan, Soco, Puyoh, Kajar, Colo, Kuwukan, Japan, Piji Pati: Gerit, Gesengan, Grogolan, Bancak, Perdopo, Gajihan, Gadu, Jepalo, Sampok, Sidomulyo, Tegalarum, Mojo, Bleber, Klumpit, Gunungsari, Cabak, Sitiluhur, Tanjungsari, Lahar, Klakankasian, Bageng, Ketanggan, Guwo, Purwosari, Pohgading, Gembong, Wonosekar, Semirejo, Kedungbulus
Biotite	Jepara: Bangsri, Tengguli, Guyangan, Banjaran, Kepuk, Plajan, Tanjung, Rajekwesi, Datar, Ngroto, Buaran (hampir seluruh bagian kabupaten Jepara) Kudus: Tergo, Cranggang, Menawan, Soco, Puyoh, Kajar, Colo, Kuwukan, Japan, Piji (hampir seluruh Kabupaten Kudus) Pati: Gerit, Gesengan, Grogolan, Bancak, Perdopo, Gajihan, Gadu, Jepalo, Sampok, Sidomulyo, Tegalarum, Mojo, Bleber, Klumpit, Gunungsari, Cabak, Sitiluhur, Tanjungsari, Lahar, Klakankasian, Bageng, Ketanggan, Guwo, Purwosari, Pohgading, Gembong, Wonosekar, Semirejo, Kedungbulus (seluruh Kabupaten Pati)
Muscovite	Jepara: Bangsri, Tengguli, Srikandang, Pendem, Guyangan, Banjaran, Kepuk, Plajan, Tanjung, Rajekwesi, Datar, Ngroto, Buaran Kudus: Tergo, Cranggang, Rahtawu, Japan Pati: Gerit, Gesengan, Grogolan, Bancak, Perdopo, Gajihan, Gadu, Jepalo, Sampok, Sidomulyo, Tegalarum, Mojo, Bleber, Klumpit, Gunungsari, Cabak, Tanjungsari, Lahar, Klakankasian, Bageng, Ketanggan, Guwo, Purwosari, Pohgading, Gembong, Wonosekar, Semirejo, Kedungbulus
Nepheline	Jepara: Bangsri, Tengguli, Guyangan, Banjaran, Kepuk, Plajan, Tanjung, Rajekwesi, Datar, Ngroto, Buaran (hampir seluruh bagian kabupaten Jepara) Kudus: Tergo, Cranggang, Menawan, Soco, Puyoh, Kajar, Colo, Kuwukan, Japan, Piji (hampir seluruh Kabupaten Kudus) Pati: Gerit, Gesengan, Grogolan, Bancak, Perdopo, Gajihan, Gadu, Jepalo, Sampok, Sidomulyo, Tegalarum, Mojo, Bleber, Klumpit, Gunungsari, Cabak, Sitiluhur, Tanjungsari, Lahar, Klakankasian, Bageng, Ketanggan, Guwo, Purwosari, Pohgading, Gembong, Wonosekar, Semirejo, Kedungbulus (seluruh Kabupaten Pati)
Glaukonite	Jepara: Bangsri, Tengguli, Guyangan, Banjaran, Kepuk, Plajan, Tanjung, Rajekwesi, Datar, Ngroto, Buaran (hampir seluruh bagian kabupaten Jepara) Kudus: Tergo, Cranggang, Menawan, Soco, Puyoh, Kajar, Colo, Kuwukan, Japan, Piji (hampir seluruh Kabupaten Kudus) Pati: Gerit, Gesengan, Grogolan, Bancak, Perdopo, Gajihan, Gadu, Jepalo, Sampok, Sidomulyo, Tegalarum, Mojo, Bleber, Klumpit, Gunungsari, Cabak, Sitiluhur, Tanjungsari, Lahar, Klakankasian, Bageng, Ketanggan, Guwo, Purwosari, Pohgading, Gembong, Wonosekar, Semirejo, Kedungbulus (seluruh Kabupaten Pati)
Orthoclase	Jepara: Bangsri, Tengguli, Guyangan, Banjaran, Kepuk, Plajan, Tanjung, Rajekwesi, Datar, Ngroto, Buaran (hampir seluruh bagian kabupaten Jepara) Kudus: Tergo, Cranggang, Menawan, Soco, Puyoh, Kajar, Colo, Kuwukan, Japan, Piji (hampir seluruh Kabupaten Kudus) Pati: Gerit, Gesengan, Grogolan, Bancak, Perdopo, Gajihan, Gadu, Jepalo, Sampok, Sidomulyo, Tegalarum, Mojo, Bleber, Klumpit, Gunungsari, Cabak, Sitiluhur, Tanjungsari, Lahar, Klakankasian, Bageng, Ketanggan, Guwo, Purwosari, Pohgading, Gembong, Wonosekar, Semirejo, Kedungbulus (seluruh Kabupaten Pati)

Figure 2. The Presence of biotite in Porphyry Andesite as a Feldspatoid Mineral.

4. Conclusions

Based on the results of data processing by Landsat 8 OLI and the results of evidence in the field, it was found that there were potassium carrier minerals around Muria Mountain that could be used as raw material for fertilizer production. The abundance that is around Mount Muria in quantity based on PSDMBP data, the element of potassium reaches 11.76 billion tons spread in three districts. And according to the location of the distribution of the most potassium is in Pati Regency.

Acknowledgments

This multidisciplinary literature review has been supported by several specific discussions in various fields. Authors wishing to encouragement from colleagues and special work with Government about this research.

Geodatabase Masterplan of Mangrove Forests in Indonesia Based on the Indonesian Geographical Element Catalog

Yusuf Hary Saputro[1]*, Soni Darmawan[1]

[1]Geodesy Engineering, Institut Teknologi Nasional, PH.H. Mustofa Street, 40124 Bandung, Indonesia

*Corresponding author's e-mail: soni_darmawan@itenas.ac.id

Abstract. The current degradation of mangrove forests is a phenomenon commonly found in developing countries such as Indonesia. Indonesia through the Ministry of Forestry has a national strategy program in the management of mangrove ecosystems (SNPEM) in Indonesia. SNPEM is an effort in the form of policies and programs to realize the management of mangrove ecosystems. However, in terms of the National Strategy for Mangrove Ecosystem Management not only mangrove mapping but also needs to be emphasized on the availability and guarantee of structured, interconnected and well integrated data and need to make masterplan geodatabase of mangrove forests. This study aims to identify spatial data and data attribute need and build a mangrove forest geodatabase to help mangrove ecosystem management. The stages of implementation include preparation from theoretical studies related with research, identification of data based on legislation and research report, normalitation of data obtained to eliminate redundacies, and database design of data entities, logical data entities to physical entities data and attributes of geodatabase design of mangrove forest in Indonesia. The result of this study is establishment of mangrove forest geodatabase in Indonesia from 9 data and 5 custodians.

Keywords: Mangrove Forest, The National Strategy for Mangrove Ecosystem Management, Geodatabase.

1. Introduction

Mangrove forest is one of the aquatic ecosystems with a number of specific environmental services, functions and ecological conditions [1]. According to Presidential Regulation No. 73 of 2012 concerning national strategies for mangrove management, mangrove ecosystems are a unity between mangrove vegetation communities associated with fauna and micro-organisms so that they can grow and develop in areas along the coast, especially in tidal areas, lagoons, river mouths that are protected with substrates mud or sandy mud in forming a sustainable environmental balance. Mangrove forests have a significant role in terms of adapting and mitigating climate change, including sources of livelihoods, food security, protection from storms and floods [1]

Indonesia is the largest archipelagic country in the world, with a coastline of more than 95,181 km, with a coastline along it, coastal resources continuously support the lives of most of Indonesia's population [2]. Based on official data from the Ministry of Forestry of the Republic of Indonesia in 2013, Indonesia's mangrove area is currently 3.2 million hectares. Previously, Indonesian mangroves were estimated at 4.2 million hectares and due to mismanagement of deforestation, it was estimated that from 1980-2005 the deforestation rate was 52,000 hectares per year. Mangrove forest degradation is currently a phenomenon that is commonly found in several countries, especially in developing countries such as Indonesia. Some of these mangroves suffered damage due to overexploitation and lack of appropriate sustainable management strategies [1].

The Ministry of Forestry has the authority in the management of mangrove forests which is affirmed in the Law of the Republic of Indonesia Number 41 of 1999 covering planning and supervision matters. The Ministry of Forestry has a national strategic program in managing mangrove ecosystems in Indonesia. The National Strategy for Mangrove Ecosystem Management, hereinafter abbreviated as SNPEM, is an effort in the form of policies and programs to realize sustainable management of mangrove ecosystems and sustainable prosperous communities based on available resources as an

integral part of the national development planning system. SNPEM also prioritizes efforts to conserve and sustainably manage and utilize mangrove ecosystems in policies and regulations and strengthen law enforcement to reduce the rate of mangrove degradation.

The National Strategy for Mangrove Ecosystem Management in regard to mangrove surveys and mapping must refer to the Indonesian National Standard on mangrove surveys and mapping. Remote sensing techniques are generally used for mangrove surveys and mapping as an approach in mapping mangroves. However, in terms of the National Strategy for Mangrove Ecosystem Management, it is not only mangrove mapping, but it needs to be emphasized in the availability and guarantee of structured, interconnected, and well integrated data and information about mangrove forest ecosystems in Indonesia in terms of sustainable mangrove forest management. In Geographic Information Systems (GIS) there are databases that have geographic references or so-called geodatabases. Geodatabase allows data to be well organized into a database and can be easily updated if there is data that needs to be updated. Geodatabase facilitates structured data management, maintains geometric data, and makes it easier to query [3]. In achieving the creation of a geodatabase that will support mangrove management, a geodatabase masterplan is needed first as a first step towards achieving a geodatabase that will support mangrove management.

This research will design a mangrove geodatabase master plan to support sustainable management of mangrove ecosystems. This research aims to know the spatial data and attribute data needed in the design of the mangrove forest geodatabase masterplan based on laws and regulations and research results and creating a geodatabase master plan for mangrove forests to assist mangrove ecosystem management activities. To achieve the research objectives, literature study needs to be done. This literature review presents an explanation of the research keywords in this case mangrove forests, the National Strategy for Mangrove Ecosystem Management, the Master Plan and Geodatabase. According to [4], mangrove forests are forest vegetation that grows in coastal areas and around river mouths, which are always or regularly inundated by sea water and are affected by tides. Mangrove forest vegetation is characterized by types of mangroves, fires, preparations, and supports. Mangrove area is not only as a collection of plants, but is one of the natural resources that can provide benefits for human life. Mangrove forests also play a role as a place to live species of shrimp and fish of commercial value. The main causes of damage to mangrove forests uncontrollably in the past there are two main causes namely, because of our ignorance about the meaning and the very important role of mangrove forests for life, including humans, and our lack of mastery of techniques for managing mangrove forests that are environmentally friendly [5].

Based on Presidential Regulation Number 73 of 2012 concerning National Strategy for Mangrove Ecosystem Management National Strategy for Mangrove Ecosystem Management, hereinafter abbreviated as SNPEM, is an effort in the form of policies and programs to realize sustainable management of mangrove ecosystems and sustainable prosperous communities based on available resources as an integral part of the planning system National development. In practice SNPEM still has issues relating to stakeholders in Indonesia and mangrove ecosystem management cannot be done unilaterally, so it needs to involve many parties or actors to control planning, management and sustainable use [6].

One approach used in the management of mangrove ecosystems to achieve sustainable regional development is to apply concepts based on social ecosystems with the aim of maintaining, preserving and maintaining ecosystem integrity, so that at the same time being able to guarantee the sustainability of the supply of resources for the socio-economic interests of the community [7]. Not only that, SNPEM also needs to emphasize on database management system and the availability and guarantee of structured, interconnected, and well integrated data and information about mangrove forest ecosystems in Indonesia in terms of sustainable mangrove forest management. According to Presidential Regulation of the Republic of Indonesia Number 32 Year 2011 concerning the master plan for the acceleration and expansion of Indonesia's development, the master plan is a planning document that has been prepared in a comprehensive (comprehensive) and integrated manner (integrative) which contains plans for the utilization or development of an area or area or a land use plan that relatively broad. The master plan

serves as a guide to the steps to realize development and as a reference for monitoring and evaluating the stages of development that have been taken. The database design process, regardless of the problem being handled, is divided into 3 (three) stages [8].

2. Material and Methods

Preparations made in the research of making the geodatabase master plan of mangrove forests are conducting theoretical studies aimed at finding and tracing the theoretical basis related to research. The literature used in this study is national legislation taken from 9 of the Ministry of Environment Legal Documentation and Information Network sources (Laws, Government Regulations, Presidential Regulations, Ministerial Regulations, and Directorate General Regulations) and 7 of research report.

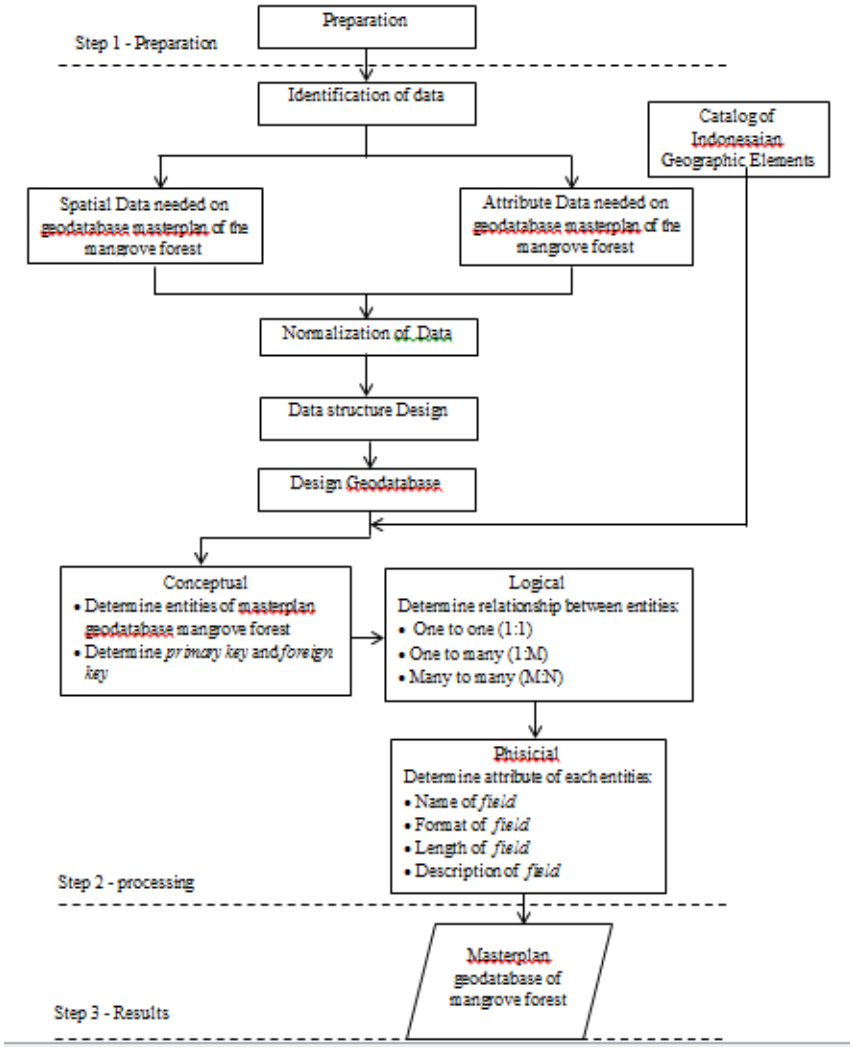

Figure 1. Methods.

2.1. Normalization of Data

The process of identifying data from statutory regulations and research results reports added up and obtained 41 data. The data contained duplicate data so that data normalization is needed. This data normalization aims to eliminate duplicate data making it easier in the next process. Normalization is done by checking one by one of the identification data if the same data is found, then the data is grouped so that it becomes a data that represents these double data. The normalization process produces 12 data.

2.2. Data Structure Design

The design of mangrove forest data structures is done by grouping the data into tables based on layers according to the data types, namely basic data, thematic data, and supporting data. The data structure in this study was built into 3 classifications:

- Basic Data
  The basic data used in the design of the mangrove forest geodatabase master plan is the administrative boundary.
- Thematic Data
  Thematic data used in the design of the mangrove geodatabase master plan are mangrove forest types and mangrove density.
- Supporting data
  Supporting data used in the design of the geodatabase master plan of mangrove forests are rainfall, pH, soil, salinity, temperature, dissolved oxygen and tides.

2.3. Conceptual Geodatabase Design

Conceptual database design consists of 2 (two) stages, namely: 1. Determine all entities in the mangrove forest geodatabase. Mangrove forest geodatabase entities, namely provincial administrative boundaries, district administrative boundaries, sub-district administrative boundaries, village administrative boundaries, mangroves, land, rainfall, salinity, dissolved oxygen, pH, temperature, and tides. 2. Defining the relationships between entities carried out through the following stages:
a) Determine the primary key or Primary Key (PK) for each entity. Entity PK is an ID (code) consisting of several digits in the form of numbers, text, or a combination of numbers and text that is unique. b) Translating relationships into Foreign Key (FK), determining the relationship between the PK of an entity and the PK of another entity. An example can be seen in the relationship between desa, sub-district, district and provincial entities can be seen in Figure 2.

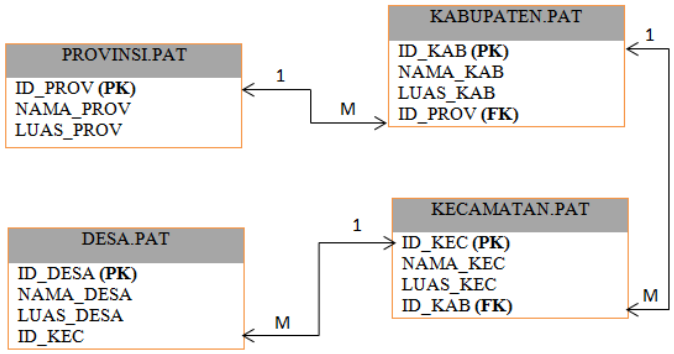

Figure 2. Relationship Entity Administrative Boundaries.

2.4. Logical Geodatabase Design

Logical database design is the stage of the process of determining relationships between entities. At this stage, there are 3 (three) types of relationships, namely one to one (1: 1) relationships, one to many (1: M) relationships, and many to many (M: N) relationships. Following is an example of designing a logical database:

- One to one relationship (1: 1)
  There are no examples of one-to-one relationships on mangrove forests because all entities only have one to many relationships and many to many relationships.
- One to many relationship (1: M)

One to many relationship (1: M), that is, between provincial and district entities, district entities with sub-district entities, sub-district entities and village entities. Relationships between entities can be seen in Figure 3.

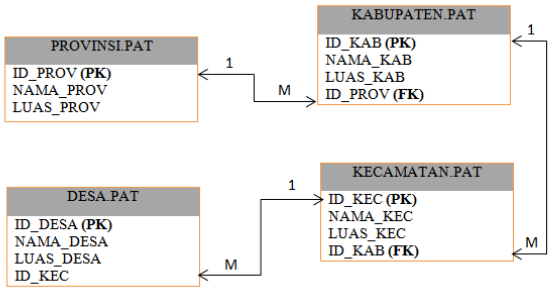

Figure 3. Relationship One to Many (1:M).

- Many to many relationships (M: N)
  The many to many relationships are the village boundary entity with mangrove and salinity entities. Relationships between entities can be seen in Figure 4.

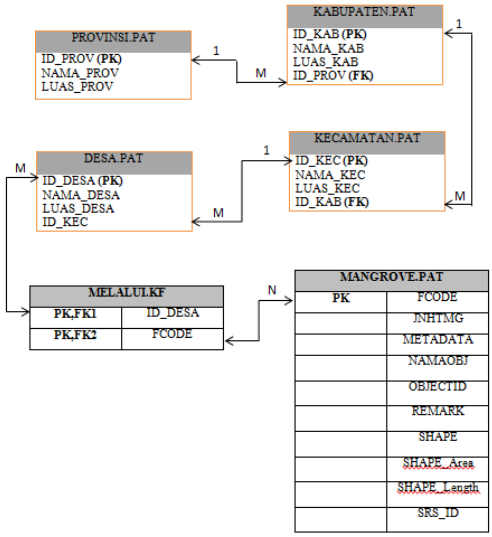

Figure 4. Relationship Many to many (M:N).

3. Results and Discussion

3.1. Identification Data of Mangrove Forest

The identification stage of mangrove forest data is carried out by identifying mangrove forest data based on a review of laws and research reports. The amount of data that has been identified based on a review of legislation is 14 data and the amount of data that has been identified is based on a study of 27 research report data.

3.2. Geodatabase Design

In the geodatabase design phase, the results are obtained in the form of tables of entities that contain attributes.

Table 1. Entity Attributes of Village Boundary.

NO	NAMA FIELD	FORMAT FIELD	PANJANG FIELD	DESKRIPSI FIELD
1	ID_DESA	Text	50	ID Desa
2	NAMA_DESA	Text	50	Nama Desa
3	LUAS_DESA	Double	10	Luas Desa
4	ID_KEC	Text	50	ID Kecamatan

Table 2. Entity Attributes of Sub-district Boundary.

NO	NAMA FIELD	FORMAT FIELD	PANJANG FIELD	DESKRIPSI FIELD
1	ID_KEC	Text	50	ID Kecamatan
2	NAMA_KEC	Text	50	Nama Kecamatan
3	LUAS_KEC	Double	10	Luas Kecamatan
4	ID_KAB	Text	50	ID Kabupaten

Table 3. Entity Attributes of District Boundary.

NO	NAMA FIELD	FORMAT FIELD	PANJANG FIELD	DESKRIPSI FIELD
1	ID_KAB	Text	50	ID Kabupaten
2	NAMA_KAB	Text	50	Nama Kabupaten
3	LUAS_KAB	Double	10	Luas Kabupaten
4	ID_PROV	Text	50	ID Provinsi

Table 4. Entity Attributes of Provincial Boundary.

NO	NAMA FIELD	FORMAT FIELD	PANJANG FIELD	DESKRIPSI FIELD
1	ID_PROV	Text	50	ID Provinsi
2	NAMA_PROV	Text	50	Nama Provinsi
3	LUAS_PROV	Double	10	Luas Provinsi

Table 5. Entity Attributes of Mangrove.

NO	NAMA FIELD	FORMAT FIELD	PANJANG FIELD	DESKRIPSI FIELD
1	FCODE	Text	50	Feature Code
2	JNHTMG	Text	50	Jenis Hutan Mangrove
4	METADATA	Text	50	Metadata
5	NAMAOBJ	Text	50	Nama Objek
6	OBJECTID	Object ID	-	ID Objek
7	REMARK	Text	50	Catatan
8	SHAPE	Geometry	-	Shape
9	SHAPE_Area	Double	10	Shape Area
10	SHAPE_Length	Double	10	Shape Length
11	SRS_ID	Text	50	Spatial Reference System Identifier

Table 6. Entity Attributes of Soil.

NO	NAMA FIELD	FORMAT FIELD	PANJANG FIELD	DESKRIPSI FIELD
1	FCODE	Text	50	Feature Code
2	JNSTNH	Text	50	Jenis Tanah
3	METADATA	Text	50	Metadata
4	NAMAOBJ	Text	50	Nama Obyek
5	OBJECTID	Object ID	-	ID Obyek
6	REMARK	Text	50	Catatan
7	SHAPE	Geometry	-	Shape
8	SHAPE_Area	Double	10	Shape Area
9	SHAPE_Length	Double	10	Shape Length
10	SRS_ID	Text	50	Spatial Reference System Identifier

Table 7. Entity Attributes of Rainfall.

NO	NAMA FIELD	FORMAT FIELD	PANJANG FIELD	DESKRIPSI FIELD
1	DATEPR	Double	10	Tanggal Perkiraan
2	FCODE	Text	50	Feature Code
3	METADATA	Text	50	Metadata
4	NAMAOBJ	Text	50	Nama Obyek
5	NRMLCH	Text	50	Normal Curah Hujan
6	OBJECTID	Object ID	-	ID Obyek
7	REMARK	Text	50	Catatan
8	SHAPE	Geometry	-	Shape
9	SHAPE_Area	Double	10	Shape Area
10	SHAPE_Length	Double	10	Shape Length
11	SRS_ID	Text	50	Spatial Reference System Identifier

Table 8. Entity Attributes of Salinity.

NO	NAMA FIELD	FORMAT FIELD	PANJANG FIELD	DESKRIPSI FIELD
1	CUACA	Text	50	Cuaca
2	DLMLAU	Text	50	Kedalaman Laut
3	DLMOBS	Text	50	Kedalaman Hasil Observasi
4	FCODE	Text	50	Feature Code
5	KODSTA	Text	50	Kode Stasiun
6	KONLAU	Text	50	Kondisi Laut
7	METADATA	Text	50	Metadata
8	NAMAOBJ	Text	50	Nama Obyek
9	OBJECTID	Object ID	-	ID Obyek
10	REMARK	Text	50	Catatan
11	SALINITAS	Double	10	NIlai Salinitas (‰)
12	SHAPE	Geometry	-	Shape
13	SRS_ID	Text	50	Spatial Reference System Identifier
14	WKTSRV	Text	50	Waktu Survei

Table 9. Entity Attributes of Disolved Oxygen.

NO	NAMA FIELD	FORMAT FIELD	PANJANG FIELD	DESKRIPSI FIELD
1	CUACA	Text	50	Cuaca
2	DLMLAU	Text	50	Kedalaman Laut
3	DLMOBS	Text	50	Kedalaman Hasil Observasi
4	FCODE	Text	50	Feature Code
5	KODSTA	Text	50	Kode Stasiun
6	KONLAU	Text	50	Kondisi Laut
7	METADATA	Text	50	Metadata
8	NAMAOBJ	Text	50	Nama Obyek
9	O2_LARUT	Text	50	NIlai Oksigen (mg/l)
10	OBJECTID	Object ID	-	ID Obyek
11	REMARK	Text	50	Catatan
12	SHAPE	Geometry	-	Shape
13	SRS_ID	Text	50	Spatial Reference System Identifier
14	WKTSRV	Text	50	Waktu Survei

Table 10. Entity Attributes of pH.

NO	NAMA FIELD	FORMAT FIELD	PANJANG FIELD	DESKRIPSI FIELD
1	CUACA	Text	50	Cuaca
2	DLMLAU	Text	50	Kedalaman Laut
3	DLMOBS	Text	50	Kedalaman Hasil Observasi
4	FCODE	Text	50	Feature Code
5	KODSTA	Text	50	Kode Stasiun
6	KONLAU	Text	50	Kondisi Laut
7	METADATA	Text	50	Metadata
8	NAMAOBJ	Text	50	Nama Obyek
9	NILAI_PH	Text	50	NIlai pH
10	OBJECTID	Object ID	-	ID Obyek
11	REMARK	Text	50	Catatan
12	SHAPE	Geometry	-	Shape
13	SRS_ID	Text	50	Spatial Reference System Identifier
14	WKTSRV	Text	50	Waktu Survei

Table 11. Entity Attributes of Temperature.

NO	NAMA FIELD	FORMAT FIELD	PANJANG FIELD	DESKRIPSI FIELD
1	CUACA	Text	50	Cuaca
2	DLMLAU	Text	50	Kedalaman Laut
3	DLMOBS	Text	50	Kedalaman Hasil Observasi
4	FCODE	Text	50	Feature Code
5	KODSTA	Text	50	Kode Stasiun
6	KONLAU	Text	50	Kondisi Laut
7	METADATA	Text	50	Metadata
8	NAMAOBJ	Text	50	Nama Obyek
9	OBJECTID	Object ID	-	ID Obyek
10	REMARK	Text	50	Catatan
12	SHAPE	Geometry	-	Shape
13	SRS_ID	Text	50	Spatial Reference System Identifier
14	SUHU	Text	50	Nilai Suhu
15	WKTSRV	Text	50	Waktu Survei

Table 12. Entity Attributes of Tides.

NO	NAMA FIELD	FORMAT FIELD	PANJANG FIELD	DESKRIPSI FIELD
1	BTSPTM	Text	50	Batas Pasang Tertinggi Bulanan
2	BTSPTY	Text	50	Batas Pasang Tertinggi Tahunan
3	BTSSRM	Text	50	Batas Pasang Terendah Bulanan
4	BTSSRY	Text	50	Batas Pasang Terendah Tahunan
5	FCODE	Text	50	Feature Code
6	METADATA	Text	50	Metadata
7	NAMAOBJ	Text	50	Nama Obyek
8	OBJECTID	Object ID	-	ID Obyek
9	REMARK	Text	50	Catatan
10	SHAPE	Geometry	-	Shape
11	SHAPE_Area	Double	10	Shape Area
12	SHAPE_Length	Double	10	Shape Length

Based on the research that has been done, an analysis of the design of the mangrove forest geodatabase master plan can be done, namely the literature used, the geographical elements of the mangrove forest geodatabase entity according to Indonesian geographical elements catalog (KUGI), and the analysis of data structure elements according to KUGI.

The literature used in the process of designing a mangrove forest geodatabase uses the National Legislation related to mangrove forests and reports on research results relating to mangrove forests. Of all the laws and regulations, there are 9 regulations that are used as a foundation in the design of mangrove forest geodatabases and for research report that is used as a basis in the design of mangrove forest geodatabases, there are 7 reports of research results. From the identification process of 9 laws and regulations and 7 research reports, 41 data on mangrove forests were obtained, which were then normalized to avoid duplicate data, so that 12 data were used in the process of building data structures and database planning. In the process of building data structures determine the basic data, secondary data, and supplementary data. In the process of designing this database there are obstacles in determining the type of data, custodial and attributes (fields) along with the content information (fields) for each data (entity) of mangrove forests. This is because there is no guideline for the Indonesian National Standard (SNI) for the design of mangrove forest geodatabases or technical workmanship or standard rules in explaining the attributes for geodatabase design. Therefore, in this study, the process carried out in the design of data structures and database designs by looking at the basic principles of the Indonesian Geographic Elements Catalog (KUGI) version 5 of 2018.

Analysis carried out on the data structure element refers based on the Indonesian Geographic Elements Catalog (KUGI) which contains 14 categories of geographic elements, namely Spatial Reference, Territorial Boundaries, Transportation, Hydrography, Hypography, Vegetation, Built Environment, Utilities, Geology, Soil, Topography, Cadastre, Disaster, and Special Dataset. In making the geodatabase data structure of the mangrove forest there are 5 categories of elements, namely in the basic data there are categories of territorial boundaries with data boundaries Village, District boundaries, Regency boundaries, and Provincial boundaries. Thematic data there are categories of vegetation with mangrove forest data. Complementary data are hydrographic categories with tidal data, soil categories with soil data, and special dataset categories with rainfall, salinity, dissolved oxygen, pH and temperature data. The design of the geodatabase master plan of the mangrove forest includes the addition of elements and attributes. These elements consist of village boundaries, sub-district boundaries, district boundaries and provincial boundaries. The process of adding and updating an element must be in accordance with the rules used to document the elements and attributes contained in the Indonesian Geographic Elements Catalog.

Data definition of village boundaries, sub-district boundaries, district boundaries, provincial boundaries, mangrove forests, soil, rainfall, salinity, dissolved oxygen, pH, temperature, and tides were obtained from KUGI sources version 5 of 2018. The following data definitions are as listed in Table 13.

Table 13. Data Definitions.

NO	DATA TYPE	DEFINITION OF DATA
1	Village Boundary	The boundaries of village government administration areas which are a series of coordinate points that are on the surface of the earth can be natural signs such as igir / mountain ridges, river medians and / or artificial elements in the field as outlined in the form of maps
	Sub-District Boundary	The boundaries of inter-sub-district government administration areas which are a series of coordinate points that are on the surface of the earth can be natural signs such as igir / mountain ridges, river medians and / or artificial elements in the field as outlined in the form of maps
	District Boundary	The boundaries of district government administration areas which are a series of coordinate points that are on the surface of the earth can be natural signs such as igir / mountain ridges, river medians and / or artificial elements in the field as outlined in the form of maps
	Provincial Boundary	The boundaries of provincial government administration areas which are a series of coordinate points that are on the surface of the earth can be natural signs such as igir / mountain ridges, river medians and / or artificial elements in the field as outlined in the form of maps
2	Mangrove	Wetland forests that lie in the lowlands that stretch along the coast in low elevation areas that are affected by tides, muddy, and brackish water.
3	Soil	The classification of the shape of the upper part of the solum based on the chemical substance, fineness, color, texture, permeability and size of the ground unit grain.
4	Rainfall	The average value of rainfall in a place in a certain time span
5	Salinity	The level of salinity or the level of salt dissolved in water. Unit of salinity per mile (%).
6	Disolved Oxygen	A value that indicates the amount of oxygen content dissolved in water
7	pH	The acidity or basicity of a solution that shows the hydrogen ion content (H +) in it (SNI 7644-2010). The degree of acidity or better known as pH has no unit
8	Temperature	The measure or degree of heat or cold of an object or system
9	Tides	Natural phenomena that occur due to the attraction of the earth to celestial bodies, especially the Moon and the Sun.

Based on the custodian, mangrove forest data types can be divided into several groups which are shown in Table 14.

Table 14. Mangrove Forest Data Types are based on Custodian.

No	Custodian	DATA TYPE
1	Badan Informasi Geospasial (BIG)	Village Boundary Sub-District Boundary District Boundary Provincial Boundary tide
2	Kementerian Lingkungan Hidup dan Kehutanan	Mangrove
3	Kementerian Pertanian	Soil
4	Badan Meteorologi dan Klimatologi Geofisika (BMKG)	Rainfall Temperature
5	Kementerian Kelautan dan Perikanan (KKP)	Disolved Oxygen pH salinity

Complete results of the geodatabase design for the design of attributes, relations, and filling examples can be seen in Figure 5.

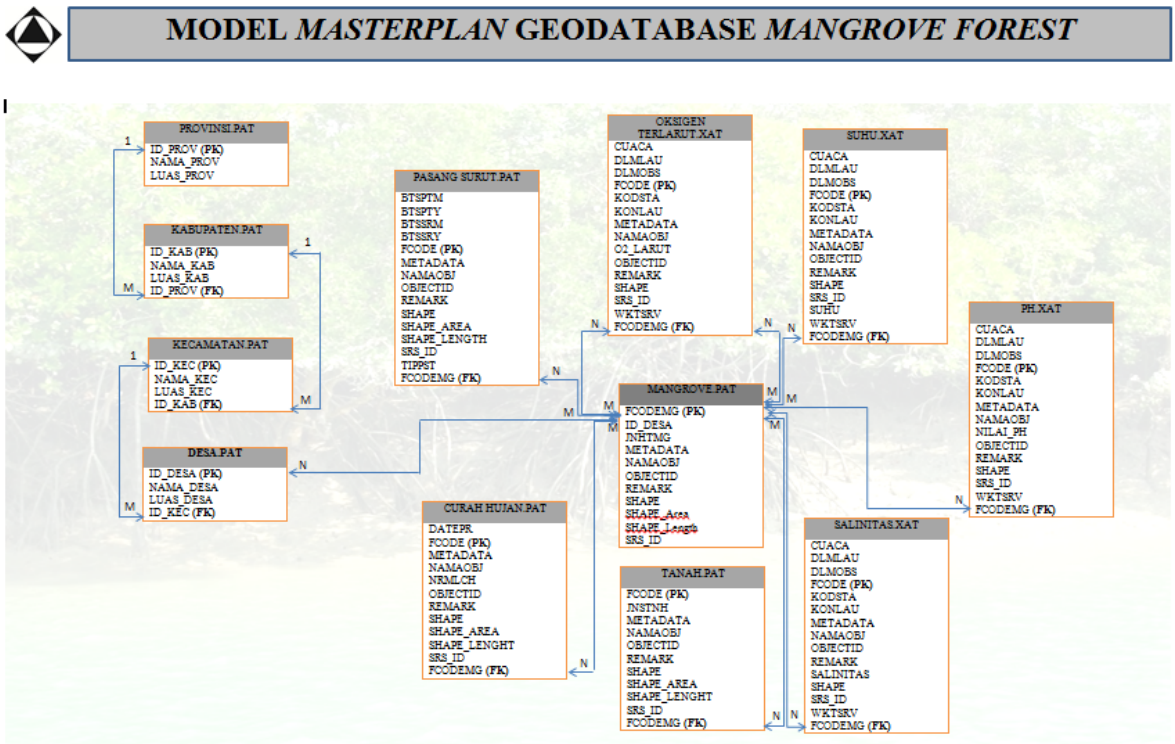

Figure 5. Results of the masterplan geodatabase.

4. Conclusions

The types of spatial data obtained are village boundaries, sub-district boundaries, district boundaries, and provincial boundaries, mangrove forests, soil, rainfall, salinity, oxygen, pH, temperature, and tides. The attribute data from spatial data were obtained from the basic principle structure of the Indonesian Geographic Elements Catalog (KUGI) Version 5 of 2018 and The design of the geodatabase master plan of mangrove forests starts from the identification of spatial data and attribute data based on legislation

and research results, data normalization, data structure design, geodatabase masterplan design conceptually, logically, and physically. The design of the geodatabase master plan of the mangrove forest is carried out by looking at the basic principle structure of the Indonesian Geographic Elements Catalog (KUGI) Version 5 of 2018.

5. References

[1] Kementrian Kehutanan, R., *Strategi Nasional PengelolaanEkosistem Mangrove Indonesia.* Jakarta: KementrianKehutanan RI, 2013.
[2] Geospasial, P.P.d.P.I.G.B.I., *BUKU I PRINSIP DASAR KATALOG UNSUR GEOGRAFI INDONESIA VERSI 5*. 2018.
[3] Guzzetti, F., et al., *Landslide inventory maps: New tools for an old problem.* Earth-Science Reviews, 2012. **112**(1-2): p. 42-66.
[4] Marsoedi and Samlawi, *Panduan Pelatihan Pelestarian dan Pengembangan Ekosistem Mangrove secara Terpadu dan Berkelanjutan. Pusat Penelitian Lingkungan Hidup*. 1997, Brawijaya University.
[5] Bengen, D.G., *Pedoman teknis pengenalan & pengelolaan ekosistem mangrove*. 2000: Pusat Kajian Sumberdaya Pesisir dan Lautan (PKSPL), Institut Pertanian Bogor ….
[6] Kustanti, A., *Evolusi hak kepemilikan dan penataan peran para pihak pada pengelolaan ekosistem hutan mangrove dengan kemunculan tanah timbul.* Bogor (ID) Institut Pertanian Bogor, 2013.
[7] Huda, N., *Strategi kebijakan pengelolaan mangrove berkelanjutan di wilayah pesisir Kabupaten Tanjung Jabung Timur Jambi*. 2008, program Pascasarjana Universitas Diponegoro.
[8] Kadir, A., *Konsep dan tuntunan praktis basis data.* Yogyakarta, Andi, 1999.

Land Suitability Analysis Using Analytical Hierarchy Process and Geographic Information System for *Coffea arabica* Linn. In Benguet Province, Philippines

Richard Dein Diaz Altarez[1*], Elvert Bugnosen Lucas[2*], John Christian Recana Pabustan[2*], Cyrx Delos Reyes Ermel Concepcion[2*], Maricor Coquilla Pabillaran[2*], Jerome Gardiola Maglinao[2*], Alexandrio Aloguin Ramirez[2*]

[1]Department of Natural Sciences, Headquarters Academic Group, Philippine Military Academy, Fort del Pilar, Baguio City, Philippines
[2]Cadet Corps Armed Forces of the Philippines, Philippine Military Academy, Fort del Pilar, Baguio City, Philippines

*Corresponding author's e-mail: rdaltarez@gmail.com, elvert.lucas239@gmail.com, atjcpabustan@yahoo.com, cycy_delosreyes14@yahoo.com, pabillaranmaricor@gmail.com, jerome20247@gmail.com, alexandrio.ramirez00@yahoo.com

Abstract. *Coffea arabica* Linn., one of the most valuable agricultural commodities worldwide, grows well in Benguet Province, Cordillera Administrative Region in the Philippines. Its yearly production decreases despite the province's potential as a center of its cultivation in the region. At present, available documented evidence about specific sites in the province where it can be ideally planted is lacking. Conventional technique on assessing site suitability for cultivation furnishes extensive spatial and descriptive data due to numerous variables affecting the growth and development of the crop. In this study, remote sensing and/or Global Information System (GIS) plays an important role as it facilitates the spatial analysis of data based on the growth requirement of the species while Analytical Hierarchy Process (AHP), a multi-criteria decision making, determines the favorable environmental conditions for the crop. The areas that are suitable for *C. arabica* cultivation were evaluated and delineated. Results indicate that the low, moderate and high suitability classes are respectively covering 15.46% (39,466.52 ha), 67.09% (171,218.90 ha) and 17.45% (44,527.31 ha) of the province. The integration of GIS and AHP in this study shows a powerful procedure in land suitability analysis for crops. However, a follow-up study undertaking on-ground validation and assessment to ensure the reliability of the output is recommended.

Keywords: Analytical Hierarchy Process, Benguet, Coffea arabica, Geographic Information System, suitability analysis

1. Introduction

Coffee is a major global consumer product [1]. In international trade, *Coffee arabica* Linn. is recognized as the most valuable agricultural commodity and accounted for 66% of the world coffee market [2]. Brazil, Vietnam, Colombia, Indonesia, and Ethiopia are the five largest coffee producers of the world that generally contribute to the 167,110.35 tons of coffee beans in [3]. In the Philippines, coffee grows well, however, its production is low and thus, accounts for only 2% of the world's production [4]. The Cordillera Administrative Region is among the top Arabica producing regions in the Philippines [5]. Arabica is well suited to provinces like Benguet in CAR due to its temperate condition and elevated terrains [4]. Coffee production of the Philippines has generally declined from 52,047 tons of green coffee beans (GCB) in 2006 to 36,171 tons of GCB in 2015 by 3.51 percent per year over the past ten (10) years. Meanwhile, in the last ten years, the area planted for coffee also fell by 1.02 percent per year. In 2014, approximately 117,451 hectares planted/harvested for coffee had declined to 113,738 hectares in 2015 by 3.16 percent. This was due to an increase in the number of coffee growers shifting to other crops, land conversion to real estate and recreation and urbanization areas [6]. In addition, other potential

contributing factors leading to low productivity include improper management of croplands and planting in areas not suitable for coffee production [7]. Although coffee is regarded so much by the international community, most of its species, including Arabica, is facing extinction because of climate change, loss of natural habitat, pest, and diseases [8, 9].

Planting coffee in Benguet requires suitable land, local environmental and geological conditions. Identification of suitable sites for such crops requires consideration of different factors such as climate, terrain, physicochemical properties of soil, among others [10, 11]. A method of identifying or prioritizing factors of planting coffee is through the use of Analytical Hierarchy Proces (AHP). The AHP is a decision-making method based on multi-criteria developed by Thomas Saaty. This is an effective method of prioritizing significance and allowing an authority to choose among the factors that are best suited for a certain problem [12, 13], in detail AHP is used to establish a hierarchical structure based on criteria, and alternatives to represent complex problems [14]. The decision-making process of AHP focuses on problem-solving and is designed to prioritize complicated hierarchical problems from objectives, criteria, and alternatives. AHP is also a tool to help appropriate decision making for problem structure with a quantitative and qualitative variable problem structure. Furthermore, AHP's advantage in decision-making can be found in many kinds of research [15]. In agriculture, weighted overlay together with the AHP gives the site suitability analysis a very promising result [11]. It has steps in determining the relative importance of weights on every criterion, before coming up with the final score [16]. Pairwise method of comparison is used to estimate the total weight of individual criteria or element. AHP and GIS integration helps to support decision-making by creating suitability maps [15, 17]. Geospatial tools can also be used to identify suitable land for coffee planting on various criteria such as soil quality, geology, drainage, location, topography. This technique can also assist in identifying and prioritizing potential coffee plantation sites [11]. Geographic Information System (GIS) is a tool for decision makers that utilize spatial data. One of its most useful applications is land use suitability mapping [18]. Integrating GIS with multi-criteria evaluation techniques are widely used in various applications such as site suitability analysis [19]. By combining AHP with GIS, an evaluation model can be constructed through thematic maps to quantitatively calculate the conditions or suitability of planting a certain crop in a given place [20].

C. arabica in Benguet, called by the locals as Benguet coffee is in the risk of extinction since farmers are unable to prune or rejuvenate their old trees, as elders think that touching the height of coffee trees can annoy the gods. Old or mature trees are not as productive as younger trees. There is also no planting of new coffee seedlings because young people prefer not to work in the agricultural sector, and suitable sites in the Province for planting coffee are not well documented. Therefore, coffee production declines every year [21]. Hence, this study aims to determine the favorable sites in the province of Benguet in the Cordillera Administrative Region for the cultivation of coffee plants using the integrated Analytical Hierarchy Process and Geographic Information System.

2. Materials and methods

2.1. Study area

The study area presenting the Province of Benguet is shown in Figure 1. Benguet lies southernmost in the Cordillera Administrative Region, sharing borders with the Province of Pangasinan in the south and Ilocos Sur and La Union in the west. It is geographically located between 16’33” north latitude and 120’33” to 120’52” east longitude. Benguet has a mountainous terrain of peaks, ridges, and canyons; and a temperate and generally pleasant climate. There are 13 municipalities with a total land area of about 2,600 square kilometers and inhabited by 446,224 people per the 2015 census, making it the most populous province in the Cordillera Administrative Region. Economic activities in the area include tourism, mining, and agriculture [22, 23].

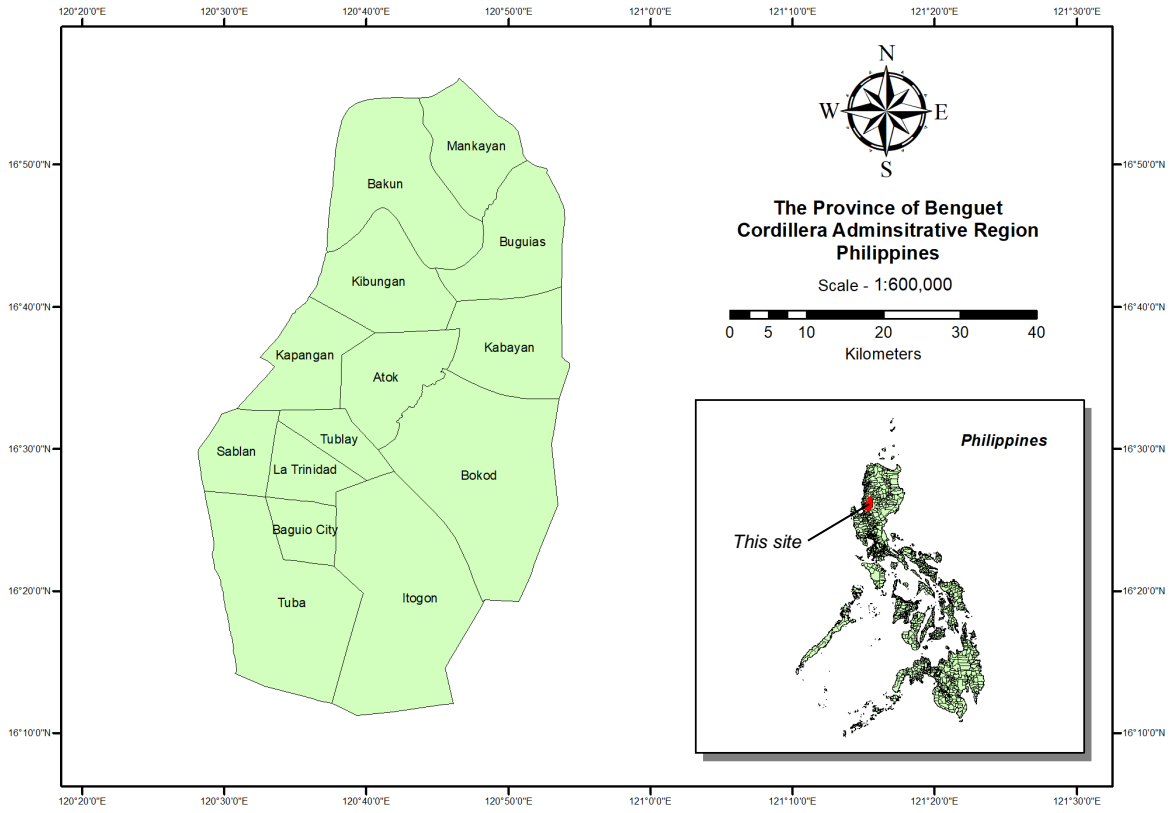

Figure 1. The location of the study area.

2.2. Software and data used

The software used for this study is ArcGIS 10.5. Shapefiles including rainfall, slope, soil, land cover, and land type were used for the suitability analysis. All the shapefiles came from the Department of Agriculture, Bureau of Agricultural Research. Likewise, all articles, journals and other available materials for *C. arabica* were examined.

2.3. Multi-criteria suitability analysis using AHP

The suitability analysis of the Province of Benguet for planting *C. arabica* was done through multi-criteria analysis, specifically AHP. This is done to identify the appropriate criteria for the growth of the said plant. Based on their importance and significance, five criteria were chosen. These criteria or factors affect the said crop. These include rainfall, slope, soil, land cover, and land type. Weights for each criterion and sub-criteria were calculated using AHP, and these weights were incorporated in the GIS environment.

The factors determined for the site suitability analysis are placed within a hierarchic system and are compared in a pairwise comparison matrix. The weights of each criterion are computed by taking the eigenvector corresponding to the largest eigenvalue of the matrix and then normalizing the sum of the components to unity [24]. The weights are generated using a scale of one to nine in which one having equal importance and nine having extreme importance (Table 1). In the AHP, there is a property of reciprocity, especially if a criterion dominates the other on the previous weights provided [25]. The relative weights of each criterion are calculated after the pairwise matrix has been finalized.

Table 1. Scale for pairwise comparison.

Variables	Preference Expressed in Linguistic Variables
1	Equally important
3	Moderately important
5	Strongly important
7	Very strongly important
9	Extremely important
2,4,6,8	Intermediate values between adjacent scale values

The AHP's one advantage is it can identify the inconsistencies made in the decision for determining the weight in the criteria used in the study [12, 17, 26]. The efficiency of the criteria is calculated using the Consistency Relationship (CR) formula: CR = CI/RI. CR represents a measure of the error made or the quality of the judgment of the decision-maker [26]. A CR lower than 0.10 is considered acceptable, and higher value will mean to redo the assessments or judgments once more. CR depends on the Consistency Index (CI) and Random Index (RI). CI is mathematically expressed as $CI = (\lambda_{max} - n)/(n-1)$, wherein λ_{max} is the largest eigenvalue on the matrix, and n is the order of the matrix [11]. RI is the average of the resulting consistency depending on the order of matrix provided by Saaty, 1980 [12] (Table 2).

Table 2. Random inconsistency index for $N = 15$.

N	1	2	3	4	5	6	7	8	9	10	11	12	13	14	15
RI	0	0	0.58	0.9	1.12	1.24	1.32	1.41	1.45	1.49	1.51	1.48	1.56	1.57	1.59

2.4. Generating land suitability map for Coffea arabica Linn.
The suitability map was generated using ArcGIS 10.5. All the criteria maps containing the weights as derived from the AHP were combined and overlaid all together in the GIS environment.

2.5. Data analysis
Using the data from the site suitability analysis by means of AHP in which incorporated in the GIS environment, the area with the highest weight was selected for planting *C. arabica* in the Province of Benguet. A map is generated that shows the spatial importance of planting the said crop with low, medium and high suitability classifications. The classification was determined through the natural breaks. This method minimizes the variation within each data. It is based on the data's intrinsic natural groupings. Class breaks identify the best comparable group values and maximize class distinctions. The characteristics are split into classes whose limits are set where the information values differ comparatively greatly. This is achieved by trying to minimize the average deviation of each class from the class meanwhile maximizing the deviation of each class from the means of the other groups. In other words, the technique aims at reducing class variance and maximizing the variance between classes [27, 28].

3. Results and discussion
The suitability analysis for planting *C. arabica* in the Province of Benguet (Figure 3) is obtained through the overlay technique in GIS, and the result of the AHP weights for criteria (Table 3) and sub-criteria (Tables 4-8). The thematic maps (figures 2.a-2.e) with weights are processed from the GIS environment through the overlay technique. The resulting suitability was classified into three: Low, Moderate and High. Red color represents the low suitability for planting the said crop. Yellow indicates moderate suitability and green represents high suitability. This classification was used in order to facilitate the interpretation of the map. In addition, the issue of classifying continuous data into classes is always

uncertain, as most scientists use their own expert opinion to create class limits [29]. In this study, the generated suitability map is classified using a natural break.

The extent and percentage area of the suitable sites for planting *C. arabica* in Benguet are shown in Table 9. More than half of the entire province is moderately suitable for planting *C. arabica*. And 17.45% comprising the Municipalities of Buguian, Mankayan, Kibungan, Kabayan, and Atok are favorable for planting the said crop. Portions of Baguio City, La Trinidad and Tublay also shows promising sites to growing *C. arabica*, however, these areas are populated and predominated by concrete structures.

While various development plans, such as comprehensive land use and urban development plan are prepared for the Province of Benguet, continuous unsustainable land conversion takes place without appropriate planning and environmental considerations. These are some of the reasons why the industry of coffee production in Benguet continuously drops every year [21]. The result of this study can be a good source of information for concerned authorities for development works related to sustainable coffee production. This, if carried with validation study, can also be used for crafting policy that will help our coffee farmers as well as the industry of the coffee in the Province as a whole.

Table 3. AHP matrix for the main criteria of factors for planting *Coffea arabica* Linn. in the Province of Province.

Factor	Land Type	Land Cover	Soil Type	Rainfall	Slope	Eigenvector
Land Type	1.00	0.50	0.33	0.20	0.50	0.06
Land Cover	2.00	1.00	0.33	0.20	0.50	0.08
Soil Type	3.00	3.00	1.00	0.20	5.00	0.25
Rainfall	5.00	5.00	5.00	1.00	2.00	0.43
Slope	5.00	2.00	0.20	0.50	1.00	0.17

Consistency Index = 0.093; Random Inconsistency Index (RI) = 1.12; Consistency Ratio (CR) = 0.08

4. Conclusions

The determination of favorable sites in the province of Benguet in the Cordillera Administrative Region for the cultivation of coffee plants using the integrated Analytical Hierarchy Process and Geographic Information System is the intention of this study. It was found that the AHP matrix with the integration of GIS for the analysis with five major criteria and 34 sub-criteria very useful. The result of this study can be used by local farmers and concerned government entities for planting *C. arabica* in the study site since it provides information on the suitable sites for growing the said crop. Though the combination of AHP and GIS is a powerful combination in land0use suitability analysis, it is still recommended to undertake validation efforts to prove the applicability of the output produced. A ground level validation with local parameters assessment can be done in the future.

5. Conflict of interest

The authors declare that they have no affiliations with or involvement in any organization or entity having any financial or non-financial interest in the topic or materials discussed in this manuscript.

Table 4. AHP matrix for the sub-criteria of land type.

Factor	Alluvial Land	Built-up	Erodible Land	Expansion Area	Gently Sloping	High Lands	Non-Agricultural	Reservoir	Unclassified	Eigenvector
Alluvial Land	1.00	3.00	3.00	3.00	0.14	0.20	1.00	3.00	3.00	0.11
Built-up	0.33	1.00	1.00	0.33	0.14	0.14	0.33	0.20	1.00	0.03
Erodible Land	0.33	1.00	1.00	0.33	0.14	0.14	0.33	0.33	1.00	0.03
Expansion Area	0.33	3.00	3.00	1.00	0.14	0.20	3.00	3.00	1.00	0.08
Gently Sloping	0.33	7.00	7.00	7.00	1.00	0.33	7.00	5.00	3.00	0.21
High Lands	3.00	7.00	7.00	5.00	3.00	1.00	7.00	5.00	3.00	0.30
Non-Agricultural	3.00	3.00	3.00	0.33	0.14	0.14	1.00	0.33	1.00	0.08
Reservoir	1.00	5.00	3.00	0.33	0.20	0.20	3.00	1.00	1.00	0.08
Unclassified	0.14	1.00	1.00	1.00	0.33	1.00	1.00	1.00	1.00	0.07

Consistency Index = 0.11; Random Inconsistency Index (RI) = 1.45; Consistency Ratio (CR) = 0.07

Table 5. AHP matrix for the sub-criteria of land cover.

Factor	Arable/Crop Land	Built-up	Forest	Grassland	Open Canopy Forest	Lake	Quarry	Riverbeds	Unclassified	Eigenvector
Arable/Crop Land	1.00	2.00	0.20	0.33	0.20	5.00	5.00	5.00	3.00	0.12
Built-up	0.50	1.00	0.14	0.14	0.20	1.00	1.00	1.00	2.00	0.04
Forest	5.00	7.00	1.00	2.00	1.00	5.00	5.00	5.00	5.00	0.23
Grassland	3.00	7.00	0.50	1.00	0.20	5.00	5.00	5.00	3.00	0.17
Open Canopy Forest	3.00	5.00	1.00	5.00	1.00	3.00	3.00	3.00	3.00	0.21
Lake	7.00	1.00	0.20	0.20	0.33	1.00	1.00	1.00	1.00	0.08
Quarry	0.50	1.00	0.20	0.20	0.33	1.00	1.00	1.00	1.00	0.04
Riverbeds	1.00	1.00	0.20	0.20	1.00	1.00	1.00	1.00	1.00	0.06
Unclassified	0.20	0.50	0.20	0.33	1.00	1.00	1.00	1.00	1.00	0.05

Consistency Index = 0.11; Random Inconsistency Index (RI) = 1.45; Consistency Ratio (CR) = 0.08

Table 6. AHP matrix for the sub-criteria of soil type.

Factor	Silt Loam	Clay Loam	Clay	Mountain Soil	Sandy Loam	Gravelly loam	Loam	Complex	Others	Eigenvector
Silt Loam	1.00	0.20	3.00	0.33	3.00	3.00	1.00	3.00	1.00	0.11
Clay Loam	5.00	1.00	5.00	2.00	5.00	0.33	0.33	5.00	1.00	0.14
Clay	0.33	0.20	1.00	0.14	0.33	0.33	0.20	3.00	1.00	0.04
Mountain Soil	3.00	0.50	7.00	1.00	5.00	3.00	0.20	5.00	1.00	0.14
Sandy Loam	3.00	0.20	3.00	0.20	1.00	1.00	0.20	3.00	1.00	0.07
Gravelly loam	0.50	3.00	3.00	0.33	1.00	1.00	0.20	3.00	1.00	0.09
Loam	7.00	3.00	5.00	5.00	5.00	5.00	1.00	6.00	1.00	0.26
Complex	1.00	0.20	0.33	0.20	0.33	0.33	0.17	1.00	1.00	0.03
Others	5.00	1.00	1.00	1.00	1.00	1.00	1.00	1.00	1.00	0.10

Consistency Index = 0.07; Random Inconsistency Index (RI) = 1.45; Consistency Ratio (CR) = 0.05

Table 7. AHP matrix for the sub-criteria slope.

Factor	Gently sloping to undulating	Level	Rolling to moderately steep	Steep	Undulating to rolling	Very steep	Eigenvector
Gently sloping to undulating	1.00	1.00	3.00	3.00	5.00	5.00	0.30
Level	1.00	1.00	3.00	3.00	5.00	5.00	0.30
Rolling to moderately steep	0.33	0.33	1.00	3.00	3.00	3.00	0.15
Steep	0.33	0.33	0.33	1.00	0.20	2.00	0.07
Undulating to rolling	0.33	0.20	0.33	5.00	1.00	3.00	0.13
Very steep	0.33	0.20	0.33	0.50	0.33	1.00	0.05

Consistency Index = 0.07; Random Inconsistency Index (RI) = 1.24; Consistency Ratio (CR) = 0.06

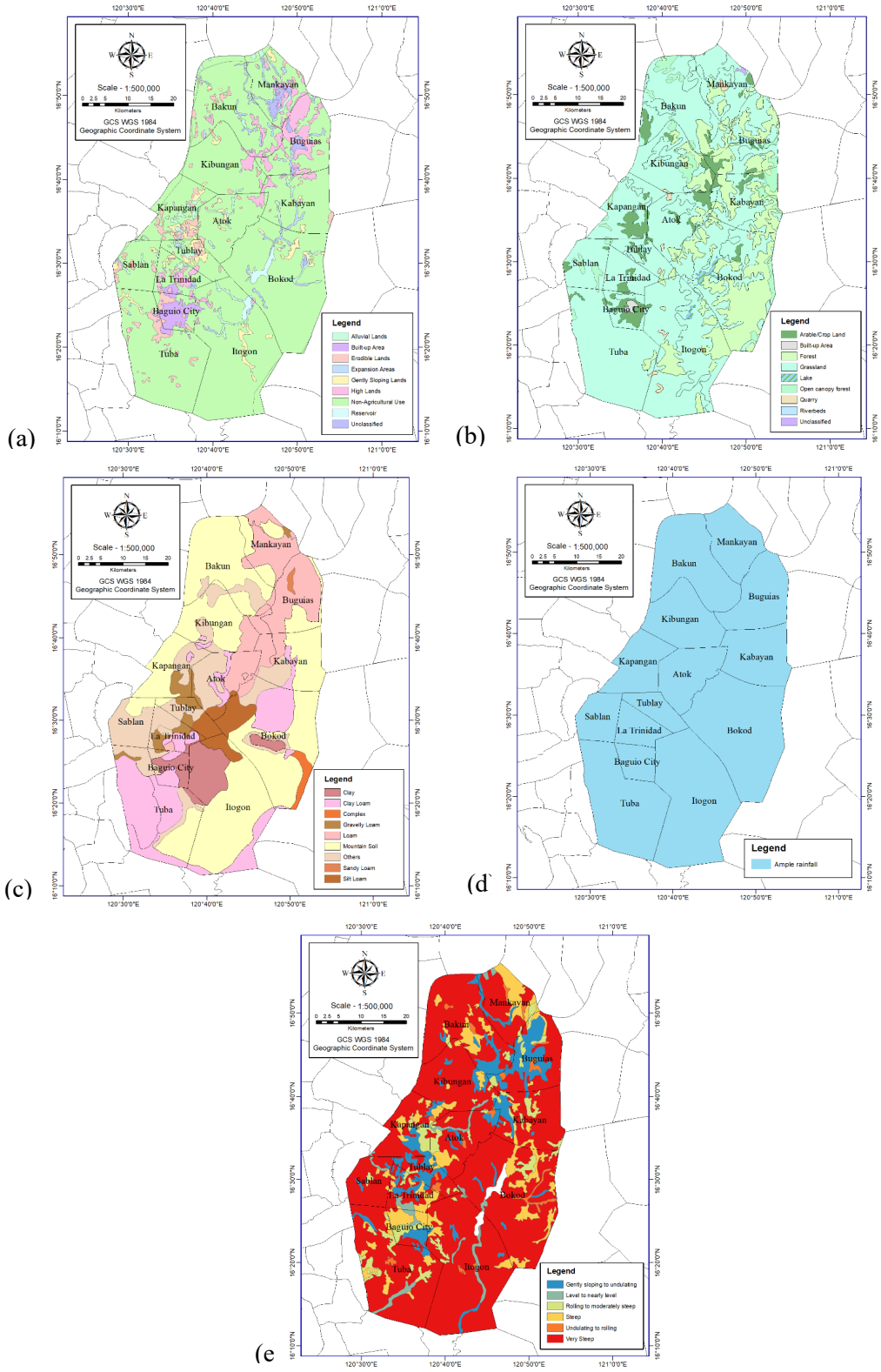

Figure 2. Thematic maps of the Province of Benguet used in the study. (a) land type. (b) land cover. (c) soil type. (d) rainfall. (e) slope

Table 8. Overall criteria weights.

Factor	W1	Sub-criteria	W2	Product Weight	Final Weight
Land Type	0.06	Alluvial Land	0.11	0.0066	0.0069
		Built-up	0.03	0.0018	0.0019
		Erodible Land	0.03	0.0018	0.0019
		Expansion Area	0.08	0.0048	0.0050
		Gently Sloping	0.21	0.0126	0.0131
		High Lands	0.30	0.0180	0.0188
		Non-Agricultural	0.08	0.0048	0.0050
		Reservoir	0.08	0.0048	0.0050
		Unclassified	0.07	0.0042	0.0044
Land Cover	0.08	Arable/Crop Land	0.12	0.0096	0.0100
		Built-up	0.04	0.0032	0.0033
		Forest	0.23	0.0184	0.0192
		Grassland	0.17	0.0136	0.0142
		Open Canopy Forest	0.21	0.0168	0.0175
		Lake	0.08	0.0064	0.0067
		Quarry	0.04	0.0032	0.0033
		Riverbeds	0.06	0.0048	0.0050
		Unclassified	0.05	0.004	0.0042
Soil Type	0.25	Silt Loam	0.11	0.0275	0.0287
		Clay Loam	0.14	0.0350	0.0365
		Clay	0.04	0.0100	0.0104
		Mountain Soil	0.14	0.0350	0.0365
		Sandy Loam	0.07	0.0175	0.0182
		Gravelly loam	0.09	0.0225	0.0235
		Loam	0.26	0.0650	0.0678
		Complex	0.03	0.0075	0.0078
		Others	0.10	0.0250	0.0261
Rainfall	0.43	Ample Rainfall	1.00	0.4300	0.4484
Slope	0.17	Gently sloping to undulating	0.30	0.0493	0.0514
		Level	0.30	0.0374	0.0390
		Rolling to moderately steep	0.15	0.0238	0.0248
		Steep	0.07	0.0136	0.0142
		Undulating to rolling	0.13	0.0119	0.0124
		Very steep	0.05	0.0085	0.0089

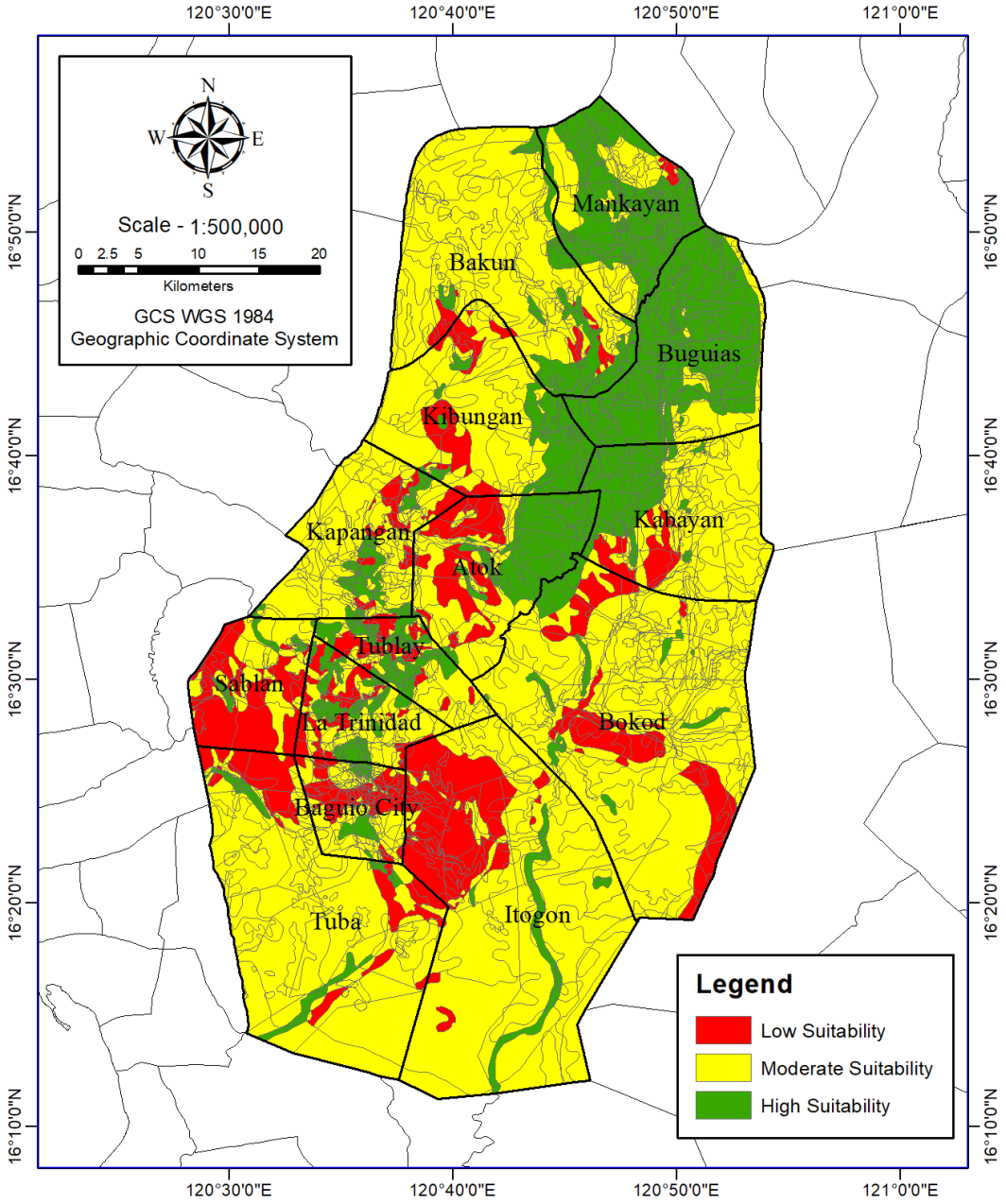

Figure 3. Suitability map for planting *Coffea arabica* Linn. in the Province of Benguet.

Table 9. Area coverage percentage of the *Coffea arabica* Linn. suitability in the Province of Benguet.

Classification	Area (Ha)	Percentage
Low Suitability	39,466.52	15.46
Moderate Suitability	171,218.90	67.09
High Suitability	44,527.31	17.45

6. References

[1] Ochoa, P.A., et al., *Estimation of suitable areas for coffee growth using a GIS approach and multicriteria evaluation in regions with scarce data.* Applied engineering in agriculture, 2017. **33**(6): p. 841-848.
[2] Labouisse, J.-P., et al., *Current status of coffee (Coffea arabica L.) genetic resources in Ethiopia: implications for conservation.* Genetic Resources and Crop Evolution, 2008. **55**(7): p. 1079.
[3] Organization, I.C., *Coffee market report*. 2007.
[4] (BAR), B.o.A.R., *Research and development, and extension agenda and programs (RDEAP 2016-2022)*. 2016.
[5] Pablo, M.P., *Coffee industry: road map localization*. 2016, Department of Trade Industry – National Industry Cluster Coordinator for Coffee.
[6] (BPI), B.o.P.I., *Philippine coffee industry roadmap 2017-2022*.
[7] Sepúlveda, R.B. and A.A. Carrillo, *Soil erosion and erosion thresholds in an agroforestry system of coffee (Coffea arabica) and mixed shade trees (Inga spp and Musa spp) in Northern Nicaragua.* Agriculture, Ecosystems & Environment, 2015. **210**: p. 25-35.
[8] Davis, A.P., et al., *High extinction risk for wild coffee species and implications for coffee sector sustainability.* Science advances, 2019. **5**(1): p. eaav3473.
[9] Moat, J., T.W. Gole, and A.P. Davis, *Least Concern to Endangered: Applying climate change projections profoundly influences the extinction risk assessment for wild Arabica coffee.* Global change biology, 2019. **25**(2): p. 390-403.
[10] Grassano, N., et al., *Evaluation of rapeseed cultivation suitability in Apulia with GIS-multicriteria analysis.* Italian Journal of Agronomy, 2011: p. e16-e16.
[11] Mishra, A.K., S. Deep, and A. Choudhary, *Identification of suitable sites for organic farming using AHP & GIS.* The Egyptian Journal of Remote Sensing and Space Science, 2015. **18**(2): p. 181-193.
[12] Saaty, T., *The Analytic Hierarchy Process*. 1980: Mc Graw Hill Inc: New York.
[13] Boonkanit, P. and A. Kengpol, *The Development and Application of a Decision Support Methodology for Product Eco-Design: A Study of Engineering Firms in Thailand.* International Journal of Management, 2010. **27**: p. 185-201.
[14] Roig-Tierno, N., et al., *The retail site location decision process using GIS and the analytical hierarchy process.* Applied Geography, 2013. **40**: p. 191-198.
[15] Boonkanit, P. and S. Kantharos. *An AHP for Prioritizing and Selecting Industrial Waste Management Method Case Study: Map Ta Phut Industrial Estate*. in *Applied Mechanics and Materials*. 2016. Trans Tech Publ.
[16] Boroushaki, S. and J. Malczewski, *Implementing an extension of the analytical hierarchy process using ordered weighted averaging operators with fuzzy quantifiers in ArcGIS.* Computers & Geosciences, 2008. **34**(4): p. 399-410.
[17] Beigbabayi, B. and M.A. Mobaraki, *Using AHP modeling and GIS to evaluate the suitability of site with climatic potential for cultivation of autumn canola in Ardabil Province.* Annals of Biological Research, 2012. **3**(5): p. 2307-2317.
[18] Javadian, M., H. Shamskooshki, and M. Momeni, *Application of sustainable urban development in environmental suitability analysis of educational land use by using AHP and GIS in Tehran.* Procedia Engineering, 2011. **21**: p. 72-80.
[19] Rad, L.K. and M. Haghyghy, *Integrated analytical hierarchy process (AHP) and GIS for land use suitability analysis.* World Applied Sciences Journal, 2014. **32**(4): p. 587-594.
[20] Xu, Y., et al., *Combining AHP with GIS in synthetic evaluation of environmental suitability for living in China's 35 major cities.* International Journal of Geographical Information Science, 2012. **26**(9): p. 1603-1623.
[21] Juan, P. *Slow Food foundation for Biodiversity: Benguet Coffee* Available from: https://www.fondazioneslowfood.com/en/ark-of-taste-slow-food/benguet-coffee/.

[22] Agency, W.P.T. *Benguet Province*. 2018; Available from: http://www.wowphilippinestravelagency.com/destinations/benguet-province/.
[23] Benguet, P.o. *Benguet Profile*. 2018; Available from: http://benguet.gov.ph/v3/.
[24] Feizizadeh, B., P. Jankowski, and T. Blaschke, *A GIS based spatially-explicit sensitivity and uncertainty analysis approach for multi-criteria decision analysis.* Computers & geosciences, 2014. **64**: p. 81-95.
[25] e Costa, C.A.B. and J.-C. Vansnick, *A critical analysis of the eigenvalue method used to derive priorities in AHP.* European Journal of Operational Research, 2008. **187**(3): p. 1422-1428.
[26] García, J.L., et al., *Multi-attribute evaluation and selection of sites for agricultural product warehouses based on an Analytic Hierarchy Process.* Computers and Electronics in Agriculture, 2014. **100**: p. 60-69.
[27] Chen, J., et al., *Research on geographical environment unit division based on the method of natural breaks (Jenks).* Int. Arch. Photogramm. Remote Sens. Spat. Inf. Sci, 2013: p. 47-50.
[28] ESRI. *Data classification methods*. 2018; Available from: https://pro.arcgis.com/en/pro-app/help/mapping/layer-properties/data-classification-methods.html.
[29] Chaudhary, P., et al., *Application of an Analytic Hierarchy Process (AHP) in the GIS interface for suitable fire site selection: A case study from Kathmandu Metropolitan City, Nepal.* Socio-Economic Planning Sciences, 2016. **53**: p. 60-71.

Total Suspended Solid Mapping Using Remote Sensing: Accuracy Comparison of Absolute and Relative Atmospheric Correction

Maria Roswita Kartika Sari Bawono[1]*, Pramaditya Wicaksono[1]*

[1]Department of Science Information Geography, Universitas Gadjah Mada, Jalan Sekip Utara, Bulaksumur, Depok, Sleman, Daerah Istimewa Yogyakarta

*Corresponding author's e-mail: mariaroswita.ksb@gmail.com, prama.wicaksono@ugm.ac.id

Abstract. The dynamic of TSS can be identified from optical reflections. One of which is Landsat 8 Operational Land Imager (OLI) imagery. Multitemporal data has characteristics of atmospheric conditions that are capable of affecting pixel values. The effect must be minimized by atmospheric correction both absolute and relative atmospheric correction. The atmospheric FLAASH, QUAC, and DOS correction methods have different approaches. FLAASH has a correlation of -0.582, DOS has a correlation of -0.579, QUAC has the highest a correlation of -0.601 and all atmospheric methods have F-significance below 0.05. Based on stepwise regression, the optimal B1/B3 transformation statistical test for all atmospheric correction methods. FLAASH accuracy test results 55.55% with SEE 21.1 mg/l, QUAC 54.58% with SEE 21.60 mg/l, and DOS at 55.95% with SEE 20.95 mg/l. Based on the results of the mapping using all methods, the spatial distribution produced shows that there are differences in the number of TSS content locations, but not too significant differences but can be considered.

Keywords: Reflectance Response, FLAASH, QUAC, DOS, Total Suspended Solid.

1. Introduction

Gajah Mungkur Reservoir has a very high sedimentation rate. The annual total sedimentation from 1993 to 2005 that entered to Gajah Mungkur Reservoir in Wonogiri was 3.1 million m^3. 21% of reservoir capacity has been reduced in 2006 and if there is no further maintenance, then by 2080, more than 50% of the reservoir capacity will be reduced [1]. Sedimentation rates need to be monitored to deal with siltation problems by mapping Total Suspended Solids (TSS). TSS is a suspension material that floats in the body of the water. The size of the suspension is 1µmeter [2].

Monitor can be done by extracting data from remote sensing images. Remote sensing data has the characteristics of certain atmospheric conditions. Atmospheric interference can affect the pixel value of the image. This is due to the interaction of electromagnetic radiation during recording, such interactions in the form of absorption, scattering, transmission, reflection, and emissions. These interactions contribute to changes in electromagnetic energy in the form of energy reduction carried out by absorption, the spread of energy in various directions by scattering, and changes in the direction of radiation by refraction [3].

Atmospheric disorders need to be considered especially for the study of quantitative analysis of remote sensing data, which is a pixel-based remote sensing analysis. The atmospheric correction needs to be done if it will detect changes in training data from one time to another or one place to another [4]. In this study, the pre-processing steps, especially in atmospheric correction, need to be considered. Atmospheric interference must be minimized so that it can return the pixel value of the remote sensing image to resemble the spectral reflection value of the actual object. In general, the atmospheric correction method is divided into two namely absolute and relative atmospheric correction. There are various atmospheric correction methods developed by experts and can be applied to minimize atmospheric disturbances, including Fast Atmospheric Analysis of Spectral Hypercubes (FLAASH) which is included in absolute atmospheric correction, QUick Atmospheric Correction (QUAC), and Dark Object Subtraction (DOS) which is included in the relative atmospheric correction.

Correction methods FLAASH, QUAC, and DOS have different approaches to minimizing atmospheric disturbances. The difference in the approach will cause the effect of atmospheric correction on the pixel value of the remote sensing image. Research on this correction method has often been done for land cover studies. Meanwhile, the third study of atmospheric correction methods for the study of Total Suspended Solid mapping has never been done. The atmospheric correction method that has been used for TSS mapping is Dark Object Subtraction (DOS). The study of the comparison of atmospheric correction methods for TSS reflectance values, we can know the difference in the spatial distribution of TSS in the three methods of correction of the atmospheric.

2. Methodology

2.1. Data and Materials

- Landsat 8 OLI Path / Row 119/66 Correction Level L1TP 26 February 2019
- Shuttle Radar Topography Mission (SRTM) 1-Arc Second to find out the location height
- Water Sample
- Boat
- Garmin 70s GPS for plotting
- 250 ml HDPE bottle for sample storage

2.2. Spectral Transformation

Pixel based mapping can be done by including multispectral classification, spectral transformation, and single band. Transformation produces new information using the main basis of feature space that can be seen from the tendency of grouping spectral values of a phenomenon [5]. NSMI was developed based on equation 2.1 using the principle of clear water having a reflection peak in the blue band, then the suspension itself will increase its reflection in the visible light spectrum especially in red and green bands and clear water increasingly absorbed by radiation [6].

$$NSMI = \frac{\rho r + \rho g - \rho b}{\rho r + \rho g + \rho b} \quad (1)$$

Note:

- ρb : Reflectance value of a blue band
- ρg : Reflectance value of a green band
- ρr : Reflectance value of a red band

In addition to the NSMI, the index transformation for TSS is NDSSI (Normalized Difference Suspended Sediment Index). Based on equation 2.2, this transformation uses a blue band because of the highest reflection of the water body in the band and the near-infrared band because it can detect the presence of TSS because the body of clear water will be absorbed maximally in this band [7].

$$NDSSI = \frac{\rho b - \rho nir}{\rho b + \rho nir} \quad (2)$$

Note:

- ρb : Reflectance value of a blue band
- ρnir : Reflectance value of a near-infrared band

In addition to using index transformation with certain formulas, one way to obtain index values is to make comparisons between bands and the use of a single band.

2.3. Diagram Method

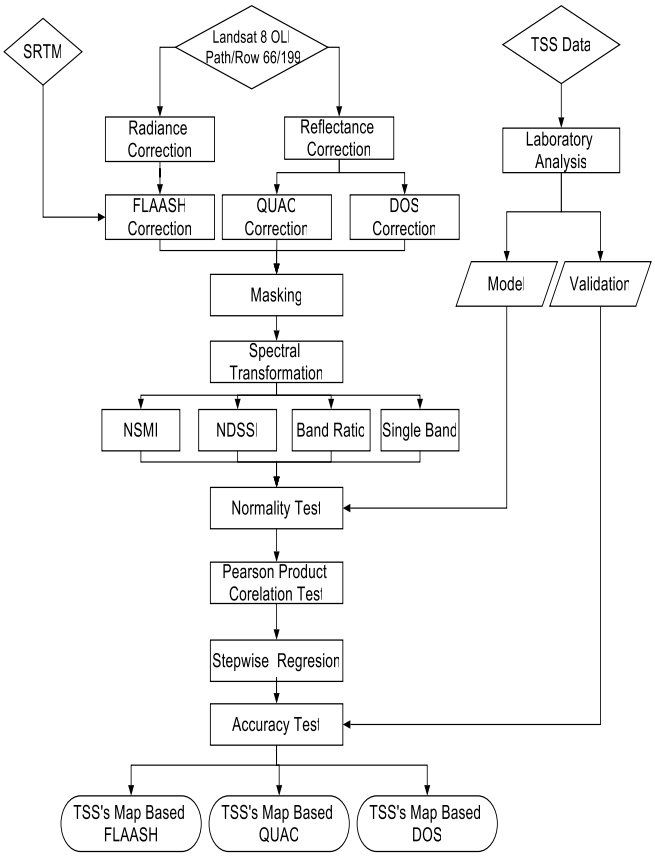

Figure 1. Diagram Method.

3. Results and Discussion

The Total Suspended Solid test uses the standard SNI 06-6989.3-2004 conducted at the Hydrology and Environmental Climatology Laboratory, Faculty of Geography, Univeristas Gadjah Mada using the gravimetric method. Based on Table 1 the results of testing 46 TSS samples carried out in the laboratory revealed that TSS content data tested were started from TSS at 12.3 - 101 mg / l. The average TSS sample tested was 37.143 mg / l.

Table 1. Result of TTS's Test Laboratory.

Code	TSS (mg/l)	Note	Code	TSS (mg/l)	Note
P01	24.8	M	P26	29.3	V
P02	23.5	M	P27	14.4	M
P04	39.3	V	P28	54.9	M
P05	24.3	M	P29	25.6	M
P07	48.1	V	P30	21.3	V
P08	25.2	M	P31	75.2	M
P09	16.7	M	P32	71.6	M
P10	12.3	V	P33	28	V
P12	24.3	M	P34	14.5	M

Code	TSS (mg/l)	Note	Code	TSS (mg/l)	Note
P13	101	M	P35	22.9	M
P14	15.7	V	P37	18.1	M
P15	42.5	M	P38	48.9	V
P16	21.6	V	P39	12.9	M
P18	20.8	M	P42	57.3	V
P19	35.5	M	P43	22.4	V
P20	15.9	M	P44	22.6	M
P22	63.1	V	P45	78.3	V
P23	43.1	M	P46	79.7	V
P24	65.3	M	P47	44.8	V

Note:

- M = Model
- V = Validation

The amount of data used is 46 samples with $\alpha = 0.05$ or a confidence level of 95%, then the value of $D_{n,\alpha}$ is 0.210. Data is said to be normal if the Dn data is maxed 0.210. Data from TSS testing results in the laboratory show that the data is normally distributed with the value of Dnmax 0.185 which means that it is smaller than $D_{n,\alpha}$ 0.210. Data can then be tested using parametric statistical methods. Based on Table 2 shows that in FLAASH atmospheric correction methods the normally distributed spectral transformations are B1/B3, B2/B3, B3/B4 and B3/B5, in the normal distributed QUAC atmospheric correction method the spectral transformation is B1/B2, B1/B3, B1/B5, B2/B3, B2/B5, B3/B2, B3/B4, B3/B5, B4/B5 and in the atmospheric correction method DOS spectral transformations that are normally distributed are B1/B2, B1/B3, B2/B3, and B3/B4.

Table 2. The Result of Normality Test from Spectral Transformation.

No	Channel	FLAASH	QUAC	DOS
		$\mathbf{Dn_{max}}$	$\mathbf{Dn_{max}}$	$\mathbf{Dn_{max}}$
1	B1	0.265	0.889	0.252
2	B2	0.286	0.276	0.278
3	B3	0.274	0.275	0.277
4	B4	0.299	0.300	0.300
5	B1/B2	0.978	0.183	0.198
6	B1/B3	0.164	0.172	0.169
7	B1/B4	0.212	0.221	0.210
8	B1/B5	0.273	0.168	0.431
9	B2/B1	0.258	0.220	0.235
10	B2/B3	0.148	0.142	0.164
11	B2/B4	0.224	0.227	0.233
12	B2/B5	0.252	0.132	0.414
13	B3/B1	0.241	0.916	0.250
14	B3/B2	0.201	0.196	0.237

No	Channel	FLAASH	QUAC	DOS
		Dn_{max}	Dn_{max}	Dn_{max}
15	B3/B4	0.177	0.184	0.181
16	B3/B5	0.168	0.124	1.857
17	B4/B1	0.283	0.266	0.279
18	B4/B2	0.292	0.293	0.282
19	B4/B3	0.218	0.214	0.216
20	B4/B5	0.207	0.137	0.389
21	NDSSI	0.359	0.232	0.293
22	NSMI	0.206	0.224	0.235

The correlation test used is the Pearson product correlation test. This correlation test compares the value of r_{count} with r_{table}. Correlation is said to be fulfilled and can be continued if $r_{count} > rt_{able}$. The number of model data carried out by the correlation test was 31 samples and a significance level of 5% with r_{table} = 0.355. Based on Table 3, it can be seen that the FLAASH atmospheric correction method that fulfills the correlation test with TSS is B1 / B3 and B2/B3, QUAC atmospheric correction variables that meet the correlation test with TSS are B1/B2, B1/B3, B2/B3 and B2/B5, and the DOS atmospheric correction method that meets the TSS correlation test are B1/B2, B1/B3, and B2/B3. All variables that meet the correlation test have an inverse relationship direction (negative) meaning that if the dependent value increases, then the independent value decreases except QUAC B2/B5. QUAC B2/B5 which has a directional relationship direction (positive) which when the dependent value increases, the independent value increases.

Table 3. The Result of The Pearson Correlation Test.

Variable		Pearson Correlation
FLAASH	B1/B3	-0.582
	B2/B3	-0.504
	B3/B4	-0.279
	B3/B5	-0.337
	B1/B2	-0.511
	B1/B3	-0.601
	B1/B5	0.284
	B2/B3	-0.530
QUAC	B2/B5	0.384
	B3/B2	-0.095
	B3/B4	-0.259
	B3/B5	-0.316
	B4/B5	-0.215
	B1/B2	-0.516
DOS	B1/B3	-0.579
	B2/B3	-0.562
	B3/B4	-0.296

The stepwise method combined method between forwarding and backward methods, namely the first variable entered is a variable that has a high correlation and significant to the dependent variable. The next incoming variable is the variable with the highest partial correlation and still significant. After that, it is evaluated if the variable is entered whether it is still significant or not. Based on the correlation test results, the optimal correlation for each atmospheric correction is B1/B3 which is then used as the main regression in the stepwise method. Stepwise regression is done after knowing the optimal partial correlation. The stepwise regression results show that in the entire band the ratio in each atmospheric correction cannot produce multiple regression. The optimal regression obtained in each atmospheric correction method is the same band ratio, namely B1/B3.

Table 4. The Result of Stepwise Regression.

Variable	Equation	Significance
FLAASH	y = -102.386x + 118.254	0.001
QUAC	y = -192.617x +132.001	0.000
DOS	y = -107.446x + 111.105	0.001

The results of statistical values for making TSS estimation models use remote sensing images using single channels B1 / B3 and B2/B3 which are optimal channels for estimating TSS with low content, while estimation of high content TSS using single band (B4) or band B4/B1 [8]. In this study the optimal transformation is the band ratio B1 / B3, this indicates that there is no optimal effect on channel B4 on TSS estimation modeling. The band B1/B3 ratio used helps estimate waters with a relatively low TSS content. This can be seen also on the spectral reflection curve from the measurement of the spectrometer that the reflection on B3 is higher than in B4, although the reflection of B4 also has a relatively high value.

Spatial distribution of TSS in each atmospheric correction method can be seen that there are here location have TSS content reaching 70 mg/l. The three locations were locations that received TSS input from the river namely the Keduang River from the north-east direction, the Tirtomoyo River from the east, and the Alang River from the south. TSS content ranging from 0 to 70 mg/l and modeling of the three atmospheric correction methods does not appear to be a very significant difference. The mapping results show the accuracy of TSS spatial distribution mapping using FLAASH 55.55% with error estimate 20.95 mg/l, QUAC 54.58% with error estimate 21.60 mg/l, and DOS 55.95% with error estimate 20.95 mg/l.

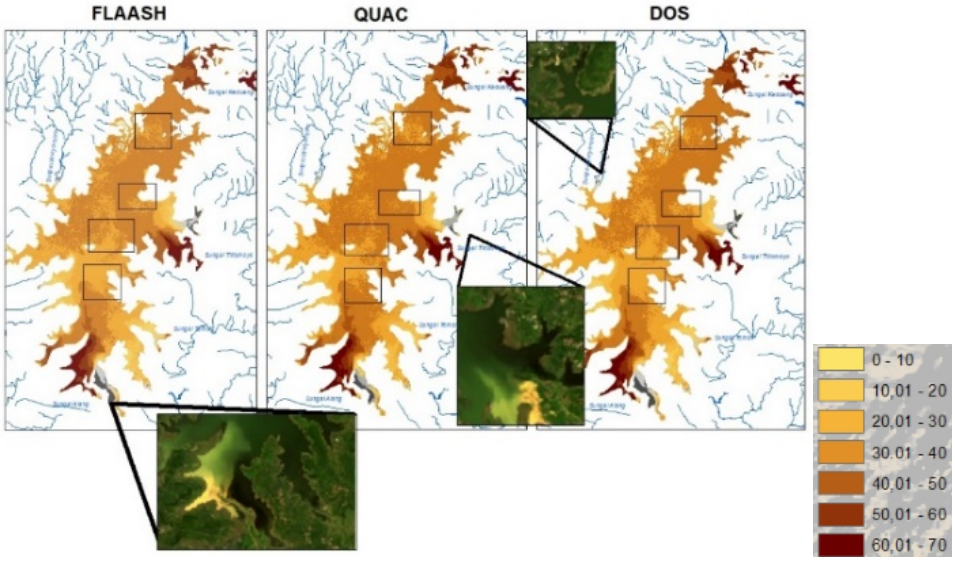

Figure 2. The Different of Spatial Distribution from The Third Method.

The difference in spatial distribution of TSS in the three methods is known that there are several pixels with different estimates of TSS content even though there are no significant differences. Maps are made with the principle of change detection to determine the difference in estimates in each class. The map shows that the FLAASH method is a method that shows a difference of 482 pixels. the QUAC method 5748 pixels, and the DOS method 2126 pixels. Overall differences are found in waters with TSS content of less than 30 mg/l or low TSS content. This shows that in waters with low TSS it has high scattering compared to those in high TSS waters (more than 30 mg/l). This is also because the data being modeled is TSS data itself. Water areas at low TSS have greater scattering, meaning that those areas are more dominant than objects other than TSS.

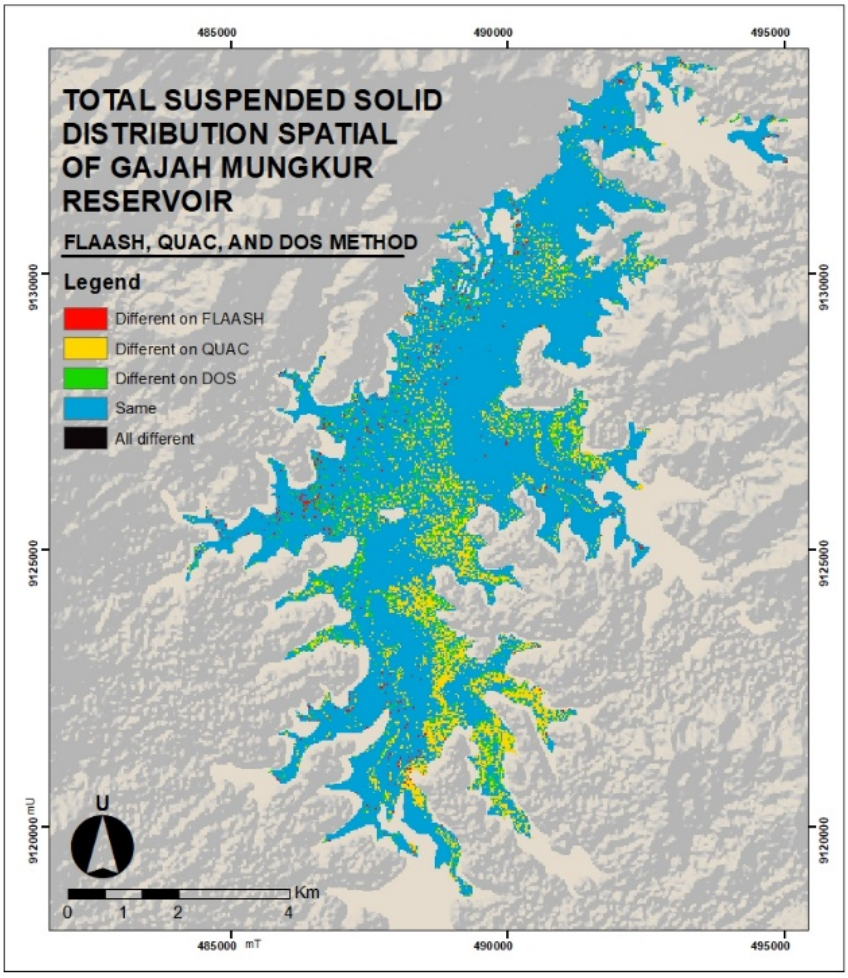

Figure 3. The Different of Spatial Distribution from The Third Method.

4. Conclusions

The results of mapping Total Suspended Solid in Landsat 8 OLI images can use the band B1/B3 ratio in all atmospheric correction methods both FLAASH, QUAC, and DOS showing the spatial distribution of high content TSS in 3 locations originating from the Keduang River, Alang River, and the Tirtomoyo River. Based on the three atmospheric correction methods, the spatial distribution shows that in several locations there are differences in distribution but the differences are not too significant. The difference is found in waters with TSS content of less than 30 mg/l or low TSS content. This is because in waters with low TSS it has a high scattering compared to those in areas with high TSS (more than 30 mg/l). Water areas at low TSS have greater scattering, meaning that those areas are more dominant than objects other than TSS.

5. References

[1] Tim Studi, J., *Studi Penanganan Sedimentasi Waduk Serbaguna Wonogiri.* Laporan Akhir Sementara, 2007. **2**.
[2] Efendi, H., *Telaah Kualitas Air.* Penerbit Kanisius. Yogyakarta, 2003.
[3] DANESHGAR, S., *Remote sensing observations for monitoring coastal zones: Volturno river mouth case study.* 2015.
[4] Song, C., et al., *Classification and change detection using Landsat TM data: when and how to correct atmospheric effects?* Remote sensing of Environment, 2001. **75**(2): p. 230-244.
[5] Danoedoro, P., *Pengantar Penginderaan Jauh*. 2010, Yogyakarta: Andi.
[6] Borges, E.F., S.D. Camila, and P.S. Santos, *Detection of Suspended Sediments in Grande River and Ondas River - Bahia/Brazil*. 2011, The Federal University of Bahia, Institute of Environmental Sciences and Sustainable Development: Brazil.
[7] Hossain, A., Y. Jia, and X. Chao. *Development of remote sensing based index for estimating/mapping suspended sediment concentration in river and lake environments*. in *Proceedings of 8th international symposium on ECOHYDRAULICS (ISE 2010)*. 2010.
[8] Wang, Y., et al., *Experimental research on quantitative inversion models of suspended sediment concentration using remote sensing technology.* Chinese geographical science, 2007. **17**(3): p. 243-249.

A New Chapter in Participatory Mapping in Indonesia

Franko Jhoner[1]*, Rahmat Kurniadi Dewantara[1]*, Fajar Harnowo[1]*

[1]The Indonesian Geospatial Information Agency, KM. 48 Jakarta-Bogor Street, 16911 Bogor, Indonesia

*Corresponding author's e-mail: franko.jhoner@big.go.id, rahmat.kurniadi@big.go.id, fajar.harnowo@big.go.id

Abstract. The enactment of the Geospatial Information Law in 2011 has opened a new chapter in the implementation of Geospatial Information in Indonesia. Various implementing rules of the Geospatial Information Law were also issued so that the Geospatial Information Law itself could be applied. Everyone as a subject of law is strongly supported by its existence in the implementation of Geospatial Information. This is supported by the enactment of a series of regulations regarding the participation of Everyone in the National Geospatial Information Network. In accordance with the Indonesian Geospatial Information Agency Regulation Number 1 of 2015, Everyone can access Participatory Mapping. Everyone can submit corrections or input to Geospatial Data or Geospatial Information through Participatory Mapping. Regarding the correction and input from Everyone, the Geospatial Information Agency will verify and validate specifically the Base Geospatial Information while the Thematic Geospatial Information will be followed up by the relevant Ministries / Institutions or Regional Governments. All of these participatory mapping activities can be accessed by everyone via the GIS-based https://petakita.big.go.id/.

Keywords: Geospatial Information Law, Participatory Mapping, Everyone.

1. Introduction

Indonesia is a big country. Indonesia has a large area, a large population, rich natural resources and diverse cultures. This is also supported by a very strategic geographical position. To develop a large and strategic Indonesian country, planning is needed that is supported by complete, up to date, reliable and maintained geospatial data and information.

The Geospatial Information Act (IG Law) aims to ensure the availability and access of IG that can be accounted for and to realize the usefulness and effectiveness of IG through cooperation, coordination, integration, and synchronization. This law encourages the use of IG in government and social life by using a single reference (single reference) includes Basic Geospatial Information (IGD) and Thematic Geospatial Information (IGT).

Participatory Mapping is a breakthrough in the administration of GIs, as long as it is in line with national policies that have been established. [1] Participatory Mapping Activities must refer to "IGD". Participatory One Map Initiative / POMI has become an element in IG infrastructure development in Indonesia. Good synergy and mutual support from all elements of society are expected to accelerate the achievement of the vision that BIG has set for the progress of the nation [2].

This paper is divided into three sections following this introduction. Section 2 draws out the theoretical tension that frames our contribution, especially in definition of Participatory Mapping based on the definition in regulation and factual activities in general public. Section 3 draw out how regulations regarding Participatory Mapping in Indonesia [3]. This paper using the normative juridical methodology. Study using existing laws and regulations [4].

2. The Definition of Participatory Mapping

There are two kind of the definition of Participatory Mapping. Firstly, the definition of Participatory Mapping in factual activities in general public. The Participatory Mapping Workshop at the Millennium Hotel, Jakarta on July 17, 2012 has defined Participatory Mapping. Participatory mapping is the public jointly or involved in the process of data collection and analysis related to problems and issues around them through the identification and depiction of geospatial features using mapping tools and technology. Secondly, the definition of Participatory Mapping in Indonesia's regulation. Based on Geospatial Information Agency Regulation Number 1 of 2015, we cannot find the definition of Participatory Mapping. But this regulation, govern how everyone is involved in Participatory Mapping.

3. Regulations regarding Participatory Mapping in Indonesia

To access Participatory Mapping site pages, everyone must register her/himself first. All of these participatory mapping activities can be accessed by everyone via the GIS-based https://petakita.big.go.id/.

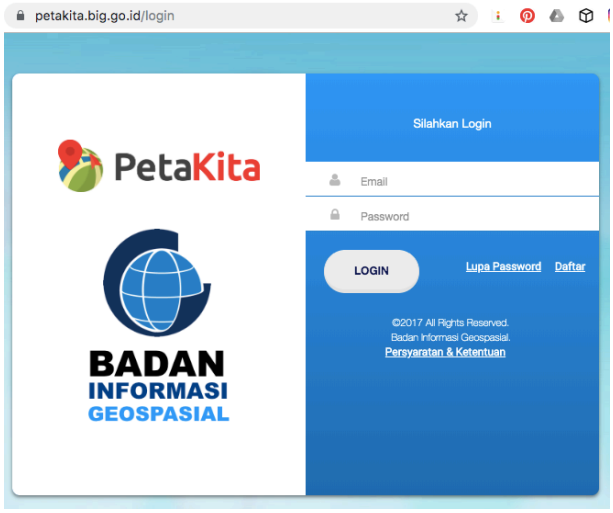

Figure 1. The Main Page of Participatory Mapping.

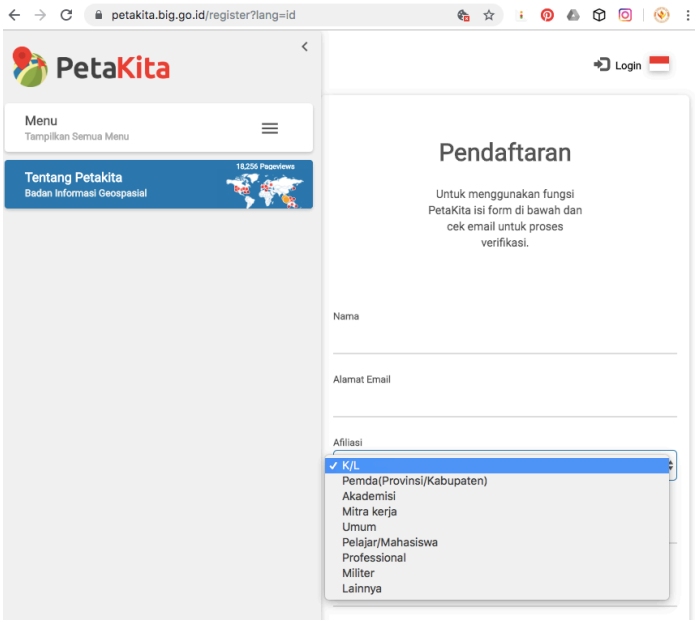

Figure 2. The Page of Participatory Mapping Registration.

After that everyone can access Participatory Mapping. Everyone can submit corrections or input to Geospatial Data or Geospatial Information through Participatory Mapping. Regarding the correction and input from everyone, the Geospatial Information Agency will verify and validate specifically the Base Geospatial Information while the Thematic Geospatial Information will be followed up by the relevant Ministries / Institutions or Regional Governments.
Data that has been through the verification and validation of DG and / or IG quality and declared to be in accordance with certain standards and / or specifications. Network Node (*simpul jaringan*) and / or Network Node Connector (*penghubung simpul jaringan*/BIG) may reject and / or delete corrections or DG and / or IG entries if it is not in accordance with the accuracy or required data standards. If it meets the standards, data can be displayed in InaGeoportal, that can access through: http://tanahair.indonesia.go.id/portal-web.

4. Conclusions

- Participatory Mapping is a breakthrough in the administration of GIs, as long as it is in line with national policies that have been established.
- Everyone can submit corrections or input to Geospatial Data or Geospatial Information through Participatory Mapping

5. References

[1] BIG, *Target Report B04, Participatory Map Publisher Pages in Geoportal*. 2017.
[2] BIG, *Target Report B04 SOP Draft: Participatory Maps in Geoportal*. 2017.
[3] BIG, K., *Peraturan Kepala Badan Informasi Geospasial No. 1 Tahun 2015 Tentang Mekanisme Peran Serta Setiap Orang Dalam Jaringan Informasi Geospasial Nasional*. 2015.
[4] Indonesia, P.R., *Undang-Undang Republik Indonesia Nomor 4 Tahun 2011 Tentang Informasi Geospasial*. 2011.

Acknowledgements
Authors wishing to acknowledge assistance or encouragement from colleagues, special work by legal staff and financial support from The Indonesian Geospatial Agency.

HOSTED BY:

SUPPORTED BY:

GOLD SPONSOR

SILVER SPONSOR

penerbit itenas
Jl. PKH. Mustapha No.23, Bandung 40124
Telp. +62 22 7272215, Fax.: +62 22 7202892
e-mail: penerbit@itenas.ac.id